

REPORT NO. GDC-MAP-80-001

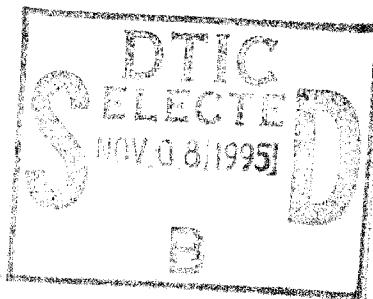
N80-334196

TIME-TEMPERATURE-STRESS CAPABILITIES OF COMPOSITE MATERIALS FOR ADVANCED SUPERSONIC TECHNOLOGY APPLICATION

PHASE I

J. R. Kerr
J. F. Haskins

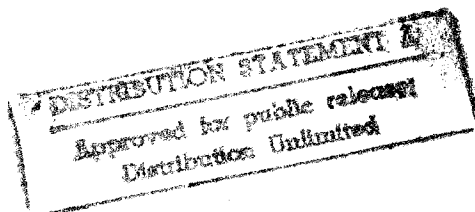
April 1980



Prepared Under
Contract NAS 1-12308

Prepared by
CONVAIR DIVISION OF GENERAL DYNAMICS
San Diego, California

for
NATIONAL AERONAUTICS AND SPACE ADMINISTRATION
Langley Research Center
Hampton, Virginia



DEPARTMENT OF DEFENSE
PLASTICS TECHNICAL EVALUATION CENTER
AERADCOM, DOVER, N. J. 07801

19951023 165

THIS QUOTE IS UNCLASSIFIED

PLASTEC

-- 1 OF 2

DTIC DOES NOT HAVE THIS ITEM

-- 1 - AD NUMBER: D430413
-- 5 - CORPORATE AUTHOR: GENERAL DYNAMICS SAN DIEGO CA CONVAIR DIV
-- 6 - UNCLASSIFIED TITLE: TIME-TEMPERATURE-STRESS CAPABILITIES OF
-- COMPOSITE MATERIALS FOR ADVANCED SUPERSONIC TECHNOLOGY APPLICATION
-- PHASE I,
--10 - PERSONAL AUTHORS: KERR, J. R. ; HASKINS, J. F. ;
--11 - REPORT DATE: APR , 1980
--12 - PAGINATION: 452P
--14 - REPORT NUMBER: GDC-MAP-80-001
--15 - CONTRACT NUMBER: NAS1-12308
--18 - MONITOR ACRONYM: NASA
--19 - MONITOR SERIES: CR-159267
--20 - REPORT CLASSIFICATION: UNCLASSIFIED
--22 - LIMITATIONS (ALPHA): APPROVED FOR PUBLIC RELEASE; DISTRIBUTION
-- UNLIMITED. ~~AVAILABILITY: NATIONAL TECHNICAL INFORMATION SERVICE,~~
-- ~~SPRINGFIELD, VA 22101. N80-33496.~~
--33 - LIMITATION CODES: 1

-- END

Y FOR NEXT ACCESSION

END

Alt-Z FOR HELP3 ANSI

3 HDX 3

3 LOG CLOSED 3 PRINT OFF 3 PARITY

1. Report No. NASA CR-159267		2. Government Accession No.		3. Recipient's Catalog No.	
4. Title and Subtitle Time-Temperature-Stress Capabilities of Composite Materials for Advanced Supersonic Technology Application — Phase I				5. Report Date April 1980	
				6. Performing Organization Code	
7. Author(s) J.R. Kerr and J.F. Haskins				8. Performing Organization Report No. GDC-MAP-80-001	
9. Performing Organization Name and Address Convair Division of General Dynamics Corporation 5001 Kearny Villa Road San Diego, California 92123				10. Work Unit No.	
				11. Contract or Grant No. NAS 1-12308	
12. Sponsoring Agency Name and Address National Aeronautics and Space Administration Langley Research Center Hampton, Virginia 23665				13. Type of Report and Period Covered	
				14. Sponsoring Agency Code	
15. Supplementary Notes Contract Monitors: B.A. Stein and D.R. Rummler					
16. Abstract Advanced composites will play a key role in the development of the technology required for the design and fabrication of future supersonic vehicles. However, implementation of the material into vehicle usage is contingent upon accelerating the demonstration of service capacity and design technology. Because of the added material complexity and lack of extensive service data, laboratory replication of the flight service will provide the most rapid method of documenting the airworthiness of advanced composite systems. A program is in progress to determine the time-temperature-stress capabilities of several high temperature composite materials. Tests included in this study are thermal aging, environmental aging, fatigue, creep, fracture, tensile, and real-time flight simulation exposure. The program has two parts. The first includes all the material property determinations and aging and simulation exposures up through 10,000 hours. The second continues these tests up to 50,000 cumulative hours. This report presents the results of the 10,000 hour phase, which has now been completed.					
17. Key Words (Suggested by Author(s)) Composite Materials, Thermal Aging, Environmental Aging, Fatigue, Creep, Tensile, Shear, Fracture, Flight Simulation Exposure, Boron, Graphite, Epoxy Resins, Polyimide Resins, Aluminum, Supersonic Vehicles, SCR				18. Distribution Statement	
19. Security Classif. (of this report) Unclassified		20. Security Classif. (of this page) Unclassified		21. No. of Pages 452	
				22. Price*	

* For sale by the National Technical Information Service, Springfield, Virginia 22151

FOREWORD

The work presented in this report was performed at General Dynamics Convair Division, San Diego, California, under Contract NAS-1-12308 for the National Aeronautics and Space Administration, Langley Research Center, Hampton, Virginia. Mr. Bland A. Stein and Mr. Donald R. Rummeler served as project monitors.

Mr. James F. Haskins served as General Dynamics program manager. Dr. James R. Kerr was the deputy program manager. Dr. Dick J. Wilkins of General Dynamics Ft. Worth Division provided the random load spectrum and assisted in the wearout theory analysis. Other key contributors to the program were:

Composite Fabrication	Chuck May
	Dr. Michael Miller
	Mike Varlas
Specimen Preparation	Charlie Maikish
Quality Assurance	Gerald O'Barr
	Jack Christian
Testing and Fixture Design	Dr. Ray Adsit
	Curt Tanner
	Ron Torgerson
	Dr. John Waszczak
	Bill Witzell
Thermal Aging	Roscoe Anderson
	Mal Campbell
Flight Simulation Exposure and Fixture Design	Don Bowers
	Charlie Dunkel
	Dick Gilbert
SEM and Metallographic Evaluation	Dr. Mike Featherby
	Bob Pettyjohn

This report was released for publication in April 1980.

Accession For	
NTIS GRA&I	<input checked="" type="checkbox"/>
DTIC TAB	<input type="checkbox"/>
Unannounced	<input type="checkbox"/>
Justification	
<i>per printout</i>	
By <i>enclosed +</i>	
Distribution/ <i>DTIC memo, 2 Nov 75</i>	
Availability Codes	
Dist	Avail and/or Special
<i>A-1</i>	

TABLE OF CONTENTS

Section	Page
1 INTRODUCTION	1-1
2 DESCRIPTION OF PROGRAM	2-1
3 MATERIAL SELECTION AND ACQUISITION	3-1
3.1 MATERIAL SELECTION	3-1
3.1.1 Metal Matrix Composite Material	3-1
3.1.2 Resin Matrix Composite Material	3-2
3.2 MATERIAL ACQUISITION	3-5
3.2.1 Metal-Matrix Composite Material	3-5
3.2.2 Resin Matrix Composite Material	3-6
4 PREPREG QUALITY ASSURANCE TESTING	4-1
4.1 BORON EPOXY	4-1
4.2 GRAPHITE EPOXY	4-2
4.3 BORON POLYIMIDE	4-2
4.4 GRAPHITE POLYIMIDE	4-3
5 LAMINATE PROCESSING AND SPECIMEN FABRICATION	5-1
5.1 LAMINATE PROCESSING	5-1
5.1.1 Boron/Epoxy	5-1
5.1.2 Graphite/Epoxy	5-1
5.1.3 Boron/Polyimide	5-3
5.1.4 Graphite/Polyimide	5-5
5.2 BORON/ALUMINUM TUBE FABRICATION	5-5
5.3 SPECIMEN FABRICATION	5-6
5.3.1 Panel Layouts and Specimen Identification	5-6
5.3.2 Machining Operations	5-7
5.3.3 Doubler Bonding	5-13
6 LAMINATE QUALITY ASSURANCE TESTING	6-1
6.1 METAL MATRIX COMPOSITE MATERIAL	6-1
6.2 RESIN MATRIX COMPOSITE MATERIALS	6-7
6.2.1 Boron/Epoxy	6-7
6.2.2 Graphite/Epoxy	6-9
6.2.3 Boron/Polyimide	6-9
6.2.4 Graphite/Polyimide	6-14
7 BASELINE TESTING	7-1
7.1 TENSILE TESTING	7-1
7.1.1 Specimen Design and Test Procedure	7-2

TABLE OF CONTENTS, Contd

Section	Page
7.1.2 Test Results and Discussion	7-10
7.2 SHEAR TESTING	7-41
7.2.1 Specimen Design and Test Procedure	7-41
7.2.2 Test Results and Discussion	7-48
7.3 FRACTURE TESTING	7-54
7.3.1 Specimen Design	7-55
7.3.2 Test Procedure, Results and Discussion	7-57
7.4 COMPRESSIVE TESTING	7-76
7.4.1 Specimen Design and Test Procedure	7-79
7.4.2 Test Results and Discussion	7-80
8 THERMAL AGING	8-1
8.1 TEST EQUIPMENT AND TEST PROCEDURE	8-1
8.2 TEST RESULTS AND DISCUSSION	8-3
8.2.1 Boron/Epoxy and Graphite/Epoxy	8-3
8.2.2 Graphite/Polyimide	8-29
8.2.3 Boron/Aluminum	8-34
9 ENVIRONMENTAL AGING	9-1
9.1 RESIN MATRIX COMPOSITE SYSTEMS	9-1
9.1.1 Specimen Design and Test Procedures	9-1
9.1.2 Test Results and Discussion	9-3
9.2 METAL MATRIX COMPOSITE SYSTEM	9-7
9.2.1 Specimen Design and Test Procedure	9-7
9.2.2 Test Results and Discussion	9-8
10 CREEP TESTING	10-1
10.1 SPECIMEN DESIGN	10-2
10.2 TEST EQUIPMENT AND TEST PROCEDURE	10-2
10.3 TEST RESULTS AND DISCUSSION	10-7
10.3.1 Boron/Epoxy	10-7
10.3.2 Graphite/Epoxy	10-12
10.3.3 Graphite/Polyimide	10-19
10.3.4 Boron/Aluminum	10-19
11 BASELINE FATIGUE TESTING	11-1
11.1 SPECIMEN DESIGN	11-1
11.2 TEST EQUIPMENT AND TEST PROCEDURE	11-2
11.3 TEST RESULTS AND DISCUSSION	11-9
11.3.1 Boron/Epoxy and Graphite/Epoxy	11-9

TABLE OF CONTENTS, Contd

Section	Page
11.3.2 Graphite/Polyimide	11-22
11.3.3 Boron/Aluminum	11-35
11.3.4 Stacking Sequence Evaluation	11-48
11.3.5 Poisson's Ratio Evaluation	11-51
12 FLIGHT SIMULATION TESTING	12-1
12.1 INTRODUCTION	12-1
12.2 DESCRIPTION OF SIMULATOR	12-3
12.2.1 Test Fixtures	12-3
12.2.2 Load Programmer and Controllers	12-4
12.2.3 Programmer Safety Features	12-4
12.2.4 Hydraulic System	12-4
12.2.5 Heating System	12-6
12.2.6 Cooling System	12-8
12.2.7 Control Console	12-8
12.2.8 Data Recording System	12-8
12.2.9 Monitor/Safety System	12-8
12.2.10 Checkout	12-11
12.2.11 Automatic Operation	12-11
12.3 SPECIMEN CONFIGURATION	12-11
12.4 RANDOM LOAD SPECTRUM	12-14
12.4.1 Spectrum Generation for the Long-Term Tests	12-16
12.4.2 Spectrum for the Short-Term Tests	12-17
12.5 WEAROUT MODEL	12-20
12.6 SHORT-TERM FLIGHT SIMULATION	12-27
12.6.1 Test Plan and Procedures	12-27
12.6.2 Short-Term Test Results	12-36
12.6.3 Short-Term Analysis	12-57
12.7 LONG-TERM FLIGHT SIMULATION	12-62
12.7.1 Test Plan and Procedures	12-62
12.7.2 Long-Term Testing	12-65
12.7.3 Long-Term Test Results	12-80
12.7.4 Phase II Test Plan	12-122
13 THERMAL EXPOSURE TEST PROGRAM SUMMARY	13-1
14 CONCLUSIONS	14-1
15 REFERENCES	15-1

TABLE OF CONTENTS, Contd

Appendix	Page
A AN ANALYSIS OF THE B/P105AC BORON POLYIMIDE SYSTEM ...	A-1
B QUALITY ASSURANCE TEST PROCEDURES	B-1

**TIME-TEMPERATURE-STRESS CAPABILITIES
OF COMPOSITE MATERIALS FOR ADVANCED
SUPERSONIC TECHNOLOGY APPLICATION — PHASE I**

J.R. Kerr and J.F. Haskins

Convair Division of General Dynamics

SUMMARY

High temperature composite materials have the potential of significantly reducing the weight of future supersonic aircraft structures. However, implementation of the material into vehicle usage is contingent upon demonstrating its airworthiness when exposed to the long-time supersonic flight service environment. The primary objective of this research was to establish the time-temperature-stress characteristics and capabilities of five classes of high temperature composite materials to determine their suitability for advanced supersonic technology consideration. The systems studied were B/E, G/E, B/PI, G/PI, and B/Al. The tests that were conducted on the composite systems were baseline tensile, notched tensile, compressive, shear, and fracture; environmental and thermal aging; constant amplitude fatigue, creep and creep rupture; and both accelerated and real-time flight simulation testing using totally random fatigue loading. Phase I of the two-phase program included the baseline, fatigue, and creep determinations and all the aging and flight simulation studies up through 10,000 hours of cumulative exposure. Phase II continues this effort up to 50,000 cumulative hours of simulated flight service. The baseline, constant amplitude fatigue, and creep tests characterized the composite materials and form a basis for comparison with the post-exposure test results. The baseline tests are also used to set the test conditions for the short-term exposures (100 and 200 hours, random fatigue at temperature). The short-term service history tests are performed to generate wearout analysis model data, and to set the stress levels for the long-term service history tests. Finally, the long-term tests provide data on the effect of 10,000- and 50,000-hour simulated supersonic flight service on residual properties of the composites. The thermal aging and the environmental aging exposures are concurrent with the service history tests. The 10,000-hour Phase I portion of the program has been completed. The considerable quantity of data that have been obtained are presented in this report.

SECTION 1

INTRODUCTION

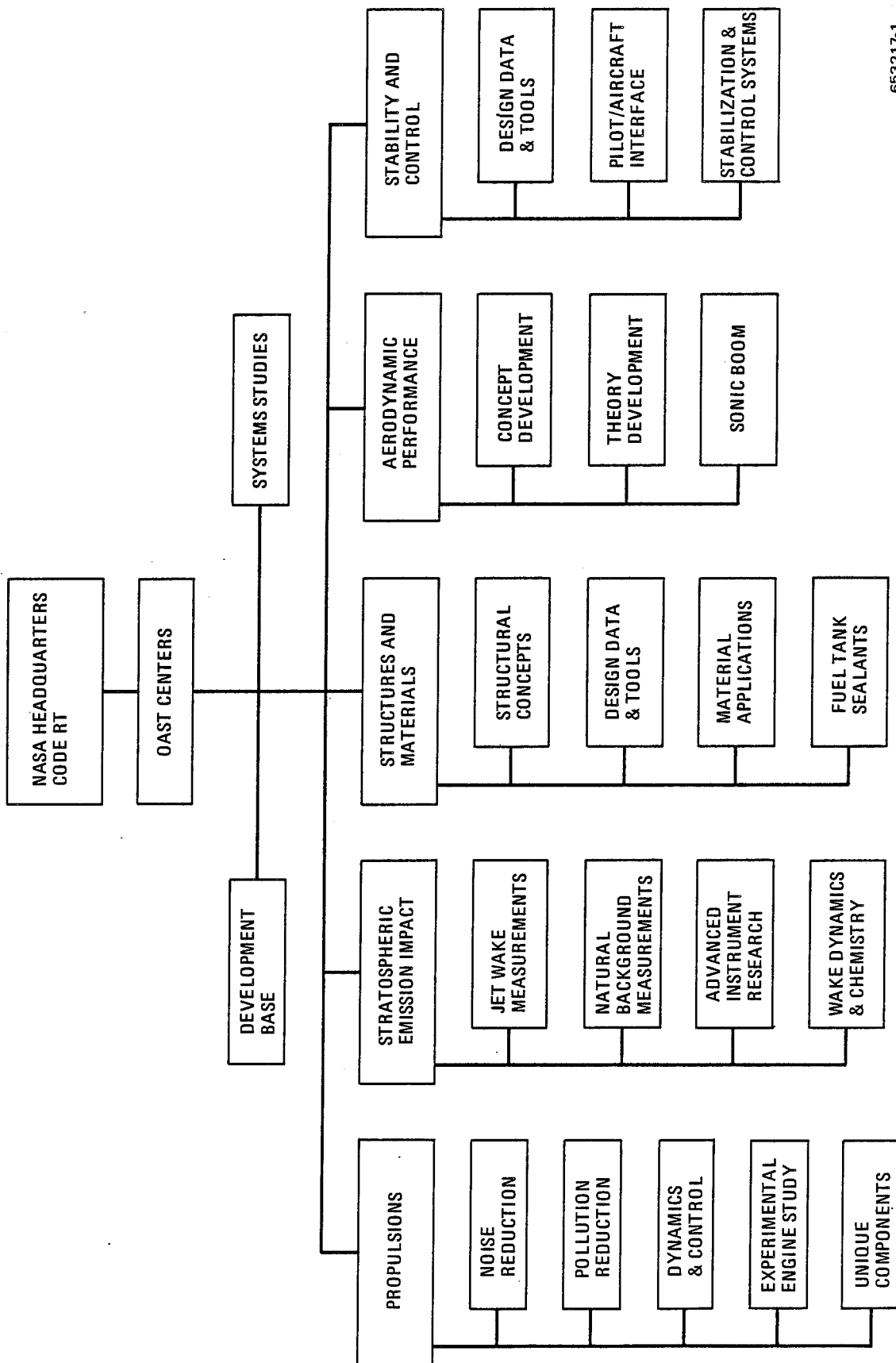
Approximately one year after the cancellation of the United States Supersonic Transport Program, the National Aeronautics and Space Administration initiated the Advanced Supersonic Technology (AST) Program. The name of the AST Program, which started in 1972, was subsequently changed to Supersonic Cruise Aircraft Research (SCAR), and more recently shortened to Supersonic Cruise Research (SCR). The overall objectives of this program were:

- a. To provide an expanded technology base for future civil and military supersonic aircraft.
- b. To provide the data needed to assess the environmental and economic impacts on the United States of present, and in particular, future foreign supersonic transport aircraft.
- c. To provide a good technical basis for any future consideration that may be given by the United States to the development of an environmentally acceptable and economically viable commercial supersonic transport.

A block diagram showing the structure of the program is given in Figure 1-1. The scope of the program included the development base, system studies and the following disciplines:

SCR PROPULSION
SCR STRATOSPHERIC EMISSIONS IMPACT
SCR STRUCTURES AND MATERIALS
SCR AERODYNAMIC PERFORMANCE
SCR STABILITY AND CONTROL

The work being reported on here was done under the Structures and Materials discipline of the SCR program. One of the primary goals in the Structures and Materials area was to advance the technology and establish a data base for advanced composites so that sound technical decisions may be made in the future regarding the use of these materials in supersonic cruise aircraft structures. Primary emphasis was placed on composites because of their high potential for reducing both weight and cost of future supersonic cruise aircraft structures. The long-time resistance to elevated temperature and other environmental factors is being investigated, and, from time to time, additional materials and tests are being added to the time-temperature-stress investigation, which is scheduled to continue into the mid 1980's. Information on the effects of long-time cyclic exposure to the environments and loads representative of long-time supersonic cruise aircraft service for composite materials of interest was not available in 1972, and, as a result, this program to generate such information was initiated in 1973. A range of baseline properties was determined for representatives of five composite materials systems: boron/epoxy, graphite/epoxy, boron/polyimide, graphite/polyimide, and boron/aluminum. Long term exposures out to 10,000 hours have now been completed in static thermal environments and in ones that simultaneously combine programmed thermal histories and mechanical load histories. Material behavior during these exposures and the post-exposure residual property tests provide exposure effects and reveal material degradation mechanisms.



653217-1

Figure 1-1 SCR Program Elements

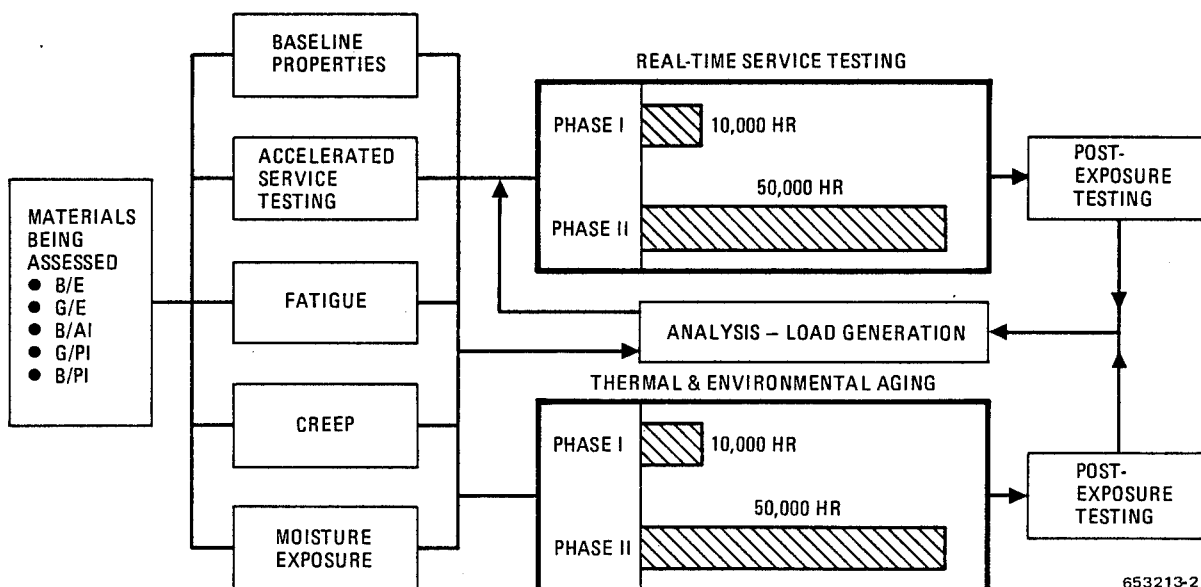
SECTION 2

DESCRIPTION OF PROGRAM

The general objective of this study is to assess the suitability of advanced filamentary reinforced composite materials for future supersonic cruise aircraft structures. The study has two phases. The first includes all material property determinations and aging simulation exposures up through 10,000 hours. The second continues these tests to 50,000 hours.

Figure 2-1 is a schematic diagram, that shows the principal elements of this work. The baseline properties are typical mechanical properties for each of the composites, and these properties are generated in sufficient detail so that any changes in them due to repeated loading and thermal or environmental aging could be measured and reported. Fatigue life is measured before and after various load and temperature histories. The materials' creep behavior is measured early in the program in order to fully evaluate filamentary composites of this type. The aging characteristics of the material are measured at various temperatures. A limited study of moisture exposure effects is included for the resin matrix materials. However, with this exception, moisture effects have been deliberately avoided by use of standard bakeout procedures prior to the various tests conducted during the program. The added costs of including moisture effects to each of the test areas was beyond the scope of the overall program.

The changes in baseline tensile, notched tensile, compressive, shear, fatigue, and fracture properties that occur during times out to 50,000 hours are being measured for environmental and thermal aging conditions, as well as random cyclic loading with cyclic temperature variations.



653213-2

Figure 2-1 Time-Temperature-Stress Capabilities of Composite Materials

These latter tests are intended to simulate conditions experienced in a lower wing surface during supersonic flight and, hence, consist almost entirely of tensile loads. For the same reason the majority of the residual property specimens are tested in tension. As will be discussed later, the failure modes and degradation mechanisms for the various exposure tests were found to be primarily matrix dominated, and, consequently, a greater percentage of compressive, shear, and transverse tensile tests would have been preferred.

In order to provide a device capable of simulating supersonic flight conditions of load and temperature, a machine was built that would be capable of not only random loading and temperature variation but could test a large number of specimens at the same time. It is desirable that the apparatus be able to accommodate a large number of test specimens because

of the expected data scatter associated with advanced composites. The machine must also be capable of operating for long periods of time with little maintenance and monitoring and be designed in such a manner as to possess adequate safeguards against either overloading or overheating the specimens.

Several assumptions are made to define the loading spectrum. The mission profile and loads were obtained from reference 1. These data were also used for the study described in reference 2. The life of a supersonic airplane is assumed to consist of 25,000 flights of two hours duration each. For this work, each flight is assumed to be an "operational flight" as defined in reference 1. Each flight consists of a 10-minute climb, a 90-minute cruise, a 20-minute descent, and a single landing load. The number of loads per flight and the number of loads in each of the segments are modeled after the reference 1 load sequence. However, the loads are randomized such that all the loads expected to occur in 25,000 flights are included. Since the 90-minute cruise is scheduled to include only about 8 loads per flight, the mean load is held for 44 minutes before and after the imposition of a 2-minute cruise loading period. The climb and descent loads are distributed over the entire climb and descent time.

The job of setting load levels for each of the composites materials for the random load spectrum so that some but not all specimens will fail during the 50,000-hour program is indeed a difficult task. This had to be done by running accelerated tests in which many loads could be applied at elevated temperature in a fairly short time. We chose to apply a $\frac{1}{2}$ lifetime of loads in 200 hours, which worked out to be about one load a second. The real-time flight spectrum is more like 20 loads per hour. The accelerated tests are run for both 100 and 200 hours at load levels such that we would have 80% survival if the tests were run to 400 hours.

The residual strength is measured for each specimen after it has been subjected to $\frac{1}{4}$ and $\frac{1}{2}$ lifetime of loads at elevated temperature. These strengths are then used to calculate, using the Halpin wearout model (ref. 3), the load levels for real-time testing, again using 80% survival at the end of 50,000 hours.

The calculated mean and peak load levels set by the 80% survival for the 50,000 hours or one lifetime are used to set the real-time load levels for the flight simulator. These differ for each composite system and also differ for the notched and unnotched specimens of the same composite. Thus each composite system will be subjected to 50,000 hours of real-time flight simulation testing using random loading and temperature described by the climb, cruise, and descent portions of the flight.

Following completion of the 10,000-hour Phase I portion of flight simulation exposure, half of the specimens are removed from test. An extensive examination of the specimens is conducted to determine the extent of damage and, for those specimens that have failed, to identify the degradation mechanisms responsible for these early failures. The specimens that survive the 10,000 hours of flight simulation exposure are used to determine residual tensile, notched tensile, compressive, shear, and fatigue properties. In this way the results of the long-term flight simulation tests can be compared with the wearout model predictions based on accelerated flight simulation exposures.

SECTION 3

MATERIAL SELECTION AND ACQUISITION

The "Structural Design Guide for Advanced Composites Applications" (ref. 4) has limited the term "advanced composites" to those systems characterized by high-strength, high-modulus fibers. For this study, advanced composites are those systems whose reinforcements have a filament tensile strength greater than 2100 MN/m² (300 ksi) and a filament modulus greater than 210 GN/m² (30 million psi).

At the time this contract was initiated, a multitude of advanced composite material systems had been developed and evaluated to various degrees. In general, five classes of material systems had been used by numerous workers in this field: boron/epoxy (B/E), graphite/epoxy (G/E), boron/polyimide (B/PI), graphite/polyimide (G/PI), and boron/aluminum (B/Al). Within each of these five classes there were several types of matrix materials and different types of fibers. The following sections discuss each of the five classes of materials and Convair's choices as to the specific advanced composite systems to be evaluated.

3.1 MATERIAL SELECTION

3.1.1 METAL MATRIX COMPOSITE MATERIAL. Table 3-1 shows the large variety of filaments and matrix materials that were available when the program was initiated. Table 3-2 lists a number of the most promising and widely used processing methods for the primary fabrication of sheet, plate, and structural shapes of metal-matrix composite materials.

Table 3-1. Metal-Matrix Composite Raw Materials

Fibers	Matrix
Boron (4 mil)	Aluminum
Boron (5.6 mil)	1100
Borsic (4.2 mil)	2024
Borsic (5.7 mil)	2219
Nitride-coated Boron	6061
Silicon Carbide	7002
Stainless Steel	7075
Graphite	7178
	713
	718
	K01
	Magnesium
	Titanium
	Nickel

Table 3-2. Primary Processing Methods

Processing Method	Typical Forms Produced
Diffusion Bonding	Mono- or multilayer tape, sheet, plate, structural shapes
Braze Bonding	Mono- or multilayer tape, sheet, plate, shapes
Eutectic Bonding	Sheet, plate, structural shapes
Plasma Spraying	Monolayer tape
Molten-metal Infiltration (Casting)	Mono- or multilayer tape, sheet, plate, structural shapes

It has been found that no one metal-matrix composite material is superior for all possible applications. However, data based on filament-matrix compatibility, comprehensive physical and mechanical property tests, primary and secondary fabrication studies, raw material and processing costs, and extensive experience in working with composite materials indicated that diffusion-bonded B/Al, in particular the large diameter (5.6-mil) boron with 6061 aluminum matrix, offered the most promise for widespread structural applications in various aircraft systems. B/Al composite material had also been found to be highly resistant to various environmental exposures, with excellent retention of properties at cryogenic and elevated temperatures, and with little or no effect of space exposures on mechanical or physical properties. Another attribute of B/Al, and metal-matrix composite material in general, was its very high transverse modulus, about 140 GN/m^2 (20 million psi) for B/Al. This enables the use of unidirectional layups in a number of structural applications that would not be possible with organic-matrix materials with their low transverse moduli. Because of these considerations (ref. 5 to 11) diffusion bonded, 5.6 mil boron/6061 aluminum was chosen for evaluation on this program.

Single-step hot pressing was the technique selected for fabricating the B/Al sheet material because of the ability to produce large panel sizes in a single pressing operation, and because of lower processing costs. In this method, boron filaments are wound over a mandrel onto thin-gage sheet material. These layers are then cut and stacked to the desired thickness and the material consolidated in a hot press. Because of more economical production of large sheet material in pressing operations, this method was chosen over the isostatic pressing technique that required consolidation of prefabricated laminates (tape material). At the beginning of the program two qualified suppliers were available. They had been using the single-step hot pressing technique to supply high-quality metal-matrix composites on a production basis for numerous hardware programs at Convair and other laboratories.

3.1.2 RESIN MATRIX COMPOSITE MATERIAL

3.1.2.1 Boron/Epoxy. At the time that this program started B/E was the most highly characterized of the advanced composite materials. As a result of approximately seven years

of evaluation, the industry had generally settled on two resin systems (Avco 5505 and 3M SP-272). 3M also provided the same resin on uncoated boron (SP-292) and maintained the same basic properties. Other 3M systems such as SP-290 had some better high-temperature properties than the SP-292 but were not as thoroughly characterized. General Dynamics had generated extensive design-allowable data on the Avco 5505 under Contracts F33615-68-C-1474 and AF33(615)-5257 (ref. 12 and 13). Convair preferred the Avco 5505 system because of its somewhat higher temperature resistance and its wide application at that time.

Most early work, conducted by Convair and elsewhere, used the 4.0-mil boron filaments. Some work had been conducted using 5.6- and 6.0-mil-diameter boron filaments, but selection of the 4.0-mil filament was made to avoid an extensive program necessary to characterize the larger diameter material. Considerable engineering data already existed on the coated 4.0-mil diameter boron including static and fatigue characteristics for many configurations with and without imperfections. IITRI (ref. 14) generated extensive data on the effects of environmental exposure on the mechanical and physical properties of the 4.0-mil Avco 5505. Since the purpose of this program was to evaluate long-term effects, selection of a fully characterized system was desirable. In addition, the long-term effects were thought to be primarily matrix dependent and independent of filament diameter.

3.1.2.2 Graphite/Epoxy. Convair had worked on high-strength, high-modulus graphite fibers as a reinforcement for epoxy and polyimide resins since 1965. In this period there had been a proliferation of graphite fibers. Early fibers based on visose rayon, such as Thornel 25, Thornel 40, and HITCO HMG-30, had been surpassed and were no longer seriously considered for structural aircraft applications. Newer fibers, primarily based on polyacrylonitrile precursors, had become the serious contenders for present and future aircraft applications. These fibers could be generally divided into four categories:

- a. Low modulus/ultra-high strength.
- b. Medium modulus/high strength.
- c. High modulus/medium strength.
- d. Ultra-high modulus/medium strength.

The first category of low modulus, 207 to 221 GN/m² (30 to 32 million psi), coupled with ultra-high strength, greater than 2760 MN/m² (400 ksi), was finding most usage in current aircraft applications because of its high strength and very low cost. Fibers that fell in this category were Hercules Type A-S and Stackpole Panex 30/A. Others having the same modules but somewhat lower strength were Thornel 300, Fortafil 30-T, and Morganite III. Type A-S had had the most usage at that time. General Dynamics has used this type of fiber extensively in the F-111 pivot fitting fairing program and the F-5 fuselage program.

The second category of fibers, those having medium modulus, 262 to 276 GN/m² (38 to 40 million psi), and high strength, greater than 2410 MN/m² (350 ksi), included such products as HT-S, Modmor Type II, and Fortafil 4-T and had been used extensively in the preceding years. They were inherently costlier than the 207 GN/m² (30 million psi) fibers and were expected to have lower utilization in the future than they had in the past.

The third category of fibers, those having high modulus, 345 to 414 GN/m² (50 to 60 million psi), and medium strength, 2070 to 2760 MN/m² (300 to 400 ksi), included such products as HM-S, Modmor Type I, and Fortafil 6-T. These fibers had not been used as extensively as the first two categories because of higher cost, lower strength, and poorer resin compatibility (lower shear strength in composites).

The fourth category of fibers, those having ultra-high modulus, greater than 483 GN/m² (70 million psi), and medium strength, 1520 to 2240 MN/m² (220 to 325 ksi), included GY-70 and Thornel 75 materials. They had the same general problems as the third category described above.

Based on the above review of available graphite fibers, Convair selected the epoxy resin-impregnated Type A-S fiber.

In the area of high-temperature 450 K (350° F) epoxy resins, there had also been a proliferation of candidate systems. Up to 1971, the prime resins evaluated and used for structural aerospace applications were Fiberite X-904, Hercules 3002, Whittaker 5205 and 5206. The 3002 was extensively evaluated for design properties by IITRI (ref. 14) and North American Rockwell (ref. 15). However, the 3002 was adversely affected by moisture, was costly, and was difficult to process into prepreg; the availability of this resin for future programs was in doubt at this time period.

In 1972 and 1973 a number of new high-temperature epoxy resins had been introduced, such as Ferro E-350 and E-450; Fiberite X-911, X-915, and X-934; Whittaker 5208; and Hercules 3501. Of these, the E-350, X-934, 5208, and 3501 were seeing the most use in evaluations and in production of aircraft parts.

Convair conducted an extensive screening of in-house data, vendor information, and outside literature relating to the newer high-temperature epoxy resins. The leading candidates were Ferro E-350 and Hercules 3501 with the E-350 appearing to be slightly better. However, at that time Ferro Corporation had recently moved its plant, lost some key personnel, and was leaving the graphite prepreg business. In addition to the favorable rating in the screening evaluation, the A-S/3501 system was currently being used in large commercial applications, was being evaluated extensively for missile applications, and was believed to be the system that would be the standard G/E composite for aircraft applications. Based on these considerations and an excellent cost picture, the A-S/3501 system was selected for the program.

3.1.2.3 Boron/Polyimide. Early studies of B/PI composites were conducted with the P13N, P10P, and 703 polyimide resin systems (ref. 16 to 20). Initially, attention was paid strictly to the fabrication of low-void laminates. As such, the prepegs were tack-free, highly imidized materials that were acceptable for making flat laminates but unacceptable for large parts. Later work led to modifications in the P13N and P10P resin systems to produce P105A, which was the first step toward developing a tacky prepreg that would yield low-void polyimide laminates. At about this time Convair under contracts NAS 8-26198 "Development of Boron and Graphite Polyimide Design Data," and NAS 8-28201, "Polyimide Compression Panel," was investigating the development and use of B/PI advanced composites. Some of the candidate resin systems evaluated were: 700, 703, 709, 710, P13N, P10P, P105A, Gemon L, 4707, and BPI-373. Two of these, P105A and 703, were selected for additional processing studies,

and some preliminary test data were developed for each system using both the 5.6- and 4.0-mil diameter boron fiber. Test results showed that 1) the data for the B/P105A composite system was significantly better than the B/703 composite system, and 2) the 4.0-mil boron fiber was superior to the 5.6-mil boron fiber in that resin contents and laminate shear properties were higher (ref. 21). For these reasons the 4.0-mil boron fiber and the P105A polyimide resin system were selected for the program. At about the time that the B/PI composite was being selected, Ciba-Geigy, the manufacturer of the resin, replaced the P105A with a newer version designated P105AC. It was this polyimide that was evaluated on the test program.

3.1.2.4 Graphite/Polyimide. Unlike the B/PI composite systems, a fully developed and characterized G/PI system was available at the time that the program was initiated. The G/PI system (HT-S/710) was developed by Convair under Contract NAS 8-26198. Substantial quantities of mechanical property, thermal aging (short time), moisture resistance, and creep data were available on this system (ref. 22). At the same time, under Contract NAS 8-28201, Convair was determining baseline design properties for A-S/710 G/PI composite systems. These data were used to design, fabricate, and analyze a large compression panel for short-term applications at 589 K (600° F). Based on the results of these two contracts, Convair selected the HT-S/710 system.

The HT-S graphite fiber was selected because of its high strength and lower weight loss at 589 K (600° F) than the Type A-S graphite fiber. Data developed and reported by Morgan Hanson of the NASA Lewis Research Center at the National SAMPE Conference in Huntsville, Alabama in 1971 indicated that the Type A-S fiber oxidized severely at 589 K (600° F). After 1000 hours, the uncoated A-S fiber had weight losses approaching 100 % (ash). What happens in a composite was unknown. However, for this program Convair believed the extra \$5 to \$10 per pound for the HT-S fiber was justified since it had higher oxidative stability than the Type A-S fiber. The A-S fiber appeared to be fully acceptable for use at 450 K (350° F) with epoxy resin systems but not for use at 589 K (600° F) with polyimide systems.

The 710 resin system was selected because it was believed to be fully characterized, compatible with graphite fibers, commercially available as prepreg from three material suppliers, and showed higher temperature stability than any of the other then available polyimide resins.

3.2 MATERIAL ACQUISITION

The following sections describe the procedures involved in purchasing the five advanced composite systems selected for evaluation on this program. For two of the materials, B/E and B/Al, little or no difficulties were encountered in procurement or during quality assurance testing. For three of the materials, however, considerable problems occurred either in acquiring the prepreps or during acceptance testing.

3.2.1 METAL-MATRIX COMPOSITE MATERIAL. The 5.6-mil boron/6061 aluminum composite, referred to as B/Al, was obtained from AVCO Corporation, Systems Division, Lowell, Massachusetts. The material, ordered to General Dynamics Specification 0-00854, was received in the form of finished sheets, 0.3 m by 0.6 m (12 in. by 24 in.) in dimensions. The requirements for the program were:

- 6 ply, $[0^\circ \pm 45^\circ]_s$ layup — 11 sheets
- 12 ply, $[0^\circ \pm 45^\circ]_{s2}$ layup — 1 sheet

6 ply, $[0^\circ]_6$ layup — 14 sheets

12 ply, $[0^\circ]_{12}$ layup — 1 sheet

Delivery of the B/AI was on schedule, and, with the exception of one 6-ply unidirectional panel, all were of acceptable quality. The one panel showed indications of poor bonding during ultrasonic C-scan testing and was returned to AVCO for replacement.

3.2.2 RESIN MATRIX COMPOSITE MATERIAL

3.2.2.1 Boron/Epoxy. The Rigidite 5505/4 boron/epoxy composite, referred to as B/E, was also obtained from AVCO Corporation, Systems Division, Lowell, Massachusetts. The material was ordered to meet the requirements of General Dynamics Specification FMS-2001B. A total of 12.7 kg (28 lb) in the form of 0.08 m (3 in.) wide prepreg tape was required for the program. The material was delivered on schedule and successfully passed all the quality assurance requirements for both the prepreg and fabricated laminates.

3.2.2.2 Graphite/Epoxy. The A-S/3501-5 graphite/epoxy, referred to as G/E, was obtained from Hercules Incorporated, Bacchus Works, Magna, Utah. Seventeen kg (37 lb) of 0.08 m (3 in.) prepreg tape was purchased to the following Hercules Specifications: fiber properties per HD-SG-2-6001; prepreg properties per HD-SG-2-6006A except flow to be run at 436 K (325 °F), 100 psi, 15 minutes; composite properties per HD-SG-6002A. This batch of material was received on schedule and checked out perfectly in the prepreg quality assurance tests. The flexural and short beam shear properties determined from the quality assurance panels were also satisfactory. Based on these quality assurance results, 12 full size panels were fabricated for the test program. The baseline tensile data, however, were widely scattered and significantly lower than normal. The transverse tensile strengths were particularly bad, with an average value of 22.8 MN/m² (3.3 ksi) at room temperature. To check that all the panels were unacceptable, resin and fiber content determinations and three tensile tests were made on each of the 6-ply unidirectional and crossply panels. The results are given in Table 3-3. The wide scatter and generally low values are clearly evident. Expected values of F_{tu} are about 1400 MN/m² (200 ksi) and 55 MN/m² (8 ksi) for the longitudinal and transverse directions of the unidirectional layups and about 550 MN/m² (80 ksi) for the crossply layups. The resin and fiber contents shown in Table 3-3 are all acceptable, although Panel No. 10 has a somewhat low fiber content. A check with the vendor (Hercules) revealed that the material was among the first to come off the line from a new prepregging process. Although the resin content was acceptable (determined during quality assurance testing), the resin distribution through the material was poor because of a lack of penetration into the graphite tows. Similar results were reported by others from material obtained during the same time period. Hercules corrected the production problem and replaced the material at no charge, but a considerable time delay was incurred because of the rejected material.

Visual examination of the replacement batch of G/E prepreg revealed none of the resin poor areas that were typical of the previously rejected batch. The material successfully passed all of the quality assurance requirements for both the prepreg and fabricated laminates. As an added check on the acceptability of the panels, tensile coupons were prepared from unused portions of the unidirectional quality assurance panel and the first full size crossply panel. The values obtained, 1655 MN/m² (240 ksi) and 579 MN/m² (84 ksi), were typical of good G/E material. Transverse tensile tests on the unidirectional panel gave an average ultimate strength of 59 MN/m² (8.6 ksi). This value is again typical of good G/E material.

Table 3-3. Quality Assurance Data for G/E Panels from Rejected Batch of A-S/3501-5 Prepreg

Panel No.	Orientation	Plies	Resin Content (wt %)	Fiber Content (vol. %)	Tensile Strength	
					MN/m ²	(ksi)
10	[0°] ₆	6	36.2	55.5	1310	190
					752	109
					696	101
11	[0°] ₆	6	32.6	59.4	1080	157
					1350	196
					1380	200
13	[0°] ₆	6	32.2	59.8	1903	276
					1510	219
					1030	150
16	[0°] ₁₂	12	27.8	64.6	a1640	a238
					a1730	a251
					a1780	a258
17	[0° ± 45°] _{s2}	12	28.5	63.8	a 786	a114
					a793	a115
					a848	a123
22	[0° ± 45°] _s	6	32.3	59.7	331	48
					379	55
					352	51
23	[0° ± 45°] _s	6	31.7	60.4	337	49
					317	46
					483	70
24	[0° ± 45°] _s	6	30.9	61.2	414	60
					434	63
					538	78
25	[0° ± 45°] _s	6	29.2	63.2	414	60
					414	60
					455	66
26	[0° ± 45°] _s	6	30.6	61.6	345	50
					538	78
					379	55

^aFlexural strength.

3.2.2.3 Boron/Polyimide. The 4.0-mil B/P105AC boron/polyimide, referred to as B/PI, was obtained from AVCO Corporation, Systems Division, Lowell, Massachusetts. As no General Dynamics procurement specification existed, the material was ordered to the following requirements:

- a. Fiber Strength: 500,000 psi minimum
- b. Resin Content: 38 to 48%
- c. Volatiles: 10 to 20%
- d. Flow 450 K (350° F) 30 to 42%

A total of 28 kg (62 lb) of prepreg in 0.3 m by 1.8 m (12 in. by 72 in.) sheets was required for the program. Delivery of the prepreg was delayed approximately three months because of difficulties encountered by AVCO in obtaining the polyimide resin from the manufacturer, Ciba-Geigy. Upon receipt of the prepreg, quality assurance testing was performed. The material was found to be acceptable and two quality assurance panels were fabricated. Quality assurance testing of the laminates was completed with the material being found acceptable. While the B/PI material passed the prepreg and laminate quality assurance requirements it was later removed from the test program because of low tensile properties and extensive thermal degradation observed during thermal aging and short-term flight simulation testing. Complete details of the problems encountered with this material system and the reasons for the poor results are found in Appendix A.

3.2.2.4 Graphite/Polyimide. The HT-S/710 graphite/polyimide composite, referred to as G/PI, was the most difficult material to procure. More than a year passed from the time of placing the initial order until completion of quality assurance testing and acceptance of the test material. One of the reasons for selecting HT-S/710 was the belief that the prepreg was readily available from at least three material suppliers. As it turned out one source was not interested in the small volume required for the program while the other two sources experienced considerable problems in fabricating acceptable prepreg. Because no General Dynamics procurement specification existed the material was ordered to the following requirements:

- a. Fiber Strength: 350,000 psi minimum
- b. Resin Content: 35-45%
- c. Volatiles: 10-20%
- d. Flow: 15-25%
- e. Acid Equivalent No.: 520 to 540

The following is a chronological account of how the material was obtained.

Jul 1973	An order for 17 kg (37 lb) of prepreg tape was placed with E.I. DuPont De Nemours and Company, Fabrics and Finishes Department, Saugus, California.
Aug 1973	The prepreg was delivered on schedule but was rejected because of low fiber volume and low acid equivalent number.

Sep 1973 A second batch was delivered. The prepreg properties were within specification requirements; however, a panel fabricated from the prepreg showed precipitation and waviness. At this time a second source of the prepreg was being checked. Hercules Incorporated quoted a 50% higher price and an 8 to 10 week delivery schedule. DuPont reported that they discovered that the resin used to fabricate the first two batches of prepreg was bad and that a third batch, made with new resin would be prepared.

Oct 1973 The third batch of prepreg delivered by DuPont failed to produce acceptable panels and was also rejected. A new order was placed with Hercules for the 17 kg (37 lb). While the price was about 50% higher, Hercules had had considerable experience with the G/PI prepreg, and no further difficulties were anticipated. Delivery, however, was not expected until December 1973.

Dec 1973 Delivery was delayed to allow the acid equivalent number of the polyimide resin to reach an acceptable value prior to manufacturing the prepreg.

Jan 1974 Delivery was further delayed when it was determined that the HT-S graphite fibers were not within specifications. A new batch of fibers was obtained and manufacture of the prepreg material was scheduled for February 1974.

Feb 1974 The first batch of prepreg manufactured by Hercules failed to meet specifications. A second batch was prepared from the remaining fiber and resin. This material was found to be acceptable, but the quantity was less than that ordered, 11 kg (24 lb) of an order of 17 kg (37 lb). Because of the high costs incurred and the small size of the order Hercules was not willing to complete the order.

Mar 1974 DuPont agreed to prepare a demonstration sample of prepreg. If the material was found to be satisfactory an order for the 17 kg (37 lb) was to be given to them.

Apr 1974 DuPont reported a delay in preparation of the demonstration sample because of out of date resin that was unacceptable for manufacturing prepreg. A new batch of resin was ordered from Monsanto.

May 1974 The small demonstration sample of prepreg was received from DuPont. The first panel fabricated from this batch was acceptable, but later panels tended to precipitate and blister. Because of these inconsistencies no order was placed with DuPont. As a result of the numerous delays encountered in obtaining the G/PI material it was decided that the 11 kg (24 lb) batch produced by Hercules would be purchased for the test program if satisfactory test panels could be fabricated. It was thought that sufficient panels could be made from the 11 kg (24 lb) to satisfy the program requirements. A small test sample was, therefore, ordered from Hercules.

Jun 1974 The sample submitted by Hercules was evaluated and found to produce an excellent laminate. To check the consistency of the prepreg a second panel was fabricated, and, again, an acceptable laminate was obtained. Based on these results the remaining 10 kg (22 lb) of prepreg were purchased from Hercules.

Jul/
Aug 1974 The material was delivered and successfully passed all of the quality assurance requirements for both the prepreg and fabricated laminates.

SECTION 4

PREPREG QUALITY ASSURANCE TESTING

The organic matrix composite materials were purchased to specific requirements on the purchase orders or, when available, to existing General Dynamics or industry specifications. To ensure that these requirements were satisfied the following properties were determined upon receipt of the prepreg:

- a. Fiber content (percentage by weight).
- b. Resin solids (percentage by weight).
- c. Volatiles (percentage by weight).
- d. Resin flow (percentage by weight).
- e. Process gel.

A description of the test methods which were used is given in Appendix B.

4.1 BORON EPOXY

B/E was purchased from AVCO Corporation to General Dynamics Specification FMS-2001B.

The FMS-2001B specification requirements, the values from the AVCO Certified Test Report received with the shipment, and the results of the Convair quality assurance tests are given in Table 4-1. Both the AVCO and Convair results satisfied the procurement specification requirements and the material was considered to be acceptable.

Table 4-1. Prepreg Requirements and Properties for Rigidite 5505 B/E Batch Number 58

Property	Requirements of Specification FMS-2001B, %	AVCO Certified Test Report Data, %	Convair Quality Assurance Test Results, %
Fiber Content (wt %)	—	—	68.1
Resin Solids Content (wt %)	29-34	31.7	31.0
Volatile Content (wt %)	2% max.	1.08	0.9
Resin Flow (wt %)	10-20	13.5	15.7

4.2 GRAPHITE EPOXY

The G/E prepreg was purchased from Hercules Incorporated to Hercules Specification HD-SG-26006A. The HD-SG-2-6006A specification requirements, the values from the Hercules Quality Assurance tests received with the shipment, and the results of the Convair Quality Assurance tests are given in Table 4-2. Both the Hercules and Convair results satisfied the procurement specification requirements and the material was considered to be acceptable.

Table 4-2. Prepreg Requirements and Properties for A-S/3501-5 G/E — Run Number 051, Spool 4C

Property	Requirements of Specification HD-SG-2-6006A, %	Hercules Quality Assurance Test Results, %	Convair Quality Assurance Test Results, %
Fiber Content (wt %)	—	58.3	57.2
Resin Solids Content (wt %)	39-45	40.5	41.6
Volatile Content (wt %)	2% max.	1.2	1.2
Resin Flow (wt %)	15-35	18	21.7

4.3 BORON POLYIMIDE

The B/PI prepreg was purchased from AVCO Corporation with a list of Convair requirements. No procurement specification or industry specification was available. Table 4-3 lists these Convair requirements, the values from the AVCO Certificate of Conformance received with the shipment, and the results of the Convair quality assurance tests. All of the AVCO and Convair results except for the slightly high Convair value for volatile content satisfied the Purchase Order requirements. The small difference, 0.7% high, was not considered to be sufficient cause for rejection of the shipment.

Table 4-3. Prepreg Requirements and Properties for B/P105AC B/PI — Resin Batch Number 5-73, Sheet Numbers AX-P105A-38 to AX-P105A-105

Property	Requirements of Convair Purchase Order, %	AVCO Certificate of Conformance Data, %	Convair Quality Assurance Test Results, %
Fiber Content (wt %)	—	—	35.7
Resin Solids Content (wt %)	38-48	38-46	43.6
Volatile Content (wt %)	10-20	14-20	20.7
Resin Flow (wt %)	30-42	—	38.3

4.4 GRAPHITE POLYIMIDE

The G/PI prepreg was purchased from Hercules Incorporated with a list of Convair specified requirements. No procurement specification or industry specification was available. Table 4-4 lists these Convair requirements and the results of the Convair quality assurance tests. No quality assurance test results from Hercules were received with the shipment. As shown in Table 4-4, the Convair results satisfied the Purchase Order requirements and the material was considered to be acceptable.

Table 4-4. Prepreg Requirements and Properties for HT-S/710 G/PI — Run Number 449, Spool Numbers 1 and 2

Property	Requirements of Convair Purchase Order, %	Convair Quality Assurance Test Results, %
Fiber Content (wt %)	—	44.4
Resin Solids Content (wt %)	35-40	40.0
Volatile Content (wt %)	10-20	15.6
Resin Flow (wt %)	15-25	17.2

SECTION 5

LAMINATE PROCESSING AND SPECIMEN FABRICATION

5.1 LAMINATE PROCESSING

All of the composite fabrications on this program were processed using autoclave curing methods. This included flat panels that ranged in size up to 0.93 m² (10 ft²), and 0.025 m (1 in.) diameter by 0.3 m (12 in.) long tubes. Two of the materials, G/E and B/PI, were fabricated into both flat panels and the torsion tube configuration. In addition, precompaction and/or "B" staging operations were included in several of the overall processes and are described in detail.

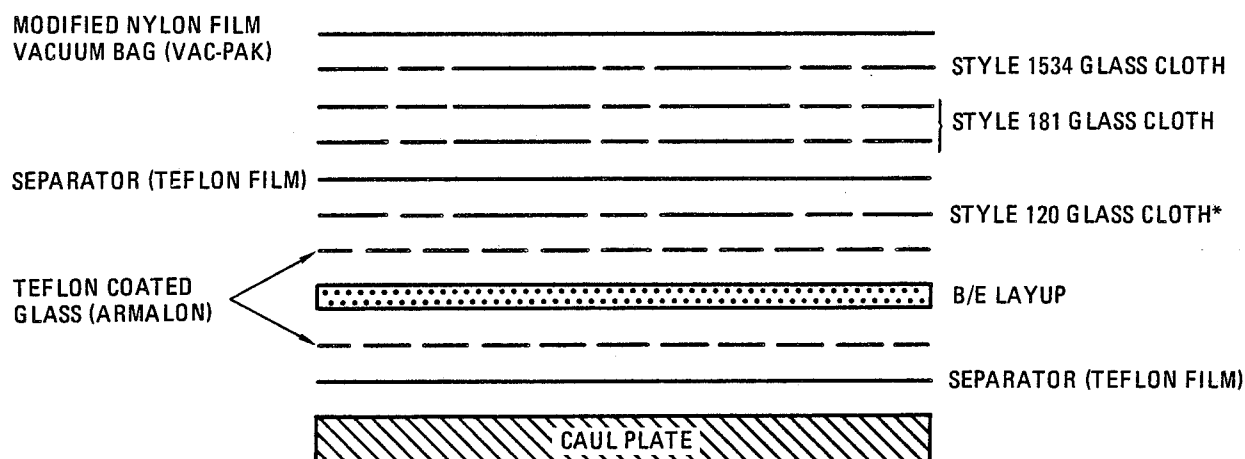
The G/E tubes and the B/PI tubes both included the precompaction operations prior to final cure. G/PI panels also required a precompaction and "B" staging of the condensation type polyimide system in order to achieve satisfactory densification during cure. The B/E and G/E systems, however, were processed using simple rapid curing schedules.

5.1.1 BORON/EPOXY. The fabrication of the B/E panels from prepreg consisting of 4-mil diameter boron and AVCO 5505 resin was accomplished using the relatively straight-forward vacuum bag and autoclave cure cycle shown below.

1. With full vacuum in the bag, heat at 1.7 to 2.8 K (3 to 5° F) per minute to 450 K (350° F).
2. Apply 0.59 MN/m² (85 psi), venting vacuum bag to atmosphere when autoclave pressure reaches 0.34 MN/m² (50 psi).
3. Hold two hours at 450 K (350° F) and 0.34 MN/m² (50 psi).
4. Cool under pressure to 353 K (175° F).

Laminates produced by this process exhibited good densification with measured specific gravities exceeding 2 and having resin contents of 26 to 32 weight percent. The layup procedure used for the 6 and 12 ply laminates (Figure 5-1) was identical except for the number of bleeder plies used. In all cases the prepreg was laid up with the scrim side down and with 0.001 m (0.04 in.) holes on 0.025 m (1 in.) centers perforating the mylar film applied above the 120 glass bleeder.

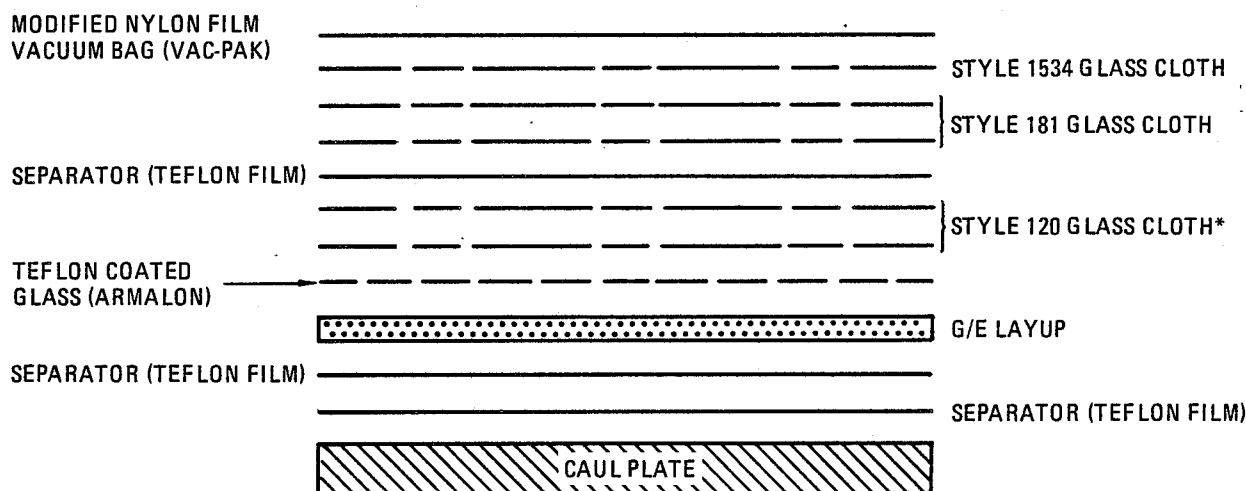
5.1.2 GRAPHITE/EPOXY. A-S/3501-5 prepreg produced by Hercules Incorporated was the G/E system used to fabricate the flat panels and the 0.025 m (1 in.) diameter by 0.3 m (12 in.) long tubes. Both the 6 and 12 ply laminate fabrications used identical cure schedules and layup procedures with one exception: the thinner panels used two 120 glass bleeders while the thicker panels used four plies of the same glass fabric for bleeders. The cure cycle used a constant heat-up rate of 1.1 to 1.7 K (2 to 3° F) per minute to 380 K (225° F) with full vacuum starting at room temperature. After applying 0.69 MN/m² (100 psi) the temperature was held one hour at 380 K (225° F) before heating to 450 K (350° F). A hold of one hour at 450 K (350° F) was followed by cooldown to below 350 K (150° F) under pressure. Details of the layup material stacking sequence are shown in Figure 5-2.



*1 PLY FOR 6 PLY B/E LAYUP; 2 PLIES FOR 12 PLY B/E LAYUP

653217-3

Figure 5-1 Schematic of B/E Cure Layup

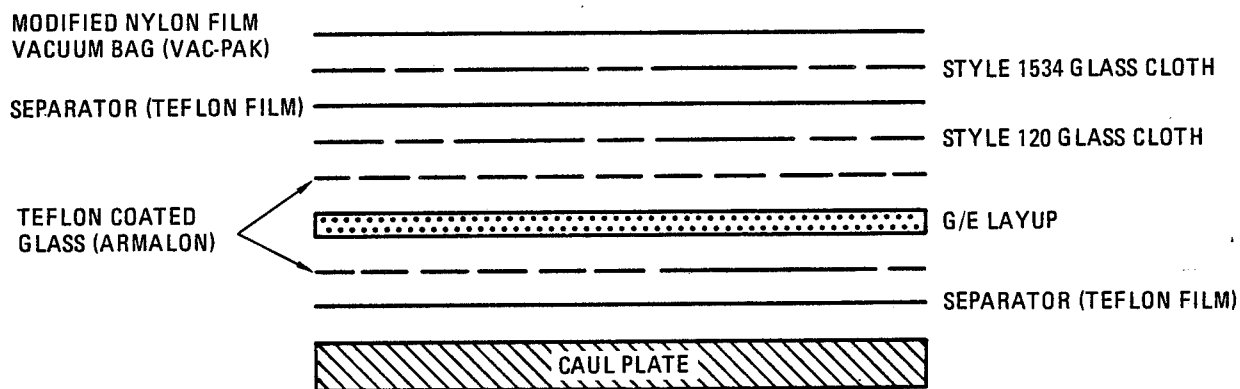


*2 PLIES FOR 6 PLY G/E LAYUP; 4 PLIES FOR 12 PLY G/E LAYUP

653213-4

Figure 5-2 Schematic of G/E Cure Layup

Fabrication of the G/E tubes was accomplished with an aluminum mandrel covered with a silicone rubber bladder. Two plies of G/E prepreg, 0.31 m (12.25 in.) by 0.30 m (12 in.) were cut and laid up with a 0.013 m (0.5 in.) offset. These plies were precompacted (Figure 5-3) in an oven at 338 K (150° F) to 344 K (160° K) for 20 minutes with full vacuum in the bag and 0.10 MN/m² (15 psi) external pressure before wrapping on the mandrel. A spiral wrap of paper bleeder 0.038 m (1.5 in.) wide was then applied over the separator covering the prepreg. Vent material addition and bagging were followed by the following short cure cycle.



653217-5

Figure 5-3 Schematic of G/E Tube Precompaction Layup

1. With full vacuum in the bag and 0.10 MN/m^2 (15 psi) in the autoclave, heat to 450 K (350° F) at 1.7 to 2.8 K (3 to 5° F) per minute.
2. Hold one hour and cool to 338 K (150° F) with vacuum in the bag and 0.10 MN/m^2 (15 psi) pressure in the autoclave.

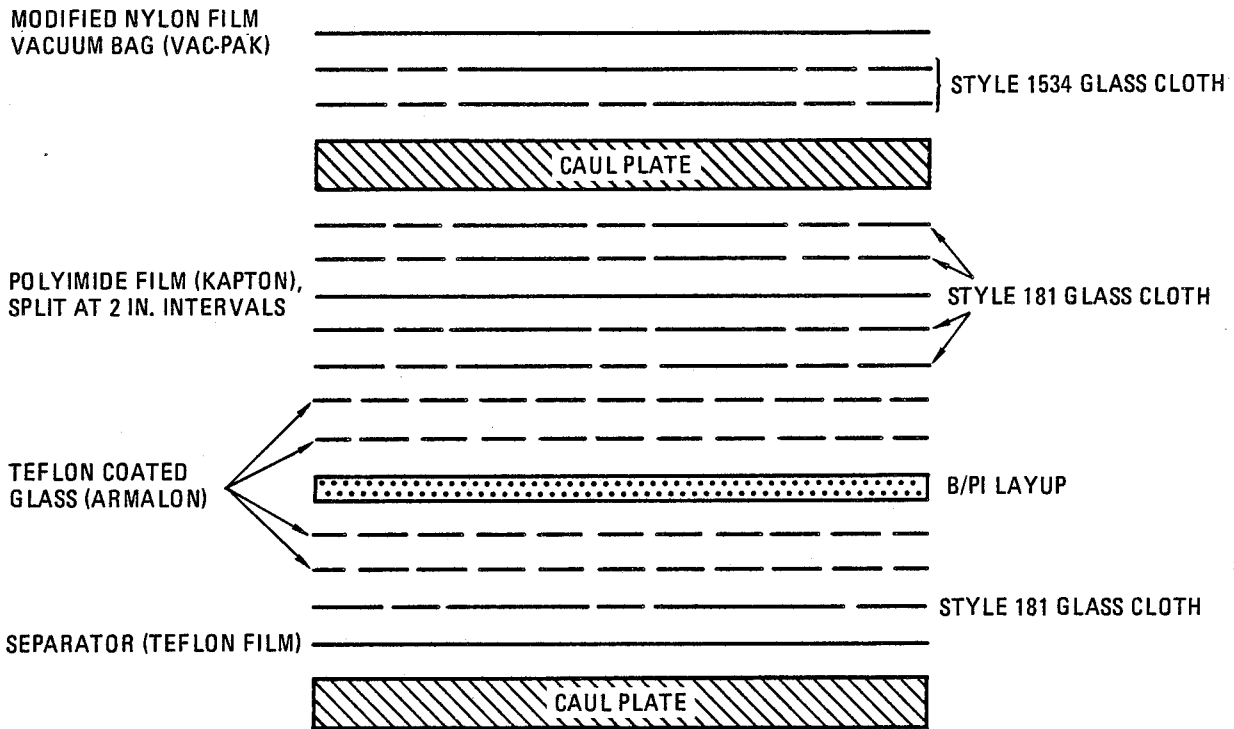
This procedure produced composite tubes having a specific gravity of 1.56, resin contents of 31 to 33 weight percent, and uniform wall thicknesses ranging from 0.00097 to 0.00102 m (0.038 to 0.040 in.).

5.1.3 BORON/POLYIMIDE. AVCO Corporation's 4.0-mil B/P105AC prepreg was the system used to fabricate the B/PI panels and tubes. The flat laminates used a top caul plate and bleeding from both sides, as shown in Figure 5-4. A single layer of 104 scrim cloth was added to the prepreg stack to balance the layup. Full vacuum in the bag was applied at room temperature and the layup was heated in the autoclave to 464 K (375° F) at 2.2 K (4° F) per minute and held there two hours. Pressure of 0.69 MN/m^2 (100 psi) was applied and the temperature was raised to 561 K (550° F), again at 2.2 K (4° F) per minute. After a two-hour hold, the layup was cooled to 353 K (175° F) at 1.1 K (2° F) per minute under autoclave pressure. Post cure consisted of a free standing heating cycle of four hours at 589 K (600° F).

Torsional tubes were fabricated using the 4.0-mil B/P105AC prepreg in a manner similar to the technique used for the G/E tubes. Aluminum mandrels covered with silicone shrink tubing were rolled with a two-ply 0.311 m (12.25 in.) by 0.308 m (12.125 in.) staggered prepreg that had been precompacted for 15-20 minutes at 383 K (230° F) with full vacuum in a bag using the layup shown in Figure 5-5. As before, bleeder paper 0.038 m (1.5 in.) wide was spirally wrapped, but two layers of bleeder were used for the more volatile polyimide resin system. One ply of a polyimide film was applied over the bleeder, followed by a venting system consisting of one layer of 1534 glass cloth, a layer of mat, and a final layer of 1534 glass fabric. The following cure and post cure cycles were used.

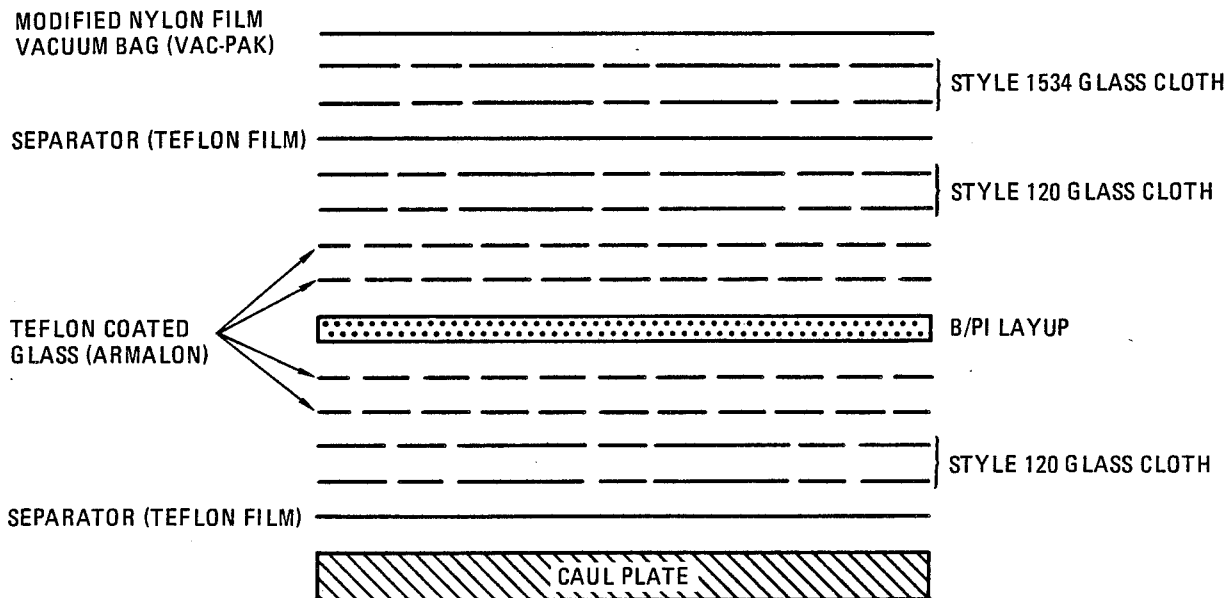
a. Cure

1. With full vacuum in the bag and 0.17 MN/m^2 (25 psi) autoclave pressure, heat to 464 K (375° F) $\pm 6 \text{ K}$ (10° F) at 2.2 K (4° F) per minute.



653213-6

Figure 5-4 Schematic of B/PI Cure Layup



653217-7

Figure 5-5 Schematic of B/PI Tube Precompaction Layup

2. Hold two hours and apply 0.69 MN/m² (100 psi).
3. Heat at 2.2 K (4° F) per minute to 561 K (550° F) and hold two hours.
4. Cool to 353 K (175° F) or below at 1.1 K (2° F) per minute under autoclave pressure.

b. Postcure

1. Heat to 589 K (600° F) at 2.2 K (4° F) per minute and hold four hours.
2. Cool below 366 K (200° F) at 1.7 K (3° F) per minute maximum.

Several of the tubes fabricated in this manner used lightweight glass sleeving as bleeder in lieu of the paper.

5.1.4 GRAPHITE/POLYIMIDE. Processing of the G/PI system required a precompaction cycle for "B" staging and volatile removal before cure. This procedure consisted of sandwiching the prepreg layup using six plies of 120 glass cloth bleeder covered by separator applied to both sides. The layup was vacuum bagged and heated to 353 K (175° F) at 2.8 K (5° F) per minute. An external pressure of 0.17 MN/m² (25 psi) was then applied and held 15 minutes before cooling to 325 K (125° F). The layup was then bagged and fresh bleeder applied (Figure 5-6) before applying the following cycle.

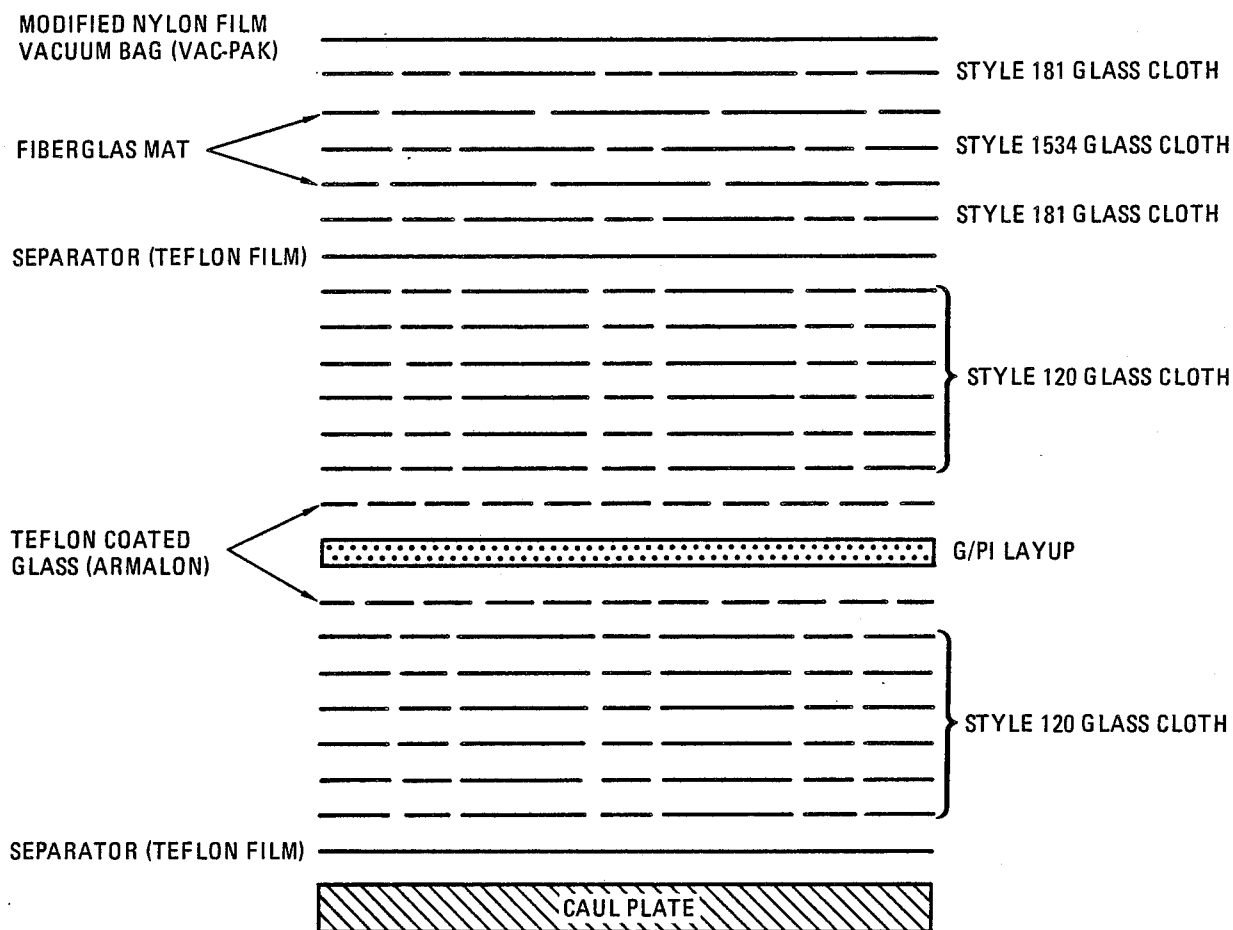
1. With full vacuum in the bag, heat to 353 K (175° F) at 1.7 K (3° F) to 2.8 K (5° F) per minute.
2. Hold 30 minutes at 353 K (175° F), heat to 400 K (260° F).
3. Hold 25 minutes at 400 K (260° F), apply 0.69 MN/m² (100 psi) autoclave pressure.
4. Heat to 450 K (350° F) and hold two hours.
5. Cool at 1.1 K (2° F) per minute under autoclave pressure to 353 K (175° F).

A slow 1.1 K (2° F) per minute, postcure in air to 644 K (700° F) completed the processing cycle.

5.2 BORON/ALUMINUM TUBE FABRICATION

The unidirectional B/Al tubes were specially designed and fabricated for the torsion tests (baseline shear) using a variation in the General Dynamics Convair B/Al tube making process. The tubular specimen was 0.15 m (6 in.) long, 0.025 m (1 in.) in diameter, and 0.001 m (0.004 in.) (6 ply) in thickness. The boron filaments were 5.6 mils in diameter and oriented in the long-axis direction of the tube. The composite was 48 volume percent boron in a 6061 aluminum matrix. A sketch of the tube is shown in Figure 5-7.

The B/Al tube with steel reinforced ends was made by winding unidirectional, single-layer tape on a thin-wall, annealed, mild steel tube (inner mandrel). The assembly was then inserted into a thick-wall steel tool (outer mandrel). The assembly was next sealed by welding rings to the ends of the inner and outer mandrels. An air evacuation tube was installed through the outer



653217-8

Figure 5-6 Schematic of G/PI Cure Layup

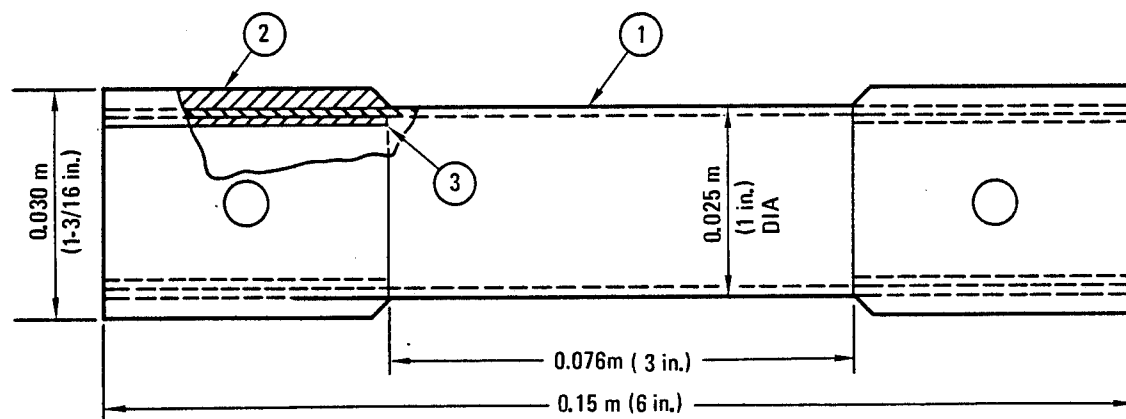
mandrel. The assembly was then helium leak tested, evacuated, heated to outgas any contaminants, and sealed (at the evacuation tube) while still under vacuum.

High temperature, high pressure autoclave bonding followed. The ductile, thin-walled inner mandrel yields during the cycle, transferring the applied pressure to the composite and its near-molten aluminum matrix. The result is complete bonding of the B/Al layers together and the bonding of the inner and outer steel tubes to the composite.

The bonded assembly was masked prior to etching by dipping each end in a molten plastic maskant to a depth of 0.038 m (1.5 in.), thus leaving the center portion free. The assembly was then submerged in a nitric acid bath that selectively dissolved both the inner and out steel jackets, leaving a B/Al tube with steel reinforced ends.

5.3 SPECIMEN FABRICATION

5.3.1 PANEL LAYOUTS AND SPECIMEN IDENTIFICATION. Cutting plans were prepared for each composite laminate showing the location and identification number of each specimen. These



- DETAIL:
- (1) 0.001 m (0.040 in.) THICKNESS (6 PLY) B/Al TUBE
 - (2) 0.0024 m (0.094 in.) THICKNESS STEEL REINFORCEMENT
 - (3) 0.00071 m (0.028 in.) THICKNESS STEEL REINFORCEMENT

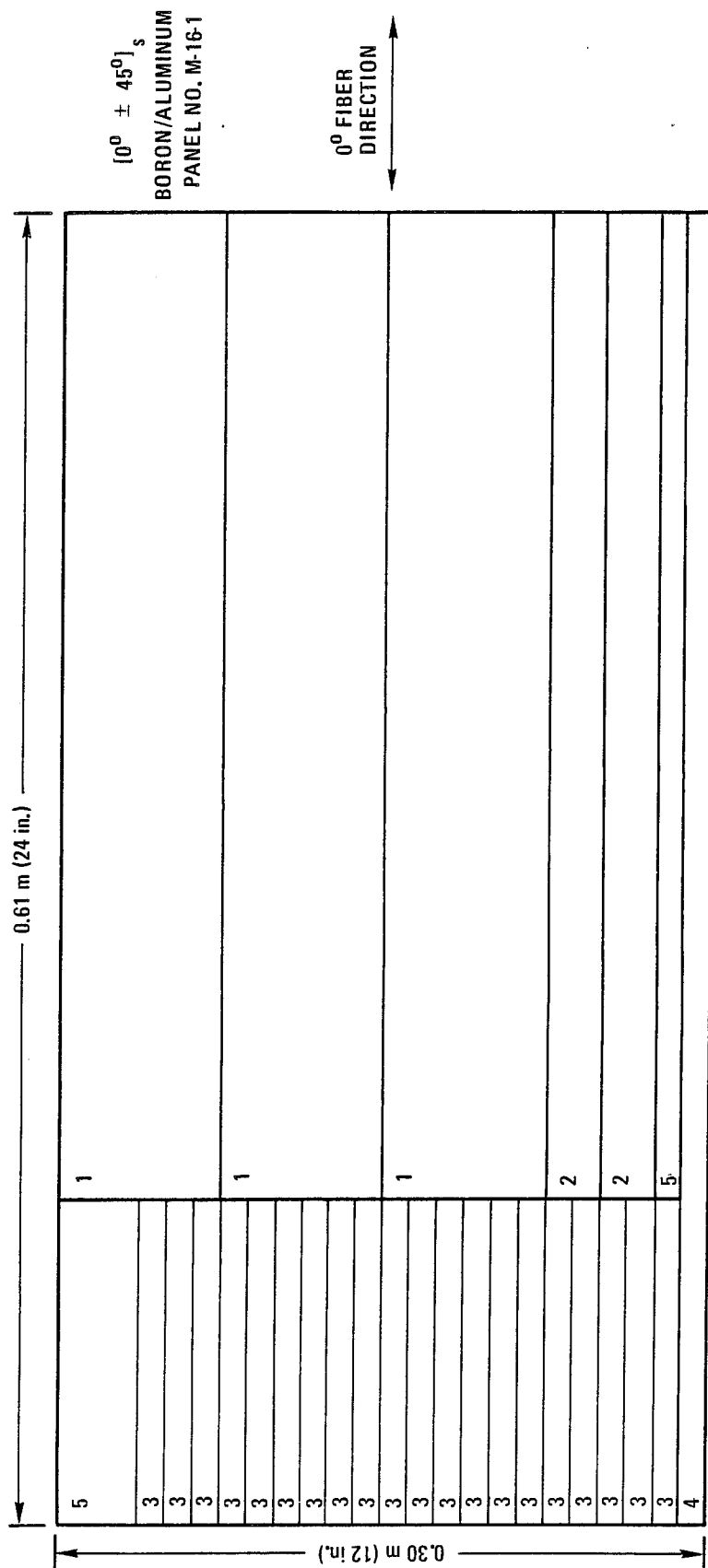
653217-9

Figure 5-7 Unidirectional B/Al Tube

plans accompanied each laminate through the cutting and machining operations and then were retained to keep a permanent record as to which panel and the specific location from which each specimen was obtained. A typical cutting plan for a B/Al laminate is shown in Figure 5-8 and for a G/E laminate in Figure 5-9. The B/Al panels had good edges and could be used without trimming. For the resin matrix composites, a 0.013 m (0.5 in.) strip was cut from the perimeter of each panel because of edge thinning. A cutting allowance of 0.0032 m (0.125 in.) was used in preparing the cutting plans. Specific gravity and resin content samples were cut from scrap pieces (not from the perimeter) for each resin matrix laminate. For the B/Al panels a 0.013 m (0.5 in.) strip in the longitudinal direction was cut from one edge of each panel for quality assurance testing (fiber content, tensile properties, and metallographic examination).

The numerous test specimens used during this program were identified according to the system described in Table 5-1. The ID numbers were placed on the resin matrix specimens with either a white pencil on the composite itself or with permanent black ink on the end doublers. For the B/Al specimens either permanent black ink on the B/Al or vibra-tool marking of the metal end doublers was used. No difficulties with unreadable ID numbers were experienced during any of the moisture or thermal exposures. Data books with a record of each specimen were prepared for the five material systems. All test results were filed in these logs, thus ensuring ready access to any of the data developed during the lengthy program.

5.3.2 MACHINING OPERATIONS. The machining operations required for the fabrication of the composite specimens included sawing, hole drilling, and slotting. Cutting of the flat laminates and torsion tubes into specimen blanks was accomplished with the large gantry-type diamond radial saw pictured in Figures 5-10 and 5-11. The resin matrix materials were cut using a 0.25 m (10 in.) diameter diamond plated blade. The diamond size was grit number 60 (270 micron).



- KEY:
1. LONG TERM FLIGHT SIMULATION - 0.076 m (3 in.) BY 0.46 m (18 in.)
 2. SHORT TERM FLIGHT SIMULATION - 0.025 m (1 in.) BY 0.46 m (18 in.)
 3. BASELINE TENSILE - 0.013 m (0.5 in.) BY 0.15 m (6 in.)
 4. QUALITY ASSURANCE - 0.013 m (0.5 in.) BY 0.61 m (24 in.)
 5. CUTTING ALLOWANCE AND SCRAP

653217-10

Figure 5-8 Cutting Plan for 6 Ply B/Al Panel



653217-11

Figure 5-9 Cutting Plan for 6 Ply G/E Panel

Table 5-1. Specimen Identification Code

Material	Laminate Orientation	Task	Test	Specimen No.
A	B/E			
B	G/E			
C	B/PI			
D	G/PI			
E	B/Al			
	U	Unidirectional		
	C	Crossply		
	aF	Notched Crossply		
		0	Baseline	1. Tensile 2. Notched Tensile 5. Fracture 6. Shear
		1	Thermal Aging	1. Tensile 2. Shear
		2	Ambient Aging	1. Control 2. 20 Weeks 3. 52 Weeks
		3	Moisture Exposure	1. 24 hr H ₂ O Boil 2. 6 Week Humidity
		4	Atmospheric Exposure	1. Resin Matrix 2. Metal Matrix
		5	Creep	
		6	Stacking Sequence	1. [45°, -45°, 0°] _s 2. [0°, 45°, -45°] _s 3. [45°, 0° -45°] _s
		7	Fatigue	1. Notched 2. Unnotched
		8	Short-Term Flight Simulation	
		9	Long-Term Flight Simulation	

Transverse specimens are marked with "T" before the regular ID No.

For example: E-C-7-1-24 is B/Al, Crossply, Notched Fatigue Specimen No. 24

^aUsed on notched flight simulation specimens only.

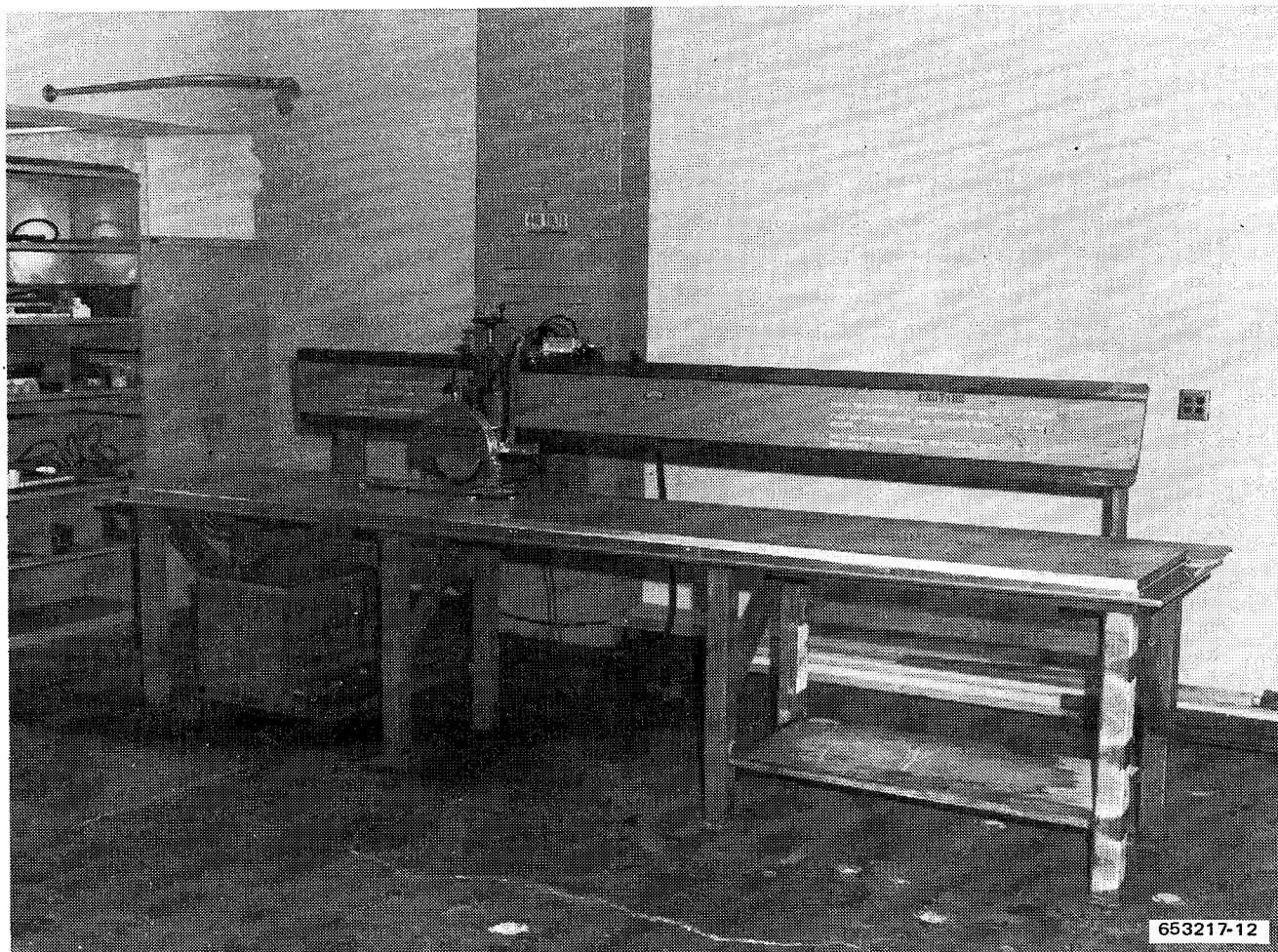
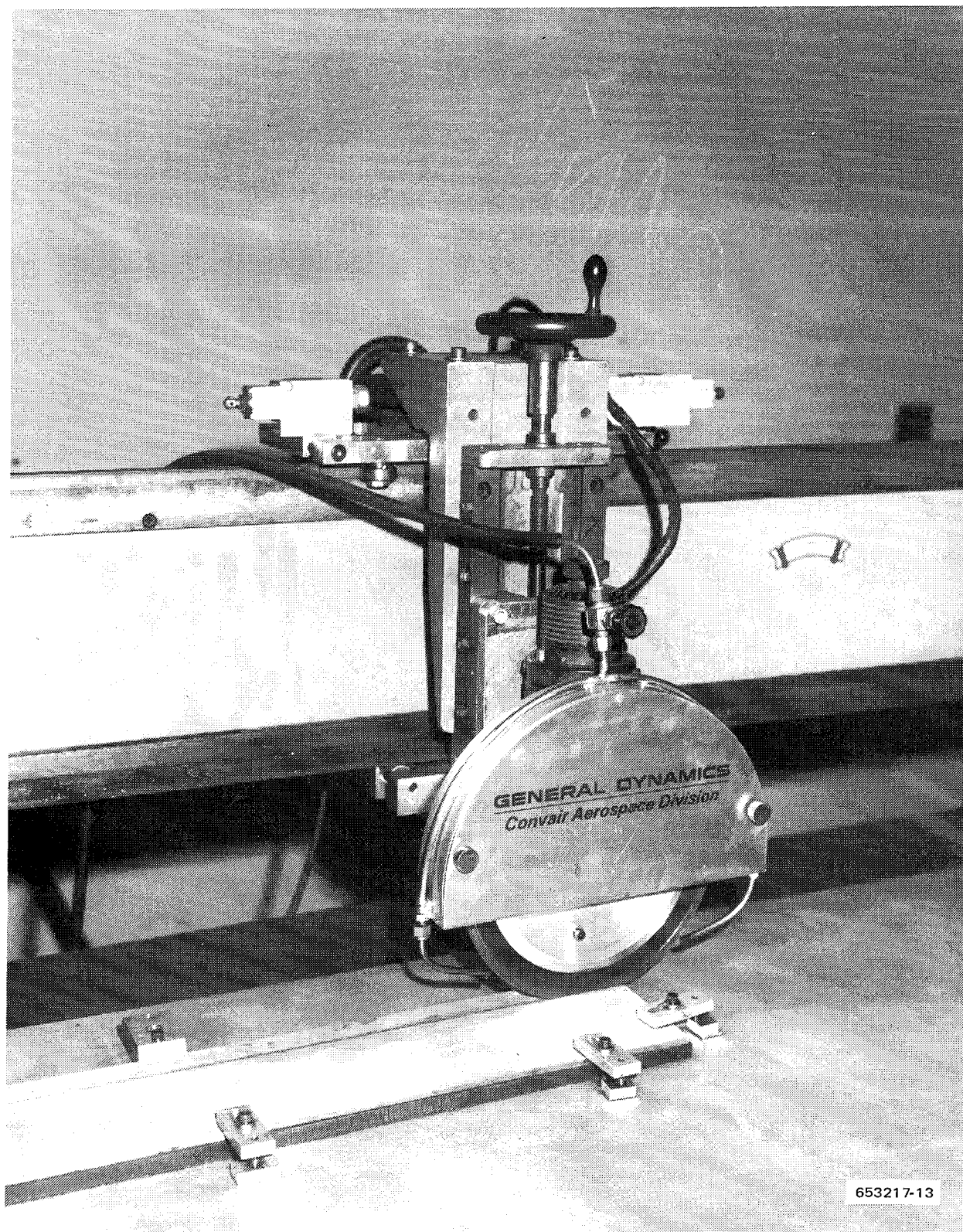


Figure 5-10 Gantry-Type Diamond Radial Saw

Sawing was done without coolant at a cutting rate of 5600 sfm with powered feed rates of 6 to 10 ipm. The specimens were cut to final size with no edge finishing required. For B/Al a 0.25 m (10 in.) diameter diamond impregnated (grit number 46 (350 micron) metal bond) saw blade was used. Cutting rates were the same as those used for the resin matrix composites. The B/Al specimens were cut wet using a 24 to 1 ratio water soluble oil with flood application. Again, good edges were obtained without additional finishing operations.

Holes were required in the notched tensile, fatigue, and flight simulation (both short- and long-term) specimens of the resin matrix materials and in the notched tensile and fatigue specimens of B/Al. Carbide and diamond coated core drills were used in a No. 2 Moore jig bore machine for fabricating the 0.0064 m (0.250 in.) holes in the resin matrix composites. No coolant was used. Electro-discharge machining (EDM) was used to produce the 0.0032 m (0.125 in.) holes in the B/Al specimens. The equipment used was an Elox HRP 104 EDM machine with a graphite electrode.



653217-13

Figure 5-11 Closeup View of Diamond Radial Saw

The other machining operations were cutting the center and edge slots in the B/Al laminate interfiber shear specimens and the center notches in the fracture specimens of all the composite materials. The B/Al shear specimens were slotted with the EDM method in a manner similar to that used for producing the holes in the notched tensile and fatigue specimens. For the fracture specimens, a rather narrow trapezoidal center notch with tip radii of approximately 0.00005 m (0.002 in.) was desired. Cutting of these notches was accomplished with a Sheffield ultrasonic impact grinding machine. The machine was operated at 20 kHz using 600 grit (17 micron) boron carbide abrasive. Optical comparator measurements of the notch radii gave values of 0.000038 m (0.0015 in.) to 0.000064 m (0.0025 in.) for both the resin matrix and the metal matrix specimens.

In addition to the machining operations required on the composite materials, it was necessary to drill loading fixture attachment pinholes in the titanium end doublers of the creep and flight simulation specimens. These holes were produced using standard drilling practices with the aid of a drill fixture that was fabricated for this purpose. The holes were drilled on the centerline of the test specimens to within ± 0.000064 m (0.0025 in.)

5.3.3 DOUBLER BONDING. With the exception of 1) short beam shear, 2) flexural, 3) fracture, and 4) laminate shear, all specimens required tapered doublers bonded to the ends to prevent failures in the gripping fixtures during testing. The major criteria considered in the selection of the doubler materials were:

- a. Temperature capability.
- b. Thermal expansion matching of doubler and specimen.
- c. Strength.
- d. Cost.

Most of the resin matrix specimens were fabricated with either epoxy-glass laminate or polyimide-quartz laminate doublers depending on the test temperature. Early in the program, two epoxy-glass laminate types were used. One, Scotchply Type 1002, was used at and below room temperature and the second, Scotchply Type 1007, a high temperature epoxy, was used for elevated temperature tests up to 450 K (350° F). To avoid the possibility of mistakenly using the Type 1002 material at elevated temperature, where its strength is quite low, a change was made midway in the program, and the Type 1007 epoxy was used for both the low and high temperature test specimens. For testing of resin matrix specimens at temperatures above 450 K (350° F) a polyimide-quartz (Skybond 703/Astroquartz) doubler material was used. Both the epoxy and the polyimide doublers were 0.0015 m (0.060 in.) in thickness. Doublers for the majority of B/Al specimens were made from 6061-T4, aluminum alloy of the same nominal thickness as the composite being tested.

The exceptions to the above described specimens were the creep and flight simulation specimens of both the resin and metal matrix systems. These specimens were pin loaded in contrast to the others, which were either clamped or loaded through a wedge action type of gripping fixture. The creep and flight simulation specimens also had the requirement of being able to sustain a long-time elevated temperature test environment. For a pin loaded application, particularly at elevated temperature, a metal doubler is far superior to either the epoxy or polyimide

types discussed above. Titanium was chosen as having the best combination of elevated temperature strength and thermal expansion match with the composite systems. For the $[0^\circ \pm 45^\circ]_s$ crossplied specimens, annealed A-70 titanium alloy (MIL-T-9046F, Type I, Composition B) was used. Because of the requirement of much higher test loads, solution treated and aged Ti-6Al-4V titanium alloy (MIL-T-9046F, Type III, Composition C) was selected for the unidirectional B/Al specimens. The thickness of the titanium alloy doublers was 0.0018 m (0.070 in.).

Of equal importance to selection of doubler material was the choice of adhesives used in bonding them to the specimen ends. The major considerations were strength at temperature and, for the creep and flight simulation specimens, long-time thermal stability. At room temperature and below, EA-9309 was selected for the resin matrix specimens and EC-2216 for the B/Al specimens. EA-9309 is a two-part epoxy paste adhesive manufactured by the Hysol Division of the Dexter Corporation. EC-2216 is a modified amine-cured filled epoxy manufactured by the 3M Company. Both were cured at room temperature for at least 72 hours prior to use. The adhesive that was considered to have had the best combination of elevated temperature strength and stability and the one selected for all elevated test specimens was HT-424. This is a modified epoxy-phenolic film adhesive with an aluminum filler on a glass carrier manufactured by the Bloomingdale Department of American Cyanamid Company. The cure cycle used for HT-424 was one hour at 450 K (350° F). The specimens were vacuum bagged and cured in an autoclave at 0.14 MN/m² (20 psi). Prior to application of the adhesive the specimens and doublers are prepared as follows:

- a. Resin-matrix specimens and doublers: lightly polished with A-1 very fine Scotch-Brite and solvent wiped.
- b. B/Al specimens and 6061-T4 Al doublers: degreased, lightly polished with A-1 very fine Scotch-Brite, solvent wiped, acid etched with Pasa-Jell 105, and rinsed with deionized water.
- c. Titanium alloy doublers: degreased, acid etched in nitric plus hydrofluoric solution, and rinsed with deionized water.

SECTION 6

LAMINATE QUALITY ASSURANCE TESTING

Quality assurance testing was performed on all purchased (B/Al) or Convair fabricated (B/E, G/E, B/PI, and G/PI) laminates to ensure good quality and, where applicable, concurrence with all specification requirements. Unacceptable material was rejected and replaced. In general, quality assurance testing consisted of visual examination, ultrasonic C-scan, volume or weight percent determinations, mechanical property testing, thickness measurement, and, for the B/Al panels, metallographic examination. The following sections describe the tests and present the results for the materials included in the program.

6.1 METAL MATRIX COMPOSITE MATERIAL

The B/Al quality assurance test program consisted of nondestructive testing, volume percent determinations, thickness measurements, tensile tests, and metallographic examinations. All the composite panels were nondestructively evaluated by ultrasonic testing. The ultrasonic technique was pulse-reflection through-transmission with a single short-focused, 5 MHz lithium sulfate transducer. The results are recorded on a C-scan recording wherein shades of gray lighter than some maximum are relatable to acoustic transmission losses within the test panel. The overall integrity of a test panel is described by an arbitrary rating system with numerical values from 0 to 5 assigned on the basis of Convair's experience in ultrasonic testing of hundreds of composite panels. The rating reflects variations from normal conditions. Normal does not necessarily mean perfect. For example, a few widely scattered stray boron filament fragments have no measurable effect on the structural performance of a given component. Although undesired from a workmanship standpoint, if small isolated defects cause no structural effects, they are judged to be normal. Degrees of variation from normalcy are subjectively determined by engineers with wide experience in the evaluation of composite materials. Ratings of 3, 4, and 5 represent severe or widespread defects judged to have detrimental effects upon the structural performance of the component. Ratings of 1 or 2 relate to scattered or isolated defects caused by faulty workmanship or minor loss of process control. These ratings apply to defects that should not adversely affect the structural performance of the component. Table 6-1 summarizes the ultrasonic test results of both the unidirectional and crossply panels. Overall panel integrity was excellent.

Volume percent (v/o) determinations were performed on each B/Al panel to determine the amount of filaments and matrix present in the composite test materials. Broken tensile specimens were used as test samples. Each specimen was washed, dried, and weighed. The filaments were leached from the samples in a 50% solution of sodium hydroxide at approximately

Table 6-1. Results of Nondestructive Evaluation of B/AI Panels

Panel No.	Orientation	No. of Plies	Intended Use (a)	Thickness mm	Thickness (in.)	Ultrasonic Rating (b)
9-1	[0°] ₆	6	0, 8, 9	0.91-0.97	0.037-0.038	0
9-2		6	0, 5, 8, 9	.91- .97	.036- .038	0
12-1		6	2, 5, 7, 8	.94- .97	.037- .038	0
12-2		6	1, 5, 7, 8	.94- .99	.037- .039	0
13-2		6	0, 1, 5, 8, 9	.91- .97	.036- .038	1
13-3		6	1, 2, 8, 9	.94- .99	.037- .039	0
14-3	[0°] ₆ [0°] ₁₂ [0° ± 45°] _s	6	7	.91- .97	.036- .038	0
14-4		6	0, 7	.91- .94	.036- .037	0
15-1		6	0, 2, 8, 9	.94- .97	.037- .038	0
15-3		6	0, 1, 2, 5, 8	.84- .99	.033- .039	0
21-4		6	2, 5, 7, 8	.97-1.02	.038- .040	0
304		6	8, 9	1.09-1.17	.043- .046	0
305		6	8, 9	1.07-1.19	.042- .047	0
306		6	8	1.09-1.17	.043- .046	0
54-1		12	7	2.06-2.11	.081- .083	0
15-2		6	0, 8, 9	.97- .99	.038- .039	0
16-1		6	0, 8, 9	.97- .99	.038- .039	1
17-1		6	0, 8, 9	.97-1.02	.038- .040	1
19-1	[0° ± 45°] _s	6	0, 1, 5, 8, 9	.99-1.04	.039- .041	1
19-2		6	1, 5, 7, 8, 9	.97- .99	.038- .039	0
19-3		6	0, 5, 7, 8	.99-1.02	.039- .040	1

Table 6-1. Results of Nondestructive Evaluation of B/AI Panels — Concluded

Panel No.	Orientation	No. of Plies	Intended Use (a)	Thickness mm	Thickness (in.)	Ultrasonic Rating (b)
20-1		6	7	.99-1.02	.039-.040	0
20-2		6	0, 7	.99-1.04	.039-.041	0
20-4		6	0, 5, 8	1.02-1.07	.040-.042	0
21-2		6	5, 7, 8	.97-1.02	.038-.040	0
21-3	$[0^\circ \pm 45^\circ]_s$	6	5, 7, 8	.99-1.04	.039-.041	0
54-2	$[0^\circ \pm 45^\circ]_{s2}$	12	7	2.06-2.11	.081-.083	0
<div> <div>a</div> <div> 0 Baseline 1 Thermal Aging 2 Ambient Aging 5 Creep </div> <div> 7 Fatigue 8 Short-Term Exposure 9 Long-Term Exposure </div> </div>						
<div> <div>b</div> <div>Rating: 0 is completely uniform, 1 to 5 is deviation from normal in increasing severity</div> </div>						

339 K (150° F). The filaments were collected, washed, dried, and weighed. Assuming the density of aluminum is 2700 kg/m³ and the density of the filaments is 2510 kg/m³ for 5.6 mil boron, the volume percentages of filaments were calculated using the following formula:

$$\text{Filament Volume Percent (v/o)} = \frac{\frac{W_F}{\rho_F}}{\frac{W_A}{\rho_A} + \frac{W_F}{\rho_F}} \times 100$$

W_F = Weight of filaments

ρ_F = Density of filaments

W_A = Weight of Aluminum

ρ_A = Density of Aluminum

The results of the v/o determinations are given in Table 6-2. For the 6 ply laminates the variation ranged from a low of 46.1 to a high of 51.4 v/o of boron with an overall average of 48.8 v/o boron. These results are typical of a nominal 50 v/o B/Al composite material. The 12 ply laminates were somewhat lower with values of 43.3 and 42.5 v/o boron.

Thickness measurements were made on the B/Al panels using micrometers. The results (Table 6-1) show relatively small differences in thickness within each panel or between the unidirectional and $[0^\circ \pm 45^\circ]_s$ crossplied B/Al panels.

Tensile tests were performed on each of the B/Al panels. The configuration of the tensile specimen used was a simple, straight-sided specimen 0.15 m (6 in.) long and 0.013 m (0.5 in.) wide cut in the longitudinal direction. Bonded doublers were utilized to minimize stress concentrations in the gripping areas. The doublers were made from 6061 T-4 bare aluminum and were of the same nominal thickness as the composite being tested. The doublers were bonded to the composite specimens with EC-2216 epoxy, a modified amine-cured filled epoxy that cures at room temperature. Tensile specimens were tested in an Instron testing machine using a head rate of 0.00025 m per minute (0.01 in. per minute). Stress-strain curves and strain measurements were made with Baldwin microformers. Modulus values were calculated from the stress-strain curves. Results of the tensile tests on the 6 ply laminates, shown in Table 6-2, indicate an average tensile strength of 1450 MN/m² (210 ksi) for the unidirectional B/Al material and 576 MN/m² (83.6 ksi) for the $[0^\circ \pm 45^\circ]_s$ crossplied layup. This is in good agreement with early work at Convair on 5.6-mil B/Al composite material. The elastic modulus values of 198 GN/m² (28.7 million psi) for the unidirectional and 123 GN/m² (17.9 million psi) for the crossplied layup, however, are about 8% less than typical of previous results. No reason could be found for the lower modulus properties. Because of the lower fiber contents, the tensile strengths of the 12 ply panels were somewhat lower than those obtained from the 6 ply panels.

Table 6-2. Results of B/Al Quality Assurance Test Program

Panel No.	Orientation	Fiber Content (Vol. %)	Tensile Strength MN/m ²	Tensile Strength (ksi)	Tensile Modulus GN/m ² (psi × 10 ⁶)	Comments on Metallographic Examination	
9-1	[0°] ₆	50.2	1480	214	193	28.0	OK
9-2		49.8	1480	214	205	29.8	OK
12-1		48.7	1300	188	213	30.9	OK
12-2		48.3	1340	194	220	31.9	OK
13-2	[0°] ₆	46.7	1540	224	—	—	Partial disbond on 2 surfaces
13-3		48.2	1540	223	207	30.0	OK
14-3		46.5	1530	222	209	30.3	OK
14-4		48.2	1430	208	170	24.7	Partial disbond on 1 surface
15-1	[0°] ₆	48.6	1330	193	181	26.3	OK
15-3		48.0	1570	228	170	24.7	Small amount of scattered disbond
21-4	[0°] ₆	48.7	1280	185	173	25.1	Scattered disbands
304		46.1	1440	209	211	30.6	OK
305		47.7	1510	219	183	26.6	OK
306		46.4	1530	222	234	34.0	OK
54-1	[0°] ₁₂	43.3	1190	173	215	31.2	OK
15-2	[0° ± 45°] _s	48.4	594	86.1	103	14.9	OK
16-1		49.0	629	91.2	150	21.7	OK
17-1		48.2	576	83.5	152	22.0	Scattered disbands
19-1		50.0	550	79.8	103	14.9	Scattered disbands

Table 6-2. Results of B/Al Quality Assurance Test Program — Concluded

Panel No.	Orientation	Fiber Content (Vol. %)	Tensile Strength MN/m ²	Tensile Strength (ksi)	Tensile Modulus GN/m ² (psi × 10 ⁶)	Comments on Metallographic Examination	
19-2		51.4	525	76.1	103	15.0	OK
19-3		50.1	544	78.9	134	19.4	OK
20-1		50.4	641	92.9	125	18.2	OK
20-2		51.2	548	79.5	149	21.6	Small amount of scattered disbands
20-4		49.8	576	83.6	109	15.8	Scattered disbands
21-2		49.1	581	84.2	123	17.8	OK
21-3	[0° ± 45°] _s	50.1	579	84.0	110	15.9	Scattered disbands
54-2	[0° ± 45°] _{s2}	42.5	495	71.8	—	—	OK

Metallographic examinations were also made of each panel to substantiate the nondestructive evaluation (NDE) tests and to observe the microstructure, layup, and filament array. Samples cut from the broken tensile specimens were metallographically mounted and polished. Several of the samples showed some disbonding, which probably occurred during tensile testing or specimen preparation. Additional samples taken from the center of the B/AI panels instead of the edge where the quality assurance (QA) test specimens were taken showed none of the disbonding present in the broken tensile specimens. Photomicrographs of typical microstructures for the unidirectional and $[0^\circ \pm 45^\circ]_s$ crossplied material are shown in Figures 6-1 and 6-2.

6.2 RESIN MATRIX COMPOSITE MATERIALS

The quality assurance test program for the resin-matrix fabricated laminates consisted of ultrasonic C-scan, resin and fiber content, and specific gravity. In addition, flexural strength (room temperature and elevated temperature) and short beam shear strength (room temperature) were determined for the 12 ply QA panels. The following sections present the results for the four resin-matrix composite systems.

6.2.1 BORON/EPOXY. Ultrasonic C-scan testing was performed on all fabricated panels to detect possible delamination or voids in the laminates. Among the most useful nondestructive test methods for locating defects aligned parallel to principal surfaces is the ultrasonic through-transmission method. A variation of this method, and the one employed for this program, is the single-transducer reflector plate method shown in Figure 6-3.

Ultrasonic energy transmitted through the specimen is returned to the transducer from a smooth reflector. If disbonds (or voids) are present, reflection of the sound at the interfaces results in less transmitted energy. The resultant energy drop is readily detected as a decrease in the strength (amplitude) of the return signal. The gated signal, input to a recorder amplifier, provides an output voltage to the recorder that is proportional to the signal amplitude.

The C-scan recorder is mechanically linked to scan and index motions of the transducer and is electrically connected to the recorder amplifier. With a signal in the gate, the recorder receives the amplified signal and "writes" during that time. A series of the line scans synchronized with the movement of the test transducer (or test specimen) produces a full scale plan of the test object and shows defects in either black and white or variable shades.

No rating system similar to that used for the B/AI C-scan evaluation was available for the resin-matrix materials. The C-scan recordings were studied by an experienced NDE engineer who rated the panels as being either acceptable or unacceptable. Areas of suspected delaminations or voids that were not sufficiently large enough to reject a laminate were marked on the panel, and these areas were avoided during specimen machining. For the B/E system all fabricated laminates were judged to be acceptable based on the ultrasonic C-scan tests.

Resin and fiber content and specific gravity determinations were made on all of the B/E panels using the test methods described in Appendix B. The results are listed in Table 6-3 along with the dimensions and intended use for each panel.

In addition to the nondestructive examination and the weight percent determinations conducted on each panel, a series of mechanical property tests was performed on the two 12 ply QA panels. Flexural strengths were determined at 297 K (75° F) and 450 K (350° F). Short

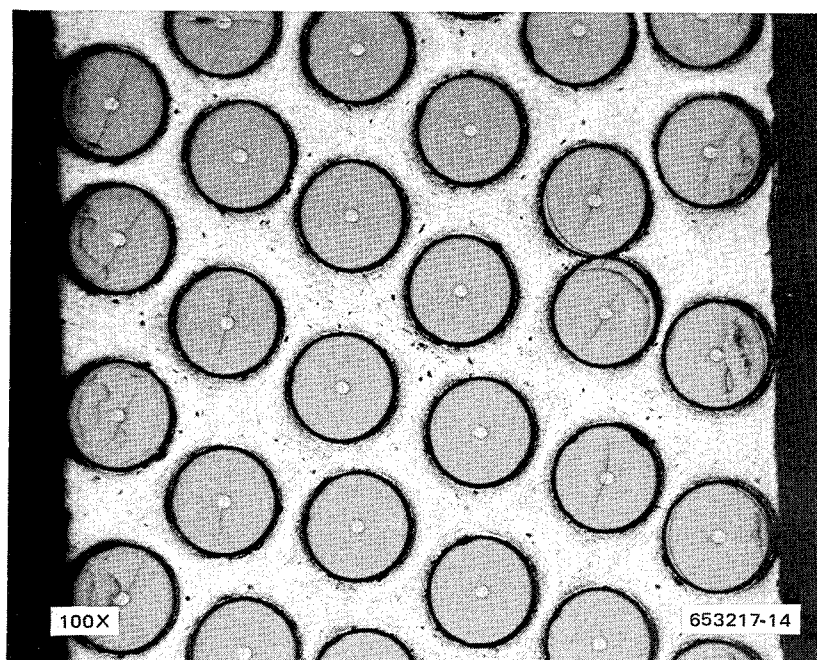


Figure 6-1 Photomicrograph Showing Typical Microstructure of Unidirectional B/Al

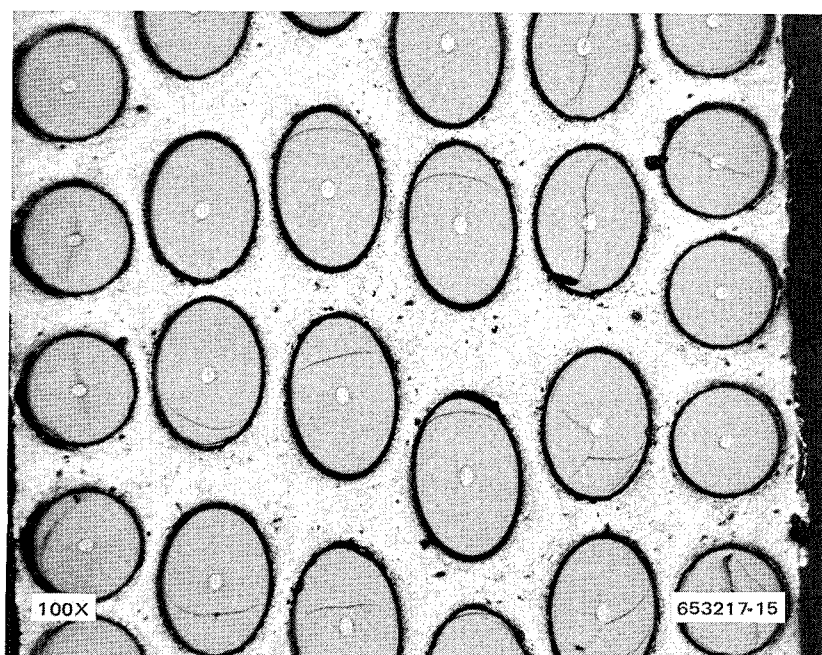


Figure 6-2 Photomicrograph Showing Typical Microstructure of $[0^\circ \pm 45^\circ]_s$ Crossplied B/Al

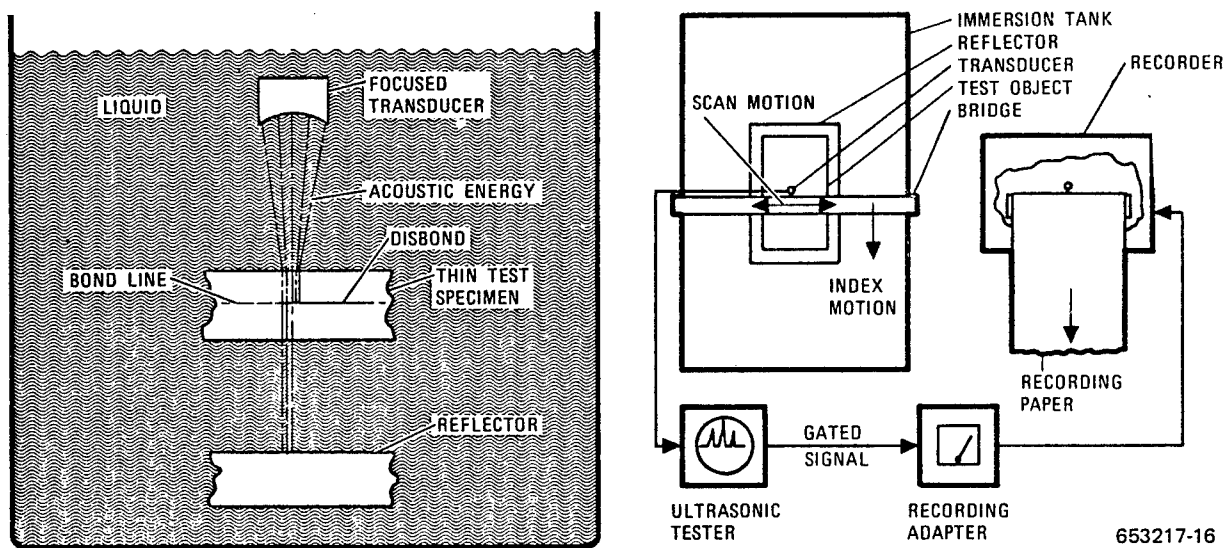


Figure 6-3 Single-Transducer Ultrasonic Technique

beam shear strength at 297 K (75° F) was also obtained for the two panels. Details of the test procedures are described in Appendix B. Table 6-4 lists the results. Based on the results of the QA tests, all of the B/E fabricated laminates were considered to be satisfactory.

6.2.2 GRAPHITE/EPOXY. Using the same technique described for the B/E material, all G/E fabricated laminates were ultrasonic C-scan tested for delaminations and voids. All panels were judged to be acceptable based on this evaluation.

The results of the remaining quality assurance tests on the G/E laminates are presented in Table 6-5 for resin and fiber contents and specific gravity values and Table 6-6 for room and elevated temperature flexural and room temperature short beam shear strengths.

In addition to the G/E panels, four G/E 8 ply unidirectional tubes were fabricated for the base-line shear tests. From each 0.30 m (12 in.) long tube, three specimens and one QA sample were obtained. Resin and fiber contents and specific gravity determinations were made on each quality assurance sample. The results are listed in Table 6-7.

Based on the results of the QA tests, all of the G/E fabricated laminates and tubes were considered to be satisfactory.

6.2.3 BORON/POLYIMIDE. Using the same technique described for the B/E material, all B/PI fabricated laminates were ultrasonic C-scan tested for delaminations and voids. All panels were judged to be acceptable based on this evaluation.

The results of the remaining QA tests on the B/PI laminates are presented in Table 6-8 for resin and fiber contents and specific gravity values and Table 6-9 for room and elevated temperature flexural and room temperature short beam shear strengths.

Table 6-3. Quality Assurance Data for B/E Laminates

Panel No.	Orientation	No. of Plies	Size m	(in.)	Intended Use (a)	Fiber Content (wt %) (b)	Resin Content (wt %)	Specific Gravity
LRC-1	[± 45°/0°] _s	6	0.23 × 0.25	9 × 10	6	71.7	28.3	2.04
LRC-2	[0° ± 45°] _s	6	.23 × .25	9 × 10	6	71.4	28.6	2.05
LRC-3	[45°/0°/-45°] _s	6	.23 × .25	9 × 10	6	70.0	30.0	2.04
LRC-4	[0°] ₆	6	.94 × 1.02	37 × 40	1, 5, 8	73.5	26.5	2.04
LRC-5	[0°] ₆	6	.51 × 1.14	20 × 45	9	72.4	27.6	2.05
LRC-6	[0°] ₆	6	.38 × .51	15 × 20	1, 5	72.7	27.3	2.03
LRC-14	[0°] ₁₂	12	.23 × .30	9 × 12	QA, 2	73.9	26.1	2.05
LRC-15	[0° ± 45°] _{s2}	12	.23 × .30	9 × 12	QA, 2	73.3	26.7	2.05
LRC-18	[0° ± 45°] _s	6	.86 × .91	34 × 36	1, 5, 8	71.5	28.5	2.01
LRC-19	[0° ± 45°] _s	6	.33 × .41	13 × 16	0	67.5	32.5	2.04
LRC-20	[0° ± 45°] _s	6	.86 × .91	34 × 36	8	71.6	28.4	2.04
LRC-21	[0° ± 45°] _s	6	.91 × 1.02	36 × 40	9	72.0	28.0	2.04

a QA	Quality Assurance	6	Stacking Sequence Evaluation
0	Baseline	8	Short-Term Exposure
1	Thermal Aging	9	Long-Term Exposure
2	Ambient Aging		
5	Creep		

b Includes approximately 9% glass fiber from scrim cloth.

Table 6-4. Quality Assurance Mechanical Property Data for B/E Laminates

Panel No.	Orientation	Temperature K	Temperature (°F)	Flexural Strength MN/m ²	Flexural Strength (ksi)	Shear Strength MN/m ²	Shear Strength (ksi)
LRC-14	[0°] ₁₂	297	75	2100	304	104	15.1
Average				2060	298	99.9	14.4
LRC-14	[0°] ₁₂	450	350	2060	299	95.8	13.9
Average				2070	300	99.9	14.5
LRC-14	[0°] ₁₂	450	350	1680	244		
Average				1740	252		
LRC-15	[0° ± 45°] _{s2}	297	75	1770	257		
Average				1730	251		
LRC-15	[0° ± 45°] _{s2}	450	350	924	134	62.7	9.1
Average				958	139	64.8	9.4
LRC-15	[0° ± 45°] _{s2}	450	350	931	135	69.6	10.1
Average				938	136	65.7	9.5
LRC-15	[0° ± 45°] _{s2}	450	350	889	129		
Average				820	119		
LRC-15	[0° ± 45°] _{s2}	450	350	882	128		
Average				864	125		

Table 6-5. Quality Assurance Data for G/E Laminates

Panel No.	Orientation	No. of Plies	Size m	(in.)	Intended Use (a)	Fiber Content (wt %)	Resin Content (wt %)	Specific Gravity
LRC 7	[±45°/0°] _s	6	0.23 × 0.25	9 × 10	6	67.5	32.5	—
LRC 8	[0° ± 45°] _s	6	.23 × .25	9 × 10	6	67.2	32.8	—
LRC 9	[45°/0°/45°] _s	6	.23 × .25	9 × 10	6	68.0	32.0	—
LRC 10A	[0°] ₆	6	.69 × .91	27 × 36	0, 5, 7	67.1	32.9	1.56
LRC11A	[0°] ₆	6	.76 × .91	30 × 36	0, 1, 7	66.8	33.2	1.56
LRC12A	[0° ± 45°] _s	6	.91 × 1.02	36 × 40	9	66.8	33.2	1.57
LRC16A	[0°] ₁₂	12	.61 × .61	24 × 24	QA, 0, 2, 7	67.4	32.6	1.55
LRC17A	[0° ± 45°] _{s2}	12	.30 × .71	12 × 28	QA, 0, 2, 7	65.6	34.4	1.56
LRC22A	[0° ± 45°] _s	6	.48 × .91	19 × 36	0, 7	65.5	34.5	1.58
LRC23A	[0° ± 45°] _s	6	.69 × .76	27 × 30	0, 7	68.2	31.8	1.56
LRC24A	[0° ± 45°] _s	6	.86 × .91	34 × 36	1, 5, 8	68.0	32.0	1.57
LRC25A	[0° ± 45°] _s	6	.91 × .91	36 × 36	8	68.7	31.3	1.56
a QA	Quality Assurance				Stacking Sequence Evaluation			
0	Baseline				6 Fatigue			
1	Thermal Aging				7 Fatigue			
2	Ambient Aging				8 Short-Term Exposure			
5	Creep				9 Long-Term Exposure			

Table 6-6. Quality Assurance Mechanical Property Data for G/E Laminates

Panel No.	Orientation	Temperature K	Temperature (°F)	Flexural Strength MN/m ²	Flexural Strength (ksi)	Shear Strength MN/m ²	Shear Strength (ksi)
LRC-16A	[0°] ₁₂	297	75	1720	249	95.2	13.8
				1716	248	99.3	14.4
Average				1620	235	101.0	14.6
				1680	244	98.5	14.3
LRC-16A	[0°] ₁₂	450	350	1220	177		
				1450	211		
Average				1210	176		
				1300	188		
LRC-17A	[0° ± 45°] _{s2}	297	75	882	128	69.6	10.1
				779	113	81.4	11.8
Average				910	132	70.3	10.2
				857	124	73.8	10.7
LRC-17A	[0° ± 45°] _{s2}	450	350	658	95.4		
				710	103		
Average				676	98.1		
				681	98.8		

Table 6-7. Quality Assurance Data for G/E Tubes

Tube No.	Fiber Content (wt %)	Resin Content (wt %)	Specific Gravity
1	66.6	33.4	1.56
2	68.6	31.4	1.55
3	67.5	32.5	1.56
4	68.2	31.8	1.56

In addition to the B/PI panels, five B/PI 8 ply unidirectional tubes were fabricated for the baseline shear tests. Resin and fiber contents and specific gravity determinations were made on two of the tubes. The other three tubes were not tested as a result of the decision to drop the B/PI system from the program because of the very low tensile properties and the extensive thermal degradation observed during thermal aging and short-term flight simulation testing. Data for the two tubes that were tested are listed in Table 6-10.

Based on the results of the quality assurance tests, all of the B/PI fabricated laminates and tubes were considered to be satisfactory.

6.2.4 GRAPHITE/POLYIMIDE. Using the same technique described for the B/E material, all G/PI fabricated laminates were ultrasonic C-scan tested for delaminations and voids. All panels were judged to be acceptable based on this evaluation.

The results of the remaining QA tests on the G/PI laminates are presented in Table 6-11 for resin and fiber contents and specific gravity values and Table 6-12 for room and elevated temperature flexural and room temperature short beam shear strengths.

Based on the results of the QA tests all of the G/PI fabricated laminates were considered to be satisfactory.

Table 6-8. Quality Assurance Data for B/PI Laminates

Panel No.	Orientation	No. of Plies	Size m	(in.)	Intended Use (a)	Fiber Content (wt %) (b)	Resin Content (wt %)	Specific Gravity
LRC-28R	[0°] ₁₂	12	0.33 × 0.56	13 × 22	QA, 0, 2	76.8	23.2	2.01
LRC-29	[0° ± 45°] _{s2}	12	.23 × .30	9 × 12	QA, 2	69.2	30.8	1.85
LRC-32	[0°] ₆	6	.46 × .69	18 × 27	0, 7	71.6	28.4	1.98
LRC-33	[0° ± 45°] _s	6	.46 × .69	18 × 27	0	67.5	32.5	1.97
LRC-34	[0°] ₆	6	.48 × .91	19 × 36	0, 7	73.1	26.9	1.93
LRC-35	[0° ± 45°] _s	6	.48 × .91	19 × 36	0, 7	69.4	30.6	1.94
LRC-36	[0° ± 45°] _s	6	.46 × .86	18 × 34	8			
LRC-37	[0° ± 45°] _s	6	.46 × .86	18 × 34	8	66.5	33.5	1.91
LRC-38	[0° ± 45°] _s	6	.46 × .86	18 × 34	8	73.7	26.3	1.98
LRC-39	[0°] ₆	6	.58 × .69	23 × 27	1, 5	73.0	27.0	1.98
LRC-40	[0° ± 45°] _s	6	.51 × .61	20 × 24	0, 5	62.8	37.2	1.90
LRC-41	[0° ± 45°] _s	6	.25 × .46	10 × 18	1	69.0	31.0	1.91
LRC-42	[0° ± 45°] _s	6	.46 × 1.02	18 × 40	9			
LRC-43	[0° ± 45°] _s	6	.46 × 1.02	18 × 40	9			

a QA	Quality Assurance	7 Fatigue
0	Baseline	8 Short-Term Exposure
1	Thermal Aging	9 Long-Term Exposure
2	Ambient Aging	
5	Creep	

b Includes approximately 9% glass fiber from scrim cloth

Table 6-9. Quality Assurance Mechanical Property Data for B/PI Laminates

Panel No.	Orientation	Temperature		Flexural Strength		Shear Strength	
		K	(°F)	MN/m ²	(ksi)	MN/m ²	(ksi)
LRC-28R	[0°] ₁₂	297	75	1770	257	55.8	8.1
Average				1860	269	53.1	7.7
LRC-28R	[0°] ₁₂			1340	195	49.0	7.1
Average				1660	240	52.6	7.6
LRC-28R	[0°] ₁₂	450	350	1400	203		
Average				1390	202		
LRC-29	[0° ± 45°] _{s2}	297	75	1550	225		
Average				1450	210		
LRC-29	[0° ± 45°] _{s2}	450	350	972	141	35.2	5.1
Average				896	130	36.5	5.3
LRC-29	[0° ± 45°] _{s2}			993	144	36.5	5.3
Average				954	138	36.1	5.2
LRC-29	[0° ± 45°] _{s2}	450	350	745	108		
Average				841	122		
LRC-29	[0° ± 45°] _{s2}			820	119		
Average				803	116		

Table 6-10. Quality Assurance Data for B/PI Tubes

Tube No.	Fiber Content (wt %)	Resin Content (wt %)	Specific Gravity
2	64.6	26	1.98
3	66.6	24	2.02

Table 6-11. Quality Assurance Data for G/PI Laminates

Panel No.	Orientation	No. of Plies	Size m	Size (in.)	Intended Use (a)	Fiber Content (wt %)	Resin Content (wt %)	Specific Gravity
LRC-50	$[0^\circ]_{12}$	12	0.46×0.58	18×23	QA, 0, 2, 7	68.8	31.2	1.41
LRC-51	$[0^\circ \pm 45^\circ]_{s2}$	12	$.46 \times .46$	18×18	QA, 2, 7	67.7	32.3	1.40
LRC-52	$[0^\circ]_6$	6	$.38 \times .69$	15×27	0, 7	67.6	32.4	1.49
LRC-53	$[0^\circ]_6$	6	$.48 \times .91$	19×36	0, 7	67.3	32.7	1.51
LRC-54	$[0^\circ \pm 45^\circ]_s$	6	$.48 \times .91$	19×36	0, 7	68.4	31.6	1.42
LRC-55	$[0^\circ \pm 45^\circ]_s$	6	$.46 \times .69$	18×27	0, 7	68.6	31.4	1.40
LRC-56	$[0^\circ \pm 45^\circ]_s$	6	$.51 \times .61$	20×24	0, 5	68.4	31.6	1.55
LRC-57	$[0^\circ \pm 45^\circ]_s$	6	$.25 \times .46$	10×18	1	67.8	32.2	1.48
LRC-58	$[0^\circ]_6$	6	$.58 \times .69$	23×27	1, 5	71.6	28.4	1.48
LRC-59	$[0^\circ \pm 45^\circ]$	6	$.46 \times .69$	18×27	8	68.3	31.7	1.43
LRC-60	$[0^\circ \pm 45^\circ]$	6	$.46 \times .69$	18×27	8	64.7	35.3	1.46
LRC-61	$[0^\circ \pm 45^\circ]$	6	$.46 \times 1.02$	18×40	9			
LRC-62	$[0^\circ \pm 45^\circ]$	6	$.46 \times 1.02$	18×40	9			

a	QA	Quality Assurance	7	Fatigue
0		Baseline	8	Short-Term Exposure
1		Thermal Aging	9	Long-Term Exposure
2		Ambient Aging		
5		Creep		

Table 6-12. Quality Assurance Mechanical Property Data for G/PI Laminates

Panel No.	Orientation	Temperature		Flexural Strength		Shear Strength	
		K	(°F)	MN/m ²	(ksi)	MN/m ²	(ksi)
LRC-50	[0°] ₁₂	297	75	1330	193	46.9	6.8
				993	144	48.3	7.0
				1220	177	49.6	7.2
Average				1180	171	48.3	7.0
LRC-50	[0°] ₁₂	450	350	869	126		
				952	138		
				807	117		
Average				876	127		
LRC-51	[0° ± 45°] _{s2}	297	75	664	96.4	40.7	5.9
				567	82.2	37.9	5.5
				703	102	33.8	4.9
Average				645	93.5	37.5	5.4
LRC-51	[0° ± 45°] _{s2}	450	350	538	78.0		
				661	95.8		
				439	63.7		
Average				546	79.2		

SECTION 7

BASELINE TESTING

The purpose of the baseline tests was threefold. First, these data served to characterize the composite materials and add to any existing data bases. Second, the baseline tests provided the scale and shape parameters necessary to define the statistical distribution of the ultimate tensile strengths for each of the material systems. These, in turn, were used to set the loads for the short-term tests, and with the short-term results, are used in a wearout analysis model to relate static and fatigue strengths. Finally, the baseline tests provided a rational starting point against which the various environmental effects may be measured.

Tests that were conducted included ultimate tensile, tensile modulus, Poisson's ratio, notched tensile ($K_t = 2.43$), transverse tensile (unidirectional laminates only), ultimate shear strength, shear modulus, and fracture. In addition to those tests that were originally planned, a limited number of compressive tests were also performed. These were added late in the program because of indications during thermal aging and flight simulation testing that matrix-dominated failure modes were operating. Testing was performed over the temperature range from 218 K (-67°F) to 450 K (350°F) for the epoxy specimens, to 616 K (650°F) for the polyimide specimens, and to 700 K (800°F) for the B/Al specimens. Because of the large amount of data already available for the B/E system, only limited testing was conducted on this material. Baseline testing of the B/PI system had not been completed when the material was removed from the test program because of low tensile properties and extensive thermal degradation during thermal aging and short-term flight simulation testing. Finally, the G/PI torsion tube tests were not run because of a lack of material with which to fabricate the test specimens. Some shear data were available at General Dynamics Convair, however, from a then current program evaluating the same HT-S/710 system.

The testing procedures used for this study were those that had been adopted by General Dynamics Convair and the composites industry at the time this contract was initiated. In general, there were no standards other than those called out in the Structural Design Guide for Advanced Composite Applications (ref. 4).

All tests were conducted on calibrated test equipment. Temperature measurements were also made with calibrated thermocouples and recording devices. The General Dynamics Standards Laboratory utilizes a fully documented system that meets all the requirements of NASA and DOD. The system has reports to establish traceability to the National Bureau of Standards or equivalent.

The baseline tests, which are discussed below, have been grouped into four categories: 1) tensile, 2) shear, 3) fracture, and 4) compressive.

7.1 TENSILE TESTING

Included in this section are the unnotched and notched tensile tests, elastic modulus determinations, and the Poisson's ratio measurements.

7.1.1 SPECIMEN DESIGN AND TEST PROCEDURE. The tensile specimen configuration was rectangular with adhesively bonded end tabs to reduce stress concentrations at the gripping fixtures. Longitudinal specimens, both notched and unnotched, were prepared from 6 ply laminates while the transverse specimens were 6 ply for B/Al and 12 ply for the epoxy and polyimide systems. The widths and lengths were dependent on the type of composite, the test direction, and the configuration, i.e., notched or unnotched. Details of the specimen geometry for the various materials and configurations are listed in Table 7-1. Based on results from numerous test programs conducted previously at General Dynamics, a width of 0.013 m (0.5 in.) was selected for the longitudinal tensile specimens of both the resin and metal matrix composites. The same width was suitable for the transverse B/Al specimens but was increased to 0.025 m (1.0 in.) for the transverse epoxy and polyimide specimens because of their low strength. The wider specimen reduced the likelihood of accidental failures during handling in the machining, doubler bonding, or testing operations. The notched configuration for the resin matrix specimens was the same as that used for the short-term flight simulation specimens. It consisted of a 0.025 m (1.0 in.) wide specimen with a 0.0064 m (0.25 in.) hole in the center. The theoretical stress concentration (K_t) for this configuration is 2.43 (ref. 23). The original plan for the B/Al system called for a side notched specimen, 0.013 m (0.5 in.) in width, with a theoretical notch acuity (K_t) of 6.3. After cutting the blanks but before machining the side notches, a decision was made to use a configuration similar to that chosen for the resin matrix specimens. To keep the hole-to-specimen width ratio the same, a 0.00318 m (0.125 in.) diameter hole was machined in the center of the B/Al specimens.

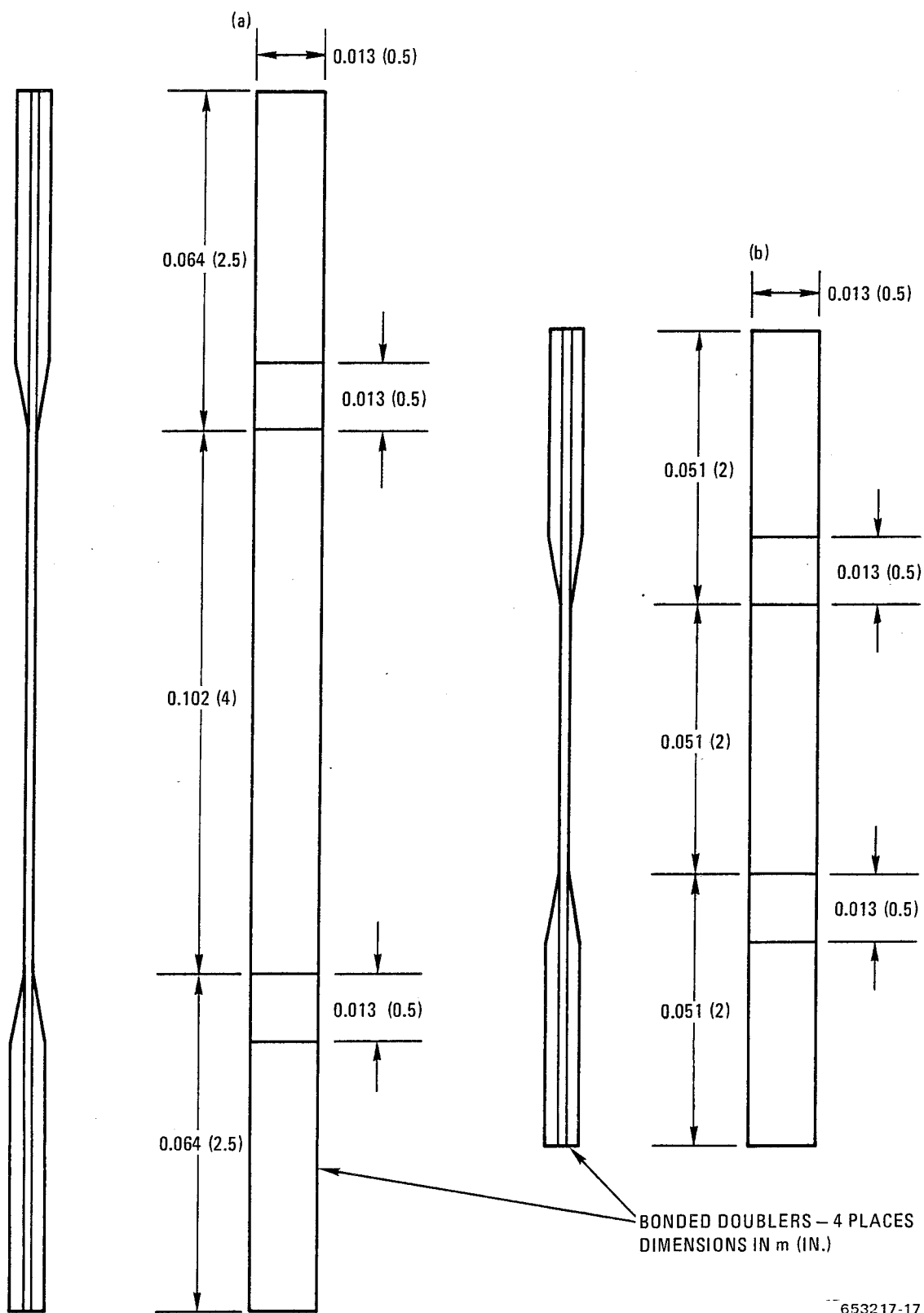
The tensile specimens used on the program are shown in Figure 7-1 for the longitudinal resin matrix and metal matrix specimens and in Figure 7-2 for the transverse resin matrix specimens. The transverse B/Al specimen is identical in dimensions to the longitudinal specimen of Figure 7-1. The notched tensile configurations are shown in Figure 7-3 for the resin and metal matrix composites.

Tensile testing was conducted in both Instron and Tinius-Olsen testing machines using Instron capstan grips with ball or universal joints to ensure axial loading of the specimens. A crosshead rate of 0.0025 m (0.01 in.) per minute was used for all tests. Strain was measured in two ways. For the specimens where Poisson's ratio was required, four strain gages were bonded to the test section. Elastic modulus values could also be determined from these specimens. A few of the G/PI and B/Al specimens were also strain gaged (two gages only) to determine modulus values at the higher temperatures where conventional extensometer measurements were not always reliable. The second method of strain measurement was with a clamp-on strain gage extensometer. The extensometer was used from 218 K (-67° F) to 561 K (550° F) with reasonably good results. At the higher temperatures, however, the bonded strain gage method was superior. An elevated temperature tensile specimen mounted in the capstan grips with a strain gage extensometer and thermocouple attached ready for test is shown in Figure 7-4.

Elevated temperature tests were conducted with either a Conrad-Missimer chamber or a small ring furnace. The advantage of the ring furnace was that the grips were not directly heated and doubler bond failures were reduced. The ring furnace was particularly beneficial at temperatures above about 561 K (550° F). All the tests at 218 K (-67° F) were performed in the Conrad-Missimer chamber. Temperature was measured with a thermocouple clipped to the specimen such that the bead was in contact with the surface. Specimens were held at temperature for a minimum of 10 minutes prior to loading.

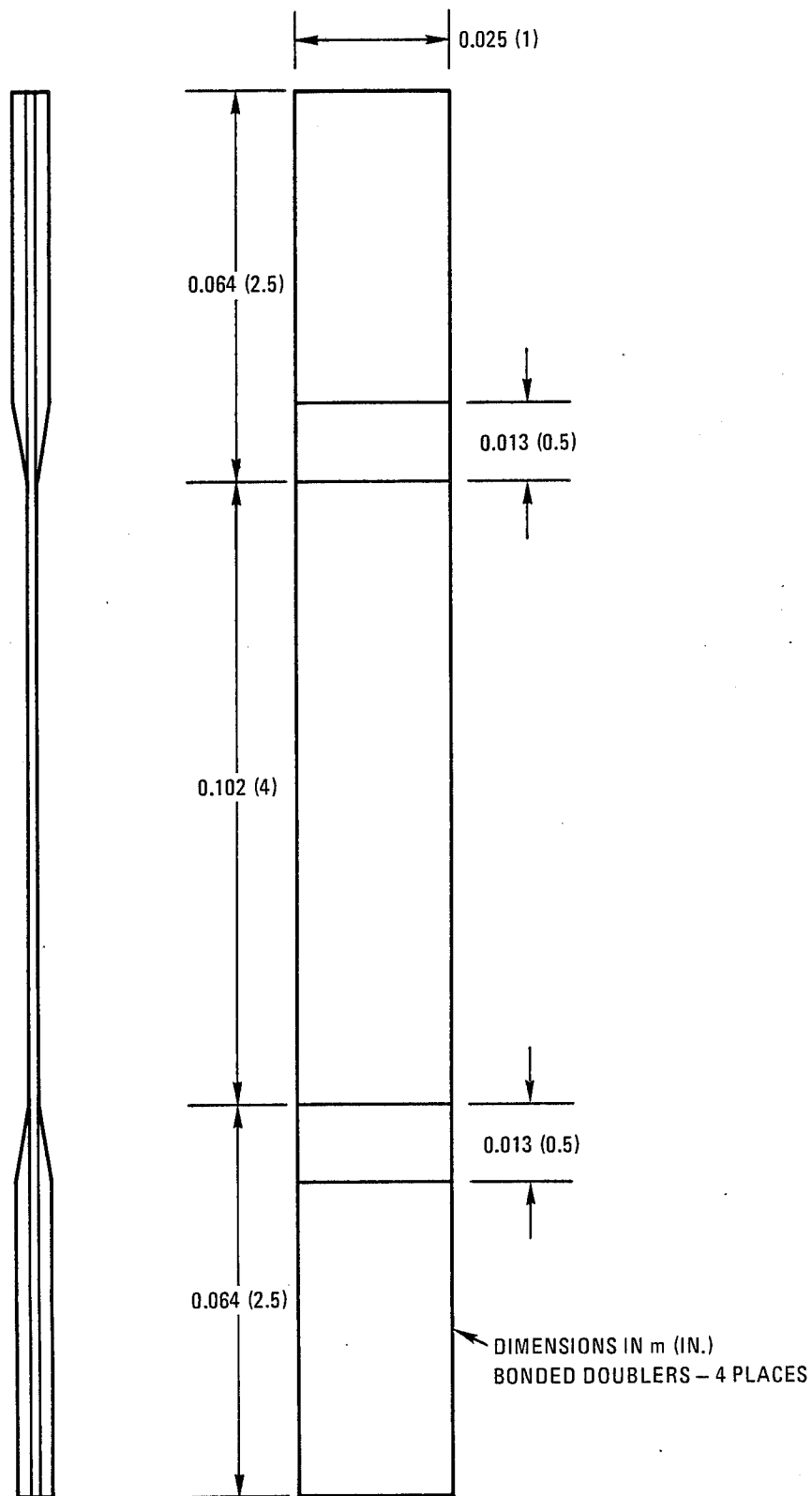
Table 7-1. Details of Tensile Specimen Geometry

Material System	Specimen Configuration	Test Direction	Length		Width		Hole Diameter		Test Section	
			m	in.	m	in.	m	in.	m	in.
Resin Matrix	Unnotched	Longitudinal	0.23	9	0.013	0.5	—	—	0.10	4
	Unnotched	Transverse	.23	9	.025	1	—	—	.10	4
	Notched	Longitudinal	.23	9	.025	1	.0064	.25	.10	4
Metal Matrix	Unnotched	Longitudinal	.15	6	.013	0.5	—	—	.051	2
	Unnotched	Transverse	.15	6	.013	.5	—	—	.051	2
	Notched	Longitudinal	.15	6	.013	.5	.00318	.125	.051	2



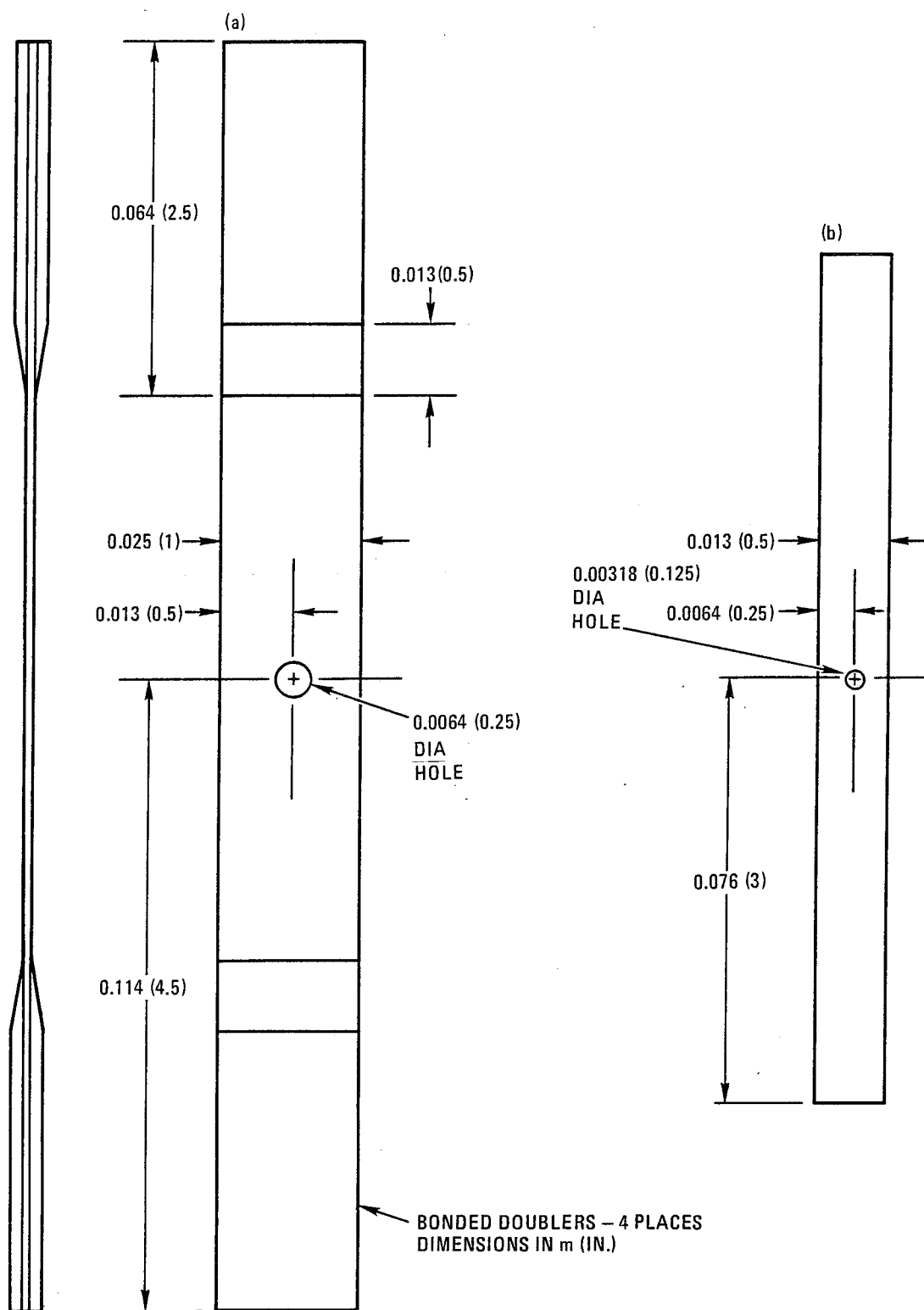
653217-17

Figure 7-1 Tensile Test Specimen for (a) Resin Matrix Composites and (b) Metal Matrix Composites



653217-18

Figure 7-2 Transverse Tensile Test Specimen for Resin Matrix Composites



653217-19

Figure 7-3 Notched Tensile Test Specimen for (a) Resin Matrix Composites and (b) Metal Matrix Composites

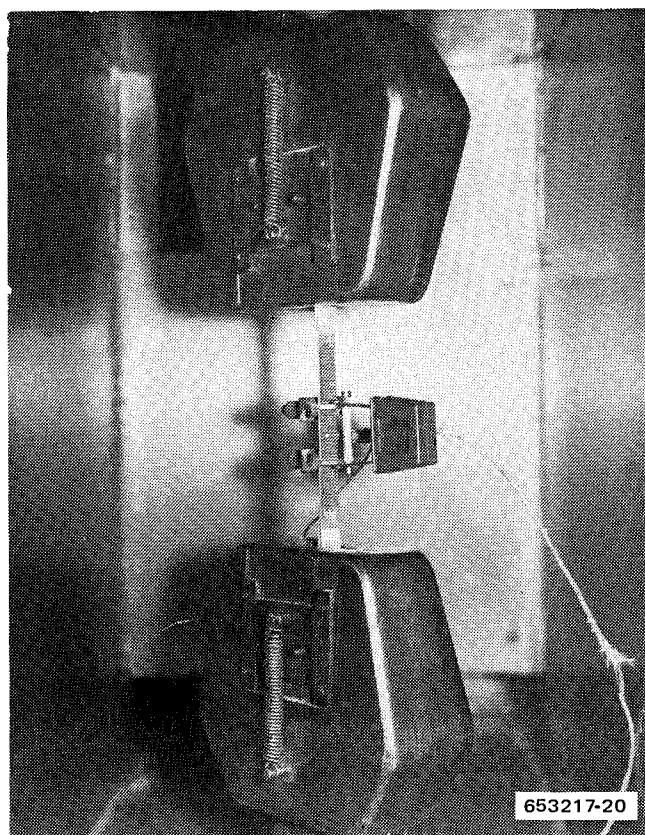


Figure 7-4 Elevated Temperature Tensile Test Setup

For the specimens that were to be strain gaged the following procedure was used. Prior to application of the gages, the specimens were lightly sanded in the gage section and precoated with M-bond 900 adhesive (manufactured by Micro-Measurement) to fill any void areas in the surface. The precoat was cured at 366 K (200° F) for two hours, and the specimens were again lightly sanded. The strain gages were then installed on the clean surfaces. Poisson's ratio specimens were instrumented with four strain gages, one longitudinal and one transverse gage on each side. For determination of elastic modulus only two gages were required, one longitudinal gage on each side.

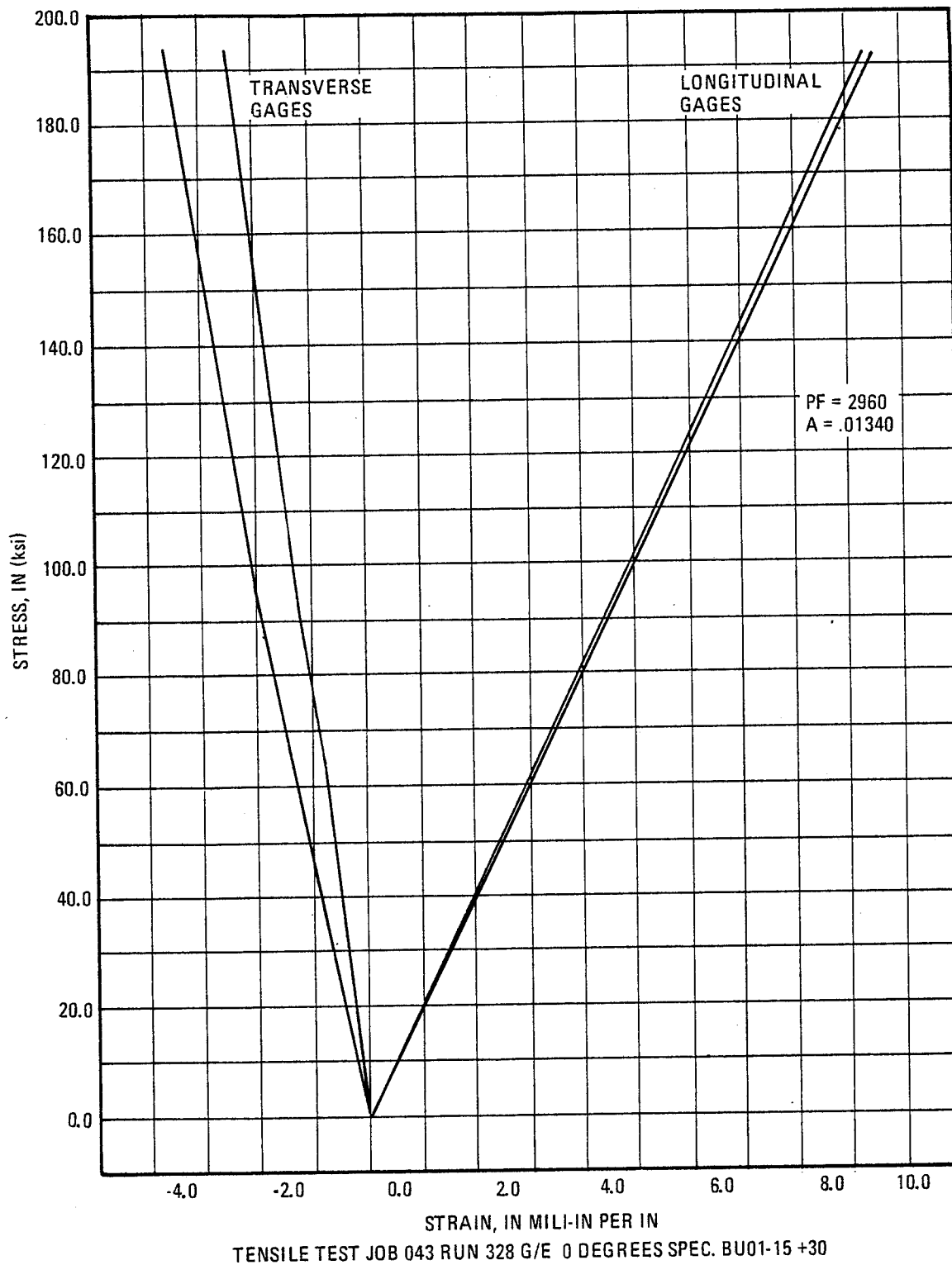
Table 7-2 lists the type of gages (manufactured by BLH Electronics, Inc.), adhesives, and cure cycles selected for the different test specimens.

Testing of the strain gaged specimens was conducted in a manner similar to that used for the specimens tested with a clamp-on extensometer except for the method of loading. These specimens were loaded incrementally to failure with strain measurements recorded automatically with a B & F Instruments, Inc. Multichannel Digital Strain Indicator, 161 Mini-System, at each load level. The output was both a typewritten recording of load versus strain and a punched paper tape that could be processed by a computer, programmed to produce a stress-strain plot. A typical computer generated plot is shown in Figure 7-5. Poisson's ratio and elastic modulus values were determined from these curves. Figure 7-6 shows the Mini-System in operation during a room temperature tensile test.

Table 7-2. Strain Gage Data for Poisson's Ratio and Elastic Modulus Testing

Material System	Orientation	Test Temperature		Type of Gage		Adhesive	Cure Cycle	
		K	(°F)	Longitudinal	Transverse		Temperature K	Time hr
B/E	$[0^\circ \pm 45^\circ]_s$	297	75	FAE-25-12-SO	FAE-12-12-SO	M-bond 200	—	—
G/E	$[0^\circ]_6$	297	75	FAE-25-12-SO	FAE-12-12-S15	M-bond 200	—	—
	$[0^\circ]_6$	394	250	FAE-25-12-SO	FAE-12-12-S15	M-bond 610	436	2
	$[0^\circ]_6$	450	350	FAE-25-12-SO	FAE-12-12-S15	M-bond 610	450	1.5
	$[0^\circ \pm 45^\circ]_s$	297	75	FAE-25-12-SO	FAE-12-12-SO	M-bond 200	—	—
G/PI	$[0^\circ]_6$	505	450	FAE-25-12-SO	FAE-12-12-S15	M-bond 610	505	1
	$[0^\circ]_6$	561	550	FSM-25-35-SO	FSM-12-35-S13	PLD-700	561	1
	$[0^\circ \pm 45^\circ]_s$	297	75	FAE-25-12-SO	FAE-12-12-SO	M-bond 200	—	—
	$[0^\circ \pm 45^\circ]_s$	505	450	FAE-25-12-SO	(a)	M-bond 610	505	1
	$[0^\circ \pm 45^\circ]_s$	561	550	FSM-25-35-SO	(a)	PLD-700	561	1
B/Al	$[0^\circ]_6$	561	550	FSM-25-35-SO	FSM-12-35-S13	PLD-700	561	1
	$[0^\circ]_6$	700	800	FSM-25-35-SO	FSM-12-35-S13	PLD-700	700	1
	$[0^\circ \pm 45^\circ]_6$	505	450	FAE-25-12-S3	(a)	M-bond 610	505	1
	$[0^\circ \pm 45^\circ]_s$	561	550	FSM-25-35-SO	(a)	PLD-700	561	1
	$[0^\circ \pm 45^\circ]_s$	616	650	FSM-25-35-SO	(a)	PLD-700	616	1
	$[0^\circ \pm 45^\circ]_s$	700	800	FSM-25-35-SO	(a)	PLD-700	700	1

a Modulus only — no transverse gage required



653217-21

Figure 7-5 Typical Stress-Strain Curve for Tensile Test

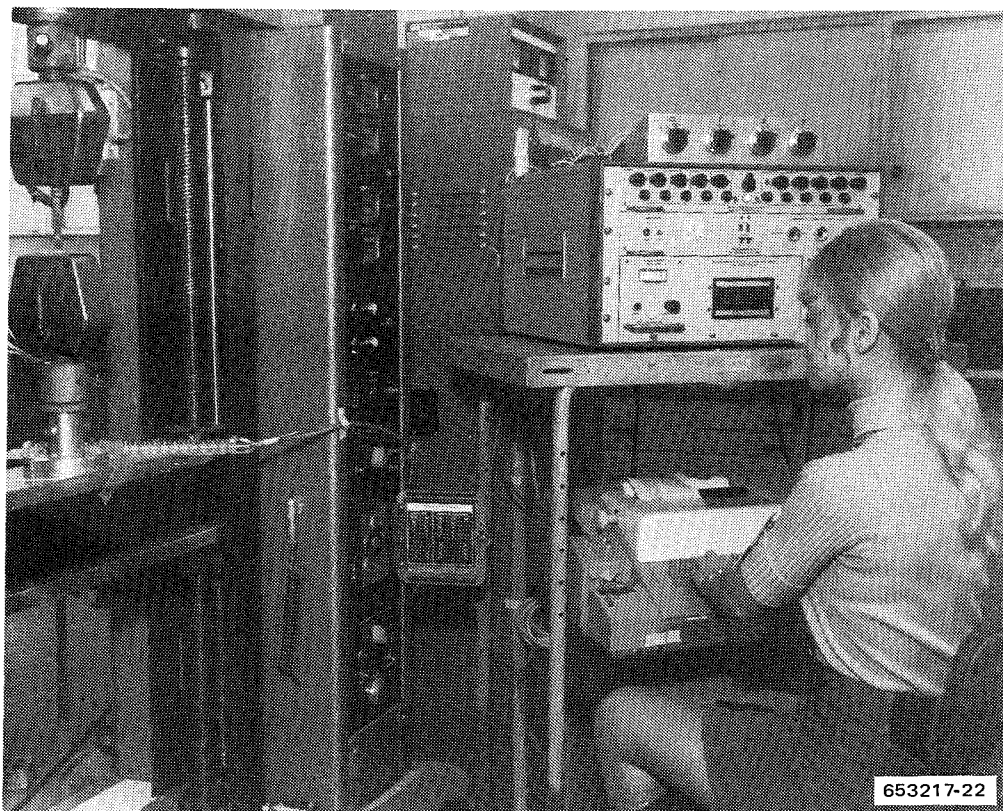


Figure 7-6 Automatic Strain Recording Instrumentation for Strain Gaged Tensile Specimen

Prior to tensile testing of the resin matrix material, all elevated temperature specimens and those room temperature specimens that were not strain gaged were heated at 394 K (250° F) for at least 24 hours to remove any absorbed moisture. The strain-gaged room temperature specimens were baked out prior to application of the gages and then stored in a desiccator until test.

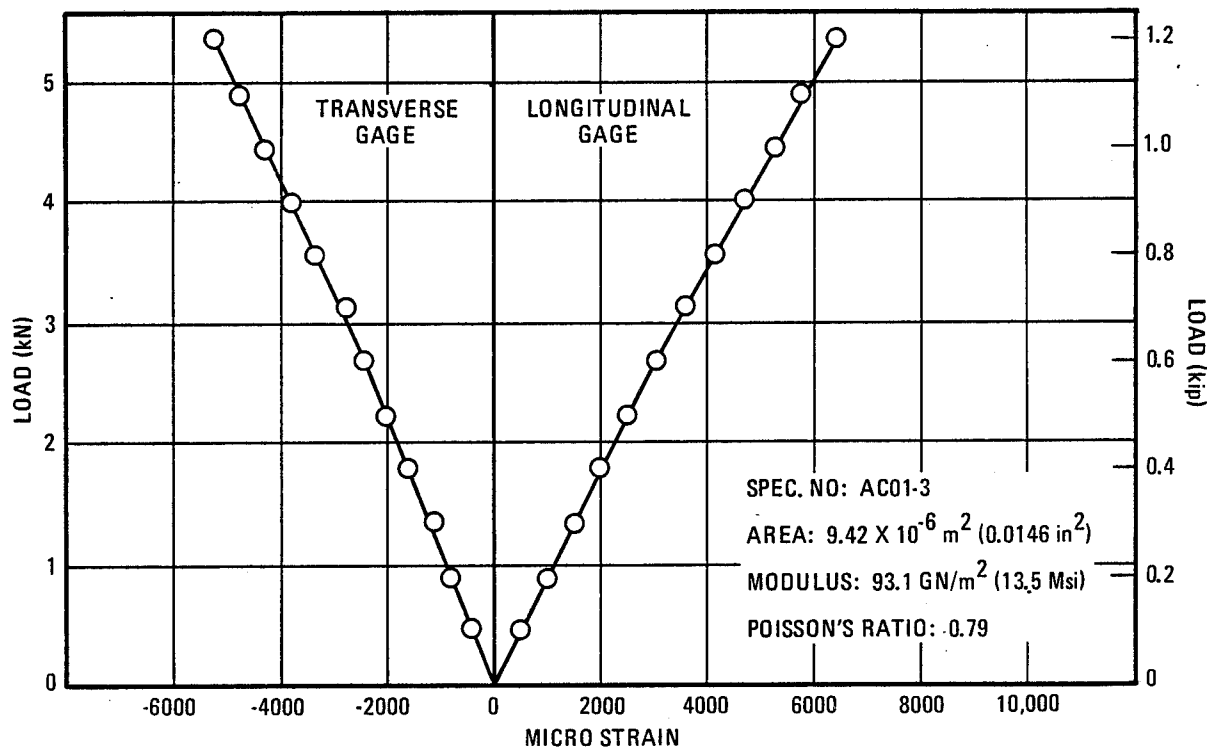
7.1.2 TEST RESULTS AND DISCUSSION

7.1.2.1 Boron/Epoxy and Graphite/Epoxy Systems. Because a large data base was already available for the B/E system, no baseline tensile testing was required. However, for later comparisons with the residual strength data from the flight simulation exposure specimens it was desirable to have baseline unnotched and notched tensile data from the same batch of material. Therefore, room temperature unnotched and notched tensile tests were conducted on $[0^\circ \pm 45^\circ]_s$ crossply material using the same test conditions and specimen configurations as were used later in evaluating the B/E flight simulation specimens after 10,000 hours of exposure. The unnotched specimens were strain gaged so that Poisson's ratio values could also be determined. The results are listed in Table 7-3. A tensile load-strain diagram is shown in Figure 7-7 for one of the strain gaged specimens. The points plotted are the average of the two longitudinal or transverse gages. Based on the few tests that were run, there is an approximately 30%

Table 7-3. Baseline Tensile Properties of $[0^\circ \pm 45^\circ]_s$ B/E at Room Temperature

Specimen Number	Configuration	Tensile Strength		Tensile Modulus		Poisson's Ratio
		MN/m ²	(ksi)	GN/m ²	(psi $\times 10^6$)	
AC01-1	Unnotched	596	86.4	^a 96.5	^a 14.0	^a 0.76
-2		617	89.5	^a 93.1	^a 13.5	^a .80
-3		643	93.2	^a 93.1	^a 13.5	^a .79
		avg	619	89.7	94.2	.78
AC02-1		399	57.9	—	—	—
-2	Notched	476	69.0	—	—	—
-3		454	65.8	—	—	—
		avg	443	64.2	—	—

^a Strain gage measurement



653217-23

Figure 7-7 Tensile Load-Strain Diagram for $[0^\circ \pm 45^\circ]_s$ B/E at 297 K (75° F)

decrease in the net tensile strength in $[0^\circ \pm 45^\circ]_s$ crossply B/E for the notched specimen configuration chosen. The Poisson's ratio values appear to be quite large (values for metals are generally about one-third) but are close to what is calculated from lamination theory for a crossplied layup.

The initial plan for the G/E baseline tensile tests was to test at four temperatures. This was later changed to seven temperatures with three specimens each (total of 21 specimens). From the tensile strength versus temperature curve obtained, two of the temperatures would then be selected for an additional seven tests each (total of 14 specimens). It was planned to select these two temperatures in the region just below that where a distinct change in the slope of the strength versus temperature curve occurred and then to use these data to set the loads for the flight simulation exposures. For G/E, however, no fall-off in strength was observed out to the maximum test temperature of 450 K (350° F). Because of the uncertainty in the maximum use temperature of G/E for very long times, the two additional tensile test temperatures were selected such as to cover a wide range of temperature. They were 394 K (250° F) and 450 K (350° F). As it later was found during the long-term flight simulation tests, both temperatures were above the maximum use temperature of the epoxy systems for 10,000 hour service.

Baseline tensile tests, both unnotched and notched, were performed on unidirectional and $[0^\circ \pm 45^\circ]_s$ crossplied specimens in the longitudinal direction. Some unnotched tensile tests were also performed in the transverse direction on unidirectional material, and a limited amount of Poisson's ratio testing was conducted. Results are listed in Tables 7-4 through 7-9. Figure 7-8 shows a typical example of a load-strain diagram obtained from one of the strain gaged Poisson's ratio specimens. The longitudinal unnotched and notched data are plotted as a function of temperature in Figures 7-9 and 7-10. A summary of all the G/E tensile properties is presented in Table 7-10.

Modulus values are given for the majority of unnotched specimens. For some specimens, however, modulus values were not determined because of the change in the test plan discussed above. Specimens that had originally been scheduled for testing at room temperature had been prepared with doublers bonded on with low temperature adhesive. To test these samples at an elevated temperature, a small ring furnace that heated only the center section of the specimen was required. With this type of heater, the clamp-on extensometer could not be accommodated. In addition to these specimens, a few others are shown without modulus values because of extensometer malfunctions. Several of the specimens were strain gaged in order to measure Poisson's ratio. The modulus values measured on these specimens are noted in the tables. In general, these values are more reliable than those determined with the mechanical extensometer.

The effect of temperature on the tensile strength of G/E is shown on Figures 7-9 and 7-10. With the exception of the 218 K (-67° F) results, the tensile strength exhibited almost no change with increasing temperature out to the maximum test temperature of 450 K (350° F). At 218 K (-67° F) the strength showed a moderate decrease for the crossplied material and a rather large one for the unidirectional material (almost 50%) for the unnotched specimens. This strength decrease at low temperatures is not uncommon for resin matrix composites. The effect is believed to be related to residual stresses in the material, which increase as the difference between the cure temperature and the test temperature is increased. Also shown on Figure 7-9 and 7-10 are the scatter bands for the various tests. For both unnotched and notched specimens the data scatter was numerically greater for the unidirectional material, but, percentagewise, the crossplied material showed a significantly greater degree of scatter. Because of the larger number of specimens tested at 394 K (250° F) and 450 K (350° F) the scatter bands at these temperature tended to be somewhat wider.

Table 7-4. Baseline Tensile Properties of $[0^\circ]_6$ G/E

Specimen Number	Temperature K (°F)		Tensile Strength MN/m ² (ksi)		Tensile Modulus GN/m ² (Msi)	
BU01-1	218	-67	917	133	—	—
-2			1050	153	—	—
-3			683	99	—	—
			avg 883	128		
BU01-4	297	75	1460	211	a143	a20.8
-5			1660	240	a134	a19.4
-6			1540	223	a145	a21.0
			avg 1550	225	141	20.4
BU01-7	394	250	1650	239	a141	a20.4
-8			1440	209	a136	a19.8
-9			1490	216	a136	a19.8
-22			1460	212	—	—
-23			1560	227	161	23.3
-24			1520	221	152	22.1
-25			1350	196	141	20.4
-26			1630	236	150	21.8
-27			1450	210	144	20.9
-28			1570	228	152	22.1
			avg 1510	219	146	21.2
BU01-10	408	275	1660	241	—	—
-11			1740	252	165	23.9
-12			1610	233	166	24.1
			avg 1670	242	166	24.0
BU01-13	422	300	1540	224	a141	a20.5
-14			1520	221	a140	a20.3
-15			1450	210	a136	a19.9
			avg 1500	218	139	20.2
BU01-16	436	325	1600	232	143	20.7
-17			1660	240	141	20.5
-18			1600	232	131	19.0
			avg 1620	235	138	20.1
BU01-19	450	350	1630	237	150	21.7
-20			1630	237	150	21.8
-21			1550	225	131	19.0
-29			1580	229	154	22.3
-30			1630	237	148	21.5
-31			1630	236	154	22.4
-32			1590	231	160	23.2
-33			1310	190	144	20.9
-34			1630	236	156	22.6
-35			1680	243	155	22.5
			avg 1590	230	150	21.8

^a Strain gage measurement

Table 7-5. Baseline Tensile Properties of $[0^\circ \pm 45^\circ]_s$ G/E

Specimen Number	Temperature		Tensile Strength		Tensile Modulus	
	K	(°F)	MN/m ²	(ksi)	GN/m ²	(Msi)
BU01-1	218	-67	416	60.4	49	7.1
-2			439	63.6	43	6.2
-3			493	71.5	50	7.3
			avg 449	65.2	47	6.9
BU01-6	297	75	578	83.8	a61	a 8.8
-7			447	64.8	a54	a 7.9
-8			463	67.2	a56	a 8.1
			avg 496	71.9	57	8.3
BU01-4	394	250	478	69.4	—	—
-5			505	73.2	—	—
-16			443	64.2	55	8.0
-22			524	76.0	46	6.6
-23			518	75.2	—	—
-24			623	90.3	43	6.2
-25			596	86.4	48	7.0
-26			541	78.4	65	9.4
-27			521	75.5	74	10.8
-28			509	73.8	62	9.0
			avg 526	76.2	56	8.1
BU01-9	408	275	494	71.6	—	—
-10			407	59.0	—	—
-17			552	80.1	54	7.8
			avg 484	70.2	54	7.8
BU01-11	422	300	569	82.5	—	—
-18			460	66.7	48	6.9
-19			497	72.1	54	7.8
			avg 509	73.8	51	7.4
BU01-12	436	325	508	73.7	—	—
-13			520	75.4	—	—
-20			477	69.2	53	7.7
			avg 502	72.8	53	7.7
BU01-14	450	350	457	66.3	—	—
-15			522	75.7	—	—
-21			499	72.4	46	6.6
-29			514	74.6	78	11.3
-30			499	72.4	70	10.1
-31			430	62.4	52	7.5
-32			470	68.1	47	6.8
-33			558	81.0	63	9.2
-34			506	73.4	53	7.7
-35			544	78.9	57	8.2
			avg 500	72.5	58	8.4

^a Strain gage measurement

Table 7-6. Baseline Notched Tensile Properties of $[0^\circ]_6$ G/E

Specimen Number	Temperature		Notched Tensile Strength	
	K	(°F)	MN/m ² (a)	(ksi)
BU02-1	218	-67	1100	159
-2			938	136
-3			1060	154
			avg 1030	150
BU02-4	297	75	1340	194
-5			1310	190
-6			1490	216
			avg 1380	200
BU02-7	394	250	1390	202
-8			1210	176
-9			1200	174
-22			1380	200
-23			1210	176
-24			1560	226
-25			1250	181
-26			1570	228
-27			1630	236
-28			1510	219
			avg 1390	202
BU02-10	408	275	1640	238
-11			1630	237
-12			1590	230
			avg 1620	235
BU02-13	422	300	1610	234
-14			1480	214
-15			1270	184
			avg 1450	211
BU02-16	436	325	1400	203
-17			1320	192
-18			1510	219
			avg 1410	205
BU02-19	450	350	b1170	b170
-20			1240	180
-21			1260	182
-29			b1160	b168
-30			1340	195
-31			b1180	b171
-32			b1260	b183
-33			1590	230
-34			1340	194
-35			b 910	b132
			avg 1350	196

^a Net section strength, i.e., based on total width less hole diameter.

^b Doubler failure, values not included in average.

Table 7-7. Baseline Notched Tensile Properties of $[0^\circ \pm 45^\circ]_s$ G/E

Specimen Number	Temperature K	Temperature (°F)	Notched Tensile Strength	
			MN/m ²	(ksi)
			(a)	
BU02-1	218	-67	317	46.0
-2			309	44.8
-3			311	45.1
			avg 312	45.3
BU02-4	297	75	367	53.2
-5			477	69.2
-6			391	56.7
			avg 412	59.7
BU02-7	394	250	461	66.9
-8			398	57.7
-9			536	77.8
-22			324	47.0
-23			360	52.2
-24			429	62.2
-25			443	64.3
-26			385	55.8
-27			319	46.2
-28			358	51.9
			avg 401	58.2
BU02-10	408	275	448	65.0
-11			367	53.3
-12			377	54.7
			avg 397	57.7
BU02-13	422	300	456	66.2
-14			372	54.0
-15			353	51.2
			avg 394	57.1
BU02-16	436	325	429	62.2
-17			425	61.6
-18			436	63.2
			avg 430	62.3
BU02-19	450	350	445	64.6
-20			396	57.5
-21			553	80.2
-29			419	60.8
-30			334	48.4
-31			403	58.4
-32			396	57.4
-33			445	64.5
-34			398	57.7
-35			369	53.5
			avg 416	60.3

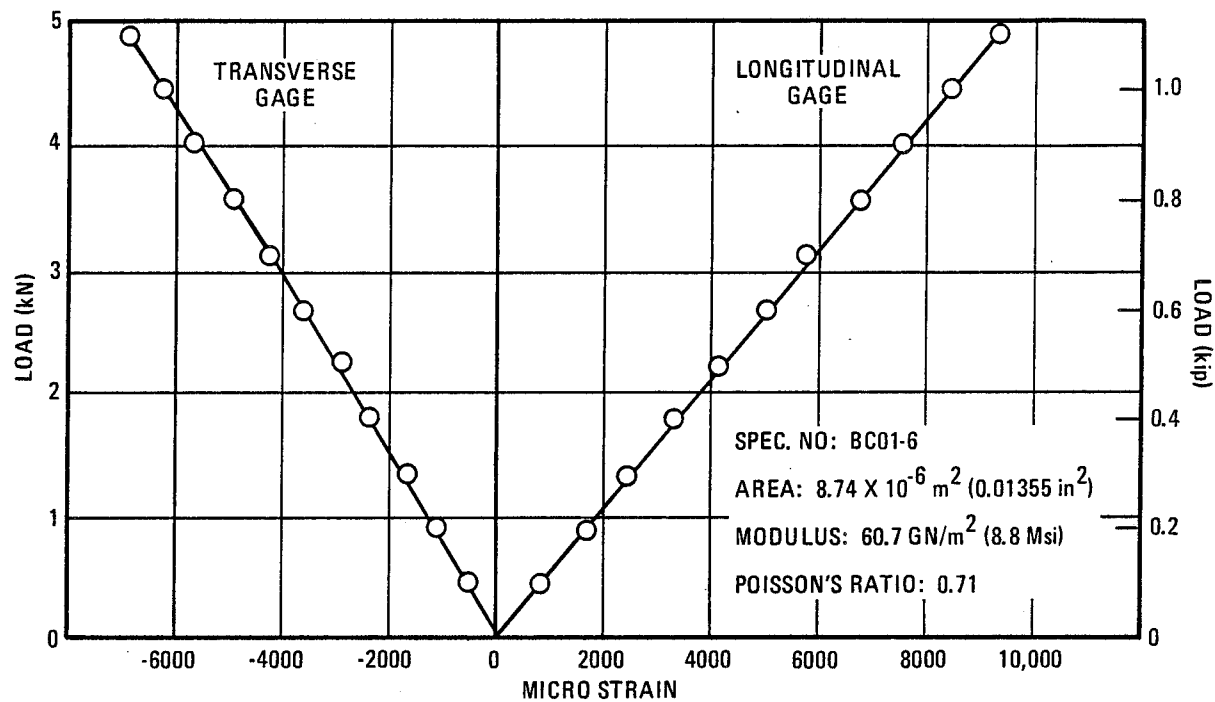
^a Net section strength, i.e., based on total width less hole diameter.

Table 7-8. Baseline Tensile Properties of $[0^\circ]_{12}$ G/E Tested in the Transverse Direction

Specimen Number	Temperature K	Temperature (°F)	Edge Condition	Specimen Width m	Specimen Width (in.)	Tensile Strength MN/m ²	Tensile Strength (ksi)
TBU01-1	297	75	Poor	0.0025	1.00	29	4.2
-2				.0025	1.00	40	5.8
-3				.0025	.99	27	3.9
-4				.0025	1.00	38	5.5
-5				.0025	1.00	38	5.5
-6				.0025	1.00	32	4.6
						avg 34	4.9
TBU01-A	297	75	Good	.0013	.50	54	7.8
-B				.0019	.75	59	8.6
-C				.0019	.75	64	9.3
-11				.0020	.80	57	8.2
-12				.0019	.75	62	9.0
						avg 59	8.6
TBU01-7	450	350	Good	.0016	.62	39	5.6
-8				.0019	.75	37	5.4
-9				.0019	.75	32	4.7
-10				.0020	.80	41	6.0
						avg 37	5.4

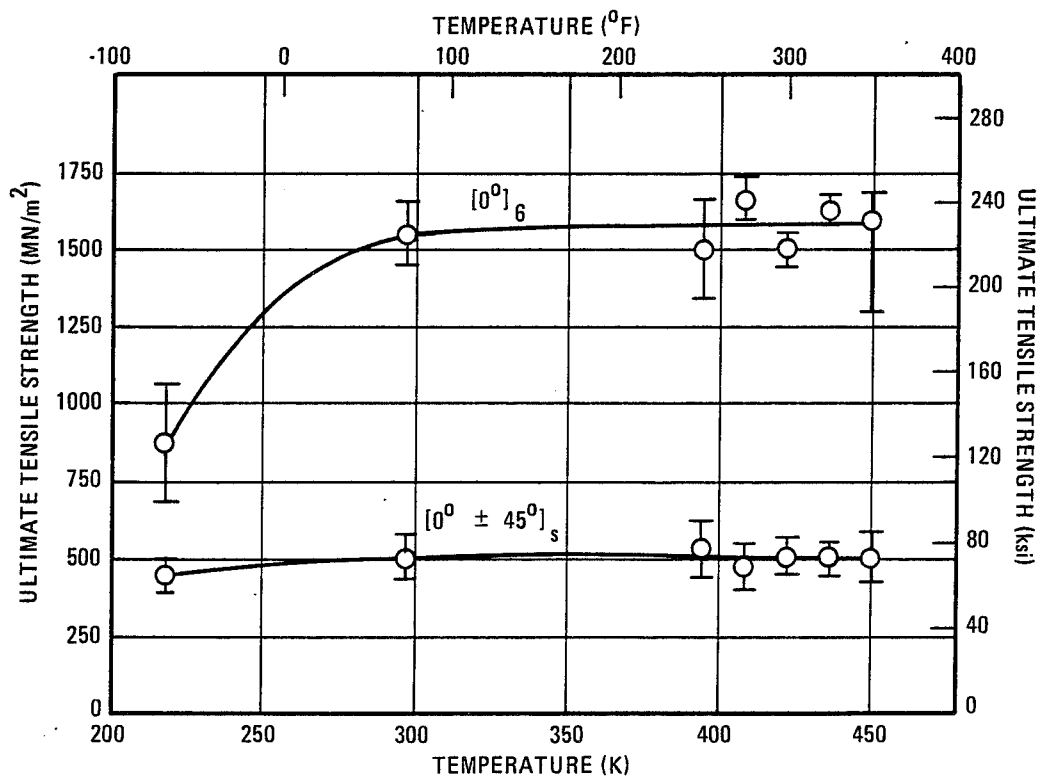
Table 7-9. Baseline Poisson's Ratio Data in Tension of G/E

Specimen Number	Laminate Orientation	Test Direction	Test Temperature K	Test Temperature (°F)	Poisson's Ratio
BU01-4	$[0^\circ]_6$	Longitudinal	297	75	0.35
-5					.33
-6					.32
					avg .33
BU01-7	$[0^\circ]_6$	Longitudinal	394	250	.30
-8					.30
-9					.37
					avg .34
BU01-13	$[0^\circ]_6$	Longitudinal	422	300	.39
-14					.32
-15					.35
					avg .35
BC01-6	$[0^\circ \pm 45^\circ]_S$	Longitudinal	297	75	.71
-7					.70
-8					.70
					avg .70



653217-24

Figure 7-8 Tensile Load-Strain Diagram for $[0^\circ \pm 45^\circ]_s$, G/E at 297 K (75° F)



653217-25

Figure 7-9 Baseline Tensile Properties of G/E

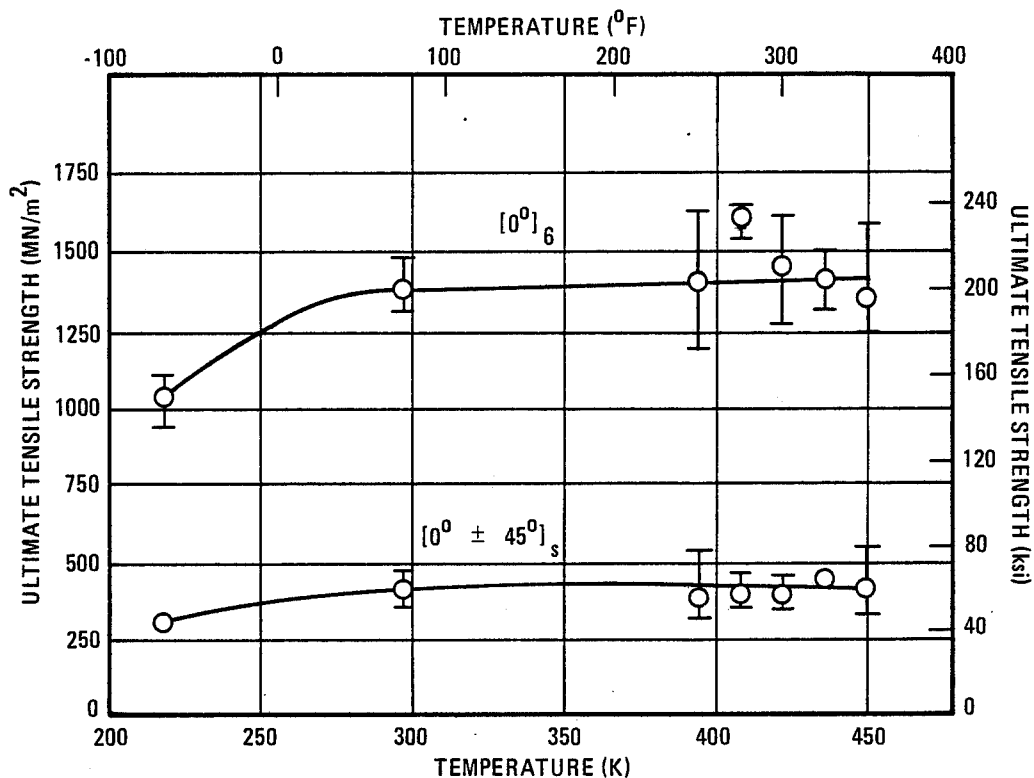


Figure 7-10 Baseline Notched Tensile Properties of G/E

In like manner to the tensile strength data, the tensile modulus was also not significantly affected by increasing temperature out to the maximum test temperatures of 450 K (350° F). At 218 K (-67° F) the average value for the crossplied material was slightly lower than those obtained at higher temperatures, but all of the 218K (-67° F) data fell within the scatter band of the tests conducted at 394 K (250° F). No modulus values were obtained from the 218 K (-67° F) tests on the unidirectional specimens because of extensometer malfunctioning.

A comparison of the ratio of the notched to the unnotched tensile strength of G/E at each of the test temperatures has been made in Table 7-11. For the unidirectional material the effect of a notch on the net section strength is quite small. The result of the notch can frequently be seen during testing, particularly fatigue testing, in that longitudinal cracks propagate tangent to the edges of the notch (center hole) along the entire length of the test section. Examples of the failure mode of the unidirectional notched specimens can be seen in Figure 7-11. Figure 7-12 is a closeup view of the bottom specimen showing the longitudinal splitting that has occurred tangent to the 0.0064 m (0.25 in.) hole. The net effect is to divide the specimen into two smaller parallel specimens. In a tensile test the two strips act as one and very little reduction in the net tensile strength was observed. During fatigue testing, however, as will be shown in Section 11, the notch was observed to either increase or decrease the fatigue life compared to unnotched specimens depending on the test conditions. For crossplied material the notched specimens gave a tensile strength that was 10 to 30% lower than the unnotched specimens. Similar effects of a center hole notch were observed for the G/PI system in both unidirectional and crossplied specimens.

Table 7-10. Summary of Baseline Tensile Properties of G/E

	218 (-67)	297 (75)	394 (250)	408 (275)	422 (300)	436 (325)	450 (350)
Tensile Strength, MN/m ² (ksi)							
[0°] ₆	882 (128)	1540 (224)	1510 (219)	1670 (242)	1500 (218)	1610 (234)	1590 (230)
[0° ± 45°] _s	449 (65.2)	496 (71.9)	525 (76.2)	484 (70.2)	509 (73.8)	502 (72.8)	500 (72.5)
[90°] ₁₂	—	59 (8.6)	—	—	—	—	37 (5.4)
Tensile Modulus, GN/m ² (Msi)							
[0°] ₆	—	141 (20.4)	146 (21.2)	166 (24.0)	139 (20.2)	139 (20.1)	150 (21.8)
[0° ± 45°] _s	48 (6.9)	57 (8.3)	56 (8.1)	54 (7.8)	51 (7.4)	53 (7.7)	58 (8.4)
Poisson's Ratio							
[0°] ₆	—	0.33	0.34	—	0.35	—	—
[0° ± 45°] _s	—	.70	—	—	—	—	—
Notched Tensile Strength, MN/m ² (ksi)							
[0°] ₆	1030 (150)	1380 (200)	1390 (202)	1620 (235)	1450 (210)	1410 (204)	1350 (196)
[0° ± 45°] _s	312 (45.3)	412 (59.7)	401 (58.2)	398 (57.7)	394 (57.1)	429 (62.3)	416 (60.3)

Table 7-11. Ratio of Notched to Unnotched Tensile Strength of G/E at Various Temperatures

Temperature		Ratio of Notched to Unnotched Strength	
K	(°F)	$[0^\circ]_6$	$[0^\circ \pm 45^\circ]_s$
218	-67	1.2	0.7
297	75	.9	.8
394	250	.9	.8
408	275	1.0	.8
422	300	1.0	.8
436	325	.9	.9
450	350	.9	.8

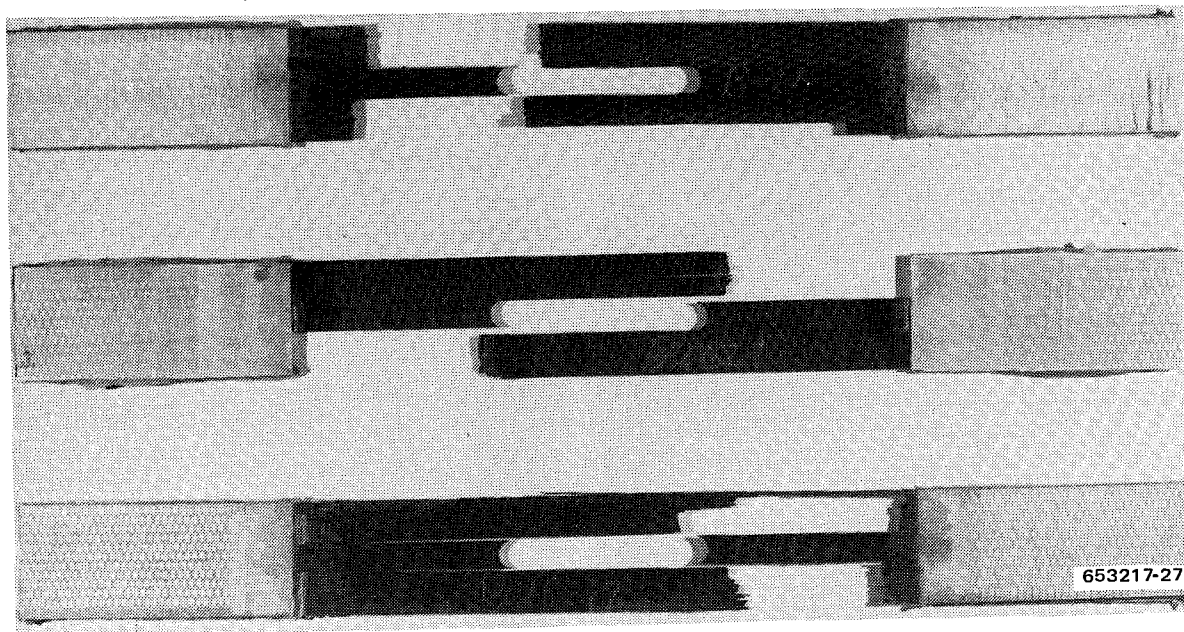


Figure 7-11 Unidirectional G/E Notched Tensile Specimens

Tensile data for the unidirectional material tested in the transverse direction are listed in Table 7-8. The plan called for six specimens each to be tested at room and one elevated temperature. The specimens, which were taken from the first G/E laminate that was fabricated, were intended to be used as a quality assurance check on the material as well as for baseline tensile property determinations. The wrong blade was used on the table saw when cutting the specimens. Six of these specimens were tested at room temperature, giving the low values shown in Table 7-8. An examination of the saw cut edges of the failed specimens revealed a very poor edge condition and one at which premature failure could readily be initiated. The remaining six untested specimens and three spares that were available were salvaged by trimming the chipped edges with the correct blade. The two types of edge conditions are shown in Figure 7-13 and 7-14. The

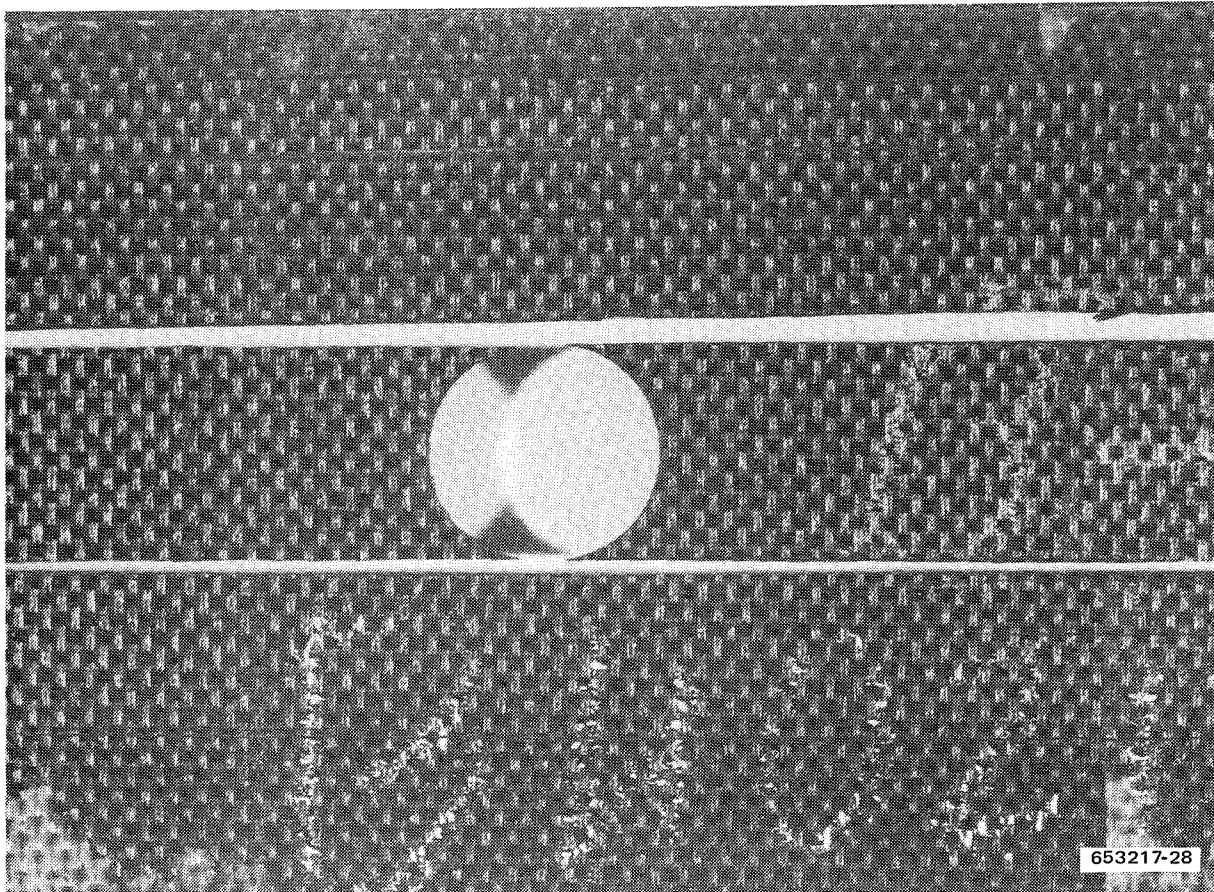


Figure 7-12 Closeup View of Unidirectional G/E Notched Tensile Specimens Showing Longitudinal Splitting Tangent to the Center Hole

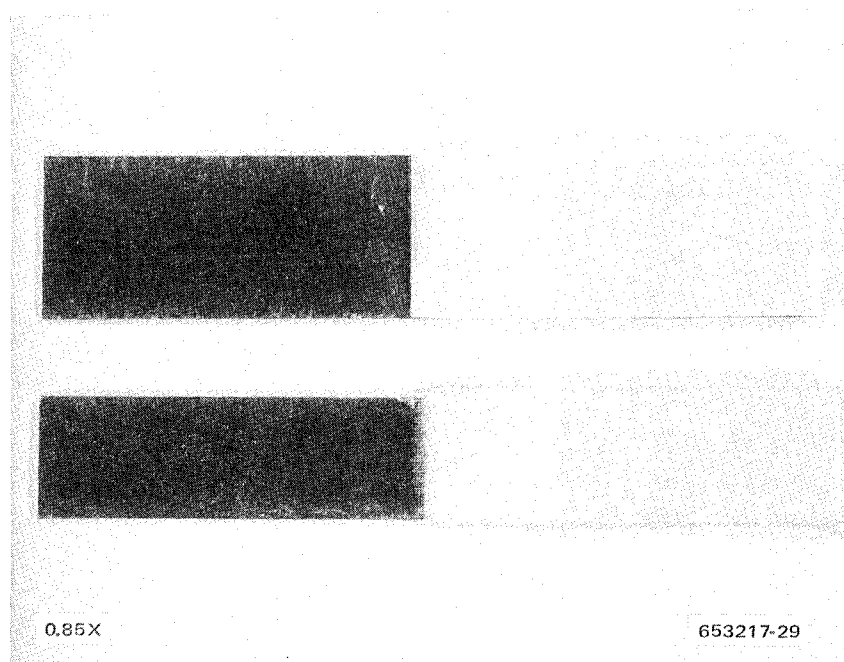


Figure 7-13 Transverse Tensile Specimens of G/E Showing Poor Edge Condition of Improperly Machined Specimen (upper) and Good Edge Condition of Properly Machined Specimen (lower)

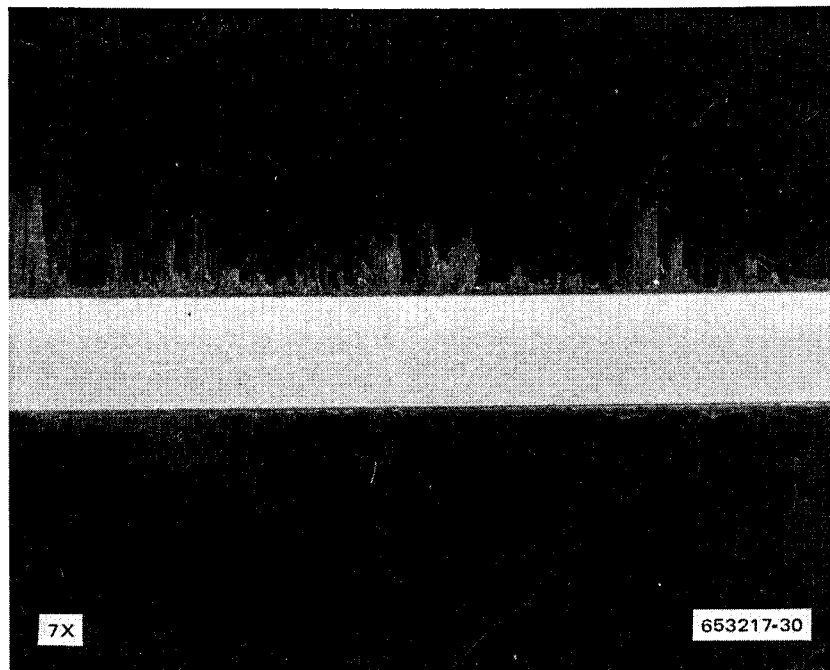


Figure 7-14 Transverse Tensile Specimens of G/E Showing Poor Edge Condition of Improperly Machined Specimen (upper) and Good Edge Condition of Properly Machined Specimen (lower)

room temperature tensile strength of the somewhat narrow specimens with good edges was nearly double that of those with the badly damaged edges. Unlike longitudinal tensile properties the transverse strength showed a considerable decrease at 450 K (350° F). The transverse strength is a matrix dominated property and would be expected to be more temperature dependent than the fiber dominated longitudinal strength.

The remaining baseline tensile data for G/E, Poisson's ratio values, are listed in Table 7-9. For the unidirectional material values of approximately $\frac{1}{3}$ (similar to that obtained for most metals) were obtained at all three temperatures. Room temperature measurements on crossplied specimens gave values that were similar to those determined for the B/E system.

7.1.2.2 Graphite/Polyimide System. The test plan for the G/PI baseline tensile specimens was similar to that used for the G/E specimens in that three tests were performed at each of seven temperatures. It differed slightly, however, in that all remaining specimens were then tested at one of the seven original temperatures rather than at two. This temperature was the one that had been selected for the flight simulation exposure tests, 505 K (450° F). Testing at one temperature was done to increase the tensile strength data base that was required for selection of the short-term flight simulation load levels. At the time these tests were performed very little data was available for the HT-S/710 system. Selection of the temperatures for the flight simulation tests is discussed in Section 12.

Baseline tensile tests, both unnotched and notched, were performed on unidirectional and $[0^\circ \pm 45^\circ]_s$ crossplied specimens in the longitudinal direction. Some unnotched tensile tests were also performed in the transverse direction on unidirectional material, and a limited amount of

Table 7-12. Baseline Tensile Properties of $[0^\circ]_6$ G/PI

Specimen Number	Temperature		Tensile Strength		Tensile Modulus	
	K	(°F)	MN/m ²	(ksi)	GN/m ²	(Msi)
DU01-1	218	-67	1300	188	144	20.9
-2			1180	171	97	14.1
-3			1100	160	134	19.4
			avg 1190	173	125	18.1
DU01-4	297	75	1260	182	a127	a18.4
-5			1190	172	a126	a18.2
66			1120	163	a126	a18.3
			avg 1190	172	126	18.3
DU01-7	505	450	1090	158	a121	a17.6
-8			1260	182	a128	a18.6
-9			1270	184	a126	a18.3
-22			1360	197	—	—
-23			1260	182	—	—
-24			1130	164	—	—
-25			1160	168	—	—
			avg 1220	176	125	18.2
DU01-10	533	500	1270	184	—	—
-11			1260	182	—	—
-12			1210	176	—	—
			avg 1250	181		
DU01-13	561	550	1370	199	a141	a20.5
-14			1400	203	a133	a19.3
-15			1190	173	a128	a18.5
			avg 1320	192	134	19.4
DU01-16	589	600	1150	167	—	—
-17			1200	174	—	—
-18			1240	180	—	—
			avg 1200	174		
DU01-19	616	650	1080	156	—	—
-20			1120	162	—	—
-21			1060	154	—	—
			avg 1090	157		

^a Strain gage measurement

Table 7-13. Baseline Tensile Properties of $[0^\circ \pm 45^\circ]_s$ G/PI

Specimen Number	Temperature		Tensile Strength		Tensile Modulus	
	K	(°F)	MN/m ²	(ksi)	GN/m ²	(Msi)
DC01-1	218	-67	387	56.1	41	5.9
-2			417	60.5	37	5.4
-3			411	59.6	36	5.2
avg			405	58.7	38	5.5
DC01-4	297	75	510	74.0	a50	a7.3
-5			505	73.2	a56	a8.1
-6			543	78.7	a53	a7.7
avg			519	75.3	53	7.7
DC01-7	505	450	423	61.3	a47	a6.8
-8			299	43.4	a39	a5.7
-9			441	63.9	a54	a7.9
-22			478	69.3	—	—
-23			525	76.2	—	—
-24			478	69.4	—	—
-25			437	63.4	—	—
-26			463	67.1	—	—
-27			496	71.9	—	—
-28			496	71.9	—	—
-29			485	70.3	—	—
-30			478	69.3	—	—
-31			560	81.2	—	—
-32			432	62.7	—	—
-33			512	74.3	—	—
-34			543	78.8	—	—
-35			449	65.1	—	—
avg			470	68.2	57	6.8
DC01-10	533	500	398	57.7	—	—
-11			410	59.5	—	—
-12			385	55.9	—	—
avg			398	57.7	—	—
DC01-13	561	550	257	37.5	a41	a6.0
-14			301	43.7	a44	a6.4
-15			463	67.2	a46	a6.7
avg			340	49.4	44	6.4
DC01-16	589	600	352	51.1	—	—
-17			432	62.6	—	—
-18			409	59.3	—	—
avg			398	57.7	—	—
DC01-19	616	650	305	44.3	—	—
-20			330	47.9	—	—
-21			345	50.0	—	—
avg			327	47.4	—	—

^a Strain gage measurement

Table 7-14. Baseline Notched Tensile Properties of $[0^\circ]_6$ G/PI

Specimen Number	Temperature K	Temperature (°F)	Notched Tensile Strength	
			MN/m ² (a)	(ksi)
DU02-1	218	-67	1180	171
-2			820	119
-3			972	141
			avg 991	144
DU02-4	297	75	1310	190
-5			1140	166
-6			1320	192
			avg 1260	183
DU02-7	505	450	1230	178
-8			1160	169
-9			1340	195
-22			986	143
-23			1250	181
-24			1040	151
-25			1110	161
-26			1130	164
-27			1060	154
-28			1080	157
-29			1120	163
-30			1210	175
-31			1240	180
-32			1190	173
-33			1140	166
-34			1070	155
-35			1050	152
			avg 1140	166
DU02-10	533	500	1240	180
-11			1240	180
-12			1140	166
			avg 1210	175
DU02-13	561	550	1040	151
-14			1120	162
-15			1280	186
			avg 1150	166
DU02-16	589	600	979	142
-17			1060	154
-18			1030	150
			avg 1020	149
DU02-19	616	650	1130	164
-20			1140	166
-21			1050	153
			avg 1110	161

^a Net section strength, i.e., based on total width less hole diameter.

Table 7-15. Baseline Notched Tensile Properties of $[0^\circ \pm 45^\circ]_s$ G/PI

Specimen Number	Temperature K	Temperature (°F)	Notched Tensile Strength	
			MN/m ² (a)	(ksi)
DC02-1	218	-67	328	47.5
-2			288	41.8
-3			339	49.1
			avg 318	46.1
DC02-4	297	75	367	53.3
-5			332	48.2
-6			372	54.0
			avg 357	51.8
DC02-7	505	450	343	49.7
-8			352	51.0
-9			330	47.8
-22			334	48.4
-23			350	50.8
-24			350	50.7
-25			301	43.7
-26			332	48.2
-27			386	56.0
-28			354	51.4
-29			305	44.2
-30			373	54.1
-31			333	48.3
-32			363	52.7
-33			303	43.9
-34			292	42.4
-35			314	45.5
			avg 336	48.8
DC02-10	533	500	361	52.3
-11			386	56.0
-12			308	44.7
			avg 352	51.0
DC02-13	561	550	250	36.3
-14			355	51.5
-15			339	49.2
			avg 315	45.7
DC02-16	589	600	242	35.1
-17			232	33.6
-18			272	39.4
			avg 249	36.1
DC02-19	616	650	221	32.0
-20			262	38.0
-21			270	39.2
			avg 251	36.4

^a Net section strength, i.e., based on total width less hole diameter.

Table 7-16. Baseline Notched Tensile Properties of $[0^\circ]_{12}$ G/PI Tested in the Transverse Direction

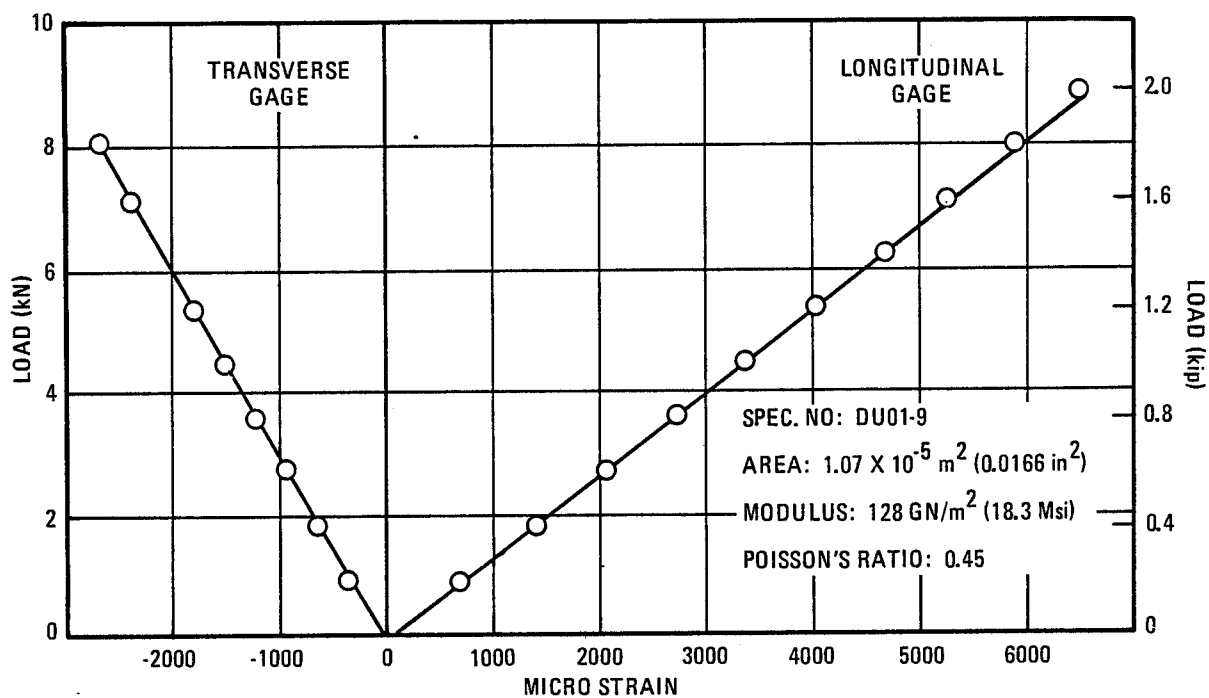
Specimen Number	Temperature		Tensile Strength		Tensile Modulus	
	K	(°F)	MN/m ²	(ksi)	GN/m ²	(Msi)
TDU01-1	297	75	21	3.0	5.2	0.75
-2			31	4.5	6.3	.91
-3			21	3.1	4.8	.69
-4			23	3.4	5.2	.76
-5			20	2.9	4.8	.69
-6			25	3.6	4.8	.69
			avg 24	3.4	5.2	.75
TDU01-7	505	450	(a)	(a)	—	—
-8			22	3.2	—	—
-9			(a)	(a)	—	—
-10			21	3.1	—	—
-11			28	4.0	—	—
-12			19	2.8	—	—
			avg 22	3.3		

^a Failed in handling

Table 7-17. Baseline Poisson's Ratio Data in Tension of G/PI

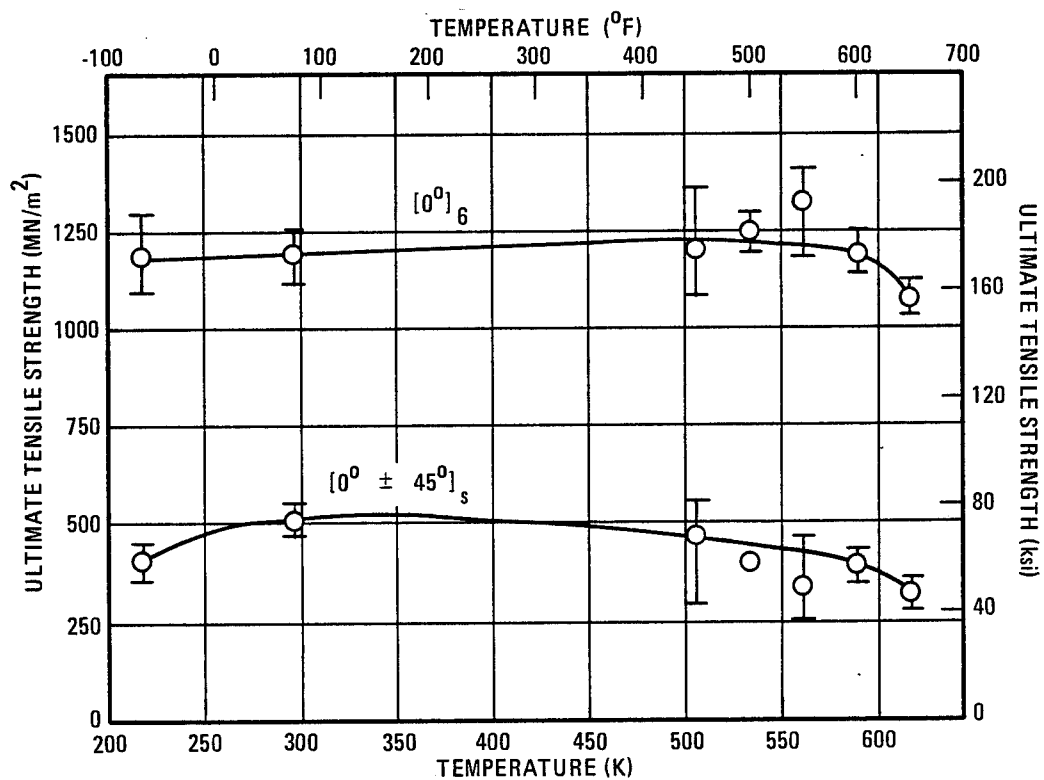
Specimen Number	Laminate Orientation	Test Direction	Test Temperature		Poisson's Ratio
			K	(°F)	
DU01-7	$[0^\circ]_6$	Longitudinal	505	450	0.38
-8					.35
-9					.45
					avg .39
DU01-13	$[0^\circ]_6$	Longitudinal	561	550	.50
-14					.45
-15					.44
					avg .46
DC01-4	$[0^\circ \pm 45^\circ]_s$	Longitudinal	297	75	.71
-5					.65
-6					.64
					avg .67

Poisson's ratio testing was conducted. Results are listed in Tables 7-12 through 7-17. A typical load-strain diagram from one of the strain gaged Poisson's ratio specimens is shown in Figure 7-15. The longitudinal unnotched and notched data are plotted as a function of temperature in Figure 7-16 and 7-17. A summary of all the G/PI tensile properties is presented in Table 7-18.



653217-31

Figure 7-15 Tensile Load-Strain Diagram for $[0^\circ]_6$, G/PI at 505 K (450° F)



653217-32

Figure 7-16 Baseline Tensile Properties of G/PI

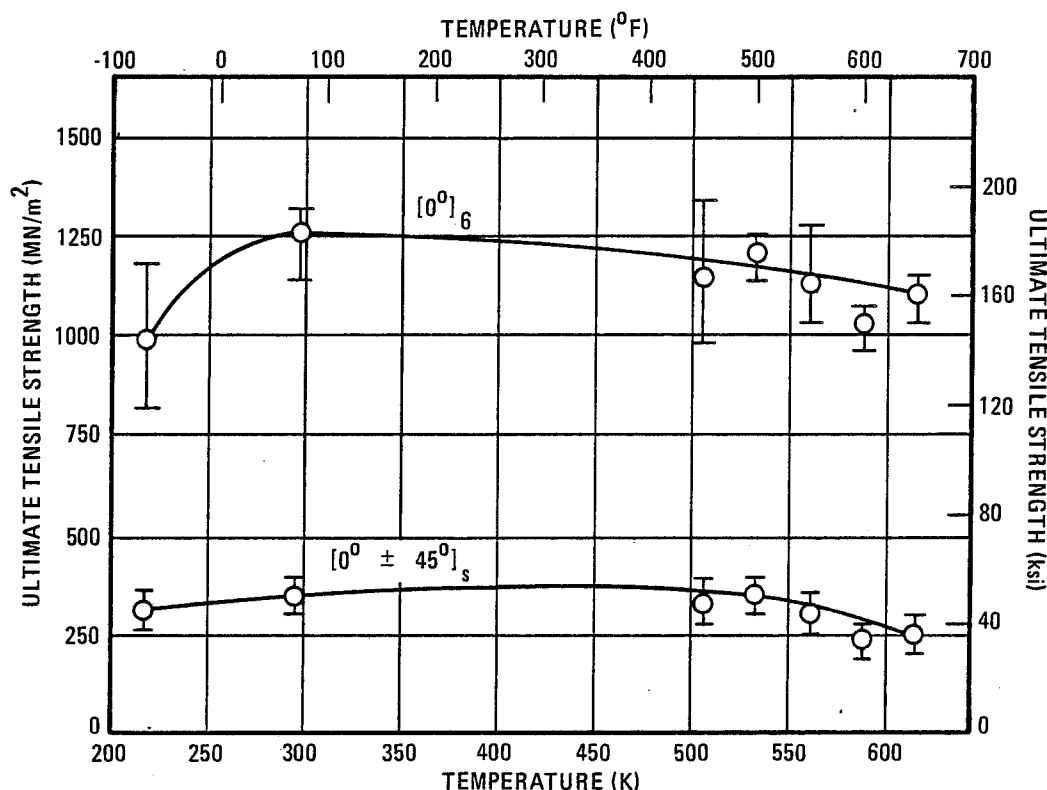


Figure 7-17 Baseline Notched Tensile Properties of G/PI

Modulus values were determined at four temperatures for the specimens tested in the longitudinal direction. A mechanical extensometer was used for the 218 K (-67° F) tests while strain gages were used at room temperature and the two elevated temperatures. Poisson's ratio values were also determined for some of these specimens. For the material tested in the transverse direction, modulus values were obtained at room temperature only. A mechanical extensometer was used for these tests.

The temperature dependence of the G/PI tensile strength is shown in Figures 7-16 and 7-17. At the maximum test temperature, 616 K (650° F), the unidirectional unnotched and notched specimens had lost approximately 10% of the room temperature strength. The loss for the crossplied specimens was somewhat higher, 37% for the unnotched and 30% for the notched specimens. Because of the limited amount of tests and the scatter in the data, the temperature at which the tensile strength begins to decrease is difficult to determine precisely. The curves indicate this decrease to occur between 561 K (550° F) and 616 K (650° F). Some decrease in strength was also observed at 218 K (-67° F) but the effect was generally less than that found for the G/E system. The spread in the G/PI tensile data as shown by the scatter bands in Figures 7-16 and 7-17 was similar to that observed for G/E. The tensile modulus for the unidirectional material was not lowered by increasing temperatures out to the maximum test temperature of 561 K (550° F). The crossplied material did show a decrease in modulus, however, of about 15% at 561 K (550° F) and nearly 30% at 218 K (-67° F).

Table 7-18. Summary of Baseline Tensile Properties of G/PI

	Temperature, K (°F)						
	218 (-67)	297 (75)	505 (450)	533 (500)	561 (550)	589 (600)	616 (650)
Tensile Strength, MN/m ² (ksi)							
[0°] ₆	1190 (173)	1190 (172)	1210 (176)	1240 (180)	1320 (191)	1200 (174)	1080 (157)
[0° ± 45°] _s	405 (58.7)	519 (75.3)	470 (68.2)	398 (57.7)	341 (49.4)	398 (57.7)	327 (47.4)
[90] ₁₂	—	23 (3.4)	23 (3.3)	—	—	—	—
Tensile Modulus, GN/m ² (Msi)							
[0°] ₆	125 (18.1)	126 (18.3)	126 (18.2)	—	134 (19.4)	—	—
[0° ± 45°] _s	38 (5.5)	53 (7.7)	47 (6.8)	—	44 (6.4)	—	—
Poisson's Ratio							
[0°] ₆	—	—	0.39	—	0.46	—	—
[0° ± 45°] _s	—	.67	—	—	—	—	—
Notched Tensile Strength, MN/m ² (ksi)							
[0°] ₆	993 (144)	1260 (183)	1140 (166)	1210 (176)	1140 (166)	1030 (149)	1110 (161)
[0° ± 45°] _s	318 (46.1)	357 (51.8)	336 (48.8)	352 (51.0)	315 (45.7)	249 (36.1)	251 (36.4)

A comparison of the ratio of the notched to unnotched tensile strength of G/PI at each of the test temperatures has been made in Table 7-19. The results are very similar to those found for the G/E system. For the unidirectional material the effect of a center hole notch was quite small except at 218 K (-67° F). The crossplied material, on the other hand, experienced decreases in tensile strength of 10 to 40% when tested in the notched configuration.

Table 7-19. Ratio of Notched to Unnotched Tensile Strength of G/PI at Various Temperatures

Temperature		Ratio of Notched to Unnotched Strength	
K	($^{\circ}$ F)	$[0^{\circ}]_6$	$[0^{\circ} \pm 45^{\circ}]_s$
218	-67	0.8	0.8
297	75	1.1	.7
505	450	.9	.7
533	500	1.0	.9
561	550	.9	.9
589	600	.9	.6
616	650	1.0	.8

Transverse tensile data are presented in Table 7-16 for room and elevated temperatures. Strength values were considerably lower than those presented earlier for the G/E system but were about 50% higher than values reported by others (ref. 21). The modulus values, however, were considerably lower than those reported in reference 21. No significant effect of temperature on the transverse strength was observed out to 505 K (450° F). Evidence of the low transverse strength of this material is shown by the two accidental specimen failures that occurred when installing the specimens in the tensile machine grips. Only slight flexing of the specimens will result in fracture.

Poisson's ratio values, Table 7-17, for unidirectional G/PI were somewhat larger than those obtained for G/E. An increase in value with increase in temperature was also observed. In like manner to the B/E and G/E data, the room temperature Poisson's ratio for crossplied material was also quite large.

7.1.2.3 Boron/Aluminum System. The baseline tensile test plan for the B/Al system as originally proposed included tests at 218 K (-67° F) and 297 K (75° F) as used for the resin matrix systems and at 561 K (550° F) and 700 K (800° F). The 700 K (800° F) temperature was considered to be the maximum short-time use temperature and 561 K (550° F) the maximum use temperature for very long time applications. Fatigue tests conducted on this program (see Section 11, however, revealed the existence of a severe surface degradation effect during fatigue cycling of B/Al at 561 K (550° F) in an air environment. The effect was not observed at 505 K (450° F). Because of this severe surface degradation the flight simulation temperature initially selected for B/Al, 561 K (550° F), was lowered to 505 K (450° F). At the time of this decision all baseline testing was completed except for the unnotched $[0^{\circ} \pm 45^{\circ}]_s$ crossplied material. A

change was made to include several tensile tests at 505 K (450 ° F) to assist in selection of the short-term flight simulation load levels. Three specimens were also tested at 616 K (650 ° F) to fill in the tensile strength versus temperature curve for unnotched $[0^\circ \pm 45^\circ]_s$ crossplied B/Al.

Baseline tensile tests, both unnotched and notched, were performed on unidirectional and $[0^\circ \pm 45^\circ]_s$ crossplied specimens in the longitudinal direction. Some unnotched tensile tests were also performed in the transverse direction on unidirectional material, and a limited amount of Poisson's ratio testing was conducted. Results are listed in Table 7-20 through 7-25. A typical load-strain diagram is plotted in Figure 7-18. The longitudinal unnotched and notched data are plotted as a function of temperature in Figures 7-19 and 7-20. A summary of all the B/Al tensile properties is presented in Table 7-26.

Table 7-20. Baseline Tensile Properties of $[0^\circ]_6$ B/Al

Specimen Number	Temperature		Tensile Strength		Tensile Modulus	
	K	(°F)	MN/m ²	(ksi)	GN/m ²	(Msi)
EU01-1	218	-67	1640	238	178	25.8
-2			1620	235	197	28.6
-3			1580	229	172	25.0
-4			1540	223	166	24.1
-5			1610	234	157	22.8
			avg 1600	232	174	25.3
EU01-6	561	550	1200	174	^a 199	^a 28.9
-7			1360	197	^a 212	^a 30.7
-8			1200	174	^a 207	^a 30.0
-9			1430	207	—	—
			avg 1300	188	206	29.9
EU01-10	700	800	1360	198	^a 192	^a 27.8
-11			1150	167	^a 194	^a 28.2
-12			1380	200	^a 214	^a 31.0
-13			1320	192	—	—
			avg 1300	189	200	29.0

^a Strain gage measurement

Modulus measurements were made using both a mechanical extensometer and strain gages at temperatures to 561 K (550 ° F). Above 561 K (550 ° F) a small number of tests was made using only strain gaged specimens. Modulus values were obtained at 218 K (-67 ° F) for the unidirectional specimens, but extensometer malfunctions during tests on the crossplied specimens gave poorly defined stress strain curves that did not allow determination of modulus. For the material tested in the transverse direction, modulus was determined only at room temperature using a mechanical extensometer.

Table 7-21. Baseline Tensile Properties of $[0^\circ \pm 45^\circ]_s$ B/Al

Specimen Number	Temperature K	Temperature (°F)	Tensile Strength		Tensile Modulus	
			MN/m ²	(ksi)	GN/m ²	(Msi)
EC01-1	218	-67	499	72.4	—	—
-2			550	79.8	—	—
-3			525	76.1	—	—
-4			554	80.4	—	—
-5			511	74.1	—	—
			avg 528	76.6		
EC01-6	297	75	487	70.7	155	22.5
-7			545	79.1	158	22.9
-8			482	69.9	160	23.2
-9			458	66.4	140	20.3
-10			552	80.0	167	24.2
-11			565	82.0	163	23.7
-12			549	79.6	169	24.5
-13			459	66.5	154	22.4
-14			545	79.1	141	20.4
-15			514	74.5	139	20.1
			avg 516	74.8	155	22.4
EC01-16	505	450	459	66.6	^a 104	^a 15.1
-17			447	64.9	142	20.6
-18			468	67.9	100	14.5
-28			454	65.9	136	19.8
-29			457	66.3	126	18.3
-30			471	68.3	116	16.9
-31			410	59.5	124	18.0
			avg 452	65.6	121	17.6
EC01-19	561	550	450	65.2	^a 103	^a 15.0
-20			365	53.0	123	17.9
-21			416	60.3	102	14.8
-32			450	65.3	120	17.4
-33			474	68.8	128	18.5
-34			455	66.0	103	15.0
-35			464	67.3	108	15.6
			avg 439	63.7	112	16.3
EC01-22	616	650	423	61.3	^a 108	^a 15.6
-23			397	57.6	—	—
-24			499	72.4	—	—
			avg 440	63.8	108	15.6
EC01-25	700	800	467	67.7	^a 93.1	^a 13.5
-26			338	49.0	—	—
-27			335	48.6	—	—
			avg 380	55.1	93.1	13.5

^a Strain gage measurement

Table 7-22. Baseline Notched Tensile Properties of $[0^\circ]_6$ B/Al

Specimen Number	Temperature K	Temperature (°F)	Notched Tensile Strength	
			MN/m ² (a)	(ksi)
EU02-1	218	-67	1200	174
-2			1210	175
-3			1240	180
-4			1230	178
-5			1210	176
			avg 1220	177
EU02-6	561	550	1190	173
-7			1130	164
-8			1140	165
-9			1130	164
			avg 1150	166
EU02-10	700	800	986	143
-11			1100	159
-12			1080	157
-13			1030	150
			avg 1050	152

^a Net section strength, i.e., based on total width less hole diameter.

Table 7-23. Baseline Notched Tensile Properties of $[0^\circ \pm 45^\circ]_5$ B/Al

Specimen Number	Temperature K	Temperature (°F)	Notched Tensile Strength	
			MN/m ² (a)	(ksi)
EC02-1	218	-67	486	70.5
-2			492	71.3
-3			460	66.7
-4			442	64.1
-5			495	71.8
			avg 475	68.9
EC02-6	297	75	470	68.1
-7			465	67.4
-8			470	68.1
-9			467	67.7
-10			455	66.0
-11			496	72.0
-12			485	70.4

Table 7-23. Baseline Notched Tensile Properties of $[0^\circ \pm 45^\circ]_s$ B/Al — Concluded

Specimen Number	Temperature		Notched Tensile Strength	
	K	(°F)	MN/m ² (a)	(ksi)
-13			490	71.0
-14			495	71.8
-15			501	72.7
			avg 479	69.5
EC02-16	561	550	434	62.9
-17			433	62.8
-18			423	61.4
-19			461	66.9
-20			454	65.9
-21			439	63.7
-22			421	61.1
-23			451	65.4
-24			455	66.0
-25			462	67.0
			avg 443	64.3
EC02-26	700	800	361	52.3
-27			361	52.4
-28			363	52.6
-29			377	54.7
-30			341	49.5
-31			361	52.3
-32			378	54.8
-33			371	53.8
-34			363	52.7
-35			351	50.9
			avg 363	52.6

^a Net section strength, i.e., based on total width less hole diameter.

Table 7-24. Baseline Tensile Properties of $[0^\circ]_6$ B/Al Tested in the Transverse Direction

Specimen Number	Temperature		Tensile Strength		Tensile Modulus	
	K	(°F)	MN/m ²	(ksi)	GN/m ²	(Msi)
TEU01-1	297	75	94.5	13.7	48.3	7.0
-2			122	17.7	67.6	9.8
-3			51.0	7.4	133	19.3
-4			74.5	10.8	121	17.6
-5			57.9	8.4	105	15.2
-6			76.5	11.1	140	20.3
			avg 79.4	11.5	102	14.9
TEU01-7	700	800	44.1	6.4	—	—
-8			31.7	4.6	—	—
-9			38.6	5.6	—	—
-10			29.0	4.2	—	—
-11			35.8	5.2	—	—
-12			33.1	4.8	—	—
			avg 35.4	5.1		

Table 7-25. Baseline Poisson's Ratio Data in Tension of B/Al

Specimen Number	Laminate Orientation	Test Direction	Test Temperature		Poisson's Ratio
			K	(°F)	
EU01-6	$[0^\circ]_6$	Longitudinal	561	550	0.31
-7					.34
-8					.34
					avg .33
EU01-10	$[0^\circ]_6$	Longitudinal	700	800	.32
-11					.30
-12					.39
					avg .34

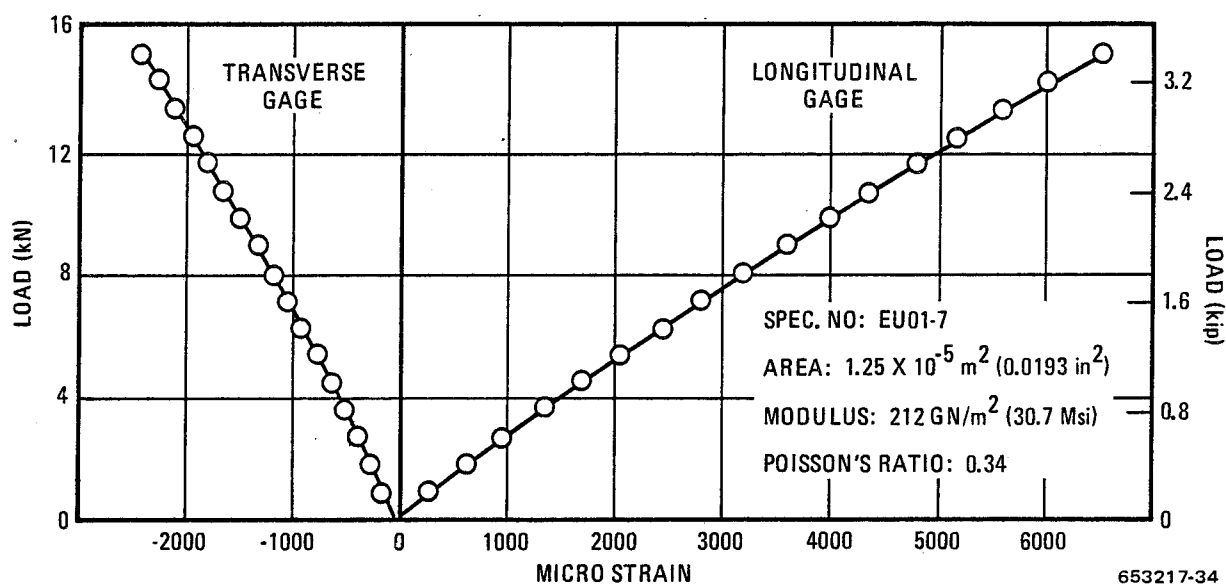


Figure 7-18 Tensile Load-Strain Diagram for $[0^\circ]_6$, B/Al at 561 K (550° F)

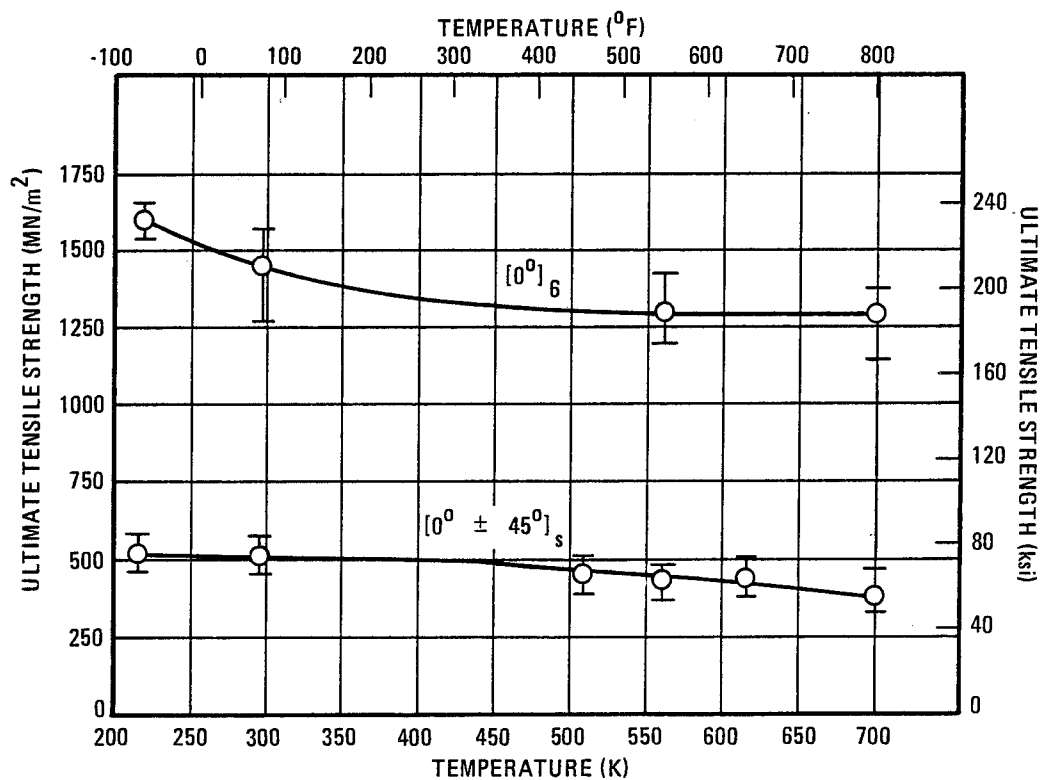
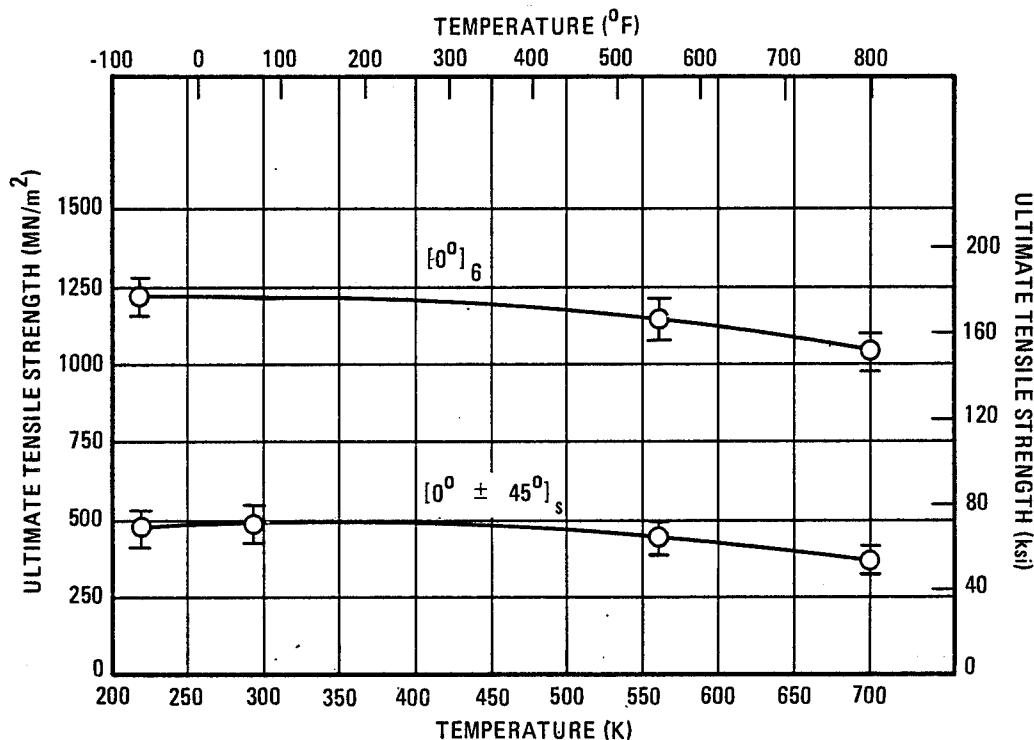


Figure 7-19 Baseline Tensile Properties of B/Al



653217-36

Figure 7-20 Baseline Notched Tensile Properties of B/Al

The effect of temperature on the tensile strength of B/Al is shown in Figures 7-19 and 7-20. No tests were conducted on the unnotched unidirectional material at room temperature, but data were available from the QA panels, and these data are plotted at room temperature in Figure 7-19. The curves show a gradual decrease in strength with increasing temperature for both orientations and configurations. The B/Al data are similar to those for G/PI in that the decrease is somewhat greater for the crossplied material, both unnotched and notched, than for the unidirectional material. The tensile strength was slightly higher at 218 K (-67°F) for the unnotched specimens but essentially unchanged for the notched specimens. In like manner to both the G/E and G/PI systems, the data scatter for B/Al was numerically greater for the unidirectional material, but, percentagewise, was greater for the crossplied material. The scatter bands for the notched tests, Figure 7-20, were considerably smaller than those obtained for the unnotched specimen tests, Figure 7-19. This effect was not observed for either of the resin matrix systems.

No decrease in tensile modulus was found for the unidirectional B/Al out to 700 K (800°F). There was a decrease of about 15% however, for tests at 218 K (-67°F). The $[0^\circ \pm 45^\circ]_s$ crossplied material exhibited a continuous decrease in modulus out to 700 K (800°F). The total change between room temperature and 700 K (800°F) was approximately 40%.

The ratios of the notched to the unnotched tensile strengths of B/Al have been calculated for several temperatures and are shown in Table 7-27. The data differ from those presented earlier for the resin matrix systems in that the crossplied specimens were not greatly affected by the notch; whereas, the unidirectional specimens experienced decreases in tensile strength of approximately 20% when tested in the notched configuration.

Table 7-26. Summary of Baseline Tensile Properties of B/Al

	218 (-67)	297 (75)	Temperature, K (°F)	616 (650)	700 (800)
			505 (450)	561 (550)	
Tensile Strength, MN/m ² (ksi)					
[0°] ₆	1600 (232)	1430 (208)	—	1300 (188)	1300 (189)
[0° ± 45°] _s	528 (76.6)	516 (74.8)	452 (65.6)	439 (63.7)	380 (55.1)
Tensile Modulus, GN/m ² (Msi)					
[0°] ₆	174 (25.3)	194 (28.2)	—	206 (29.9)	200 (29.0)
[0° ± 45°] _s	—	154 (22.4)	121 (17.6)	112 (16.3)	93 (13.5)
Poisson's Ratio					
[0°] ₆	—	0.23	—	0.33	0.34
Notched Tensile Strength, MN/m ² (ksi)					
[0°] ₆	1220 (177)	1210 (176)	—	1140 (166)	1050 (152)
[0° ± 45°] _s	475 (68.9)	479 (69.5)	—	443 (64.3)	363 (52.6)

Table 7-27. Ratio of Notched to Unnotched Tensile Strength of B/Al at Various Temperatures

Temperature		Ratio of Notched to Unnotched Strength	
K	(°F)	[0°] ₆	[0° ± 45°] ₅
218	-67	0.8	0.9
297	75	^a .8	.9
561	550	.9	1.0
700	800	.8	1.0

^aEstimated from curves of tensile strength versus temperature

Tensile data for unidirectional material tested in the transverse direction are given in Table 7-24. The effect of temperature on the transverse tensile strength was much more pronounced than that for longitudinal strength with values at 700 K (800° F) approximately half of those measured at room temperature.

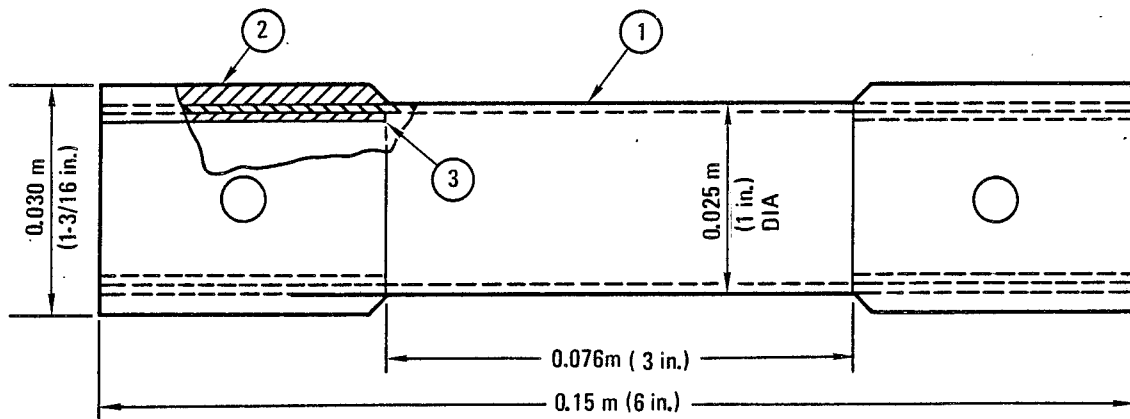
Results of the Poisson's ratio tests are listed in Table 7-25. Values at both test temperatures were approximately 1/3, similar to what is found for most unreinforced metals.

7.2 SHEAR TESTING

Two methods of shear testing were utilized for both the resin matrix and the metal matrix systems. For the resin matrix materials, a torsion tube specimen configuration that measures interfiber shear and a short beam configuration that measures interlaminar shear were tested. For B/Al the torsion tube specimen and a slotted rectangular interfiber shear specimen were used. Specimens, test procedures, and results are presented in the following sections for the methods that used the tube and rectangular interfiber shear specimens. The short beam method is discussed in Appendix B, Quality Assurance Test Procedures.

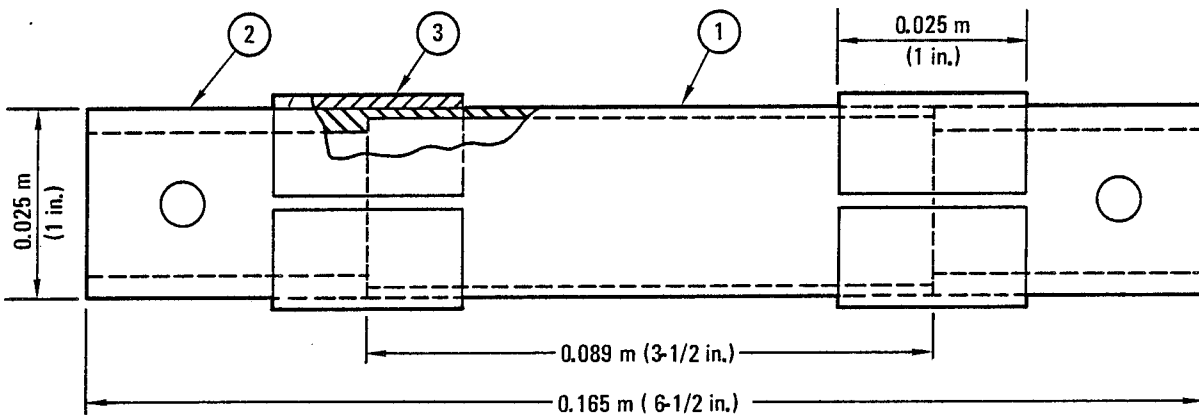
7.2.1 SPECIMEN DESIGN AND TEST PROCEDURE. The B/Al torsion tube specimen was 0.15 m (6 in.) long by 0.024 m (1 in.) outside diameter with a nominal 0.001 m (0.040 in.) wall thickness. The specimens were fabricated from 6 plies of B/Al tape oriented with the boron filaments in the long-axis direction of the tube. Steel end fittings were diffusion bonded to the tube in the manufacturing process. Loading was accomplished by cylindrical male fixtures that were pin-attached to the steel reinforced tube ends with 0.0064 m (0.25 in.) steel bolts. A sketch of the B/Al tube is shown in Figure 7-21.

The G/E torsion tube specimen, also shown in Figure 7-21, was similar to the B/Al tube except for the length and end fittings. These specimens were 0.089 m (3.5 in.) in length and had steel fittings adhesively bonded to the ends after fabrication and cutting to the correct lengths. To obtain a wall thickness of 0.001 m (0.040 in.) (to prevent buckling during test) it was necessary to use an 8 ply tube for the G/E specimens rather than the 6 plies used for the B/Al specimens.



- DETAIL:
- (1) 0.001 m (0.040 in.) THICKNESS (6 PLY) B/AI TUBE
 - (2) 0.0024 m (0.094 in.) THICKNESS STEEL REINFORCEMENT
 - (3) 0.00071 m (0.028 in.) THICKNESS STEEL REINFORCEMENT

(a)



- DETAIL:
- (1) 0.001 m (0.040 in.) THICKNESS (8 PLY) A-S/3501 G/E TUBE
 - (2) 0.0032 m (1/8 in.) WALL STEEL TUBE
 - (3) 0.0016 m (1/16 in.) WALL SPLIT STEEL COLLAR

(b)

653217-37

Figure 7-21 Torsion Tube Configurations (a) B/AI Specimen and (b) G/E Specimen

To determine the shear modulus, all of the torsion tube specimens were strain gaged prior to test. A half bridge, shear-torque rosette strain gage was bonded to each tube with M-bond 610 adhesive. The gages and adhesive cure cycles that were used are:

a. Gages:

B/Al — FAED-12C-12-S3

G/E — FAED-12C-12-SO

b. Cure Cycles:

Test Temperature	Cure Cycles
297 K (75° F)	2 hours at 394 K (250° F)
394 K (250° F)	2 hours at 394 K (250° F)
450 K (350° F)	1.5 hours at 450 K (350° F)
505 K (450° F)	1 hour at 505 K (450° F)

Application techniques were the same as those described earlier for the Poisson's ratio and tensile modulus specimens.

Testing of the strain gaged tube specimens was conducted in an MTS Closed-Loop Tension-Torsion machine. The specimens were loaded (in torsion) incrementally to failure with strain readings recorded automatically at each load step with a B & F Instruments, Inc. Multi-channel Digital Strain Indicator, 161 Mini-System. The output was both a typewritten recording of torque versus strain and a punched paper tape that could be processed by a computer, programmed to produce a shear stress versus strain plot. In addition, a torque-twist curve was also recorded for each test. Typical torque-twist and stress-strain curves are shown in Figures 7-22 and 7-23. An overall view of the torsion testing machine and the Mini-System strain recorder is presented in Figure 7-24. For elevated temperature tests the specimens were heated in the mid-section with a small ring furnace and held 10 minutes prior to twisting. A closeup view of a B/Al tube installed in the test machine is shown in Figure 7-25 prior to testing at room temperature and in Figure 7-26 before testing at elevated temperature. The white material packed around the tube above and below the ring furnace in Figure 7-26 is Fiberfrax insulation batting for maintaining good temperature uniformity. Temperature was monitored with a chromel-alumel thermocouple attached to the center of the tube and controlled manually to ± 3 K ($\pm 5^\circ$ F) during the short time period required for the test.

Shear strengths were calculated from the torsion test data and tube dimensions by using the following thin walled tube approximation of the torsion formula for circular shafts:

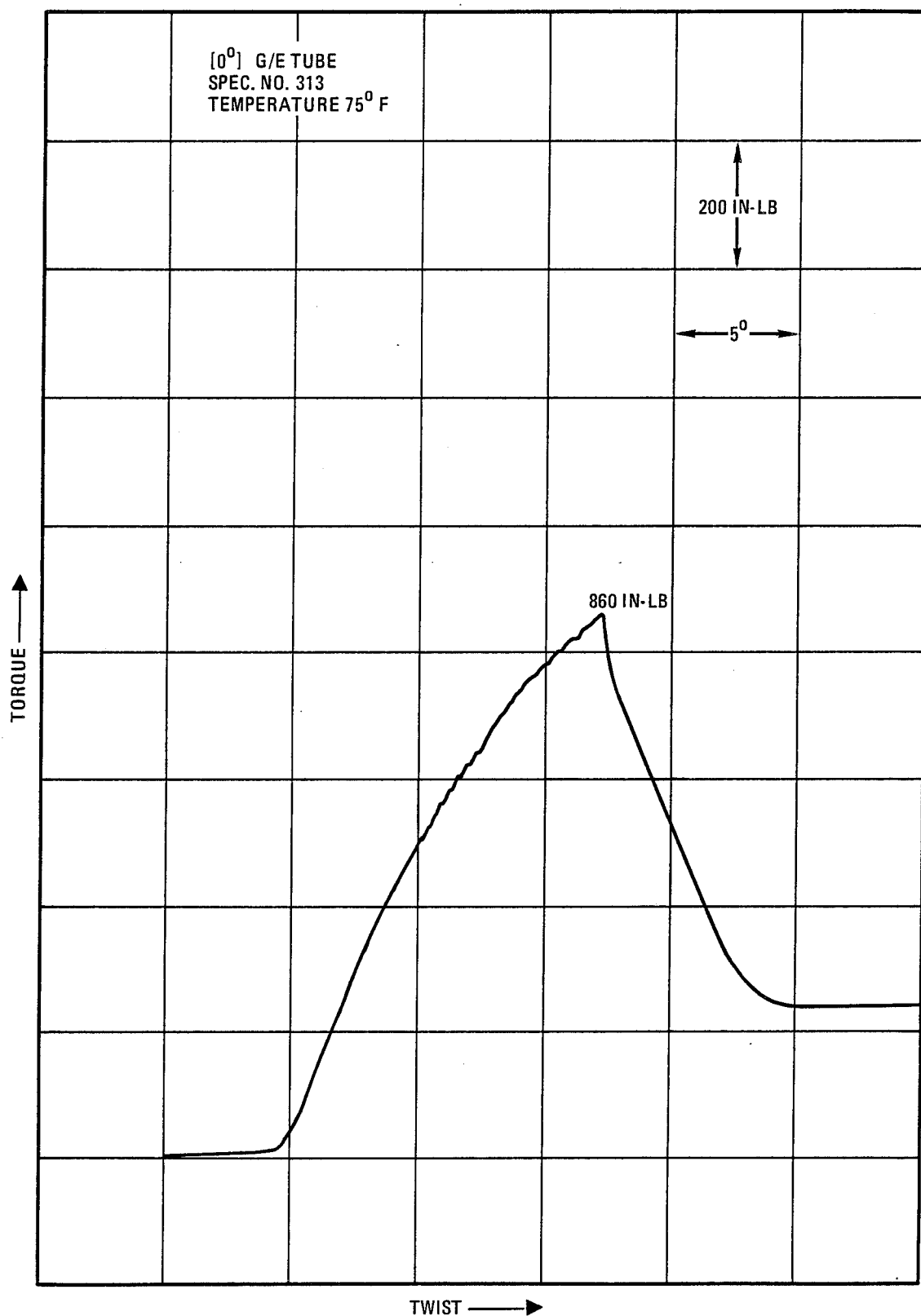
$$\tau = \frac{2 T D_o}{\pi t (D_o - t)^3}$$

τ = ultimate shear strength, N/m² (lb/in²)

T = Maximum torque, Nm (in-lb)

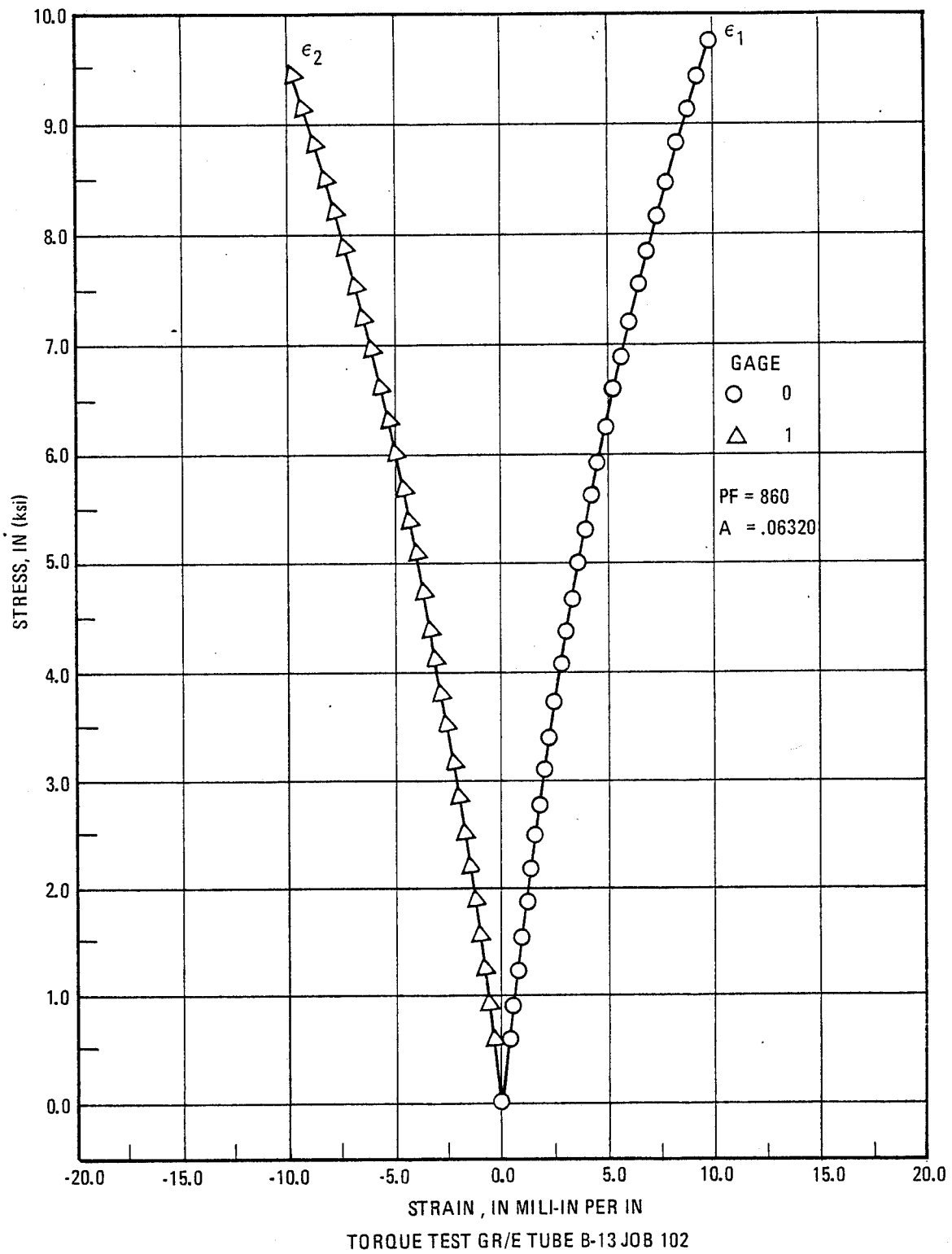
D_o = Outside diameter of tube, m (in.)

t = Wall thickness of tube, m (in.)



653217-38

Figure 7-22 Typical Torque-Twist Curve for Torsion Test of Unidirectional G/E Tube Specimen BU06-13



653217-39

Figure 7-23 Typical Stress-Strain Curve for Torsion Test of Unidirectional G/E Tube, Specimen BU06-13

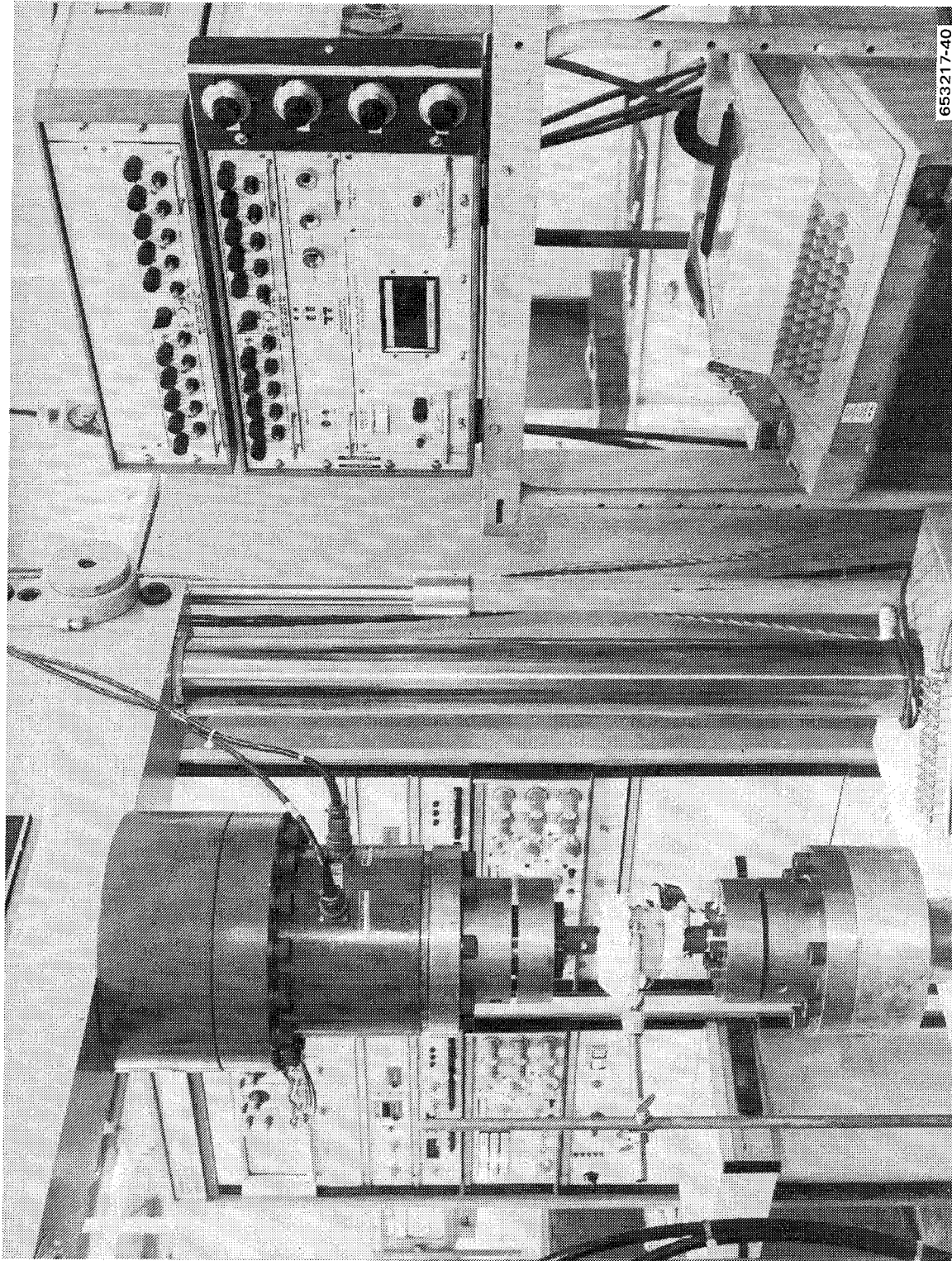


Figure 7-24 Test Apparatus for Torsion Testing of Unidirectional Tubes

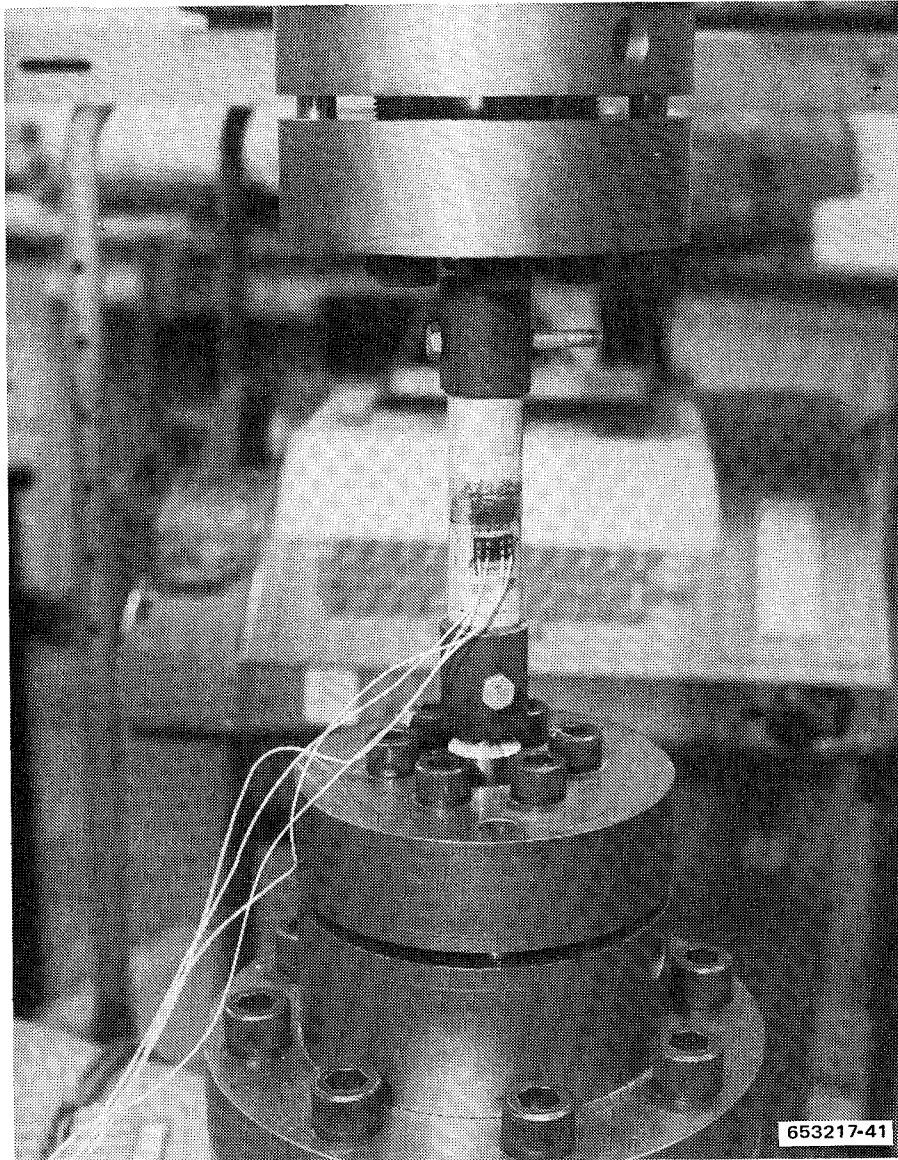


Figure 7-25 Strain Gaged B/Al Tube Specimen Installed in Torsion Test Machine

The shear modulus, G , was determined from the stress-strain curves as follows:

$$G = \frac{\tau}{\gamma} = \frac{\tau}{\epsilon_1 - \epsilon_2}$$

where γ (equal to $\epsilon_1 - \epsilon_2$) is the angle of twist and ϵ_1 and ϵ_2 are strain readings taken at a value of shear stress, τ , in the linear portions of the stress-strain curves (see Figure 7-23).

The second type of shear specimen, which was used only for the B/Al system, is shown in Figure 7-27. The slots were cut in the specimens by the EDM method. All specimens were prepared from six-ply unidirectional material with the boron filaments oriented in the long direction of the specimen. No end doublers were required because of the low failure loads. These low

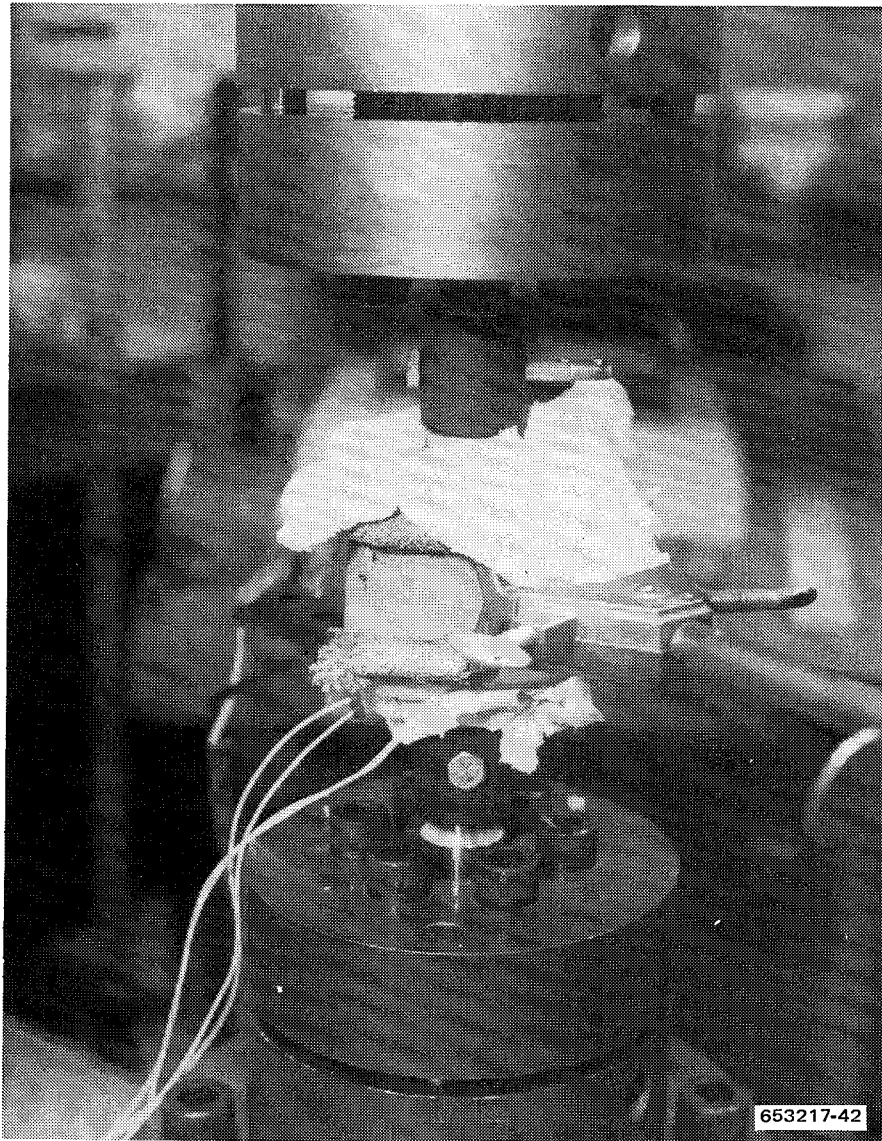
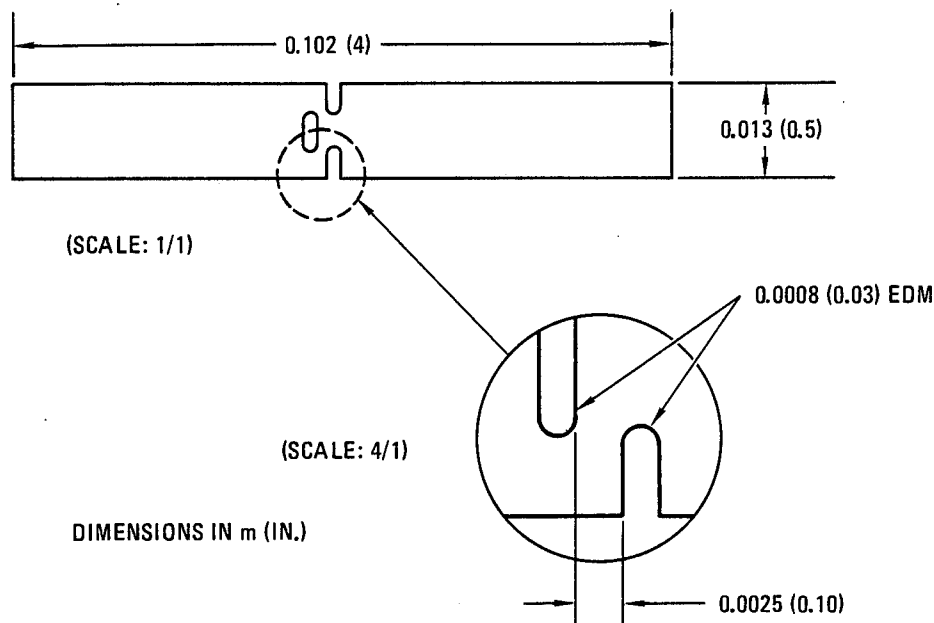


Figure 7-26 Test Setup for Elevated Temperatures Torsion Testing of B/Al Tube

loads ensured failure in the test sections rather than the grips. The specimens were tested in Instron or Tinius-Olsen testing machines using Instron capstan grips with ball or universal joints to ensure axial loading. A head rate of 0.0025 m (0.01 in.) per minute was used. No strain measurements were made during testing of these B/Al interfiber shear specimens. Tests at 218 K (-67° F) and 561 K (550° F) were conducted in a Conrad-Missimer Chamber. The 700 K (800° F) tests were performed with a small ring furnace. As in the tensile tests, temperature was measured with a thermocouple clipped to the surface of the specimen. Temperature was maintained at the desired level for 10 minutes prior to loading.

7.2.2 TEST RESULTS AND DISCUSSION

7.2.2.1 Graphite/Epoxy System. The initial plan for the G/E system was to test six tubes each at room temperature and 450 K (350° F). This was later changed such that at elevated temperature three were tested at 394 K (250° F) and three at 450 K (350° F). The revision was made to



653217-43

Figure 7-27 B/Al Interfiber Shear Specimen

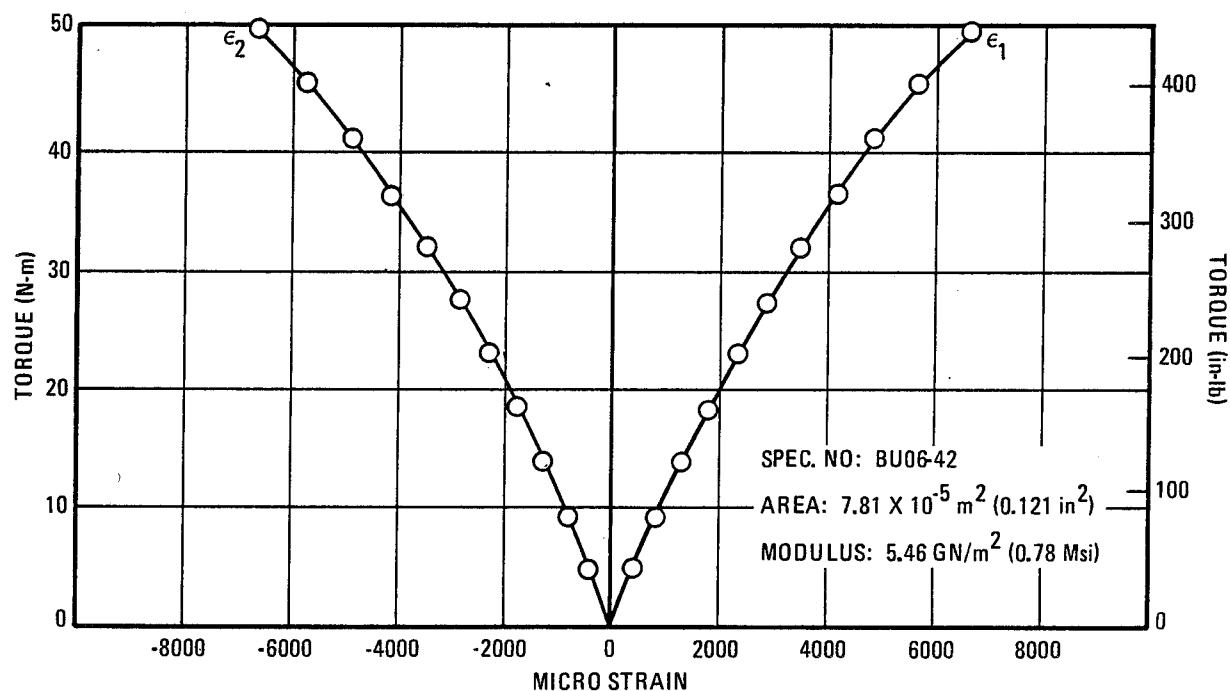
better define the shear strength versus temperature relationship. Shear strength and shear modulus data for G/E are presented in Table 7-28. Shear modulus values were obtained from torque-strain diagrams such as the one shown in Figure 7-28. The effect of temperature was to reduce the strength by approximately 30% at both 394 K (250° F) and 450 K (350° F). While the strength leveled off at 394 K (250° F) and 450 K (350° F), the shear modulus exhibited a continuous decrease out to 450 K (350° F). The percentage change in modulus was, however, significantly less than that for the shear strength. Data from one of the tests (tube no. BU06-37) was not usable because of overheating of the tube. The overheated tube failed at a torque level that was less than one-tenth that of the other tubes tested at 450 K (350° F).

7.2.2.2 Boron/Aluminum System. Data for the two types of shear specimen used in testing of B/Al are listed in Tables 7-29 and 7-30. Strain measurements for determination of shear modulus were made only on the tube tests. A typical torque-strain diagram is shown in Figure 7-29. The initial test plan was to conduct laminate shear tests at the four temperatures shown in Table 7-30 and to conduct the tube tests at 297 K (75° F) and 561 K (550° F). As discussed in the baseline tensile section, 561 K (550° F) was considered to be the maximum use temperature of B/Al for very long time applications. Because of a surface degradation of the B/Al observed during fatigue testing on this program at 561 K (550° F), the maximum use temperature was lowered to 505 K (450° F). At the time of this decision all shear testing was completed except for the elevated temperature tube tests. A change was made to conduct these tests at the lower temperature, 505 K (450° F).

Table 7-28. Baseline Interfiber Shear Properties of G/E Unidirectional Tubes

Specimen Number	Temperature		Shear Strength		Shear Modulus	
	K	(°F)	MN/m ²	(ksi)	GN/m ²	(Msi)
BU06-11	297	75	94	13.7	5.1	0.74
-12			94	13.6	6.1	.88
-13			106	15.4	5.4	.78
-24			89	12.9	5.5	.80
-25			92	13.4	5.5	.80
-26			86	12.5	5.9	.85
			avg 94	13.6	5.6	.81
BU06-38	394	250	52	7.6	4.7	.68
-40			72	10.5	4.8	.70
-42			70	10.1	5.4	.78
			avg 65	9.4	5.0	.72
BU06-37	450	350	(a)	(a)	(a)	(a)
-39			67	9.7	4.4	.64
-41			70	10.2	4.5	.65
			avg 68	9.9	4.4	.64

^aSpecimen overheated



653217-44

Figure 7-28 Shear Load-Strain Diagram for [0°]₈, G/E at 394 K (250° F)

Table 7-29. Baseline Interfiber Shear Properties of B/Al Unidirectional Tubes

Specimen Number	Temperature		Shear Strength		Shear Modulus	
	K	(°F)	MN/m ²	(ksi)	GN/m ²	(Msi)
EU06-1	297	75	61	8.8	5.0	7.3
-2			90	13.0	(a)	(a)
-3			66	9.5	4.3	6.2
-4			61	8.8	4.5	6.5
-5			63	9.1	4.6	6.7
-6			61	8.8	4.2	6.1
			avg 67	9.7	4.5	6.6
EU06-7	505	450	82	11.9	4.1	5.9
-8			64	9.3	3.2	4.6
-9			70	10.1	3.6	5.2
-10			65	9.4	2.8	4.1
-11			77	11.1	5.2	7.5
-12			^b 74	^b 10.8	4.5	6.4
			avg 72	10.4	3.9	5.6

^aStrain gage malfunction

^bTorque still rising — machine at maximum twist

The shear strength of B/Al as determined from the tube tests, Table 7-29, was not lowered by increasing the temperature from room temperature to 505 K (450° F). There was a decrease in shear modulus, however, of approximately 15%. For the laminate specimen tests, Table 7-30, a decrease in shear strength of 30 to 40% was observed at elevated temperatures. At room temperature higher shear strengths were obtained with the laminate specimen configuration than with the tubular configuration although, presumably, the two measure the same property. The two groups of specimens were from different batches of material, which could account for some of the difference. Another possible reason for the lower values obtained from the tube tests was the presence of some small longitudinal cracks on the outside surface of half of the tubes. These cracks, shown in Figure 7-30, were shallow and did not extend beyond the first ply. Whether or not other cracks were present in any of the inner plies of the 6 ply tubes could not be determined. There was no correlation between the individual values of shear strength and the presence or absence of the surface cracks, however. While the longitudinal cracks in the tubes may well have been responsible for low values of ultimate shear strength, it is not believed that the cracks had much effect during the early portions of the tests where the shear modulus was determined. In the past, agreement of shear strength values determined by different test methods has generally been poor for composite systems.

One of the tube specimens, EU06-12, did not fail before the test machine had reached its limit of twist, 100°. At this point the torque was still increasing slightly. Consequently, the value of ultimate shear strength reported in Table 7-29 is slightly low. The unfailed, but twisted, specimen is shown in Figure 7-31 with a similar specimen that has failed in shear in the longitudinal direction of the tube.

Table 7-30. Baseline Interfiber Shear Strength of $[0^\circ]_6$ B/Al Laminates

Specimen Number	Temperature		Shear Strength	
	K	(°F)	MN/m ²	(ksi)
EU06-13	218	-67	90	13.1
-14			100	14.5
-15			91	13.2
-16			100	14.5
-17			93	13.5
			avg 95	13.8
EU06-18	297	75	97	14.0
-19			100	14.5
-20			94	13.6
-21			94	13.7
-22			81	11.8
			avg 93	13.5
EU06-23	561	550	61	8.9
-24			52	7.5
-25			54	7.8
-26			62	9.0
-27			50	7.2
			avg 56	8.1
EU06-28	700	800	66	9.5
-29			64	9.5
-30			66	9.6
-31			63	9.1
-32			(a)	(a)
			65	9.4

^aSpecimen improperly machined

Data from one of the laminate specimens, EU06-32, was not reported because of improper machining. The slot on one side of the specimen was not sufficiently deep and several continuous boron filaments remained across the test section. With this configuration a shear failure was not possible thus invalidating the test.

One interesting point in comparing the B/Al data with that for the resin matrix materials is the striking difference in values of shear modulus. Values for the metal matrix material are almost an order of magnitude higher than those obtained for the resin matrix systems. Shear strength values (at room temperature), on the other hand, differ by no more than 30%. Similar results are obtained when comparing transverse tensile data (modulus and strength) of metal and resin matrix systems.

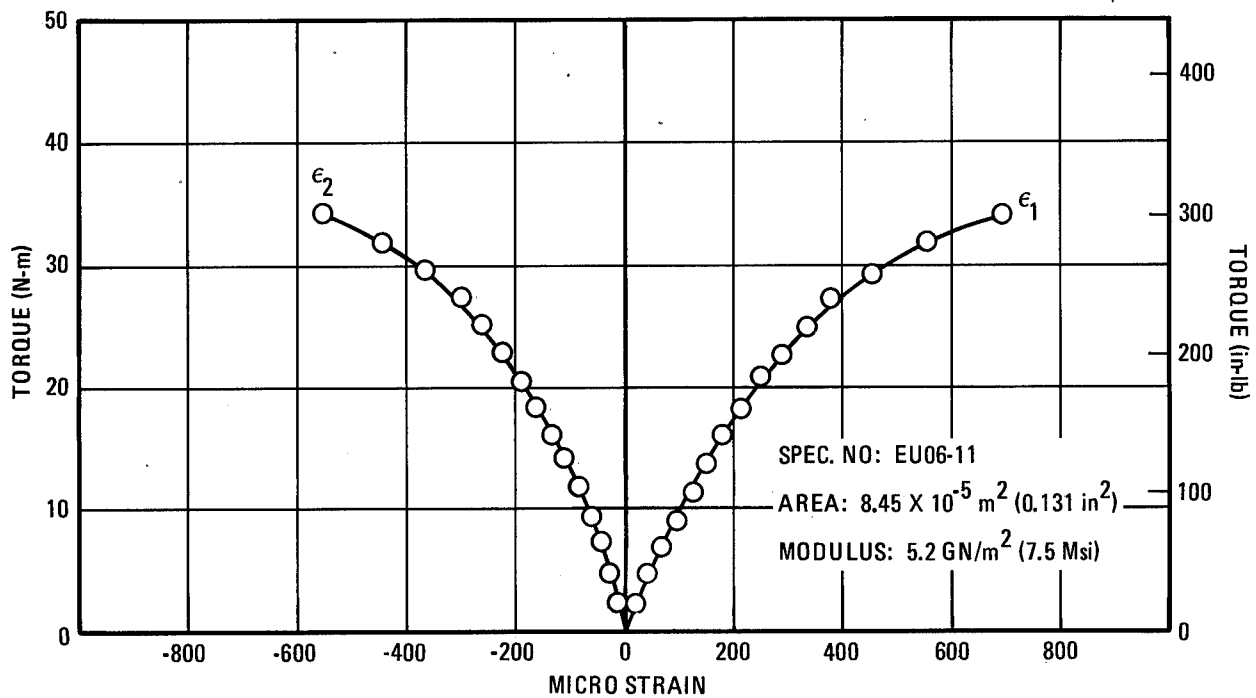


Figure 7-29 Shear Load-Strain Diagram for $[0^\circ]_6$, B/Al at 505 K (450° F)

653217-45

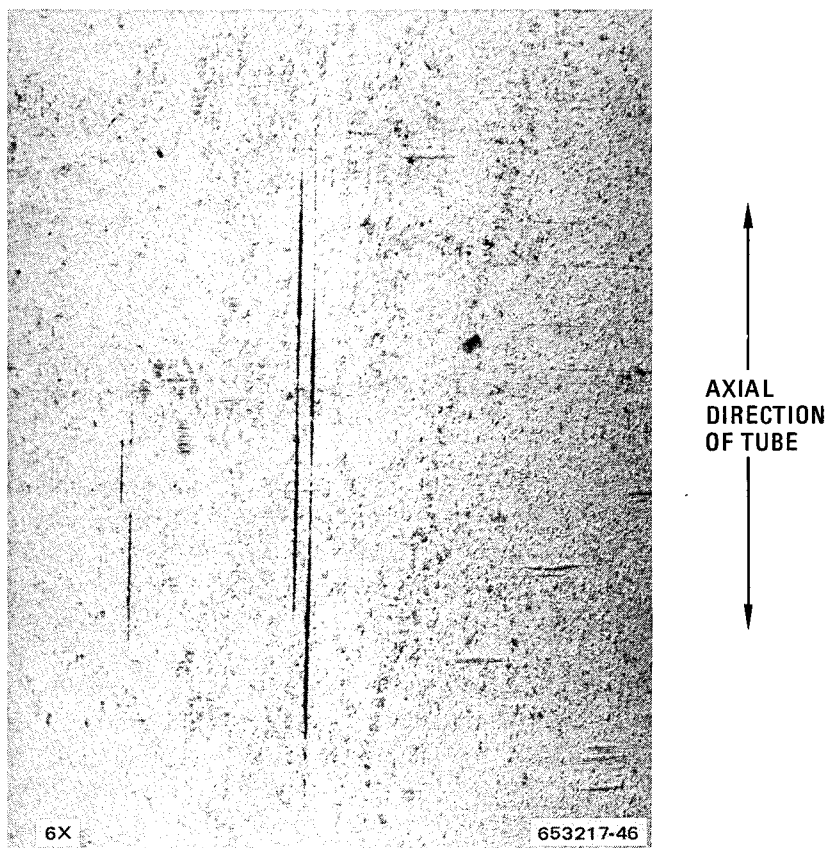


Figure 7-30 B/Al Tube Specimen, EU06-12, Showing Longitudinal Surface Cracks

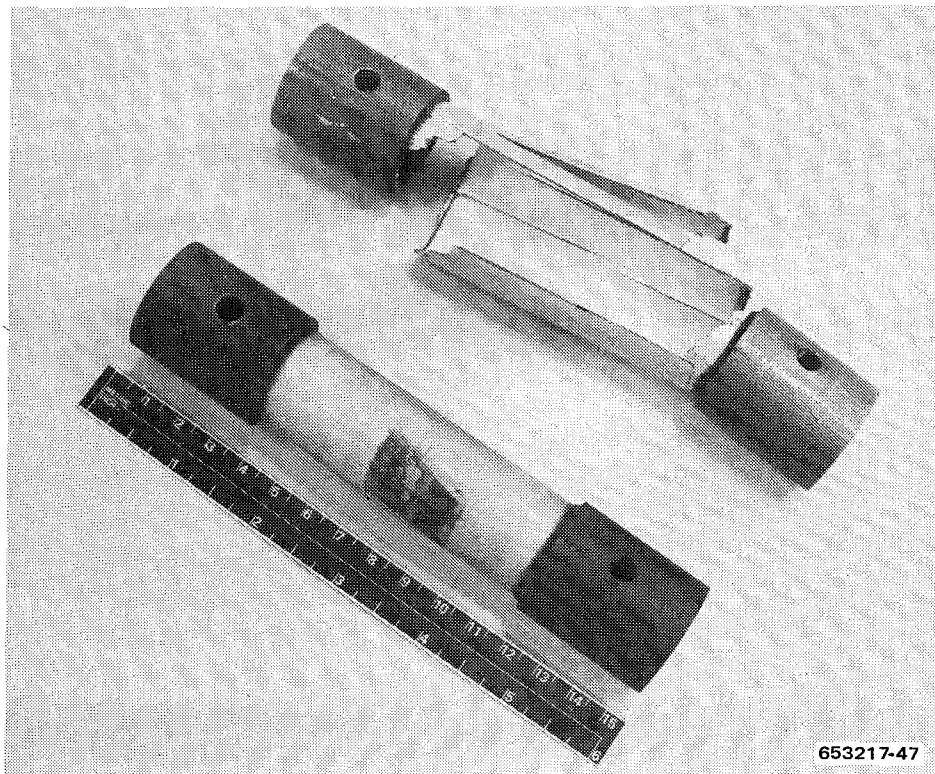


Figure 7-31 B/Al Tube Specimens After Shear Testing: Upper, Specimen EU06-1, Twisted to Failure in Shear; Lower, Specimen EU06-12, Twisted to Maximum Capability of Test Machine

7.2.2.3 Graphite/Polyimide System. Because sufficient HT-S/710 prepreg was unavailable, it was not possible to fabricate the tube specimens necessary to conduct the G/PI shear tests. However, some shear data, for the same HT-S/710 system, had been obtained in a study performed at General Dynamics Convair during 1973. These dates are listed in Table 7-31 (unpublished data from W.G. Scheck). The G/PI tubular specimens were processed using the same fabrication techniques described in Section 5 for G/E and B/PI tubes and the autoclave cure cycle given in Section 5 for the HT-S/710 G/PI laminates. The tubes were 0.15 m (6 in.) long by 0.025 m (1 in.) outside diameter with a nominal wall thickness of 0.001 m (0.040 in.). Test techniques were similar to those described above for the B/Al and G/E tubes (Section 7.2.1).

The data of Table 7-31 show a decrease in shear strength of G/PI of approximately 30% of the room temperature value for specimens tested at both 77 K (-320°F) and 589 K (600°F). The modulus, on the other hand, decreases slightly as the test temperature is raised from 77 K (-320°F) to 589 K (600°F).

7.3 FRACTURE TESTING

The effects of stress risers (cutouts, cracks, damage zones, material discontinuities, etc.) in composite materials has been the subject of a number of recent investigations. Methods are

Table 7-31. Interfiber Shear Properties of G/PI Unidirectional Tubes

Specimen Number	Temperature		Shear Strength		Shear Modulus	
	K	(°F)	MN/m ²	(ksi)	GN/m ²	(Msi)
TU-1	77	-320	52	7.6	6.8	0.98
A-3			44	6.4	7.2	1.04
A-4			50	7.3	7.2	1.05
avg			49	7.1	7.1	1.02
TU-4	297	75	87	12.6	5.8	.84
TU-5			68	9.9	6.6	.96
TU-6			57	8.2	6.1	.89
avg			71	10.2	6.2	.90
TU-7	589	600	49	7.1	7.2	1.04
A-5			49	7.1	4.8	.69
avg			49	7.1	6.0	.86

being sought to predict both the static and fatigue behavior of composite materials which contain such stress risers. Waddoups, Eisenman, and Kaminski (ref. 24) have developed a fracture mechanics based model, the Wearout Model, which has been moderately successful in predicting the degradation of coupon strength as a function of loading. Whereas in metals, crack growth rate (i.e., da/dn) is normally measured and used as an indication of strength degradation such is not the case for composites. Flaw growth is usually not observed in composites, even though such crack growth has been observed for both B/Al and B/E (ref. 25 and 26).

The objective of this study was to attempt to observe damage accumulation in flawed composite tension coupons and to reduce the data to a da/dn format. Since crack growth is not readily observed in composites, changes in material compliance (load, P, divided by crack opening displacement, COD) were to be related to changes in effective crack length. Given da/dn data for a composite material, conventional fracture mechanics theories can then be applied to predict effective crack length as a function of loading history, and failure characteristics.

7.3.1 SPECIMEN DESIGN. The study included six specimens each of the four different materials to determine fracture behavior. The four materials investigated are described in Table 7-32. For each material, six ($0^\circ \pm 45^\circ$)_s specimens measuring 0.064 m (2.5 in.) by 0.30 m (12 in.) were fabricated and identified by dash numbers as shown in Table 7-33. Specimen configuration is shown in Figure 7-32.

Table 7-32. Composite Materials Studied

Material	Layup	Panel Thickness		Material ID
		m	in.	
B/E	$[0^\circ \pm 45^\circ]_s$	0.00076	0.030	AC05
G/E	$[0^\circ \pm 45^\circ]_s$.00076	.030	BC05
G/PI	$[0^\circ \pm 45^\circ]_s$.00076	.030	DC05
B/Al	$[0^\circ \pm 45^\circ]_s$.00107	.042	EC05

Table 7-33. Specimen Identification

Material	Specimens
B/E	AC05-1, AC05-2, AC05-3, AC05-4, AC05-5, AC05-6
G/E	BC05-1, BC05-2, BC05-3, BC05-4, BC05-5, BC05-6
G/PI	DC05-1, DC05-2, DC05-3, DC05-4, DC05-5, DC05-6
B/Al	EC05-1, EC05-2, EC05-3, EC05-4, EC05-5, EC05-6

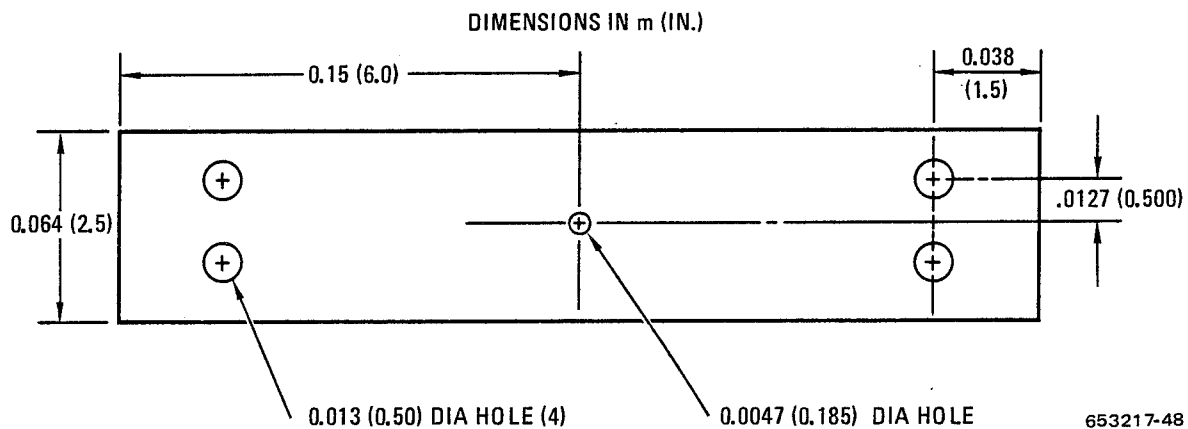


Figure 7-32 Test Specimen Configuration

Initial flaws were applied by drilling a No. 13 hole, 0.0047 m (0.185 in.) diameter, in the center of the specimen and then extending symmetrical narrow slits, 0.00066 m (0.026 in.), from each side of the hole by ultrasonic impact grinding. The end of a flaw made in this manner in B/E is shown in Figure 7-33. Dash three specimens required that the slots be progressively increased during testing without losing the clip gage instrumentation. This was done by hand with a 0.00013 m (0.005 in.) diameter diamond coated wire. All flaw lengths at the beginning of each test sequence are shown in Table 7-34.

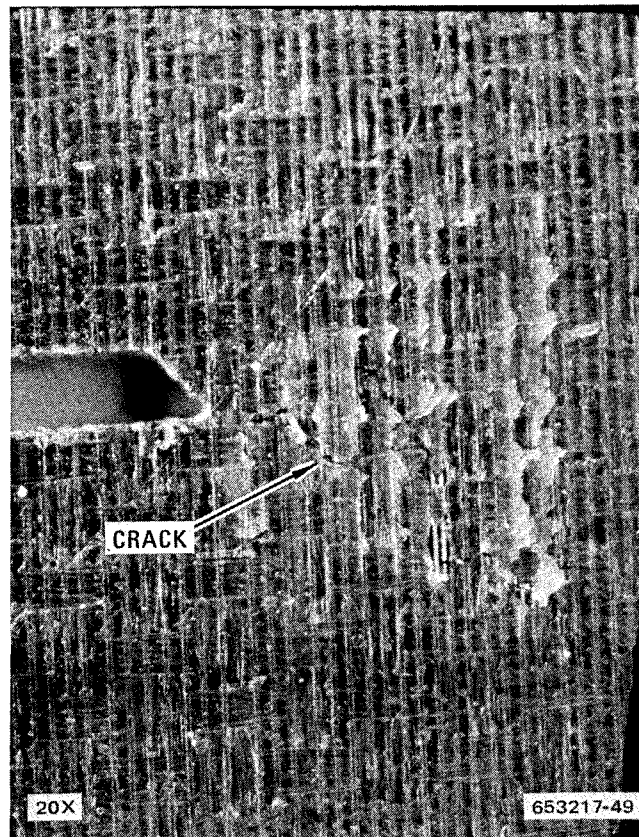


Figure 7-33 End of Slot in Specimen AC05-1 Showing Crack

7.3.2 TEST PROCEDURE, RESULTS AND DISCUSSION. The test plan is summarized in Table 7-35. The procedure for -1 and -2 tests was to try to initiate crack growth, either visual or effective delta length, by progressively increasing static loads and then applying cyclic fatigue loads to extend the effective crack length. Clip gages were used to monitor COD, and any change in compliance, P/COD, was considered to represent an increase in effective crack length. These specimens would then be static pulled to determine their residual strengths.

Table 7-36 shows results of compliance testing of -1 and -2 specimens. The expected systematic damage growth and corresponding change in slope of the compliance curve did not occur. Only isolated damage growth was observed, and this was mostly in the form of cracks parallel to surface fibers. More recent experiments suggest that synergistic effects of moisture and cyclic rate play a large role in damage growth in composites. The failed specimens are shown in Figures 7-34 and 7-35.

The purpose of the -3 specimens was to determine load versus COD for progressively increased crack lengths. Clip gages were used to measure COD and flaws (slits) were lengthened in small increments by hand sawing with a diamond coated wire. For each flaw length the specimen was slowly cycled, three times, up to a maximum load of 1000 pounds. Test results for the four

Table 7-34. Initial Flaw Configuration and Length

SPECIMEN IDENTIFICATION	INITIAL FLAW CONFIGURATION	INITIAL FLAW LENGTH, 2a, m (in.)									
		SEQ. 1	2	3	4	5	6	7	8	9	10
AC05-1 B D E		0.0222(.875)	0.0222(.875)	0.0222(.875)	0.0239(.94)	0.0239(.94)	0.0236(.93)	0.0222(.875)	0.0381(1.50)		
		.0222(.875)	.0236(.93)	.0236(.93)	.0236(.93)	.0222(.875)	.0222(.875)	.0222(.875)			
		.0222(.875)	.0222(.875)	.0222(.875)	.0222(.875)	.0222(.875)	.0222(.875)				
		.0222(.875)	.0222(.875)	.0222(.875)	.0222(.875)	.0222(.875)	.0222(.875)				
AC05-2 B D E		.0222(.875)	.0222(.875)	.0222(.875)	.0222(.875)	.0222(.875)	.0222(.875)	.0222(.875)			
		.0222(.875)	.0249(.98)	.0249(.98)	.0249(.98)	.0249(.98)	.0249(.98)	.0249(.98)			
		.0222(.875)	.0222(.875)	.0222(.875)	.0222(.875)	.0222(.875)	.0222(.875)				
		.0222(.875)	.0222(.875)	.0222(.875)	.0222(.875)	.0222(.875)	.0222(.875)				
AC05-3 B D E		.0047(.185)	.00724(.285)	.00978(.385)	.0123(.485)	.0149(.585)	.0174(.685)	.0225(.885)	.0276(1.085)	.0326(1.285)	.033(1.30)
		.0047(.185)	.00724(.285)	.00978(.385)	.0123(.485)	.0149(.585)	.0174(.685)	.0225(.885)	.0276(1.085)	.0326(1.285)	.033(1.30)
		.0047(.185)	.00724(.285)	.00978(.385)	.0123(.485)	.0149(.585)	.0174(.685)	.0225(.885)	.0276(1.085)	.0326(1.285)	.033(1.30)
		.0047(.185)	.00724(.285)	.00978(.385)	.0123(.485)	.0149(.585)	.0174(.685)	.0225(.885)	.0276(1.085)	.0326(1.285)	.033(1.30)
AC05-4 B D E		.0047(.185)	.0047(.185)	.0047(.185)	.0047(.185)	.0047(.185)	.0047(.185)	.0047(.185)	.0047(.185)	.0047(.185)	
		.0047(.185)	.0047(.185)	.0047(.185)	.0047(.185)	.0047(.185)	.0047(.185)	.0047(.185)	.0047(.185)	.0047(.185)	
		.0047(.185)	.0047(.185)	.0047(.185)	.0047(.185)	.0047(.185)	.0047(.185)	.0047(.185)	.0047(.185)	.0047(.185)	
		.0047(.185)	.0047(.185)	.0047(.185)	.0047(.185)	.0047(.185)	.0047(.185)	.0047(.185)	.0047(.185)	.0047(.185)	
AC05-5 B D E		.0286(1.125)									
		.0286(1.125)									
		.0286(1.125)									
		.0286(1.125)									
AC05-6 B D E		.0349(1.375)									
		.0349(1.375)									
		.0349(1.375)									
		.0349(1.375)									

a: Flaw length — see table.

b: Specimen width — 2b = 0.064m (2.5 in.)

c: Hole diameter — c = 0.0047m (.185 in.)

Table 7-35. Matrix of Tests Performed

Material	Identification	No. of Sizes	Static Strength	Number of Tests/Sequences			Objectives
				Compliance Sequences	Fatigue Sequences	Residual Strength	
B/E	AC05-1	2		3	1	1	$\Delta \frac{P}{(COD)}, R.S.$
	-2	1		4	3	1	$\Delta \frac{P}{(COD)}, R.S.$
	-3	10		9		1	P vs COD
	-4	1			8	1	Fat., R.S.
	-5	1	1				UTS
	-6	1	1				UTS
G/E	BC05-1	2		3	3	1	$\Delta \frac{P}{(COD)}, R.S.$
	-2	2		4	4	1	$\Delta \frac{P}{(COD)}, R.S.$
	-3	10		9		1	P vs COD
	-4	1			8	1	Fat., R.S.
	-5	1	1				UTS
	-6	1	1				UTS
G/PI	DC05-1	2	1	5	3	1	$\Delta \frac{P}{(COD)}, R.S.$
	-2	2		4	1		$\Delta \frac{P}{(COD)}, R.S.$
	-3	10		9		1	P vs COD
	-4	1			8	1	Fat., R.S.
							UTS

Table 7-35. Matrix of Tests Performed — Concluded

Material	Identification	No. of Sizes	Static Strength	Number of Tests/Sequences			Objectives
				Compliance Sequences	Fatigue Sequences	Residual Strength	
B/Al	-5	1	1				UTS
	-6	1	1				UTS
	EC05-1	1		4	1	1	$\Delta \frac{P}{(COD)^P}$ R.S.
	-2	1		5	4	1	$\Delta \frac{P}{(COD)^P}$ R.S.
	-3	10		9		1	P vs COD
	-4	1			8	1	Fat., R.S.
	-5	1	1				UTS
	-6	1	1				UTS

Table 7-36. Results of Compliance Tests

SPECIMEN IDENTIFICATION	LOAD MN (Kip)	FATIGUE R = + 0.1		N = 1	COMPLIANCE, $\Delta \frac{P}{(GOD)}$, MN/m (KIP/in.)									
		CYCLES	P MAX MN (Kip)		2	3	4	5	6	7	8	9	10	
AC05-1 B/E	0.0062(1.4)	0	0	74(420)	74(420)	74(420)	74(420)	74(420)	74(420)	74(420)	75(430)	74(420)	74(420)	
	.0080(1.8)	0	0	72(410)	72(410)	72(410)	72(410)	72(410)	72(410)	72(410)	72(410)	72(410)	72(410)	
	.0098(2.2)	0	0	70(400)	67(380)	(a)								
AC05-2 B/E	.0062(1.4)	56 000	0.0098(2.2)	74(420)	74(420)	74(420)	74(420)	74(420)	74(420)	74(420)	74(420)	74(420)	72(410)	
	.0080(1.8)	0	0	74(420)	74(420)	74(420)	74(420)	74(420)	74(420)	74(420)	74(420)	74(420)	74(420)	
	.0080(1.8)	10 000	.0090(1.8)	70(400)	74(420)	74(420)	(b)							
BC05-1 G/E	.0080(1.8)	100 000	.0080(1.8)	67(380)	67(380)	67(380)								
	.0080(1.8)	2 565 000	.0080(1.8)											
	.0051(1.15)	0	0	44(250)	44(250)	44(250)	44(250)	44(250)	44(250)	44(250)	44(250)	44(250)	44(250)	
BC05-2 G/E	.0051(1.15)	10 000	.0051(1.15)	42(240)	42(240)	42(240)	(c)							
	.0051(1.15)	100 000	.0051(1.15)	40(230)	40(230)	40(230)								
	.0051(1.15)	2 515 000	.0051(1.15)											
DC05-1 G/P	.0042(1.95)	0	0	44(250)	44(250)	44(250)	44(250)	44(250)	44(250)	44(250)	44(250)	44(250)	44(250)	
	.0058(1.25)	0	0	40(226)	40(226)	40(226)								
	.0069(1.55)	10 000	.0062(1.39)	37(210)	34(195)	39(220)								
DC05-2 G/P	.0062(1.39)	105 000	.0062(1.39)	37(210)	37(210)	37(210)								
	.0062(1.39)	2 515 000	.0062(1.39)	(e)										
	.0042(1.95)	0	0	40(230)	42(240)	42(240)	42(240)	42(240)	42(240)	42(240)	42(240)	42(240)	42(240)	
EC05-1 B/A	.0058(1.25)	0	0	40(230)	40(230)	40(230)	40(230)	40(230)	40(230)	40(230)	40(230)	40(230)	40(230)	
	.0069(1.55)	0	0	30(169)	39(225)	42(240)	42(240)	42(240)	42(240)	42(240)	42(240)	42(240)	42(240)	
	.0069(1.55)	10 000	.0024(1.55)	43(248)	44(250)	39(224)	36(206)	36(206)	36(206)	36(206)	36(206)	36(206)	36(206)	
EC05-2 G/P	.0069(1.55)	100 000	.0069(1.55)	40(226)	39(224)	39(224)	36(206)	36(206)	36(206)	36(206)	36(206)	36(206)	36(206)	
	.0069(1.55)	2 611 000	.0069(1.55)	38(216)	38(216)	38(216)	38(216)	38(216)	38(216)	38(216)	38(216)	38(216)	38(216)	
	.0039(1.875)	0	0	38(215)	40(228)	40(230)	40(230)	40(230)	40(230)	40(230)	40(230)	40(230)	40(230)	
EC05-1 B/A	.0058(1.25)	0	0	35(200)	37(211)	37(211)	37(211)	37(211)	37(211)	37(211)	37(211)	37(211)	37(211)	
	.0069(1.55)	0	0	39(220)	46(262)	46(261)	46(260)	46(261)	46(261)	46(261)	46(261)	46(261)	46(261)	
	.0080(1.79)	0	0	NG	NG	NG	NG	NG	NG	NG	NG	NG	NG	
EC05-1 B/A	.0044(1.0)	<1 000	.0080(1.79)	FAILURE	FAILURE	FAILURE	FAILURE	FAILURE	FAILURE	FAILURE	FAILURE	FAILURE	FAILURE	
	.0067(1.5)	0	0	154(880)	175(1000)	175(1000)	228(1300)	228(1300)	175(1000)	180(1030)	184(1050)	184(1050)	184(1050)	
	.0089(2.0)	0	0	147(840)	145(830)	149(850)	151(860)	149(850)	149(850)	149(850)	149(850)	149(850)	149(850)	
EC05-2 B/A	.0089(2.0)	0	0	154(880)	165(940)	165(940)	170(970)	166(950)	166(950)	165(940)	165(940)	165(940)	165(940)	
	.0111(2.5)	0	0	149(850)	154(880)	154(880)	154(880)	156(890)	156(890)	154(880)	152(870)	152(870)	154(880)	
	.0111(2.5)	2 500 000	.0111(2.5)	CRACK INITIATION, ONE BROKEN FIBER, CRACK ON ONE SIDE OF NOTCH, BOTH FACES	CRACK INITIATION, ONE BROKEN FIBER, CRACK ON ONE SIDE OF NOTCH, BOTH FACES	CRACK INITIATION, ONE BROKEN FIBER, CRACK ON ONE SIDE OF NOTCH, BOTH FACES	CRACK INITIATION, ONE BROKEN FIBER, CRACK ON ONE SIDE OF NOTCH, BOTH FACES	CRACK INITIATION, ONE BROKEN FIBER, CRACK ON ONE SIDE OF NOTCH, BOTH FACES	CRACK INITIATION, ONE BROKEN FIBER, CRACK ON ONE SIDE OF NOTCH, BOTH FACES	CRACK INITIATION, ONE BROKEN FIBER, CRACK ON ONE SIDE OF NOTCH, BOTH FACES	CRACK INITIATION, ONE BROKEN FIBER, CRACK ON ONE SIDE OF NOTCH, BOTH FACES	CRACK INITIATION, ONE BROKEN FIBER, CRACK ON ONE SIDE OF NOTCH, BOTH FACES	CRACK INITIATION, ONE BROKEN FIBER, CRACK ON ONE SIDE OF NOTCH, BOTH FACES	
EC05-2 B/A	.0044(1.0)	0	0	203(1160)	191(1090)	191(1090)	187(1070)	191(1090)	187(1070)	187(1070)	191(1090)	187(1070)	187(1070)	
	.0067(1.5)	0	0	165(940)	179(1020)	179(1020)	171(1010)	179(1020)	175(1000)	175(1000)	175(1000)	179(1020)	171(1010)	
	.0089(2.0)	0	0	155(890)	170(970)	166(950)	166(950)	166(950)	166(950)	172(980)	172(980)	172(980)	168(960)	
EC05-2 B/A	.0089(2.0)	10 000	.0089(2.0)	173(990)	173(990)	173(990)	173(990)	173(990)	173(990)	173(990)	173(990)	173(990)	173(990)	
	.0089(2.0)	100 000	.0089(2.0)	172(980)	172(980)	172(980)	172(980)	172(980)	172(980)	172(980)	172(980)	172(980)	172(980)	
	.0089(2.0)	500 000	.0089(2.0)	LONG CRACK AT END OF SLOT	LONG CRACK AT END OF SLOT	LONG CRACK AT END OF SLOT	LONG CRACK AT END OF SLOT	LONG CRACK AT END OF SLOT	LONG CRACK AT END OF SLOT	LONG CRACK AT END OF SLOT	LONG CRACK AT END OF SLOT	LONG CRACK AT END OF SLOT	LONG CRACK AT END OF SLOT	

a Longitudinal cracks at end of slot.

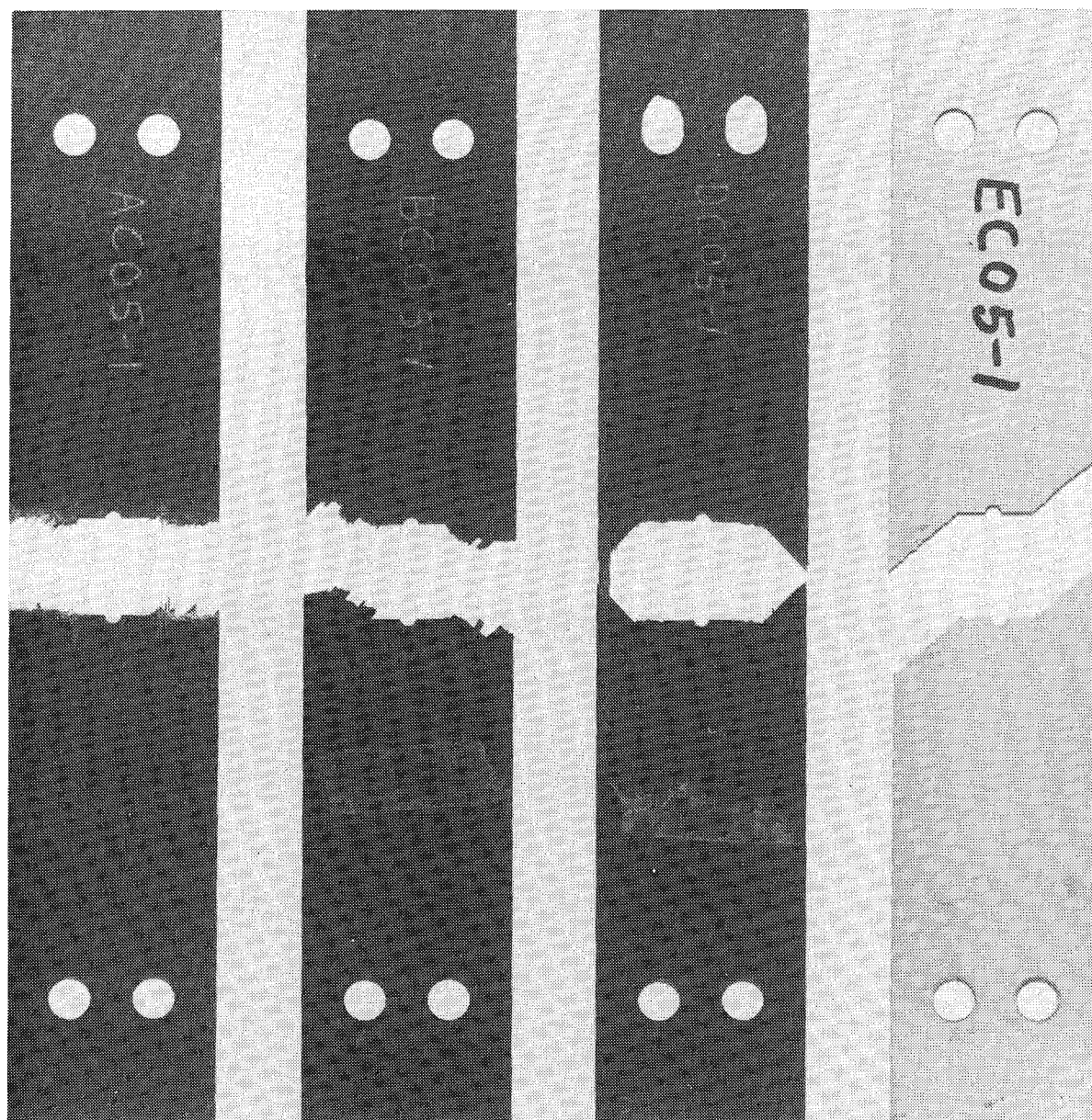
b No cracks.

c Crack at end of slot, CL = 0.000177m (0.0697 in.).

d Cracks at end of slot, CL = 0.000200m (0.0787 in.).

e CL = 0.000198m (0.078 in.) and 0.0000790m (0.0311 in.).

f Crack at end of slot, CL = 0.0000549m (0.0216 in.).



B/E

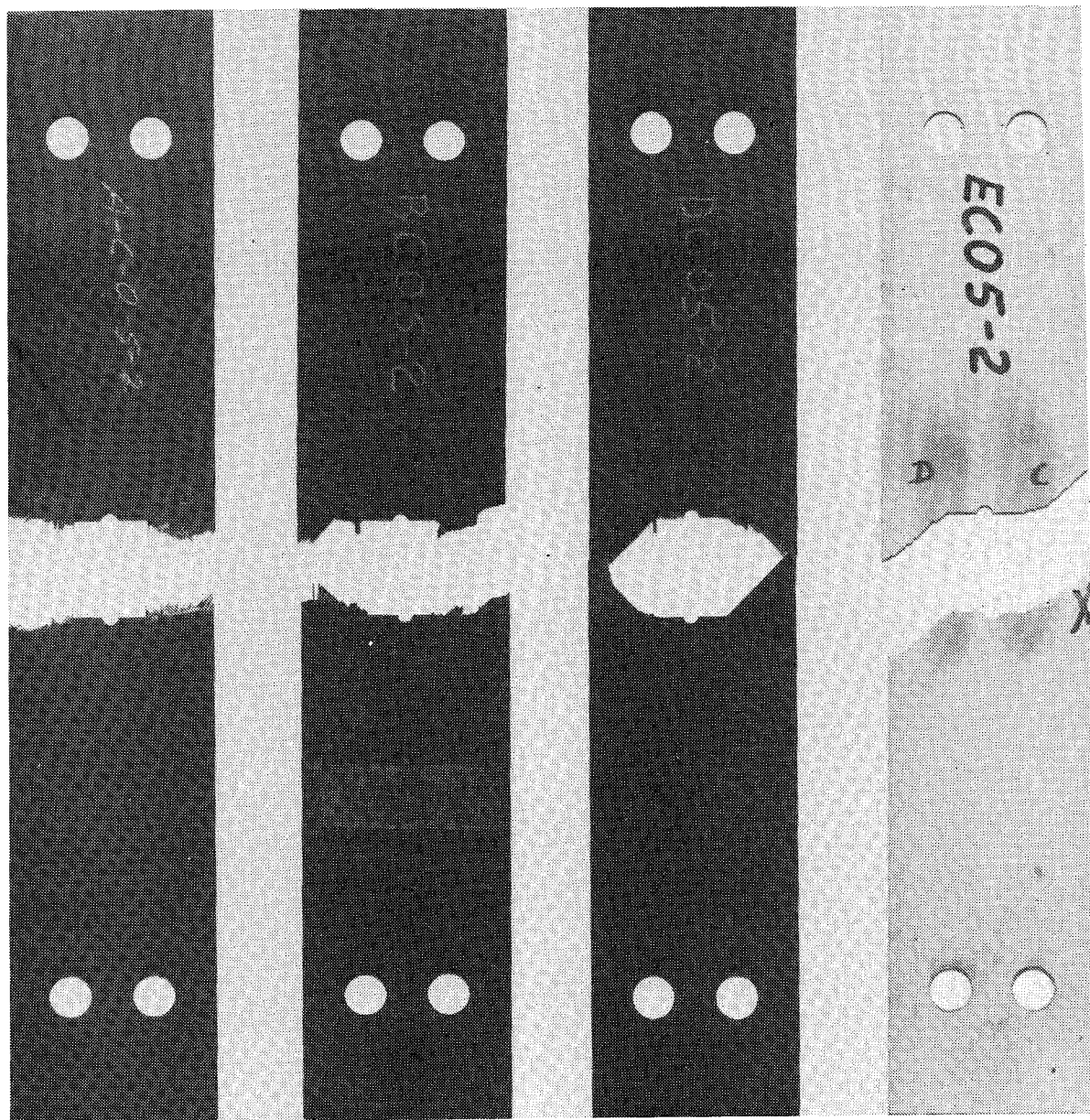
G/E

G/PI

B/AI

653217-52

Figure 7-34 Compliance Specimens (-1's) After Failure in Residual Strength Tests



B/E

G/E

G/PI

B/AI

653217-53

Figure 7-35 Compliance Specimens (-2's) After Failure in Residual Strength Tests

specimens are shown in Figures 7-36, 7-37, 7-38, and 7-39. Load divided by COD versus flaw length was then plotted for each material as shown in Figure 7-40. All four specimens yielded an exponential decaying type of curve with the data points of the G/E and G/PI specimens lying on the same curve. The consistent shape of these curves warrants further investigation of a $\text{Load/COD} = A e^{-\text{flaw size}}$ fatigue model. The failed specimens are shown in Figure 7-41.

The -4 specimens were fatigue tested with the 0.0047 m (0.185 in.) diameter hole only. No slits were applied. COD was measured after cycle numbers 1, 2, 19, 100, 1000, 10,000 and 2,500,000. Specimens were then static pulled to determine residual strengths.

Fatigue test results are shown in Table 7-37. There was no fatigue crack growth observed in any of the four specimens. When these specimens were static pulled for residual strength, only one, AC05-4, failed at the 0.0047 m (0.185 in.) diameter hole. The other three failed in or near the grips. The failed specimens are shown in Figure 7-42.

The objective of -5 and -6 specimen tests was to determine static strengths at two different flaw lengths. The -5's had 0.0286 m (1.125 in.) flaws and the -6's had 0.00349 m (1.375 in.) flaws. All were simply pulled to static failure.

Results of static strength tests are shown in Table 7-38, and the failed specimens are shown in Figures 7-43 and 7-44. Results of all residual strength tests are shown in Table 7-39. The effect of flaw length on gross area static failure stress is plotted in Figure 7-45.

Values for the apparent stress intensity factor, K_Q , were calculated for each notched specimen that was pulled to failure. The following equation from reference 27 was used.

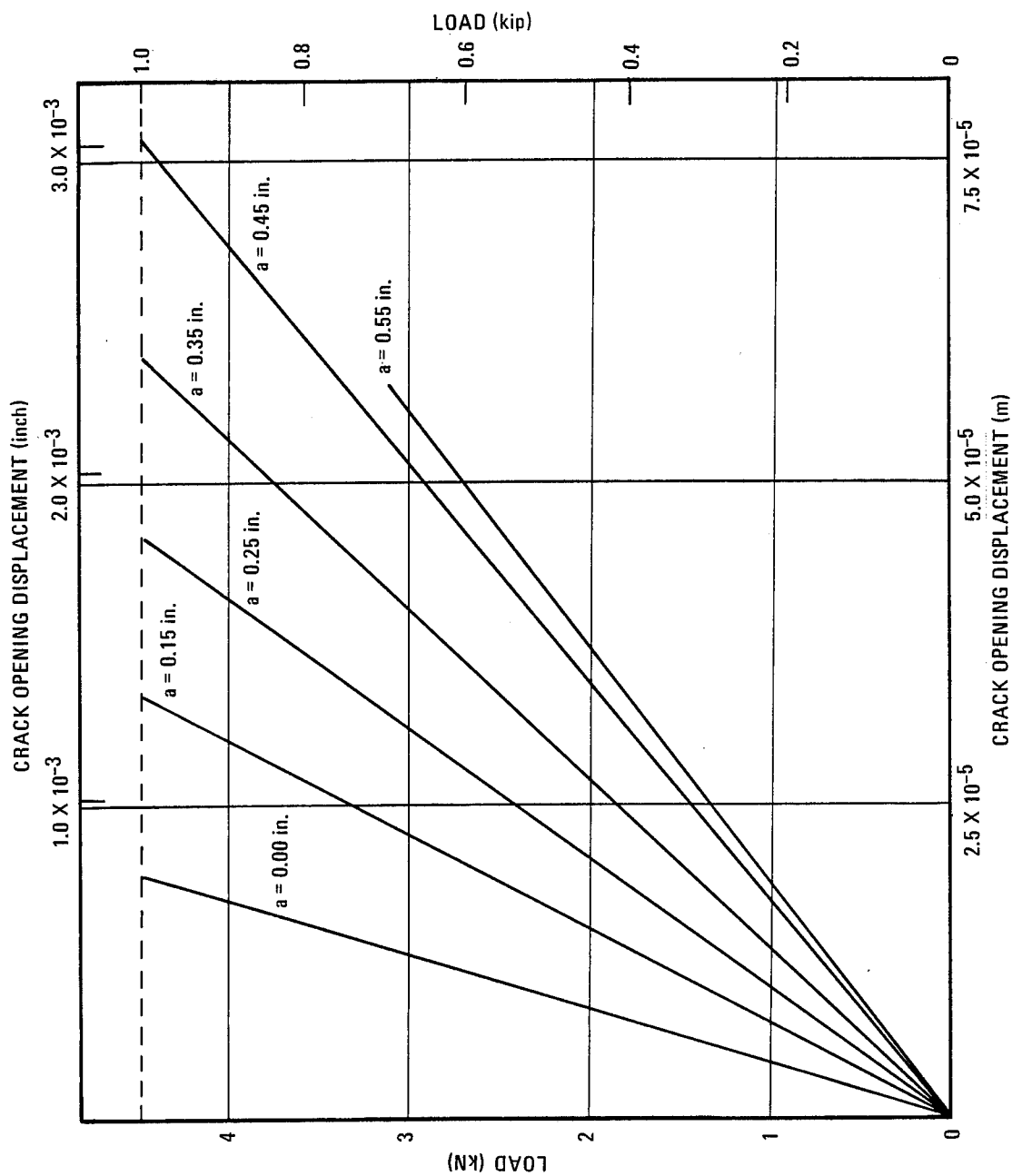
$$K_Q = \sigma \sqrt{\pi a} \left(\frac{2b}{\pi a} \tan \frac{\pi a}{2b} \right)^{1/2}$$

where K_Q = apparent stress intensity factor, $\text{MN/m}^2 \sqrt{\text{m}}$ (ksi $\sqrt{\text{in.}}$)
 σ = gross stress, MN/m^2 (ksi)
 $2a$ = crack length, m (in.)
 $2b$ = specimen width, m (in.)

Figure 7-46 shows the variation of K_Q with crack length for both fatigued and nonfatigued specimens.

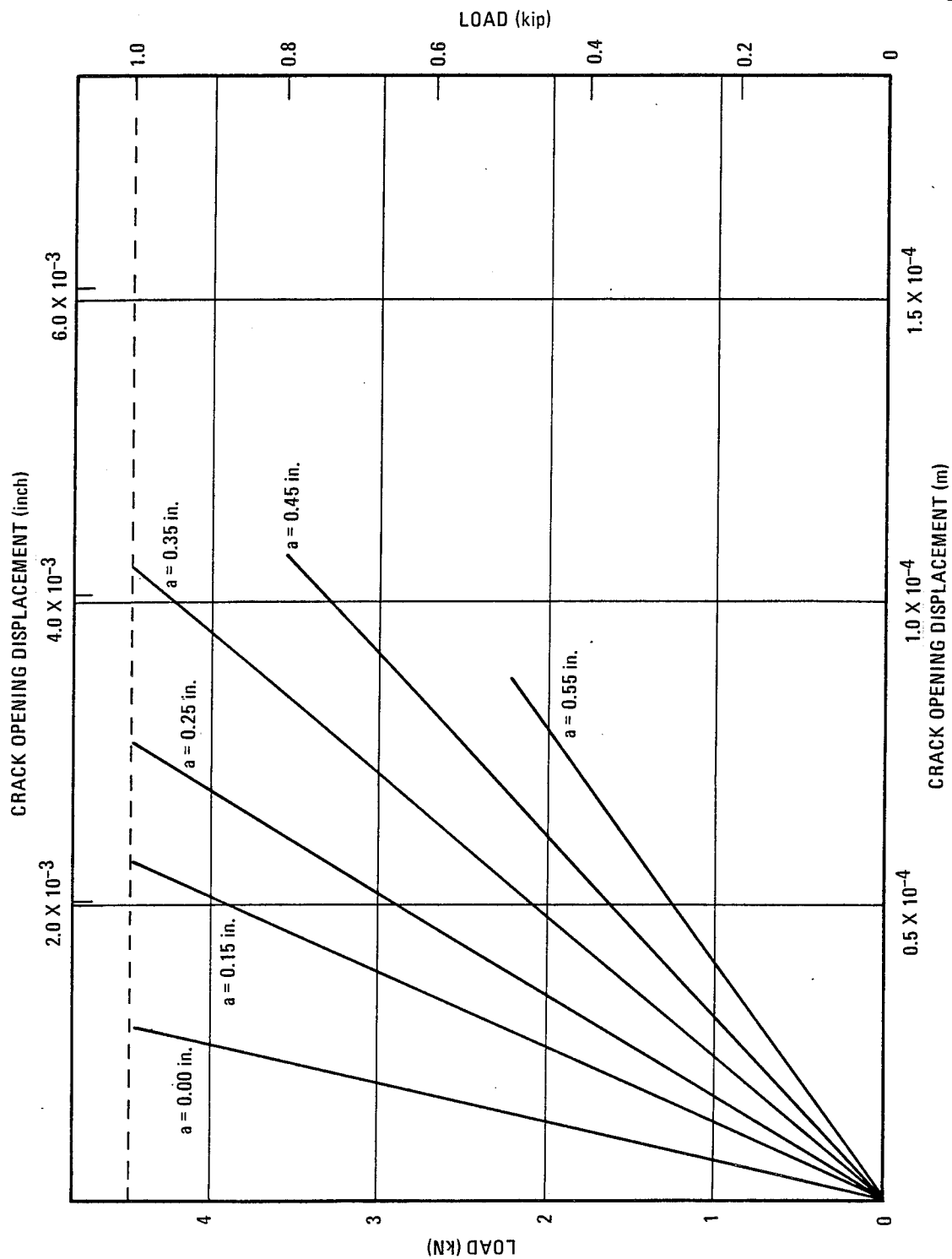
Four composite laminates were studied to determine their flaw growth and fracture behavior. All tests were run at room temperature and moisture was not controlled. All fatigue cycling was at $R = 0.1$ and 30 Hz. Based on the test program and data reduction presented above, the following conclusions are drawn:

1. Under these test conditions, cracks (or effective cracks) in crossplied composite laminates grow only when applied cyclic loads are very near the breaking strength.



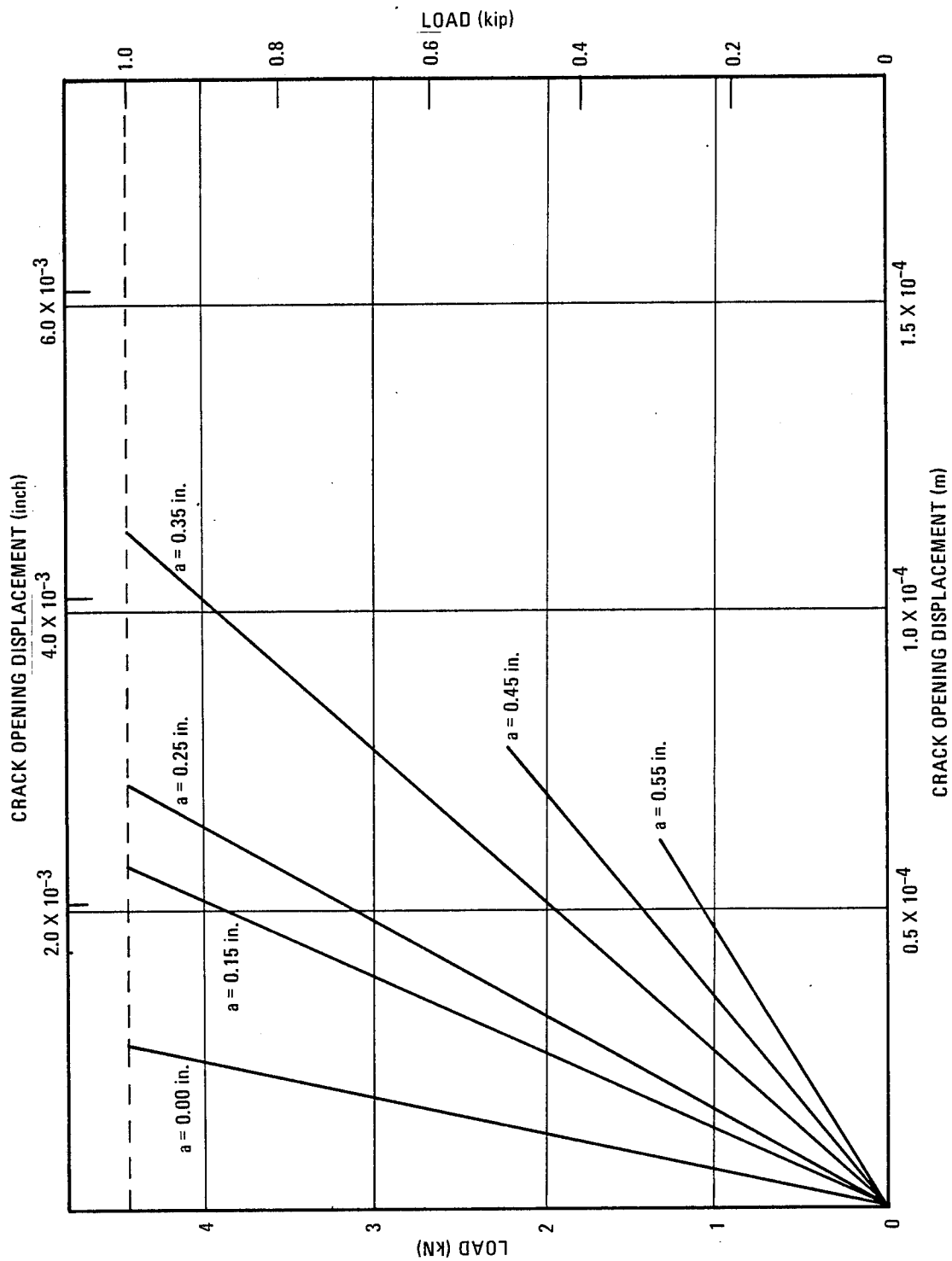
653217-54

Figure 7-36 Load Versus Crack Opening Displacement for Specimen AC05-3



653217-55

Figure 7-37 Load Versus Crack Opening Displacement for Specimen BC05-3



653217-56

Figure 7-38 Load Versus Crack Opening Displacement for Specimen DC05-3

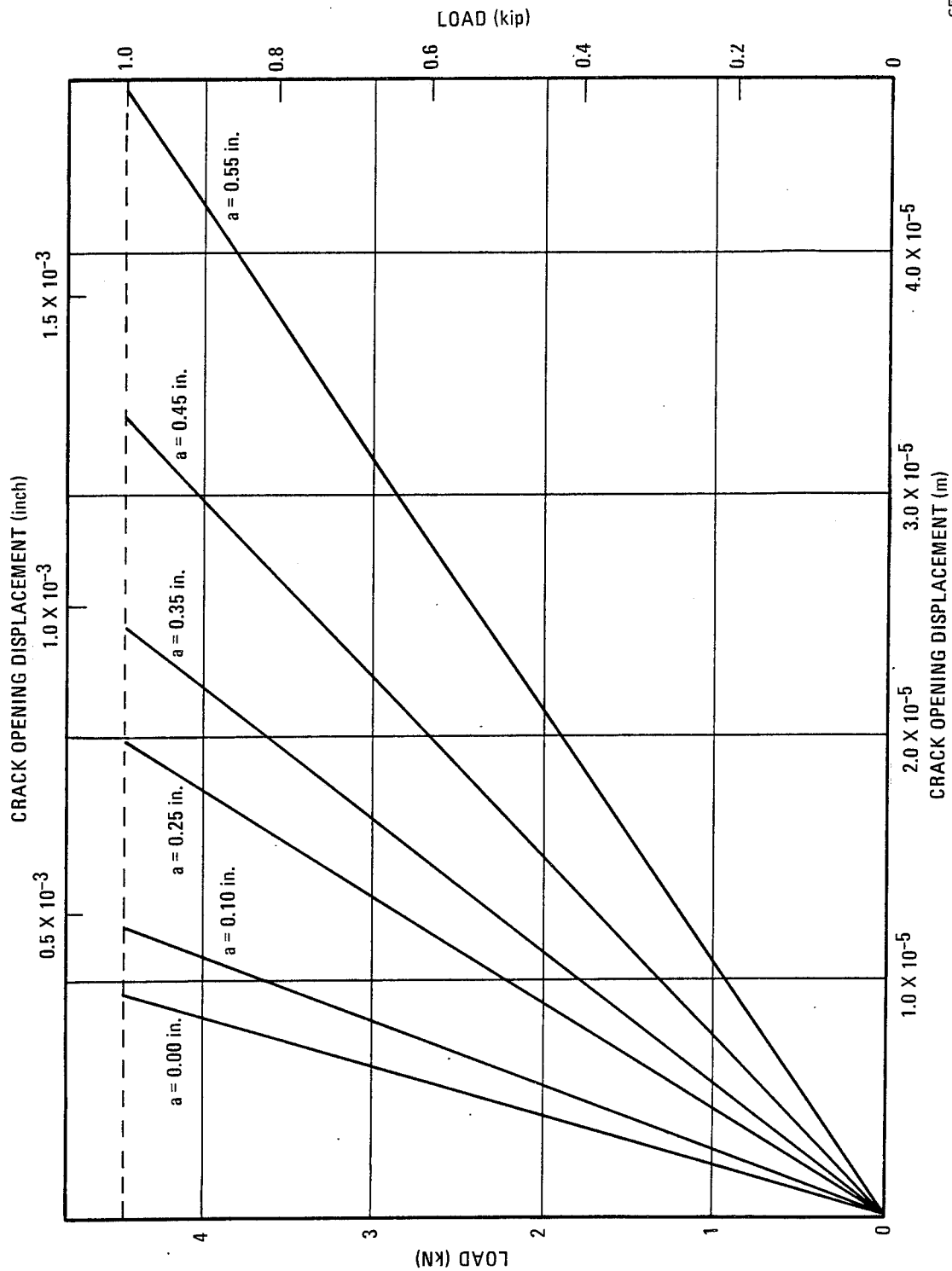
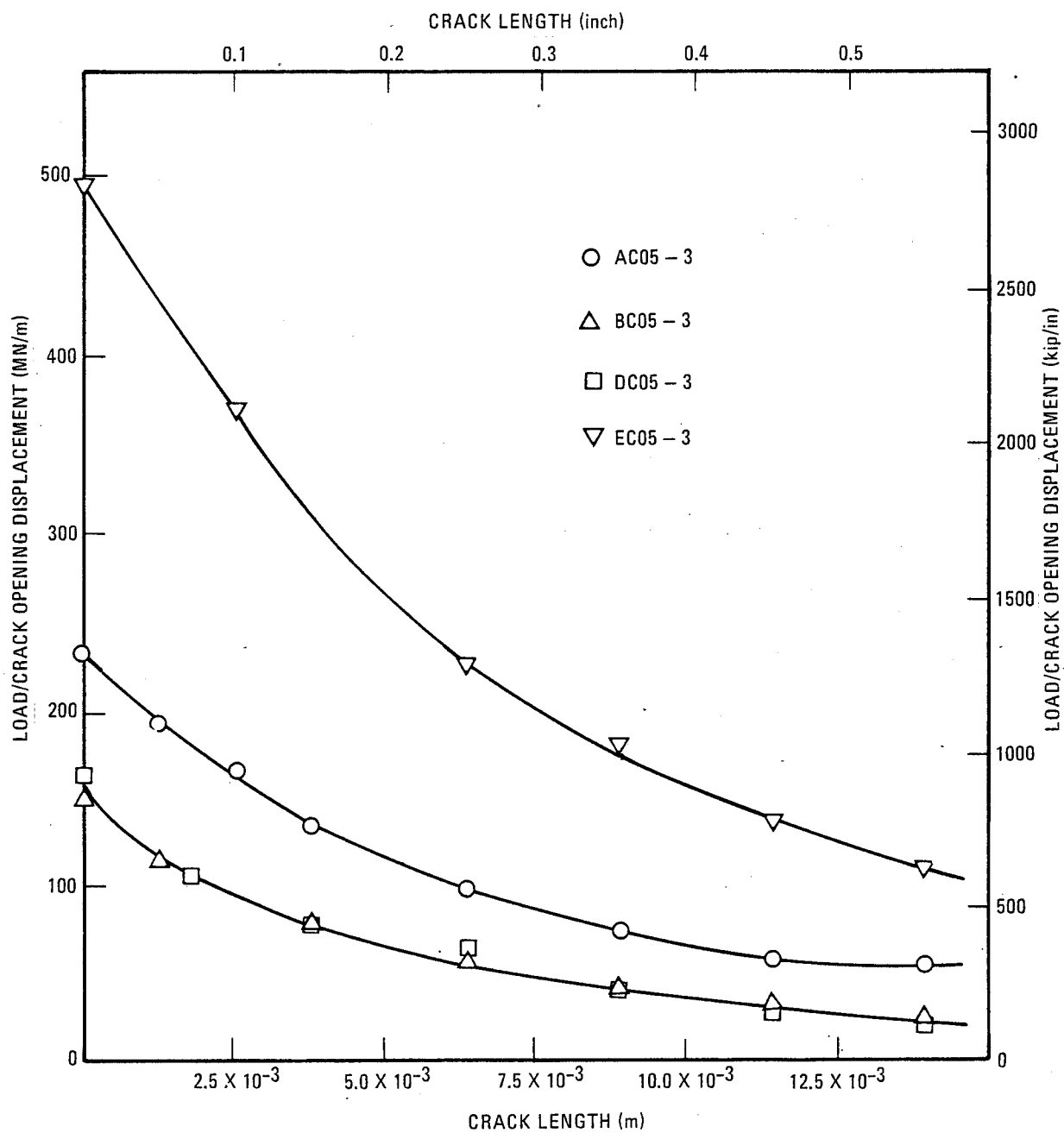


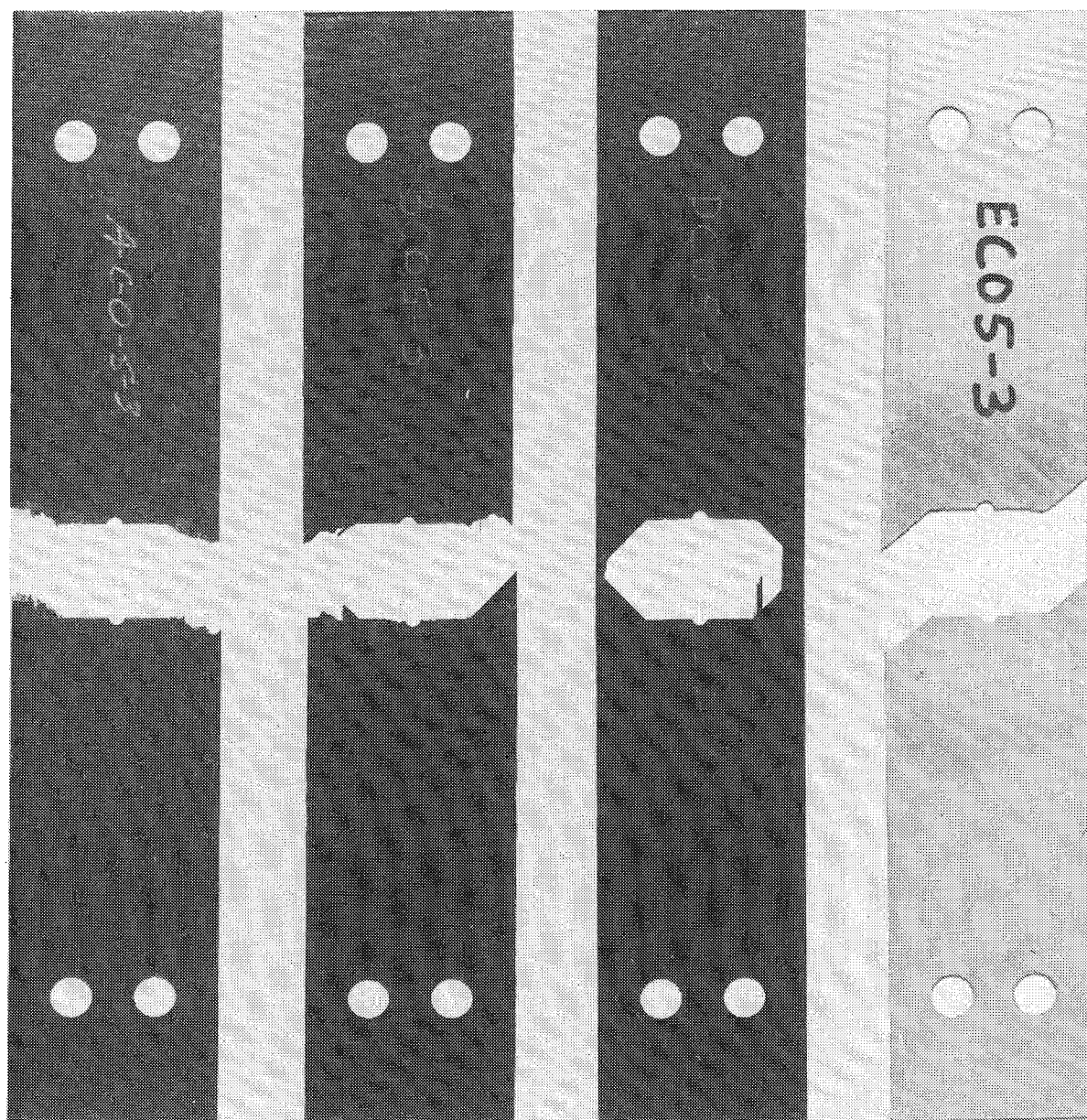
Figure 7-39 Load Versus Crack Opening Displacement for Specimen EC05-3

653217-57



653217-58

Figure 7-40 Load/Crack Opening Displacement Versus Cracks Length



B/E

G/E

G/PI

B/AI

653217-59

Figure 7-41 Compliance Specimens (-3's) After Failure in Residual Strength Tests

Table 7-37. Results of Fatigue Tests^a

MATERIAL	SPECIMEN IDENTIFICATION	SEQUENCE NO. 1			SEQUENCE NO. 2			SEQUENCE NO. 3		
		INITIAL FLAW 2a _i m (in.)	MAX. LOAD, P MN (Kip)	CYCLES N	INITIAL FLAW 2a _i m (in.)	MAX. LOAD, P MN (Kip)	CYCLES N	INITIAL FLAW 2a _i m (in.)	MAX. LOAD, P MN (Kip)	CYCLES N
B/E	AC05-1 -2 -4	0.0239(.94)	0.00979(2.2)	56 000	0.0222(.875)	0.00801(1.8)	100 000			
		.0222(.875)	.00801(1.8)	10 000						
G/E	BC05-1 -2 -4	.00470(1.85)	.0125(2.8)	2 611 121						
		.0236(.93)	.00512(1.15)	10 000	.0236(.93)	.00512(1.15)	100 000			
G/PI	DC05-1 -2 -4	.0249(.98)	.00618(1.39)	10 000	.0249(.98)	.00618(1.39)	100 000			
		.00470(.185)	.0111(2.5)	2 611 121						
B/AI	EC05-1 -2 -4	.0222(.875)	.00689(1.55)	10 000	.0222(.875)	.00689(1.55)	100 000			
		.0292(1.15)	.00796(1.79)	d < 1 000						
		.00470(.185)	.0111(2.5)	2 611 121						
		.0222(.875)	.0111(2.5)	250 000	.0222(.875)	.00890(2.0)	100 000	0.0222(.875)	0.00890(2.0)	f 600 000
		.00470(.185)	.0171(3.84)	2 611 125						

^a R = +.1 for all fatigue tests.

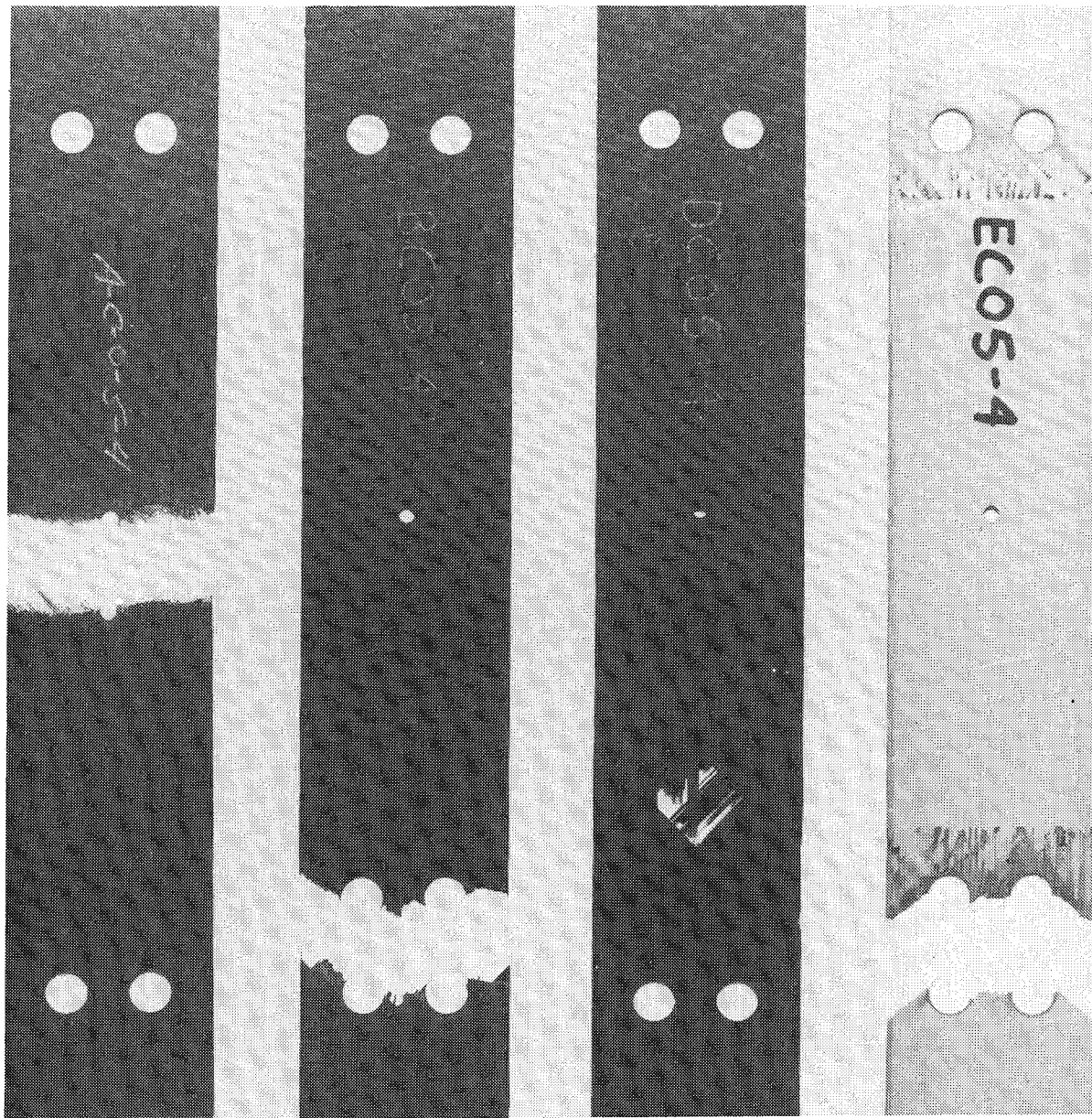
^b Failed in grips.

^c Flaw extended to 2a = 0.0381m (1.50 in) before residual strength test.

^d Failed during this sequence.

^e Failed near grips. Damage was evident around hole.

^f Crack growing parallel to fibers, L = 0.0025m (0.10 in).



B/E

G/E

G/PI

B/AI

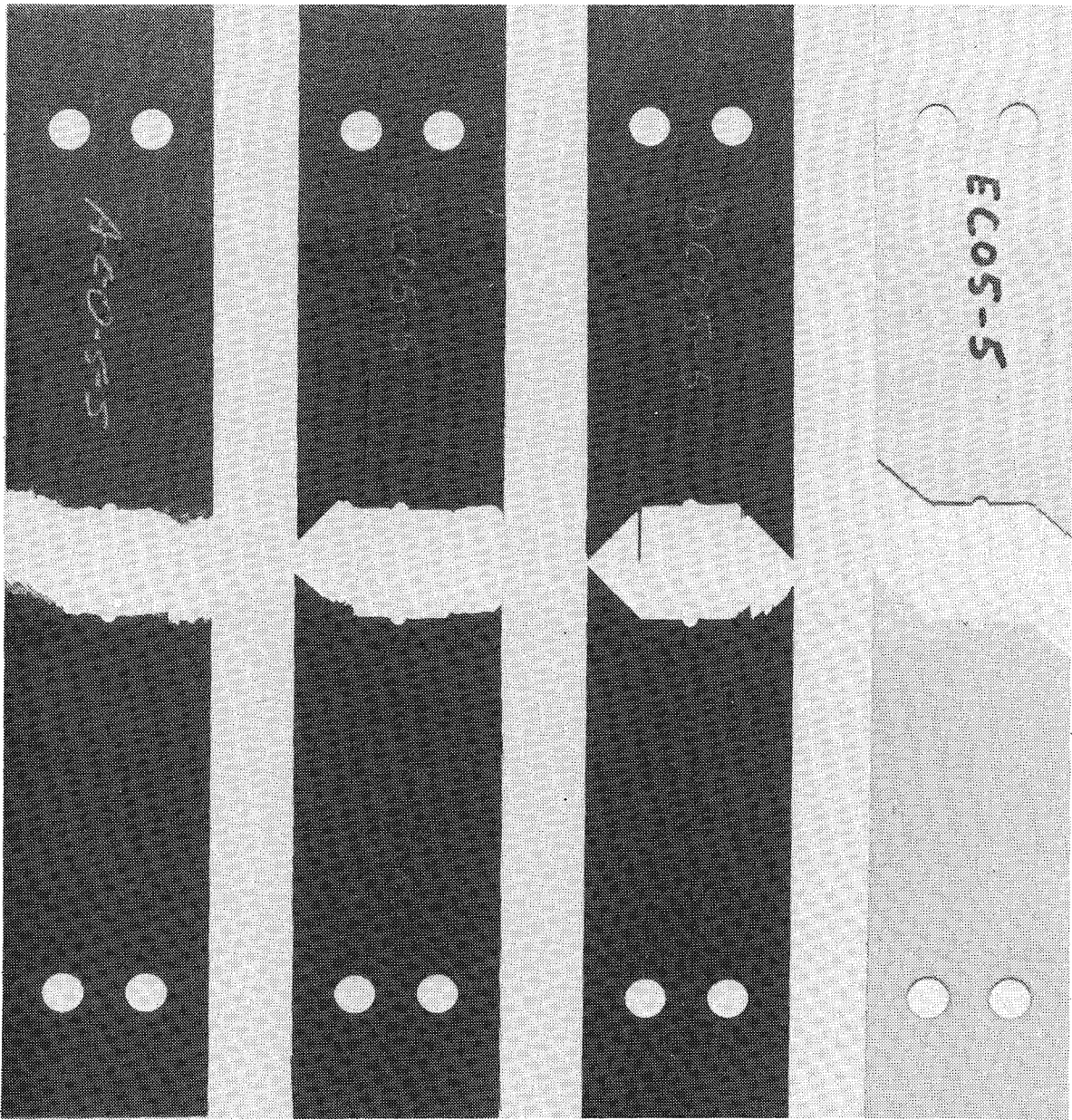
653217-61

Figure 7-42 Fatigue Specimens (-4's) After Failure in Residual Strength Tests

Table 7-38. Results of Static Tests

Material	Specimen Identification	Flaw Length		Failure Load		Gross Area Stress		Net Area Stress		K _Q	
		m	2a (in.)	MN	(kip)	MN/m ²	(ksi)	MN/m ²	(ksi)	MN/m ² √m	(ksi√in.)
B/E	AC05-5-6	0.0286	1.125	0.00910	2.045	188	27.3	342	49.6	43.8	39.9
		.0349	1.375	.00694	1.56	143	20.8	319	46.2	39.0	35.5
G/E	BC05-5-6	0.0286	1.125	0.00656	1.475	136	19.7	247	35.8	31.6	28.8
		.0349	1.375	.00411	.925	84.8	12.3	189	27.4	23.1	21.0
G/PI	aDC05-1-5-6	0.0381	1.500	0.00420	.945	86.9	12.6	217	31.5	25.6	23.3
		.0286	1.125	.00605	1.36	125	18.1	228	33.0	29.0	26.4
		.0349	1.375	.00489	1.10	101	14.7	225	32.6	27.6	25.1
B/Al	EC05-5-6	0.0286	1.125	0.0148	3.325	219	31.7	397	57.6	50.9	46.3
		.0349	1.375	.0117	2.625	172	25.0	383	55.6	46.9	42.7

^a This specimen was fatigue cycled with a smaller flaw, 2a = 0.0222m (0.875 in.).



B/E

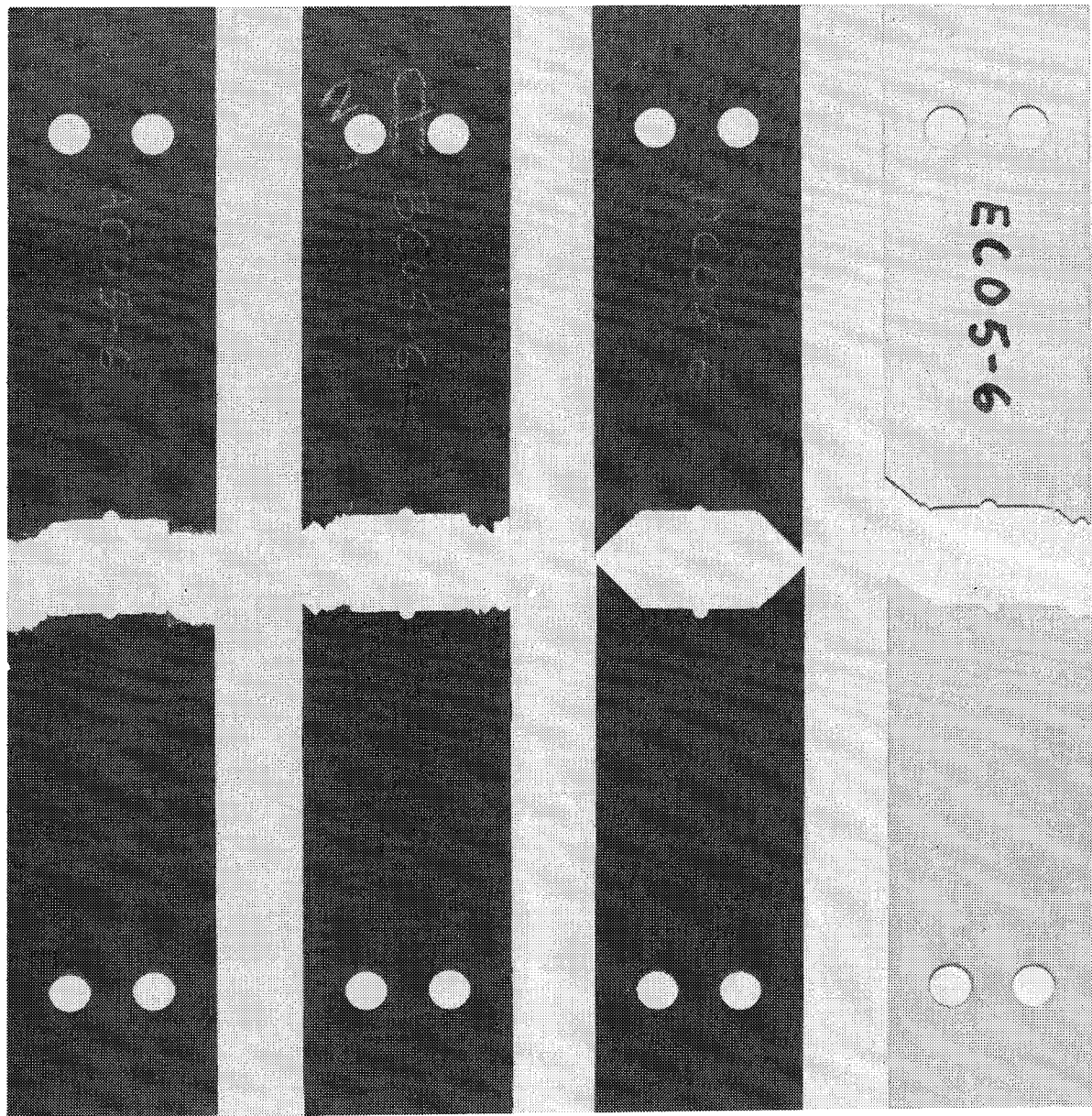
G/E

G/PI

B/AI

653217-62

Figure 7-43 Static Strength Specimens (-5's) After Failure



B/E

G/E

G/PI

B/AI

653217-63

Figure 7-44 Static Strength Specimens (-6's) After Failure

Table 7-39. Results of Residual Strength Tests

MATERIAL	SPECIMEN IDENTIFICATION	INITIAL FLAW SIZE $2a_i$ m (in.)	NO. OF FATIGUE & COMPLIANCE CYCLES	FINAL FLAW SIZE $2a_f$ m (in.)	FAILURE LOAD MN (Kip)	GROSS AREA STRESS MN/m ² (ksi)	NET AREA STRESS MN/m ² (ksi)	K_Q MN/m ² √m (ksi√in)
B/E	AC05-1	0.0222(.875)	56 022	0.0239(.94)	0.0110(2.475)	228(33.0)	365(52.9)	46.9(42.7)
	-2	.0222(.875)	110 000	.0222(.875)	.0107(2.40)	221(32.0)	339(49.2)	43.5(39.6)
	-3	.0047(.185)	27	^a .0330(1.30)	.00667(1.50)	138(20.0)	288(41.7)	35.8(32.6)
	-4	.0047(.185)	2 611 121	.0047(.185)	.0209(4.70)	432(62.7)	467(67.7)	- -
G/E	BC05-1	.0222(.875)	110 016	.0236(.93)	.00773(1.737)	159(23.0)	254(36.9)	32.5(29.6)
	-2	.0222(.875)	110 017	.0249(.98)	.00775(1.742)	160(23.2)	263(38.2)	33.8(30.8)
	-3	.0047(.185)	27	^a .0330(1.30)	.00540(1.215)	112(16.2)	233(33.8)	29.0(26.4)
	-4	.0047(.185)	2 611 121	.0047(.185)	^b .00992(2.23)	205(29.7)	221(32.1)	- -
G/PI	DC05-1	.0222(.875)	110 056	^a .0381(1.50)	.00420(0.945)	86.9(12.6)	217(31.5)	25.6 23.3
	-2	.0222(.875)	<1 030	.0292(1.15)	^c .00796(1.79)	165(23.9)	305(44.2)	38.9 35.4
	-3	.0047(.185)	27	^a .0330(1.30)	.00533(1.198)	110(16.0)	230(33.3)	28.7 26.1
	-4	.0047(.185)	2 611 121	.0047(.185)	^d .0147(3.30)	303(44.0)	328(47.5)	- -
B/Al	EC05-1	.0222(.875)	2 500 040	.0222(.875)	.0175(3.94)	258(37.5)	398(57.7)	51.0 46.4
	-2	.0222(.875)	710 036	^e .0222(.875)	.0162(3.635)	239(34.6)	248(35.9)	47.0 42.8
	-3	.0047(.185)	27	^a .0330(1.30)	.0129(2.90)	190(27.6)	396(57.5)	- -
	-4	.0047(.185)	2 611 125	.0047(.185)	^b .0265(5.95)	391(56.7)	423(61.3)	- -

^a Flaw extended to this length by hand with diamond coated wire.^b Failure in grips.^c Failed during fatigue cycling.^d Failure not at flaw but damage at flaw was noted.^e Crack parallel to fiber, 0.0025m (0.1 in.) in length.

653217-64

- The apparent stress intensity factor, K_Q , calculated from fracture tests does not lie on a straight horizontal line when plotted versus *visual* crack length. The testing showed only very limited evidence of growth of *effective* crack length. This leads to the conclusion that the fracture mechanics approach is not appropriate for characterizing crack growth in composite materials. Delaminations were not investigated, hence, no conclusions can be made regarding that type of flaw.
- Fatigue cycling showed no trend effects on stress intensity factors calculated from residual strength tests when compared to results from uncycled static tests.
- Results from the "-3" specimens, Figure 7-40, indicate that the B/Al is more resistive to crack opening displacement than the B/E. The G/E and G/PI possess the same resistance to crack opening displacement and are less resistant than the B/E. As the two graphite reinforced systems were the same, this would indicate that the fibers dominate the fatigue mechanism, i.e., whether the matrix is epoxy or polyimide is of less importance. The large difference between the B/Al and B/E materials, on the other hand, indicates that for boron reinforced systems the matrix, either a ductile metal or a brittle resin, plays a major role in the fatigue mechanism.

7.4 COMPRESSIVE TESTING

Results of the thermal aging and flight simulation tests indicated that matrix properties such as compressive and shear strength were affected to a greater degree than tensile strength, a fiber dominated property. For this reason it was decided to include a limited number of

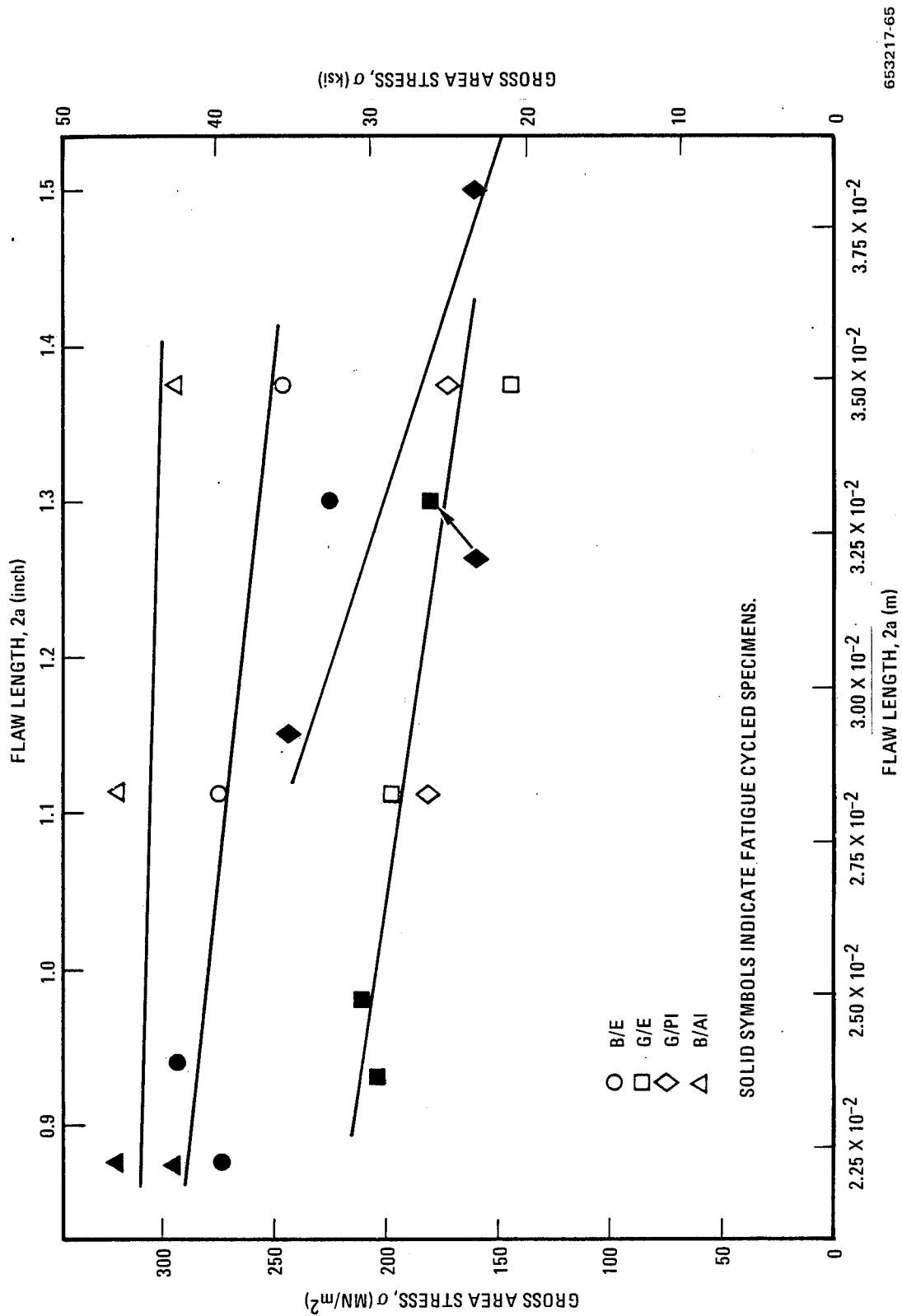
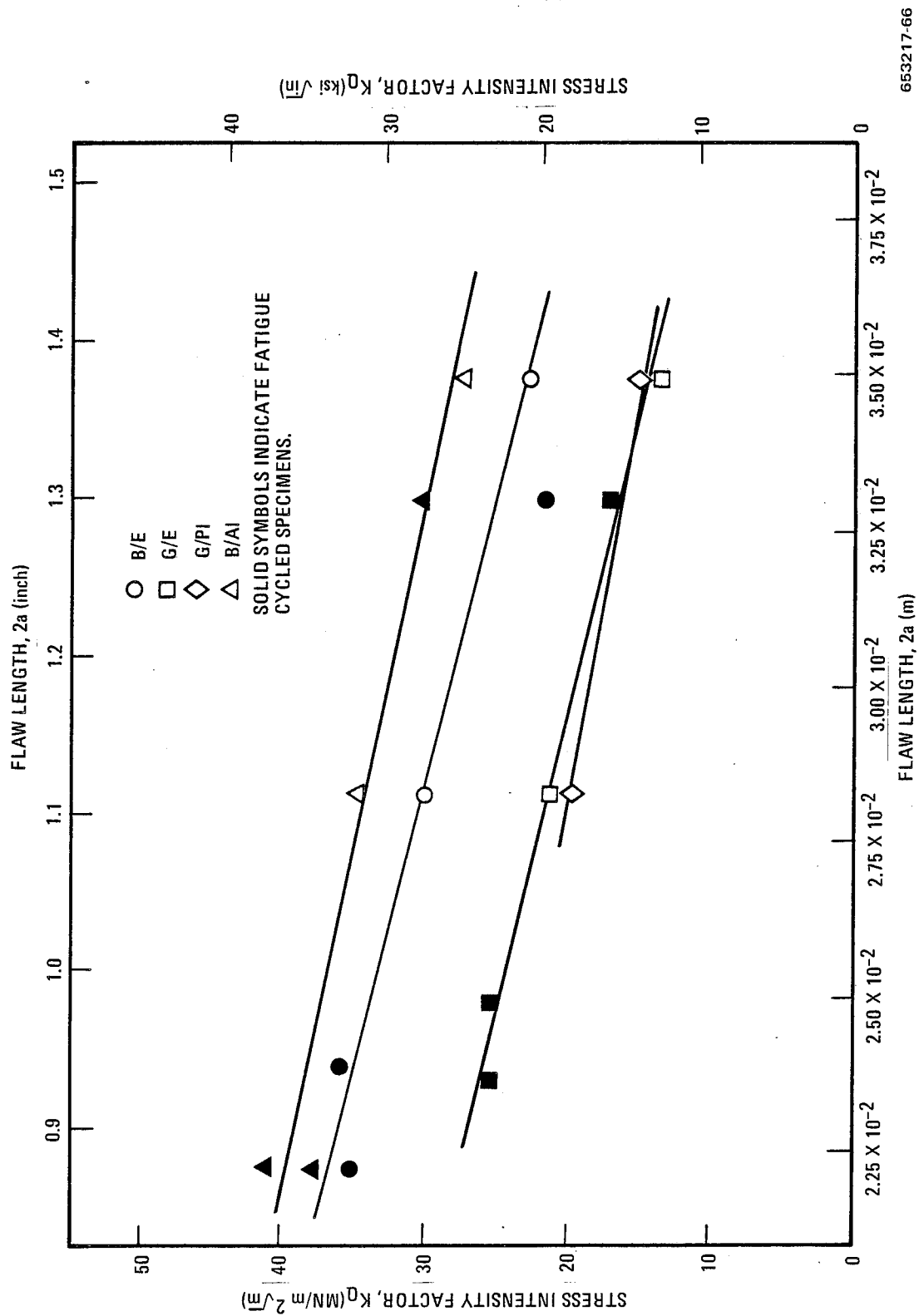


Figure 7-45 Effect of Flaw Length on Gross Area Static Failure Stress



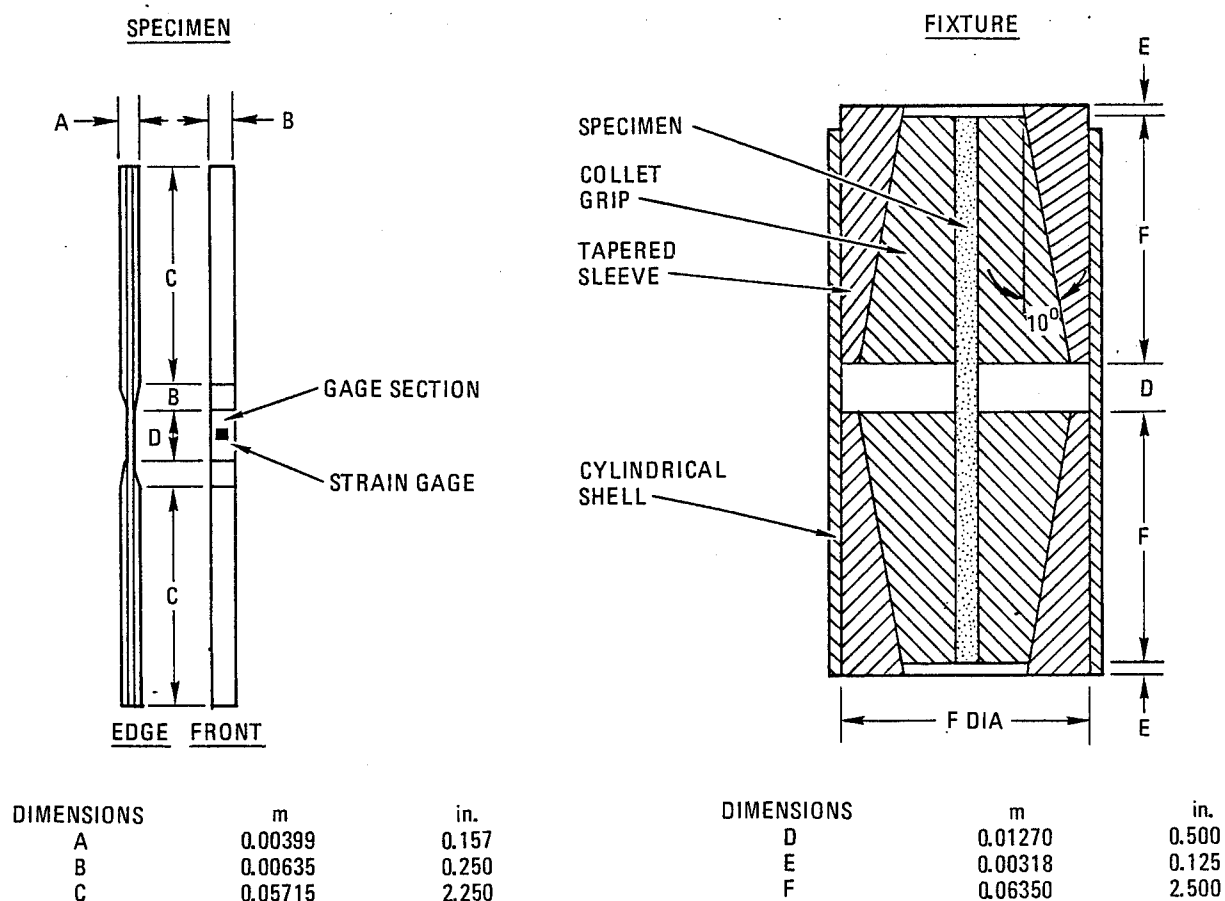
653217-66

Figure 7-46 Effect of Flaw Length on Stress Intensity Factor

residual compressive tests in the 10,000 hour flight simulation test program. To check out the feasibility of determining compressive strength of a six ply laminate such as that used in the flight simulation exposures, a series of baseline compressive tests were conducted on laminated B/E, G/E, and G/PI specimens. No baseline B/Al compressive tests were made.

7.4.1 SPECIMEN DESIGN AND TEST PROCEDURE. At the time that the compressive tests were performed, an ASTM standard test method, D3410-75, had been prepared for determination of compressive properties of oriented fiber composites. The specimen configuration, test fixture, and procedure used in the baseline tests were those called out in this ASTM Specification. Figure 7-47 shows the test specimen and test fixture. To obtain the required specimen thickness of 0.0015 m (0.060 in.) to 0.003 m (0.120 in.) it was necessary to bond together several pieces of the 6 ply laminates. For the B/E and G/E systems, four layers were used while for the somewhat thicker G/PI only three were required. The procedure for fabrication of the specimens was:

1. Cut three or four pieces of $[0^\circ \pm 45^\circ]_s$ composite approximately 0.038 m (1.5 in.) by 0.140 m (5.5 in.) with 0° plies in long direction.



653217-67

Figure 7-47 Compression Test Specimen and Fixture

2. Heat at 394 K (250 °F) for 24 hours to remove any absorbed moisture.
3. Bond pieces together with fiberglass doublers at each end using EA 9309 adhesive.
4. Cut 0.0064 m (0.25 in.) wide specimens from the 18 or 24 ply laminates.
5. Apply two strain gages to each specimen using the procedures described in Section 7.1.1. Gages used were B/E, FAE-12-12-S3; G/E and G/PI, FAE-12-12-S0.
6. Store in desiccator until tested.

The compressive tests were conducted in an Instron testing machine using a fixture of the type described in Figure 7-47. The test setup is shown in Figure 7-48. After the specimen is loaded into the fixture, a slight preload is applied to exercise the gages and ensure that the specimen is properly positioned. The specimen is then loaded incrementally to failure with strain measurements recorded automatically with the same equipment that was used for the tensile tests. The output was both a typewritten recording of load versus strain and a punched paper tape that could be processed by a computer, programmed to produce a stress-strain plot. Compressive modulus values were determined from the stress-strain curves.

7.4.2 TEST RESULTS AND DISCUSSION. Compressive strength and modulus data for the three resin matrix systems are given in Table 7-40, and typical load-strain curves for each system are shown in Figures 7-49 to 7-51. In agreement with results of others, the strength and modulus

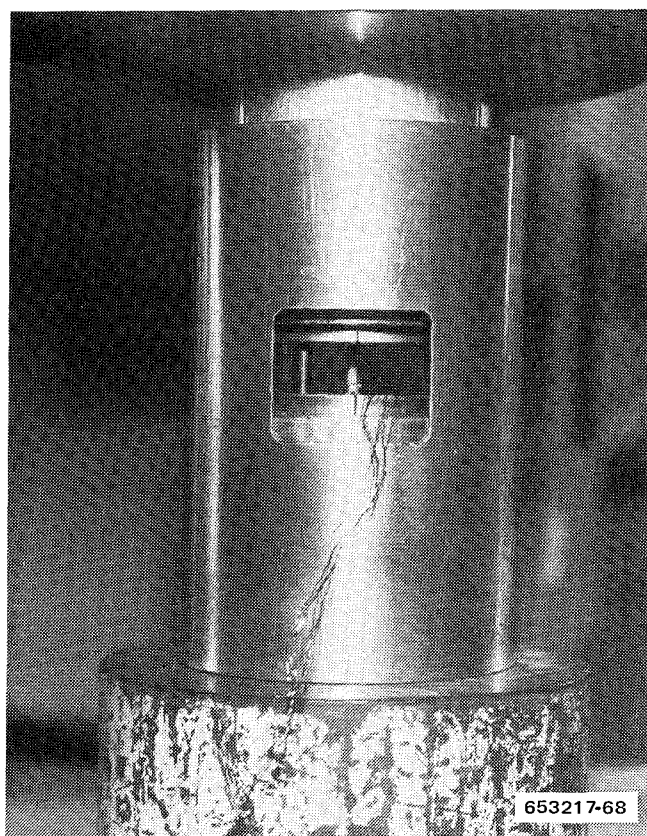
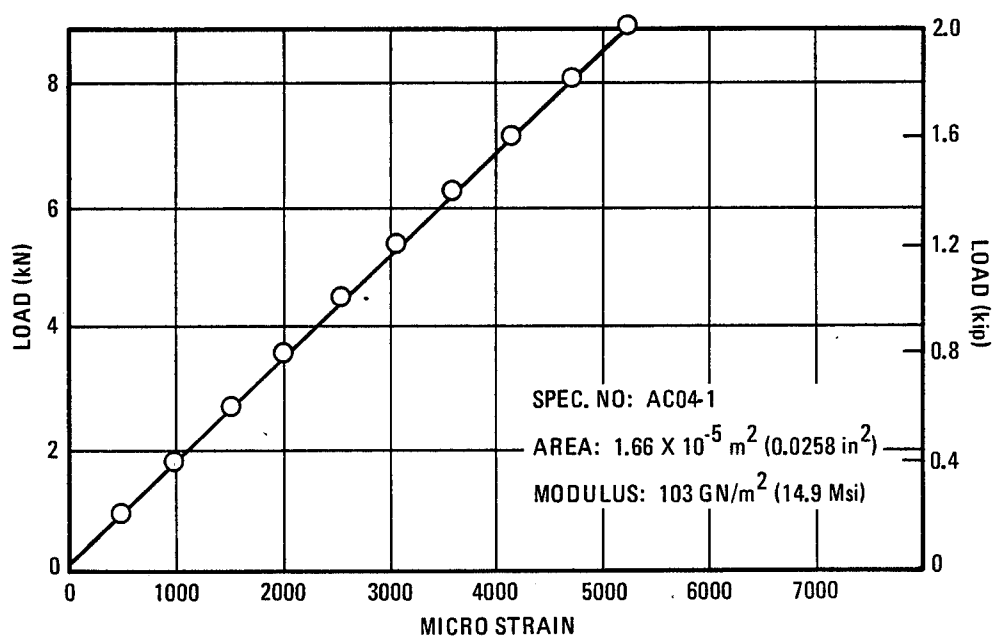


Figure 7-48 Test Setup for Compressive Tests

Table 7-40. Baseline Compressive Properties of Laminated $[0^\circ \pm 45^\circ]_s$ Crossplied Composite Systems at Room Temperature

Material System	Specimen Number	Compressive Strength		Compressive Modulus	
		MN/m ²	(ksi)	GN/m ² (a)	(Msi) (a)
B/E	AC04-1	1459	211.6	103	14.9
	-2	1665	241.5	101	14.7
	-3	1497	217.1	101	14.7
	avg	1540	223.4	102	14.8
G/E	BC04-1	571	82.8	47	6.8
	-2	570	82.6	43	6.3
	avg	570	82.7	45	6.6
G/PI	DC04-1	382	55.4	46	6.6
	-2	363	52.6	48	7.0
	-3	386	56.0	44	6.4
	avg	377	54.7	46	6.7

^aStrain gage measurements



653217-69

Figure 7-49 Compressive Load-Strain Diagram for $[0^\circ \pm 45^\circ]_{s2s}$, B/E at 297 K (75° F)

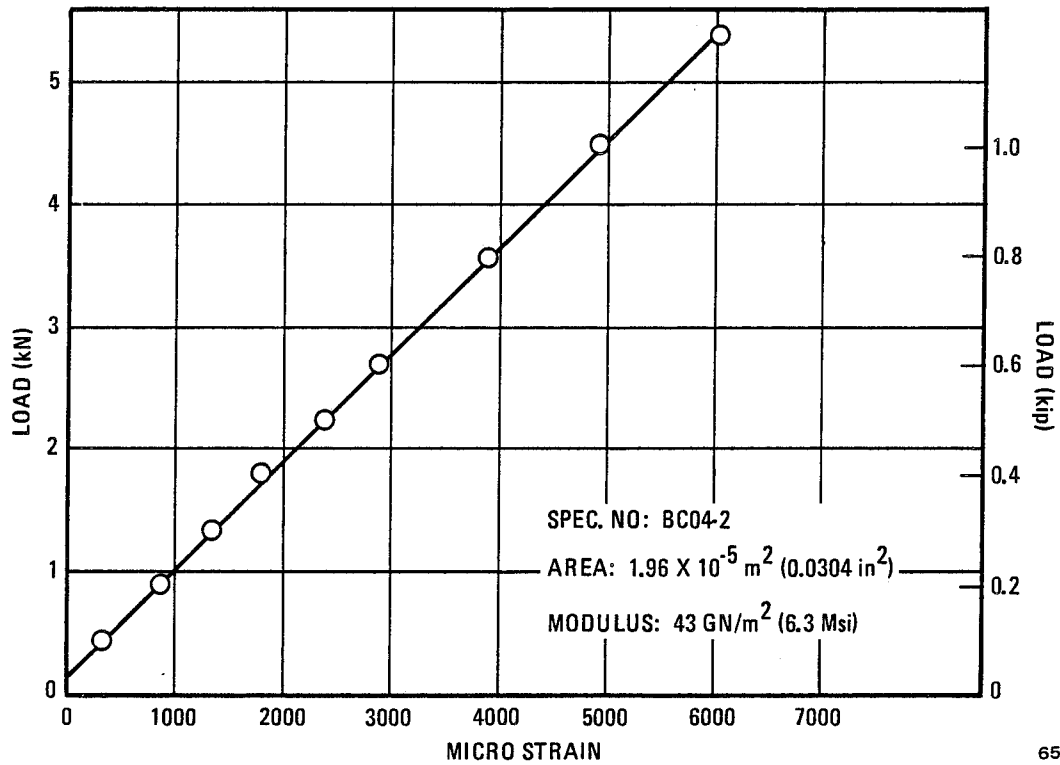


Figure 7-50 Compressive Load-Strain Diagram for $[0^\circ \pm 45^\circ]_{s2s}$, G/E at 297 K (75° F)

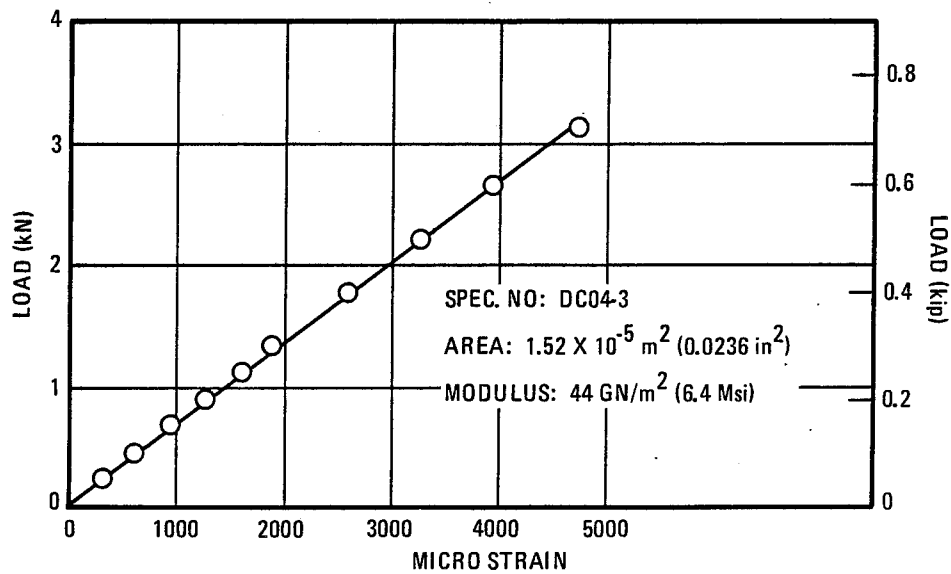


Figure 7-51 Compressive Load-Strain Diagram for $[0^\circ \pm 45^\circ]_{s3}$, G/PI at 297 K (75° F)

values of the boron reinforced system are considerably larger than either of the graphite reinforced systems. The higher compressive properties of the B/E over the G/E and G/PI would be anticipated from a comparison of the reinforcing fibers. The boron fibers in the 0° plies are aligned along their entire length in the loading direction, whereas the much smaller diameter graphite fibers that are twisted into multi-filament tows are, on a micro scale, generally aligned slightly off axis to the compressive load. Both the strength and modulus values of the graphite systems are less than half of the values for the boron system.

SECTION 8

THERMAL AGING

To determine the effects of elevated temperature exposure on the stability of advanced composites an extensive thermal aging study was conducted. It was thought that these data, together with the fatigue data also generated during the program, would be very valuable in understanding the results of the flight simulation exposures.

All of the composite materials were thermally aged for 10,000 hours during Phase I of the contract. Additional exposures, out to 50,000 hours, will be carried out during Phase II of the contract and will be described in a future report. At various times during the 10,000 hours, specimens were removed for examination and determination of residual tensile strength and, for B/Al, also residual interfiber shear strength. Test specimens were taken from both unidirectional and $[0^\circ \pm 45^\circ]_s$ crossplied laminates. All were 6 ply in thickness. The aging temperatures were: epoxy, 394 K (250° F) and 450 K (350° F); polyimide 505 K (450° F) and 561 K (550° F); and B/Al, 450 K (350° F), 561 K (550° F), and 700 K (800° F). The resin matrix composites were aged at ambient pressure and at a reduced pressure of 0.014 MN/m² (2 psi) to simulate high altitude flight conditions. The B/Al system was aged at ambient pressure only. A second oxygen pressure was selected for the thermal aging of the organic composites because, in general, the organics are oxidation prone. Previous work had shown a direct correlation of thermal aging and oxygen pressure on residual strength of resin matrix composites (ref. 28). In actual use, a SCR vehicle would be at very high altitude during much of the time at which the structure has reached its maximum temperature. Thus, if oxygen pressure is taken into account, the organic materials can likely be used at higher temperatures and for longer times.

The following sections describe the test procedures and equipment for the thermal aging studies and present and discuss the experimental results.

8.1 TEST EQUIPMENT AND TEST PROCEDURE

The 700 K (800° F) thermal age of B/Al was carried out in a small, commercial, electrical resistance oven. The built-in "on/off" temperature controller was replaced by a more accurate controller. After modifying the control system, the entire oven was enclosed with ceramic bricks to improve the temperature stability over the 10,000-hour aging period. With this arrangement the temperature was held to 700 ± 6 K ($800^\circ \pm 10^\circ$ F).

All other exposures were conducted in specially constructed aging furnaces similar to the sketch in Figure 8-1. The heater plates consist of insulated wire sandwiched between two thin aluminum plates. The reduced pressure specimens are enclosed in containers consisting of an aluminum picture frame with vacuum fittings and thin aluminum covers. The top cover is sealed with a weld after the specimens are in place. The top is cut off and rewelded periodically during the 50,000 hours to remove specimens for testing. This is less expensive and more reliable than a gasket sealed container. The reduced pressure is obtained by a vacuum pump simultaneously pumping on one side of each container. Bleed air is valved into the other side of

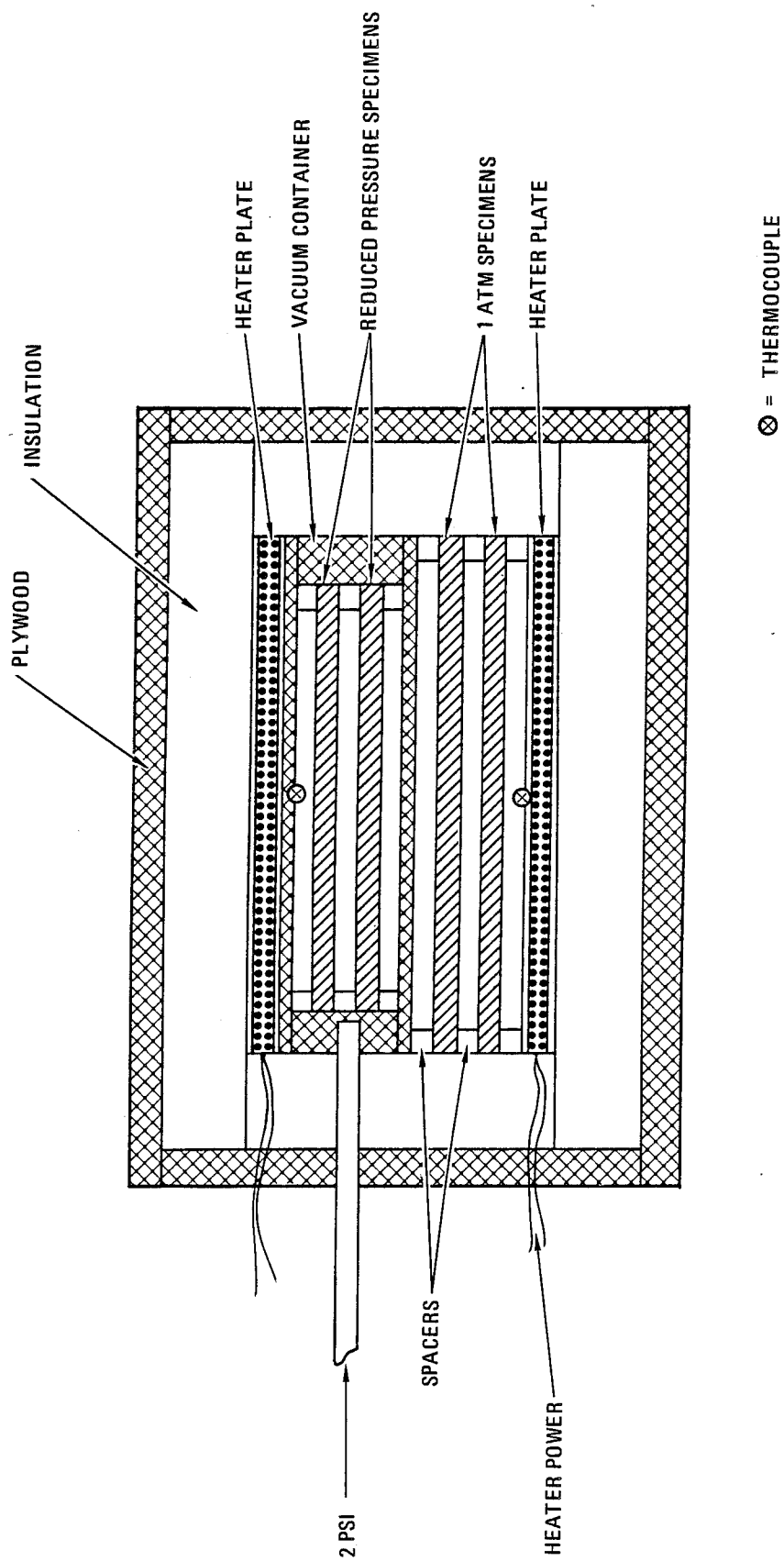


Figure 8-1 Thermal Aging Furnace Configuration

653217-72

each to maintain 0.014 MN/m² (2 psi). This assures a constant fresh supply of air to each container. All furnace temperatures were initially equilibrium controlled, i.e., a constant amount of power was supplied to the heaters. The power equals that lost through the insulation at equilibrium temperature. This method does not require the use of expensive controllers, and temperature fluctuations are generally smaller than those achieved with active controls. There is also essentially zero probability of a malfunction allowing the specimens to overheat. However, there was a problem that developed on very warm days when the temperature could rise slightly above the desired limits. To prevent this from happening while still retaining the assurance that a failure in a power supply, thermocouple, or some control element would not cause overheating, a small modification was made. This was to add a controller to the system on about 10% of the available power. The furnace would operate as before, except when the outside temperature rose too high the controller would override the system and maintain the desired temperature range. The temperatures were generally maintained to ± 3 K ($\pm 5^\circ$ F) with infrequent excursions to a maximum of ± 6 K ($\pm 10^\circ$ F).

The procedure followed for the exposures was to cut the specimen blanks to final size including machining of the B/Al interfiber shear specimens (Figure 7-27), drying the resin matrix composites at 394 K (250° F) for 24 hours, and loading into the aging furnaces. The specimens were supported at their ends by narrow strips of stainless steel so that almost the entire surface was exposed to the air atmosphere within the furnaces. At the required time intervals the ovens were shut down, opened, and the specimens were removed and stored in a desiccator until doubler bonding and tensile testing. Only the resin matrix specimens were placed in the desiccator, as moisture absorption was not a problem with the B/Al. Residual strength testing was performed at 297 K (75° F) for the B/Al, 450 K (350° F) for the epoxies, and 505 K (450° F) and 561 K (550° F) for the polyimides. The tensile and shear specimen configurations and test procedures were the same as those described in Section 7.

8.2 TEST RESULTS AND DISCUSSION

8.2.1 BORON/EPOXY AND GRAPHITE/EPOXY. Residual tensile strength data for the epoxy systems are presented in Table 8-1 and 8-2 for B/E aged at ambient pressure, Table 8-3 for B/E aged at reduced pressure, Table 8-4 and 8-5 for G/E aged at ambient pressure, and Table 8-6 for G/E aged at reduced pressure. Aging was carried out at 394 K (250° F) and 450 K (350° F) for both unidirectional and $[0^\circ \pm 45^\circ]_s$ crossplied specimens. The tensile strength data have also been plotted as a function of aging time for the two epoxy systems. These curves are found in Figures 8-2 through 8-5. A summary of the effects of 10,000 hours of thermal aging on the tensile strength retention of B/E and G/E is shown in Table 8-7. In Table 8-7 and in others throughout the report that list percentage strength retention, whenever residual strength is greater than baseline strength a value of 100% retention has been used.

The results shown in Figures 8-2 and 8-3 for B/E are typical of both the epoxy systems. At 394 K (250° F) and ambient pressure no degradation has occurred for either the unidirectional or crossplied material during the 10,000 hours. Examination of the specimens after removal from the furnace revealed no changes in appearance during the first 5000 hours. After 10,000 hours only slight color changes were observed in both the B/E and the G/E specimens. The excellent condition of the specimens after 10,000 hours is shown in Figure 8-6 and 8-7. Failed tensile specimens of B/E and G/E before and after aging show no significant differences.

Table 8-1. Thermal Aging Data for $[0^\circ]_6$ B/E in 0.10 MN/m^2 (14.7 psi) Air

Aging Temperature K (°F)		Test Temperature K (°F)		Aging Time (hr)	Tensile Strength MN/m^2 (ksi)	
394	250	450	350	Baseline avg	1380	200
				100	1390	202
					1350	196
					1370	198
					avg 1370	199
				500	1460	212
					1360	197
					1340	194
					avg 1390	201
				1,000	1330	193
					1390	201
					1380	200
					avg 1370	198
				5,000	1480	214
					1450	210
					1520	220
					avg 1480	215
				10,000	1410	204
					1430	208
					1450	211
					avg 1430	208
450	350	450	350	5,000	1230	179
					1240	180
					1250	182
					avg 1240	180
				10,000	1010	146
					1010	147
					1080	156
					avg 1030	150

Table 8-2. Thermal Aging Data for $[0^\circ \pm 45^\circ]_s$ Crossply B/E in 0.10 MN/m^2 (14.7 psi) Air

Aging Temperature K (°F)		Test Temperature K (°F)		Aging Time (hr)	Tensile Strength MN/m ² (ksi)	
394	250	450	350	Baseline avg	550	79.8
				100	510	73.9
					496	71.9
					493	71.5
					avg 500	72.4
				500	478	69.4
					428	62.1
					474	68.7
					avg 460	66.7
				1,000	512	74.2
					504	73.1
					539	78.2
					avg 518	75.2
				5,000	535	77.6
					527	76.4
					533	77.3
					avg 532	77.1
450	350	450	350	10,000	538	78.1
					534	77.4
					522	75.7
					avg 531	77.1
				500	544	78.9
					461	66.9
					517	75.0
					avg 507	73.6
				1,000	581	84.2
					508	73.7
					493	71.5
					avg 527	76.5
				5,000	310	44.9
					319	46.3
					309	44.8
					avg 313	45.3
				10,000	339	49.2
					342	49.6
					314	45.6
					avg 332	48.1

Table 8-3. Thermal Aging Data for B/E Aged in 0.014 MN/m² (2 psi) Air

Aging Temperature		Orientation	Test Temperature		Aging Time (hr)	Tensile Strength	
K	(°F)		K	(°F)		MN/m ²	(ksi)
450	350	[0°] ₆	450	350	Baseline avg	1380	200
						1520	220
						1290	187
						1400	203
					5,000	avg 1400	203
						1390	201
						1340	195
						1400	203
						avg 1380	200
					10,000	1390	201
						1340	195
						1400	203
						avg 1380	200
						1390	201
						1340	195
450	350	[0° ± 45°] _s	450	350	Baseline avg	550	79.8
						519	75.3
						529	76.7
						590	85.6
					5,000	avg 546	79.2
						379	54.9
						367	53.2
						381	55.3
						avg 376	54.5
					10,000	379	54.9
						367	53.2
						381	55.3
						avg 376	54.5

Table 8-4. Thermal Aging Data for [0°]₆ G/E in 0.10 MN/m² (14.7 psi) Air

Aging Temperature			Test Temperature		Aging Time (hr)	Tensile Strength	
K	(°F)		K	(°F)		MN/m ²	(ksi)
394	250	450	350		Baseline avg	1590	230
						1520	220
						1590	230
						1540	224
					500	avg 1550	225
						1260	182
						1270	184
						1470	213
						avg 1330	193
					1,000	1480	214
						1560	227
						1450	210
						avg 1500	217

Table 8-4. Thermal Aging Data for $[0^\circ]_6$ G/E in 0.10 MN/m^2 (14.7 psi) Air — Concluded

Aging Temperature K (°F)		Test Temperature K (°F)		Aging Time (hr)	Tensile Strength MN/m ² (ksi)	
450	350	450	350	5,000	1630	236
					1600	232
					1440	209
					avg 1560	226
				10,000	1650	240
					1650	239
					1850	268
					avg 1720	249
				100	1500	218
					1650	239
					1460	212
					avg 1540	223
				500	1630	236
					1620	235
					1550	225
					avg 1600	232
				1,000	1260	182
					1500	218
					1540	223
					avg 1430	208
				5,000	1210	175
					1370	199
					1300	188
					avg 1290	188
				10,000	1360	198
					1270	184
					1210	176
					avg 1280	186

Table 8-5. Thermal Aging Data for $[0^\circ \pm 45^\circ]_s$ Crossply G/E in 0.10 MN/m² (14.7 psi) Air

Aging Temperature K (°F)		Test Temperature K (°F)		Aging Time (hr)	Tensile Strength MN/m ² (ksi)	
394	250	450	350	Baseline avg	500	72.5
				100	496	72.0
					542	78.6
					483	70.0
					avg 507	73.5
				500	475	68.9
					492	71.4
					494	71.7
					avg 487	70.7
				1,000	494	71.6
					552	80.0
					626	90.8
					avg 557	80.8
				5,000	589	85.4
					559	81.1
					536	77.7
					avg 561	81.4
				10,000	559	81.1
					593	86.0
					585	84.9
					avg 579	84.0
450	350	450	350	500	494	71.6
					608	88.2
					559	81.1
					avg 554	80.3
				1,000	552	80.0
					501	72.6
					563	81.6
					avg 539	78.1
				5,000	485	70.3
					440	63.8
					474	68.7
					avg 466	67.6
				10,000	265	38.5
					60	8.7
					238	34.5
					avg 188	27.2

Table 8-6. Thermal Aging Data for G/E Aged in 0.014 MN/m² (2 psi) Air

Aging Temperature		Orientation	Test Temperature		Aging Time (hr)	Tensile Strength		
K	(°F)		K	(°F)		MN/m ²	(ksi)	
450	350	[0°] ₆	450	350	Baseline avg	1590	230	
					5,000	1730	251	
						1740	252	
						1560	227	
						avg 1680	243	
					10,000	1770	257	
						1870	271	
						1760	255	
						avg 1800	261	
					[0° ± 45°] _s	Baseline avg	500	72.5
						5,000	584	84.7
							596	86.4
		571					82.8	
		avg 584					84.6	
		10,000				535	77.6	
					498	72.3		
					548	79.5		
					avg 527	76.5		

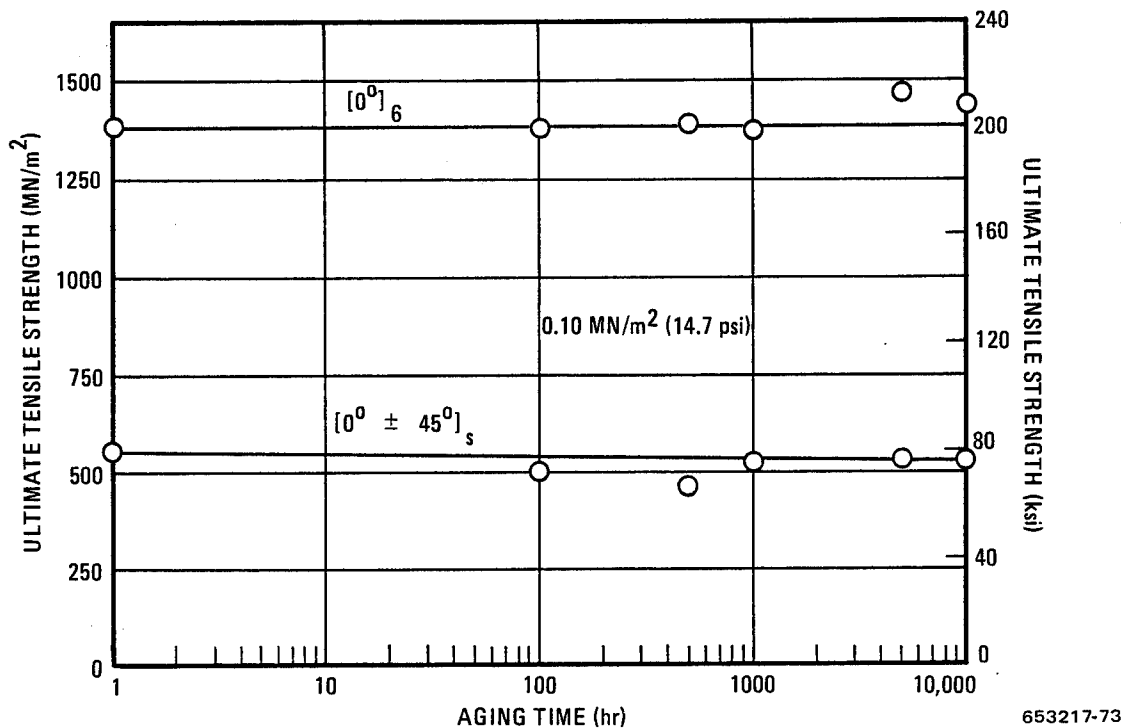
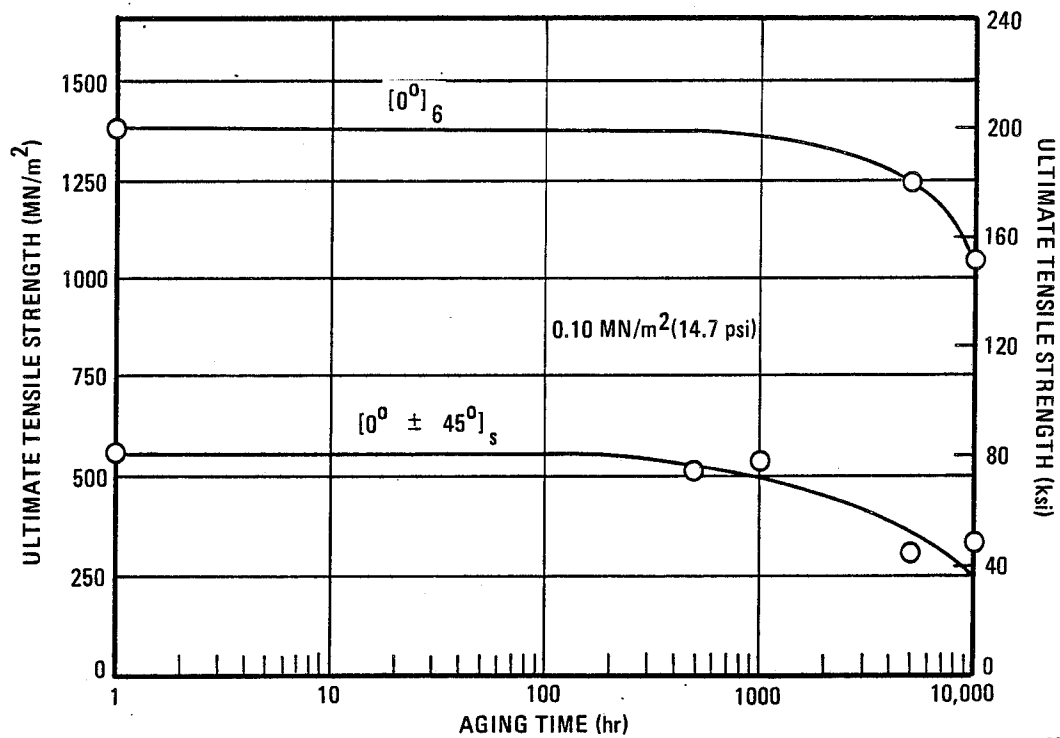
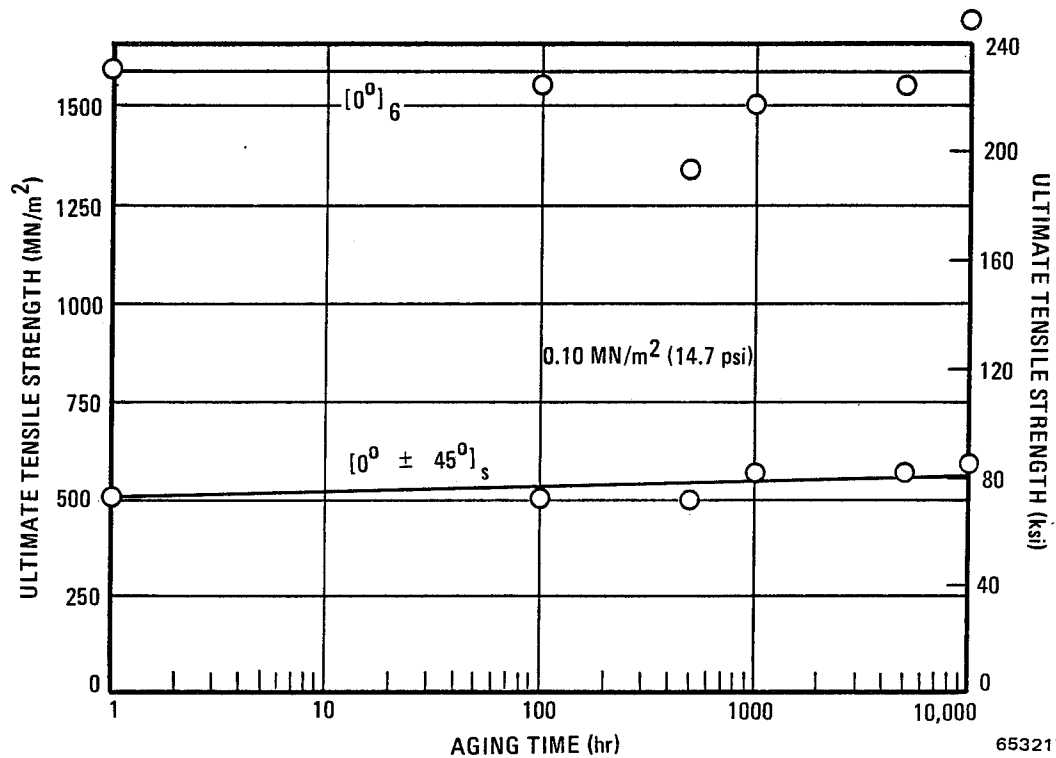


Figure 8-2 Tensile Strength of B/E at 450 K (350° F) After Thermal Aging at 394 K (250° F)



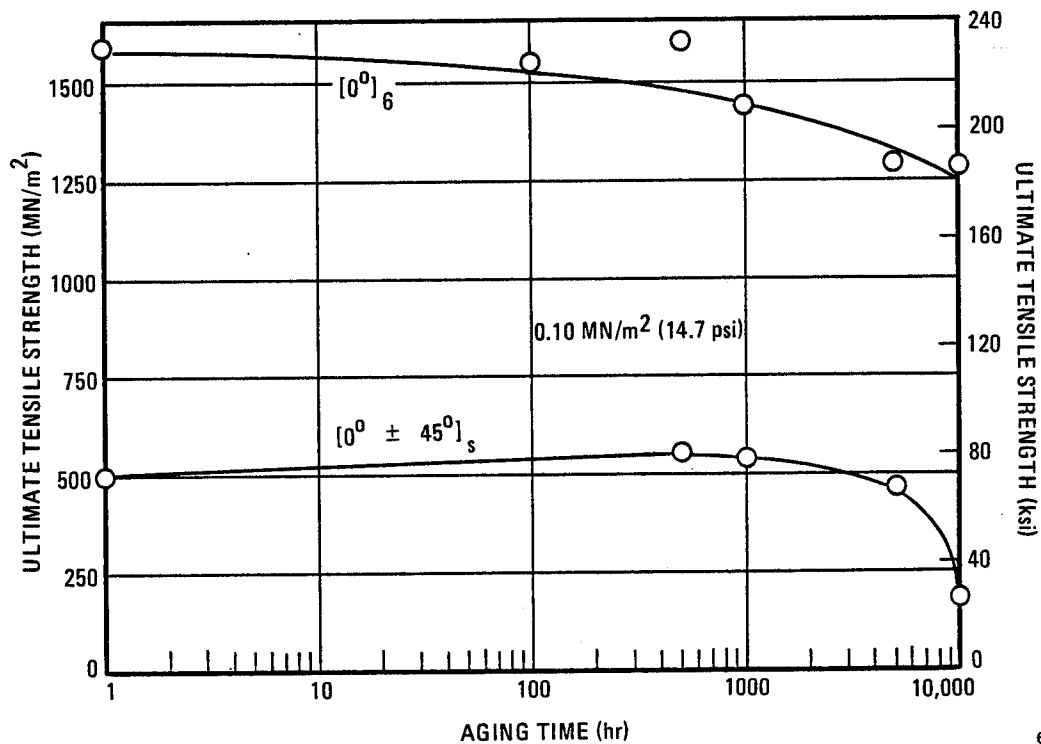
653217-74

Figure 8-3 Tensile Strength of B/E at 450 K (350° F) After Thermal Aging at the Same Temperature



653217-75

Figure 8-4 Tensile Strength of G/E at 450 K (350° F) After Thermal Aging at 394 K (250° F)



653217-76

Figure 8-5 Tensile Strength of G/E at 450 K (350° F) After Thermal Aging at the Same Temperature

Table 8-7. Summary of Tensile Strength Retention After 10,000 Hours of Thermal Aging for B/E and G/E

Material System	Orientation	Aging Temp.		Aging Pressure MN/m ²	Test Temp.		Retention of Tensile Strength (%)
		K	(°F)		K	(°F)	
B/E	[0°] ₆	394	250	0.10	450	350	100
	[0° ± 45°] _s	394	250	0.10	450	350	97
	[0°] ₆	450	350	0.10	450	350	75
	[0° ± 45°] _s	450	350	0.10	450	350	60
	[0°] ₆	450	350	0.014	450	350	100
	[0° ± 45°] _s	450	350	0.014	450	350	68
G/E	[0°] ₆	394	250	0.10	450	350	100
	[0° ± 45°] _s	394	250	0.10	450	350	100
	[0°] ₆	450	350	0.10	450	350	81
	[0° ± 45°] _s	450	350	0.10	450	350	38
	[0°] ₆	450	350	0.014	450	350	100
	[0° ± 45°] _s	450	350	0.014	450	350	100

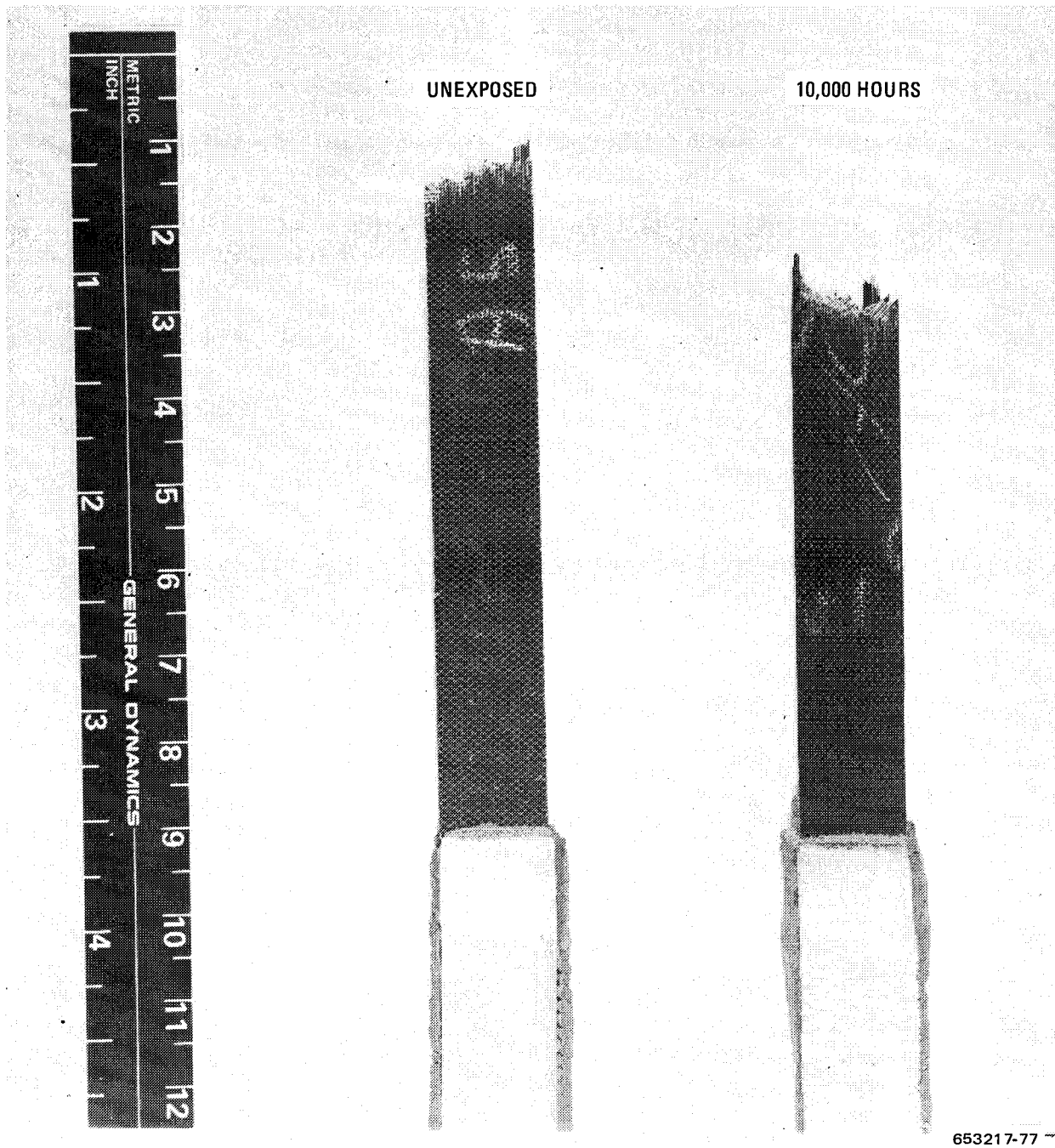


Figure 8-6 B/E Before and After 10,000 hr of Thermal Aging at 394 K (250° F) in 1 atm Air and Tensile Testing at 450 K (350° F)

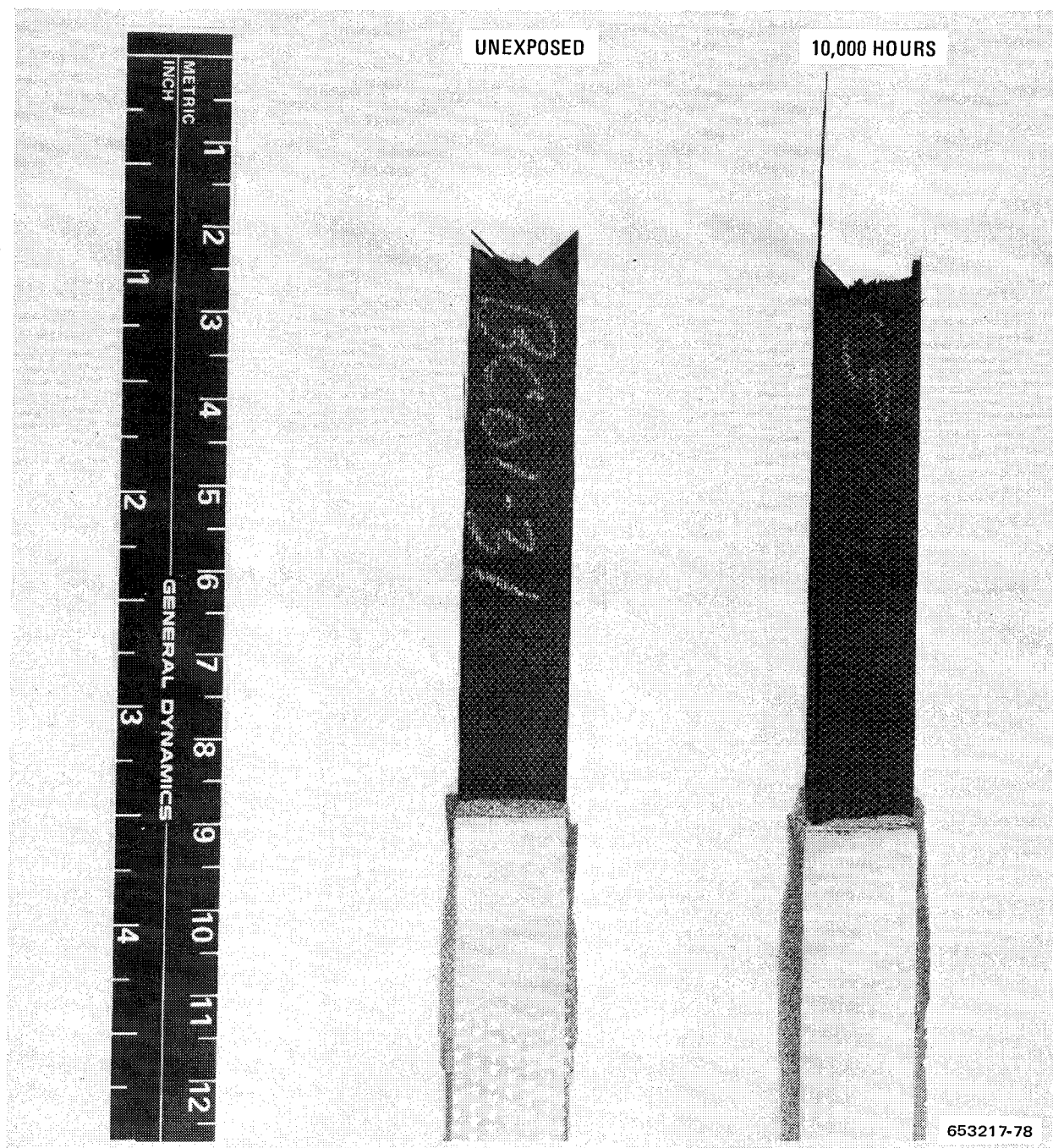


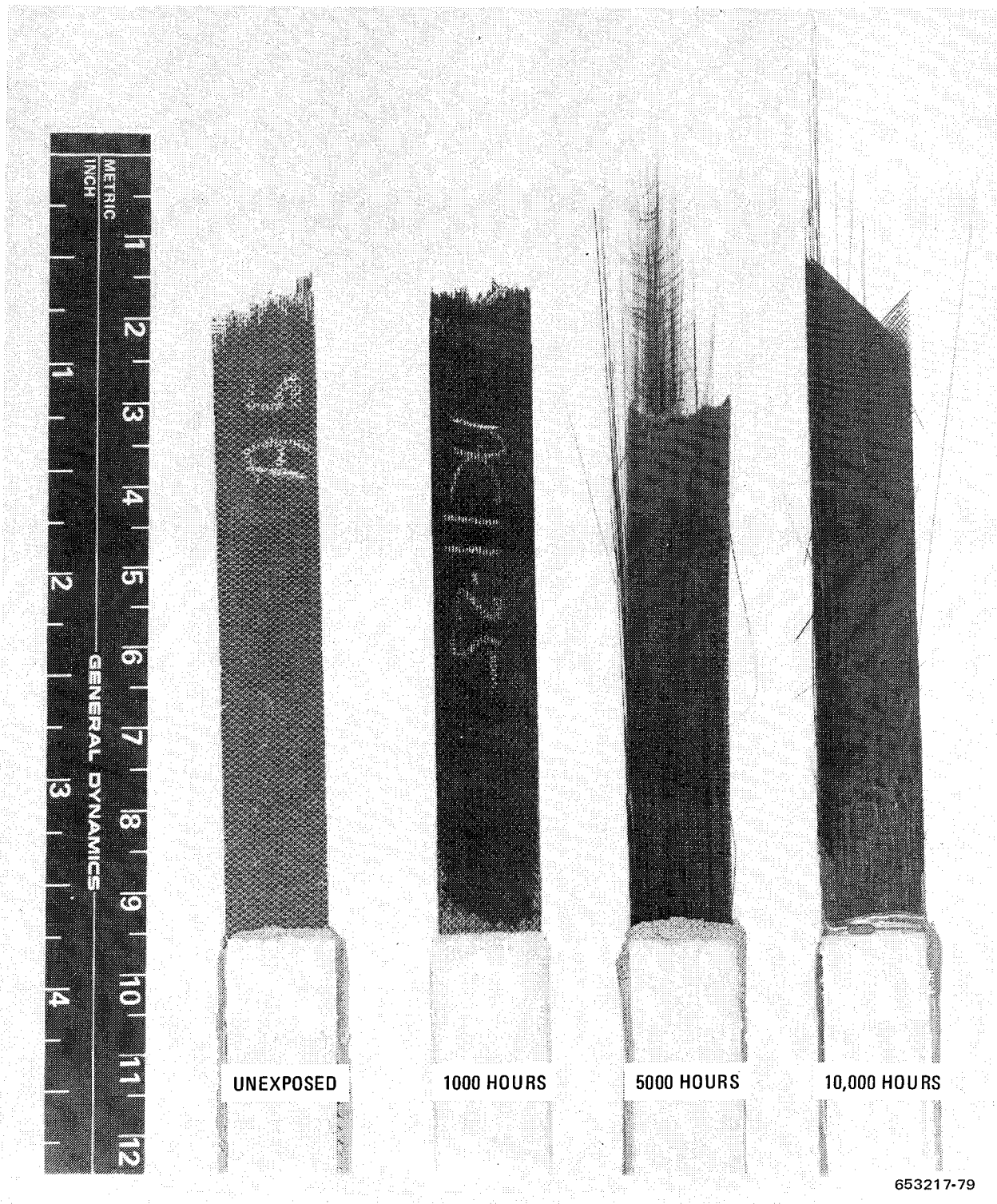
Figure 8-7 G/E Before and After 10,000 hr of Thermal Aging at 394 K (250° F) in 1 atm Air and Tensile Testing at 450 K (350° F)

Thermal aging of the epoxy systems at 450 K (350° F) produced significant degradation when exposure was carried out at ambient pressure but almost no effects when aging was done at a reduced pressure of 0.014 MN/m² (2 psi). The degradation in tensile properties combined with a significant change in appearance of the specimens, particularly after tensile testing, occurred after 5000 hours at 450 K (350° F) in a 0.10 MN/m² (14.7 psi) air environment. For the same time and temperature, but at a reduced pressure of 0.014 MN/m² (2 psi), similar specimens showed essentially no reduction in 450 K (350° F) tensile strength. Specimens exposed at the reduced pressure failed in a manner typical of unexposed material. The samples aged in air at ambient pressure, on the other hand, were dramatically different. For these specimens the epoxy resin matrix, in many areas, crumbled away during tensile testing exposing the boron or graphite filaments. Portions of failed test specimens of each material before and after aging at 450 K (350° F) are shown in Figures 8-8 and 8-9. The change in appearance of the failed specimens between 1000 hours and 5000 hours of exposure is quite distinct. While not apparent from Figure 8-8 and 8-9, the loss of resin after 5000 hours was somewhat greater for the B/E than for the G/E material. One other observation was made during bonding of doublers to the 5000-hour tensile specimens. Prior to applying the adhesive, the ends were lightly polished with Scotch-Brite. For the B/E samples exposed at ambient pressure, just a slight amount of rubbing removed the outer powdery layer of resin and revealed the boron fibers of the outer plies. Such an effect was not observed for the G/E specimens or the reduced pressure B/E specimens.

After 10,000 hours of thermal aging at 450 K (350° F) further degradation of the epoxy materials was observed. The G/E specimens showed a slight color change (to a darker brown) but, otherwise, were visually unchanged by the 10,000 hour exposure. However, during doubler bonding the $[0^\circ \pm 45^\circ]_s$ specimens aged at ambient pressure all delaminated. Figure 8-10 shows the poor condition of these specimens. The tensile strength of these crossplied specimens was very low, while the unidirectional specimens showed a decrease of about 25%. The appearance of the specimens after test was similar to those aged for 5000 hours at 450 K (350° F), see Figure 8-9.

The epoxy matrix crumbled away during tensile testing leaving the bare graphite tows looking like a bundle of yarn. The relatively high tensile strength of the unidirectional specimens, 1680 MN/m² (186 ksi), after 10,000 hours exposure is somewhat misleading as to the actual quality of the material. A transverse tensile or shear test that measures the matrix strength would undoubtedly give extremely poor results. For the same time and temperature, but at a reduced pressure of 0.014 MN/m² (2 psi), similar specimens showed no reduction in 450 K (350° F) tensile strength. These specimens failed in a manner typical of unexposed material, see Figure 8-11.

The B/E specimens aged in ambient air were in very poor condition after the 10,000-hour exposure at 450 K (350° F). Two of the crossplied specimens were delaminated when removed from the aging furnace, and slight flexing of the third specimen during handling also resulted in delamination. Figure 8-12 shows the two delaminated crossplied specimens prior to doubler bonding. For the unidirectional specimens much of the resin was gone from the surface exposing many of the outer boron filaments. Some of these outer filaments were lost during the doubler bonding operation. The unidirectional specimens had very little transverse stiffness and could easily be bent by hand. Again, the crossplied specimens showed a greater decrease in tensile properties than the unidirectional specimens. In like manner to the G/E material, the tensile results don't indicate how badly the B/E had been degraded by the 10,000 hours in ambient air at 450 K (350° F). The resin matrix has retained almost no strength after the aging



653217-79

Figure 8-8 B/E Before and After Thermal Aging at 450 K (350° F) in 1 atm Air and Tensile Testing at the Same Temperature

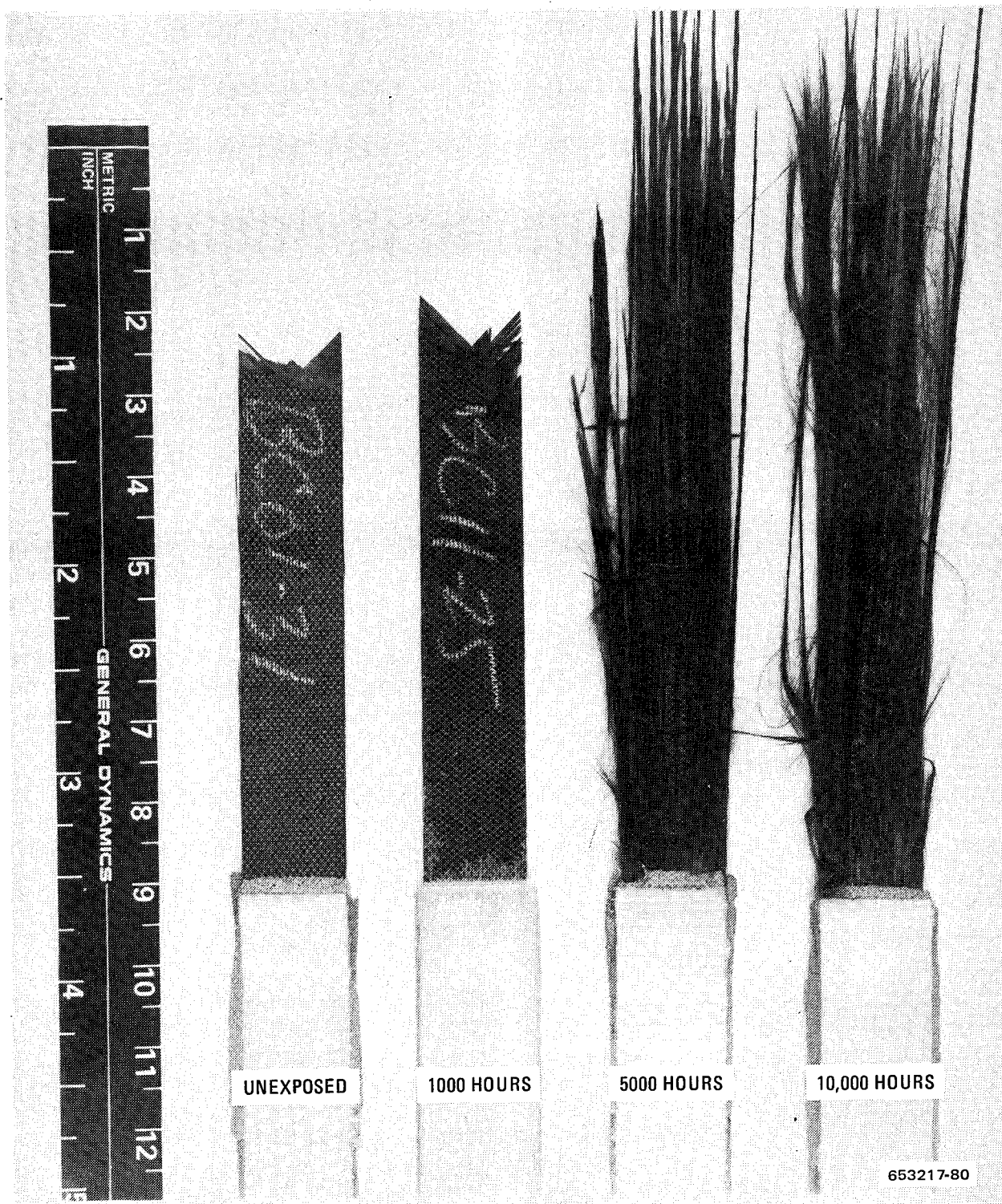


Figure 8-9 G/E Before and After Thermal Aging at 450 K (350° F) in 1 atm Air and Tensile Testing at the Same Temperature

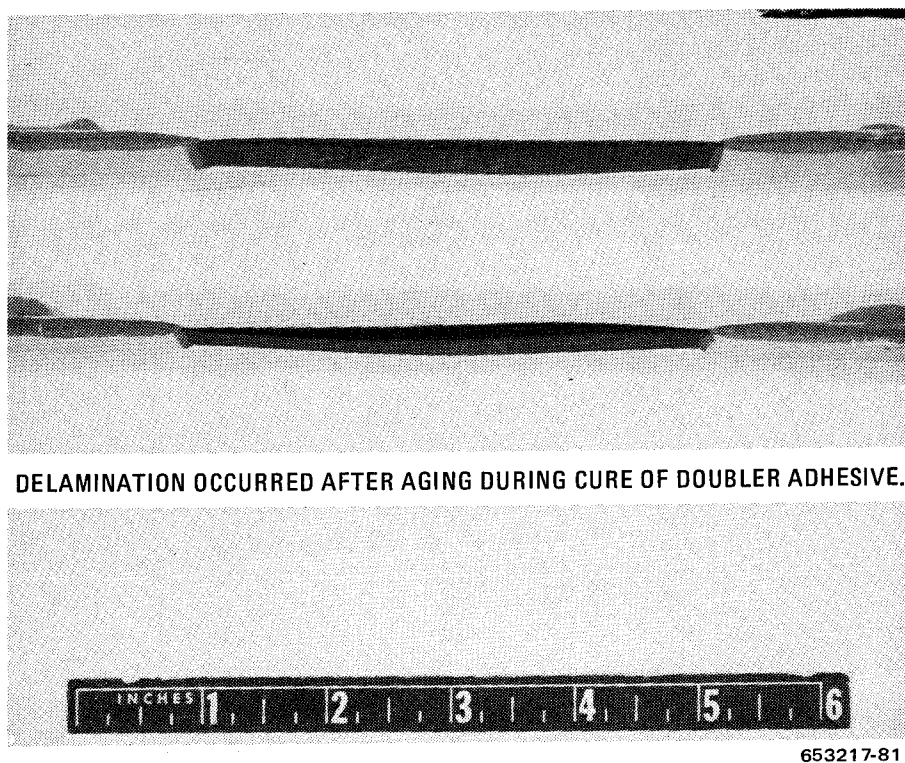


Figure 8-10 G/E Tensile Specimens After 10,000 hr of Thermal Aging at 450 K (350° F) in 1 atm Air

exposure. Figure 8-8 shows failed tensile specimens after various exposure times at 450 K (350° F) in ambient air. The 10,000-hour specimens consist primarily of broken boron fibers and scrim cloth with most of the epoxy matrix having crumbled and fallen away from the test section between the doublers.

In contrast to the G/E material, the B/E specimens aged for 10,000 hours at 450 K (350° F), but at a reduced pressure of 0.014 MN/m² (2 psi), did show a reduction in strength and a change in failure appearance. The unidirectional specimens retained 100% of the 450 K (350° F) tensile strength, but the crossplied specimens only approximately 70%. Many bare filaments were visible in the failed specimens of both layups where the resin matrix had broken up. The effect was not as pronounced as that observed for the ambient tests, but compared to unexposed specimens where almost no bare filaments occur, the indications are clear that the matrix is starting to degrade even at the reduced pressure. The 5000-hour specimens showed no property degradation and failed in a manner similar to unexposed material. The difference between the 5000-hour and 10,000-hour failure appearance can be seen in Figure 8-13.

The results from these aging tests show conclusively that the B/5505 boron epoxy and AS/3501 graphite epoxy systems are not suitable for long-term service in one atmosphere air at 450 K (350° F). At a reduced pressure of 0.014 MN/m² (2 psi) air, the G/E appears to be unaffected for at least 10,000 hours, while the B/E begins to experience some matrix degradation between 5000 and 10,000 hours.

8.2.1.1 Microscopic Examination of the Thermal Aging Specimens. After tensile testing, many of the thermal aging specimens were sectioned and mounted for study using both an optical

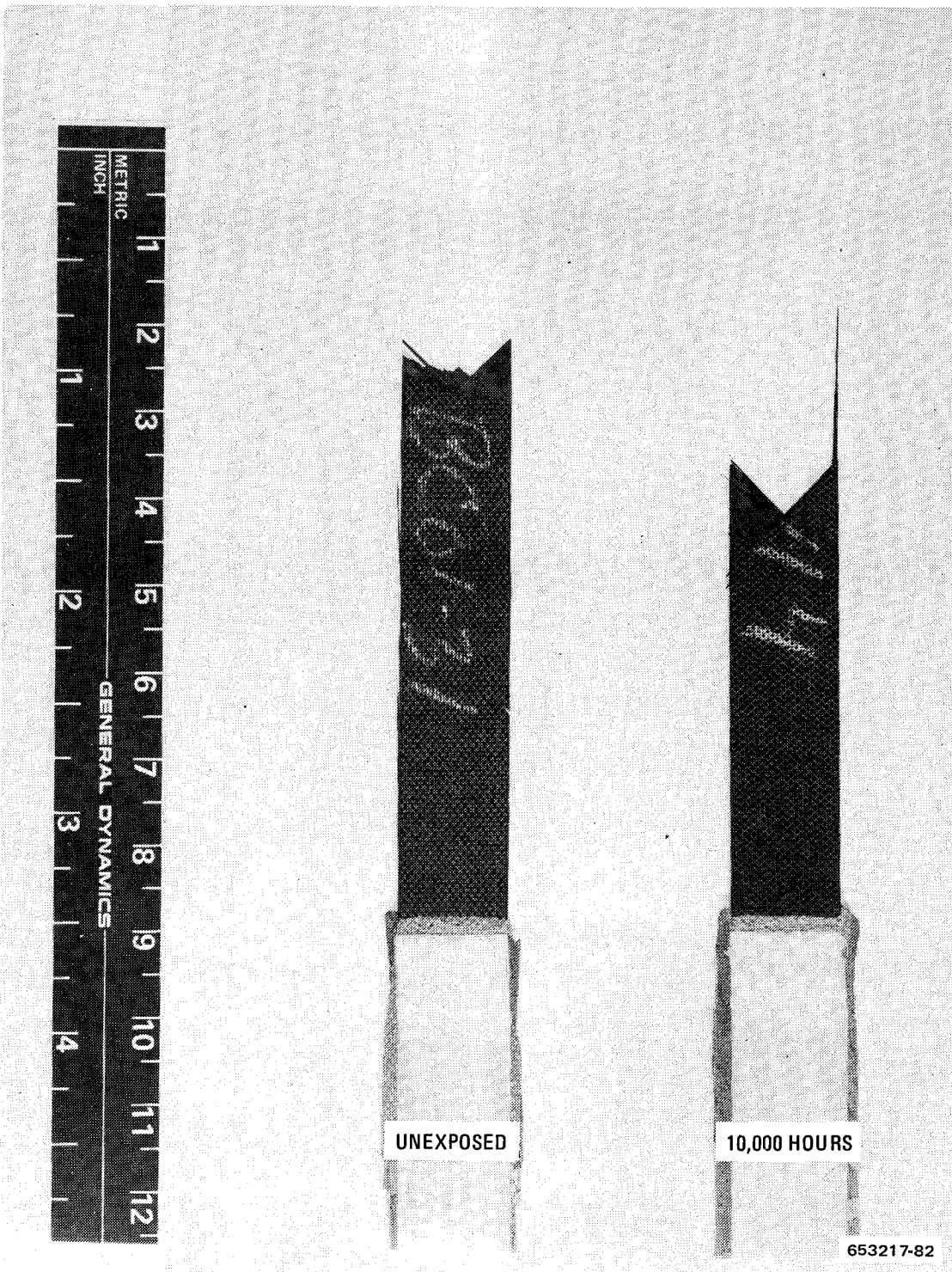


Figure 8-11 G/E Before and After Thermal Aging at 450 K (350° F) in 0.014 MN/m² (2 psi) Air and Tensile Testing at the Same Temperature

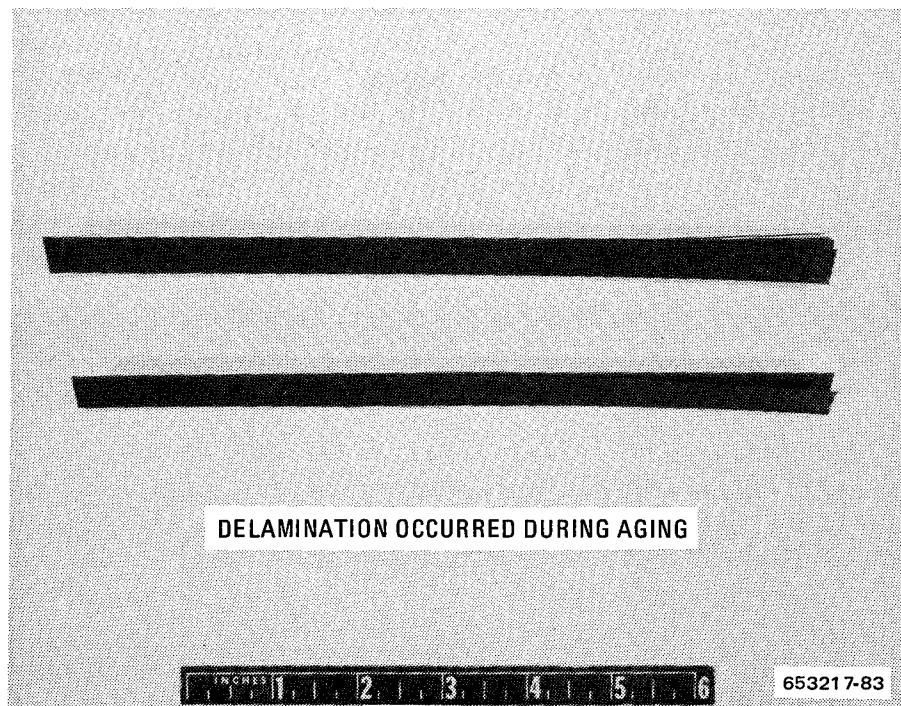


Figure 8-12 Crossplied B/E After 10,000 hr of Thermal Aging at 450 K (350° F) in 1 atm Air

microscope (metallograph) and scanning electron microscope (SEM). These studies were intended to detect changes that occurred in the composites during exposure in order to assist in identifying degradation mechanisms. Additional examinations were conducted of the fractured surfaces (primarily with the SEM) to determine failure modes and to further study the degradation processes.

Figure 8-14 shows photomicrographs of G/E aging specimens using a metallograph and a SEM at 100X and 500X magnifications. These pictures are for 10,000 hours exposure at 450 K (350° F) and 0.014 MN/m² (2 psi) pressure. Close examination of these photomicrographs shows only surface changes in the resin and some cracking, which probably occurred during post exposure tensile testing. Some of the cracks are located at boundaries between lamina and others within a particular lamina, as shown in the upper two photomicrographs. The lighter cast at the specimen edges in the SEM pictures will be shown later to be oxidation. Here it has occurred only at the surfaces exposed to oxygen.

The pictures in Figure 8-15 taken at 100X with the metallograph show good examples of how oxidation of the epoxy resin can proceed inward as a function of time and temperature. The upper pictures show that there is little difference between the as-received material and that aged for 10,000 hours at 394 K (250° F) in one atmosphere air. The lower pictures, on the other hand, show extensive degradation in the outside plies after 5000 hours at 450 K (350° F), and considerable degradation in both the inner and outer layers after 10,000 hours. The SEM pictures in Figure 8-16 taken from the same specimens show the identical effects, but even more clearly than the metallographic pictures. For example, the slight amount of surface oxidation after 10,000 hours at 394 K (250° F) is easily distinguished in the SEM photograph in Figure 8-16, while scarcely visible in Figure 8-15.

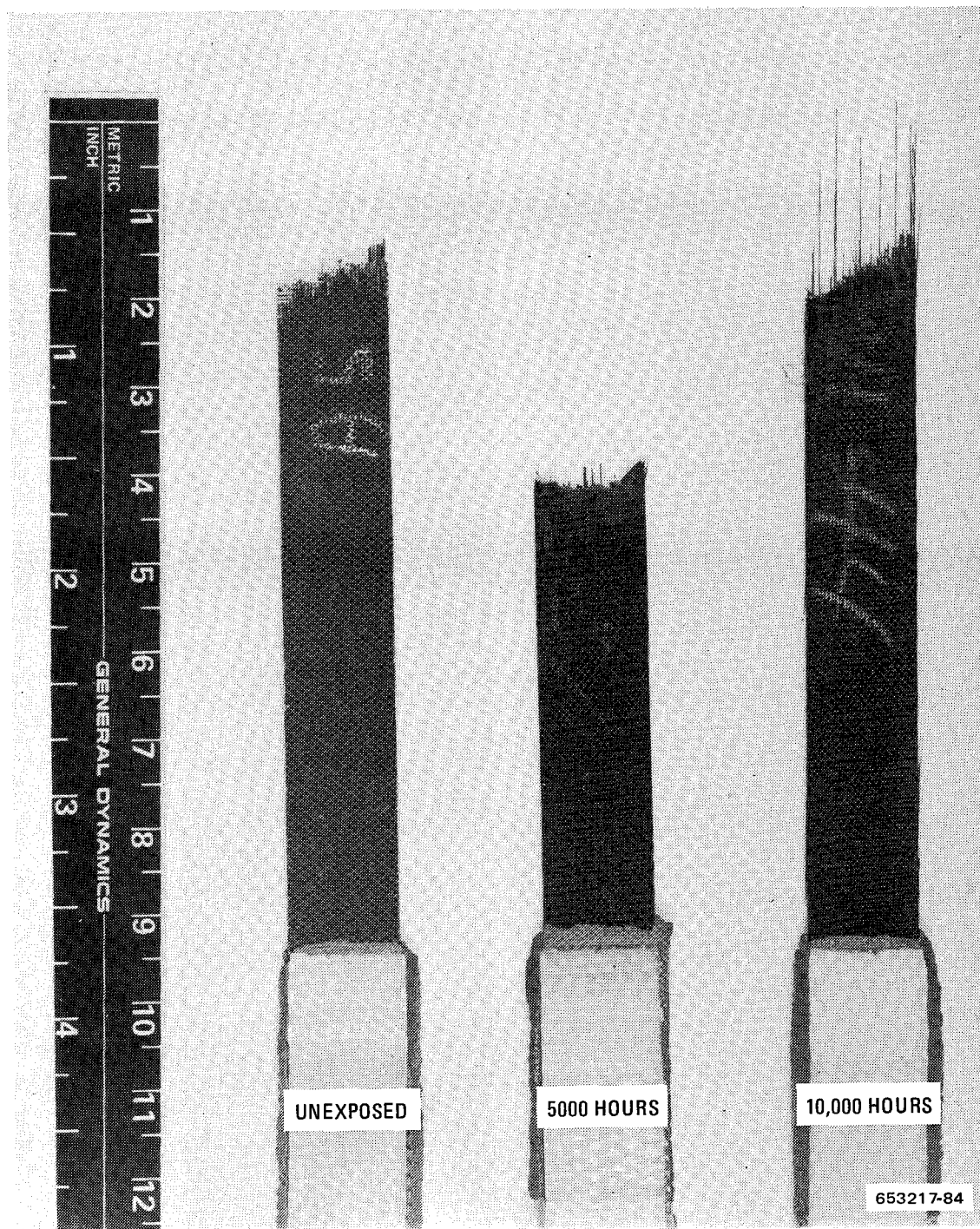
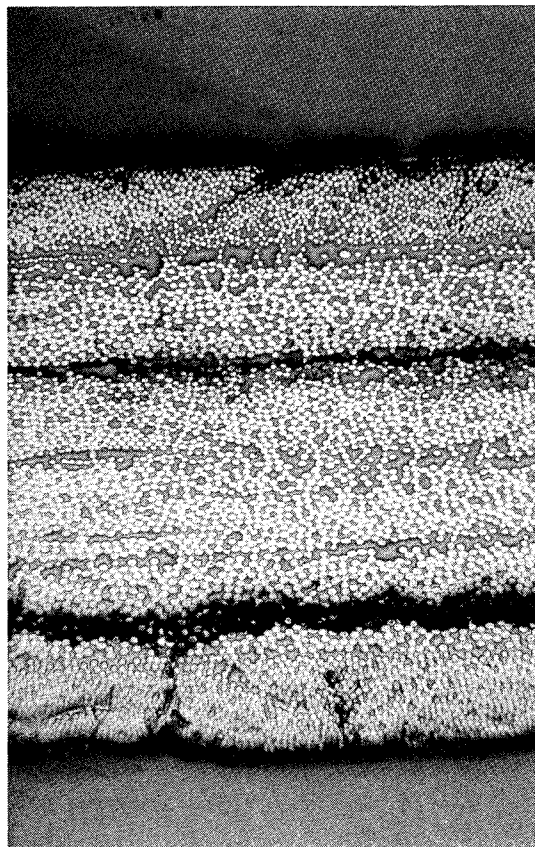
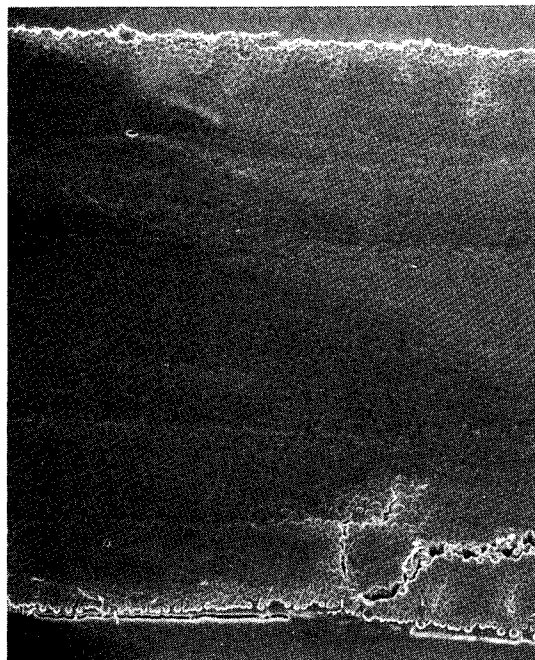


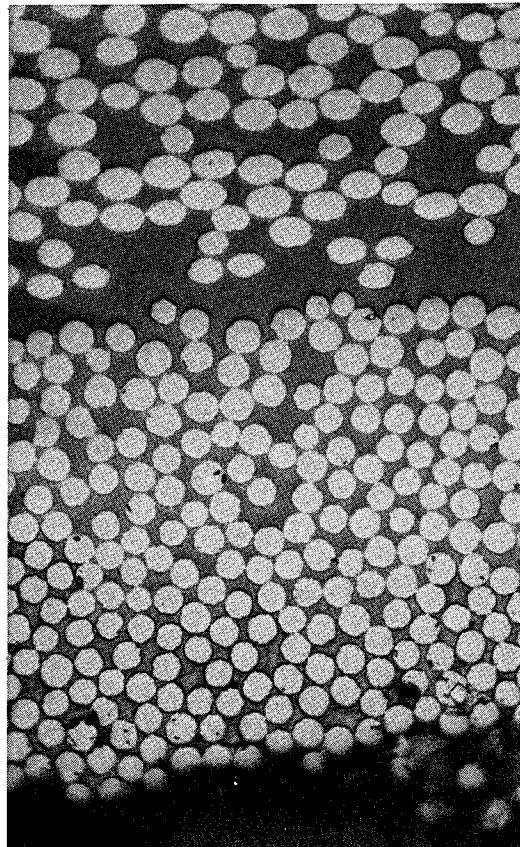
Figure 8-13 B/E Before and After Thermal Aging at 450 K (350° F) in 0.014 MN/m² (2 psi) Air and Tensile Testing at the Same Temperature



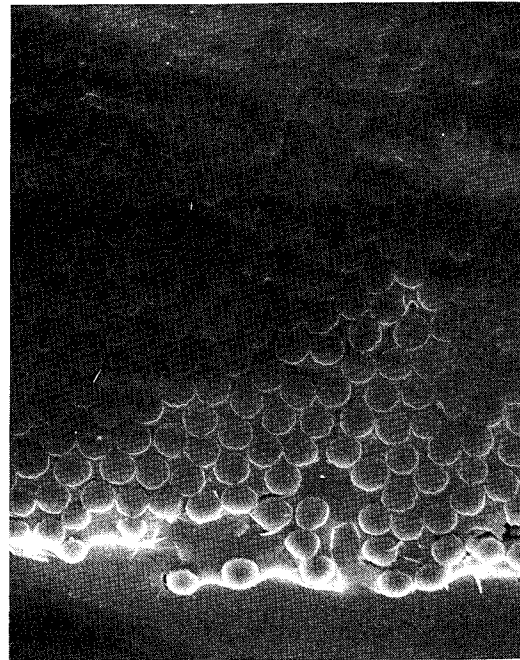
100X (METALLOGRAPH)



100X (SEM)



500X (METALLOGRAPH)

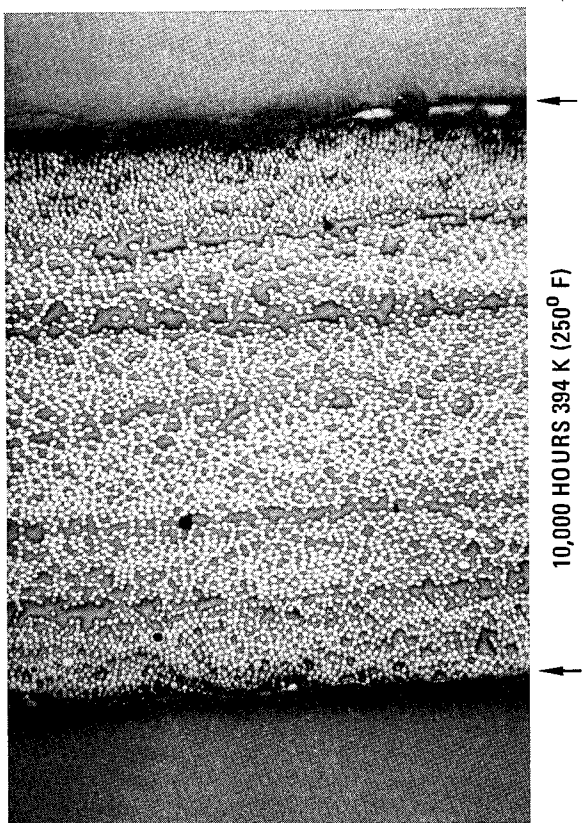


500X (SEM)

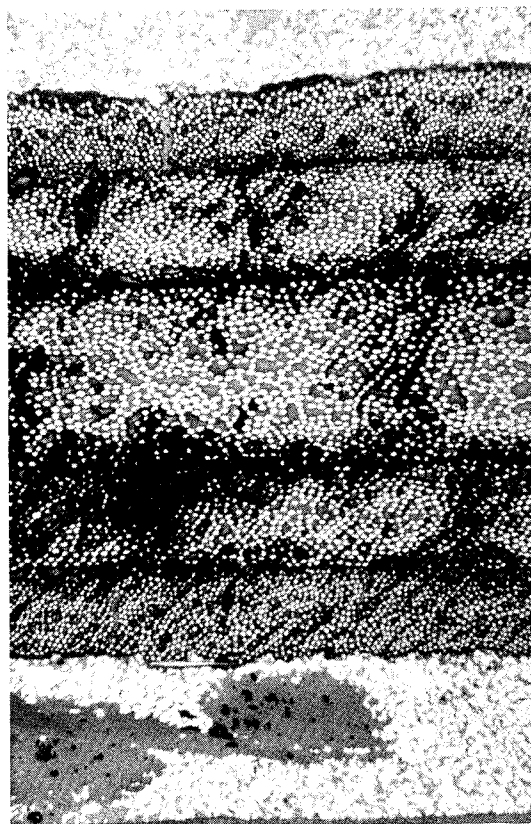
ARROWS INDICATE SPECIMEN EDGES

653217-85

Figure 8-14 Photomicrographs of G/E After Thermal Aging at 450 K (350° F) in 0.014 MN/m² (2 psi) Air for 10,000 hr



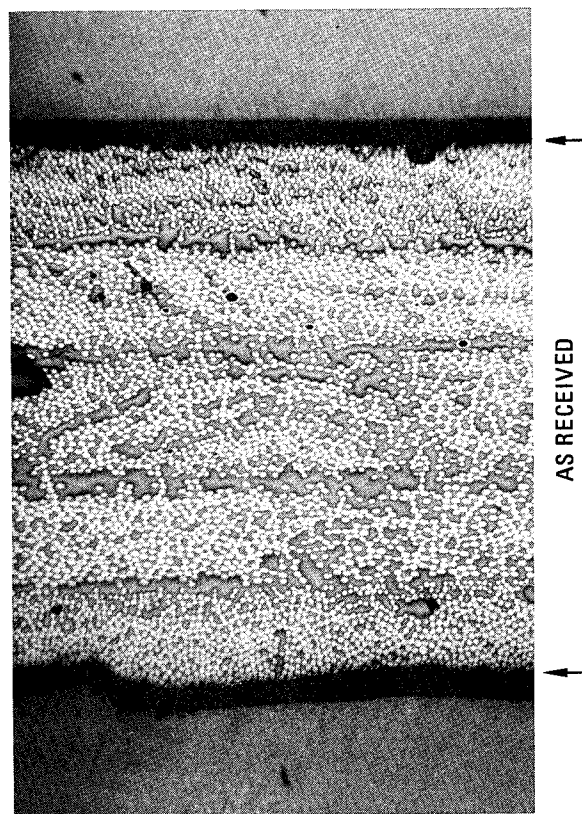
↑ 10,000 HOURS 394 K (250° F) ↑



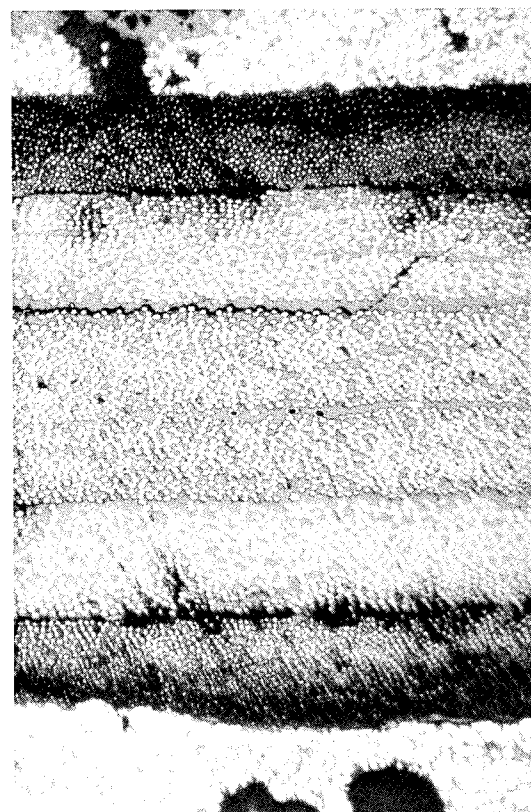
↑ 10,000 HOURS 450 K (350° F) ↑

ARROWS INDICATE SPECIMEN EDGES

653217-86

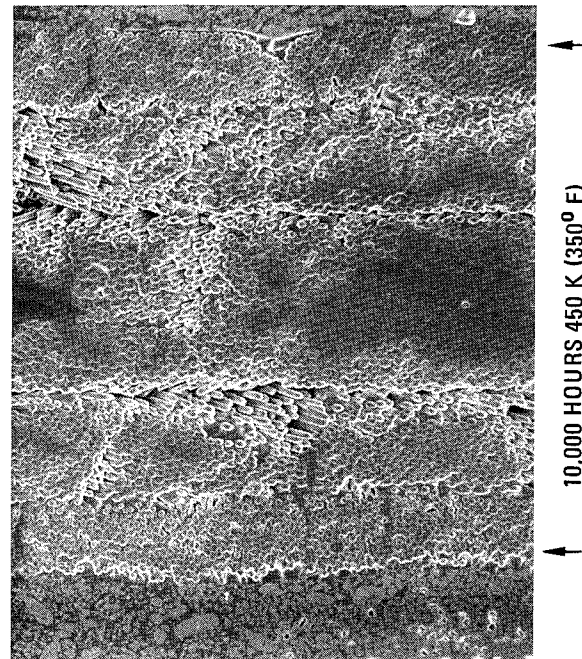
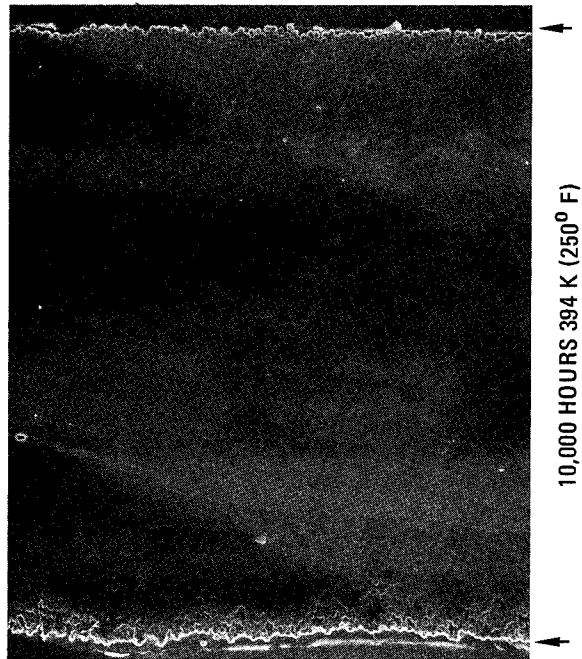
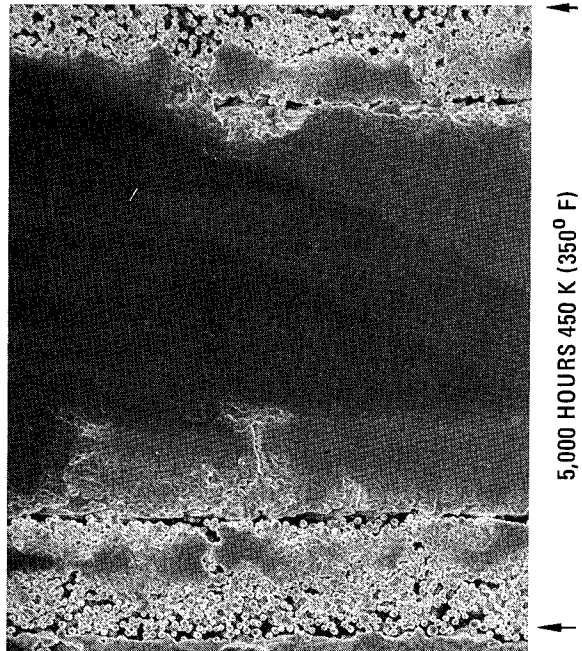
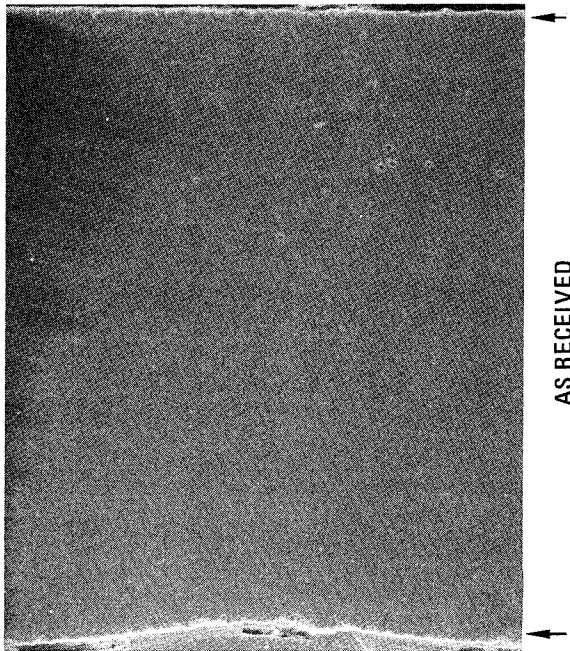


↑ AS RECEIVED ↑



↑ 5,000 HOURS 450 K (350° F) ↑

Figure 8-15 Photomicrographs (Metallograph) of G/E After Thermal Aging in One Atmosphere Air at Indicated Temperature. 100X



ARROWS INDICATE SPECIMEN EDGES

Figure 8-16 Photomicrographs (SEM) of G/E After Thermal Aging in One Atmosphere Air at Indicated Temperature. 100X

653217-87

The changes from light to dark for pictures taken using the metallograph and dark to light using the SEM are explained by the amount of relief polishing around the individual fibers that increases with the degree of oxidation. When the epoxy resin oxidizes, it is more prone to crumble, and differences in the amount of oxidation in the polished mounts can easily be detected using the SEM at higher magnifications.

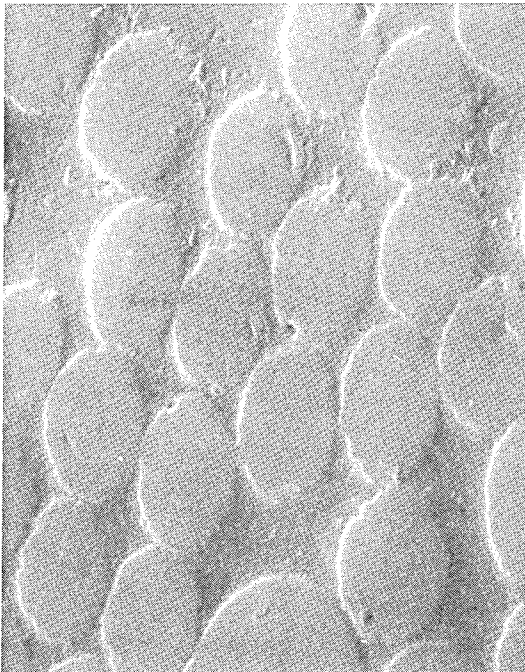
Figure 8-17 shows typically how this occurs. The as-received specimen has little and uniform relief for all plies as shown at 2500X using the SEM to examine a typical polished surface. The inner plies of a specimen aged for 10,000 hours at 394 K (250° F) look much the same except for the filaments being oriented at 45° to the surface. If one moves to the outer ply, the relief has increased as shown at the lower right of Figure 8-17. This effect becomes more pronounced for specimens aged at 450 K (350° F) and 10,000 hours as shown in the lower left picture. The magnification was lowered to a 1000X for clarity.

8.2.1.2 Fractographs. In addition to the metallographic cross sectional examinations, a study was also made of the fracture surfaces of several of the specimens. Examples are presented in Figures 8-18 and 8-19. Typical fractographs of G/E unaged and aged at 394 K (250° F) and ambient pressure for 10,000 hours are shown in the upper portion of Figure 8-18. As might be predicted from the tensile results, the appearance of the fracture surfaces are very similar for the two specimens. The matrix is relatively intact and there is little fiber pullout. For specimens aged at 450 K (350° F) and ambient pressure for either 5000 or 10,000 hours, it was not possible to get a good SEM picture of the fracture. The very brittle resin had crumbled away from the filaments in the area of the fracture so that only a few filament ends would have appeared in the field of view.

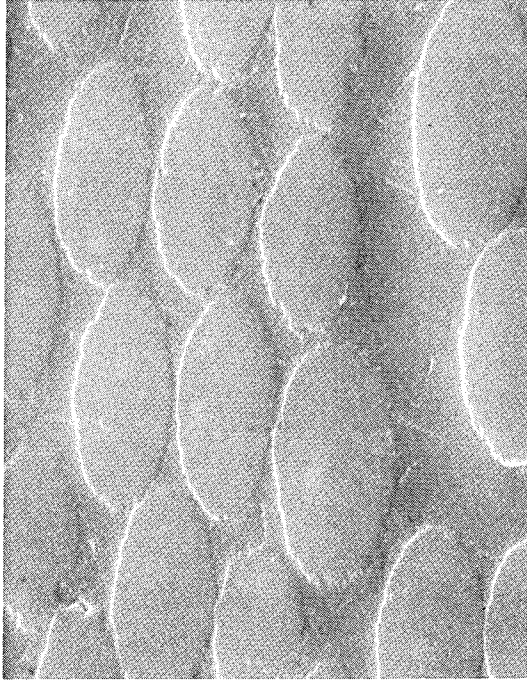
The pictures in the lower portion of Figure 8-18 show some of the filaments near the fracture locations in specimens aged at 450 K (350° F). The filaments are quite different in appearance than those in the upper two photographs in the amount of resin adhering to the surface. The presence of this much resin on the graphite filaments indicates a severe degradation of the epoxy matrix, which accounts for the failure within the matrix rather than at the fiber/resin interface.

An interesting example of the gradient of oxidation into the specimens is illustrated in the fractographs of Figure 8-19. These pictures were taken from areas near the surface of specimens aged at 394 K (250° F) and ambient pressure and at 450 K (350° F) and reduced pressure. As shown in Figure 8-14 and 8-16, only a slight amount of oxidation (only at the outer surfaces) had occurred in these specimens in 10,000 hours. In Figure 8-19 the depth to which the oxidation had progressed is readily visible. The resin near the outer surface has been embrittled by oxidation and has broken away from the filaments during tensile testing. Deeper into the specimen the fracture surface more closely resembles that of an unaged specimen.

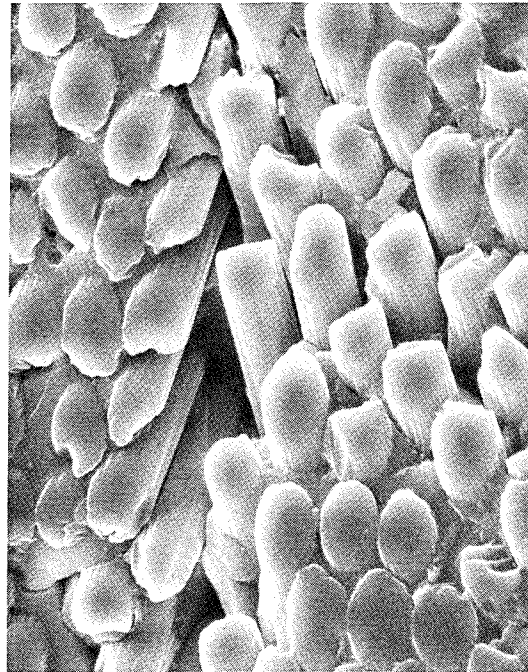
8.2.1.3 Glass Transition Temperature Studies. Further studies of the changes in the epoxy resin were made by measuring the glass transition temperature (T_g) of small samples cut from the G/E thermal aging specimens. These tests were performed using a DuPont 942 Thermomechanical Analyzer module in conjunction with a DuPont 990 Thermal Analyzer. The results are tabulated in Table 8-8. For aging at 394 K (250° F) no change was observed for aging times out to 10,000 hours, in agreement with the tensile results. For the reduced pressure, 0.014 MN/m² (2 psi), exposures at 450 K (350° F), however, significant increases in T_g were found. These changes in the resin were not detected by either the mechanical property tests or microscopic



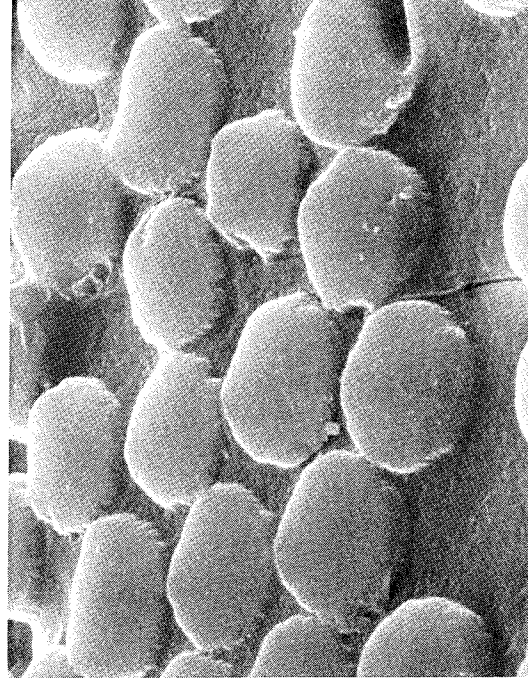
AS RECEIVED (2500X) ANY PLY



10,000 HOURS 394 K (250° F) (2500X) INNER PLY



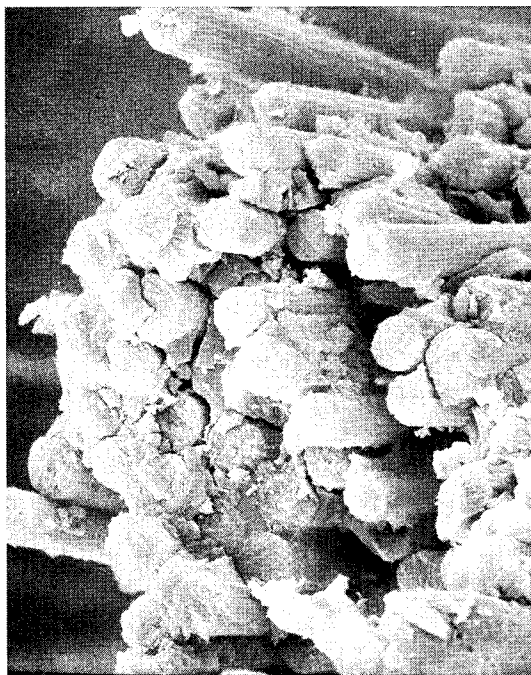
10,000 HOURS 450 K (350° F) (1000X)
INNER PLIES



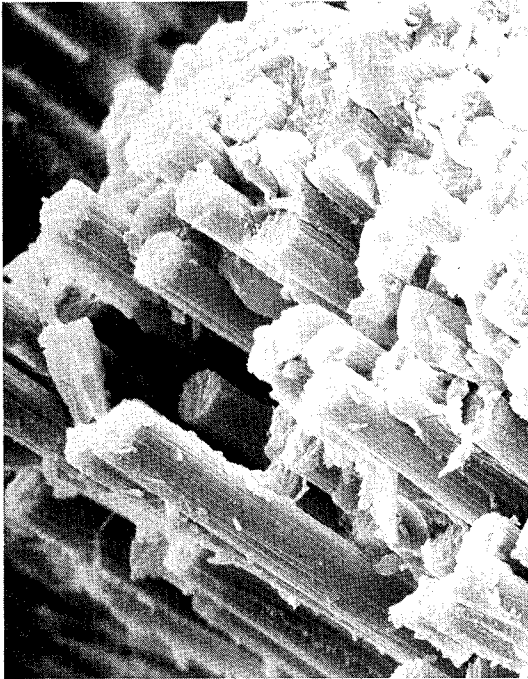
10,000 HOURS 394 K (250° F) (2500X)
OUTSIDE PLY

653217-88

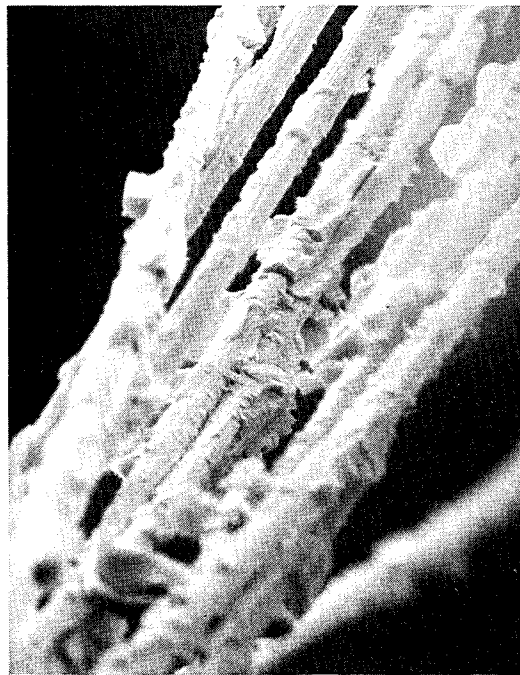
Figure 8-17 Photomicrographs (SEM) of G/E After Thermal Aging in One Atmosphere Air at Indicated Temperature



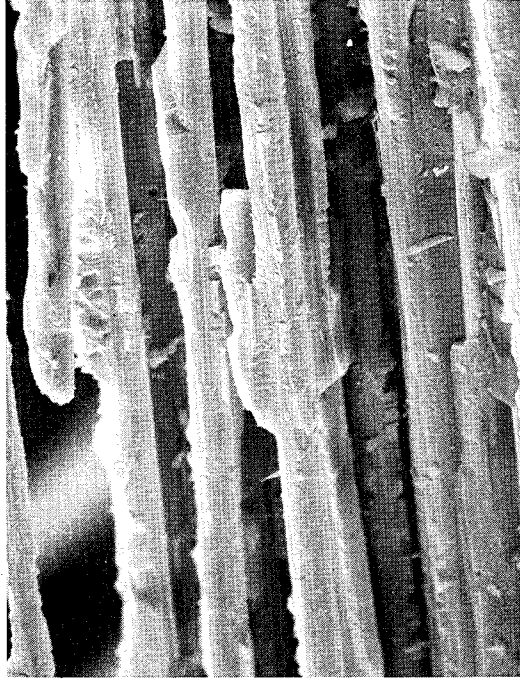
AS RECEIVED TESTED AT 450 K (350° F) (900X)



10,000 HOURS 394 K (250° F) (1000X)



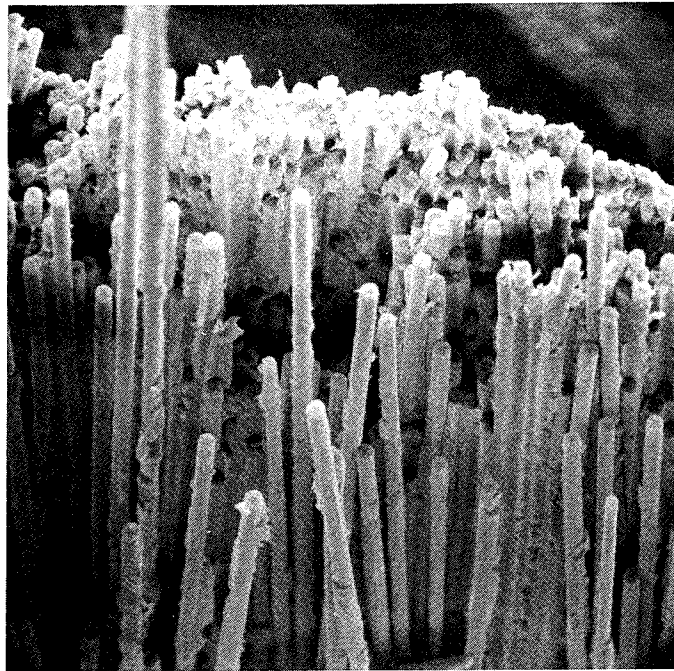
5,000 HOURS 450 K (350° F) (500X)



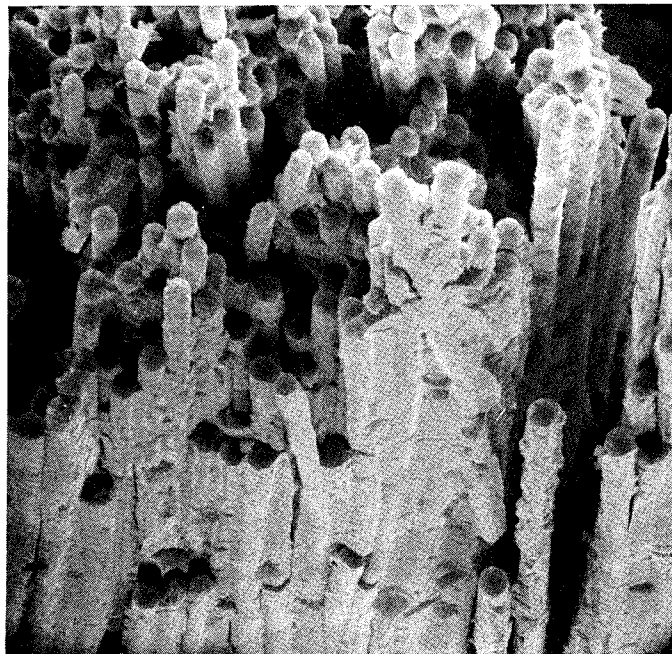
10,000 HOURS 450 K (350° F) (600X)

653217-89

Figure 8-18 SEM Fractographs of G/E After Thermal Aging in One Atmosphere Air at Indicated Temperature



10,000 HOURS 394 K (250° F), 101 kN/m² (14.7 psi)
(250X)



10,000 HOURS 450 K (350° F), 13.8 kN/m² (2 psi)
(400X)

653217-90

Figure 8-19 SEM Fractographs of G/E (Surface of Specimen Toward Viewer)

examinations. No measurements could be made on the 5000-hour and 10,000-hour specimens aged at ambient pressure and 450 K (350° F) because of the damage that occurred during tensile testing. The full significance of the changes in the T_g values and their relationship to the changes in the resin systems during aging are not clearly understood at this time. It is hoped, however, that this analytical technique will assist in the study of the processes that take place during elevated temperature exposure.

Table 8-8. Glass Transition Temperature, T_g , Data for $[0^\circ \pm 45^\circ]_s$ G/E

Condition	Aging Temperature K	(°F)	Aging Pressure MN/m ²	(psi)	Aging Time (hr)	T_g K	(°F)
As-Received						463	374
Aged	394	250	0.10	14.7	5,000	463	374
Aged	394	250	.10	14.7	10,000	464	375
Aged	450	350	.014	2	5,000	490	422
Aged	450	350	.014	2	10,000	505	449
Aged	450	350	.10	14.7	5,000	(a)	(a)
Aged	450	350	.10	14.7	10,000	(a)	(a)
Flight Simulation	408	275	.10	14.7	4,500	498	436

^aSpecimens were unsuitable for T_g determination

The last entry in Table 8-8 is for a flight simulation specimen (aging plus random fatigue loading) which failed in approximately 4500 hours, see Section 12. The rather large increase in T_g obtained from this specimen is the first indication that the combined effects of heat and load may be much larger than one would predict.

8.2.2 GRAPHITE/POLYIMIDE. Residual tensile strength data for the G/PI system are presented in Tables 8-9 and 8-10 for aging at ambient pressure and Table 8-11 for aging at reduced pressure. Aging was carried out at 505 K (450° F) and 561 K (550° F) for both unidirectional and $[0^\circ \pm 45^\circ]_s$ crossplied specimens. Residual tensile strength testing was performed at the same temperatures that were used for the thermal aging exposures. The tensile data have been plotted as a function of aging time and are presented in Figure 8-20 and 8-21. A summary of the effects of 10,000 hours of thermal aging on the tensile strength retention of G/PI is shown in Table 8-12.

In like manner to the epoxy systems the G/PI material exhibited very little decrease in tensile strength at the lower aging temperature, 505 K (450° F), but significant decreases at the higher temperature, 561 K (550° F). These decreases were observed as early as 200 hours for the 561 K (550° F) specimens aged at ambient pressure. Although the strength decreases were quite large, very little change in the appearance of the specimens was observed. The color and surface texture remained almost unchanged after 10,000 hours at both aging temperatures.

Table 8-9. Thermal Aging Data for $[0^\circ]_6$ G/PI in 0.10 MN/m^2 (14.7 psi) Air

Aging Temperature K (°F)		Test Temperature K (°F)		Aging Time (hr)	Tensile Strength MN/m^2 (ksi)	
505	450	505	450		Baseline avg	1210 176
				500		827 120
						752 109
						758 110
					avg	779 113
				1,000		1210 175
						990 144
						1370 198
					avg	1190 172
				5,000		1190 173
						1420 206
						1240 180
					avg	1280 186
				10,000		1280 185
						1390 201
						1350 196
					avg	1340 194
561	550	561	550		Baseline avg	1320 191
				200		1290 187
						1280 185
						1350 196
					avg	1310 189
				500		1170 170
						1300 189
						1200 174
					avg	1220 178
				1,000		1100 159
						1170 169
						1190 173
					avg	1150 167
				5,000		1170 169
						1070 155
						1010 147
					avg	1080 157
				10,000		1117 162
						876 127
						807 117
					avg	933 135

Table 8-10. Thermal Aging Data for $[0^\circ \pm 45^\circ]_s$ Crossply G/PI in 0.10 MN/m² (14.7 psi) Air

Aging Temperature K (°F)		Test Temperature K (°F)		Aging Time (hr)	Tensile Strength MN/m ² (ksi)						
505	450	505	450		Baseline avg	470 68.2					
					1,000		521 75.5				
							443 64.3				
						328 47.5					
					avg	431 62.4					
					5,000		435 63.1				
							501 72.6				
						576 83.5					
					avg	504 73.1					
					10,000		335 48.6				
							525 76.2				
						454 65.9					
					avg	438 63.6					
					561	550	561	550		Baseline avg	434 63.0
										1,000	
	474 68.7										
	394 57.1										
	avg	437 63.3									
	5,000		276 40.0								
			276 40.0								
		258 37.4									
	avg	270 39.1									
	10,000		192 27.8								
			211 30.6								
		274 39.7									
	avg	226 32.7									

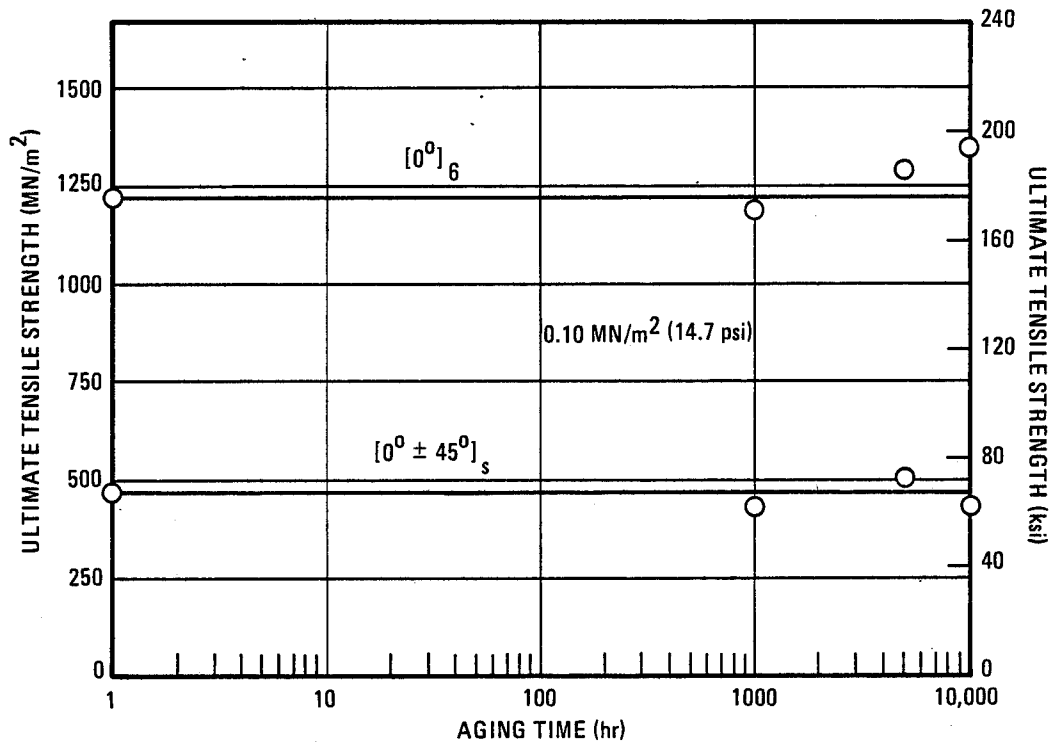
slight edge cracks appeared after 1000 hours at 561 K (550° F) and 5000 hours at 505 K (450° F). After 5000 hours at 561 K (550° F) both the ambient and reduced pressure specimens had some small spots on the surface that could not be accounted for. At 20X magnification the small spots had a somewhat charred appearance. Neither the small spots nor the slight edge cracks were believed to be detrimental, and aside from these the specimens were not appreciably different in appearance from the unexposed material. Portions of failed tensile specimens before and after exposure at the two aging temperatures and pressures are shown in

Table 8-11. Thermal Aging Data for G/PI Aged in 0.014 MN/m² (2 psi) Air

Aging Temperature K (°F)		Orientation	Test Temperature K (°F)		Aging Time (hr)	Tensile Strength MN/m ² (ksi)	
505	450	[0°] ₆	505	450		Baseline avg	1210 176
							1370 198
							1210 175
							1480 215
					5,000	avg 1350	196
							1280 185
							1140 166
							1180 171
						avg 1200	174
					10,000		1320 191
							1300 188
							980 142
							1300 188
561	550	[0°] ₆	561	550		Baseline avg	1320 191
							1300 188
							980 142
							1300 188
					5,000	avg 1190	173
							1060 154
							1010 146
							970 140
					10,000	avg 1010	147

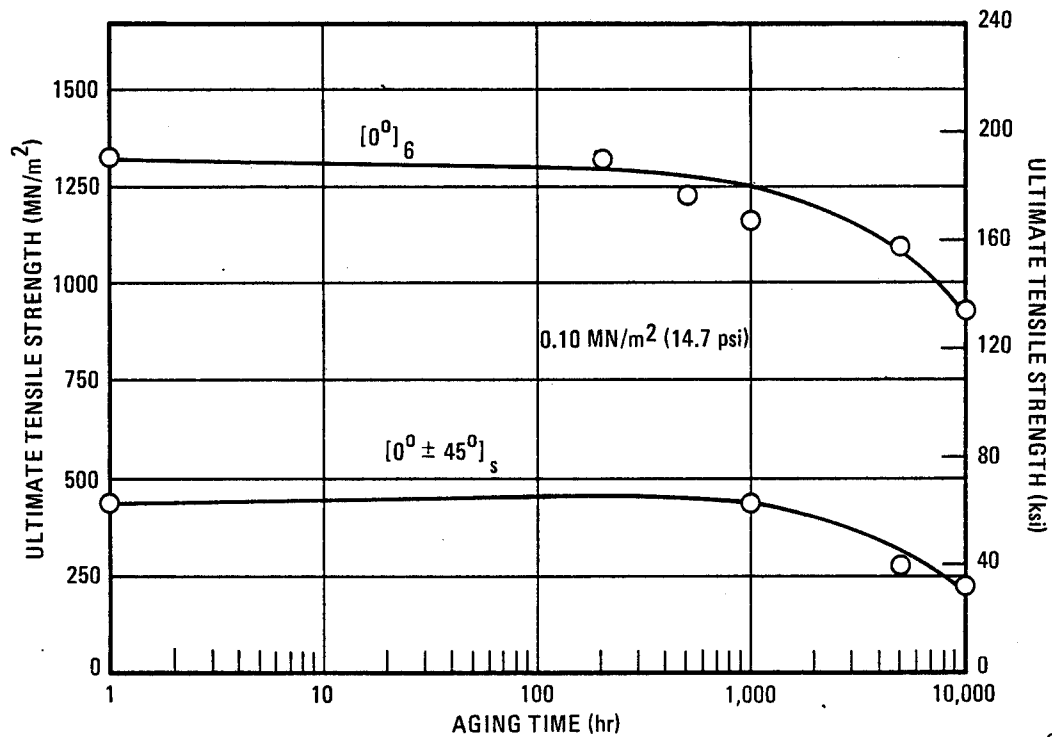
Table 8-12. Summary of Tensile Strength Retention After 10,000 Hours of Thermal Aging for G/PI

Orientation	Aging Temperature K (°F)		Aging Pressure MN/m ² (psi)		Test Temperature K (°F)		Retention of Tensile Strength (%)
[0°] ₆	505	450	0.10	14.7	505	450	100
[0° ± 45°] _s	505	450	.10	14.7	505	450	93
[0°] ₆	505	450	.014	2	505	450	99
[0°] ₆	561	550	.10	14.7	561	550	71
[0° ± 45°] _s	561	550	.10	14.7	561	550	52
[0°] ₆	561	550	.014	2	561	550	77



653217-91

Figure 8-20 Tensile Strength of G/PI at 505 K (450° F) After Thermal Aging at the Same Temperature



653217-92

Figure 8-21 Tensile Strength of G/PI at 561 K (550° F) After Thermal Aging at the Same Temperature

Figures 8-22 to 8-25. Aside from a few of the small spots that are barely visible on the 5000-hour and 10,000-hour, 561 K (550° F) specimens, no difference is apparent in either the appearance of the specimen or the failure mode as a result of the exposure.

There was one group of three specimens that gave unusually poor results. These were the unidirectional specimens aged for 500 hours at 505 K (450° F). Residual strength values were obtained that were considerably lower than either the unexposed material or the specimens aged for 1000 hours, 5000 hours, or 10,000 hours. Examination of the broken specimens and the test data, as well as careful review of the specimen preparation and test procedures failed to reveal the cause of this anomaly. Because the 500-hour data appeared to be in error, they were not included on the aging plot in Figure 8-20.

No significant reductions in the average 505 K (450° F) tensile strengths were observed for the G/PI system after a 10,000-hour thermal age at 505 K (450° F) in ambient air. One of the crossplied specimens gave a low value, but the other two were quite high and their average was approximately 93% of the unexposed material. The unidirectional specimens actually showed an increase in strength after aging in one atmosphere air. Aging at the reduced pressure of 0.014 MN/m² (2 psi) had essentially no effect on the tensile strength. The specimens aged for 10,000 hours at 561 K (550° F) exhibited a decrease in strength of about one-third when aged at 0.10 MN/m² (14.7 psi) and about one-fourth for the reduced pressure exposures. In summary of these data, HT-S/710 graphite/polyimide should be limited to 505 K (450° F) for exposures greater than 10,000 hours because of loss of residual tensile strength during thermal aging.

Metallographic and SEM examinations were conducted on G/PI specimens before and after thermal aging exposures. Unlike the G/E material, the changes in appearance as a result of the thermal exposures were far less obvious. Figure 8-26 shows SEM photomicrographs of G/PI tensile specimens of unexposed material and material aged for 10,000 hours at 561 K (550° F) and 0.10 MN/m² (14.7 psi). While considerable porosity is visible in both photomicrographs, the amount observed in aged material was greater than unexposed material. Careful study of these and other specimens also indicated an increase in the amount of fibers that had separated from the matrix material after aging. When examined at higher magnification numerous, fine cracks were observed at the fiber-matrix interface in the aged material, Figure 8-27. None were found in the unexposed material, Figure 8-27. It was not determined whether these cracks appeared during aging or were the result of the tensile testing or polishing operations. Either way, they indicate the likelihood of the initiation of matrix embrittlement by oxidation during aging in a manner similar to that observed in the G/E system.

8.2.3 BORON/ALUMINUM. Thermal aging studies were conducted on unidirectional and $[0^\circ \pm 45^\circ]_s$ crossplied laminates of B/Al for time periods of 5000 and 10,000 hours. Exposures were carried out in one atmosphere air at temperatures of 450 K (350° F), 561 K (550° F), and 700 K (800° F). Following aging, residual tensile and interfiber shear tests were performed at room temperature. Longitudinal tensile strengths of the unidirectional and crossplied materials were determined to evaluate fiber degradation while transverse tensile and longitudinal shear properties of the unidirectional material were obtained to study matrix effects. The data from the various exposures are presented in Table 8-13 to 8-16. A summary of the effects of 10,000 hours of thermal aging on the strength retention of B/Al is given in Table 8-17. The tensile and shear strength data have also been plotted as a function of aging time. These curves are shown in Figures 8-28 to 8-30.

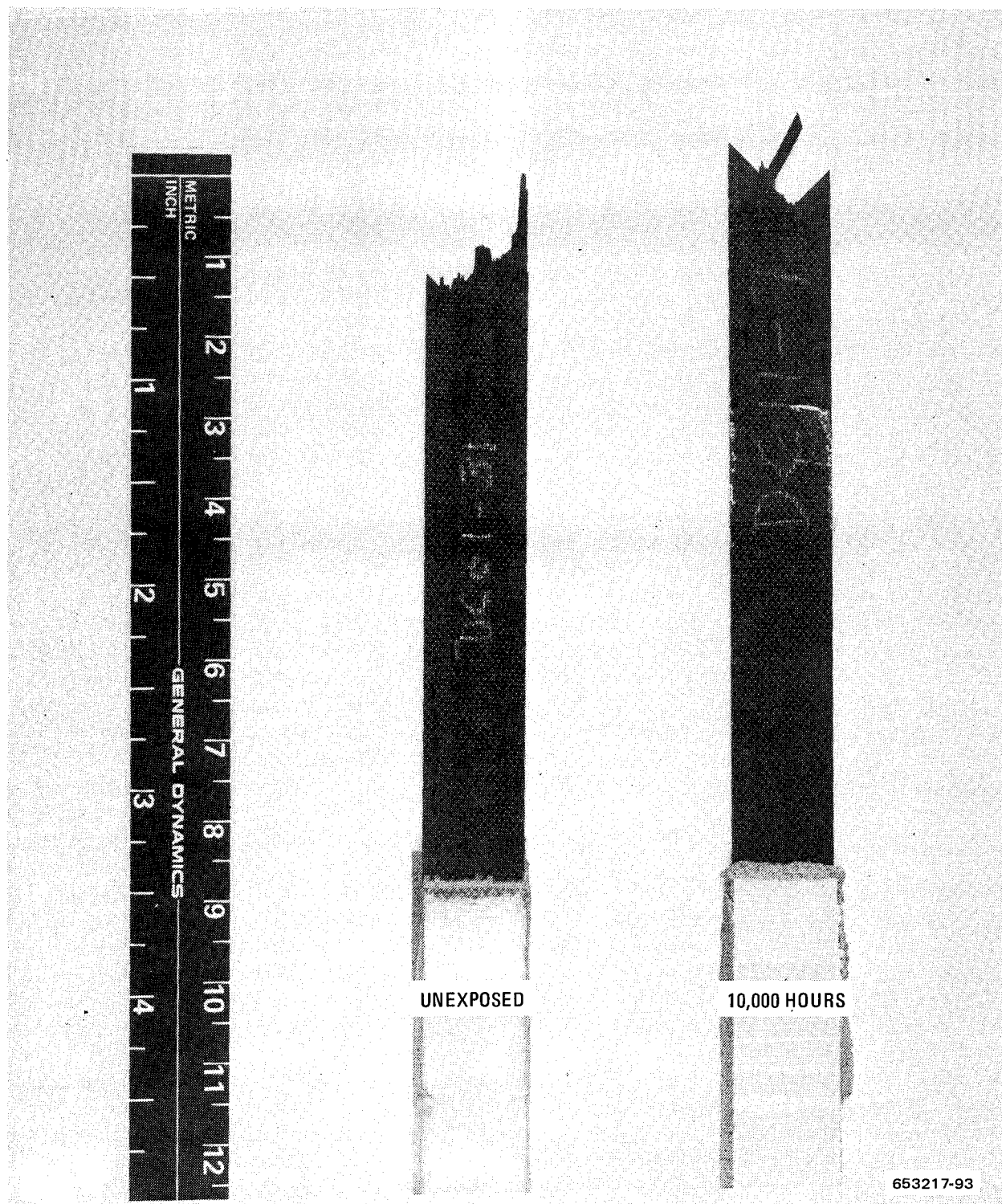


Figure 8-22 G/PI Before and After 10,000 hr of Thermal Aging at 505 K (450° F) in 1 atm Air and Tensile Testing at the Same Temperature

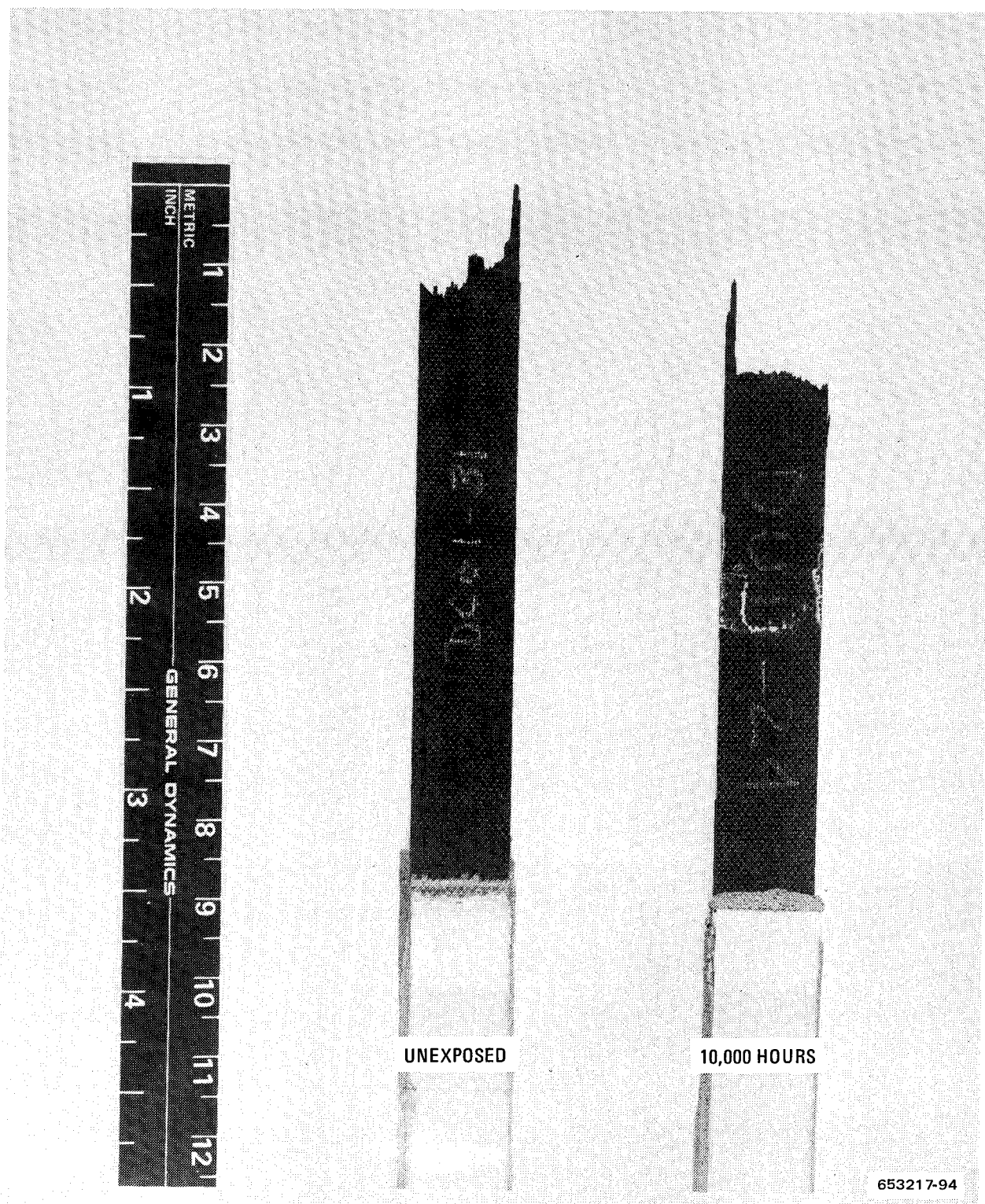


Figure 8-23 G/PI Before and After 10,000 hr of Thermal Aging at 505 K (450° F) in 0.014 MN/m² (2 psi) Air and Tensile Testing at the Same Temperature

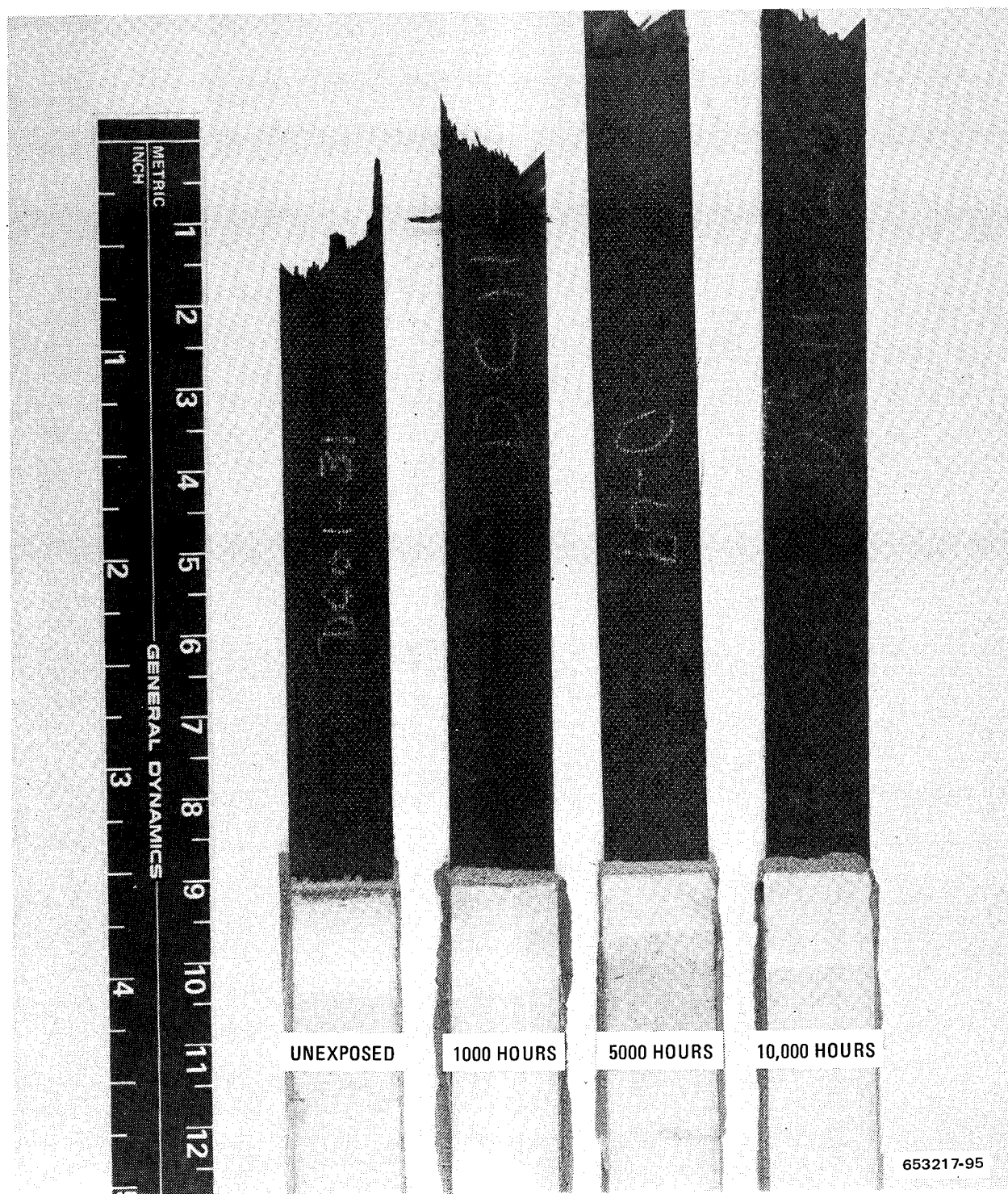


Figure 8-24 G/PI Before and After Thermal Aging at 561 K (550° F) in 1 atm Air and Tensile Testing at the Same Temperature

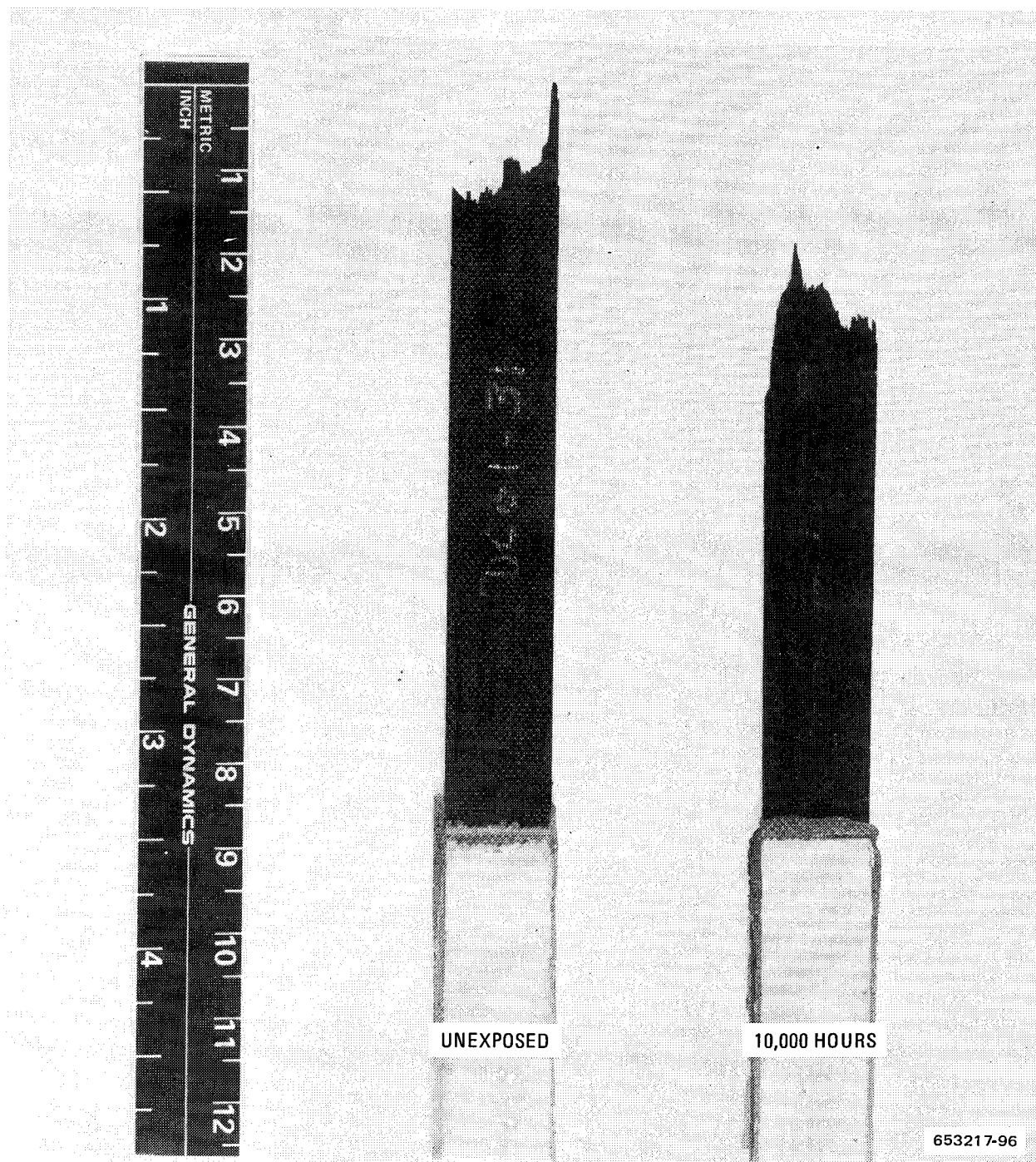
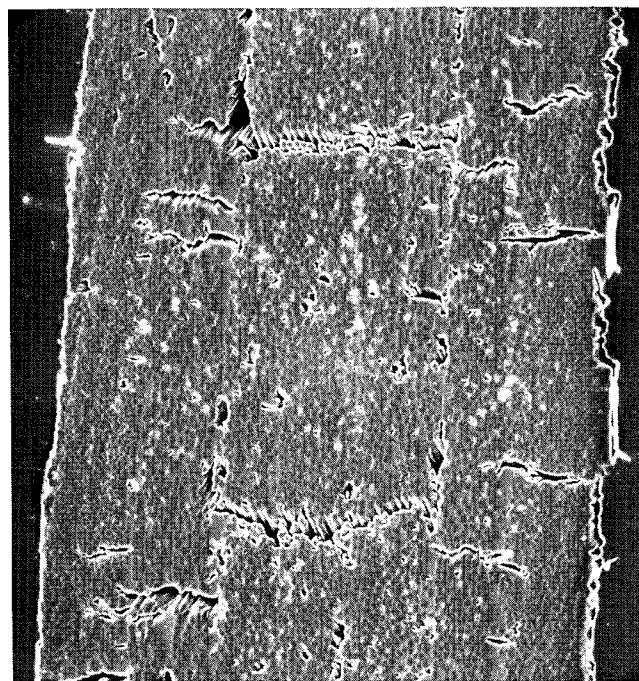
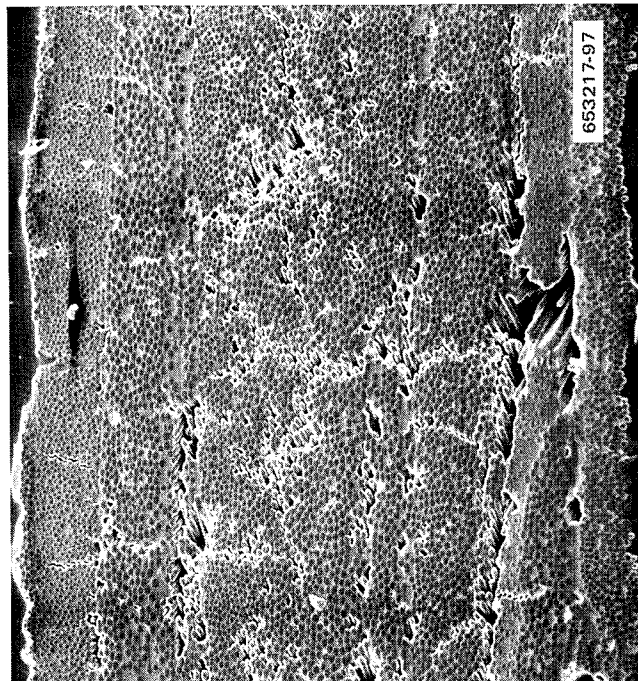


Figure 8-25 G/PI Before and After 10,000 hr of Thermal Aging at 561 K (550° F) in 0.014 MN/m² (2 psi) Air and Tensile Testing at the Same Temperature

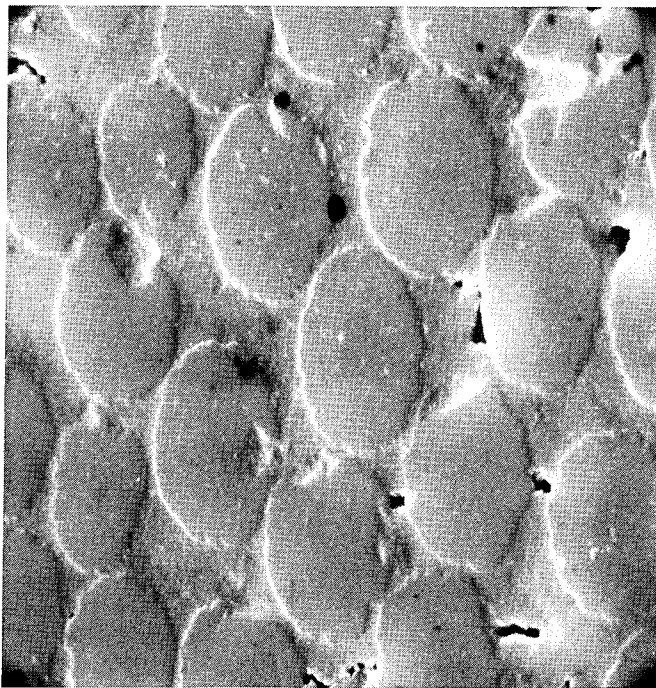


AS RECEIVED

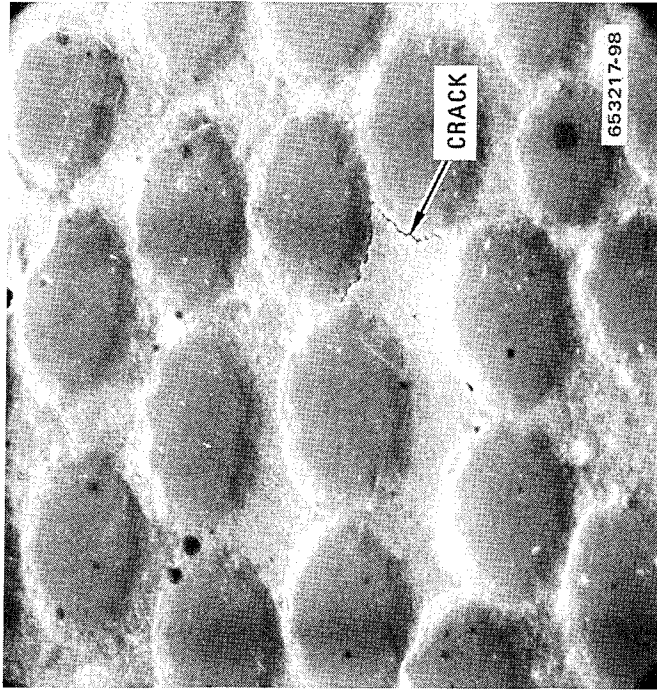


10,000 HOURS 561 K (550° F)

Figure 8-26 Photomicrographs (SEM) of G/PI After Thermal Aging in One Atmosphere Air at Indicated Temperature. 100X



AS RECEIVED



10,000 HOURS 561 K (550° F)

Figure 8-27 Photomicrographs (SEM) of G/PI After Thermal Aging in One Atmosphere Air at Indicated Temperature. 2500X

Table 8-13. Thermal Aging Data for $[0^\circ]_6$ B/Al Aged in One Atmosphere Air and Tested at 297 K (75° F) — Longitudinal Test Direction

Aging Temperature K (°F)		Aging Time (hr)	Tensile Strength MN/m ² (ksi)	
450	350	Baseline avg	1450	210
			1320	191
			1230	179
			1070	155
		5,000	avg 1210	175
			1010	146
			986	143
			869	126
		10,000	avg 955	138
			841	122
			855	124
			889	129
561	550	5,000	avg 862	125
			855	124
			703	102
			786	114
		10,000	avg 781	113
			327	47.4
			631	91.5
			315	45.7
		5,000	avg 424	61.5
			263	38.1
			320	46.4
			318	46.1
700	800	10,000	avg 300	43.5
			327	47.4
			631	91.5
			315	45.7
		5,000	avg 424	61.5
			263	38.1
			320	46.4
			318	46.1
		10,000	avg 300	43.5
			327	47.4
			631	91.5
			315	45.7

Table 8-14. Thermal Aging Data for $[0^\circ]_6$ B/Al Aged in One Atmosphere Air and Tested at 297 K (75° F) — Transverse Test Direction

Aging Temperature K (°F)		Aging Time (hr)	Tensile Strength MN/m ² (ksi)	
450	350	Baseline avg	79.3	11.5
		5,000	159	23.1
			143	20.7
			116	16.8
			avg 139	20.2
		10,000	104	15.1
			93.8	13.6
			121	17.5
			avg 106	15.4
561	550	5,000	98.6	14.3
			102	14.8
			104	15.1
			avg 102	14.7
		10,000	108	15.7
			74.5	10.8
			75.2	10.9
			avg 85.9	12.5
		5,000	104	15.1
			101	14.7
			94.5	13.7
			avg 100	14.5
700	800	10,000	80.0	11.6
			76.5	11.1
			100	14.5
			avg 85.5	12.4

Table 8-15. Thermal Aging Data for $[0^\circ]_6$ B/Al Aged in One Atmosphere Air and Tested at 297 K (75° F) — Interfiber Shear in Longitudinal Direction

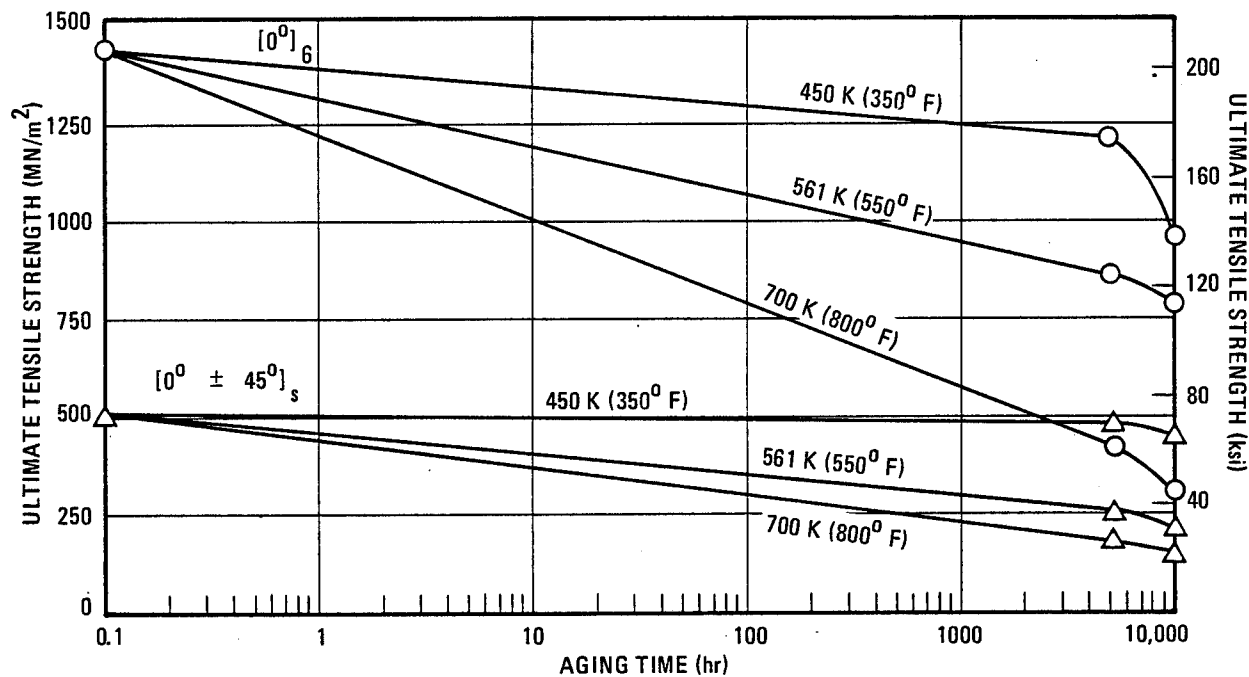
Aging Temperature		Aging Time (hr)	Tensile Strength	
K	(°F)		MN/m ²	(ksi)
450	350	Baseline avg	93.1	13.5
		5,000	82.0	11.9
			93.1	13.5
			109	15.8
			avg 94.7	13.7
		10,000	109	15.8
			100	14.5
			108	15.7
			avg 106	15.3
561	550	5,000	85.5	12.4
			93.8	13.6
			91.7	13.3
			avg 90.3	13.1
		10,000	97.2	14.1
			91.7	13.3
			91.0	13.2
			avg 93.3	13.5
700	800	5,000	42.1	6.1
			77.2	11.2
			79.3	11.5
			avg 66.2	9.6
		10,000	71.7	10.4
			18.6	2.7
			24.8	3.6
			avg 38.4	5.6

Table 8-16. Thermal Aging Data for $[0^\circ \pm 45^\circ]_s$ Crossplied B/Al Aged in One Atmosphere Air and Tested at 297 K (75° F) — Longitudinal Test Direction

Aging Temperature		Aging Time (hr)	Tensile Strength			
K	(°F)		MN/m ²	(ksi)		
450	350	Baseline avg	516	74.8		
		5,000	430	62.3		
			467	67.7		
			535	77.6		
			avg 477	69.2		
		10,000	459	66.6		
			444	64.4		
			428	62.1		
			avg 444	64.4		
561	550	5,000	276	40.1		
			251	36.4		
			257	37.3		
			avg 261	37.9		
		10,000	184	26.7		
			214	31.1		
			210	30.4		
			avg 203	29.4		
		700	800	5,000	168	24.4
					185	26.8
198	28.7					
avg 184	26.6					
10,000	142			20.6		
	143			20.7		
	154			22.3		
	avg 146			21.2		

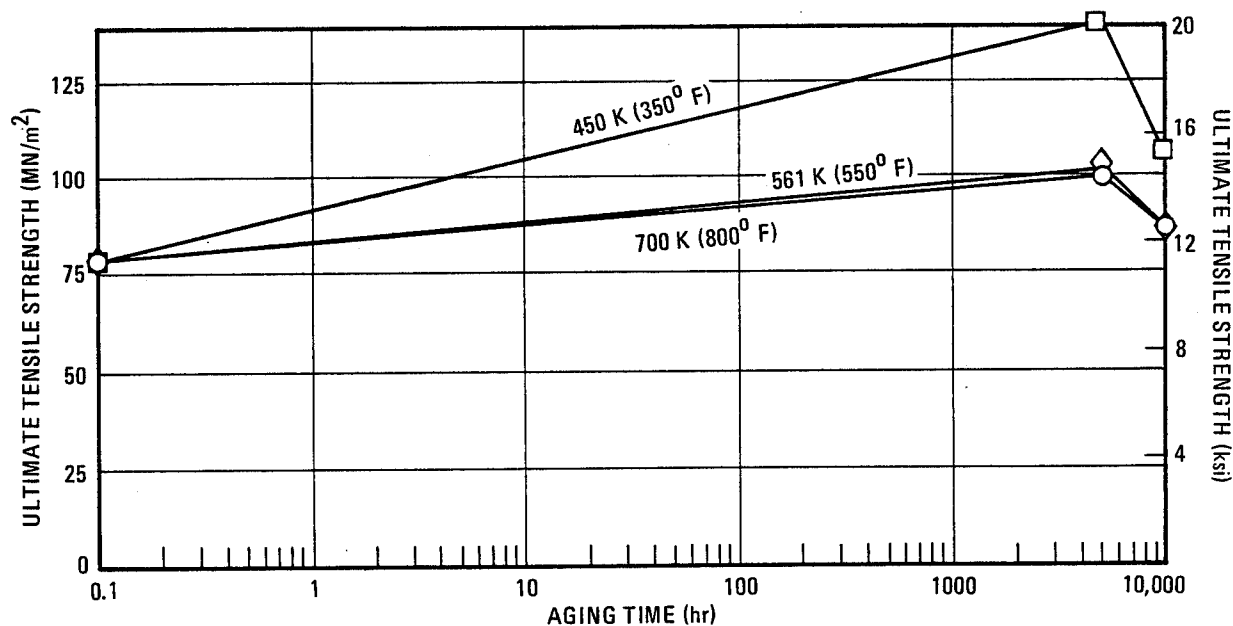
Table 8-17. Summary of Room Temperature Strength Retention After 10,000 Hours of Thermal Aging in One Atmosphere Air for B/Al

Laminate Orientation	Test Direction	Property	Strength Retention (%) After 10,000 Hours		
			450 K (350° F)	561 K (550° F)	700 K (800° F)
$[0^\circ]_6$	$[0^\circ]$	Tensile	66	54	21
$[0^\circ]_6$	$[90^\circ]$	Tensile	100	100	100
$[0^\circ]_6$	$[0^\circ]$	Shear	100	100	41
$[0^\circ \pm 45^\circ]_s$	$[0^\circ]$	Tensile	86	39	28



653217-99

Figure 8-28 Tensile Strength of B/Al at 297 K (75° F) After Thermal Aging at Indicated Temperature



653217-100

Figure 8-29 Transverse Tensile Strength of B/Al at 297 K (75° F) After Thermal Aging at Indicated Temperature

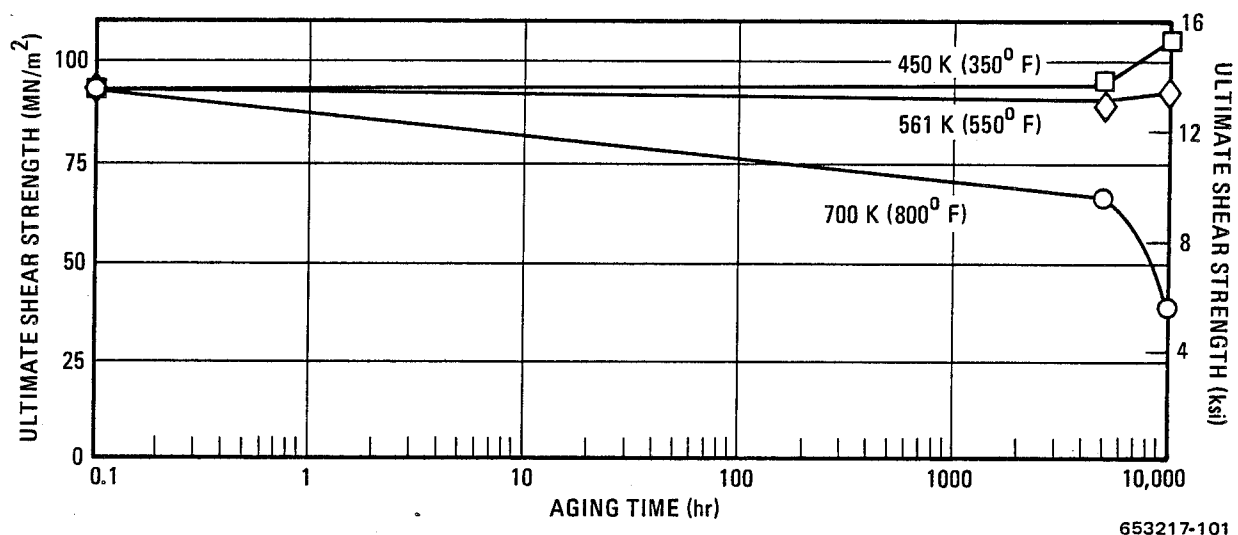


Figure 8-30 Shear Strength of Unidirectional B/Al at 297 K (75° F) After Thermal Aging at Indicated Temperature

At 561 K (550° F) and 700 K (800° F) extensive degradation was observed in the tensile strength of material tested in the 0° direction of both layups. These decreases were as high as 80% at 700 K (800° F) and 60% at 561 K (550° F). Decreases were also observed (particularly in the unidirectional material) at 450 K (350° F), although not as large. The physical appearance of the specimens was unchanged after 10,000 hours of aging at the two lowest temperatures. At the highest temperature, 700 K (800° F), some surface discoloration was observed. Of more importance, however, was oxidation and loss of the exposed ends of the boron fibers in the transverse tensile and interfiber shear specimens. Figure 8-31 is a SEM photomicrograph of the edge of a transverse tensile specimen that was aged for 5000 hours at 700 K (800° F). The boron fibers are oxidized to a depth of approximately 0.00064 m (0.025 in.). After 10,000 hours of aging, loss of the boron fibers extends to a depth of approximately 0.0015 m (0.06 in.). No oxidation of the boron was found in specimens aged at the other temperatures.

Because the notches in the interfiber shear specimens were fabricated prior to aging, oxidation of the boron filaments had a significant effect on the residual shear strength. At 450 K (350° F) and 561 K (550° F), where no oxidation was found, no decrease in shear strength was observed. However, at 700 K (800° F) decreases of 30 and 60% were measured after 5000 and 10,000 hours respectively. The machined edges at each end of the shearing regions were exposed to the air environment during aging and extensive oxidation of the boron occurred. This can be seen in the fracture surfaces of shear specimens shown in Figures 8-32 and 8-33. These figures show samples of B/Al after aging periods of 5000 and 10,000 hours and, for comparison, one that had not been exposed prior to shear testing. The length of the shear region is approximately 0.0025 m (0.10 in.) as shown in Figure 2-27. For the unexposed specimen, Figure 8-32, where no oxidation of the boron has occurred, the fracture surface is uniform along its length. The primary failure mode was matrix failure with some failure at the filament-matrix interface. In the specimen aged for 5000 hours at 700 K (800° F), Figure 8-32, loss of boron by oxidation is readily visible at either end of the sheared region. This attack extends for approximately 0.00064 m (0.025 in.) from each end and has consumed about half of the fiber length. With the

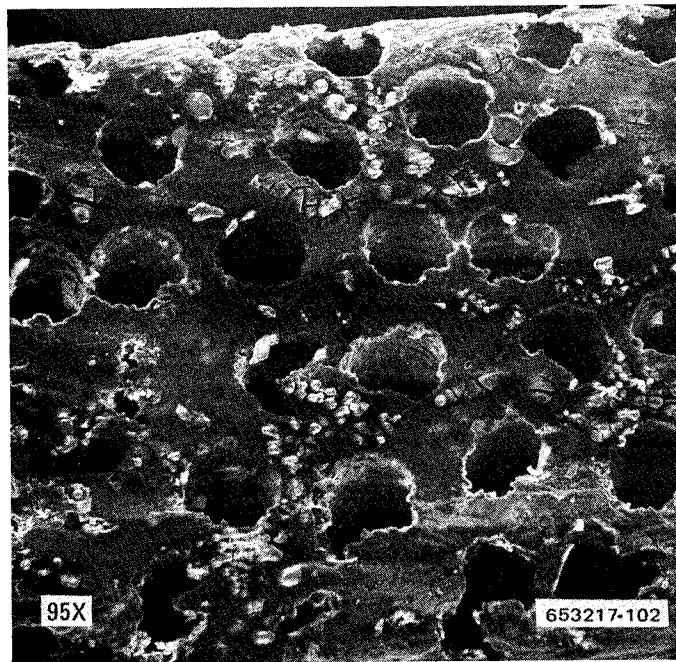
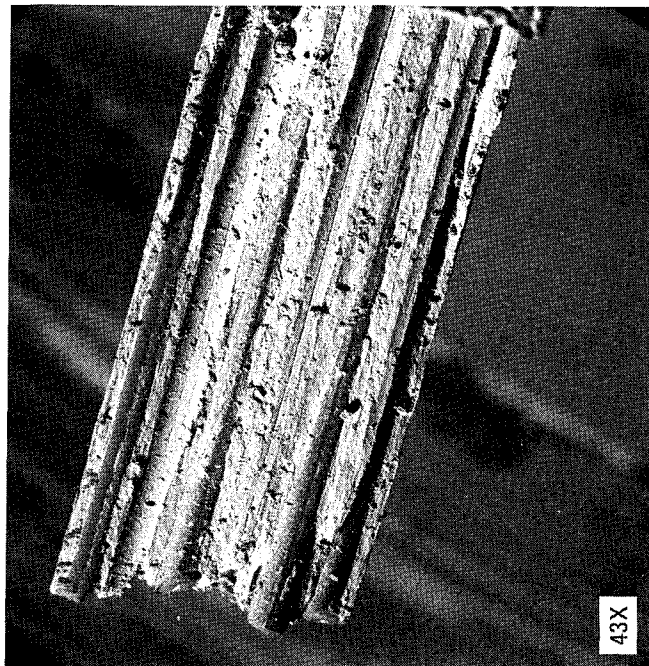


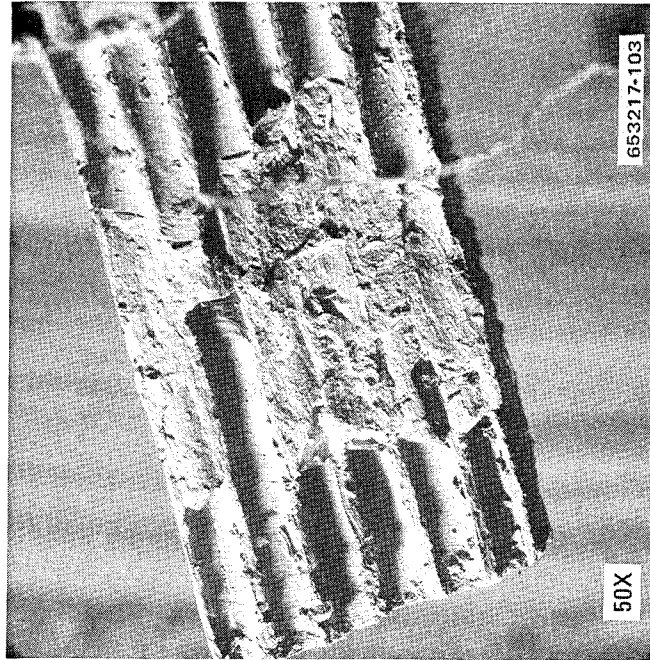
Figure 8-31 Edge View of B/Al After 5000 hr of Thermal Aging at 700 K (800° F) in 1 atm Air Showing Loss of Boron Through Oxidation

loss of the filaments the area over which fracture occurred was considerably reduced and the specimen had lower strength. The residual shear stress was calculated using the original shearing area. It is this effect that accounts for the apparent 30% decrease in shear strength after 5000 hours at 700 K (800° F). Had the notches been machined in the specimens after aging, the residual shear strengths would probably have shown little change from the unexposed values. The failure mode in the center portion of the aged specimen is similar to that of the unexposed specimen in Figure 8-32 with the addition of a small amount of filament splitting. In the two end portions, failure has occurred in the narrow aluminum regions between the hollow areas previously occupied by the oxidized boron filaments. Figure 8-33 shows the two fracture surfaces (specimens are tested in double shear — Figure 7-27) of a specimen aged for 10,000 hours at 700 K (800° F). For this specimen oxidation of the boron was more extensive on one side than on the other. As can be seen in Figure 8-33, oxidation has consumed almost all the boron on the surface on the left. The opposite sheared surface, on the right in Figure 8-33, shows somewhat less filament oxidation. The failure mode of the specimens aged for 10,000 hours was again matrix dominated but showed an increase in the amount of filament splitting over that observed after 5000 hours.

Table 8-17 shows 100% retention of the transverse tensile strength for all the thermal aging exposures. These results, however, are somewhat misleading because of the low values obtained from the baseline tests. The baseline specimens were taken from a different panel than was used for the thermal aging tests and showed considerable scatter when tensile tested. The transverse tensile data from aged material, Table 8-14, indicate some decrease in strength has occurred for the 10,000-hour exposures, at 561 K (550° F) and 700 K (800° F). These decreases are thought to be the result of changes in the boron and boron-aluminum interface



UNEXPOSED



5000 HOURS

Figure 8-32 Fracture Surface of Interfiber Shear Specimens of B/Al Before and After Thermal Aging at 700 K (800° F) in 1 atm Air

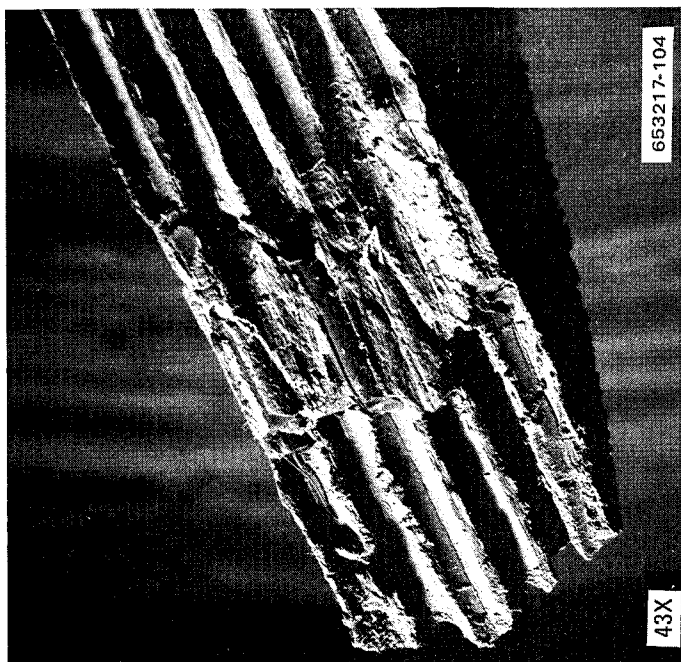
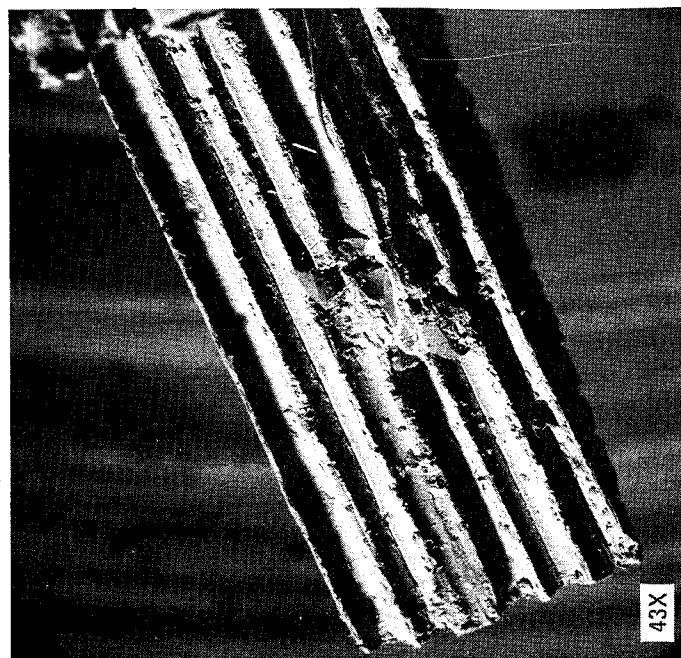


Figure 8-33 Fracture Surfaces of Interfiber Shear Specimen of B/AI After 10,000 hr of Thermal Aging at 700 K (800° F) in 1 atm Air (Specimen was Tested in Double Shear)

rather than degradation of the aluminum matrix. Figures 8-34 through 8-36 show the fracture surfaces of transverse tensile specimens that were tested after the following thermal treatments:

- a. Figure 8-34, unexposed.
- b. Figure 8-35, 5000 hours at 450 K (350°).
- c. Figure 8-36, 10,000 hours at 561 K (550°F).

In the unexposed specimen, Figure 8-34, the primary failure mode is matrix failure with some failure near, but not quite at, the filament-matrix interface. As thermal aging temperatures and times increase the failure mode changes from primarily matrix dominated to one in which, first, increased fracture at the filament-matrix interface occurs and, second, for more severe exposures, considerable filament splitting is observed. Figure 8-35 shows the increased interface fracture. A good example of filament splitting is illustrated by Figure 8-36. Two boron fibers have fractured lengthwise through their centers revealing the fine tungsten cores used in fabricating the filaments. An element scan taken with the SEM is also shown in Figure 8-36. With this technique the higher the atomic number of the constituent of the specimen the lighter the trace that is shown on the screen of the SEM. The two very light lines indicate the tungsten cores, the darkest areas are the low atomic number boron fibers, and the remaining grey area is the aluminum matrix. The change in the failure mode and the accompanying decrease in transverse tensile strength apparently occurs because the boron filaments become weakened as a result of interdiffusion between the boron and the 6061 aluminum alloy at the

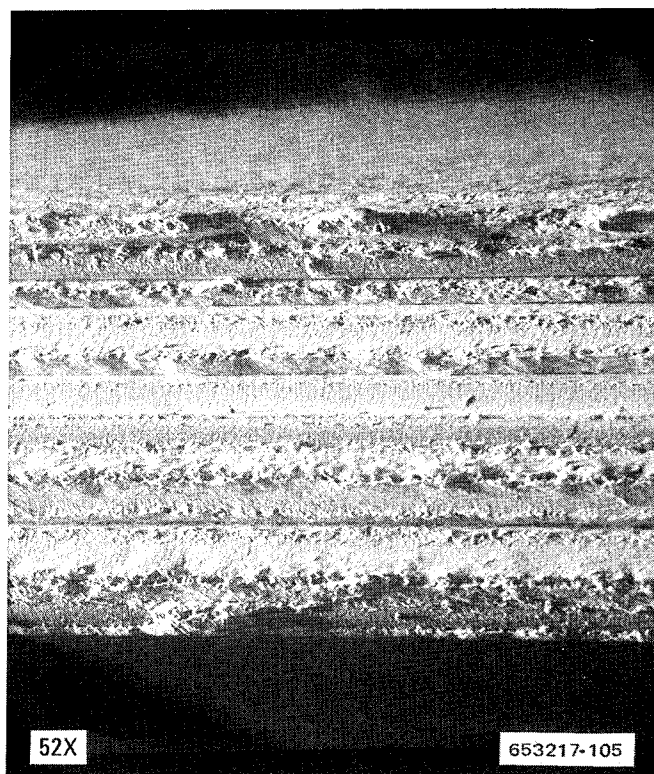


Figure 8-34 Fracture Surface of Transverse Tensile Specimen of Unexposed B/Al Showing Predominantly Matrix Failure

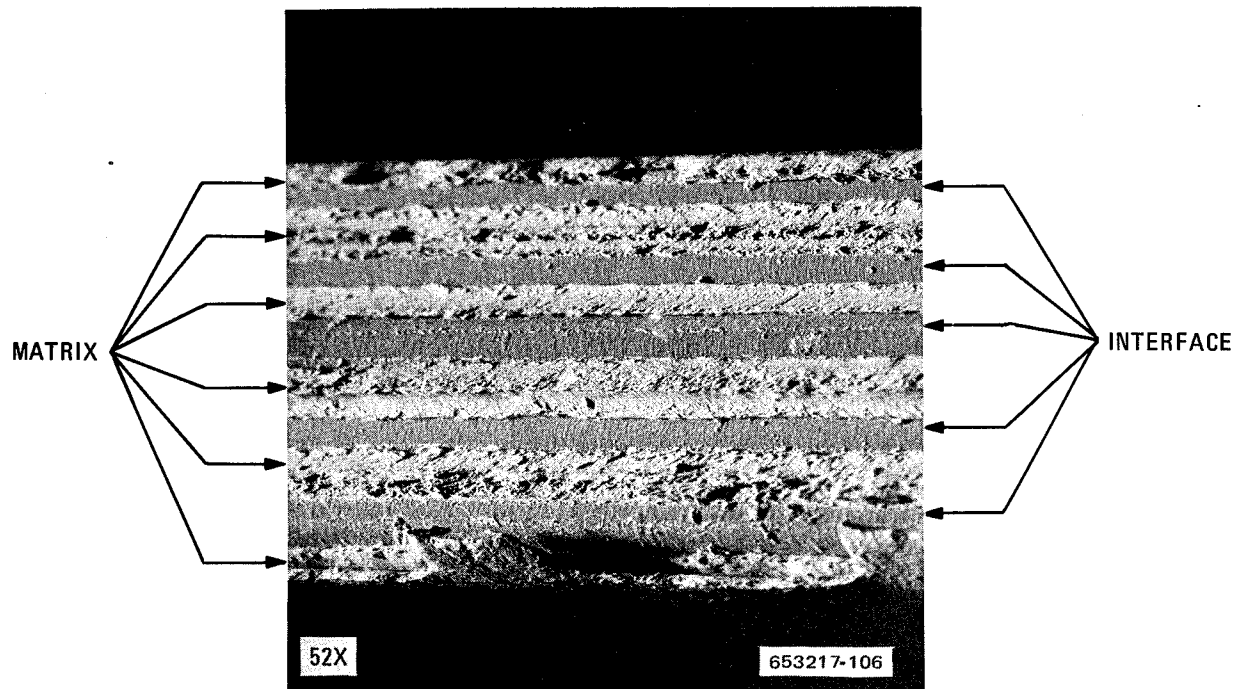


Figure 8-35 Fracture Surface of Transverse Tensile Specimen of B/Al After 5000 hr of Thermal Aging at 450 K (350° F) in 1 atm Air Showing Both Matrix and Interface Failure Modes

fiber-matrix interface during thermal exposure. Electron microprobe studies (ref. 29) have shown that degradation of boron fibers can occur at elevated temperatures as a result of the diffusion of various elements from the aluminum alloy to the filaments. An excellent review of interfacial effects on the strength of B/Al after thermal exposure can be found in reference 30.

The effect of boron fiber oxidation during aging at 700 K (800° F) was shown to have contributed considerably to the decrease in shear strength. For the transverse tensile specimens aged at 700 K (800° F) the contribution was considerably less because of the lower percentage of test section affected, e.g., after 5000 hours at 700 K (800° F) oxidation has consumed approximately 0.00064 m (0.025 in.) from each end of the test section or 50% of the 0.0025 m (0.10 in.) long shear region but only 10% of the 0.0127 m (0.50 in.) wide tensile specimen. Figure 8-37 shows the extent of oxidation inward from the surface of transverse tensile specimens aged for 5000 and 10,000 hours. The appearance of split hollow tubes is similar to that of Figure 8-32 and 8-33 for the shear specimens. The fracture surface away from the ends again reveals filament splitting and interfacial fracture in addition to the matrix failure.

Further evidence that the decrease in tensile and shear strength of B/Al during thermal aging was the result of degradation of the boron filaments rather than the aluminum matrix was found during examination of the failed $[0^\circ \pm 45^\circ]_s$ crossplied specimens aged for 5000 hours at 561 K (550° F). The outer 0° ply (on both sides) showed a series of closely spaced, 0.0013 m (0.05 in.) to 0.0025 m (0.10 in.), cracks across the width of the specimens. An overall view of these specimens showing the surface cracks as well as the necking that occurred during tensile testing is presented in Figure 8-38. Magnified views of the surface cracks are shown in Figure 8-39. Examination of the cracks with a stereographic microscope revealed that the cracks

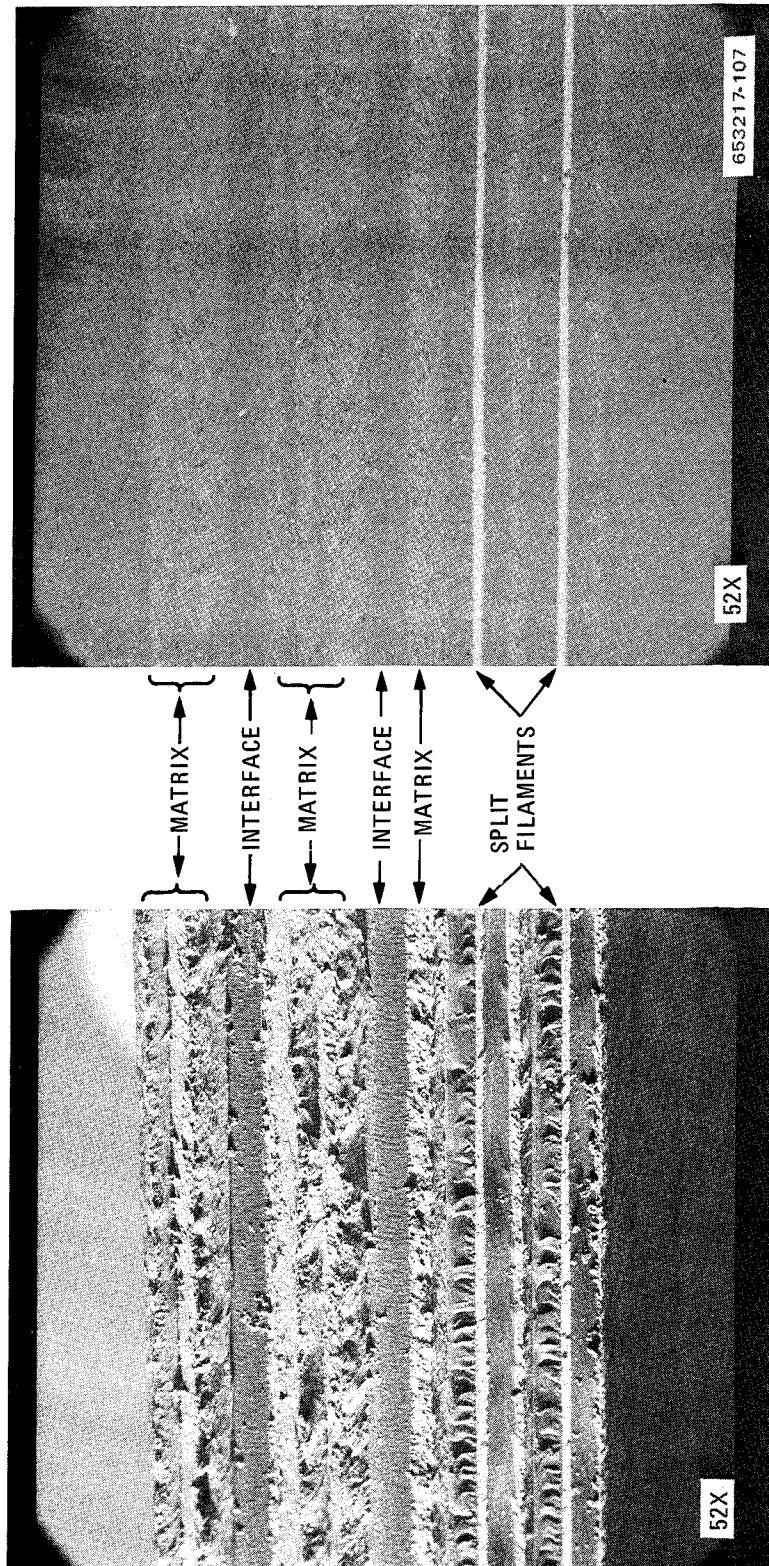
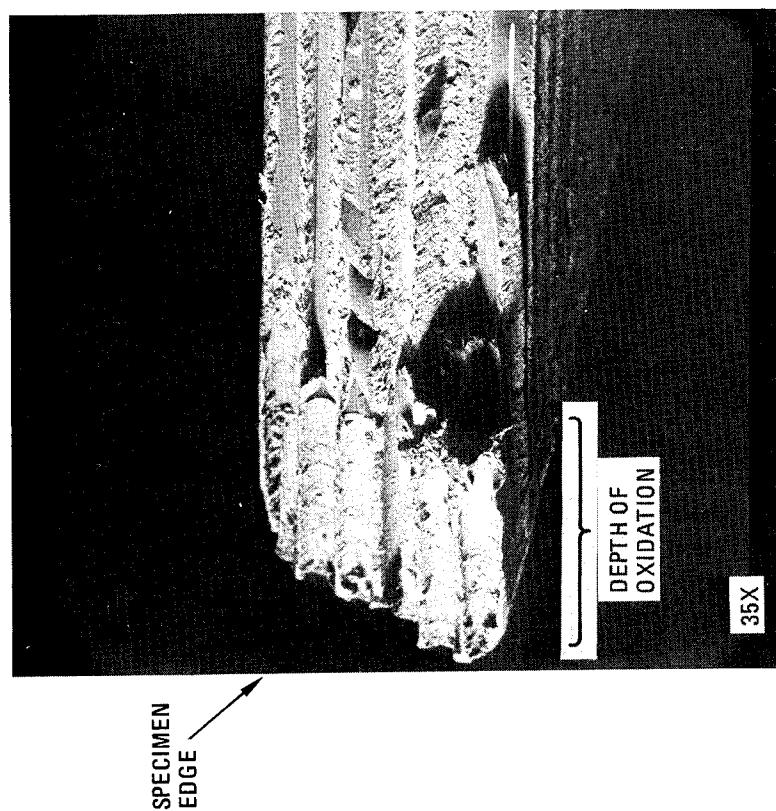
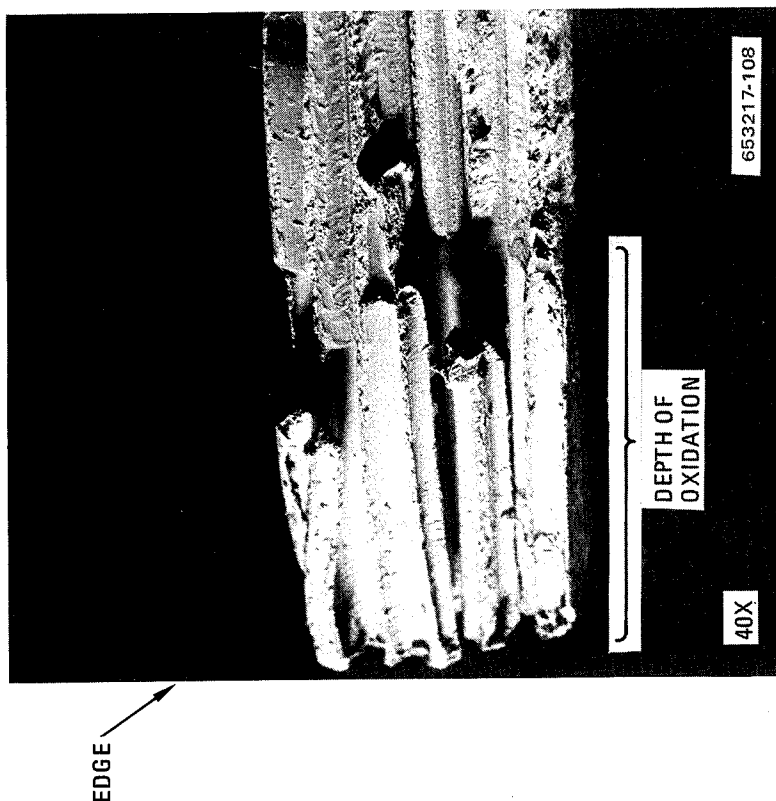


Figure 8-36 Fracture Surface of Transverse Tensile Specimen of B/AI After 10,000 hr of Thermal Aging at 561 K (550° F) in 1 atm Air Showing Matrix, Interface, and Filament Failure Modes



5000 HOURS 35X MAGNIFICATION



10,000 HOURS 40X MAGNIFICATION

Figure 8-37 Portion of Fracture Surface of Transverse Tensile Specimens of B/Al After Thermal Aging at 700 K (800° F) in 1 atm Air Showing Extent of Loss of Boron Through Oxidation

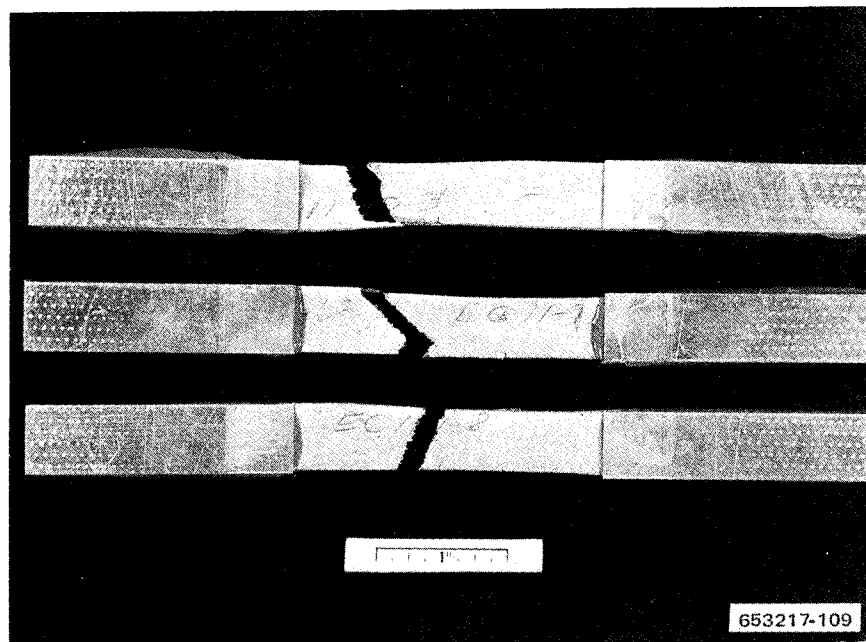


Figure 8-38 B/AI After 5000 hr of Thermal Aging at 561 K (550° F) in 1 atm Air and Tensile Testing at Room Temperature Showing Transverse Surface Cracks and Necking in the Test Section

extended only through the outer 0° plies and that the boron filaments in these outside plies were broken at each one of the surface cracks. This can be seen on the right in Figure 8-39. It is believed that the boron filaments became weakened as a result of diffusion to the filament-matrix interface during thermal exposure. Following the multiple failures along the brittle filaments in the outside 0° layers, the load was picked up by the 45° plies. With the 0° plies no longer active, the specimens necked down considerably prior to final failure. This necking, which is not typical of $[0^\circ \pm 45^\circ]_s$ material that has not been exposed, is clearly visible in Figure 8-38. In the specimens aged for 10,000 hours at 561 K (550° F), surface cracks were not as prevalent as those observed in the 5000-hour specimens but were similar in appearance. A very small number of surface cracks were also found after tensile testing the specimens aged at 450 K (350° F) while none were observed in the specimens aged at 700 K (800° F). Apparently the fracturing of the 0° outer boron filaments with the attendant surface cracks is highly dependent on the degree of filament embrittlement and is optimum after 5000 hours of exposure at 561 K (550° F).

In summary of these data, B/6061 boron/aluminum should be limited to 450 K (350° F) for supersonic cruise aircraft cumulative exposures greater than 10,000 hours because of loss of residual tensile strength during thermal aging.

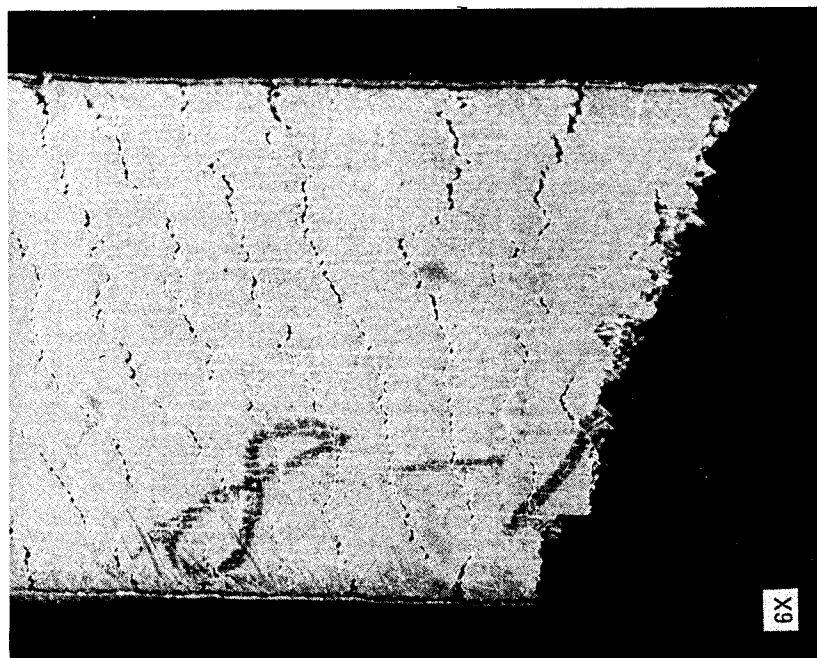


Figure 8-39 B/Al After 5000 hr of Thermal Aging at 561 K (550° F) in 1 atm Air and Tensile Testing at Room Temperature Showing Transverse Surface Cracks

1. The first part of the paper discusses the importance of the study of the history of the United States. It is argued that the study of history is essential for a full understanding of the present and for the development of a sense of national identity. The author points out that the study of history can help us to understand the causes of the problems we face today and to find ways to solve them. It can also help us to appreciate the achievements of our ancestors and to learn from their mistakes.

2. The second part of the paper discusses the importance of the study of the history of the United States. It is argued that the study of history is essential for a full understanding of the present and for the development of a sense of national identity. The author points out that the study of history can help us to understand the causes of the problems we face today and to find ways to solve them. It can also help us to appreciate the achievements of our ancestors and to learn from their mistakes.

3. The third part of the paper discusses the importance of the study of the history of the United States. It is argued that the study of history is essential for a full understanding of the present and for the development of a sense of national identity. The author points out that the study of history can help us to understand the causes of the problems we face today and to find ways to solve them. It can also help us to appreciate the achievements of our ancestors and to learn from their mistakes.

SECTION 9

ENVIRONMENTAL AGING

At the time that this study was initiated, most of the data generated on advanced composite materials had been initial strength data without regard to environmental conditions. The small amount that was available was generally for only relatively short periods of exposure compared to the lifetime of a commercial airliner. This portion of the program was intended to evaluate the composite systems as a function of exposure to moisture, ambient aging, and atmospheric contaminants over relatively long periods of time.

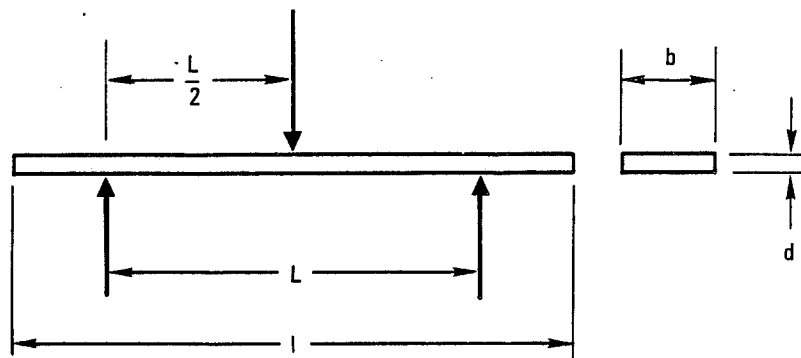
For the resin matrix composites, 24-hour water boil, 6-week humidity, and 20-week and 52-week ambient aging tests were conducted as accelerated means of simulating long-term ambient exposures. Residual strength testing (flexure) of unidirectional and $[0^\circ \pm 45^\circ]_{s2}$ crossplied specimens at room and elevated temperatures was performed after exposure and compared to tests on control (unexposed) specimens.

For the B/Al system an environmental study was conducted to determine the effects of corrosion and atmospheric contaminants. Tensile and shear specimens of both coated and bare B/Al were placed in an outdoor industrial seacoast atmosphere corrosion test facility maintained by General Dynamics Convair Division in San Diego, California. Residual strength was determined on one set of specimens after 10,000 hours of exposure. A second set of B/Al specimens will be tested at the completion of 50,000 hours on Phase II of the overall test program. Also included in the Phase II portion of the program will be residual tensile properties of the B/E, G/E, and G/PI systems after 50,000 hours of outdoor exposure to atmospheric contaminants.

The following sections describe the test procedures for the environmental aging studies and present and discuss the experimental results.

9.1 RESIN MATRIX COMPOSITE SYSTEMS

9.1.1 SPECIMEN DESIGN AND TEST PROCEDURES. The longitudinal flexure specimen was used for all the Phase I environmental aging studies of the resin matrix composites. The flexure specimen does not provide data that can be used directly for design but is an effective and relatively inexpensive method for making comparisons between materials or evaluating effects of various exposures. The specimen configuration is shown in Figure 9-1. As no universally accepted specification for flexural testing of composites was available, the test methods that were used were generally in accordance with ANSI/ASTM D 790-71 and Federal Test Method Standard No. 406, Method 1031. Details of the test procedure are given in Appendix B.



SPECIMEN DIMENSIONS

LENGTH (l) = 0.076 m (3.0 in.)

WIDTH (b) = 0.01270 m (0.500 in.)

THICKNESS (d) = APPROXIMATELY 0.0015 m (0.060 in.)

SPAN/THICKNESS RATIO ($\frac{L}{d}$) = 32 TO 1

LOADING HEAD AND REACTION SUPPORTS ARE 0.00635 m (0.250 in.)
DIAMETER STEEL ROD

OVERHANG MUST BE THE SAME OVER EACH END

653217-111

Figure 9-1 Longitudinal Flexural Specimen

Prior to conducting the moisture environmental exposures, the flexure specimens were heated at 394 K (250° F) for 24 hours to ensure that all were in a dry condition at the start of exposure. The control specimens were also dried for 24 hours at 394 K (250° F) before testing. All testing after exposure was accomplished within four hours after the exposure cycle had been completed.

The 24-hour water boil exposures were carried out in a reflux condenser using deionized water. An American Instrument Co., Inc. Climate-Lab, Complete Humidity-Temperature Apparatus was used to conduct the 6-week humidity exposures. The chamber was maintained at 322 K (120° F) with a controlled environment of 95 to 100% relative humidity. The ambient aging test specimens were kept in a desiccator at 294 ± 3 K (70 ± 5 ° F) and 52% relative humidity. The humidity level was maintained by a saturated aqueous solution of $\text{Na}_2\text{Cr}_2\text{O}_7 \cdot 7\text{H}_2\text{O}$. Specimens were removed from the desiccator and tested after 20 weeks and a second batch after 52 weeks.

The environmental aging exposures were conducted with 12 specimens cut from both unidirectional and $[0^\circ \pm 45^\circ]_{s2}$ crossplied panels. Residual strength testing was done at 297 K (75° F) and 450 K (350° F) on the unidirectional specimens for all exposure conditions. For the crossplied specimens, only 450 K (350° F) tests were performed for the humidity and ambient

aging exposures. The 24-hour water boil crossplied specimens were tested at both 297 K (75° F) and 450 K (350° F). Testing at elevated temperature was accomplished by heating the specimens to the test temperature in a Conrad-Missimer chamber (held in a standard test machine—Instron, Tinius-Olsen or Baldwin), holding at temperature for 10 minutes before test, and then loading to failure. It has been found that the 10-minute hold is a good compromise for getting good stabilization without driving off all the moisture.

9.1.2 TEST RESULTS AND DISCUSSION. Residual flexural strength data after 24-hour water boil, 6-week humidity, and 20-week and 52-week ambient aging exposures are presented in Table 9-1 for B/E, Table 9-2 for G/E, and Table 9-3 for G/PI. Listed in the tables are the control and exposed values and the percent retention of flexural strength after the different environmental ages. In order of increasing effect on mechanical properties, the various exposures are ranked as one might predict, i.e., 20-week ambient, 52-week ambient, and either 6-week humidity or 24-hour water boil. The results are typical of those obtained by others (ref. 21 and 31).

For epoxy systems, crossplied laminates traditionally have shown better 450 K (350° F) strength retention after exposure than unidirectional laminates. No definite theory has been advanced to explain this, but contributing factors might include specimen configuration, built-in thermal stresses from curing, compressive mode of failure after exposure, etc. An examination of the epoxy flexural strength data (Tables 9-1 and 9-2) shows that after long term aging, the failure strengths for both unidirectional and crossplied laminates are nearly the same. This would be anticipated for a matrix dominated failure mode. The room temperature flexural strengths were nearly unaffected by any of these exposures, while those at 450 K (350° F) were, in general, severely degraded; the only exceptions were the crossplied B/E material after the 20- and 52-week ambient age. The unidirectional specimens were particularly affected with losses in the 450 K (350° F) flexural strength of from 77 to 41% depending on the type of exposure.

Table 9-1. Effects of Moisture and Ambient Aging on B/E Laminates

Exposure	Orientation	Flexural Strength/Temperature				Retention %
		297 K	(75° F)	450 K	(350° F)	
		MN/m ²	(ksi)	MN/m ²	(ksi)	
Control	[0°] ₁₂	2100	304	1680	244	
		2060	298	1740	252	
		2060	299	1770	257	
		2070	300	1730	251	
	[0° ± 45°] _{s2}	924	134	889	129	
		958	139	820	119	
		931	135	882	128	
		938	136	864	125	

Table 9-1. Effects of Moisture and Ambient Aging on B/E Laminates — Concluded

Exposure	Orientation	297 K		Flexural Strength/Temperature (75° F)		450 K (350° F)		Retention %
		MN/m ²	(ksi)			MN/m ²	(ksi)	
24-Hour Water Boil	[0°] ₁₂	1900	276			415	60.2	
		1990	288			341	49.4	
		1960	284			428	62.1	
		1950	283	94		395	57.2	23
	[0° ± 45°] _{s2}	924	134			431	62.5	
		896	130			437	63.4	
		820	119			758	110	
		880	128	94		542	78.6	63
6-Week Humidity	[0°] ₁₂	2060	298			724	105	
		2190	318			738	107	
		2130	309			586	85.0	
		2130	308	103		683	99.0	39
	[0° ± 45°] _{s2}		—			690	100	
			—			648	94.0	
			—			586	85.0	
						641	93.0	74
20-Week Ambient Age	[0°] ₁₂	2190	317			1060	154	
		2120	308			1000	145	
		2220	322			1030	149	
		2180	316	105		1030	149	59
	[0° ± 45°] _{s2}		—			869	126	
			—			834	121	
			—			952	138	
						885	128	102
52-Week Ambient Age	[0°] ₁₂	2210	320			965	140	
		2300	334			862	125	
		2320	337			896	130	
		2280	330	110		908	132	53
	[0° ± 45°] _{s2}		—			882	128	
			—			772	112	
			—			772	112	
						809	117	94

Table 9-2. Effects of Moisture and Ambient Aging on G/E Laminates

Exposure	Orientation	Flexural Strength/Temperature					
		297 K	(75° F)	Retention	450 K	(350° F)	Retention
		MN/m ²	(ksi)	%	MN/m ²	(ksi)	%
Control	[0°] ₁₂	1720	294		1220	177	
		1710	248		1460	211	
		1620	235		1210	176	
		1680	244		1230	188	
	[0° ± 45°] _{s2}	882	128		658	95.4	
		779	113		710	103	
		910	132		676	98.1	
		857	124		681	98.8	
24-Hour Water Boil	[0°] ₁₂	1850	268		424	61.5	
		1620	235		405	58.7	
		1580	229		464	67.3	
		1680	244	100	431	62.5	33
	[0° ± 45°] _{s2}	855	124		345	50.1	
		834	121		415	60.2	
		820	119		334	48.4	
		836	121	98	365	52.9	54
6-Week Humidity	[0°] ₁₂	1720	250		405	58.7	
		1640	238		372	54.0	
		1680	244		388	56.3	
		1680	244	100	388	56.3	30
	[0° ± 45°] _{s2}	—	—		268	38.9	
		—	—		289	41.9	
		—	—		272	39.4	
					276	40.1	41
20-Week Ambient Age	[0°] ₁₂	1960	284		634	91.9	
		1690	245		690	100	
		1900	275		793	115	
		1850	268	110	706	102	54
	[0° ± 45°] _{s2}	—	—		609	88.3	
		—	—		479	69.5	
		—	—		535	77.6	
					541	78.5	79
52-Week Ambient Age	[0°] ₁₂	1670	242		605	87.8	
		1660	240		564	81.8	
		1540	223		598	86.7	
		1620	235	96	589	85.4	45
	[0° ± 45°] _{s2}	—	—		394	57.1	
		—	—		392	56.8	
		—	—		376	54.5	
					387	56.1	57

Table 9-3. Effects of Moisture and Ambient Aging on G/PI Laminates

Exposure	Orientation	297 K		Flexural Strength/Temperature (75° F)		450 K (350° F)		Retention %
		MN/m ²	(ksi)			MN/m ²	(ksi)	
Control	[0°] ₁₂	1330	193			869	126	
		993	144			952	138	
		1220	177			807	117	
		1180	171			876	127	
	[0° ± 45°] _{s2}	665	96.4			538	78.0	
		567	82.2			661	95.8	
		701	101.7			439	63.7	
		644	93.4			546	79.2	
24-Hour Water Boil	[0°] ₁₂	1140	166			848	123	
		1020	148			986	143	
		841	122			938	136	
		1000	145	85		924	134	106
	[0° ± 45°] _{s2}	578	83.9			476	69.0	
		567	82.3			374	54.3	
		351	50.9			385	55.9	
		499	72.4	78		412	59.7	75
6-Week Humidity	[0°] ₁₂	938	136			1080	156	
		889	129			848	123	
		1190	172			848	123	
		1010	146	85		925	134	106
	[0° ± 45°] _{s2}		—			348	50.6	
			—			501	72.6	
			—			486	70.5	
						445	64.5	81
20-Week Ambient Age	[0°] ₁₂	1150	167			703	102	
		1210	176			690	100	
		1280	186			827	120	
		1210	176	103		740	107	84
	[0° ± 45°] _{s2}		—			523	75.9	
			—			703	102	
			—			590	85.5	
						605	87.8	111
52-Week Ambient Age	[0°] ₁₂	1290	187			869	126	
		1180	171			931	135	
		1100	159			1020	148	
		1190	172	101		940	136	107
	[0° ± 45°] _{s2}		—			537	77.9	
			—			523	75.9	
			—			458	66.4	
						506	73.4	93

The effects of the moisture exposures on the polyimide specimens were generally less damaging than for the epoxy systems. Some decreases in flexural strength of the crossplied material were observed at 450 K (350° F) after the 24-hour water boil and 6-week humidity tests, but no significant effects were observed as a result of the 20- and 52-week ambient ages.

Fiber reinforced resin matrix composites (particularly epoxies) absorb moisture from the atmosphere. This absorption causes two basic problems, i.e., 1) losses in matrix dominated mechanical properties and, 2) changes in physical dimensions. The effects are mostly reversible in that heat or vacuum will drive off the moisture and will return the composites to their dry control properties and dimensions. The absorption of moisture primarily occurs in the resin matrix, and the resulting changes in composite mechanical and physical properties are a result of this absorption by the resin. Therefore, the type of reinforcement does not greatly influence the moisture effects. This was seen in the results presented earlier in that both the boron and graphite reinforced epoxies exhibited considerable property degradation from the absorbed moisture.

The general moisture problem was discovered by General Dynamics Convair Division in 1970 (ref. 5 and 21). The problem manifested itself initially by unusually low longitudinal flexure strength at 450 K (350° F) in G/E after short terms of aging at ambient temperature and humidity in air conditioned laboratories. Extensive work on this problem (ref. 31) led to the conclusion that the cause of the problem was plasticization of the epoxy resin by moisture, which subsequently lowers the glass transition temperature of the resin. The high temperature composite properties generally affected by moisture absorption are shear strength and modulus, edge compressive strength, bolt bearing and flat-wise tensile strengths. Since the initial work at General Dynamics Convair significant efforts have been made and are still in progress at several laboratories in this country to determine moisture effects on mechanical properties of polymer matrix composites. Many of these early results were presented in 1975 at a U.S. Air Force Materials Laboratory and Society of Aerospace Materials and Process Engineers Workshop, which examined the environmental durability of resin matrix composites. A summary of the data presented along with the conclusions and recommendations of the participants can be found in reference 32.

9.2 METAL MATRIX COMPOSITE SYSTEM

9.2.1 SPECIMEN DESIGN AND TEST PROCEDURE. The tensile and interfiber shear specimen configurations used for the B/Al environmental study were identical to those described previously in Section 7, Baseline Testing. All specimens were machined from 6 ply unidirectional B/Al. Tensile specimens were cut from both the longitudinal and transverse directions while the interfiber shear specimens were cut from only the longitudinal direction.

In addition to determining the susceptibility of B/Al composite material to corrosion and atmospheric contaminants, an objective of the study was to evaluate an elevated temperature corrosion protection system for B/Al. In previous work at General Dynamics Convair (ref. 33) it was found that B/Al composite materials are somewhat more susceptible to corrosion than aluminum structures, especially at the edges, where both boron and aluminum are exposed to the corrosive environment. In these same studies, effective corrosion resistance was achieved by a paint finish system applied over a chemical film treatment. These systems, however, were effective to only approximately 422 K (300° F), somewhat below the range desired for the SCR

application. Later work on a corrosion protection system for B/Al composites serviceable up to 589K (600° F) was also accomplished at Convair (ref. 34). While not completely effective in preventing corrosion of the aluminum, the polyimide, silicone, and fluorocarbon coating systems studied showed promise. Using these results as a starting point, a limited test program was conducted to develop a coating for use on these environmental exposures. The finish system that was selected consisted of a chemical conversion coating followed by an epoxy primer and a polyimide topcoat. Before the chemical conversion coating, the specimens were degreased, alkaline cleaned, and deoxidized. The epoxy primer was applied over the chemical conversion coating and allowed to dry. Aluminum powder pigment (5% by weight) was added to the polyimide coating material before application over the primer. After application of the aluminized polyimide coating, the specimens were cured at 436 K (325° F) for 14 hours. This coating has a maximum use temperature of about 589 K (600° F). Half of the B/Al specimens used for the environmental exposure tests were coated and the other were bare.

Painted redwood racks were made to hold the specimens during exposure. The racks were placed in an outdoor industrial-seacoast atmosphere, corrosion test facility (Figure 9-2) maintained by General Dynamics Convair on the rooftop of a building in San Diego, California approximately 800 meters (0.5 miles) from San Diego Bay. Half of the coated and half of the bare B/Al specimens were removed after 10,000 hours for examination and residual strength testing. The other half will be tested after 50,000 hours of exposure in Phase II of the program. Tensile and interfiber shear tests were conducted at room temperature using the procedures described in Section 7.

9.2.2 TEST RESULTS AND DISCUSSION. After 10,000 hours of outdoor exposure no change in appearance was observed in the coated B/Al specimens, but the bare specimens all showed

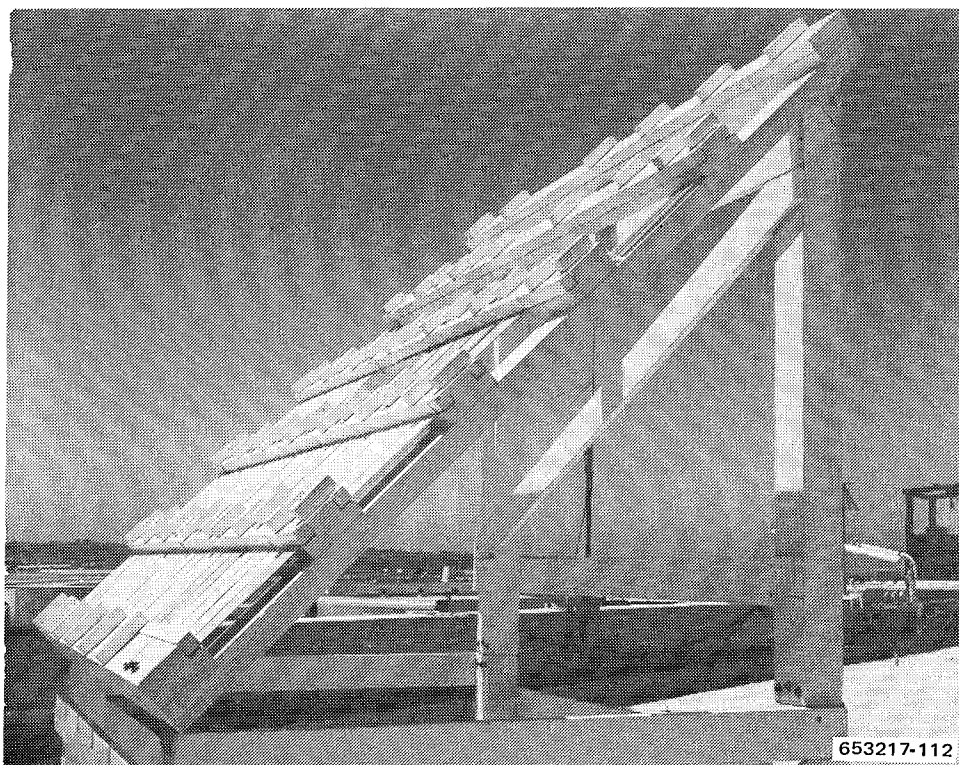


Figure 9-2 Outdoor Corrosion Test Facility

evidence of extensive surface corrosion with some concentrated attack at localized areas (pitting). This attack was much heavier on the side of the specimen facing away from the rack. The samples were held in the racks only on the ends so that both front and back surfaces were exposed to the environment. Photographs of the specimens mounted in the wooden racks before exposure are shown in Figure 9-3, and after 10,000 hours in Figure 9-4. The corrosion of the uncoated specimens is clearly visible in Figure 9-4.

The results of post exposure tensile and shear testing are presented in Tables 9-4 and 9-5. Only typical values of the unexposed strengths are given because the environmental aging specimens were cut from different panels than those used for the baseline tests. No effects to either tensile or shear properties were observed for the coated samples. For the uncoated specimens, significant decreases were found in the transverse tensile strength and the shear strength, while the longitudinal tensile strength was unaffected by the 10,000-hour exposure. A surface effect such as corrosion of the bare aluminum would be expected to decrease the matrix controlled properties, i.e., transverse tensile and shear, but have little effect on longitudinal tensile, a fiber controlled property.

To check the extent and nature of the surface corrosion, a metallographic examination of bare and coated specimens was performed. No change in appearance was found for the coated specimen after the 10,000-hour exposure as the coating had provided complete protection. Examination of the uncoated specimen, on the other hand, revealed extensive intergranular attack at the surface, which extended to a depth of approximately 0.00007 m (0.003 in.). An example of these corrosion crack regions is shown in Figure 9-5. Some surface disruption has also occurred near one of the boron filaments.

The uncoated interfiber shear specimens, see Figure 7-27, had been prepared prior to placing in the test facility so that the machined edges as well as the surfaces were exposed to the atmosphere. These specimens showed a decrease in shear strength of approximately one-third. Later, a second set of shear specimens was prepared by re-machining half of each of the three failed specimens. For these specimens, only the surface of the test area had been exposed and subjected to corrosive attack. The shear strength of these specimens, Table 9-5, was only slightly lower than the coated material. The configuration of the shear specimen used for these tests is one in which stress concentrations build up at the machined surfaces at either end of the shearing regions. If these surfaces are exposed to a corrosive environment, the subsequent corrosion cracks can initiate failures at loads substantially lower than those obtained from undamaged specimens. It is this phenomenon that is believed to have been responsible for the significant effect on shear strength of machining the notch before or after exposure.

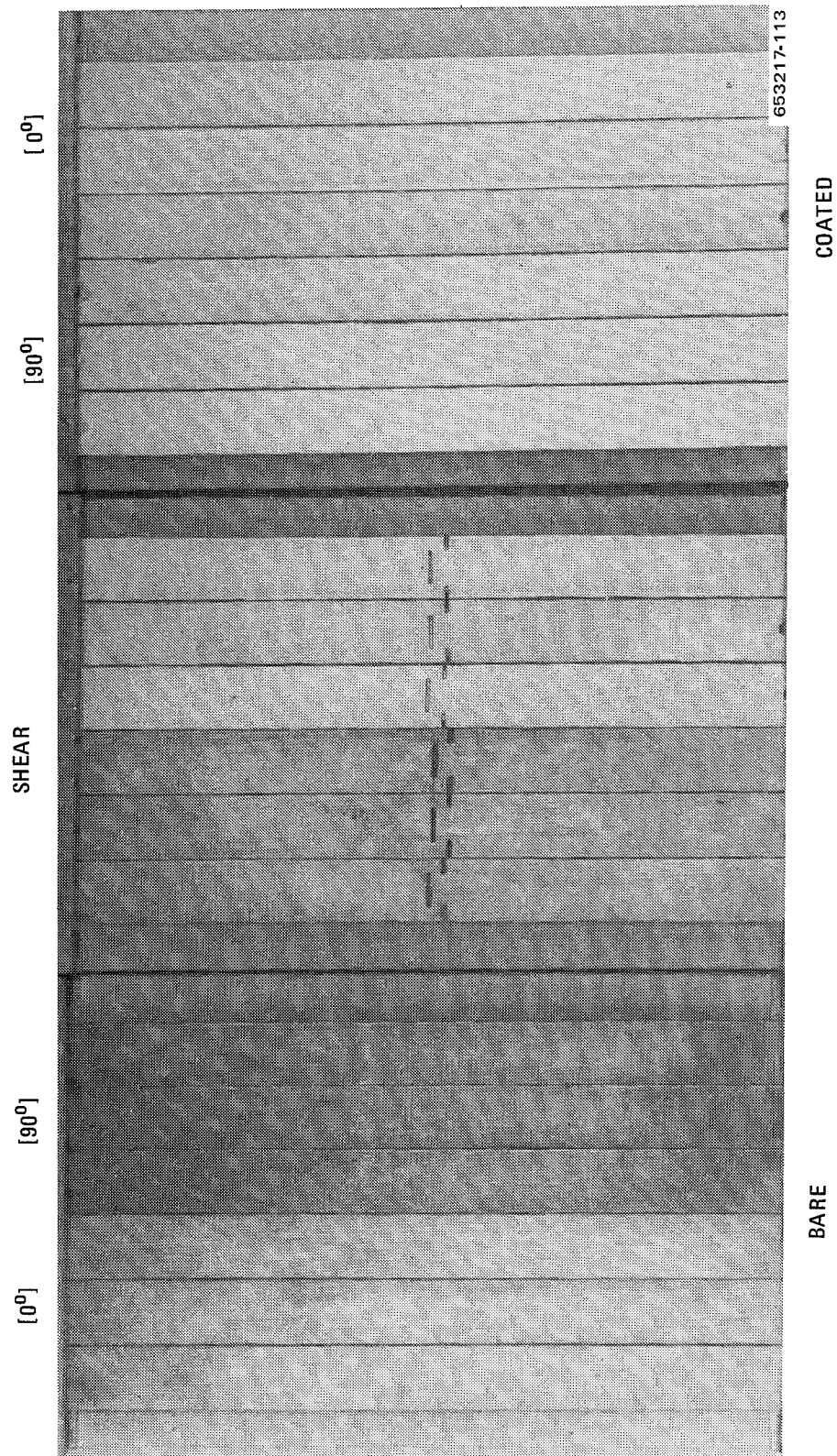


Figure 9-3 Corrosion Racks Containing Unidirectional B/AI Specimens—Before Exposure

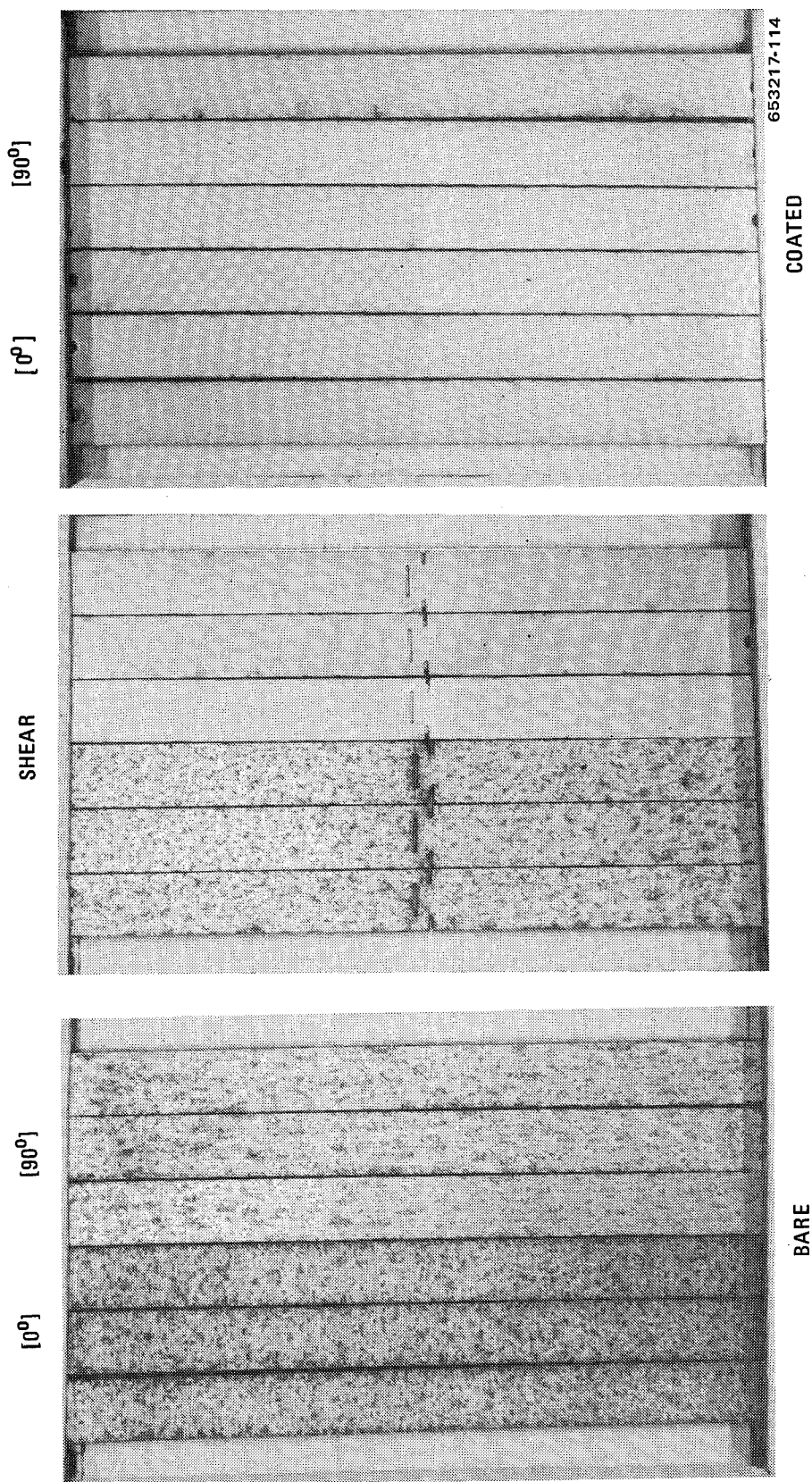


Figure 9-4 Corrosion Racks Containing Unidirectional B/AI Specimens—Exposed for 10,000 hr. in an Industrial-Seacoast Atmosphere

Table 9-4. Tensile Data for Bare and Coated [0°]₆ B/Al After 10,000 Hours of Atmospheric Contaminants Exposure in an Industrial-Seacoast Environment

Condition	Orientation	Strength		Typical Strength Unexposed	
		MN/m ²	(ksi)	MN/m ²	(ksi)
Bare	[90°]	121	17.6	152	22
		127	18.4		
		134	19.5		
		127	18.5		
Coated	[90°]	176	25.6	152	22
		156	22.7		
		167	24.2		
		166	24.2		
Bare	[0°]	1410	205	1450	210
		1400	203		
		1560	226		
		1460	211		
Coated	[0°]	1500	217	1450	210
		1500	218		
		1390	202		
		1460	212		

Table 9-5. Shear Data for Bare and Coated [0°]₆ B/Al After 10,000 Hours of Atmospheric Contaminants Exposure in an Industrial-Seacoast Environment

Condition	Orientation	Strength		Typical Strength Unexposed	
		MN/m ²	(ksi)	MN/m ²	(ksi)
Bare, Machined Before Exposure	[0°]	82.0	11.9	110	16
		75.2	10.9		
		77.2	11.2		
		78.1	11.3		
Bare, Machined After Exposure	[0°]	109	15.8	110	16
		102	14.8		
		106	15.4		
		106	15.3		
Coated	[0°]	119	17.3	110	16
		108	15.7		
		97.2	14.1		
		108	15.7		

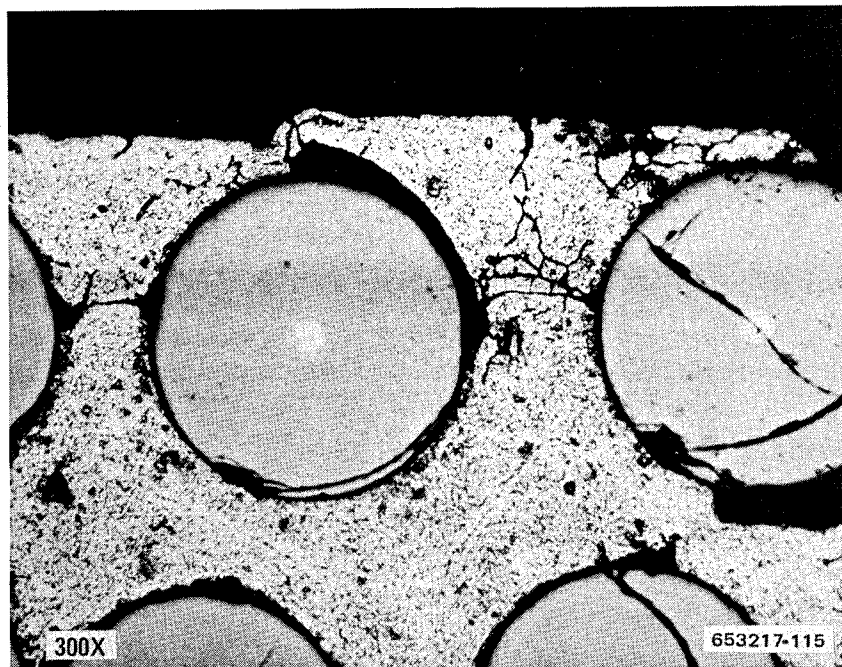


Figure 9-5 Intergranular Corrosion Cracks in Unidirectional B/Al After 10,000 hr. of Atmospheric Contaminants Exposure in an Industrial-Seacoast Environment

SECTION 10

CREEP TESTING

The objective of this task was to determine experimentally the creep and creep rupture behavior of the four advanced composite materials selected for evaluation in the SCR program. Axial creep tests were performed at two temperatures for exposure times of 100 and 1000 hours for each system. The two test temperatures were the proposed maximum use temperature for each material and one selected lower temperature in the potential application range. Results obtained during Phase I of this contract study have since proven these proposed maximum use temperatures to have been overly optimistic for all four composites. The lower temperatures were, however, well chosen, and agree quite closely with those used for the flight simulation tests. Creep properties were determined for two layups, unidirectional and $[0^\circ \pm 45^\circ]_s$ crossply, of each material. All specimens were taken from 6 ply laminates. The creep/creep rupture test program is summarized in Table 10-1.

Table 10-1. Summary of Creep/Creep Rupture Test Program

Material	Laminate Orientation	Temperature		Time	Number of	
		K	(°F)	(hr)	Specimens	
B/E	[0° ± 45°] _s	394	250	100	2	
				1000	3	
		450	350	100	6	
				1000	1	
	[0°] ₆	450	350	100	4	
				1000	2	
	G/E	[0° ± 45°] _s	394	250	100	5
					1000	2
450			350	100	4	
				1000	1	
[0°] ₆		394	250	100	5	
				1000	1	
		450	350	100	4	
				1000	2	
G/PI	[0° ± 45°] _s	505	450	1000	6	
		561	550	100	6	
	[0°] ₆	505	450	100	6	
		561	550	100	6	
	B/Al	[0° ± 45°] _s	505	450	100	3
					1000	3
561			550	100	3	
				1000	3	
[0°] ₆		505	450	100	6	
		561	550	100	6	

10.1 SPECIMEN DESIGN

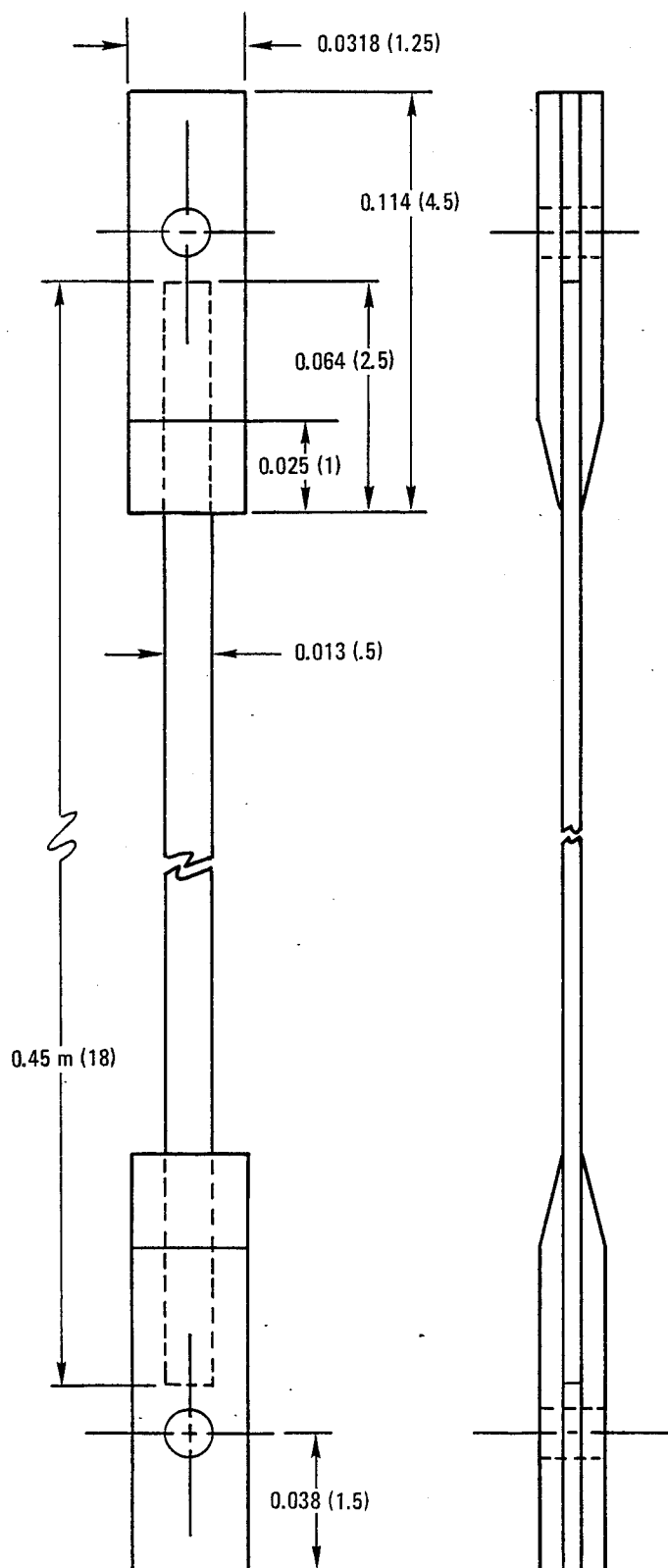
No standard specimen for creep testing of composites had been established at the time the creep testing task was initiated. Previous work at General Dynamics Convair (ref. 21 and 33) with a straight sided specimen similar to that used for tensile testing had given good results for material with no fibers aligned in the loading direction. For specimens with fibers in the loading direction the high loads required resulted in frequent bond failures in the end doublers. A slightly modified specimen was used for this program. To reduce misalignment and ensure axial loading the grips were changed from wedge to pin loaded. Tapered titanium doublers were bonded to the grip areas to minimize stress concentrations. The length of the specimens was such that it would help prevent premature grip failures by permitting the grip ends to extend outside the furnace. A length of 0.56 m (22 in.) was selected, and the B/E and B/AI specimens were prepared. No problems were encountered with bond failures in the B/E specimens, but four of the B/AI specimens failed prematurely in the doubler bonds. As heating of the adhesive during testing was thought to have contributed to the problem, the length of the G/E and G/PI specimens was increased to 0.71 m (28 in.) to further extend the grip ends outside the furnace. While the longer specimen undoubtedly helped, the combination of high loads and temperatures also resulted in several bond failures in both the G/E and G/PI systems. The configuration of the creep specimen is shown in Figure 10-1.

10.2 TEST EQUIPMENT AND TEST PROCEDURE

All creep tests were performed in air using Arcweld Creep Testing Machines, Model JE, 5440 kg (12,000 lb) or Model EE, 9070 kg (20,000 lb), and Arcweld Power Positioning Furnaces, Model F8. The furnaces are 0.43 m (17 in.) in length with 0.064 m (2.5 in.) diameter ceramic muffle tubes in which the specimens are radiant heated. The resistance heated furnaces have three zones that can be manually adjusted to minimize temperature gradients along the central test section of the specimens. A centrally located viewing port is available for optical measurements. Temperature control for the furnaces is provided by Wheelco controllers using chromel-alumel thermocouples inserted through the wire heating elements and in contact with the outside of the muffle tube. The test temperature was measured with three chromel-alumel thermocouples attached at 0.0444 m (1.75 in.) intervals to the gage section of the test specimen with high temperature fiberglass tape. Temperature variations at any one location were generally less than ± 1.75 K (3° F) while temperature uniformity along the 0.0889 m (3.50 in.) section was generally maintained to ± 2.8 K (5° F). Strain measurements were made with an optical method employing a platinum sliding-strip extensometer mechanically attached to the specimen. The optical equipment consisted of a Gaertner filar micrometer 50X magnification microscope mounted on the furnace and sighted through the central viewing port. Illumination of the platinum extensometer was provided by a lamp system within the microscope.

A creep machine and furnace with a specimen in test is shown in Figure 10-2. A closeup view of the Gaertner microscope in place on the furnace can be seen in Figure 10-3. Figure 10-4 shows the platinum sliding-strip extensometer attached to a composite specimen prior to loading into the creep testing apparatus. Also visible are the chromel-alumel thermocouples.

Prior to testing, the resin matrix composite specimens were dried at 394 K (250° F) for 24 hours. The specimen dimensions were measured, and the creep machine loads were calculated for the particular stress level desired. Fiducial marks were lightly penciled at 0.0508 m (2 in.)



LOADING HOLES ON
CENTER LINE OF
SPECIMEN TO WITHIN
 ± 0.000064 m (0.0025 in.)

BONDED DOUBLERS-
4 PLACES

DIMENSIONS
IN m (in.)

653217-116

Figure 10-1 Creep Test Specimen



Figure 10-2 Creep Testing Apparatus

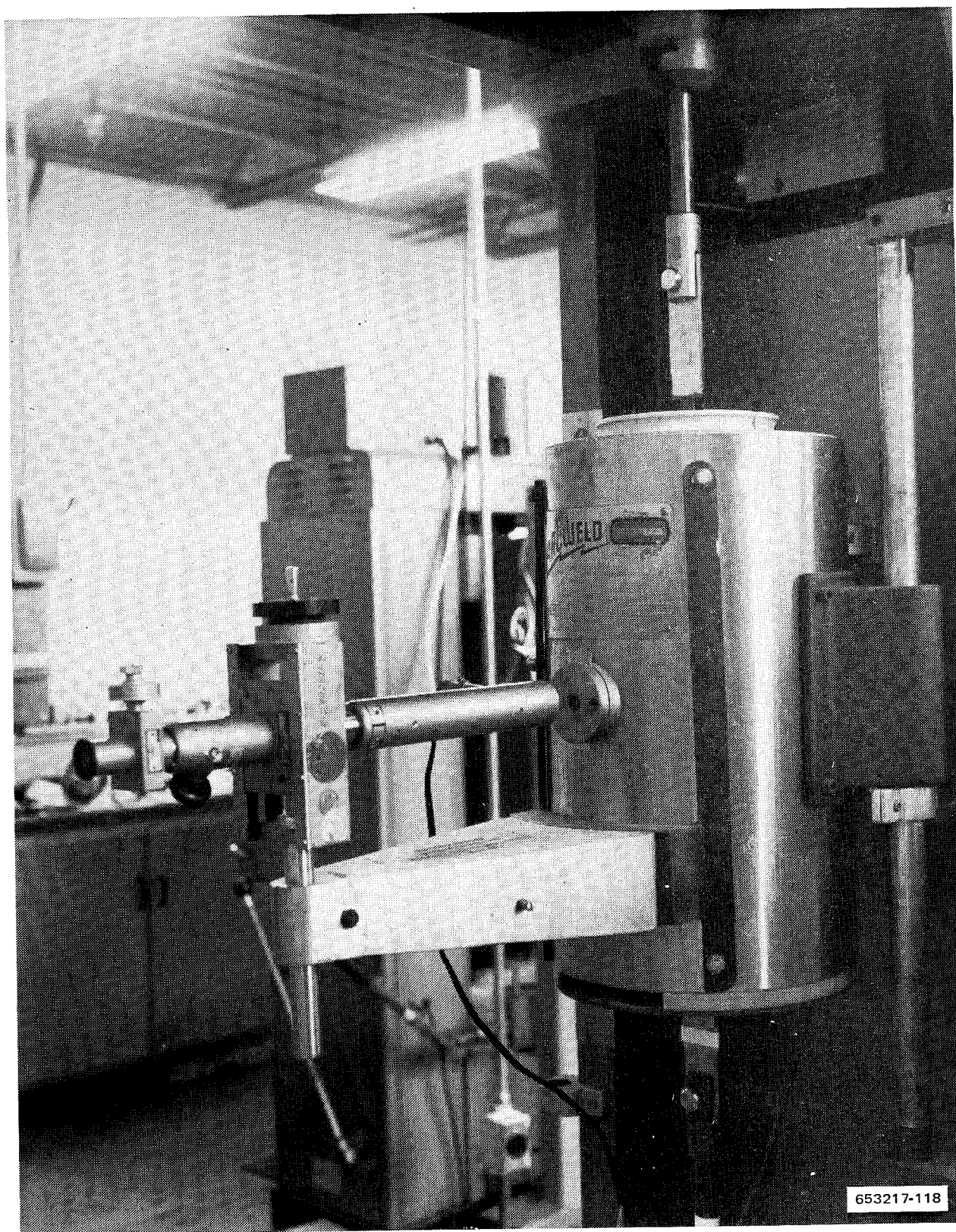


Figure 10-3 Furnace Mounted Filar Micrometer Microscope for Creep Measurements

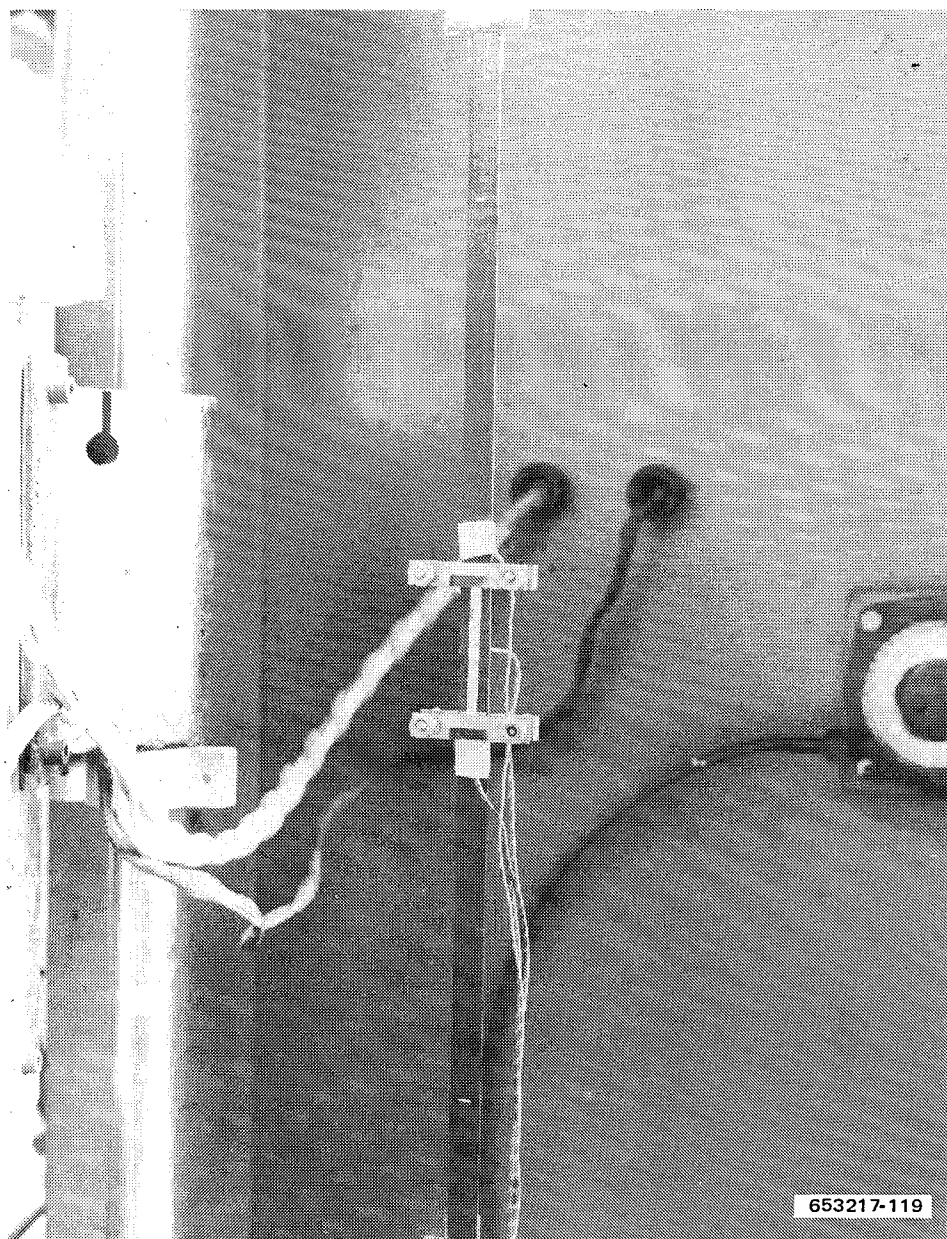


Figure 10-4 Creep Specimen with Platinum Sliding-Strip Extensometer and Thermocouples Attached

intervals in the region where the platinum extensometer was to be attached in order to determine the total strain by before and after measurements with a cathotometer. These measurements were later discontinued when the scatter in the readings was found to be of the same magnitude as the total strains obtained during creep testing. The platinum extensometer was attached, and the three thermocouples were taped to the specimen, above, below, and opposite the extensometer. The specimen, which was connected to the upper and lower pullrods, was then carefully loaded through the preheated furnace and attached to the loading arms of the creep machine. A small load, 0.45 kg (1 lb), was applied while the temperature was stabilized, and the microscope was focused and positioned on the platinum extensometer. The full load was then gradually applied, and strain measurements were begun immediately. The elapsed

time between the initial small load application and the full load application was approximately 0.25 hour. The difference in measurements between zero and full load is due to elastic strain. These values are shown on the individual creep curves but are not reported in the total strain values presented in the tables. Optical measurements were continued for either 100 hours or for 1000 hours or until specimen failure. At the conclusion of the tests for those specimens that did not fail, the load, except for 0.45 kg (1 lb), was removed, and a final strain measurement was recorded. The final measurement was generally not made at exactly 100 or 1000 hours because of a one shift operation in the testing laboratory. Consequently, the creep curves are plotted out to the times of the last measurement. The values listed in the data tables for total creep strain, however, have been, when possible, taken from the creep versus time curves at either 100 or 1000 hours.

10.3 TEST RESULTS AND DISCUSSION

The creep testing program, which is summarized in Table 10-1, consisted of 100- and 1000-hour tests at two temperatures and two layups for each of the four material systems. The data are presented in tabular form and as creep strain versus time curves. The elastic strain values obtained during loading are shown on the individual creep curves but are not reported in the total creep strain values presented in the tables. Also shown on the creep curves are the strain values after unloading at the conclusion of a test in which failure did not occur. The difference between the initial full load strain and the final unloaded strain should be equal to the permanent plastic creep strain. However, as a result of the very small creep strains obtained in these tests the agreement was generally poor. Only for the $[0^\circ \pm 45^\circ]_s$ crossplied B/Al and B/E was the agreement reasonably close. Again, these values were not reported in the tabular data but can be obtained from the creep curves.

The specimens that failed during load application and for which no curves could be drawn are identified in the tables. Also noted in both the tables and on the curves are the specimens that failed during testing or that experienced doubler bond failures during testing.

10.3.1 BORON/EPOXY. Results of creep testing of B/E at 394 K (250° F) and 450 K (350° F) are listed in Table 10-2. Data are presented for 18 specimens.

Creep strain versus time curves are presented in Figures 10-5 and 10-6 for crossplied material at 394 K (250° F), in Figures 10-7 through 10-9 for unidirectional material at 450 K (350° F), and in Figures 10-10 and 10-11 for crossplied material at 450 K (350° F).

The data show that the amount of creep obtained in B/E material with boron filaments aligned in the loading direction is very small. No specimen gave values of more than a few tenths of a percent of permanent creep strain. For example, specimen AC5-8 (crossplied) exhibited only 0.13% creep in 1000 hours at 394 K (250° F) when loaded at 79% of the average ultimate tensile strength, and specimen AU5-5 (unidirectional) exhibited only 0.27% creep in 1000 hours at 450 K (350° F) when loaded at 88% of the average ultimate tensile strength. Specimens that failed prior to completing 100 hours of exposure also underwent very little creep as indicated by measurements just before fracture. See, for example, Figures 10-6 and 10-9. One specimen, AU5-3, Figure 10-7, did show a sharp rise in the creep curve before failure, but the total creep strain was still less than 0.2%. Before-after measurements were not successful in determining the total creep strain of failed specimens. For specimens that fractured in the gage section the combination of low creep strain and the difficulty of accurate fit-back of the failed specimen halves made the measurements unreliable.

Table 10-2. Summary of Creep Test Results for B/E

Specimen Number	Orientation	Test Temperature		Stress		Time (hr)	Total Creep Strain (%)	Comments
		K	(°F)	MN/m ²	(ksi)			
AC5-11	[0° ± 45°] _s	394	250	310	45	1000	0.08	Failed in 9 hours
-9				345	50	100	.08	
-7				379	55	1000	.22	
-8				414	60	1000	.13	
-10				448	65	a8	a.03	
AU5-1	[0°] ₆	450	350	896	130	100	.07	Failed in 97 hours Failed in 2.2 hours
-4				931	135	552	.17	
-2				965	140	100	.11	
-5				1000	145	1000	.27	
-6				1020	147.5	a93	a.23	
-3				1030	150	a1.8	a.15	
AC5-13	[0° ± 45°] _s	450	350	345	50	1000	.18	Failed in 14 hours Failed in 18 hours Failed in 0.03 hour Failed on loading Failed in 0.17 hour
-6				379	55	a4.5	a.08	
-5				396	57.5	a5	a.08	
-1				414	60	100	.19	
-3				431	62.5	—	—	
-4				431	62.5	—	—	
-2				448	65	—	—	
aLast measurement prior to failure								

^aLast measurement prior to failure

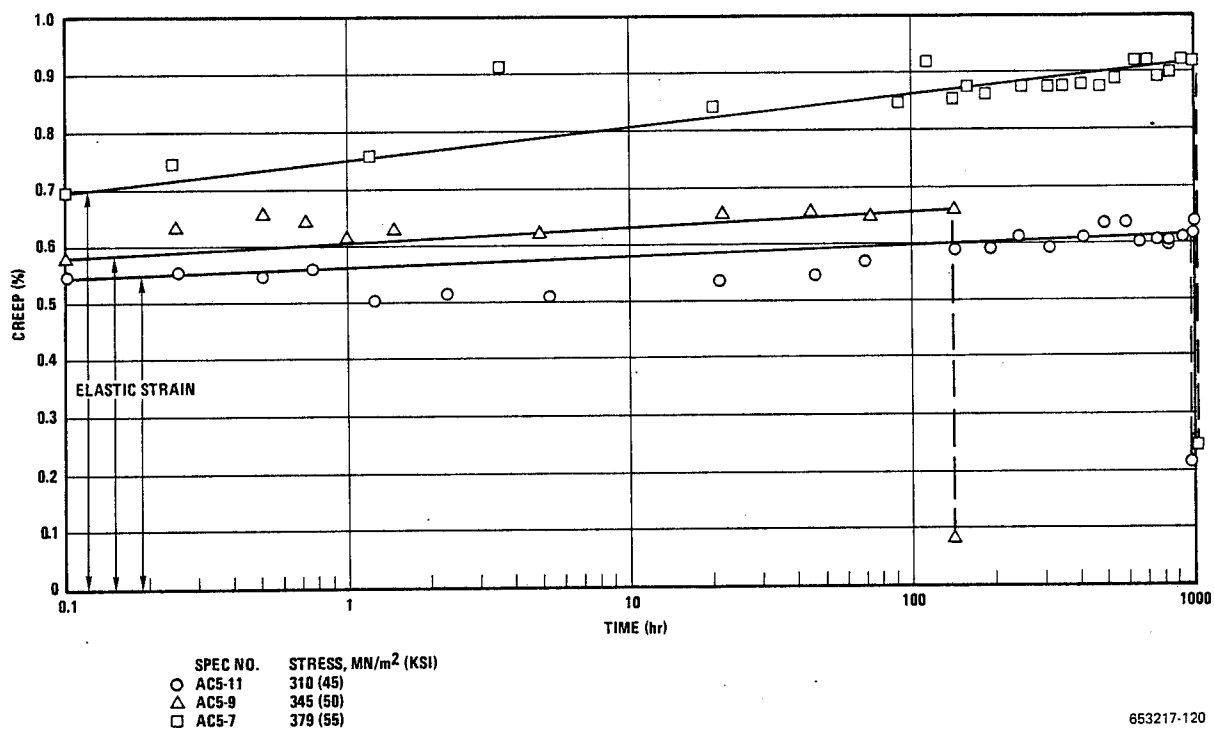


Figure 10-5 Creep Strain for $[0^\circ \pm 45^\circ]_s$ B/E at 394 K (250° F)

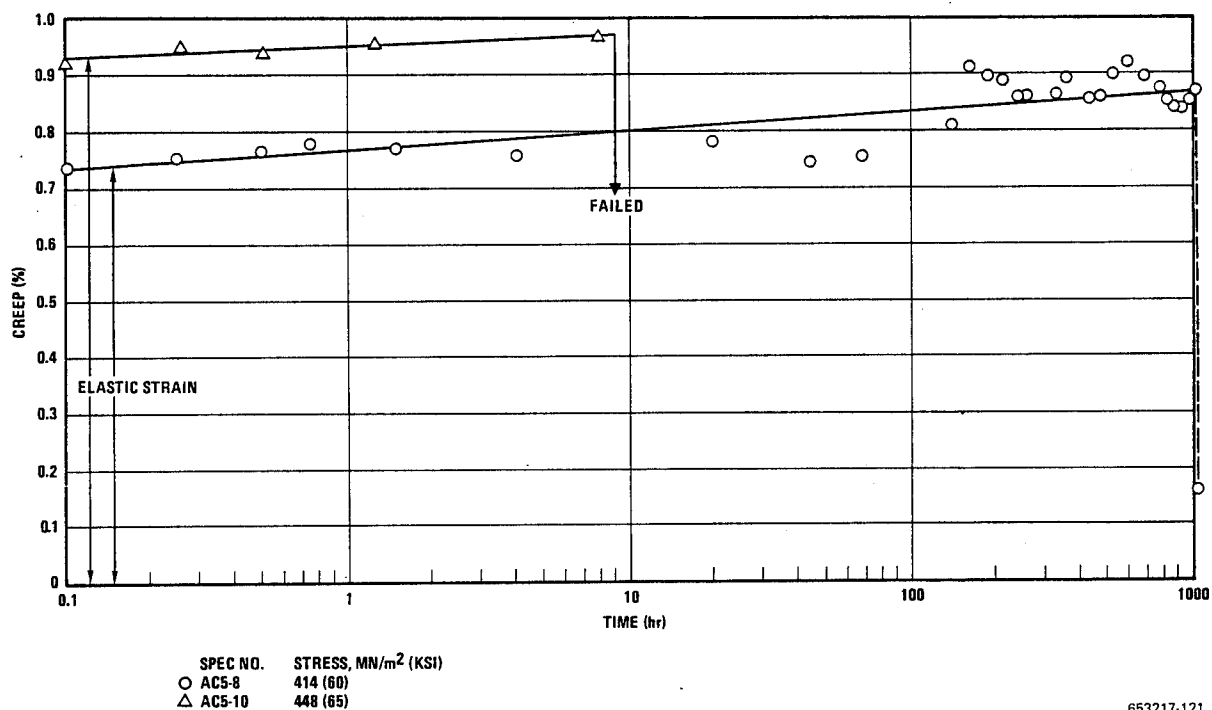


Figure 10-6 Creep Strain for $[0^\circ \pm 45^\circ]_s$ B/E at 394 K (250° F)

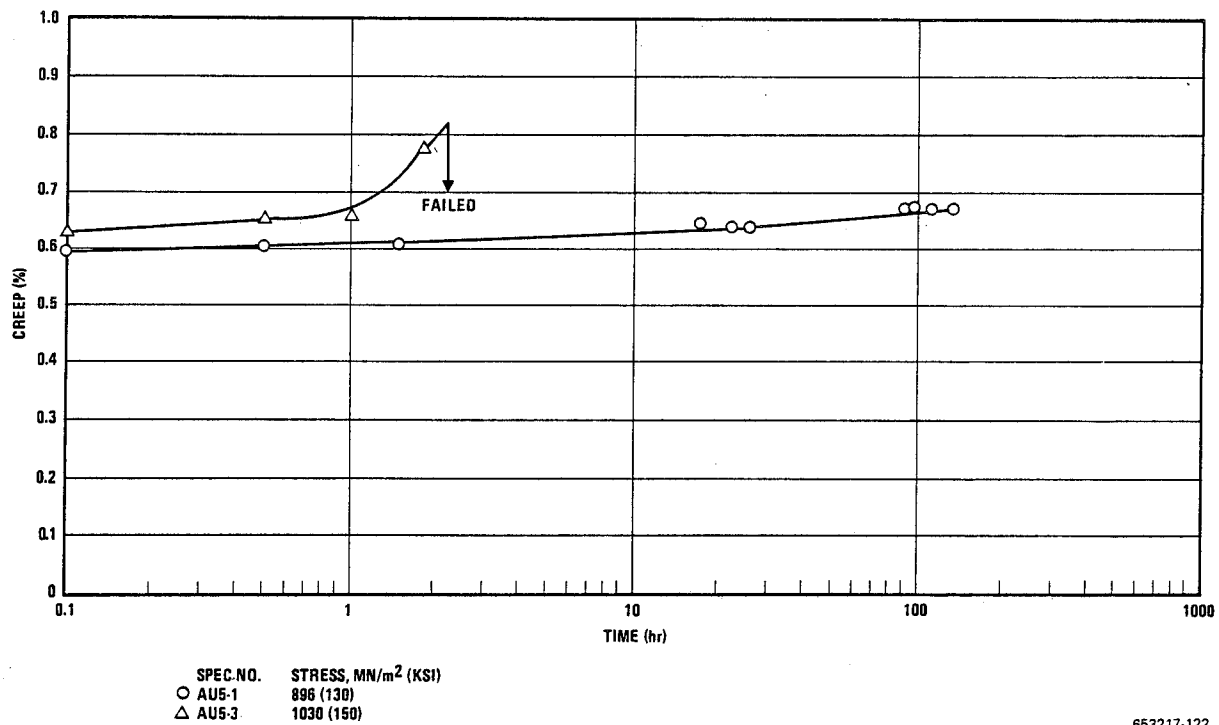


Figure 10-7 Creep Strain for $[0^\circ]_6$ B/E at 450 K (350° F)

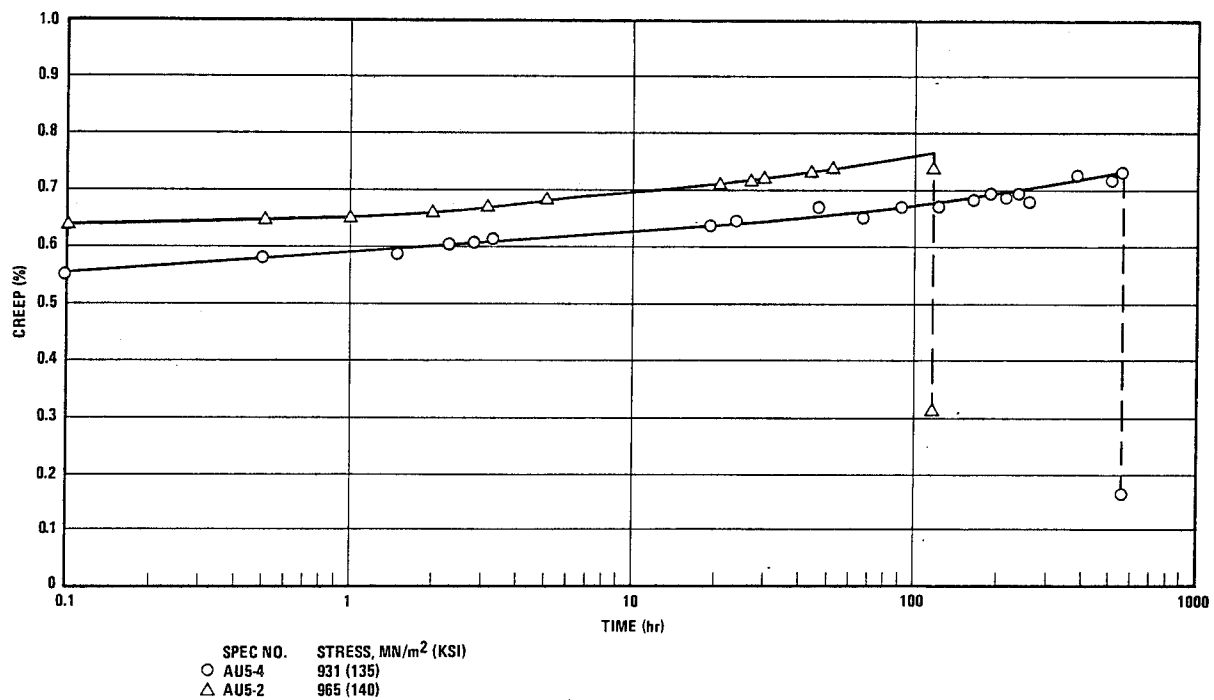


Figure 10-8 Creep Strain for $[0^\circ]_6$ B/E at 450 K (350° F)

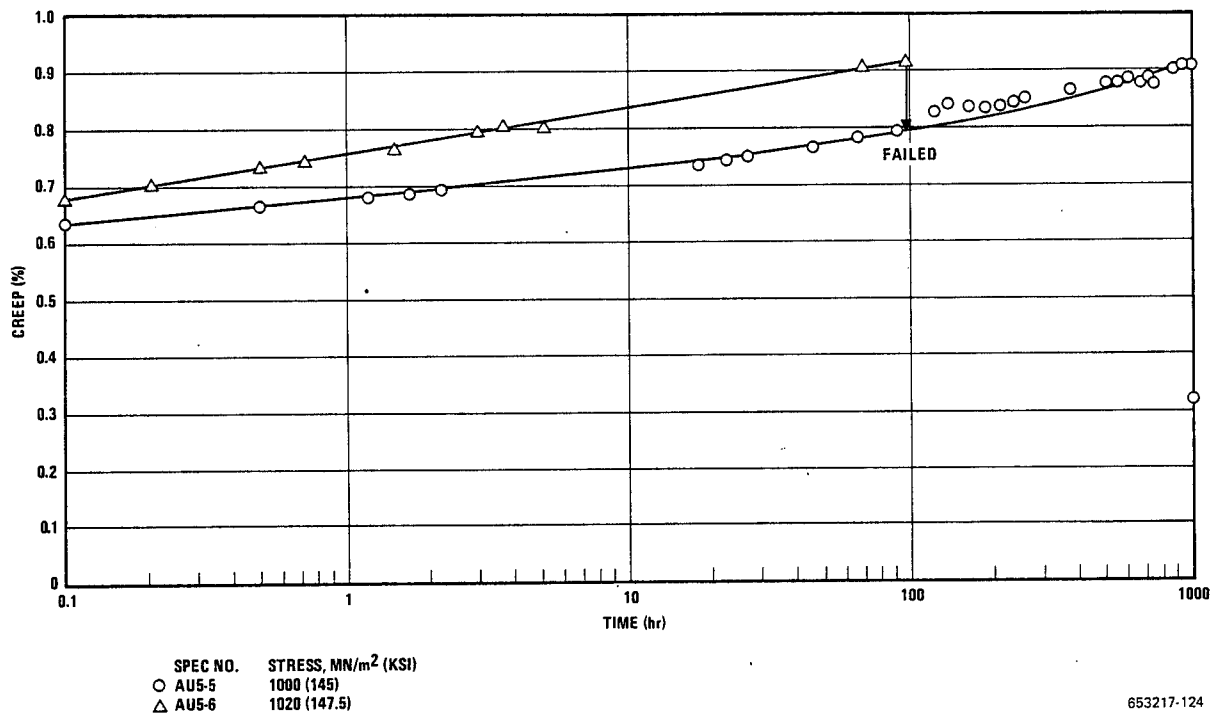


Figure 10-9 Creep Strain for $[0^\circ]_6$ B/E at 450 K (350° F)

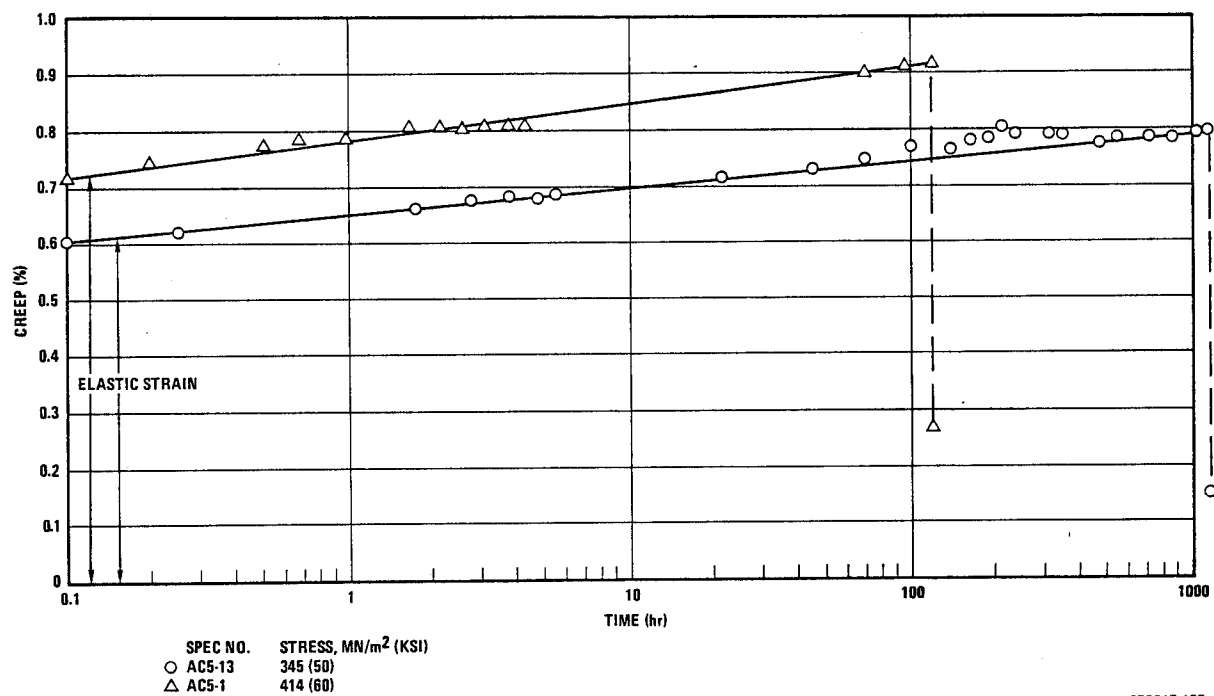
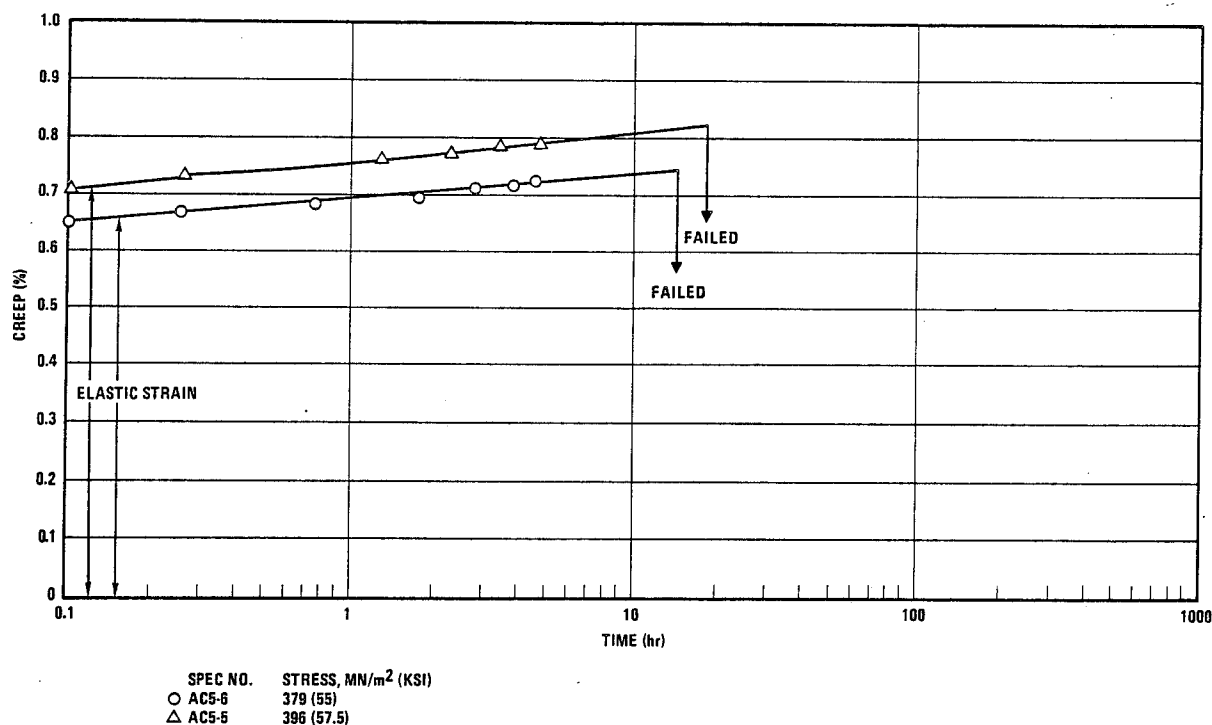


Figure 10-10 Creep Strain for $[0^\circ \pm 45^\circ]_5$ B/E at 450 K (350° F)



653217-126

Figure 10-11 Creep Strain for $[0^\circ \pm 45^\circ]_s$ B/E at 450 K (350° F)

In analyzing the creep data an effort was made to prepare composite creep curves for 0.05, 0.10, 0.15, 0.20, and 0.25% creep by determining the time periods required for varying amounts of creep strain as a function of stress level. The limited amount of creep data available, the small amount of creep strain measured, and the scatter in the data combined to give results that were unsuitable for the plotting of this type of creep curve. This was found to apply to all the other composite systems as well as the B/E.

10.3.2 GRAPHITE/EPOXY. Results of creep testing of G/E at 394 K (250° F) and 450 K (350° F) are listed in Table 10-3. Data are presented for 24 specimens.

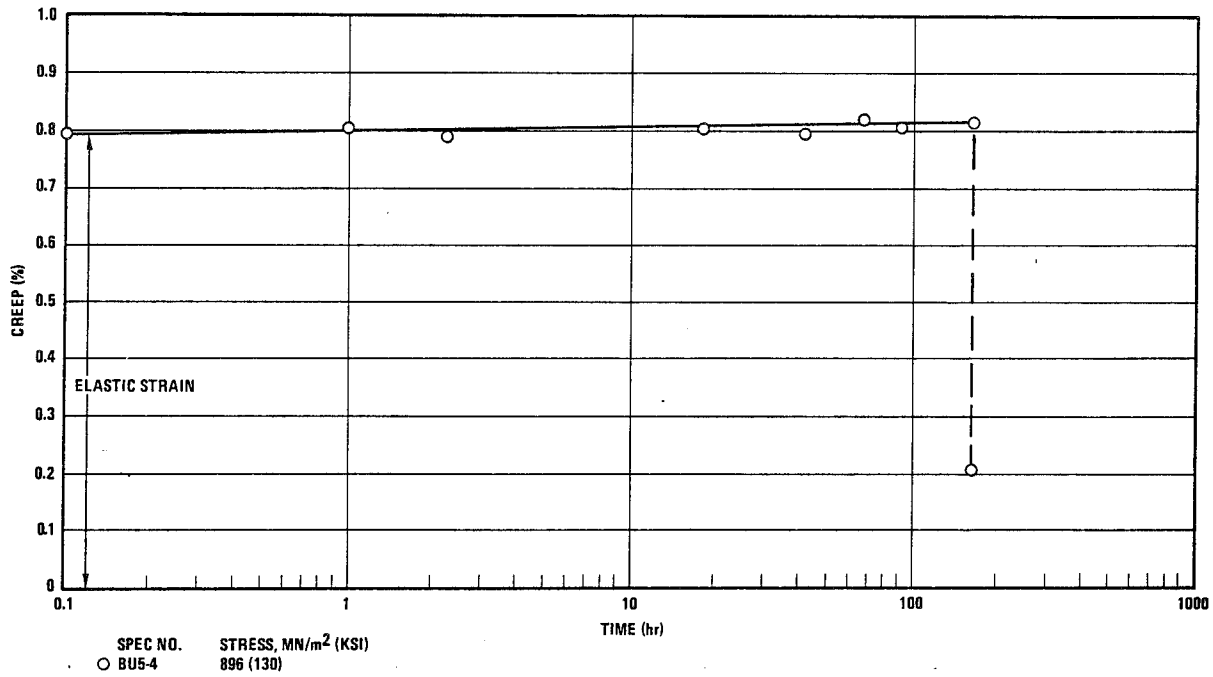
Creep strain versus time curves are presented in Figures 10-12 through 10-14 for unidirectional material at 394 K (250° F), in Figures 10-15 through 10-18 for crossplied material at 394 K (250° F), in Figures 10-19 and 10-20 for unidirectional material at 450 K (350° F), and in Figure 10-21 for crossplied material at 450 K (350° F).

The G/E data are very similar to those for B/E in that the amount of permanent creep strain was very small for all test conditions. For only two specimens was the creep greater than 0.1% and for these specimens the values were below 0.2%. An example of the small amount of creep observed in the G/E material can be seen for specimen BC5-10 (crossplied). This specimen showed only 0.17% creep in 570 hours when loaded to 500 MN/m² (72.5 ksi) or 95% of the average ultimate tensile strength. A similar specimen, when tested at 517 MN/m² (75 ksi), failed during application of the load in the test machine. Two of the crossplied specimens failed in this manner (during loading) but at stresses that were within the scatter band found during baseline testing at the same temperatures. Three of the unidirectional specimens also failed

Table 10-3. Summary of Creep Test Results for G/E

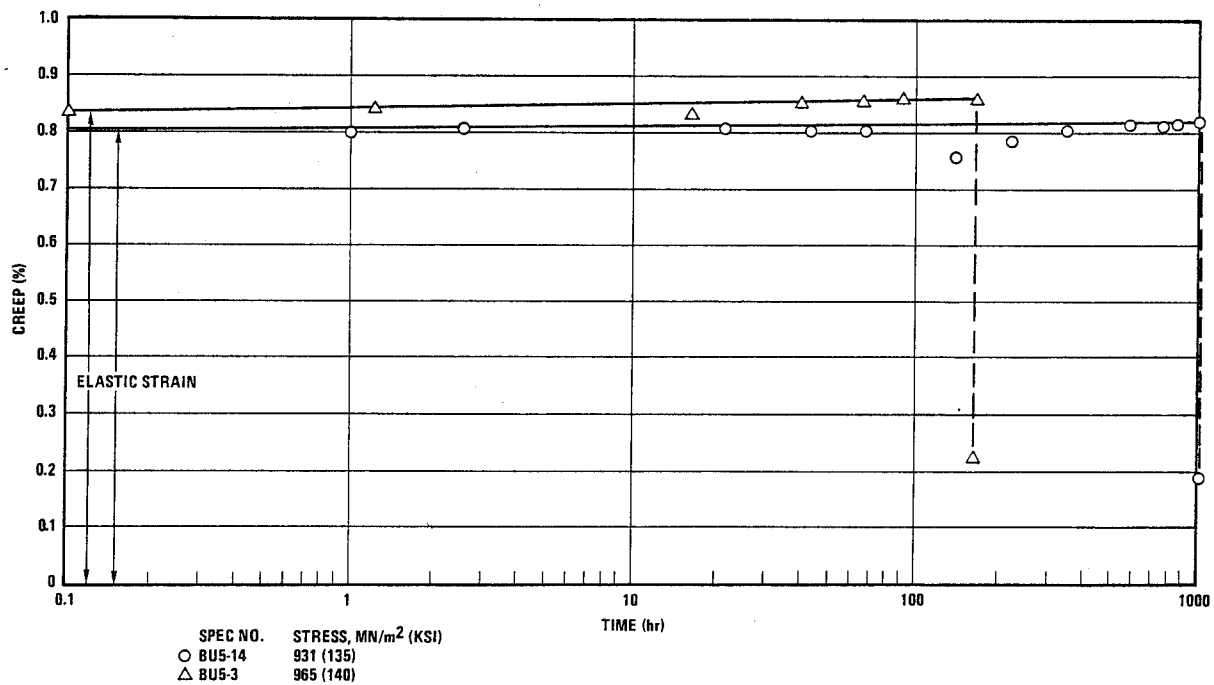
Specimen Number	Orientation	Test Temperature		Stress MN/m ²	(ksi)	Time (hr)	Total Creep Creep Strain (%)	Comments
		K	(°F)					
BU5-4	[0°] ₆	394	250	896	130	100	0.01	
-14				931	135	1000	.01	
-3				965	140	100	.02	
-6				1000	145	100	.01	
-2				1030	150	—	—	Failed on loading
-1				1100	160	—	—	Failed on loading
BC5-7	[0° ± 45°] _s	394	250	414	60	100	.04	
-13				448	65	1000	.02	
-8				448	65	100	.07	
-11				465	67.5	100	.03	
-9				483	70	100	.08	
-10				500	72.5	570	.17	
-12				517	75	—	—	Failed on loading
BU5-12	[0°] ₆	450	350	896	130	1000	.01	
-7				965	140	100	.01	
-10				1000	145	a1.6	.02	Bond failure in 3 hours
-11				1000	145	—	—	Failed on loading
-9				1030	150	1000	.02	
-13				1070	155	100	.06	
BC5-5	[0° ± 45°] _s	450	350	396	57.5	—	—	Bond failure on loading
-1				414	60	100	.05	Bond failure in 170 hours
-4				431	62.5	1000	.15	
-3				448	65	—	—	Failed on loading
-2				448	65	—	—	Bond failure on loading

aLast measurement prior to failure



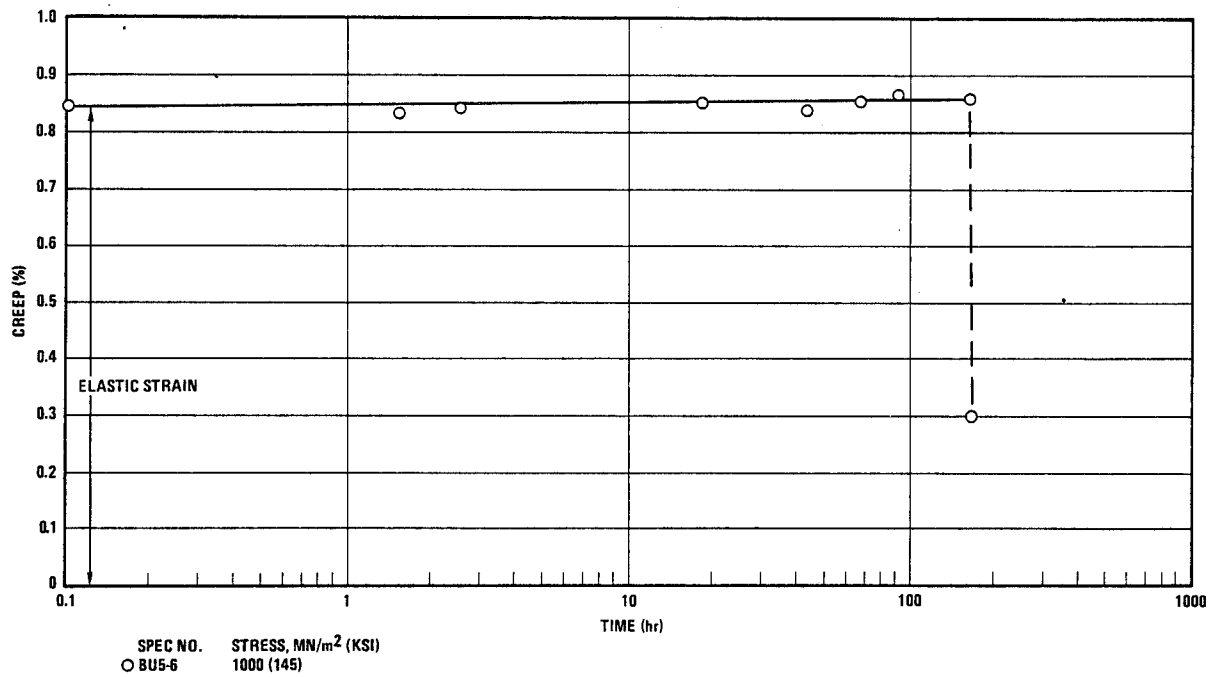
653217-127

Figure 10-12 Creep Strain for [0°]₆ G/E at 394 K (250° F)



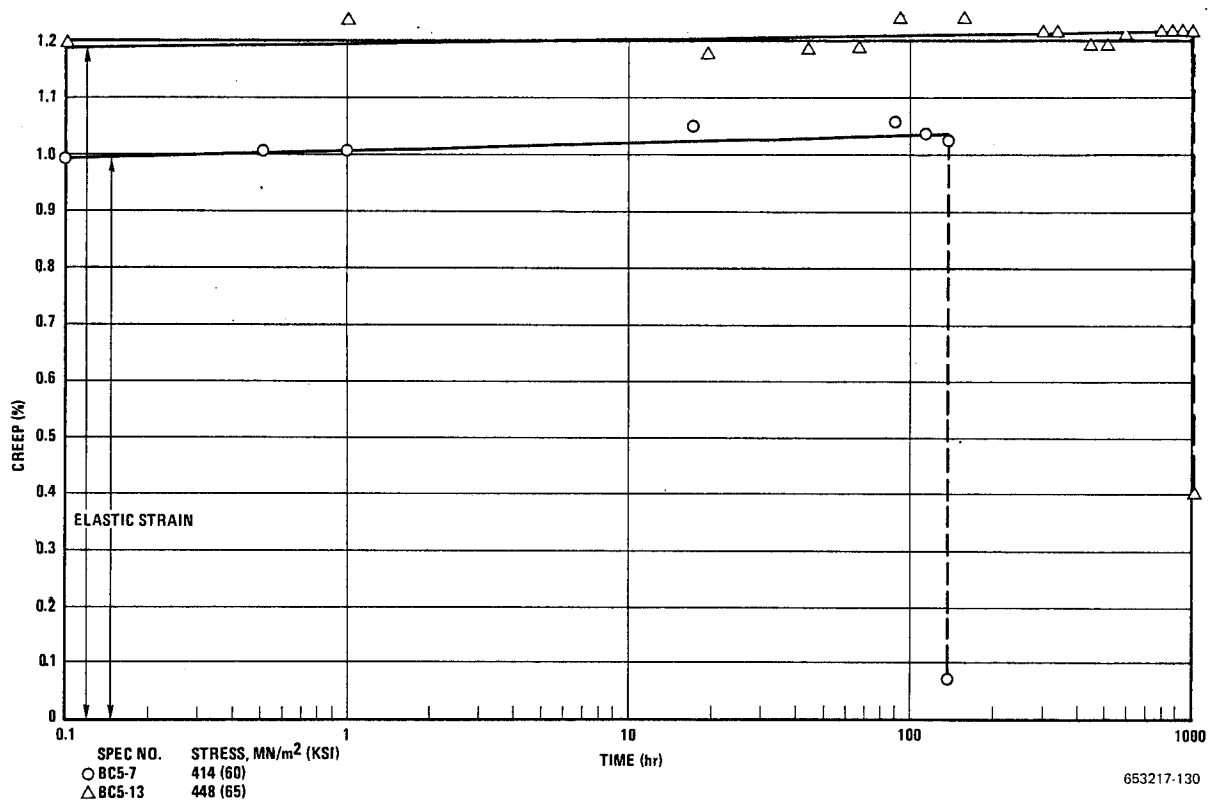
653217-128

Figure 10-13 Creep Strain for [0°]₆ G/E at 394 K (250° F)



653217-129

Figure 10-14 Creep Strain for $[0^\circ]_6$ G/E at 394 K (250° F)



653217-130

Figure 10-15 Creep Strain for $[0^\circ \pm 45^\circ]_6$ G/E at 394 K (250° F)

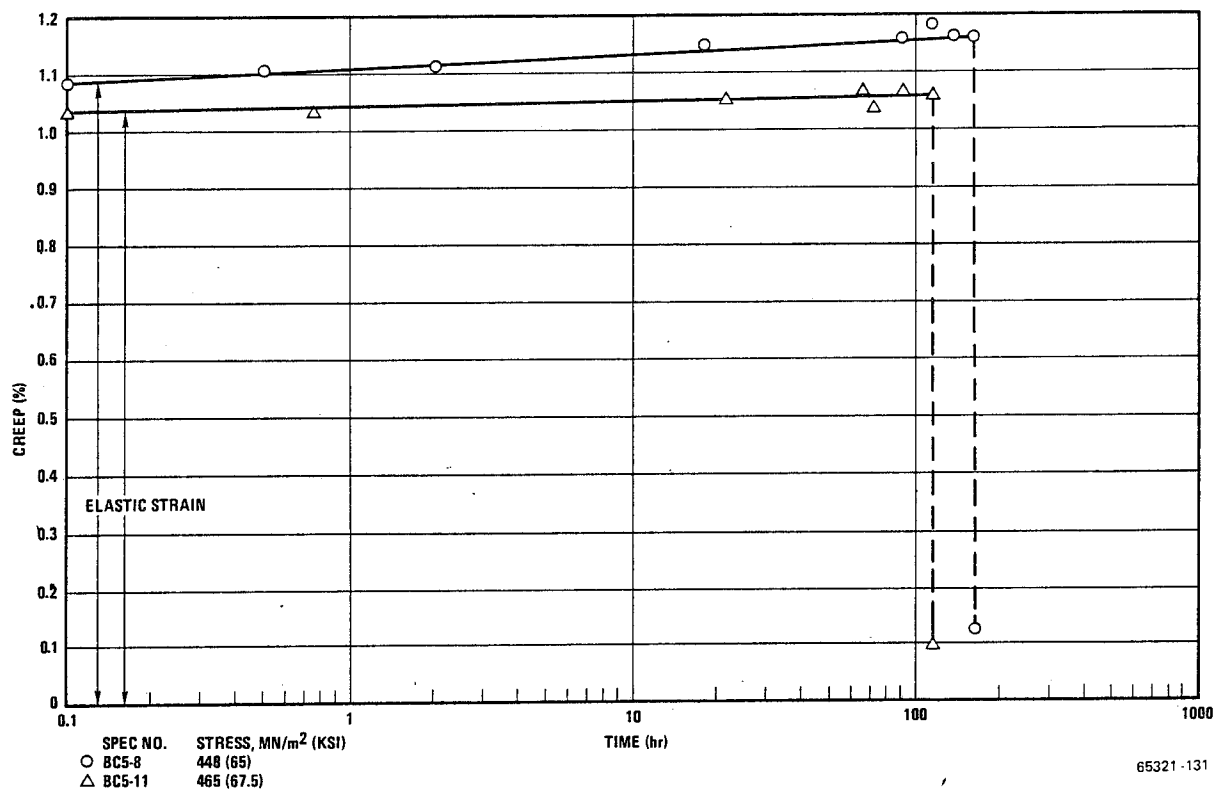


Figure 10-16 Creep Strain for $[0^\circ \pm 45^\circ]$, G/E at 394 K (250° F)

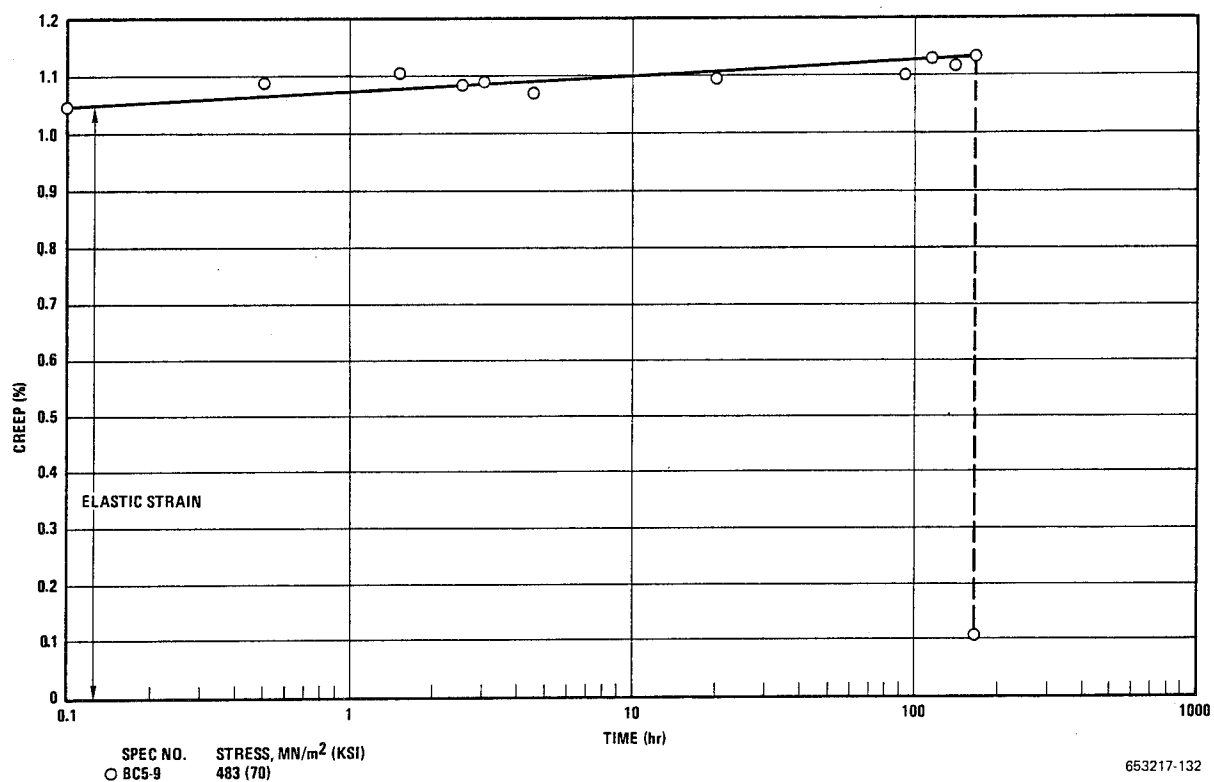


Figure 10-17 Creep Strain for $[0^\circ \pm 45^\circ]$, G/E at 394 K (250° F)

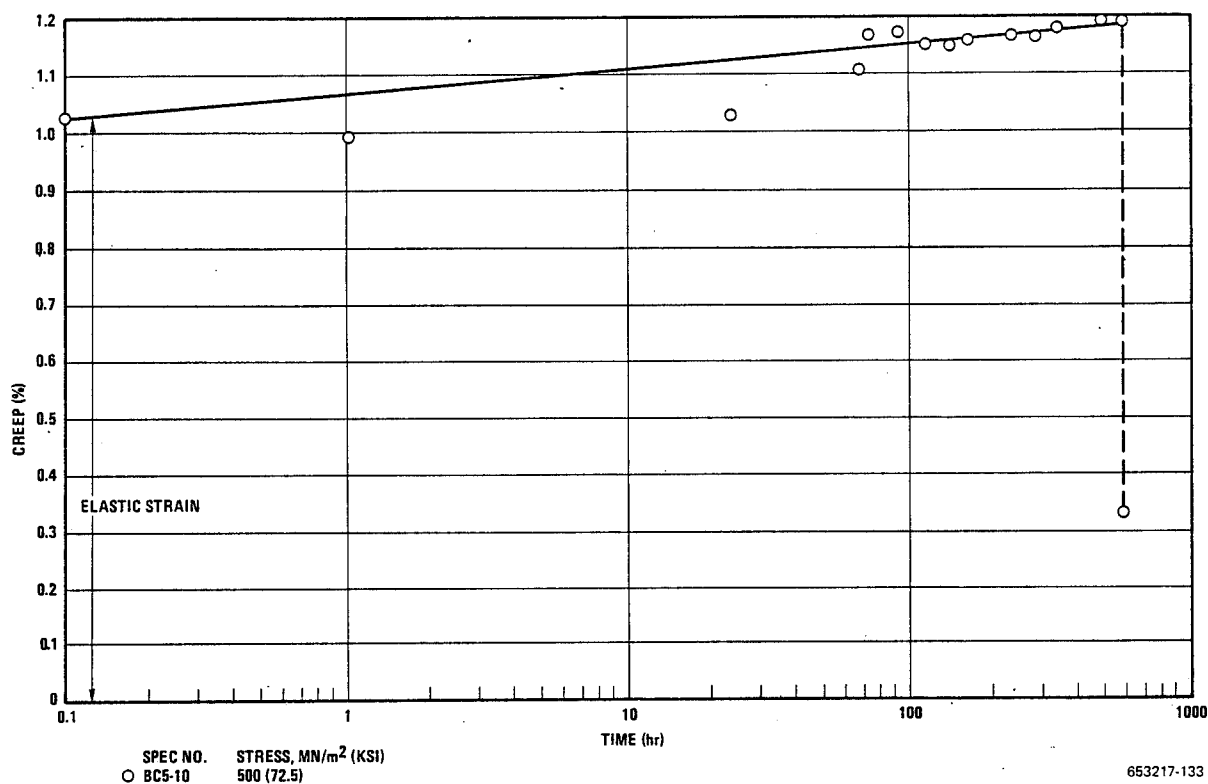


Figure 10-18 Creep Strain for $[0^\circ \pm 45^\circ]$, G/E at 394 K (250° F)

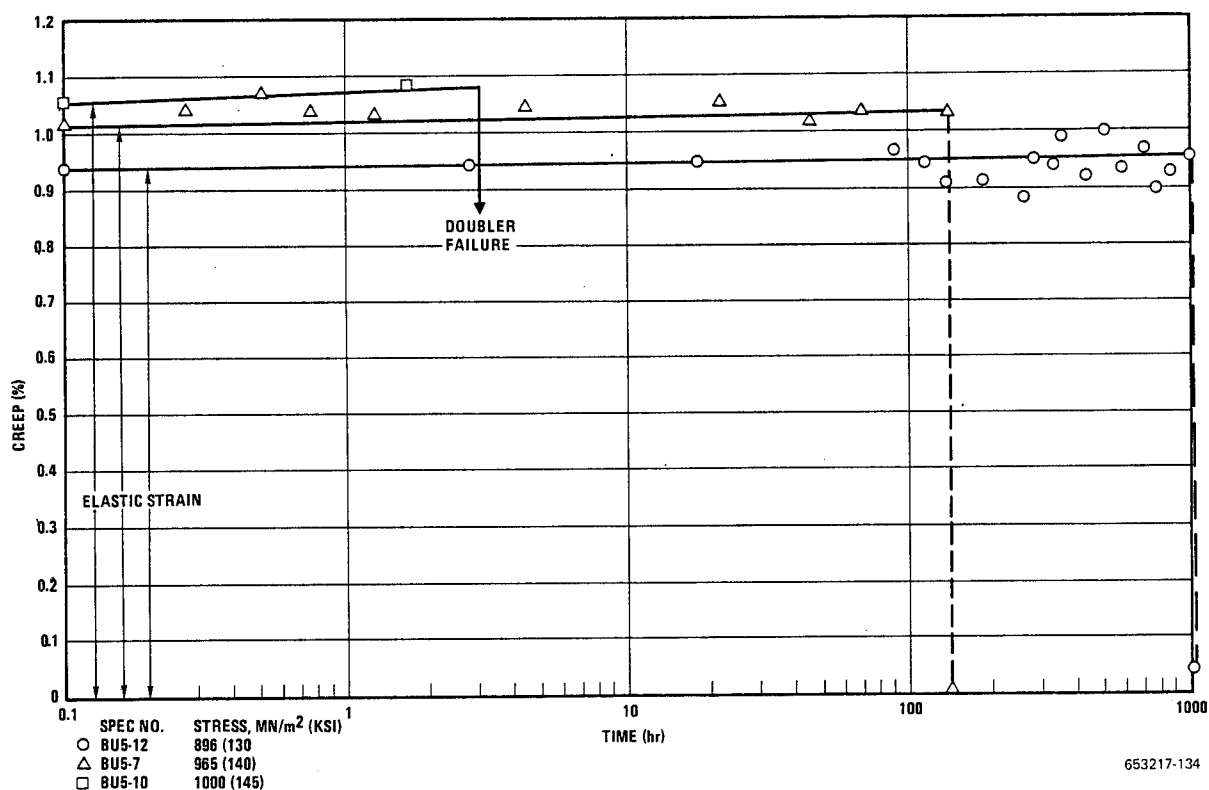


Figure 10-19 Creep Strain for $[0^\circ]$, G/E at 450 K (350° F)

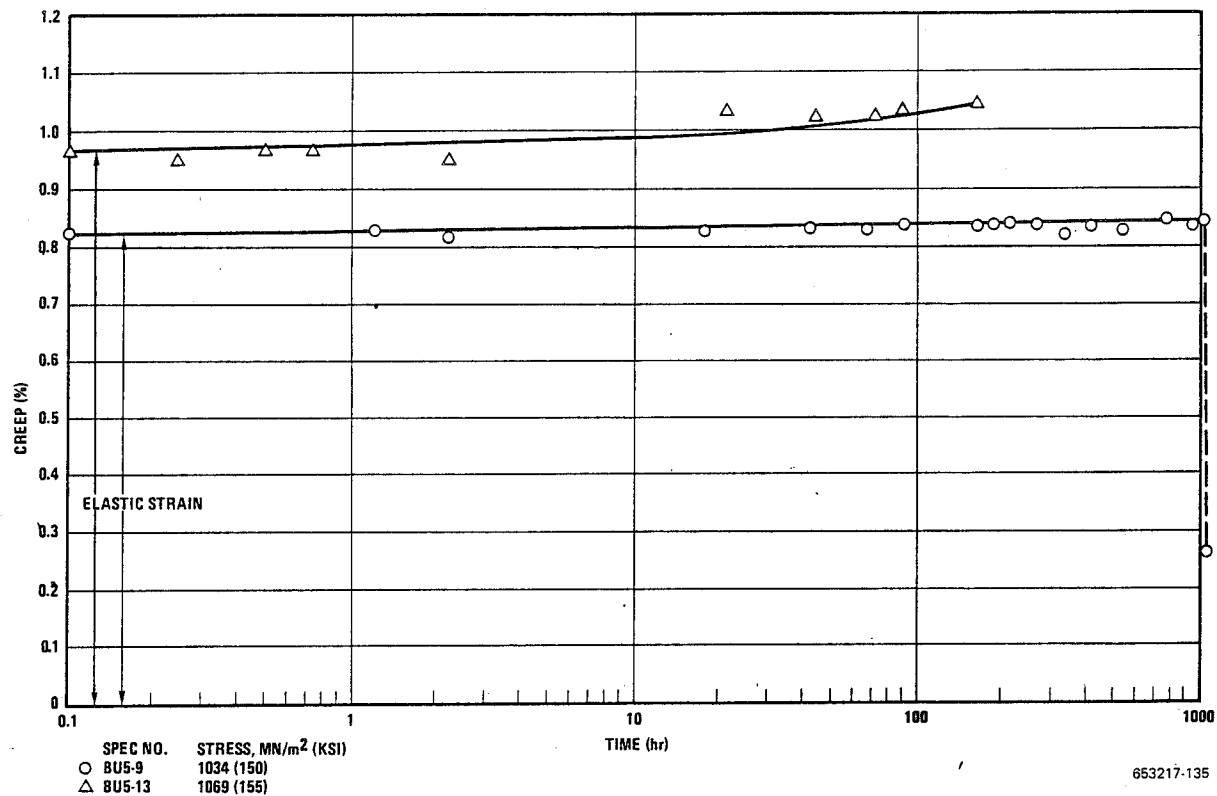


Figure 10-20 Creep Strain for $[0^\circ]_6$ G/E at 450 K (350° F)

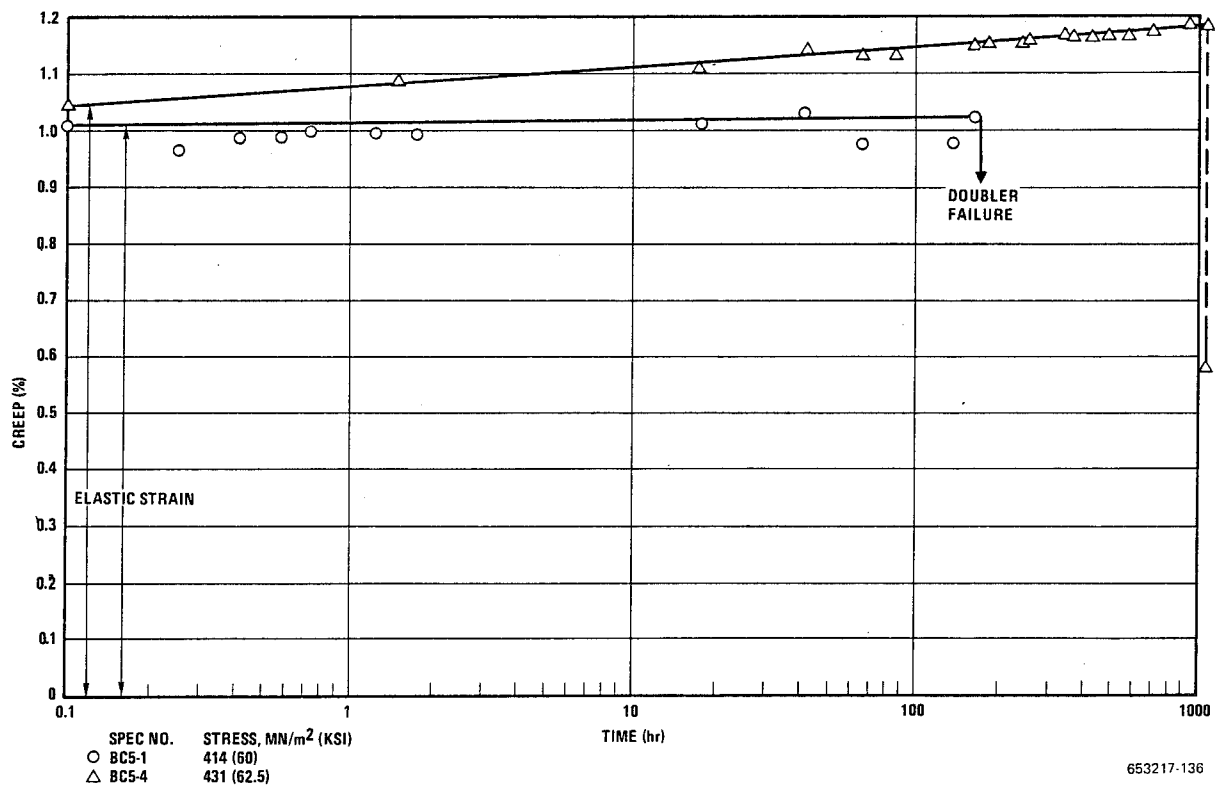


Figure 10-21 Creep Strain for $[0^\circ \pm 45^\circ]_s$ G/E at 450 K (350° F)

during loading. These failures, however, occurred at stresses well below the scatter band obtained in the baseline test program. Differences in material strengths were not the cause of the premature failures because both the baseline and the creep specimens were all cut from the same panel, LRC-10A. Of the three specimens that failed on loading, one failed at the center, the second failed in two locations — at the center and approximately 0.04 m (1.5 in.) from the top doubler, and the third, also failing at two locations, at the edge of each doubler. It may have been the rapid application of load that led to the early failure of these specimens. The loads were added in incremental steps of 181 kg (400 lb) to reach a value of slightly more than 907 kg (2000 lb).

10.3.3 GRAPHITE/POLYIMIDE. Results of creep testing G/PI at 505 K (450° F) and 561 K (550° F) are listed in Table 10-4. Data are presented for 24 specimens.

Creep strain versus time curves are presented in Figure 10-22 for unidirectional material at 550 K (450° F), in Figures 10-23 through 10-27 for crossplied material at 550 K (450° F), in Figures 10-28 and 10-29 for unidirectional material at 561 K (550° F), and in Figure 10-30 for crossplied material at 561 K (550° F).

Creep strain values obtained for the G/PI system at both test temperatures were also very low. For only one specimen, DC5-1 (crossplied), was a value greater than 0.1% recorded. Examples of the small creep extensions that were measured are the 0.03% creep for specimen DU5-1 (unidirectional) in 100 hours at 550 K (450° F) when loaded at 85% of the average ultimate tensile strength and the 0.07% creep for specimen DC5-8 (crossplied) in 100 hours at 561 K (550° F) when loaded at 91% of the average ultimate tensile strength.

The data obtained for the G/PI system were somewhat limited because of several doubler bond failures in the unidirectional specimens. These were caused by the combination of high shear stresses in the adhesive because of the high applied test loads and heating from the furnaces. Several specimens failures also occurred during application of the loads at the beginning of testing. In like manner to the G/E loading failures, the G/PI crossplied specimens failed at stresses within the baseline tensile data scatterband while the unidirectional specimens failed at stresses slightly below the baseline scatterband.

10.3.4 BORON/ALUMINUM. Results of creep testing of B/Al at 505 K (450° F) and 561 K (550° F) are listed in Table 10-5. Data are presented for 24 specimens.

Creep strain versus time curves are presented in Figures 10-31 and 10-32 for unidirectional material at 505 K (450° F), in Figures 10-33 and 10-34 for crossplied material at 505 K (450° F), in Figures 10-35 through 10-37 for unidirectional material at 561 K (550° F), and in Figures 10-38 through 10-40 for crossplied material at 561 K (550° F).

Creep strains measured for B/Al specimens were somewhat higher than for other systems but were still quite small. The unidirectional material gave values less than 0.2% with the crossplied material reaching a maximum value of only 0.31%. Several failures were recorded during test prior to completing the required 100- or 1000-hour time periods. There were also several doubler bond failures in the more highly loaded unidirectional specimens. These failures, both in the B/Al composite material at each test temperature and in the doubler bonds at 561 K (550° F), occurred at stress levels above approximately 85% of the average ultimate

Table 10-4. Summary of Creep Test Results for G/PI

Specimen Number	Orientation	Test Temperature		Stress		Time (hr)	Total Creep		Comments
		K	(°F)	MN/m ²	(ksi)		Creep Strain (%)		
DU5-5	[0°] ₆	505	450	965	140	—	—		Bond failure in 0.15 hr
-6				965	140	—	—		Bond failure in 0.22 hr
-4				1000	145	100	.02		
-1				1030	150	100	.03		
-3				1070	155	—	—		Failed on loading
-2				1100	160	—	—		Failed on loading
DC5-6	[0° ± 45°] _s	505	450	259	37.5	1000	.08		
-3				276	40	1000	.06		
-5				293	42.5	1000	.05		
-2				310	45	1000	.00		
-4				328	47.5	986	.10		
-1				345	50	a428	a.18		Failed in 471 hours
DU5-11	[0°] ₆	561	550	862	125	a46	a.00		Bond failure in 58 hours
-8				896	130	100	.01		
-9				931	135	100	.00		
-12				948	137.5	—	—		Bond failure on loading
-7				965	140	a22	a.02		Bond failure in 33 hours
-10				1000	145	—	—		Failed on loading
DC5-12	[0° ± 45°] _s	561	550	207	30	100	.03		
-11				241	35	100	.04		
-7				276	40	100	.04		
-8				310	45	100	.07		
-10				328	47.5	—	—		Failed on loading
-9				345	50	—	—		Failed on loading

Last measurement prior to failure

aLast measurement prior to failure

tensile strength for the 505 K (450° F) tests and above approximately 75% for the 561 K (550° F) tests. One specimen, EC5-12, failed during loading at a stress level, 421 MN/m² (61 ksi), slightly below the average ultimate tensile strength, 439 MN/m² (63.7 ksi), of cross-plyed B/Al at 561 K (550° F). The specimen had been mistakenly identified as an unidirectional specimen and was intended to have been tested at a much higher load.

The conclusion drawn from creep testing of the four composite materials is that boron or graphite filament reinforced materials with 0° plies aligned in the direction of loading undergo very little creep even at stress levels that result in fracture in short exposure times. Because of the low creep strains observed in these materials, it would appear that stress rupture tests could well be substituted for creep measurements. A plot of creep stress versus time for various creep strains from 0.05% to rupture would likely show a family of curves that were very closely spaced. Since the expense in obtaining creep data is far greater than that for stress rupture testing, a considerable savings could be realized.

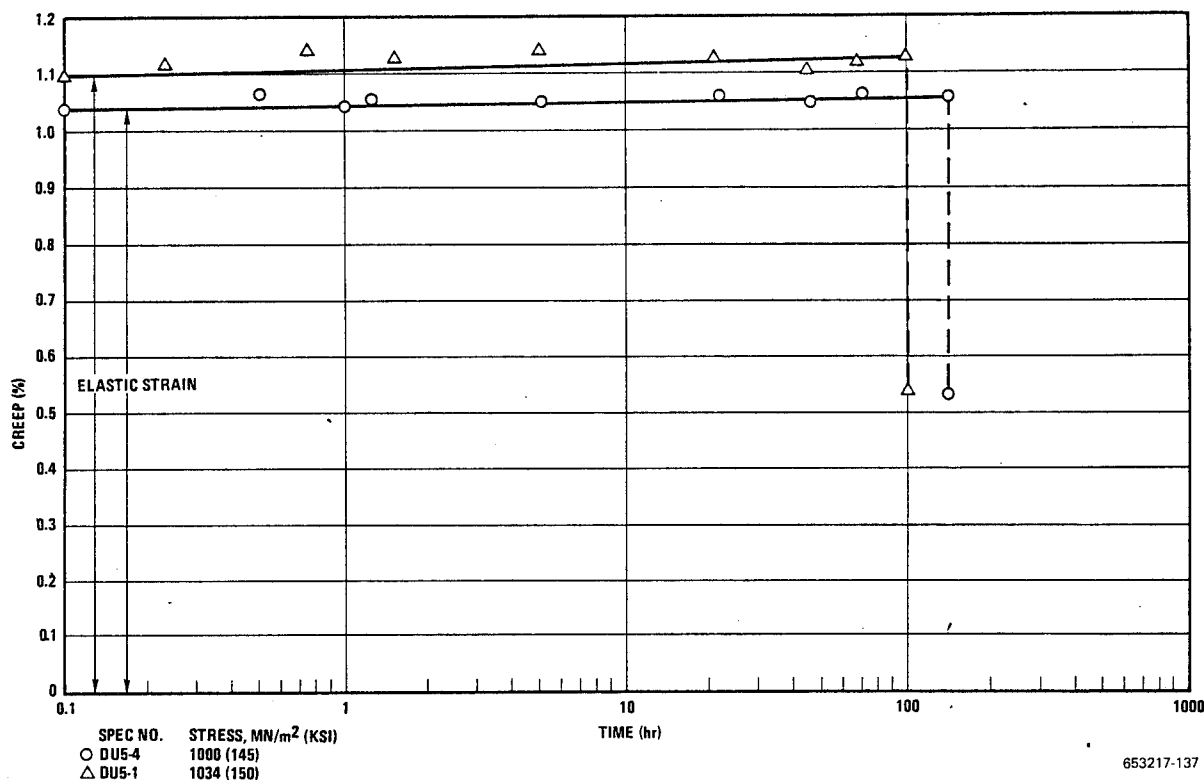


Figure 10-22 Creep Strain for [0°]₆ G/PI at 505 K (450° F)

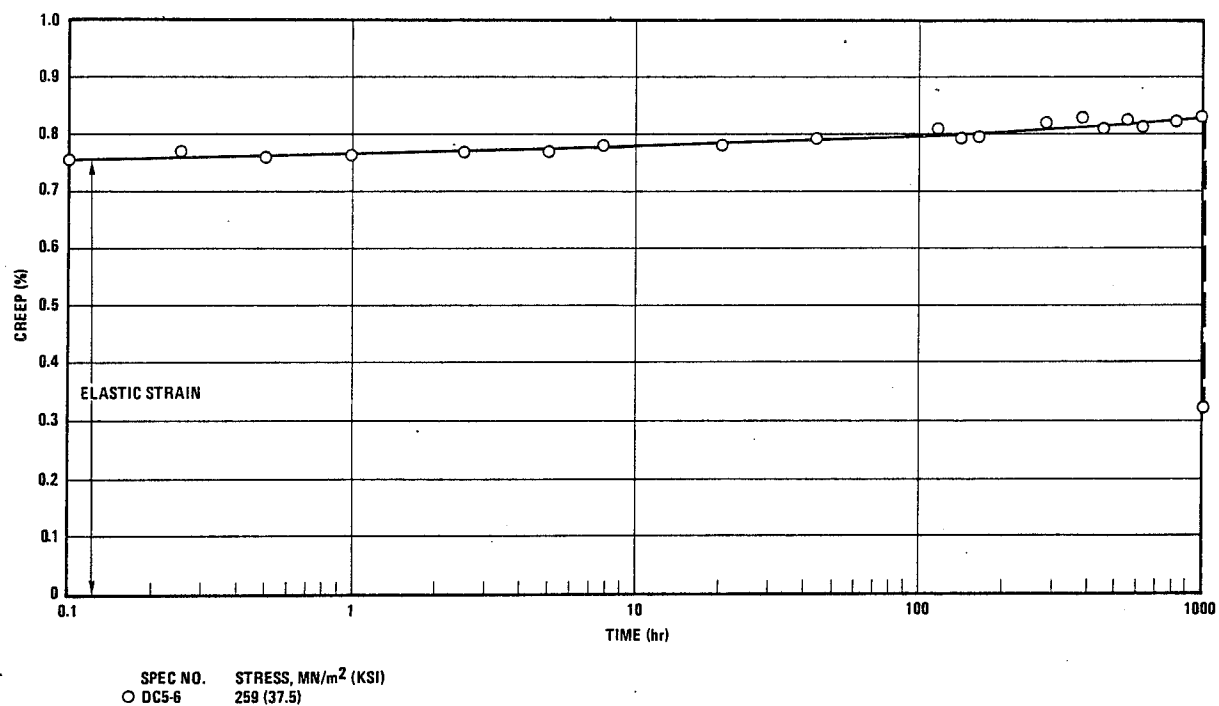


Figure 10-23 Creep Strain for $[0^\circ \pm 45^\circ]_s$ G/PI at 505 K (450° F)

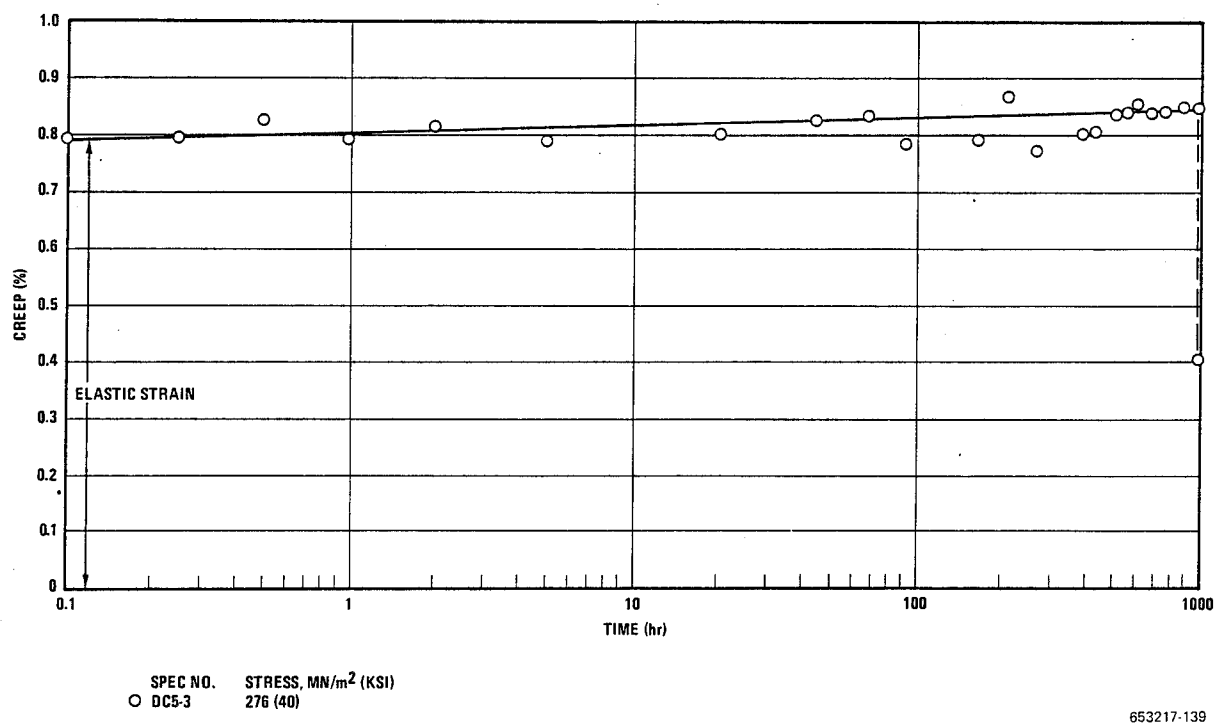


Figure 10-24 Creep Strain for $[0^\circ \pm 45^\circ]_s$ G/PI at 505 K (450° F)

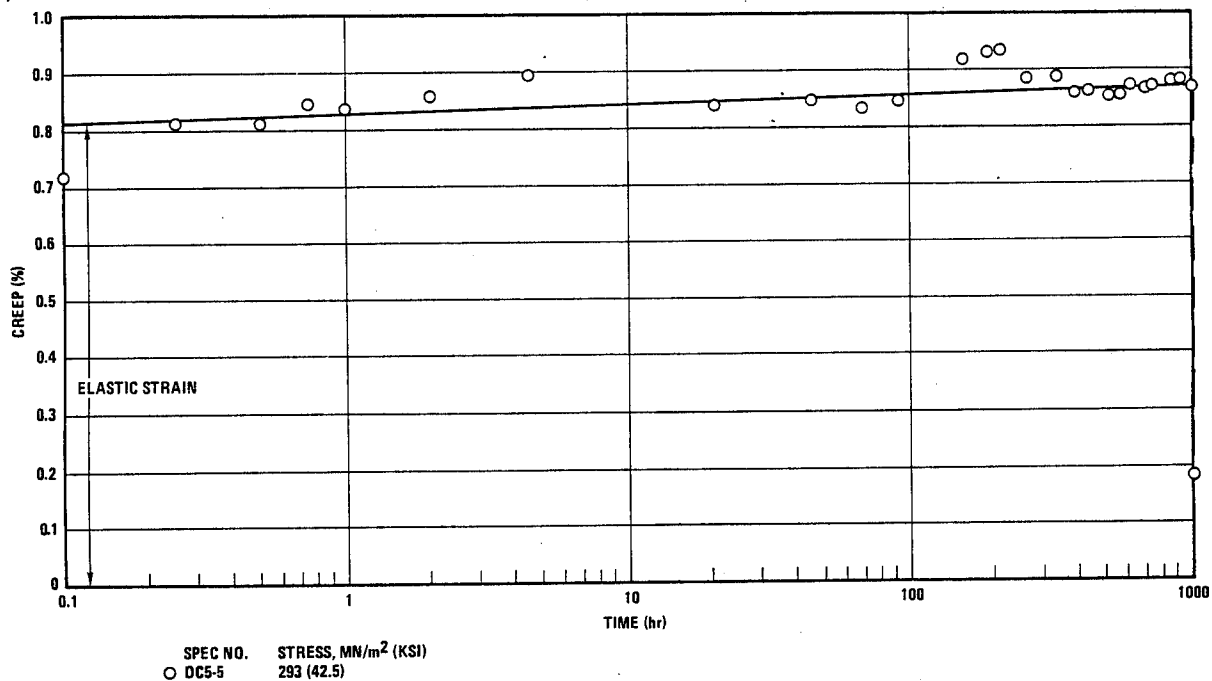


Figure 10-25 Creep Strain for $[0^\circ \pm 45^\circ]_s$ G/PI at 505 K (450° F)

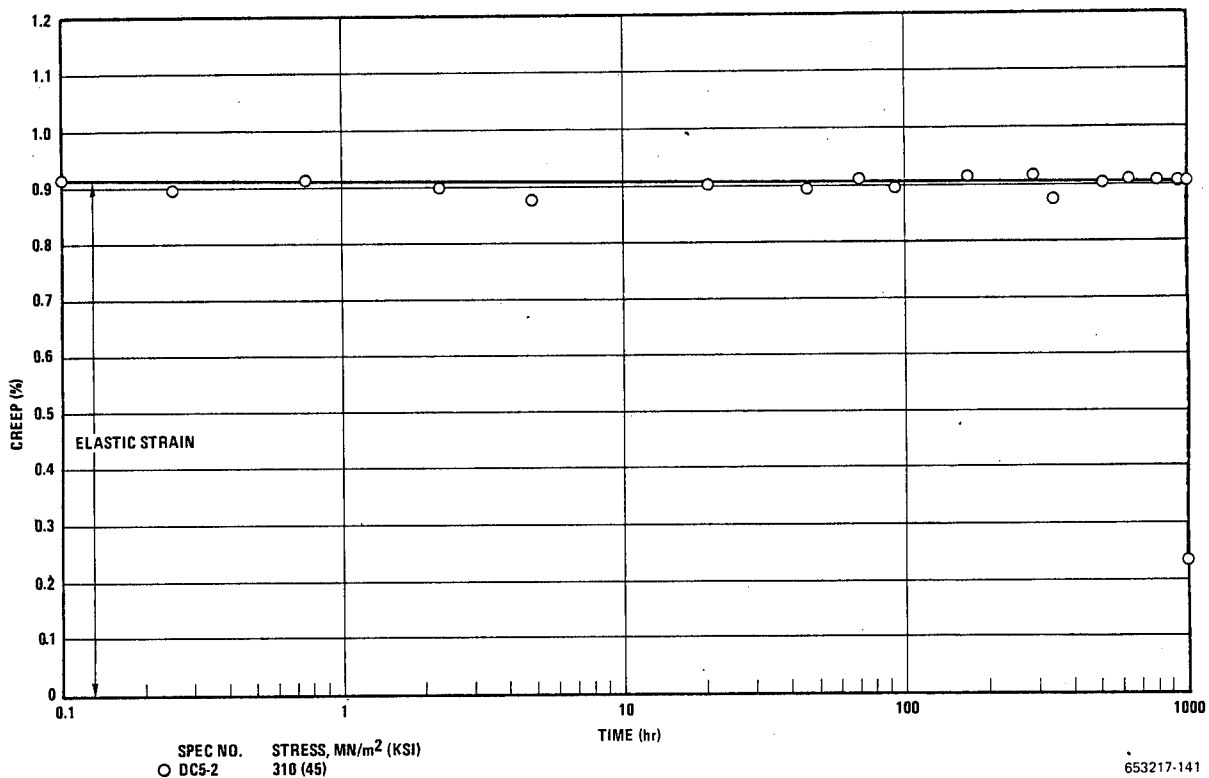


Figure 10-26 Creep Strain for $[0^\circ \pm 45^\circ]_s$ G/PI at 505 K (450° F)

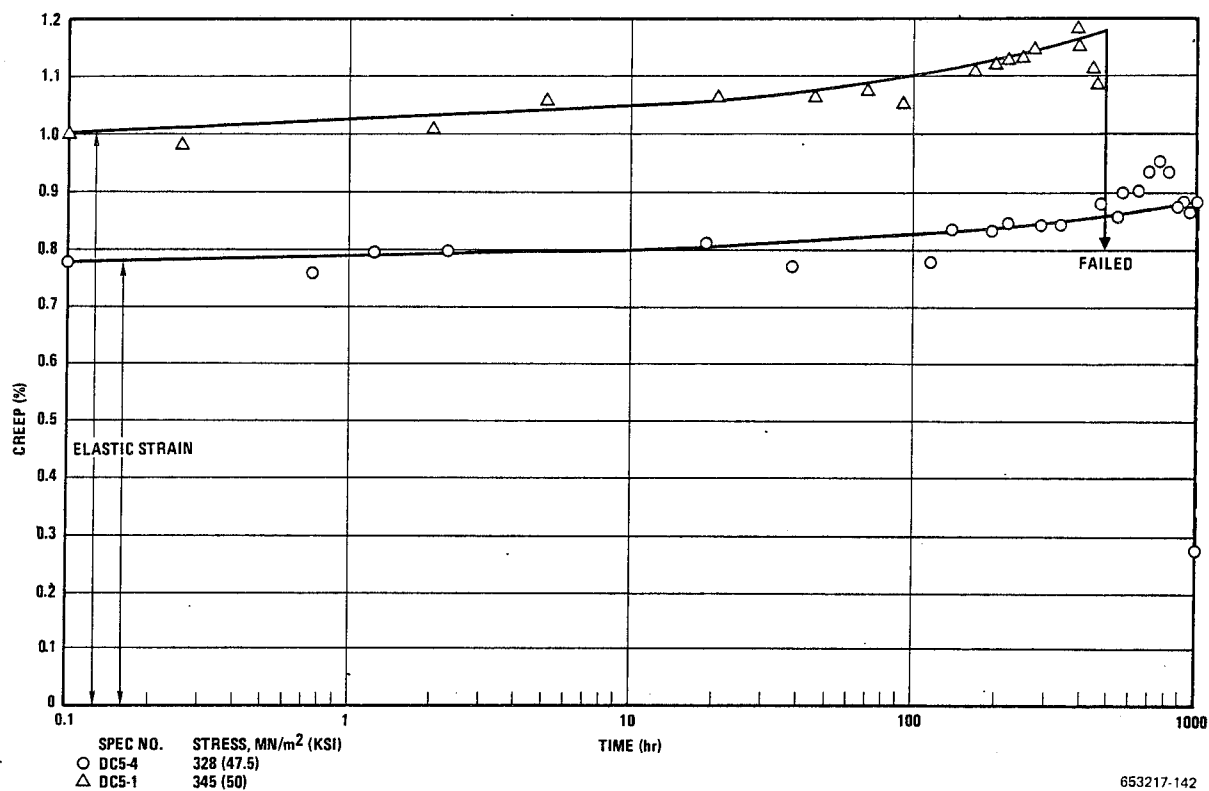


Figure 10-27 Creep Strain for $[0^\circ \pm 45^\circ]_s$ G/PI at 505 K (450° F)

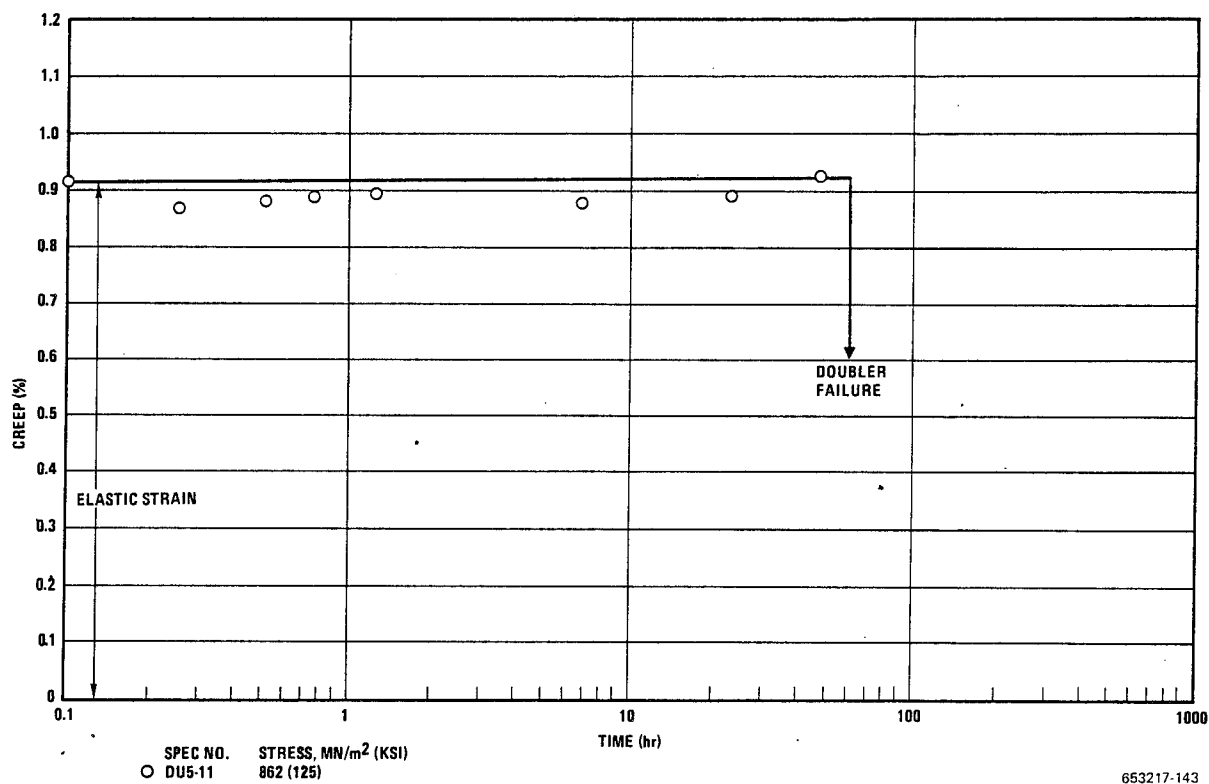


Figure 10-28 Creep Strain for $[0^\circ]_6$ G/PI at 561 K (550° F)

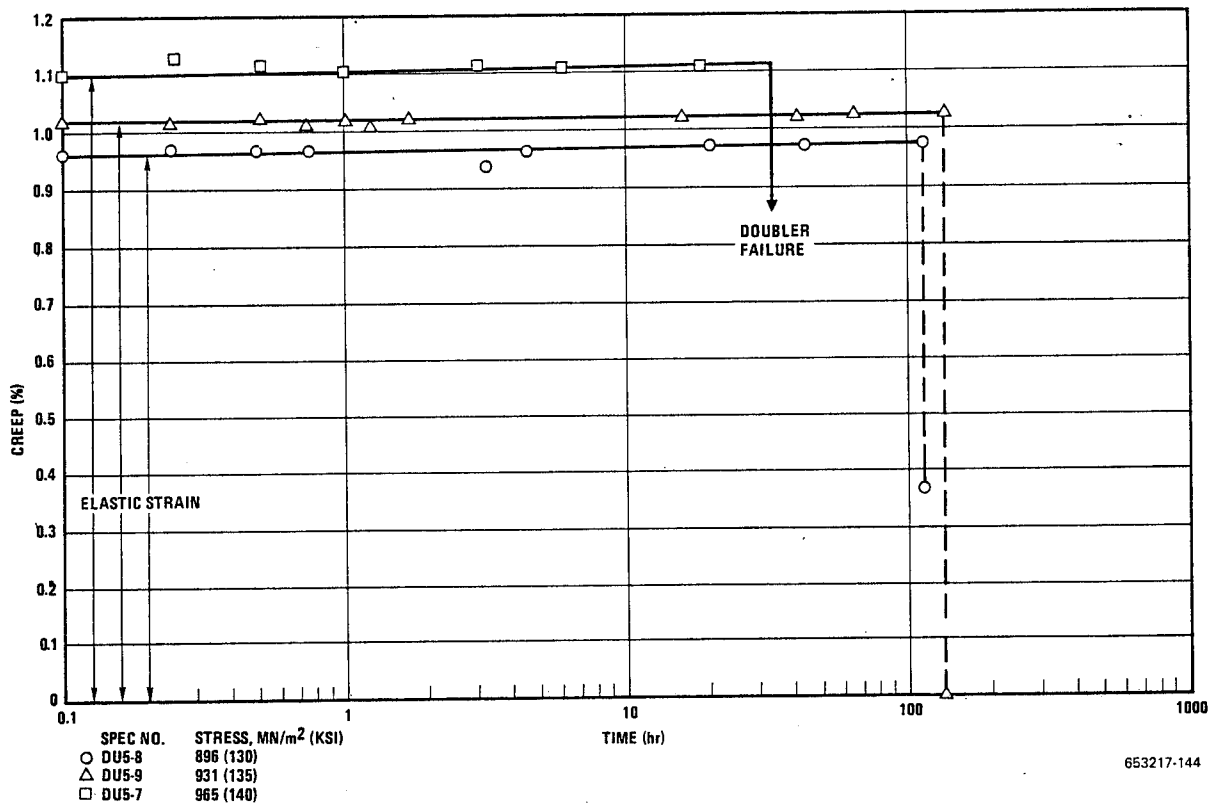


Figure 10-29 Creep Strain for $[0^\circ]_6$ G/PI at 561 K (550° F)

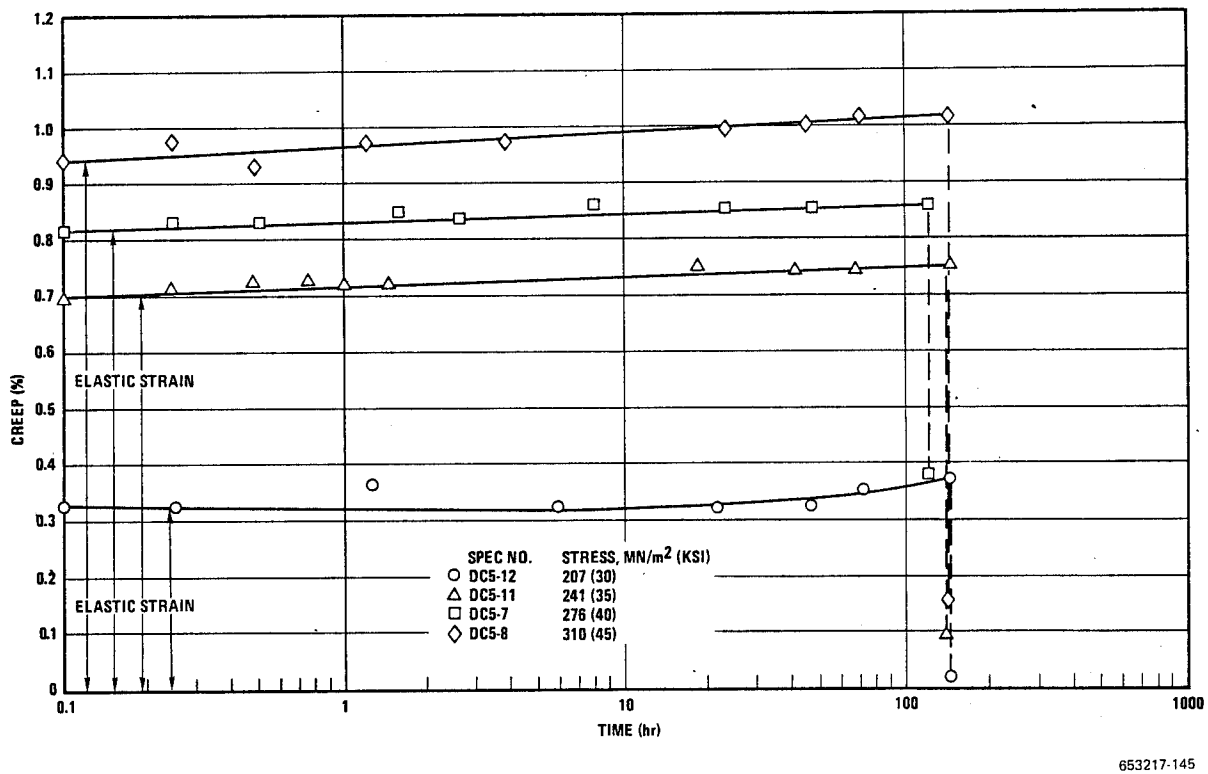


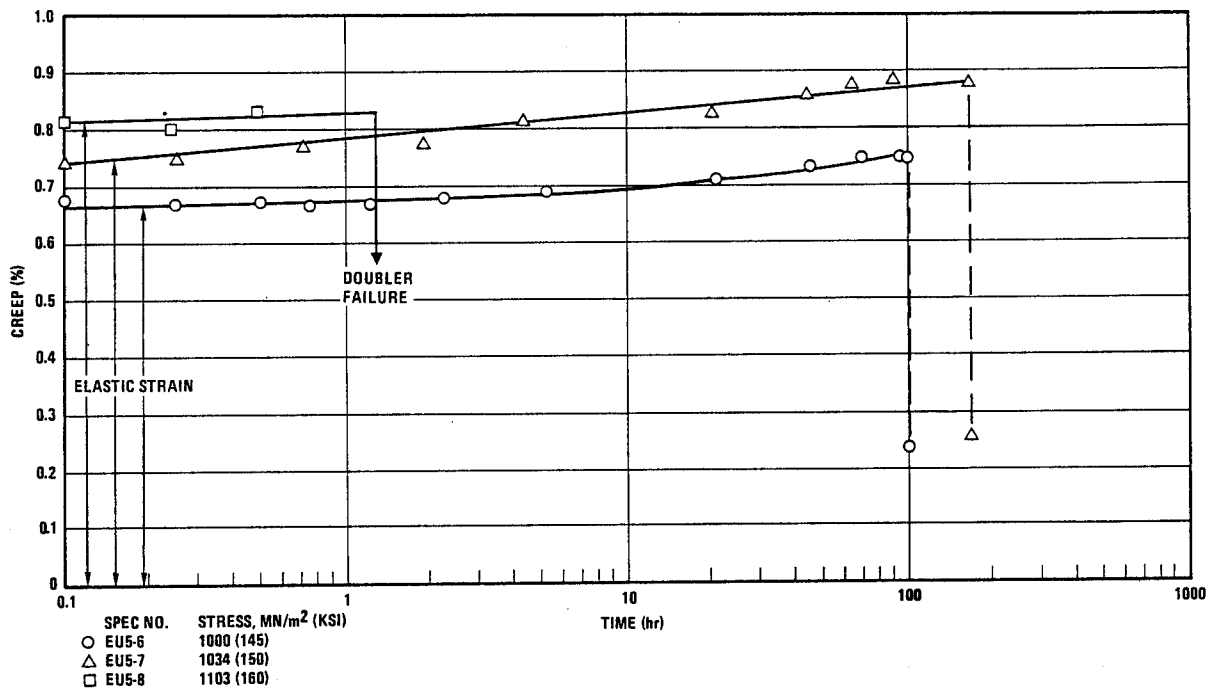
Figure 10-30 Creep Strain for $[0^\circ \pm 45^\circ]_6$ G/PI at 561 K (550° F)

Table 10-5: Summary of Creep Test Results for B/Al

Specimen Number	Orientation	Test Temperature		Stress		Time (hr)	Total Creep		Comments
		K	(°F)	MN/m ²	(ksi)		Creep Strain (%)		
EU5-6	[0°] ₆	505	450	1000	145	100	0.08	Bond failure in 0.17 hr.	
-7				1030	150	100	.13		
-12				1070	155	—	—		
-8				1100	160	a.5	a.01	Bond failure in 1.3 hr.	
-9				1100	160	100	.18		
-10				1170	170	a.21	a.19	Failed in 45 hours	
EC5-5	[0° ± 45°] _s	505	450	276	40	100	.12		
-11				310	45	1000	.24		
-7				345	50	1000	.24		
-8				379	55	100	.19		
-10				414	60	a.648	a.31	Failed in 714 hours	
-6				448	65	a1.2	a.09	Failed in 2.7 hours	
EU5-4	[0°] ₆	561	550	827	120	100	.09		
-3				862	125	100	.13		
-5				896	130	100	.13		
-11				896	130	100	.16		
-2				965	140	a2.5	a.07	Bond failure in 8 hours	
-1				1030	150	—	—	Bond failure in 0.07 hour	
EC5-9	[0° ± 45°] _s	561	550	276	40	1000	.29		
-4				293	42.5	1000	.18		
-1				310	45	1000	.25		
-3				328	47.5	100	.15	Failed in 114 hours	
-2				345	50	a18	a.13	Failed in 30 hours	
-12				421	61	—	—	Failed on loading	

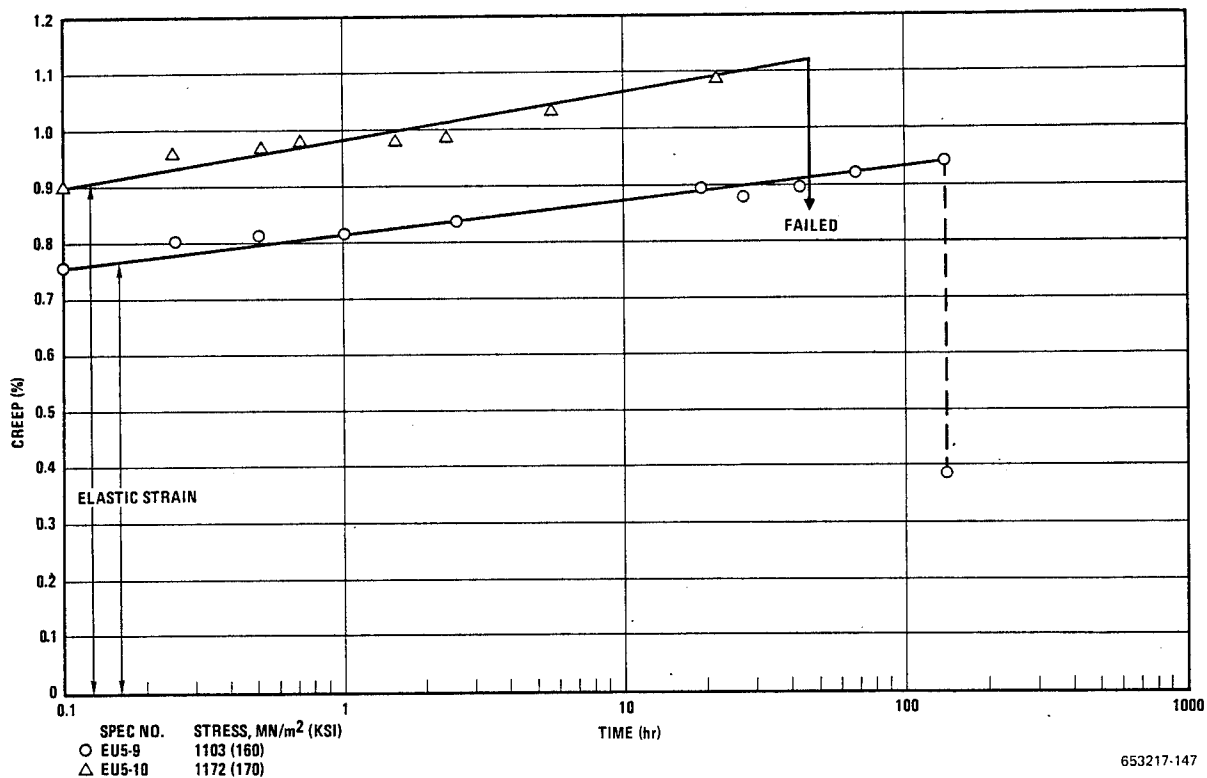
^aLast measurement prior to failure

aLast measurement prior to failure



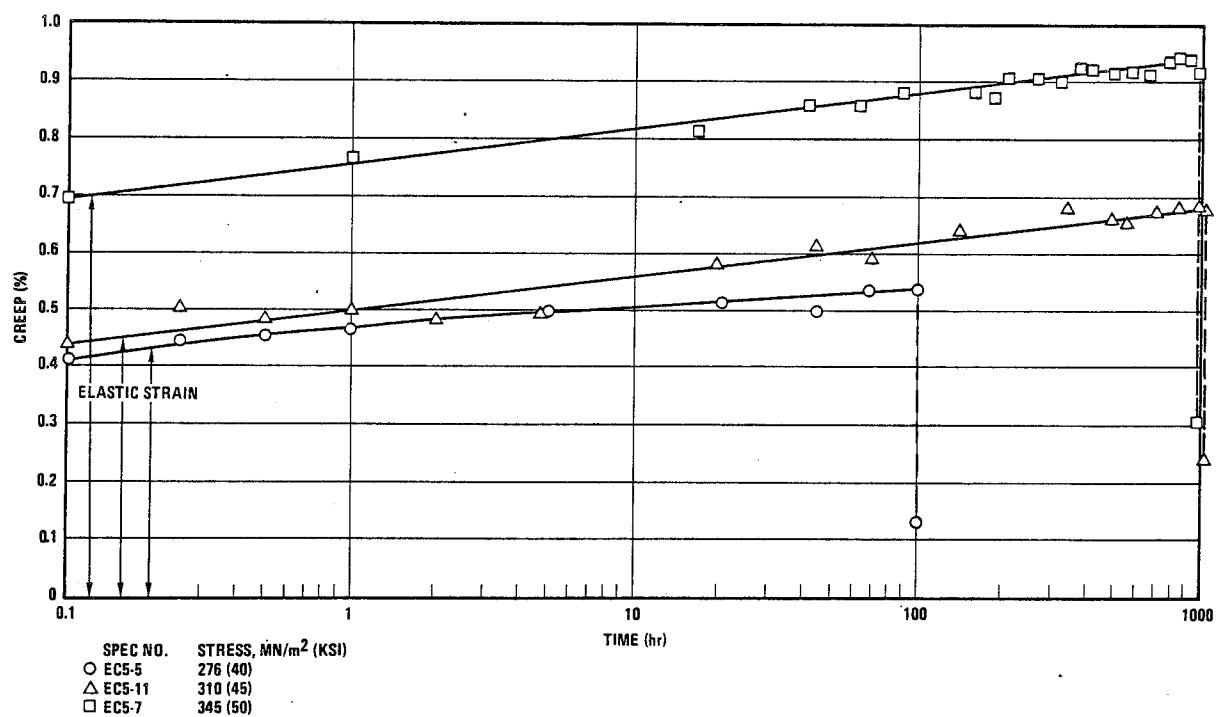
653217-146

Figure 10-31 Creep Strain for $[0^\circ]_6$ B/Al at 505 K (450° F)



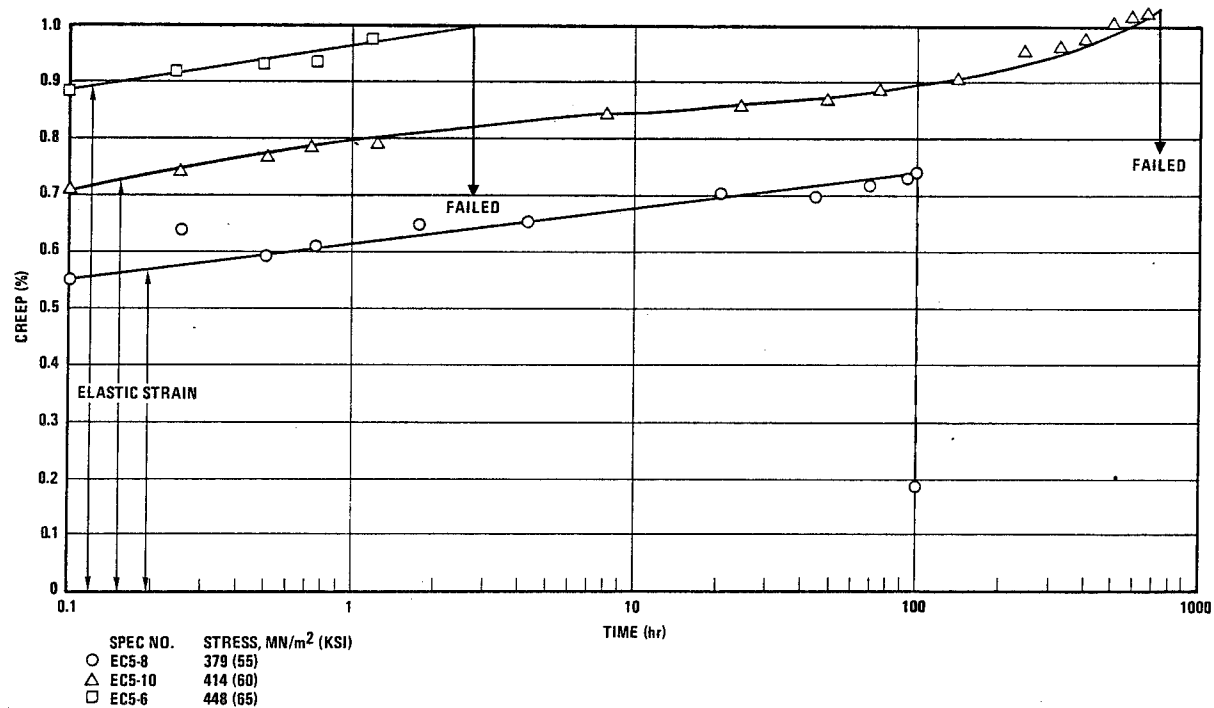
653217-147

Figure 10-32 Creep Strain for $[0^\circ]_6$ B/Al at 505 K (450° F)



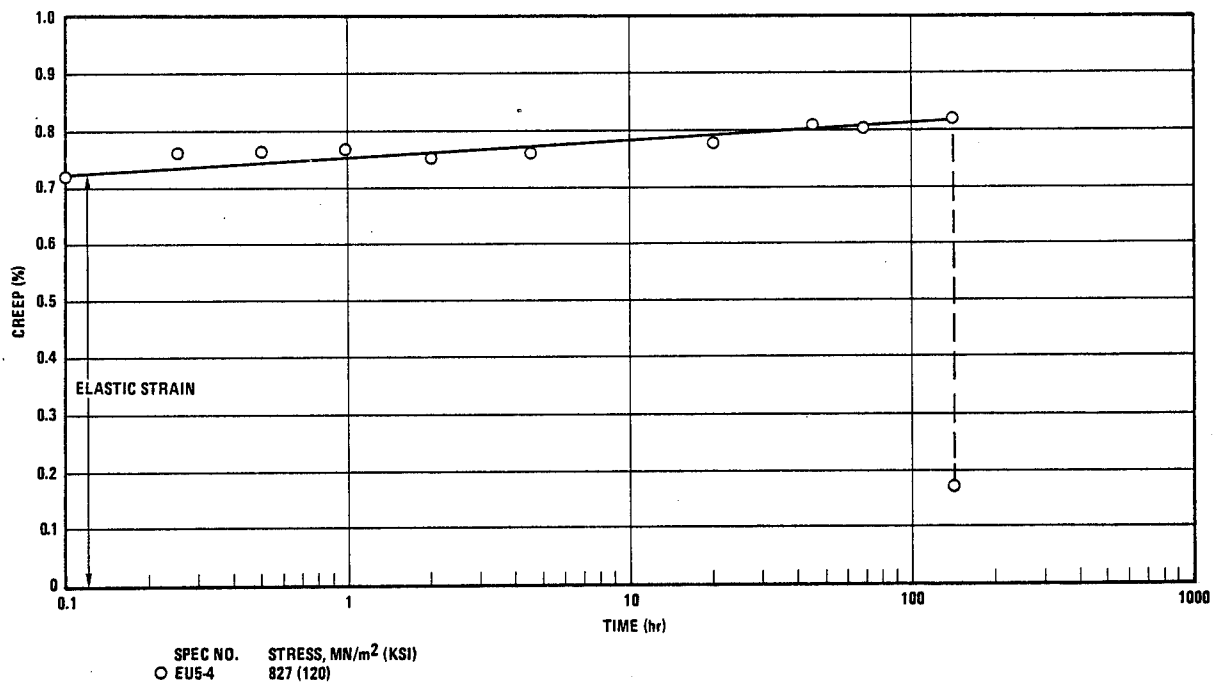
653217-148

Figure 10-33 Creep Strain for $[0^\circ \pm 45^\circ]_s$ B/Al at 505 K (450° F)



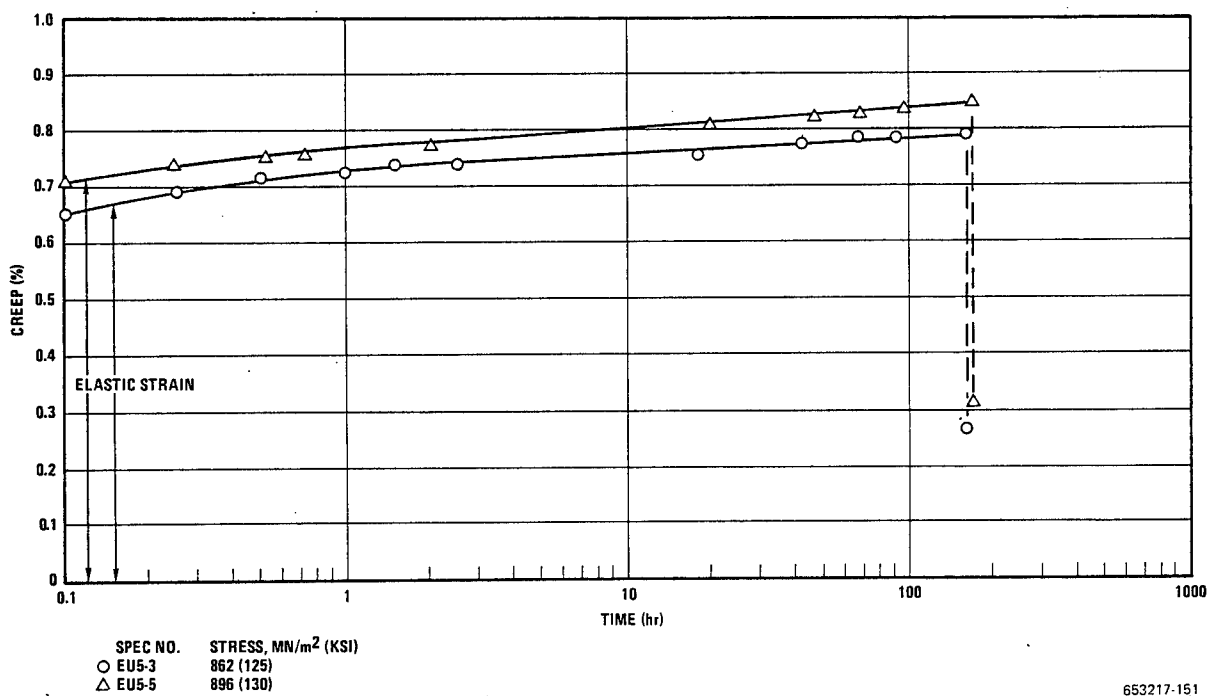
653217-149

Figure 10-34 Creep Strain for $[0^\circ \pm 45^\circ]_s$ B/Al at 505 K (450° F)



653217-150

Figure 10-35 Creep Strain for $[0^\circ]_6$ B/Al at 561 K (550° F)



653217-151

Figure 10-36 Creep Strain for $[0^\circ]_6$ B/Al at 561 K (550° F)

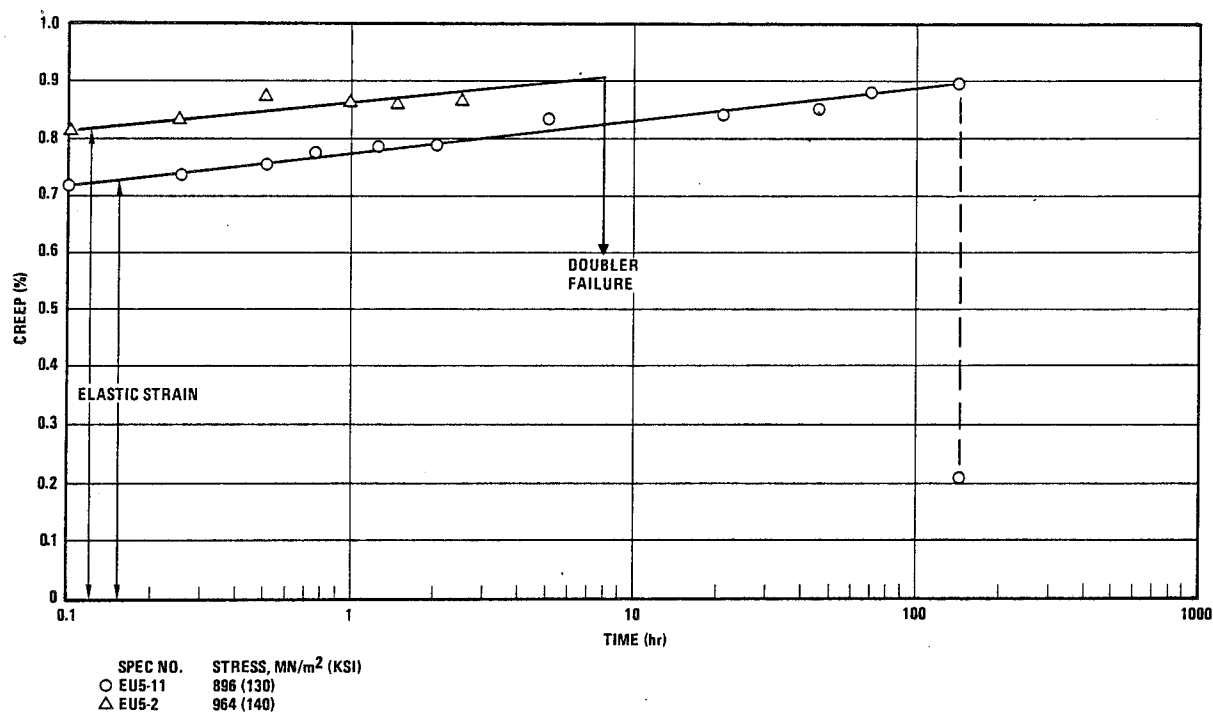


Figure 10-37 Creep Strain for $[0^\circ]_6$ B/Al at 561 K (550° F)

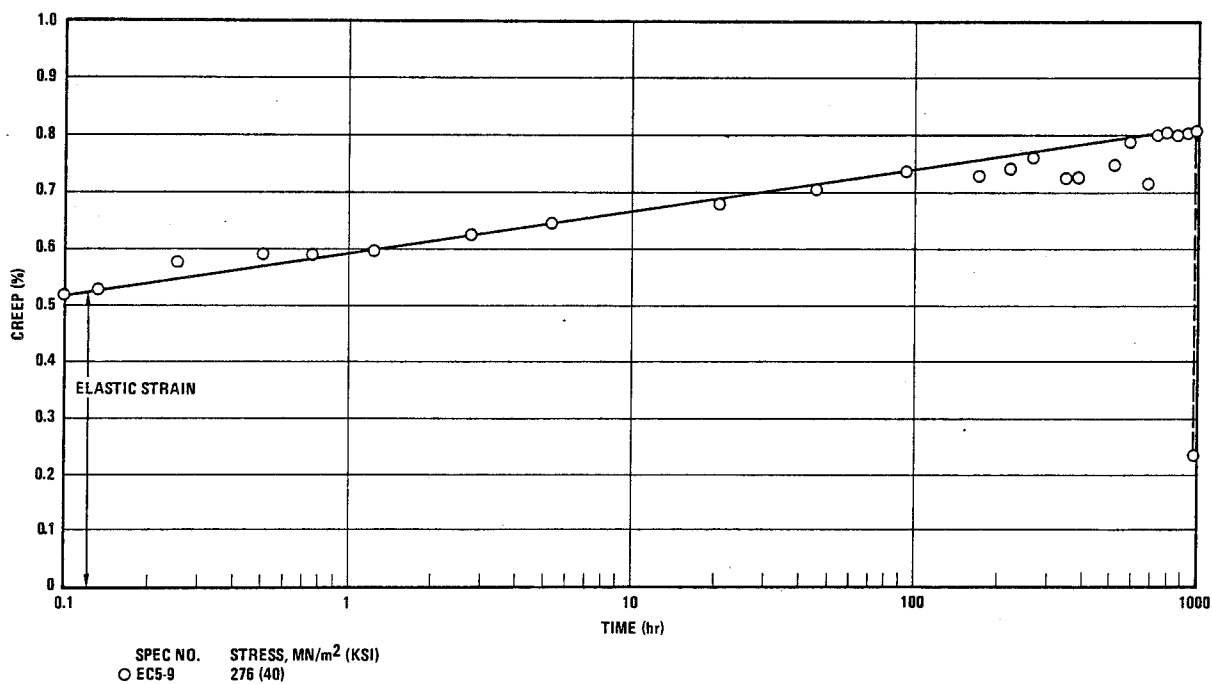


Figure 10-38 Creep Strain for $[0^\circ \pm 45^\circ]_5$ B/Al at 561 K (550° F)

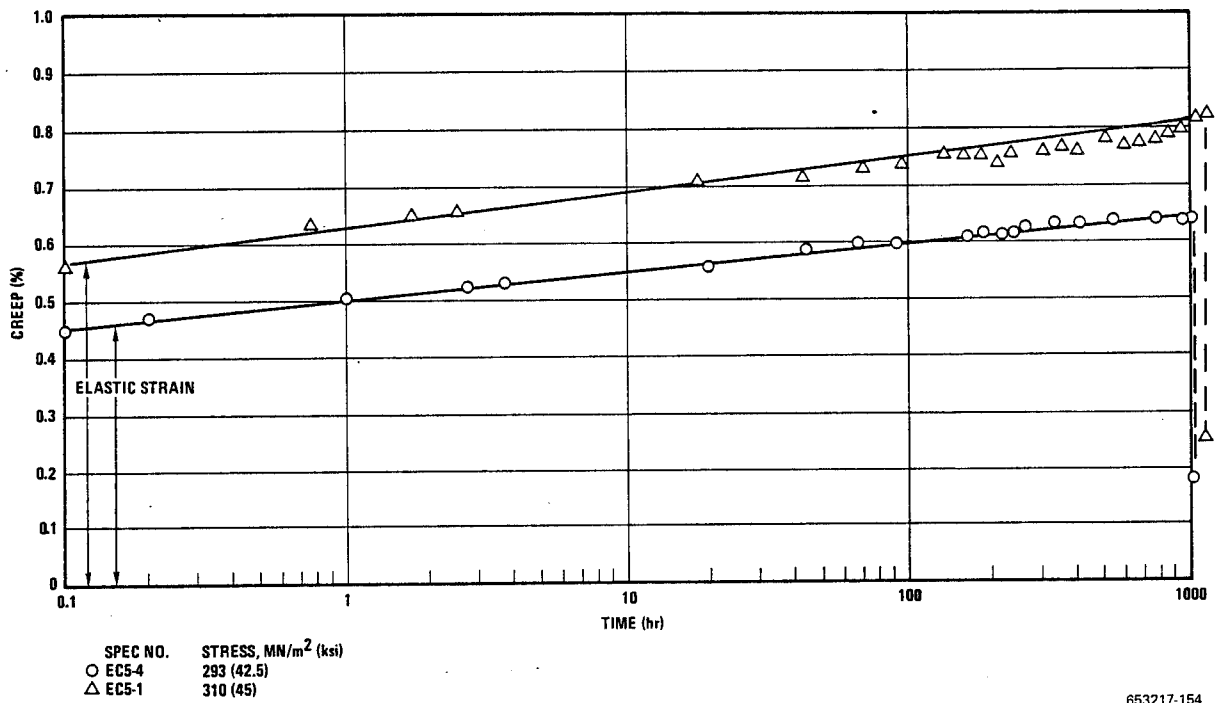


Figure 10-39 Creep Strain for $[0^\circ \pm 45^\circ]_s$ B/Al at 561 K (550° F)

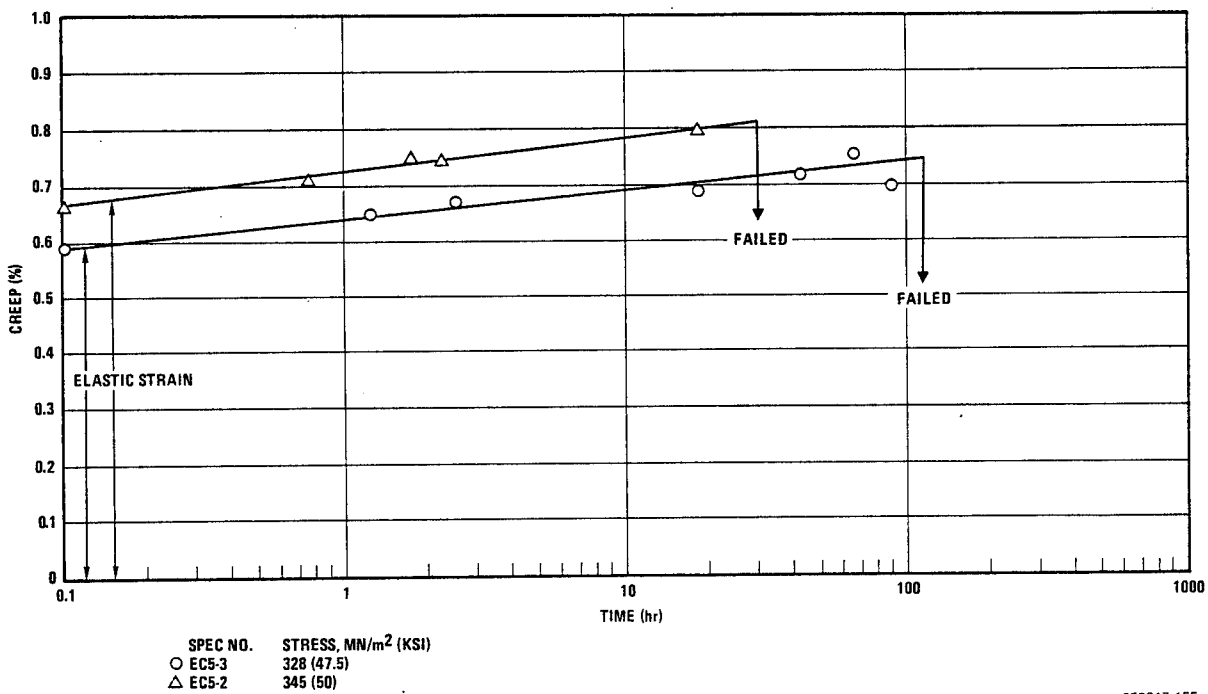


Figure 10-40 Creep Strain for $[0^\circ \pm 45^\circ]_s$ B/Al at 561 K (550° F)

SECTION 11

BASELINE FATIGUE TESTING

Fatigue testing made up a significant portion of the SCR study with four distinct parts: 1) conventional constant amplitude tests at room and elevated temperatures with flawed and unflawed test specimens; 2) constant amplitude tests on material that survived 10,000 hours of flight simulation exposure; 3) short-term flight simulation tests (random fatigue loads, constant elevated temperature) of 100 and 200 hours; and 4) long-term flight simulation (random fatigue loads, cyclic temperature) for 10,000 hours. The constant amplitude tests on unexposed material characterize the composites. Tests after exposure to 10,000 hours of flight simulation provide data to compare the residual fatigue properties to original properties. The short-term flight simulation tests generate wearout analysis model data necessary to set the stress levels for the long term flight simulation tests. Finally, the long-term tests provide data on the effect of 10,000-hour simulated supersonic flight service environments for each composite system. The bulk of these tests, those that serve as baseline for later comparisons, were performed on unexposed composite materials. It is these tests that are described in this section. In some cases, the data were available in the literature, and no additional tests were required. As a result of considerable early testing and extensive use, the B/E material fitted this category and only limited testing was necessary (ref. 35 and 36).

Test parameters that were considered in the baseline constant amplitude fatigue tests were 1) specimen layup, 2) specimen configuration, 3) test temperature, and 4) stress ratio. Specimens of both unidirectional and $[0^\circ \pm 45^\circ]$ crossply layups were evaluated. All test specimens were loaded in the direction of the 0° fibers. Flawed and unflawed specimens were included. The flawed specimens were fabricated with a center hole having a diameter equal to one-fourth of the specimen width. For isotropic material a specimen with this configuration would have a theoretical stress concentration factor, K_t , of 2.43 (ref. 23). Testing was conducted at room temperature for all systems and, in addition, at 450 K (350° F) for G/E and at 505 K (450° F) for G/PI and B/Al. Fatigue tests were performed at stress ratios (R) of 0.1 and -1 , where R is defined as the algebraic ratio of the minimum stress to the maximum stress in one cycle (thus loading for the $R = 0.1$ tests is tension-tension while for $R = -1$ the loading is fully reversed tension-compression).

In addition to the baseline tests described above, two other fatigue studies are included in this section. The first was a limited program to investigate the effects of stacking sequence on fatigue strength of the $[0^\circ \pm 45^\circ]$ family of laminates. The second was a determination of Poisson's ratio of specimens after 10 million fatigue cycles (runout).

11.1 SPECIMEN DESIGN

Specimens tested at a stress ratio, R , of 0.1 were fabricated from 6 ply $[0^\circ]_6$ and $[0^\circ \pm 45^\circ]_s$ laminates. For $R = -1$ tests, where compressive as well as tensile loads are applied, a thicker specimen was used. Information obtained from IITRI (private communication from K.E. Hofer, 1973) indicated that fatigue testing 6 ply composite material at $R = -1$ gave unreliable results. The problem was related to compressive buckling and could be overcome by the use of

thicker material. For this reason the $R = -1$ specimens were cut from 12-ply $[0^\circ]_{12}$ and $[0^\circ \pm 45^\circ]_{s2}$ laminates. Cutting, hole machining, and doubler bonding techniques were those described in Section 5. Details of the specimen geometry for the various configurations and test conditions are listed in Table 11-1. The length of the $R = 0.1$ specimens that were tested at elevated temperature was twice that of the room temperature specimens to allow the ends to extend well away from the furnace during testing. With this technique doubler bond failures were eliminated. Because of the compressive loads present during the $R = -1$ testing it was not feasible to extend the length of these specimens for the elevated temperature conditions. Doubler bond heating of these specimens was minimized by reducing the size of the furnace as described in Section 11.2. The widths of the various specimens were the same as those chosen for the baseline unnotched and notched tensile tests (Section 7) except that the $R = -1$, unnotched specimens were all 0.025 m (1.0 in.) in the fatigue tests rather than 0.013 m (0.5 in.).

Table 11-1. Details of Fatigue Specimen Geometry

Specimen Configuration	R Value	Test Temperature	Thickness (Plies)	Length m (in.)	Width m (in.)	Hole Diameter m (in.)	Test Section m (in.)
Unnotched	0.1	R.T.	6	0.23 9	0.013 0.5	—	0.10 4
	.1	Elevated	6	.46 18	.013 0.5	—	.33 13
	-1	R.T.	12	.10 4	.025 1	—	.013 0.5
	-1	Elevated	12	.10 4	.025 1	—	.013 0.5
Notched	.1	R.T.	6	.23 9	^a .025 1	^b .0064 0.25	.10 4
	.1	Elevated	6	.46 18	^a .025 1	^b .0064 0.25	.33 13
	-1	R.T.	12	.10 4	.025 1	.0064 0.25	.013 0.5
	-1	Elevated	12	.10 4	.025 1	.0064 0.25	.013 0.5

^afor B/Al: 0.013 (0.5)
^bfor B/Al: 0.00318 (0.125)

11.2 TEST EQUIPMENT AND TEST PROCEDURE

All tests were performed on Baldwin-Sonntag SF1U and SU10U fatigue machines at a constant frequency of 30 Hz. Both grip ends of the specimens were placed between two L-shaped steel fixtures that were bolted to the machine loading platens. The specimens were secured to the steel plates by two .013 m (0.5 in.) diameter bolts that straddle the edges of the grip ends of the specimen. To further increase the gripping power of the fixtures, a special abrasive cloth (Bay State Gritcloth, size 320 grit) was placed at each specimen-to-fixture interface. This cloth had two beneficial features for a secure grip: 1) the open weave design, which increases the frictional holding force, and 2) the abrasive coating on both surfaces of the cloth, which becomes embedded in the contact surfaces of both the fixtures and tabs. The two bolts were torqued to a level that just secured the specimen, the alignment of the specimen was carefully checked to ensure axial loading, and final tightening was completed. Figures 11-1 through 11-3 show one of the fatigue testing machines and close-up views of the gripping fixtures with both $R = 0.1$ and $R = -1$ specimens in place.

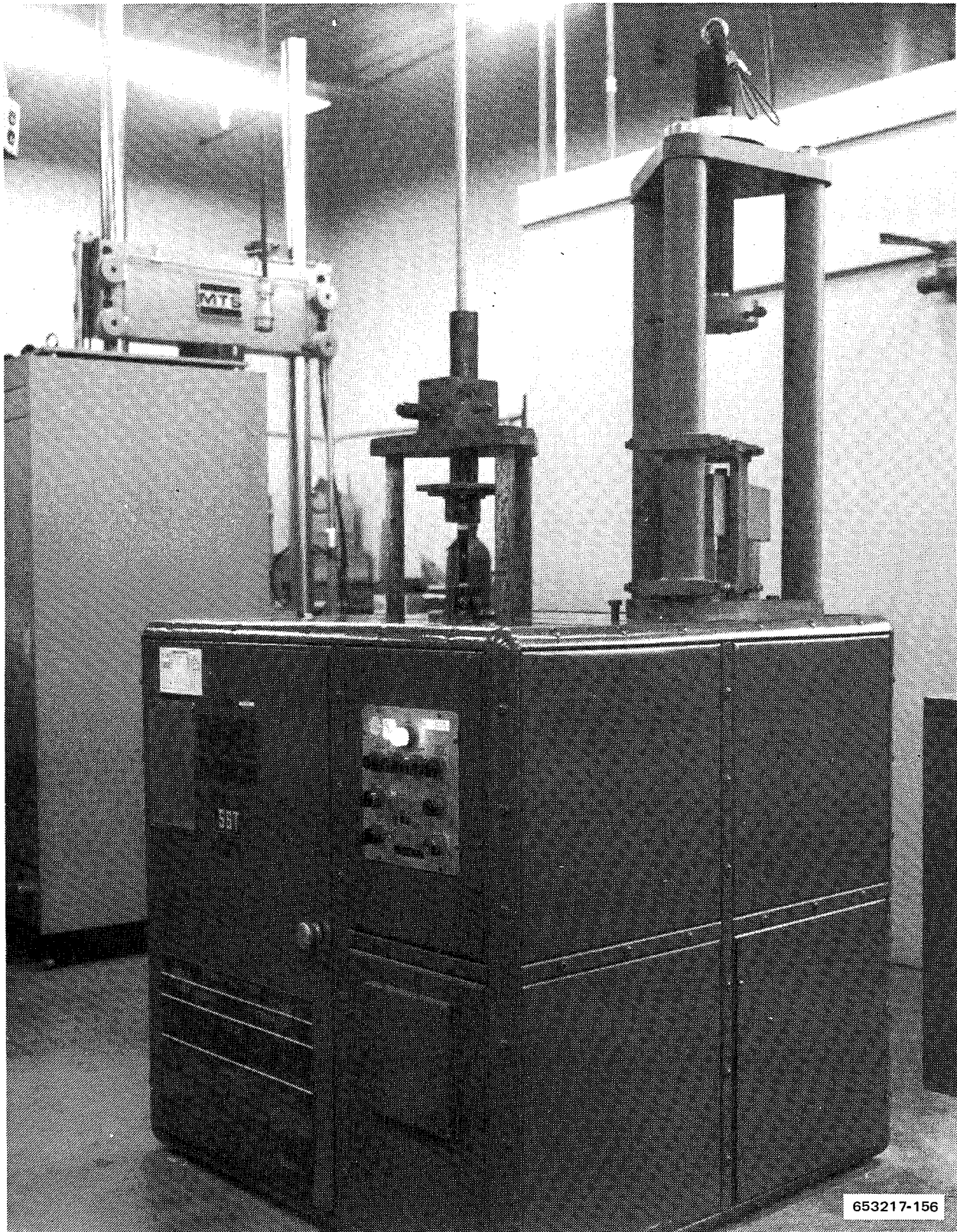


Figure 11-1 Fatigue Testing Apparatus

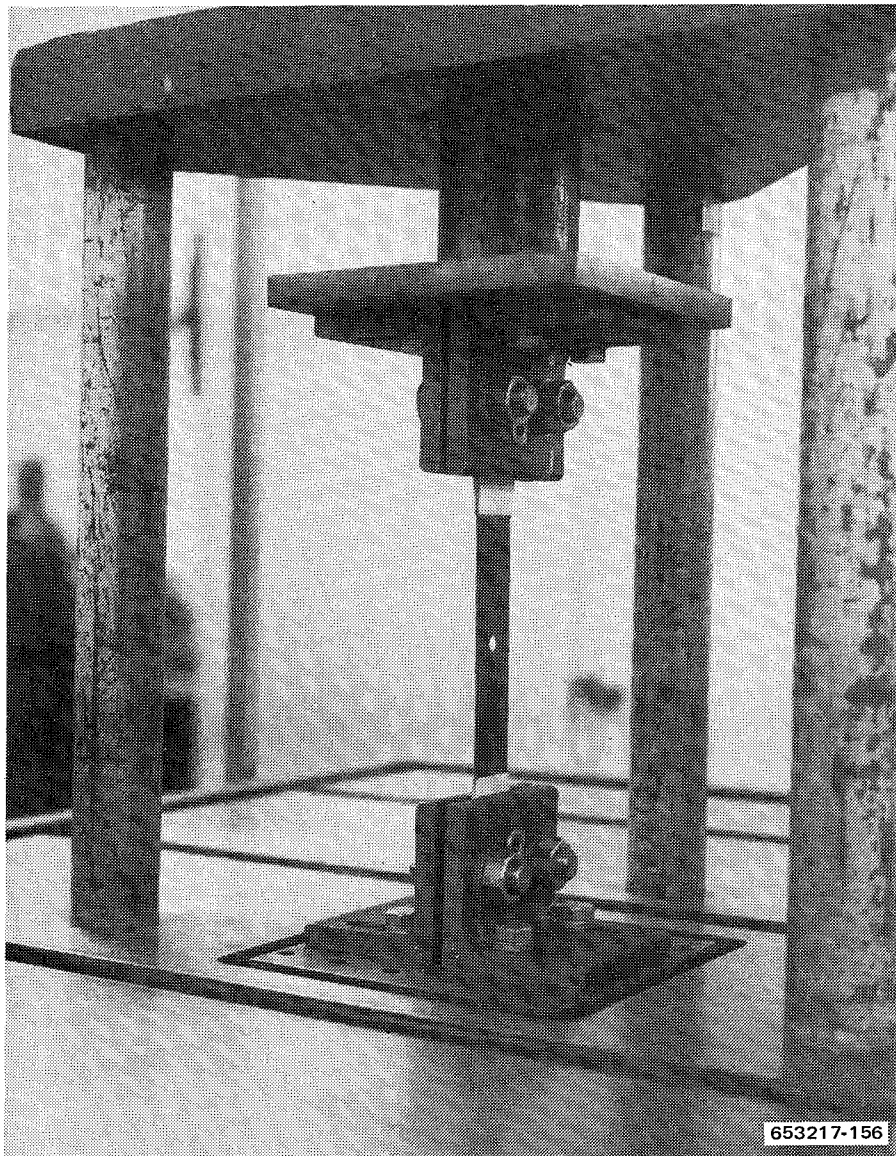


Figure 11-2 Fatigue Specimen Mounted in Gripping Fixture for $R = 0.1$ Test at Room Temperature

For elevated temperature tests of the $R = 0.1$ specimens a 0.15 m (6 in.) long clamshell furnace was used. The length of the specimens was such as to allow the ends to extend out of the furnace far enough to prevent excessive heating of the doubler adhesive. This factor and the excellent gripping power of the end fixtures combined to eliminate doubler bond failures at elevated temperature. Figure 11-4 shows the furnace arrangement with a specimen loaded in the fatigue machine. Temperature was controlled to ± 3 K ($\pm 5^\circ$ F) with a Minneapolis Honeywell Brown Electronik controller using a chromel-alumel thermocouple attached to the specimen at the center of the gage section.

For the $R = -1$ specimens a much smaller furnace was required for the elevated temperature tests because of the limited amount of space available between the gripping fixtures. Most

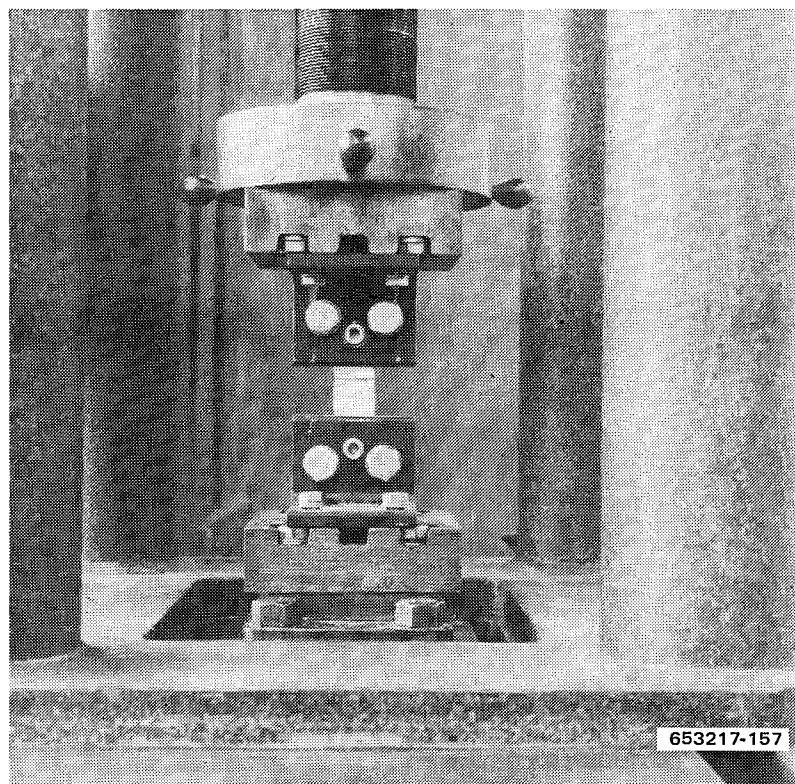


Figure 11-3 Fatigue Specimen Mounted in Gripping Fixture for $R = -1$ Test at Room Temperature

tests were conducted using a small ring furnace of the type shown in Figure 11-5. This could be used on all tests that were run in the smaller SF1U fatigue machine but not in the larger SF1OU because of space limitations. The unidirectional B/Al specimen loads were such as to require the larger SF1OU fatigue machine. For these specimens a successful technique for elevated temperature testing was developed by using a flexible heating tape, which was wrapped around the short test section of the specimens. The heater was 0.61 m (24 in.) in length, 0.013 m (.5 in.) wide, rated at 200 watts and had a maximum use temperature of 873 K (1112° F). Figure 11-6 shows a specimen with the heating tape in place ready for test.

Prior to testing, the resin matrix composite specimens were dried at 394 K (250° F) for 24 hours. No baking of the B/Al specimens was required. The specimen dimensions were measured, and the static and dynamic loads calculated for the particular stress level and R value desired. The notched stress values were based on net section, i.e., width minus hole diameter. After loading the specimen in the machine and carefully checking the alignment, the load levels were set, and the test initiated. The tests were continued to failure or until a maximum of 10 million cycles was obtained. The number of load cycles was measured with a counter driven by the motor rotating the dynamic load. This counter had a least count of 1000 cycles so that any failures below this value were not registered. Nine specimens were tested for each combination of: 1) material system, 2) laminate orientation, 3) specimen type (unflawed or flawed), 4) R value, and 5) test temperature. The test data were plotted on semi-logarithmic paper to obtain the characteristic S-N curves.

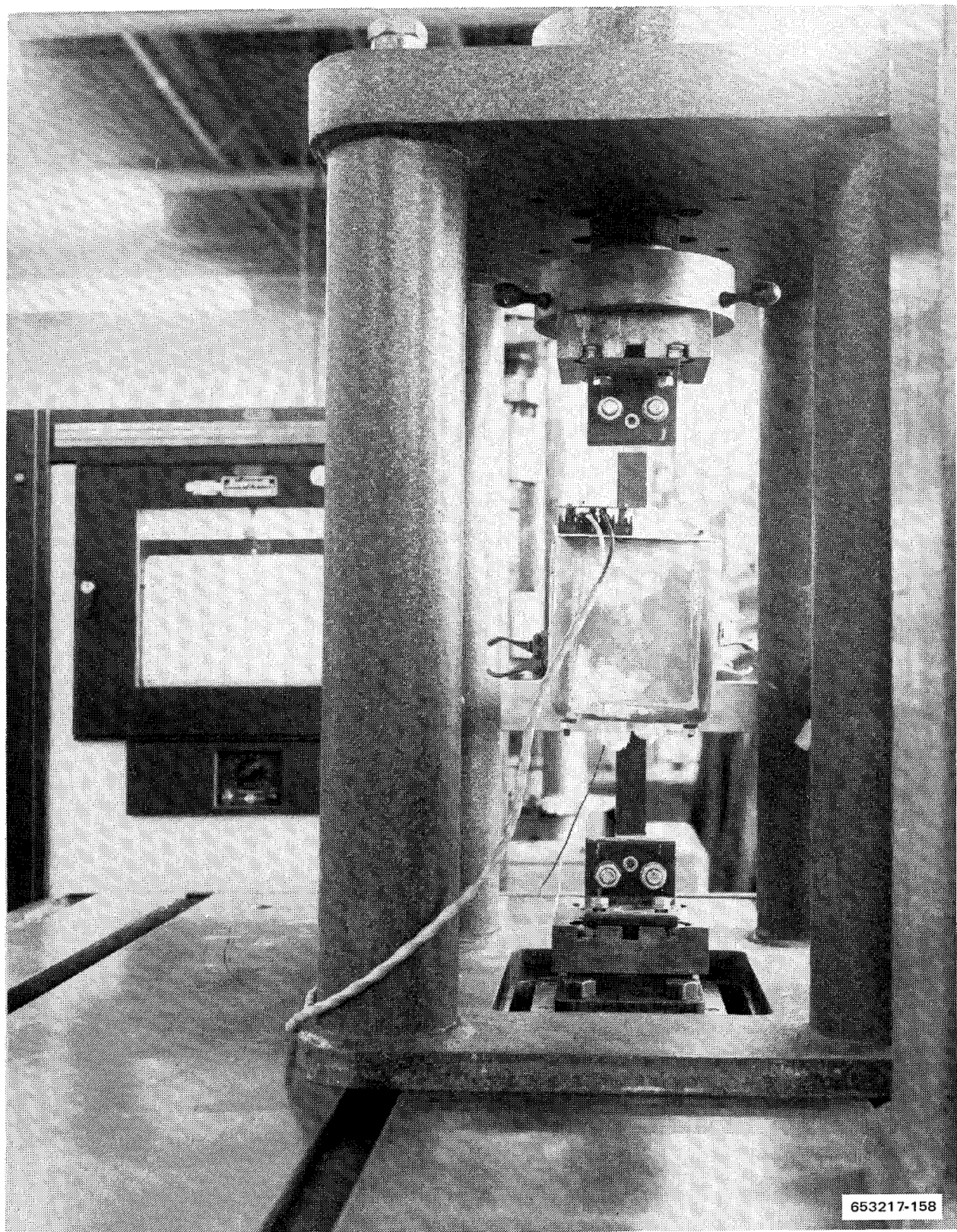


Figure 11-4 Furnace Arrangement for $R = 0.1$ Fatigue Test at Elevated Temperature

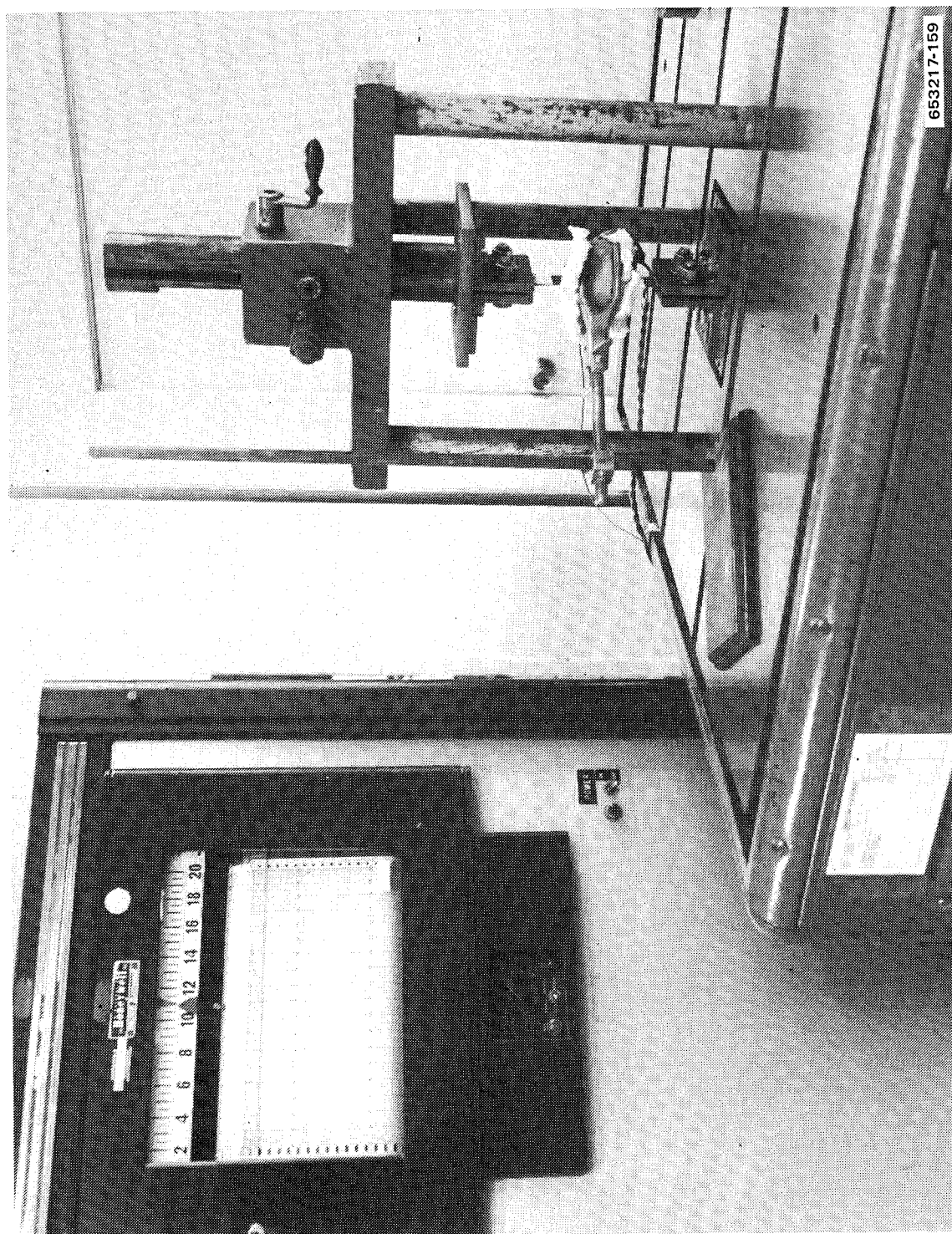


Figure 11-5 Small Ring Furnace for Elevated Temperature Fatigue Testing

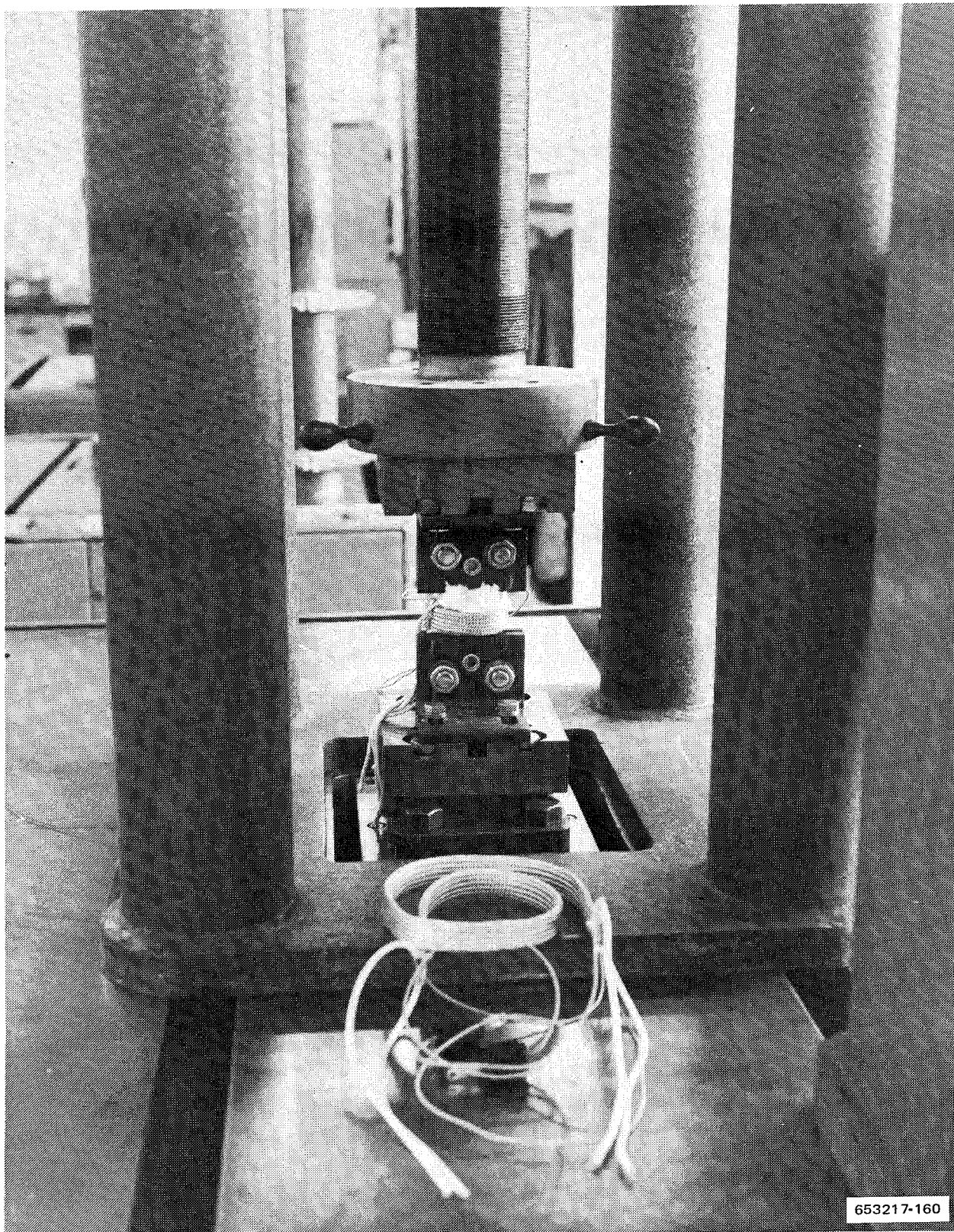


Figure 11-6 Elevated Temperature, $R = -1$ Fatigue Test Setup Showing Use of Flexible Heating Tape

Initially the S-N curves were drawn to show a straight line of best fit of the data points as determined by linear regression analysis. The high degree of scatter in some of the data sets and the uncertainty of how to input the runout specimens often gave S-N curves that did not appear to be consistent with those from data sets with little scatter. For this reason the method was changed, and all curves have been drawn by hand. They are intended only as eye pointers to the, at times, rather scattered fatigue data.

11.3 TEST RESULTS AND DISCUSSION

The overall baseline fatigue testing program is summarized in Table 11-2. This table shows the number of specimens and stress ratios that were employed at each test temperature for the four material systems. Of the total number of test specimens shown in Table 11-2, all are included in the data presented in this section although a few are not valid because of equipment malfunctions, doubler bond failures, or incorrect test loads or temperatures. These specimens are identified in the tables and figures. The data are presented in both tabular form and as S-N curves, one for each stress ratio and temperature.

Table 11-2. Summary of Fatigue Test Program

Material System	Laminate Orientation	Specimen Configuration	Number of Tests per Stress Ratio					
			297 K R = 0.1	(75° F) -1.0	450 K (350° F) 0.1	-1.0	505 K (450° F) 0.1	-1.0
B/E	[0° ± 45°]	Unnotched	5	—	—	—	—	—
		Notched	5	—	—	—	—	—
G/E	[0° ± 45°]	Unnotched	9	9	9	9	—	—
		Notched	9	9	9	9	—	—
	[0°]	Unnotched	9	9	9	9	—	—
		Notched	9	9	9	9	—	—
G/PI	[0° ± 45°]	Unnotched	9	9	—	—	9	9
		Notched	9	9	—	—	9	9
	[0°]	Unnotched	9	9	—	—	9	9
		Notched	9	9	—	—	9	9
B/Al	[° ± 45°]	Unnotched	9	9	—	—	a9	9
		Notched	9	9	—	—	a9	9
	[0°]	Unnotched	9	9	—	—	a9	9
		Notched	9	9	—	—	a9	9

^aTest Temperature was 561 K (550°)

11.3.1 BORON/EPOXY AND GRAPHITE/EPOXY. Because of the large amount of testing previously conducted by others on the B/E system, no baseline fatigue testing was required. However, to determine more precisely the effects of the flight simulation exposure it was desirable to have baseline fatigue data from this same batch of material using the same specimen configuration and test technique as used during the post exposure evaluation. For this reason baseline fatigue data were determined for B/E for the same test conditions and specimen configurations as were later used in evaluating the B/E flight simulation specimens after 10,000 hours of exposure. These were room temperature tests on unnotched and notched

$[0^\circ \pm 45^\circ]_s$ crossply material tested at an R value of 0.1. The results are listed in Table 11-3 and plotted in Figure 11-7. The slopes of the S-N curves are quite different for the two specimen configurations. The notched material has a relatively flat curve lying near 414 MN/m^2 (60 ksi). The S-N curve for the unnotched material is much steeper, with fatigue strengths below 10^5 cycles greater than the notched specimens but with lower strength for lifetimes greater than 10^5 cycles.

Table 11-3. Axial Fatigue Data for $[0^\circ \pm 45^\circ]_s$ B/E, R = 0.1

Specimen Number	Test Temperature K (°F)	Specimen Type	Maximum MN/m ² (ksi)	Cycles	Comments
AC72-1	297 75	Unnotched	414 60	227,000	
-2			448 65	31,000	
-3			345 50	3,534,000	
-4			483 70	8,000	
-5			310 45	10,116,000	Did not fail
AC71-4	297 75	Notched	345 50	10,090,000	Did not fail
-5			414 60	1,386,000	
-6			483 70	<1,000	
-7			431 62.5	462,000	
-8			448 65	<1,000	

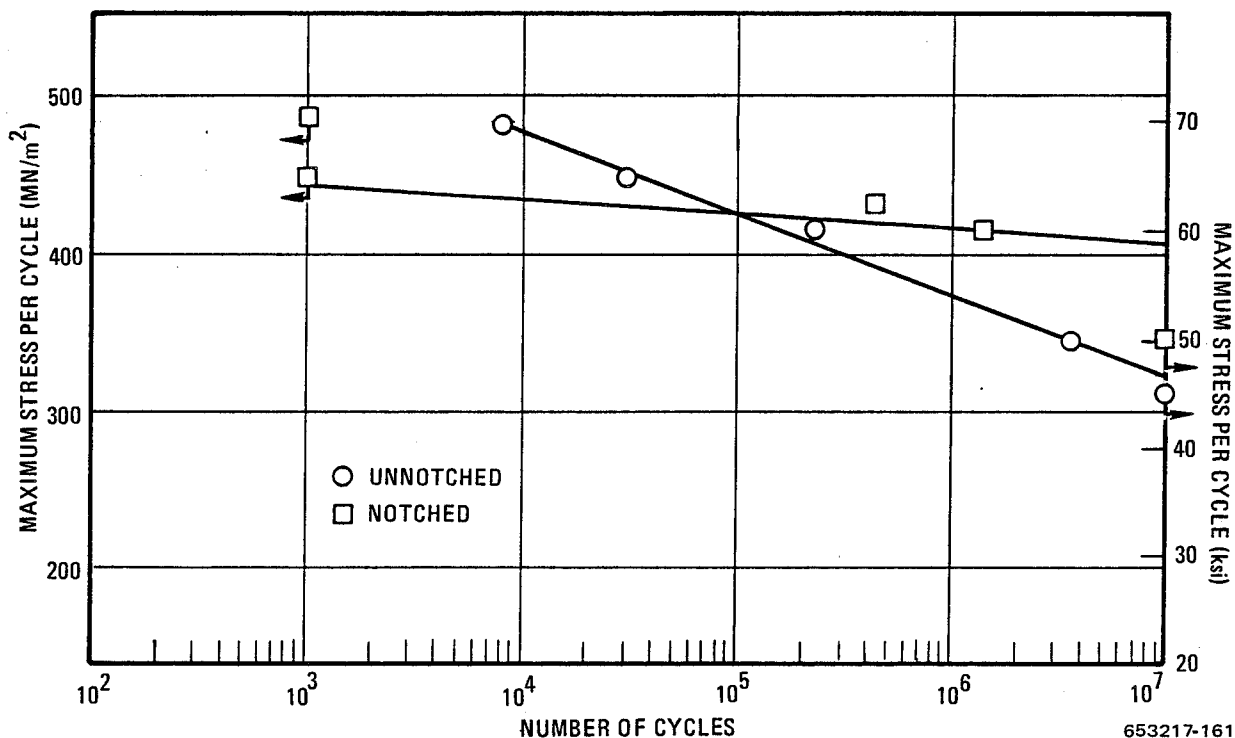


Figure 11-7 Axial Fatigue Properties of $[0^\circ \pm 45^\circ]_s$ B/E at 297 K (75° F) and a Stress Ratio, R, of 0.1

For G/E a complete set of fatigue tests was performed. The results are listed in Tables 11-4 through 11-11 and individual S-N curves are plotted in Figures 11-8 through 11-15. On these S-N curves the individual data points have been included. In the discussion of the fatigue data, several of the S-N curves have been combined to more clearly show the effects of the test parameters, i.e., stress ratio, temperature, or specimen configuration. On these curves the data points have been omitted for clarity.

Several points are apparent from an examination of the G/E baseline fatigue data. The test parameter that exhibited the greatest influence on the fatigue strength was the stress ratio, R . In every case the tests conducted at $R = -1$ gave considerably lower fatigue properties than those run at R values of 0.1. Generally, the effect of a notch (center hole) was to reduce the fatigue strength, and an increase in temperature from 297 K (75° F) to 450 K (350° F) also caused a drop in strength. Figures 11-16 and 11-17 compare the results of axial fatigue testing at room temperature and stress ratios of $R = 0.1$ and $R = -1$ for both unnotched and notched specimens. These data show the fatigue life for a stress ratio of $R = -1$ to be much lower than for $R = 0.1$. For both stress ratios, the fatigue life for notched specimens is less than for unnotched specimens except the unidirectional material tested at $R = -1$, where no notch effect was observed. Similar data are presented in Figures 11-18 and 11-19 for testing at 450 K (350° F). Again the fatigue strength is greatly reduced for the $R = -1$ tests compared to those conducted at a stress ratio of $R = 0.1$. The presence of a notch is shown to reduce the fatigue strength for the $R = 0.1$ tests, but not for the $R = -1$ tests. Further, the unidirectional notched specimens performed better than those that were unnotched. The reason for this behavior is not clearly understood at this time, but may be related to the phenomenon of crack blunting brought on by the combination of high compressive loading and a matrix softened because of elevated temperature exposure. Additional studies of this effect are needed.

Two problems were experienced early in the G/E fatigue test program. The first was doubler bond failures in the room temperature, $R = -1$, unnotched, crossply specimens. After the first two specimens failed, the remaining doublers were removed and rebonded using a modification of the bonding procedure and substituting a higher shear strength adhesive. These specimens gave satisfactory results. The second problem occurred with the room temperature, $R = 0.1$, unnotched, unidirectional specimens. Six of these nine specimens failed in the G/E but inside the doublers. These failures are thought to have been caused, in part, by nonuniform clamping pressure applied by the test machine grips because of the warped condition of the doublers. Changes in the adhesive bonding process were made to eliminate this problem in the remaining specimens.

One measure of the fatigue resistance of a material is the percent of the ultimate strength at which the fatigue limit or endurance limit (run-out) occurs. Fatigue limit is the limiting value of the stress below which a material can presumably endure an infinite number of stress cycles, i.e., the stress at which the S-N curve becomes horizontal. For certain materials and test conditions no fatigue limit occurs and some value of N (number of cycles) is chosen. Many of the S-N curves obtained during testing of the composites in this study were of this type. For these curves a value of 10^7 cycles was used.

The percentages of the ultimate strengths at 10^7 cycles have been calculated for each of the groups of G/E specimens and are listed in Table 11-12. For $[0^\circ \pm 45^\circ]$ crossply material tested in tension-tension fatigue, $R = 0.1$, the values average 86% for both room and elevated temperature and unnotched and notched configurations. Similar tests on unidirectional material

Table 11-4. Axial Fatigue Data for $[0^\circ \pm 45^\circ]_s$ G/E, Unnotched, $R = 0.1$

Specimen Number	Test Temperature		Maximum Stress		Cycles	Comments
	K	(°F)	MN/m ²	(ksi)		
BC72-20	297	75	414	60	11,830,000	
-21			483	70	<1,000	
-22			448	65	<1,000	
-23			431	62.5	12,165,000	Did not fail
-24			448	65	<1,000	
-25			431	62.5	340,000	
-26			431	62.5	<1,000	
-27			448	65	1,121,000	
-28			465	67.5	10,140,000	Did not fail
BC72-47	450	350	445	50	1,274,000	
-48			276	40	10,165,000	Did not fail
-49			414	60	60,000	
-50			379	55	6,181,000	
-51			310	45	10,000,000	Did not fail
-52			396	57.5	1,000	
-53			362	52.5	3,000	
-54			328	47.5	10,000,000	Did not fail
-55			379	55	1,000	

Table 11-5. Axial Fatigue Data for $[0^\circ \pm 45^\circ]_{s2}$ G/E, Unnotched, $R = -1$

Specimen Number	Test Temperature		Maximum Stress		Cycles	Comments
	K	(°F)	MN/m ²	(ksi)		
BC72-11	297	75	414	60	<1,000	
-12			276	40	16,000	
-13			345	50	1,000	
-14			310	45	3,000	
-15			276	40	3,000	
-16			241	35	28,000	Bond failure
-17			241	35	5,000	
-18			207	30	87,000	Bond failure
-19			172	25	10,400,000	
BC72-38	450	350	207	30	5,000	
-39			138	20	10,159,000	Did not fail
-40			172	25	15,560,000	Did not fail
-41			241	35	3,000	
-43			190	27.5	2,131,000	
-44			207	30	38,000	
-45			190	27.5	38,000	
-46			172	25	10,007,000	Did not fail
-47			224	32.5	9,000	

Table 11-6. Axial Fatigue Data for $[0^\circ \pm 45^\circ]_s$ G/E, Notched, $R = 0.1$

Specimen Number	Test Temperature		Maximum Stress		Cycles	Comments
	K	(°F)	MN/m ²	(ksi)		
BC71-10	297	75	276	40	10,468,000	Did not fail
-11			345	50	<1,000	
-12			310	45	12,723,000	Did not fail
-13			328	47.5	10,313,000	Did not fail
-14			345	50	10,116,000	Did not fail
-15			379	55	15,284,000	Did not fail
-16			448	65	<1,000	
-17			414	60	<1,000	
-18			396	57.5	<1,000	
BC71-28	450	350	345	50	10,006,000	Did not fail
-29			362	52.5	<1,000	
-30			379	50	1,000	
-31			310	45	13,368,000	Did not fail
-32			328	47.5	10,125,000	Did not fail
-33			345	50	<1,000	
-34			345	50	26,000	Failed under doubler
-35			345	50	<1,000	
-36			336	48.75	<1,000	

Table 11-7. Axial Fatigue Data for $[0^\circ \pm 45^\circ]_{s2}$ G/E, Notched, $R = -1$

Specimen Number	Test Temperature		Maximum Stress		Cycles	Comments
	K	(°F)	MN/m ²	(ksi)		
BC71-1	297	75	276	40	17,000	
-2			207	30	164,000	
-3			138	20	282,000	
-4			69	10	15,418,000	Did not fail
-5			172	25	127,000	
-6			241	35	24,000	
-7			207	30	4,000	
-8			103	15	17,308,000	Did not fail
-9			121	17.5	10,500,000	Did not fail
BC71-19	450	350	207	30	17,000	
-20			172	25	1,000	Machine malfunction
-21			172	25	665,000	
-22			190	27.5	434,000	
-23			155	22.5	12,160,000	Did not fail
-24			172	25	1,689,000	
-25			190	27.5	670,000	
-26			207	30	89,000	
-27			155	22.5	12,470,000	Did not fail

Table 11-8. Axial Fatigue Data for $[0^\circ]_6$ G/E, Unnotched, $R = 0.1$

Specimen Number	Test Temperature		Maximum Stress		Cycles	Comments
	K	(°F)	MN/m ²	(ksi)		
BU72-20	297	75	1,030	150	42,000	
-21			965	140	17,000	Failed under doubler
-22			965	140	8,000	Failed under doubler
-23			896	130	14,620,000	Did not fail
-24			931	135	70,000	Failed under doubler
-25			931	135	10,184,000	Did not fail
-26			965	140	17,000	Failed under doubler
-27			1,000	145	47,000	Failed under doubler
-28			1,070	155	19,000	Failed under doubler
BU72-47	450	350	965	140	1,073,000	
-48			896	130	10,156,000	Did not fail
-49			1,030	150	2,000	
-50			1,000	145	5,000	
-51			979	142	316,000	
-52			948	137.5	9,482,000	Did not fail
-53			983	142.5	103,000	
-54			1,000	145	1,000	
-55			965	140	8,548,000	

Table 11-9. Axial Fatigue Data for $[0^\circ]_{12}$ G/E, Unnotched, $R = -1$

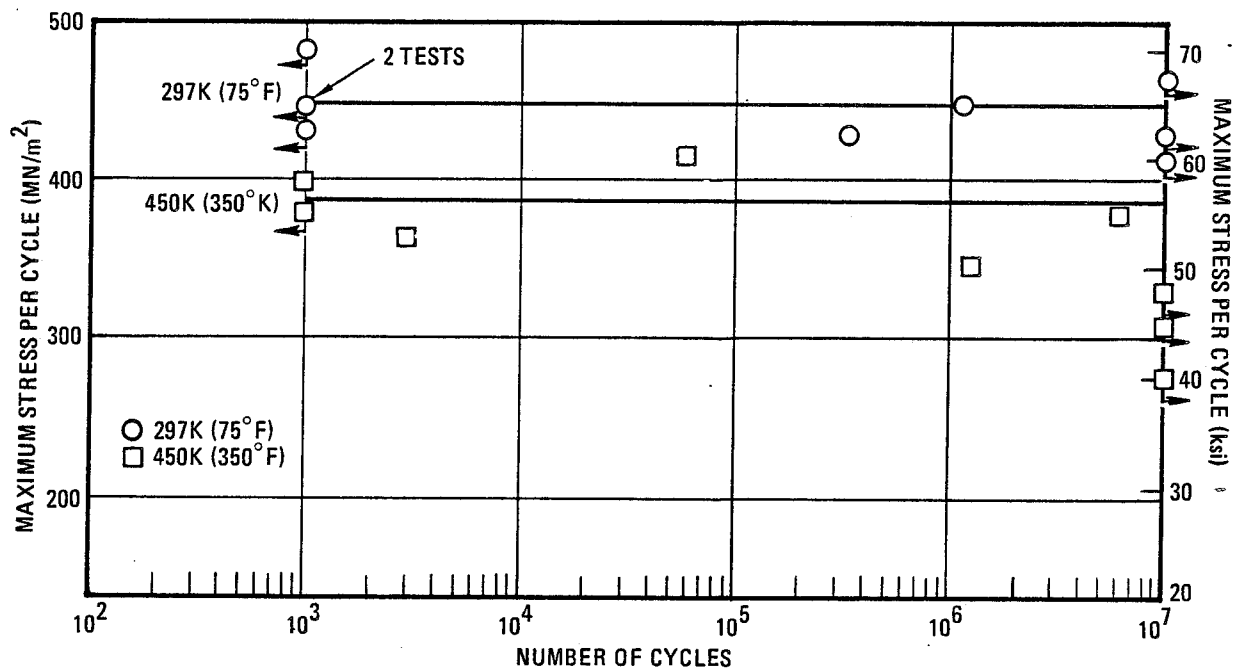
Specimen Number	Test Temperature		Maximum Stress		Cycles	Comments
	K	(°F)	MN/m ²	(ksi)		
BU72-11	297	75	620	90	<1,000	
-12			483	70	10,003,000	Did not fail
-13			517	75	12,000	
-14			448	65	3,517,000	
-15			414	60	12,592,000	Did not fail
-16			448	65	10,202,000	Did not fail
-17			500	72.5	3,000	
-18			500	72.5	19,000	
-19			534	77.5	5,000	
BU72-38	450	350	552	80	<1,000	
-39			379	55	75,000	
-40			414	60	37,000	
-43			483	70	3,000	
-44			448	65	31,000	
-45			345	50	307,000	
-46			310	45	56,000	
-1			276	40	3,215,000	
-2			241	35	5,269,000	
-3			207	30	10,904,000	Did not fail

Table 11-10. Axial Fatigue Data for $[0^\circ]_6$ G/E, Notched, $R = 0.1$

Specimen Number	Test Temperature		Maximum Stress		Cycles	Comments
	K	(°F)	MN/m ²	(ksi)		
BU71-10	297	75	896	130	507,000	
-11			862	125	1,688,000	
-12			931	135	36,000	
-13			965	140	183,000	
-14			879	127.5	401,000	
-15			914	132.5	26,000	
-16			862	125	625,000	Failed under doubler
-17			845	122.5	1,116,000	
-18			827	120	12,630,000	Did not fail
BU71-28	450	350	965	140	1,000	
-29			896	130	425,000	
-30			827	120	55,000	
-31			827	120	15,415,000	Did not fail
-32			931	135	1,000	
-33			862	125	1,000	
-34			862	125	1,071,000	
-35			879	127.5	12,143,000	Did not fail
-36			914	132.5	11,050,000	Did not fail

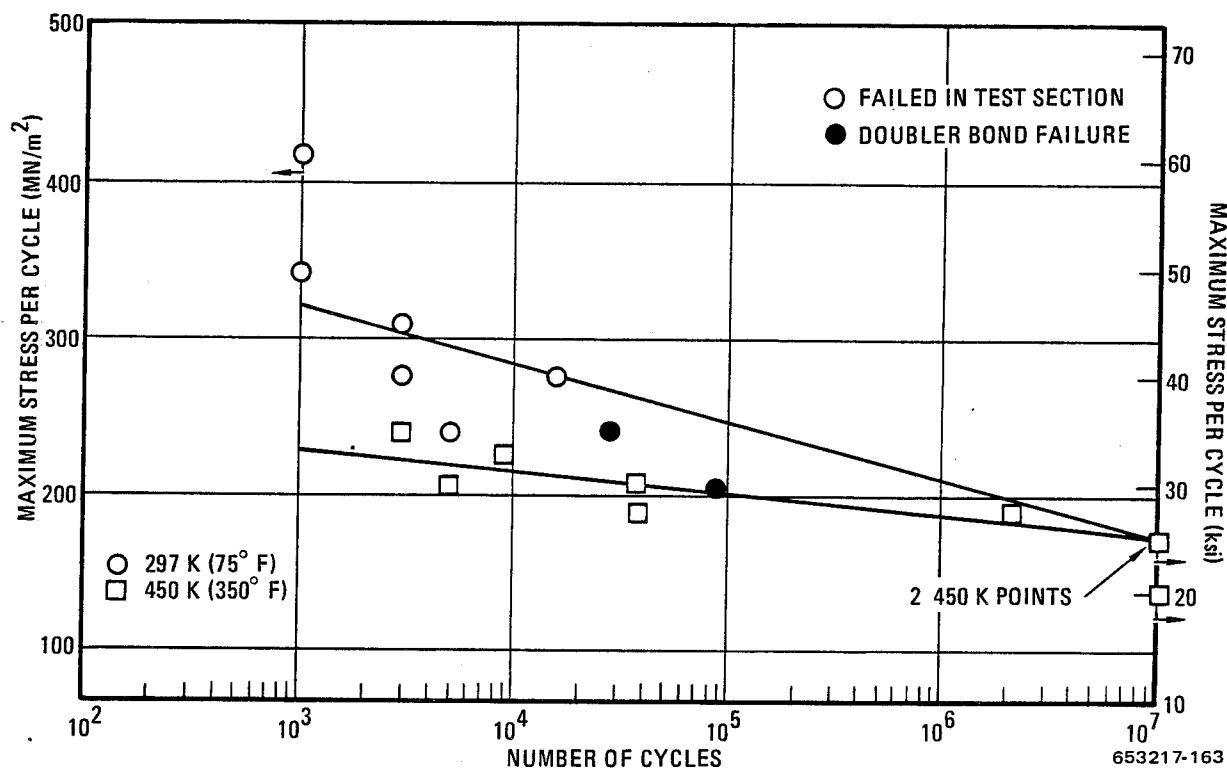
Table 11-11. Axial Fatigue Data for $[0^\circ]_{12}$ G/E, Notched, $R = -1$

Specimen Number	Test Temperature		Maximum Stress		Cycles	Comments
	K	(°F)	MN/m ²	(ksi)		
BU71-1	297	75	827	120	<1,000	
-2			552	80	3,000	
-3			483	70	10,000,000	Did not fail
-4			517	75	25,000	
-5			500	72.5	17,000	
-6			500	72.5	35,000	
-7			517	75	14,000	
-8			483	70	92,000	
-9			483	70	2,382,000	
BU71-19	450	350	552	80	2,000	
-20			483	70	58,000	
-21			414	60	9,770,000	
-22			448	65	2,000	
-23			448	65	5,020,000	
-24			517	75	17,000	
-25			465	67.5	448,000	
-26			431	62.5	10,155,000	Did not fail
-27			534	77.5	12,000	



653217-162

Figure 11-8 Axial Fatigue Properties of Unnotched $[0^\circ \pm 45^\circ]_s$ G/E at a Stress Ratio, R , of 0.1



653217-163

Figure 11-9 Axial Fatigue Properties of Unnotched $[0^\circ \pm 45^\circ]_{s2}$ G/E at a Stress Ratio, R , of -1

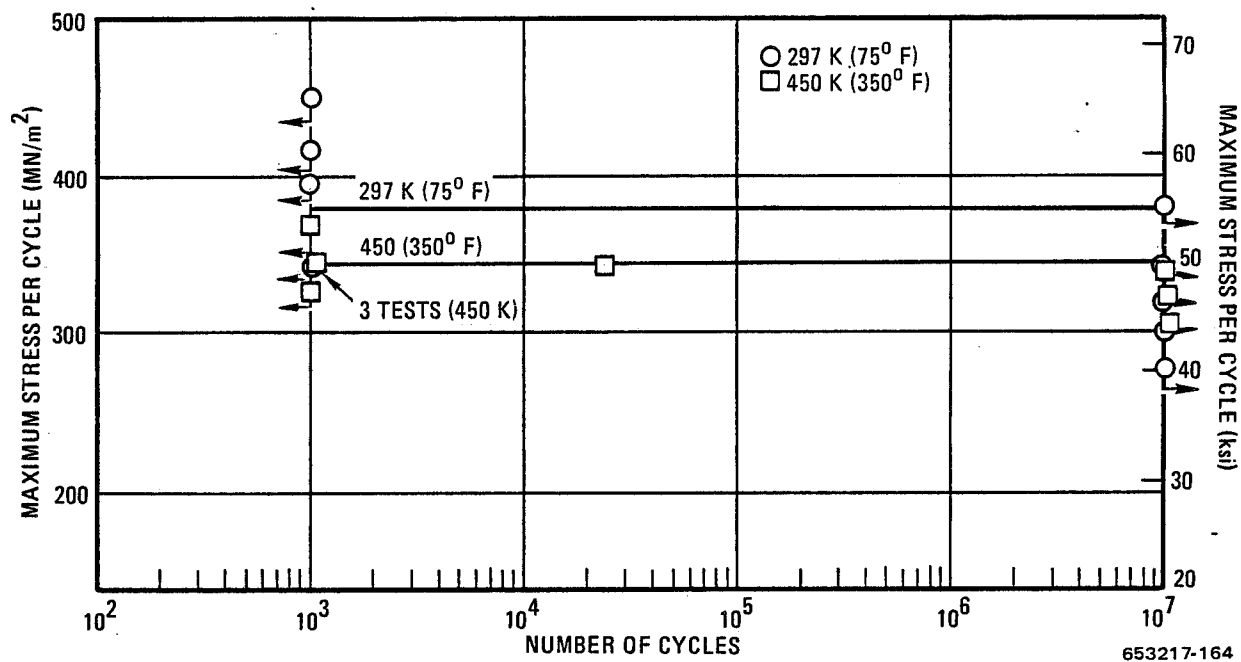


Figure 11-10 Axial Fatigue Properties of Notched $[0^\circ \pm 45^\circ]_s$ G/E at a Stress Ratio, R , of 0.1

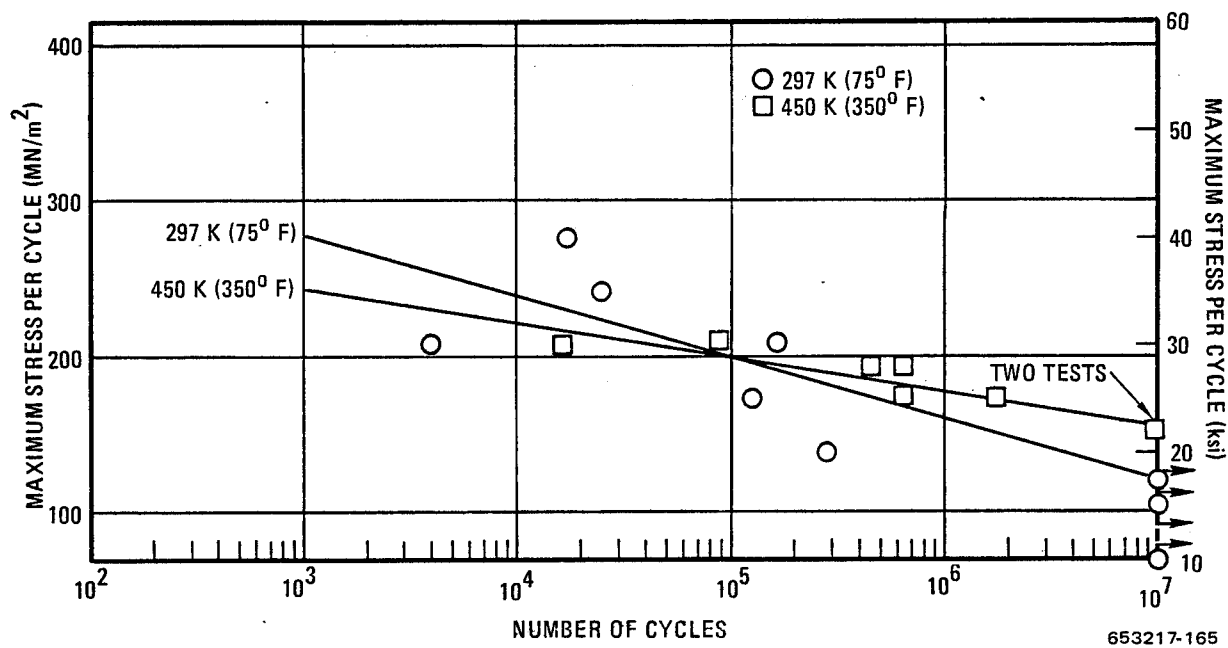
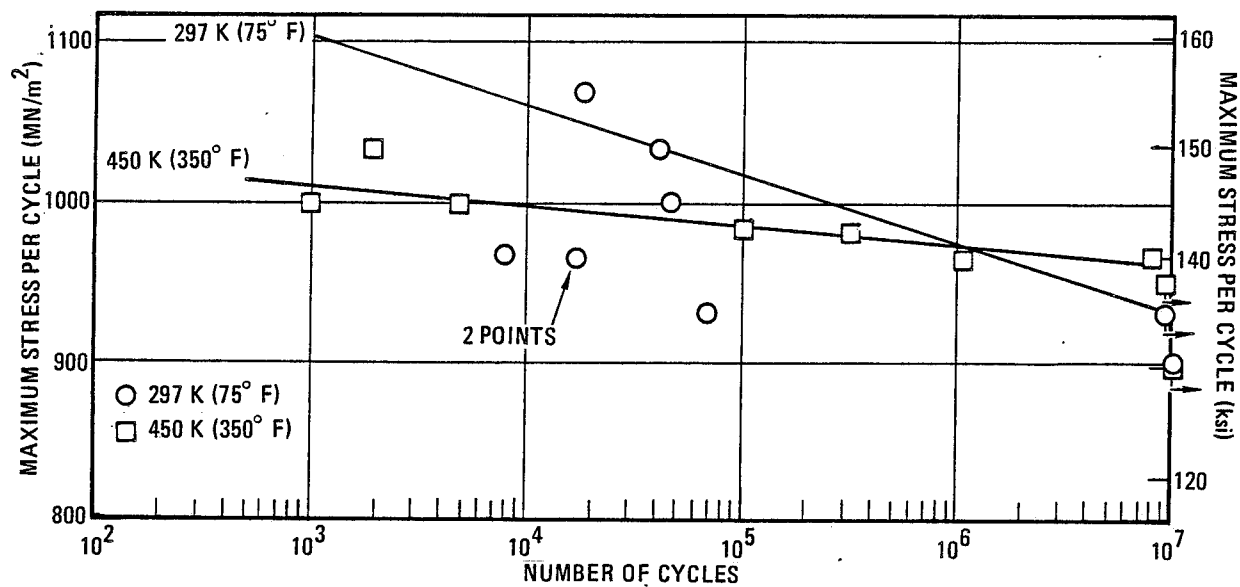
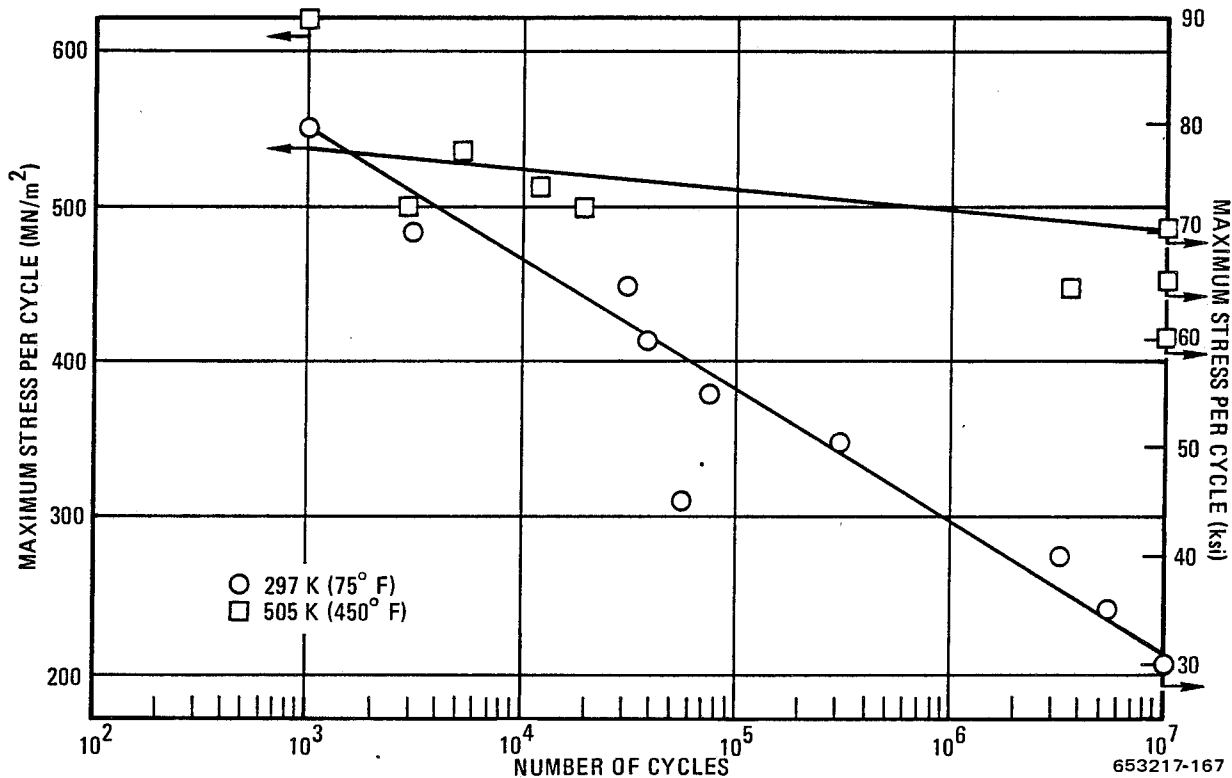


Figure 11-11 Axial Fatigue Properties of Notched $[0^\circ \pm 45^\circ]_{s2}$ G/E at a Stress Ratio, R , of -1



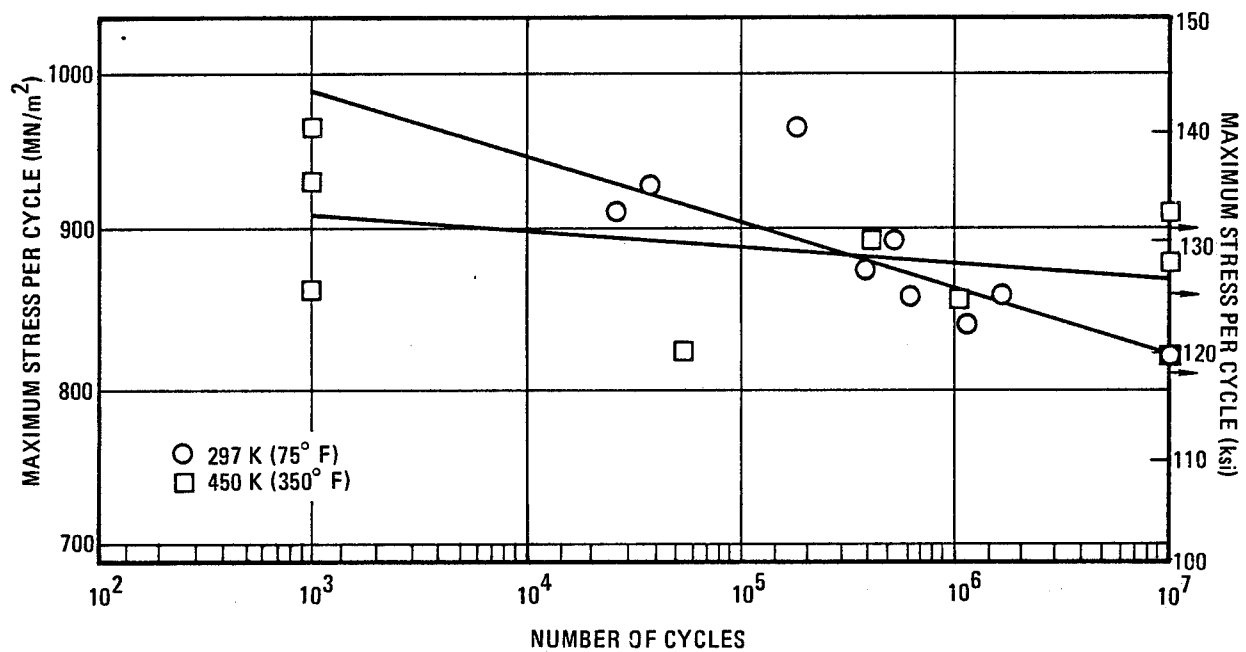
653217-166

Figure 11-12 Axial Fatigue Properties of Unnotched $[0^\circ]_6$ G/E at a Stress Ratio, R , of 0.1



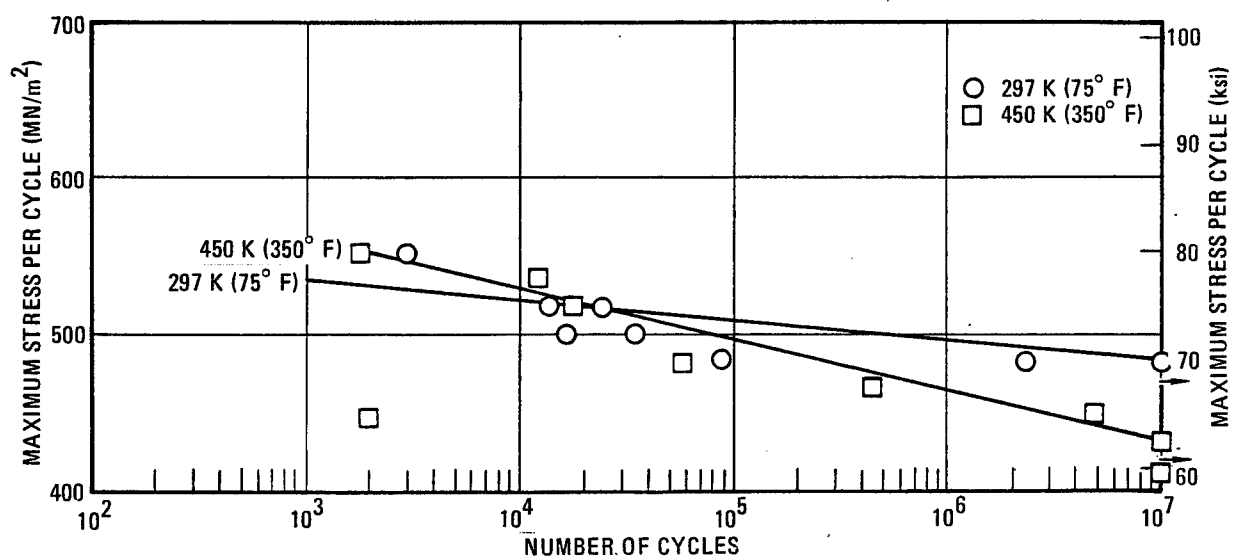
653217-167

Figure 11-13 Axial Fatigue Properties of Unnotched $[0^\circ]_{12}$ G/E at a Stress Ratio, R , of -1



653217-168

Figure 11-14 Axial Fatigue Properties of Notched $[0^\circ]_6$ G/E at a Stress Ratio, R , of 0.1



653217-169

Figure 11-15 Axial Fatigue Properties of Notched $[0^\circ]_{12}$ G/E at a Stress Ratio, R , of -1

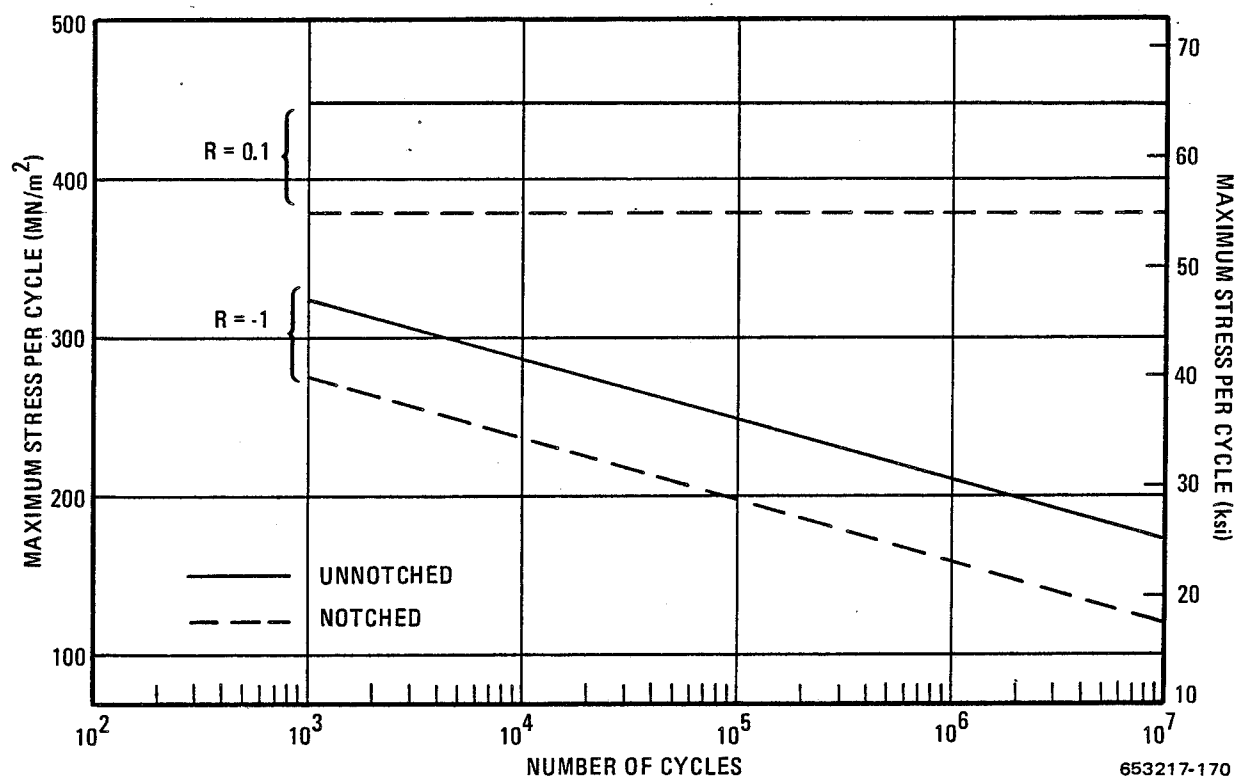


Figure 11-16 Axial Fatigue Properties of $[0^\circ \pm 45^\circ]$ G/E at 297 K (75° F)

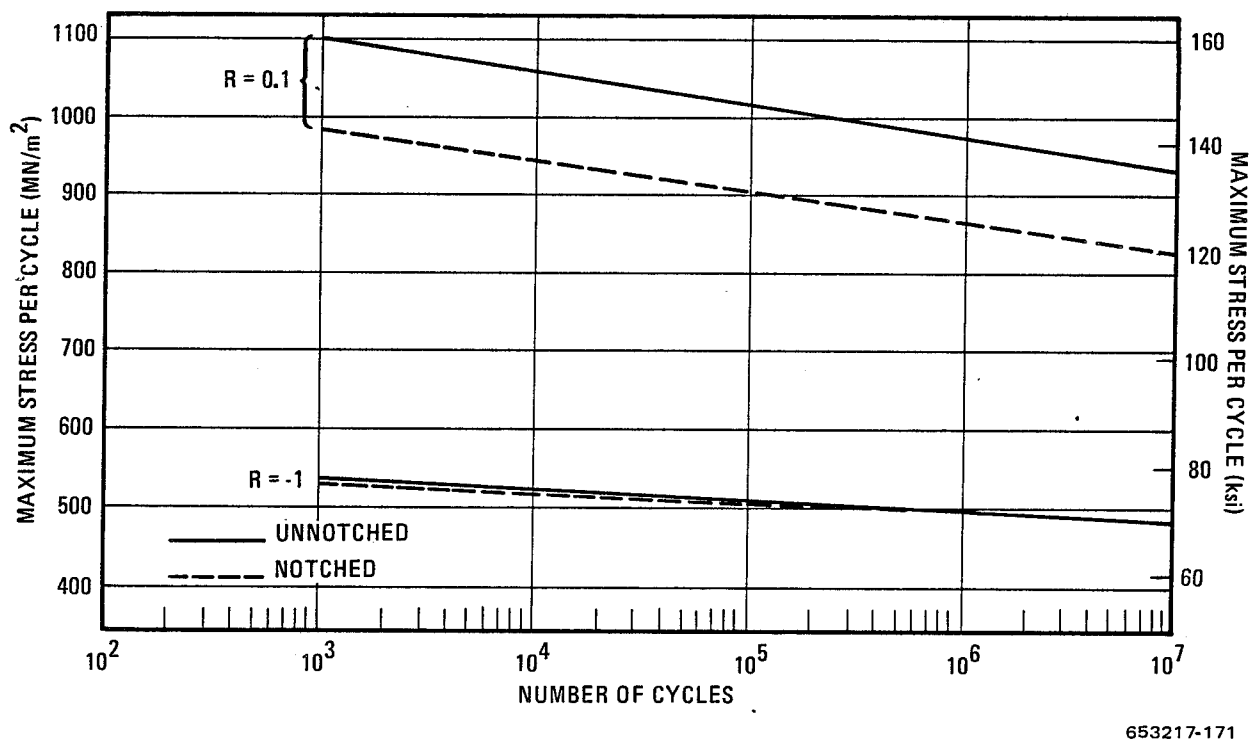


Figure 11-17 Axial Fatigue Properties of $[0^\circ]$ G/E at 297 K (75° F)

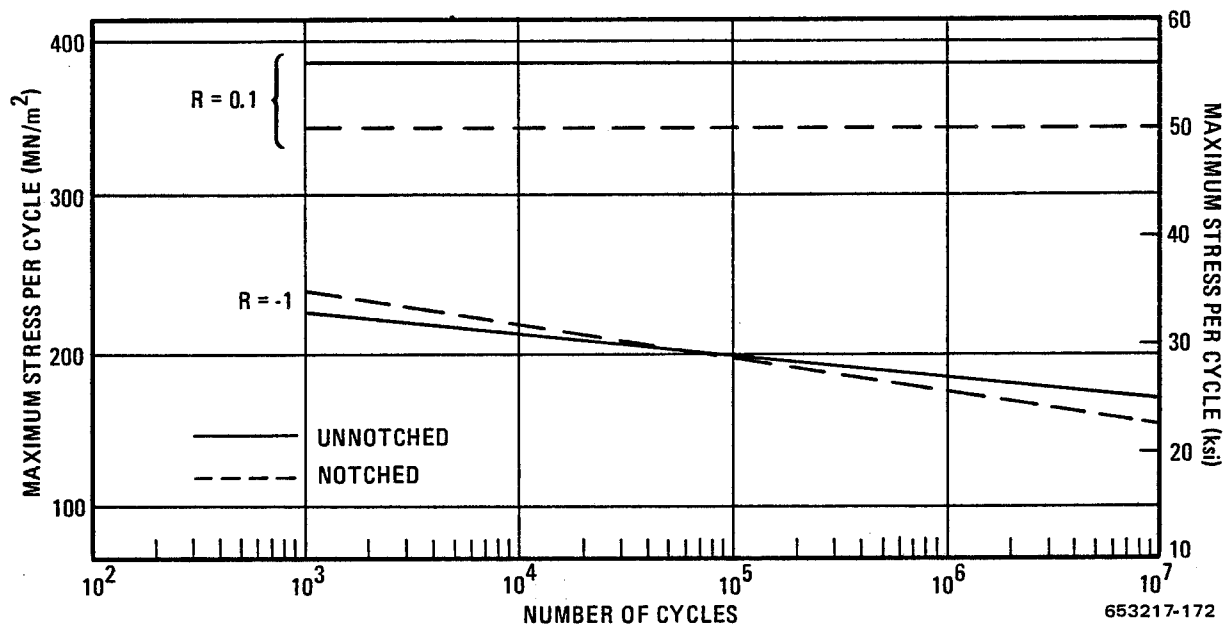


Figure 11-18 Axial Fatigue Properties of $[0^\circ \pm 45^\circ]$ G/E at 450 K (350° F)

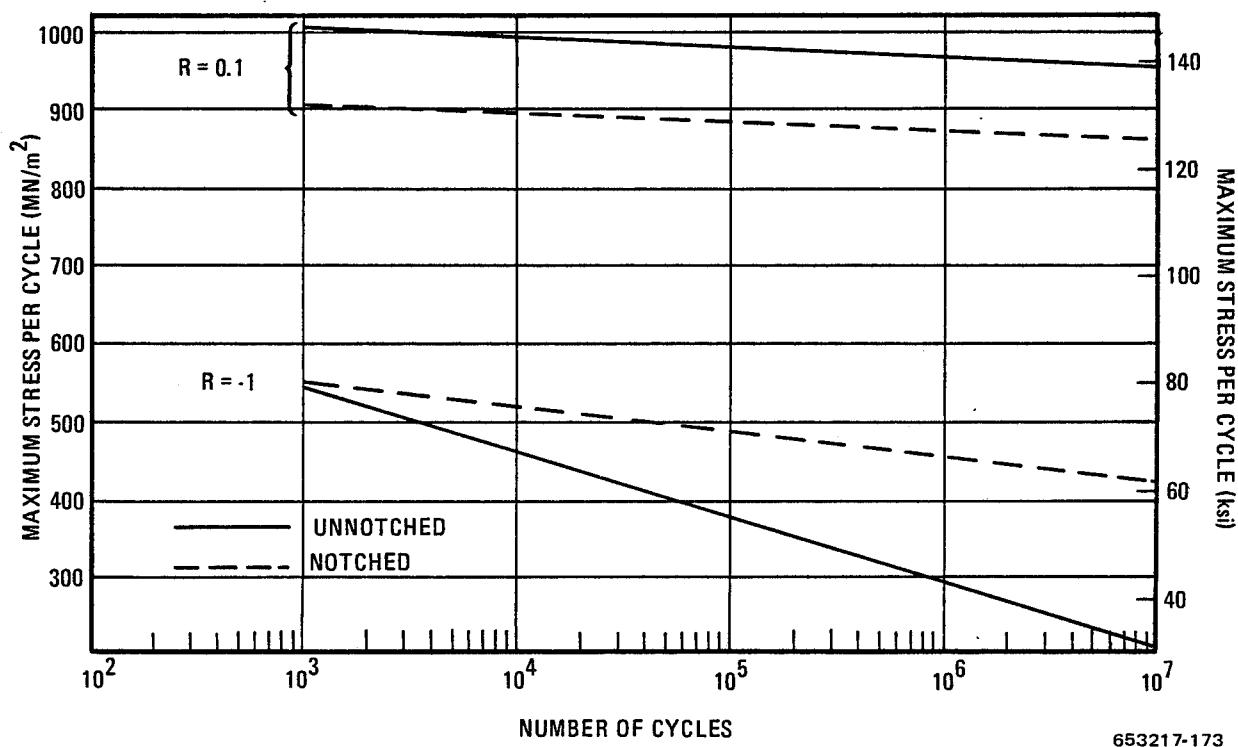


Figure 11-19 Axial Fatigue Properties of $[0^\circ]$ G/E at 450 K (350° F)

Table 11-12. Strength at Fatigue Limit or 10^7 Cycles Expressed as Percentage of Ultimate Tensile Strength for G/E

Orientation	Specimen Configuration	Temperature K	Temperature (°F)	R Value	Fatigue Strength at 10^7 Cycles (%)
[0° ± 45°]	Unnotched	297	75	0.1	90
	Notched	297	75	.1	92
	Unnotched	450	350	.1	77
	Notched	450	350	.1	83
	Unnotched	297	75	-1.0	35
	Notched	297	75	-1.0	29
	Unnotched	450	350	-1.0	34
	Notched	450	350	-1.0	37
[0°]	Unnotched	297	75	.1	60
	Notched	297	75	.1	60
	Unnotched	450	350	.1	60
	Notched	450	350	.1	64
	Unnotched	297	75	-1.0	31
	Notched	297	75	-1.0	35
	Unnotched	450	350	-1.0	13
	Notched	450	350	-1.0	32

averaged about 60% of the ultimate strength at 10^7 cycles. Values for the same types of tests except for tension-compression fatigue, $R = -1$, were considerably lower, 34% for crossply and 28% for unidirectional. To show how these values compare to typical aircraft aluminum sheet alloys, Table 11-13 was prepared. Data were obtained (ref. 37) for 0.0023 m (0.090 in.) thick 2024-T3 and 7075-T6 aluminum alloy sheet at room temperature. For tension-tension fatigue the G/E composite is far superior to the aluminum alloys particularly for notched configurations. For tension-compression fatigue the advantage is not as great although the notched G/E is still considerably higher than either of the notched aluminum alloys. For either type of fatigue loading the G/E material is less sensitive to a notch than the aluminum alloys.

11.3.2 GRAPHITE/POLYIMIDE. A complete set of fatigue data was also obtained for the G/PI system. For this material the elevated temperature selected was 505 K (450° F). The results of the numerous tests are listed in Tables 11-14 through 11-21 and individual S-N curves are plotted in Figures 11-20 through 11-27. Again, all the data points have been included in these S-N plots. These curves have been combined in Figures 11-28 through 11-31 to show the effects of the different test parameters.

Table 11-13. Comparison of Strength at Fatigue Limit or 10^7 Cycles Expressed as Percentage of Ultimate Tensile Strength for G/E and Two Aluminum Alloys Tested at Room Temperature

Specimen Configuration	R Value	Fatigue Strength at 10^7 Cycles (% of F_{tu})			
		Graphite/Epoxy [$0^\circ \pm 45^\circ$] [0°]		Aluminum Alloy 2024-T3 7075-T6	
Unnotched	0.1	90	60	49	47
^a Notched	.1	92	60	27	24
Unnotched	-1.0	35	31	29	24
^a Notched	-1.0	29	35	16	13

^aG/E, center notch, theoretical $K_t = 2.43$
Al Alloys, edge notch, $K_t = 2$

Table 11-14. Axial Fatigue Data for [$0^\circ \pm 45^\circ$], G/PI, Unnotched, $R = 0.1$

Specimen Number	Test Temperature		Maximum Stress		Cycles	Comments
	K	($^\circ$ F)	MN/m ²	(ksi)		
DC72-20	297	75	414	60	<1,000	
-21			345	50	1,000	
-22			276	40	5,622,000	
-23			310	45	1,000	
-24			293	42.5	12,045,000	Did not fail
-25			310	45	10,184,000	Did not fail
-26			328	47.5	3,000	
-27			328	47.5	14,000	
-28			328	47.5	3,000	
DC72-47	505	450	345	50	1,000	
-48			276	40	18,000	
-49			207	30	10,008,000	Did not fail
-50			310	45	4,000	
-51			241	35	14,974,000	
-52			259	37.5	10,230,000	Did not fail
-53			276	40	6,764,000	
-54			276	40	6,000	Failed under doubler
-55			276	40	30,000	

Table 11-15. Axial Fatigue Data for $[0^\circ \pm 45^\circ]_{s2}$ G/PI, Unnotched, $R = -1$

Specimen Number	Test Temperature		Maximum Stress		Cycles	Comments
	K	(°F)	MN/m ²	(ksi)		
DC72-11	297	75	172	25	169,000	
-12			190	27.5	77,000	
-13			121	17.5	10,150,000	Did not fail
-14			155	22.5	15,394,000	Did not fail
-15			190	27.5	20,000	
-16			172	25	56,000	
-17			155	22.5	4,647,000	
-18			207	30	1,000	
-19A			138	20	1,036,000	
DC72-38	505	450	138	20	2,908,000	
-39			103	15	245,000	
-40			69	10	10,004,000	Did not fail
-41			172	25	58,000	
-42			121	17.5	10,200,000	Did not fail
-43			155	22.5	1,419,000	
-44			207	30	5,000	
-45			241	35	<1,000	
-46			190	27.5	3,000	

Table 11-16. Axial Fatigue Data for $[0^\circ \pm 45^\circ]_s$ G/PI, Notched, $R = 0.1$

Specimen Number	Test Temperature		Maximum Stress		Cycles	Comments
	K	(°F)	MN/m ²	(ksi)		
DC71-10	297	75	310	45	<1,000	
-11			276	40	10,200,000	Did not fail
-12			293	42.5	10,141,000	Did not fail
-13			310	45	<1,000	
-14			302	43.75	3,000	
-15			297	43.125	2,000	
-16			293	42.5	10,175,000	Did not fail
-17			276	40	10,288,000	Did not fail
-18			297	43.125	15,370,000	Did not fail
DC71-28	505	450	276	40	15,375,000	Did not fail
-29			310	45	3,068,000	Failed near doubler
-30			345	50	14,604,000	Did not fail
-31			379	55	<1,000	
-32			362	52.5	<1,000	
-33			345	50	1,000	
-34			345	50	117,000	
-35			328	47.5	6,000	
-36			310	45	<1,000	

Table 11-17. Axial Fatigue Data for $[0^\circ \pm 45^\circ]_{s2}$ G/PI, Notched, $R = -1$

Specimen Number	Test Temperature		Maximum Stress		Cycles	Comments
	K	(°F)	MN/m ²	(ksi)		
DC71-1	297	75	41	6	10,256,000	Did not fail
-2			207	30	<1,000	
-3			138	20	462,000	
-4			121	17.5	330,000	
-5			103	15	3,421,000	
-6			138	20	114,000	
-7			172	25	1,000	
-8			155	22.5	47,000	
-9			86	12.5	12,532,000	
DC71-19	505	450	103	15	2,591,000	Did not fail
-20			121	17.5	1,137,000	
-21			86	12.5	10,220,000	
-22			138	20	27,000	
-23			155	22.5	11,000	
-24			172	25	1,000	
-25			129	18.75	60,000	
-26			112	16.25	2,018,000	
-27			95	13.75	2,569,000	

Table 11-18. Axial Fatigue Data for $[0^\circ]_6$ G/PI, Unnotched, $R = 0.1$

Specimen Number	Test Temperature		Maximum Stress		Cycles	Comments
	K	(°F)	MN/m ²	(ksi)		
DU72-20	297	75	758	110	3,000	Did not fail
-21			690	100	3,000	
-22			620	90	17,648,000	
-23			655	95	9,000	
-24			655	95	10,290,000	
-25			672	97.5	7,000	
-26			690	100	2,000	
-27			672	97.5	2,000	
-28			655	95	52,000	
DU72-47	505	450	690	100	10,180,000	Did not fail
-48			758	110	12,000	
-49			724	105	4,000	
-50			724	105	17,256,000	
-51			741	107.5	100,000	
-52			724	105	12,015,000	
-53			776	112.5	3,480,000	
-54			810	117.5	70,000	
-55			845	122.5	<1,000	

Table 11-19. Axial Fatigue Data for $[0^\circ]_{12}$ G/PI, Unnotched, $R = -1$

Specimen Number	Test		Maximum Stress		Cycles	Comments
	Temperature K	(°F)	MN/m ²	(ksi)		
DU72-11	297	75	345	50	19,000	
-12			241	35	8,404,000	Failed under doubler
-13			276	40	39,000	Failed under doubler
-14			259	37.5	70,000	
-15			207	30	10,584,000	Did not fail
-16			483	70	1,000	
-17			448	65	<1,000	
-18			379	55	22,000	
-19A			310	45	39,000	Failed under doubler
-46			138	20	10,257,000	Did not fail
DU72-38	505	450	276	40	1,154,000	
-39			310	45	6,452,000	
-40			345	50	155,000	
-41			414	60	<1,000	
-42			379	55	7,000	
-43			276	40	3,000	
-44			207	30	12,232,000	Did not fail
-45			293	42.5	6,000	

Table 11-20. Axial Fatigue Data for $[0^\circ]_6$ G/PI, Notched, $R = 0.1$

Specimen Number	Test		Maximum Stress		Cycles	Comments
	Temperature K	(°F)	MN/m ²	(ksi)		
DU71-10	297	75	655	95	10,160,000	Did not fail
-11			724	105	10,000,000	Did not fail
-12			793	115	10,175,000	Did not fail
-13			862	125	685,000	
-14			896	130	4,000	
-15			879	127.5	1,000	
-16			827	120	3,000	
-17			810	117.5	634,000	
-18			845	122.5	421,000	
DU71-28	505	450	758	110	2,000	
-29			620	90	58,000	
-30			552	80	10,111,000	Did not fail
-31			690	100	6,000	
-32			586	85	9,000	
-33			586	85	4,000	
-34			569	82.5	3,640,000	
-35			655	95	5,885,000	
-36			586	85	10,000,000	Did not fail

Table 11-21. Axial Fatigue Data for $[0^\circ]_{12}$ G/PI, Notched, $R = -1$

Specimen Number	Test Temperature		Maximum Stress		Cycles	Comments
	K	(°F)	MN/m ²	(ksi)		
DU71-1	297	75	83	a12	10,268,000	Did not fail
-2			110	a16	15,377,000	Did not fail
-3			414	60	2,000	Failed under doubler
-4			345	50	12,000	Failed under doubler
-5			310	45	1,443,000	Failed under doubler
-6			328	47.5	3,000	Failed under doubler
-7			379	55	25,000	Failed near doubler
-8			345	50	12,000	Failed under doubler
-9			414	60	1,068,000	
DU71-19	505	450	483	70	<1,000	
-20			345	50	7,000	
-21			414	60	2,000	
-22			276	40	1,893,000	
-23			310	45	6,000	
-24			241	35	3,867,000	
-25			207	30	10,149,000	Did not fail
-26			310	45	10,021,000	Did not fail
-27			345	50	10,173,000	Did not fail

^aLow stress levels were the result of an error in calculating the fatigue machine loads.

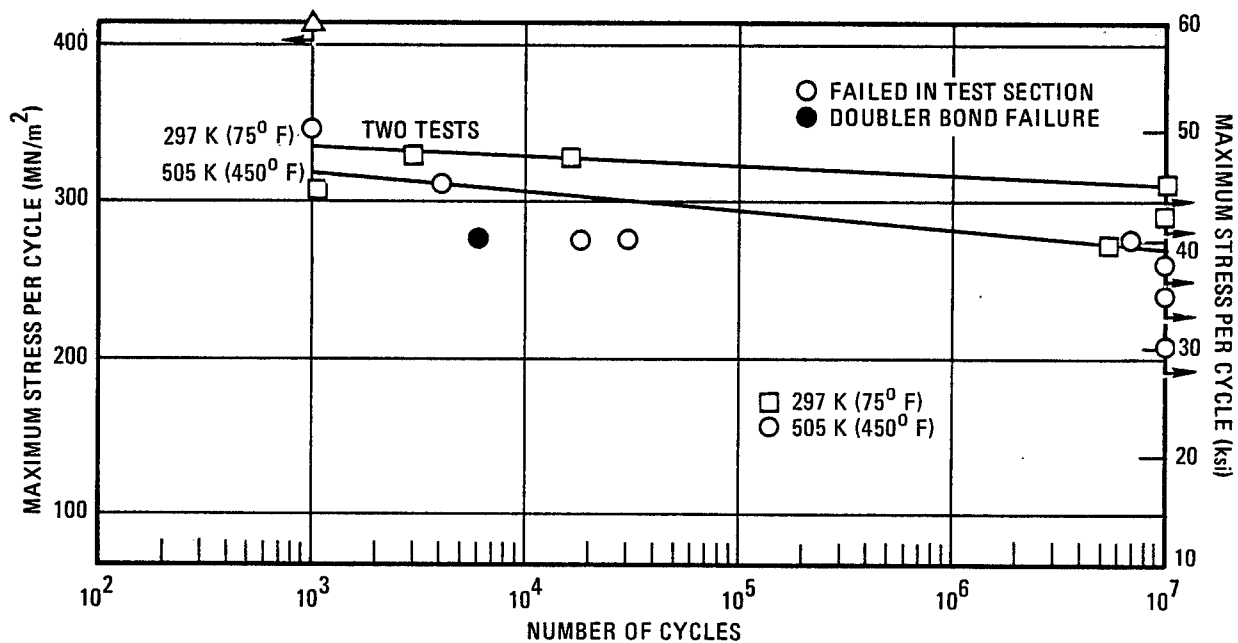


Figure 11-20 Axial Fatigue Properties of Unnotched $[0^\circ \pm 45^\circ]_s$ G/PI at a Stress Ratio, R , of 0.1

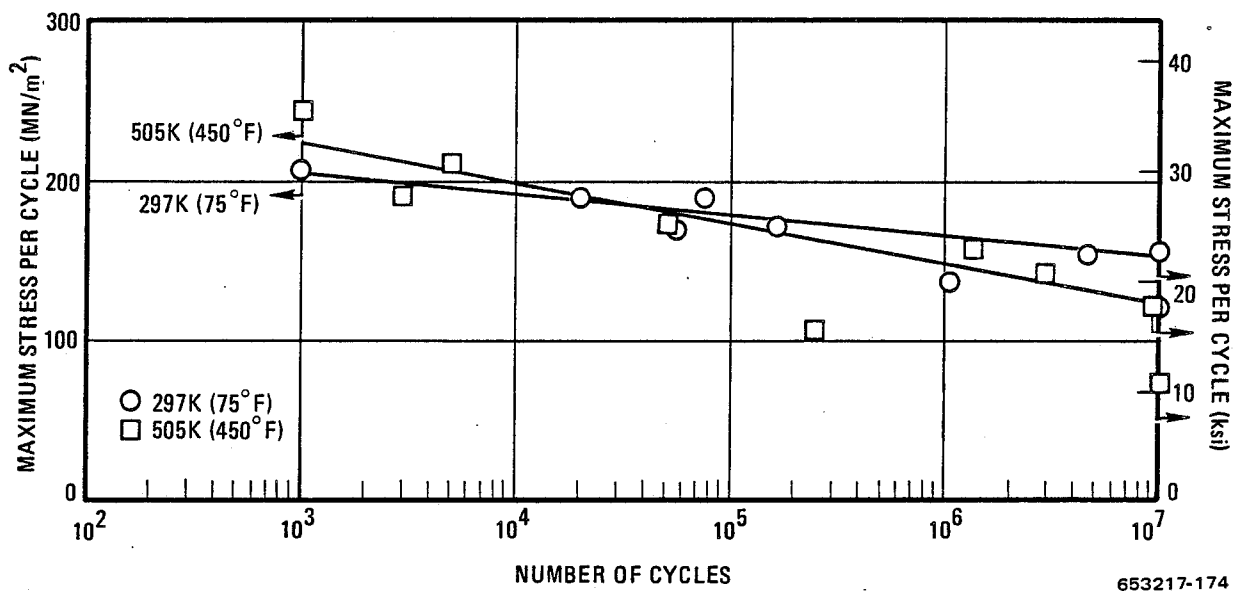


Figure 11-21 Axial Fatigue Properties of Unnotched $[0^\circ \pm 45^\circ]_{s2}$ G/PI at a Stress Ratio, R , of -1

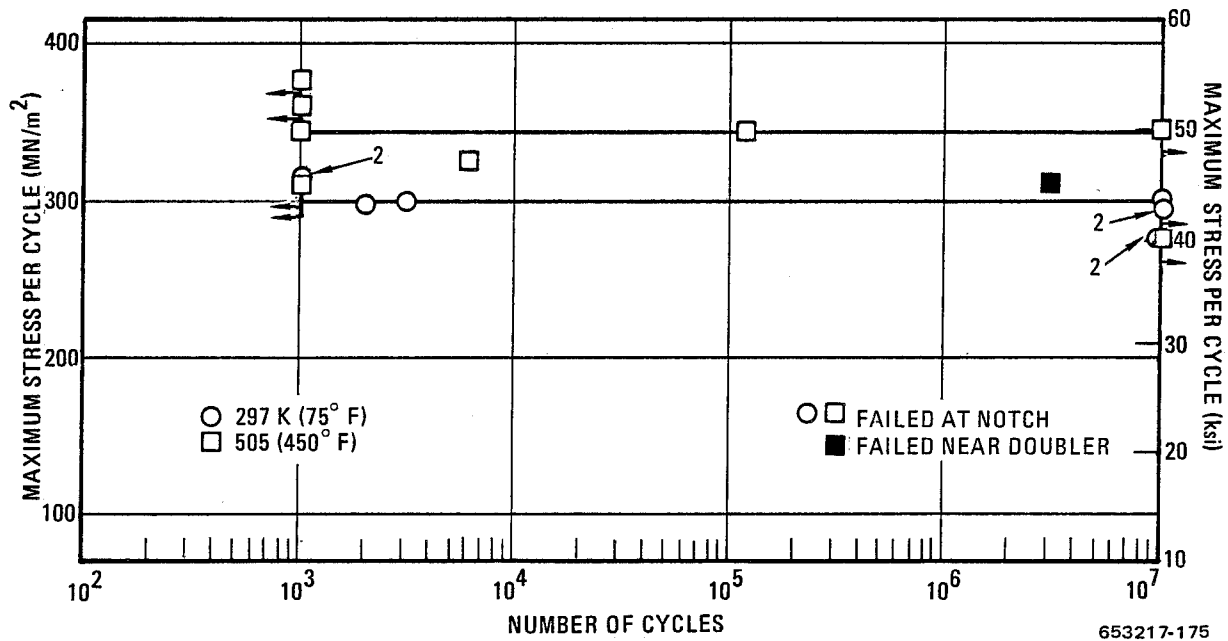


Figure 11-22 Axial Fatigue Properties of Notched $[0^\circ \pm 45^\circ]_s$ G/PI at a Stress Ratio, R , of 0.1

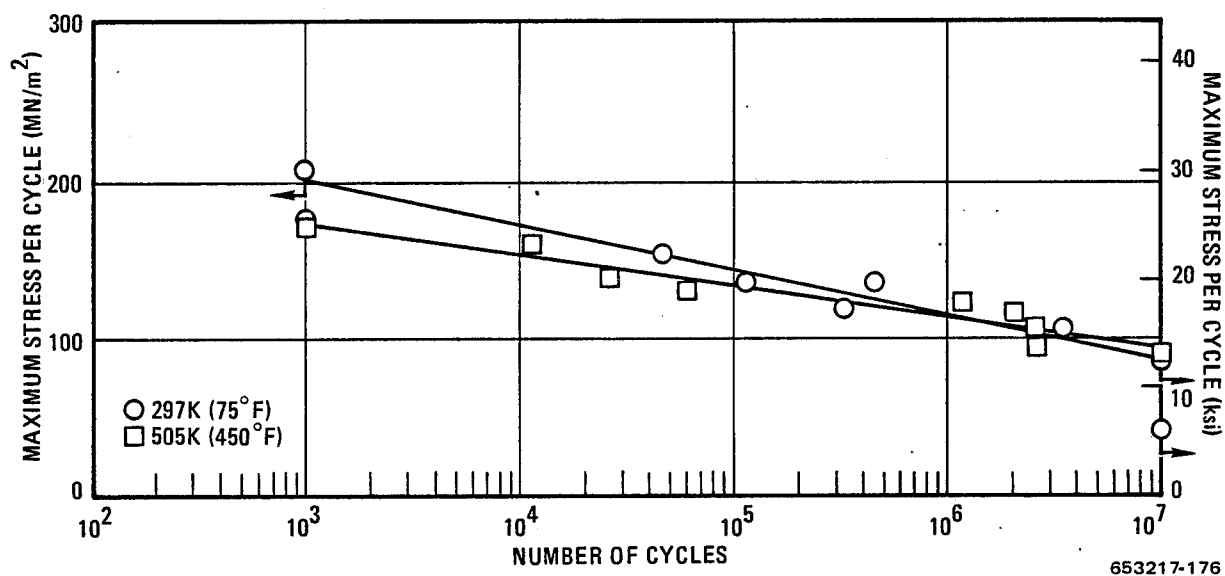


Figure 11-23 Axial Fatigue Properties of Notched $[0^\circ \pm 45^\circ]_{s2}$ G/PI at a Stress Ratio, R , of -1

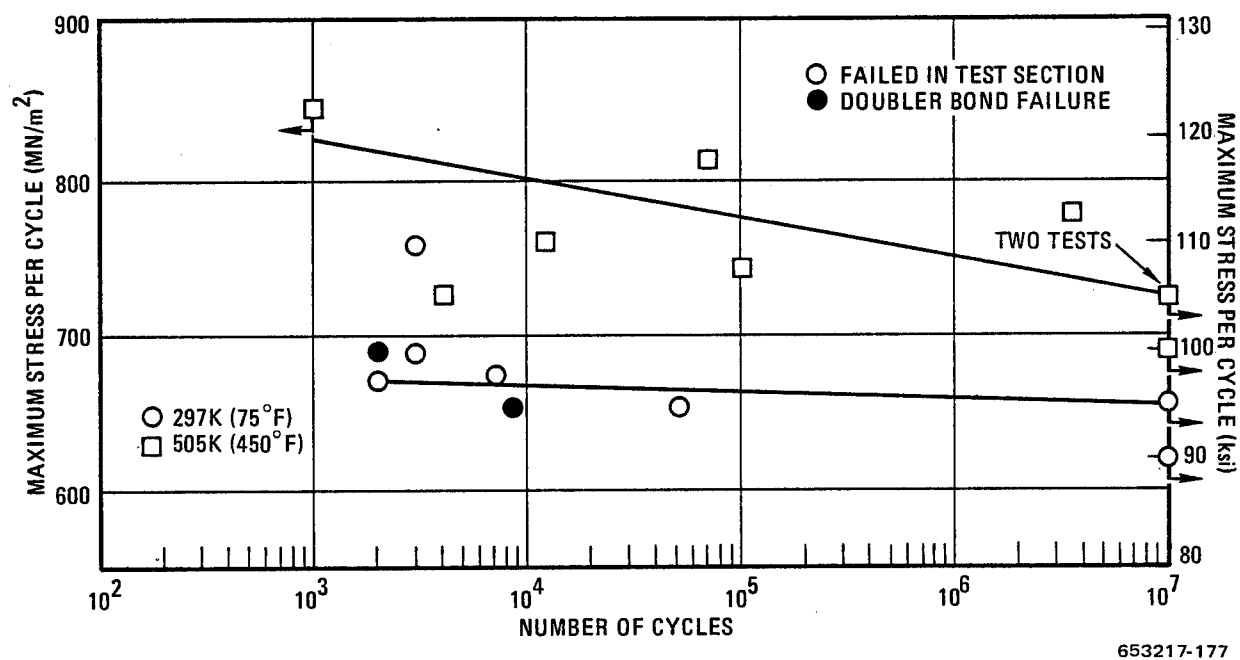


Figure 11-24 Axial Fatigue Properties of Unnotched $[0^\circ]_6$ G/PI at a Stress Ratio, R , of 0.1

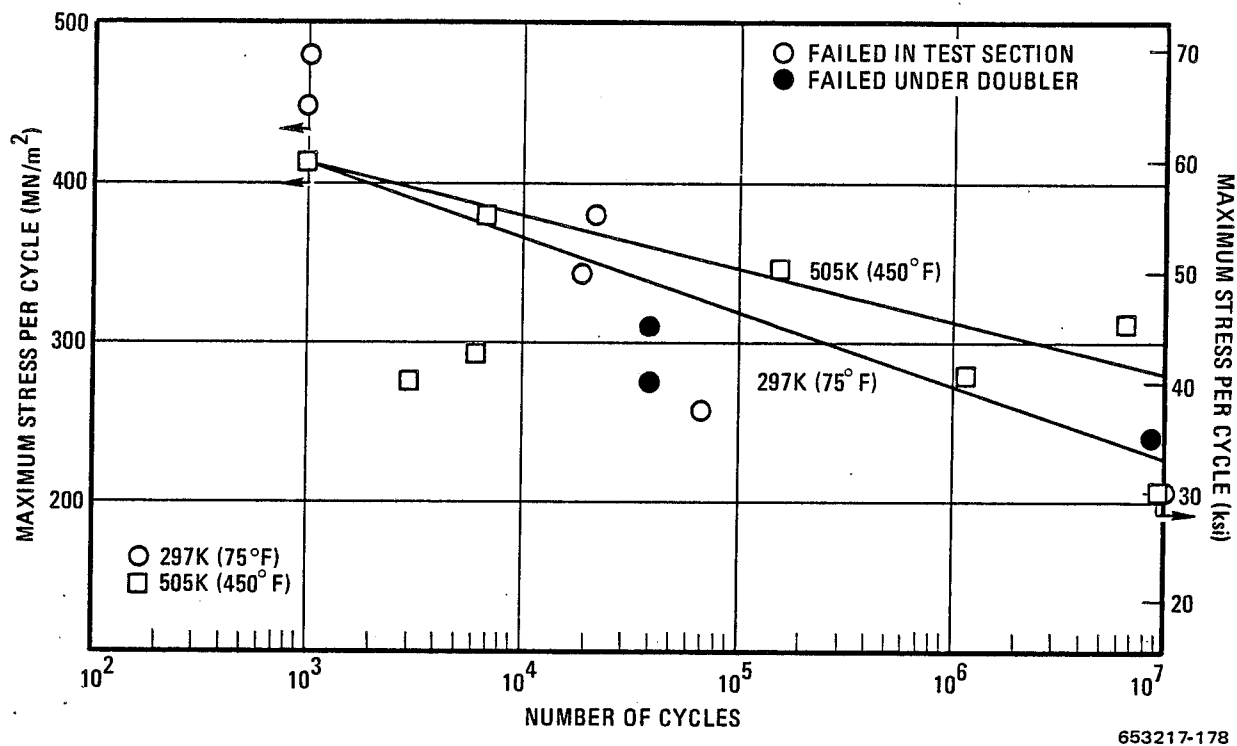


Figure 11-25 Axial Fatigue Properties of Unnotched $[0^\circ]_{12}$ G/PI at a Stress Ratio, R , of -1

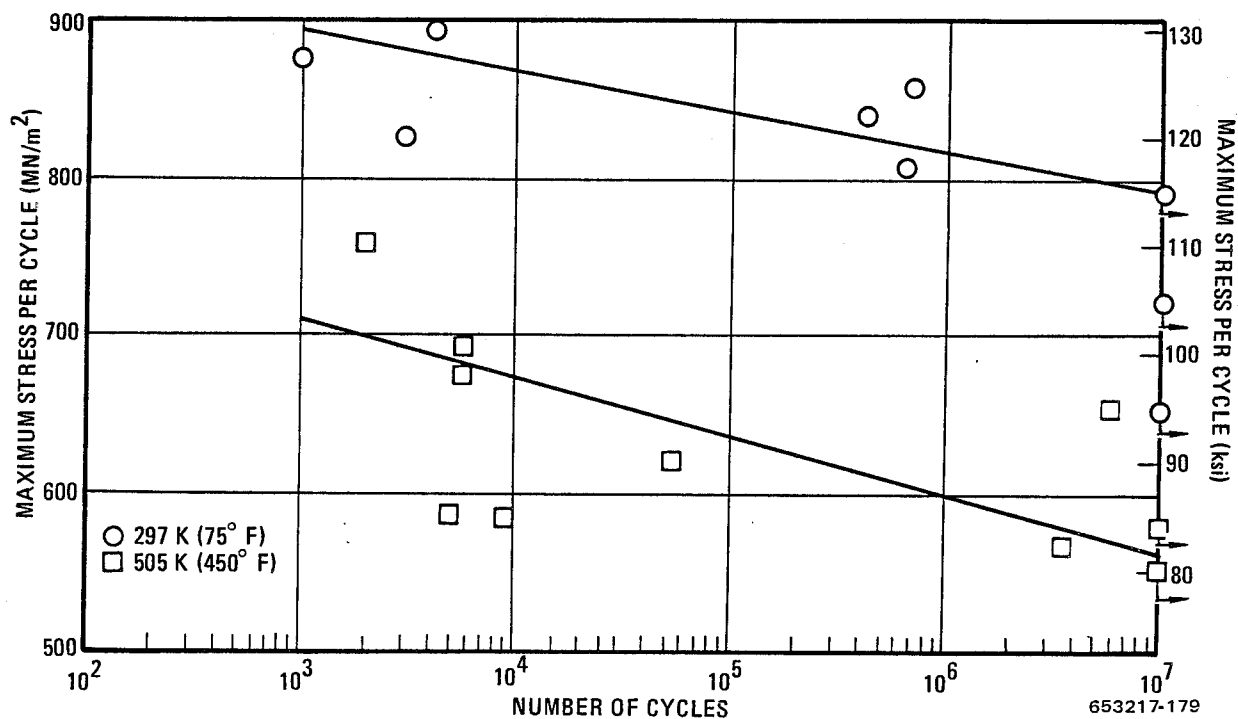


Figure 11-26 Axial Fatigue Properties of Notched $[0^\circ]_6$ G/PI at a Stress Ratio, R , of 0.1

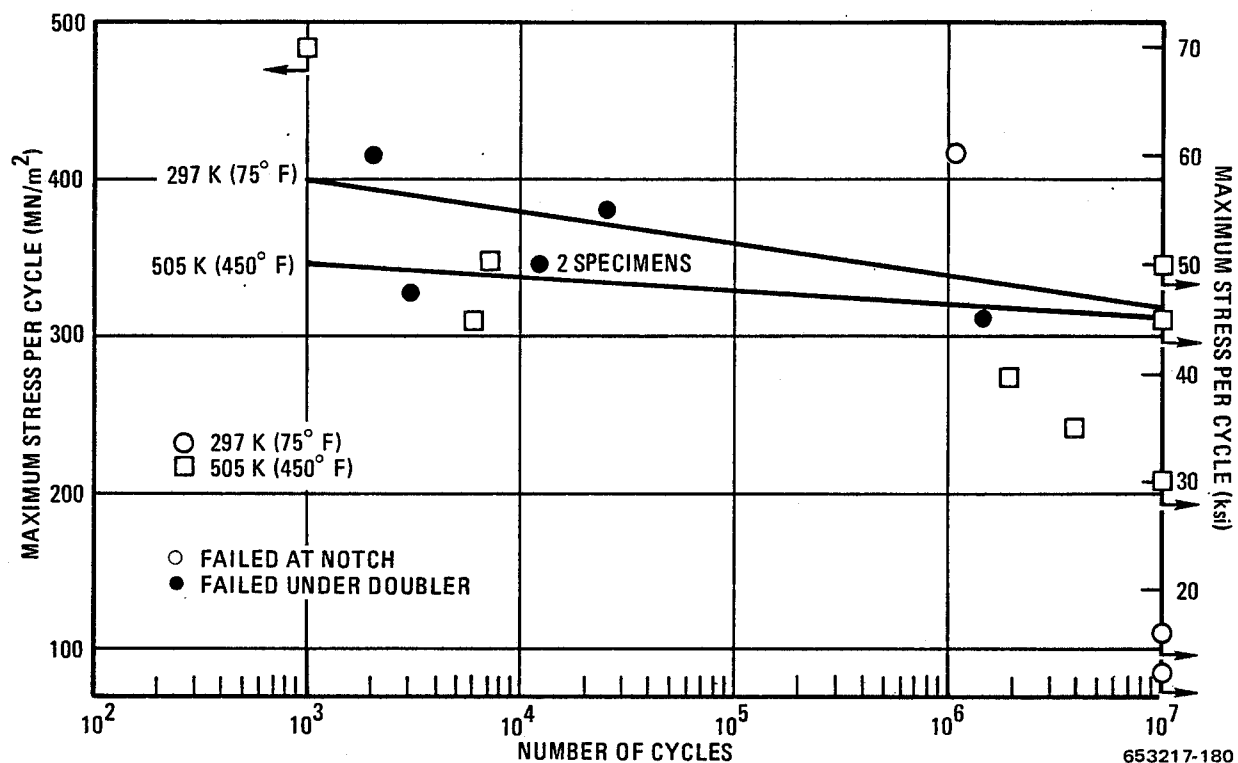


Figure 11-27 Axial Fatigue Properties of Notched $[0^\circ]_{12}$ G/PI at a Stress Ratio, R , of -1

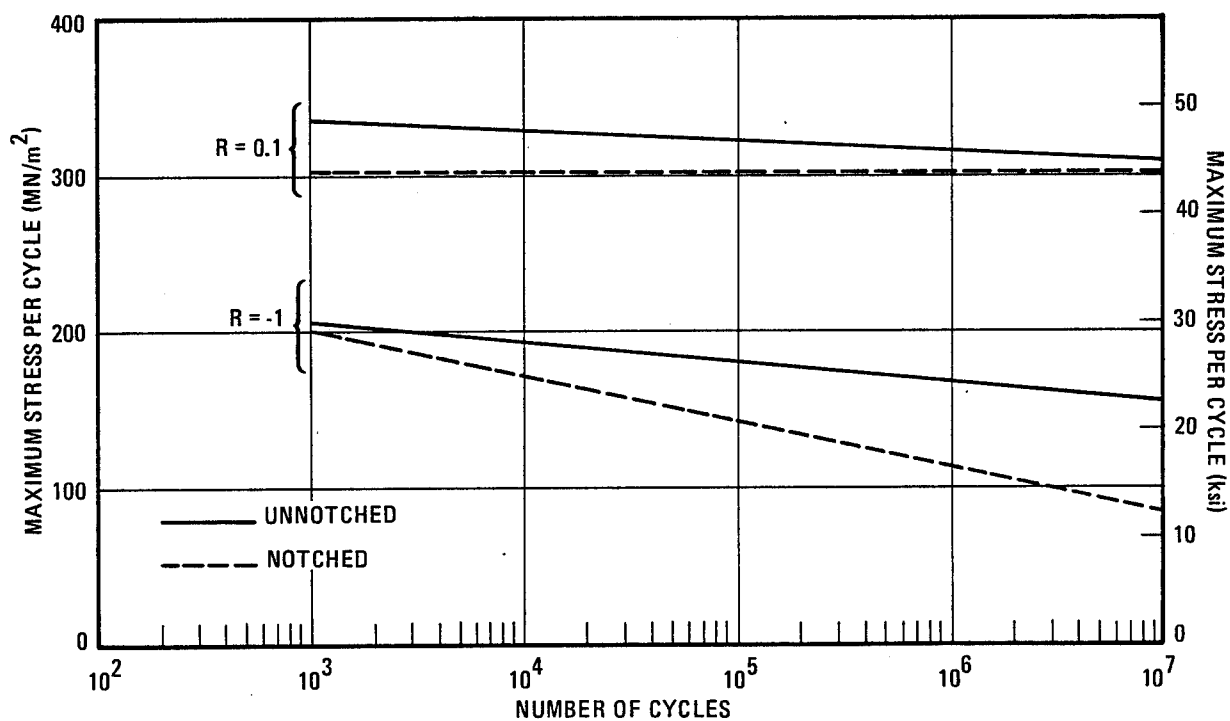
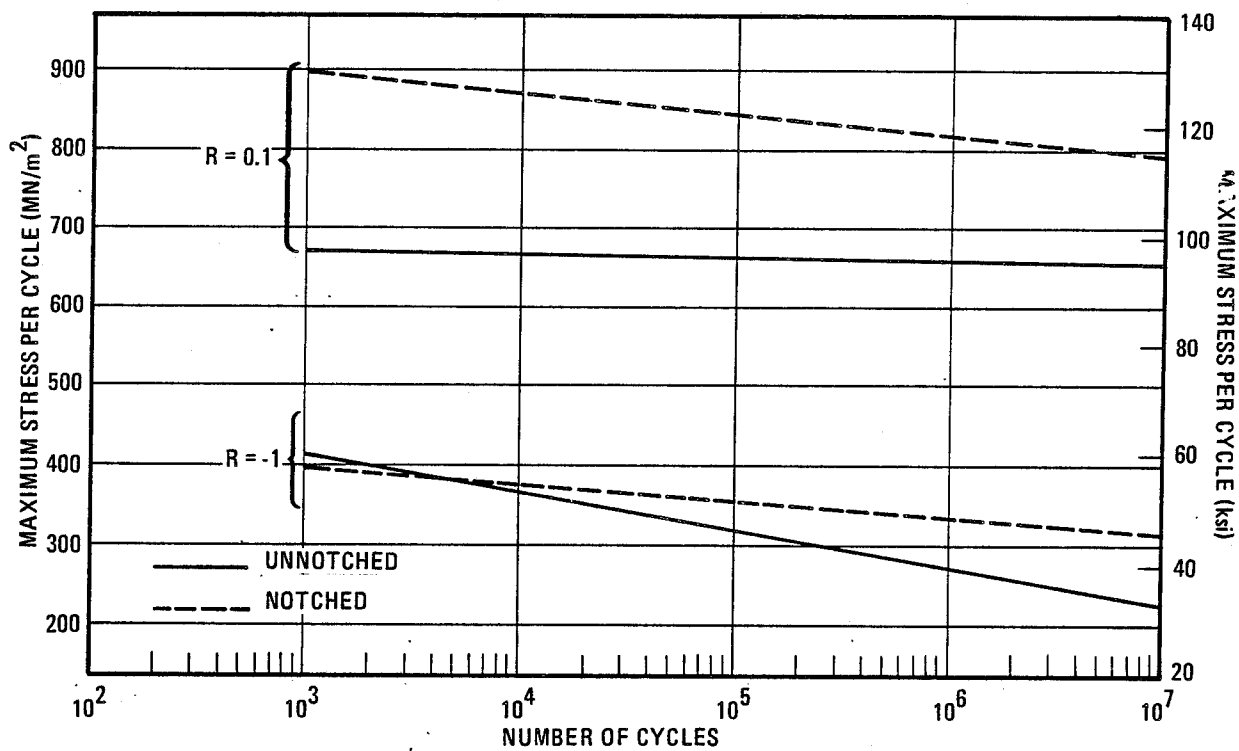
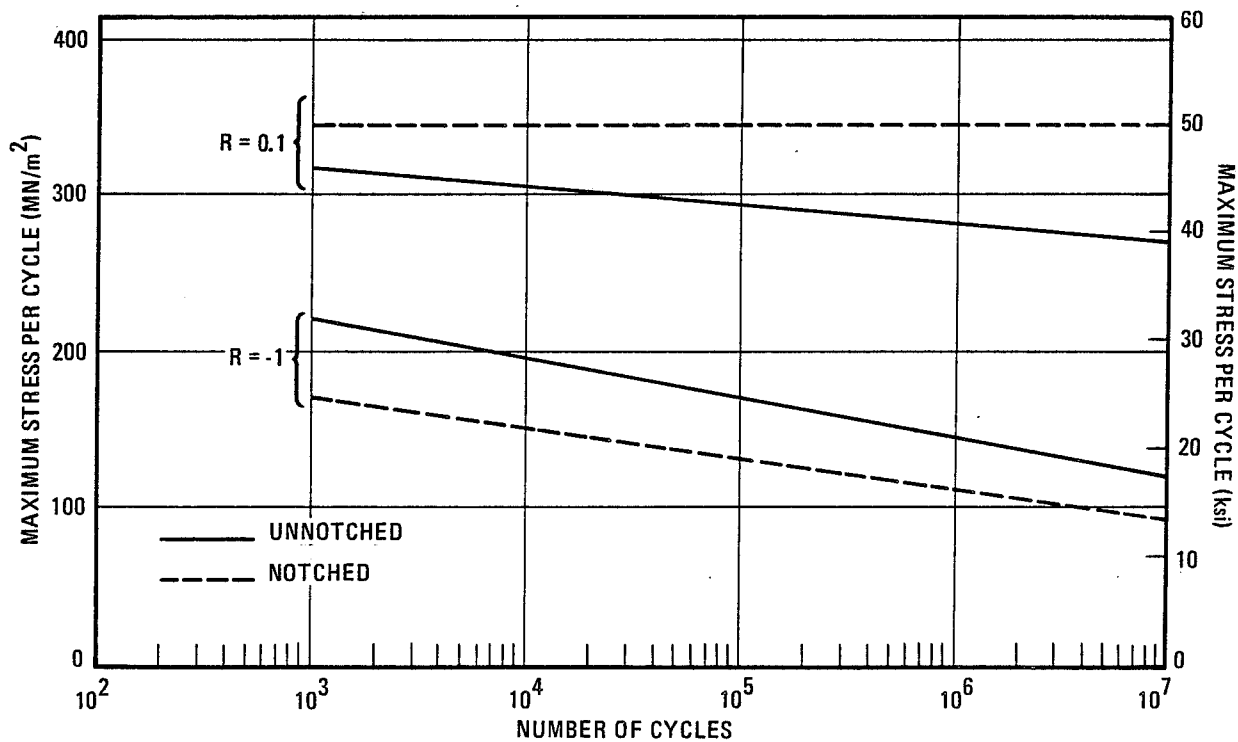


Figure 11-28 Axial Fatigue Properties of $[0^\circ \pm 45^\circ]$ G/PI at 297 K (75° F)



653217-182

Figure 11-29 Axial Fatigue Properties of $[0^\circ]$ G/PI at 297 K (75° F)



653217-183

Figure 11-30 Axial Fatigue Properties of $[0^\circ \pm 45^\circ]$ G/PI at 505 K (450° F)

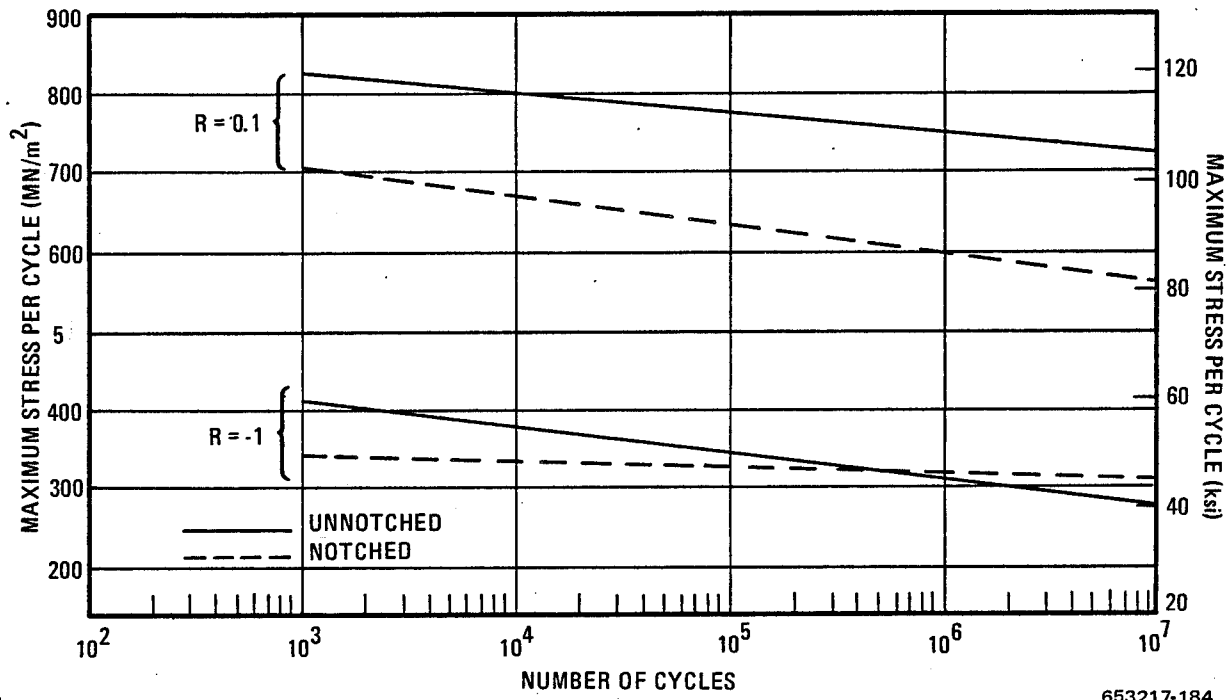


Figure 11-31 Axial Fatigue Properties of [0°] G/PI at 505 K (450° F)

In like manner to the results obtained with the G/E material, the factor having the most pronounced effect on fatigue strength was the stress ratio, R . In all cases, with the other parameters identical, specimens tested in an R value of -1 gave fatigue strengths at 10^3 cycles (determined from S-N curve) that were less than those obtained at 10^7 cycles for specimens tested at an R value of 0.1 . The effect of a notch was generally to reduce the fatigue strength but, again, there were exceptions. Notched specimen curves were higher than unnotched for both $[0^\circ]$ material at 297 K (75° F) and $R = 0.1$, Figure 11-29, and $[0^\circ \pm 45^\circ]$ material at 505 K (450° F) and $R = 0.1$, Figure 11-30. For $[0^\circ]$ material at 297 K (75° F) and $R = -1$, Figure 11-29, and at 505 K (450° F) and $R = -1$, Figure 11-31, the unnotched and notched curves crossed each other. The G/PI fatigue data, primarily the $[0^\circ]$ results, showed a good deal more scatter than was found in the G/E data, and this may have contributed to the inconsistencies in the effects of a notch on G/PI fatigue strength. The effect of increasing the temperature for the $R = -1$ tests was a slight reduction in fatigue strength. For the $R = 0.1$ tests both decreases and increases in fatigue properties were observed depending on the laminate orientation and the specimen configuration. Additional fatigue testing would be useful in determining the effects that a notch or an increase in test temperature contribute to the fatigue strength of G/PI.

In testing one group of specimens (12 ply, unidirectional, notched, $R = -1$, room temperature, Table 11-21, Figure 11-27) many of the failures occurred in the composite under the bonded end doublers rather than in the test section through the center hole. This type of failure is not uncommon for unidirectional composites tested in fatigue. During fatigue cycling vertical cracks initiate at the edges of, and tangent to, the center hole, dividing the specimen into three parallel strips. Failure can then occur anywhere along the two outside load carrying strips and

often is initiated at the highly stressed regions at the end doublers. The same failure mechanism was prevalent in the unidirectional B/Al specimens tested under the same conditions.

A table similar to the one presented earlier for the G/E data has been prepared to show the percentage of the G/PI ultimate strengths at which the fatigue limit (or 10^7 cycles) occurred. The results, Table 11-22, were quite similar to the G/E system except for being slightly lower in value. Tests at an R value of 0.1 give approximately 75% for the crossply material and 60% for the unidirectional material. Again, for stress ratios of -1 the values were considerably lower, 27% and 24% respectively for the crossply and unidirectional layups. In a comparison with similar data for typical aircraft aluminum sheet alloys (Table 11-13) the G/PI is superior, particularly for the notched material. While the advantage is not as great as that shown by the G/E system, G/PI retains these excellent fatigue properties up to 505 K (450° F), well above the maximum use temperatures of either the epoxy or aluminum systems. To show the same comparison with a structural material having a higher maximum use temperature than the aluminum alloys, Table 11-23 was prepared. Data were obtained (ref. 37) for 0.0016 m (0.063 in.) thick Ti-6Al-4V titanium alloy sheet at 297 K (75° F) and 589 K (600° F). The G/PI composite is as good or better than the titanium alloy up to 505 K (450° F) for all comparisons except the unnotched unidirectional material tested in tension-compression fatigue. Again, data scatter in the $[0^\circ]$ results may be a factor. In like manner to the G/E — aluminum alloy comparison the advantage held by the G/PI over the titanium alloy is particularly evident in the notched data.

Table 11-22. Strength at Fatigue Limit or 10^7 Cycles Expressed as Percentage of Ultimate Tensile Strength for G/PI

Orientation	Specimen Configuration	Temperature K	($^\circ$ F)	R Value	Fatigue Strength at 10^7 Cycles (%)
$[0^\circ \pm 45^\circ]$	Unnotched	297	75	0.1	60
	Notched	297	75	.1	85
	Unnotched	505	450	.1	57
	Notched	505	450	.1	100
	Unnotched	297	75	-1.0	30
	Notched	297	75	-1.0	24
	Unnotched	505	450	-1.0	26
	Notched	505	450	-1.0	28
$[0^\circ]$	Unnotched	297	75	.1	55
	Notched	297	75	.1	63
	Unnotched	505	450	.1	60
	Notched	505	450	.1	50
	Unnotched	297	75	-1.0	19
	Notched	297	75	-1.0	25
	Unnotched	505	450	-1.0	23
	Notched	505	450	-1.0	27

11.3.3 BORON/ALUMINUM. Results of the B/Al fatigue testing program are listed in Tables 11-24 through 11-31. These data have been plotted in S-N diagrams in Figures 11-32 through 11-39. The fatigue curves have also been combined in Figures 11-40 through 11-43 to show the effects of the different test parameters. The elevated temperature initially selected for testing was 561 K (550° F), but this was later reduced to 505 K (450° F) because of severe surface degradation of the aluminum. Consequently, half of the elevated temperature tests (those at $R = 0.1$) were conducted at 561 K (550° F) and the other half ($R = -1$) at 505 K (450° F).

Figures 11-40 through 11-43 again show the pronounced effect that the stress ratio, R , has on the fatigue strength. For all combinations of orientation, temperature, and specimen configuration that were evaluated, the $R = -1$ tests gave values well below those of $R = 0.1$. The effect of the center hole in the notched specimens, generally, was a decrease in fatigue strength. For some groups of specimens the effect was slight and for one, the unidirectional material tested at 297 K (75° F) and $R = -1$, the notched fatigue strength was well above the unnotched strength at the lower end of the S-N curve. The effect of raising the test temperature from 297 K (75° F) to 561 K (550° F) was to significantly reduce the fatigue strength at 10^7 cycles. For fatigue lives of 10^5 or less and at an R value of 0.1, the effect of temperature on fatigue life was not very great. The specimens, however, exhibited extensive surface attack in the outer aluminum layer. Because of this poor performance the $R = -1$ test temperature was lowered to 505 K (450° F). As shown in Figures 11-42 and 11-43 the slopes of the S-N curves for these tests were similar to those obtained at room temperature, and the fatigue strengths were only slightly lowered.

Examination of the B/Al specimens that were fatigue tested at 561 K (550° F) revealed severe degradation of the aluminum matrix material, as shown in Figures 11-44 and 11-45. The surface of the specimens showed multiple cracks and roughness caused by localized deformation.

Table 11-23. Comparison of Strength at Fatigue Limit or 10^7 Cycles Expressed as Percentage of Ultimate Tensile Strength for G/PI and Ti-6Al-4V Titanium Alloy at Room and Elevated Temperatures

Specimen Configuration	R Value	Fatigue Strength at 10^7 Cycles (% of F_{tU})					
		Graphite/Polyimide				Ti-6Al-4V Alloy	
		[0° ± 45°]		[0°]		Solution-treated and aged	
		297 K (75° F)	505 K (450° F)	297 K (75° F)	505 K (450° F)	297 K (75° F)	589 K (600° F)
Unnotched	0.1	60	57	55	60	50	52
^a Notched	0.1	85	100	63	50	23	29
Unnotched	-1.0	30	26	19	23	32	25
^a Notched	-1.0	24	28	25	27	16	19

^aG/PI, center notch, theoretical $K_t = 2.43$
Ti-6Al-4V Alloy, center notch, $K_t = 2.82$

Table 11-24. Axial Fatigue Data for $[0^\circ \pm 45^\circ]_s$ B/Al, Unnotched, $R = 0.1$

Specimen Number	Test Temperature		Maximum Stress		Cycles	Comments
	K	(°F)	MN/m ²	(ksi)		
EC72-20	297	75	262	38	17,451,000	Did not fail
-21			379	55	1,876,000	
-22			414	60	72,000	
-23			345	50	33,360,000	
-24			448	65	716,000	
-25			483	70	1,686,000	
-26			517	75	17,000	
-27			465	67.5	122,000	
-28			414	60	2,627,000	
EC72-47	561	550	414	60	53,000	
-48			379	55	201,000	
-49			345	50	571,000	
-50			310	45	1,780,000	
-51			276	40	2,691,000	
-52			241	35	9,385,000	
-53			224	32.5	9,341,000	
-54			207	30	10,551,000	
-55			448	65	66,000	

Table 11-25. Axial Fatigue Data for $[0^\circ \pm 45^\circ]_{s2}$ B/Al, Unnotched, $R = -1$

Specimen Number	Test Temperature		Maximum Stress		Cycles	Comments
	K	(°F)	MN/m ²	(ksi)		
EC72-11	297	75	345	50	38,000	
-12			379	55	8,000	
-13			310	45	72,000	
-14			276	40	448,000	
-15			207	30	6,610,000	
-16			241	35	788,000	
-17			190	27.5	15,437,000	
-18			414	60	1,000	
-19			362	52.5	2,000	
EC72-38	505	450	276	40	58,000	
-39			207	30	861,000	
-40			345	50	4,000	
-41			379	55	2,000	
-42			310	45	7,000	
-43			241	35	52,000	
-44			138	20	10,006,000	
-45			172	25	10,111,000	
-46			259	37.5	38,000	

Table 11-26. Axial Fatigue Data for $[0^\circ \pm 45^\circ]_2$ B/Al, Notched, $R = 0.1$

Specimen Number	Test Temperature		Maximum Stress		Cycles	Comments
	K	(°F)	MN/m ²	(ksi)		
EC71-10	297	75	345	50	492,000	
-11			276	40	10,150,000	Did not fail
-12			414	60	24,000	
-13			379	55	1,192,000	
-14			310	45	10,130,000	Did not fail
-15			448	65	5,000	
-16			396	57.5	901,000	
-17			362	52.5	2,913,000	
-18			328	47.5	10,085,000	Did not fail
EC71-28	561	550	345	50	No data	Temp. over-shoot
-29			276	40	2,634,000	
-30			241	35	5,490,000	
-31			207	30	10,100,000	Did not fail
-32			310	45	790,000	
-33			345	50	477,000	
-34			414	60	91,000	
-35			448	65	79,000	
-36			224	32.5	8,247,000	

Table 11-27. Axial Fatigue Data for $[0^\circ \pm 45^\circ]_{22}$ B/Al, Notched, $R = -1$

Specimen Number	Test Temperature		Maximum Stress		Cycles	Comments
	K	(°F)	MN/m ²	(ksi)		
EC71-1	297	75	276	40	247,000	
-2			310	45	60,000	
-3			241	35	547,000	
-4			345	50	8,000	
-5			207	30	6,480,000	
-6			379	55	< 1,000	Failed under doubler
-7			172	25	10,195,000	Did not fail
-8			328	47.5	7,000	
-9			224	32.5	1,227,000	
EC71-19A	505	450	207	30	739,000	
-20			241	35	42,000	
-21			276	40	10,000	
-22			172	25	2,309,000	
-23			138	20	12,710,000	Did not fail
-24			310	45	4,000	
-25			345	50	2,000	
-26			224	32.5	26,000	
-27			259	37.5	12,000	

Table 11-28. Axial Fatigue Data for $[0^\circ]_6$ B/Al, Unnotched, R = 0.1

Specimen Number	Test Temperature		Maximum Stress		Cycles	Comments
	K	(°F)	MN/m ²	(ksi)		
EU72-20	297	75	758	110	12,140,000	Did not fail
-21			1,000	145	302,000	
-22			931	135	54,000	
-23			862	125	76,000	
-24			827	120	2,000	
-25			827	120	798,000	Did not fail
-26			1,030	150	48,000	
-27			896	130	30,559,000	
-28			1,100	160	181,000	
EU72-47	561	550	862	125	2,185,000	Nitrogen Atmosphere
-48			827	120	3,209,000	
-49			793	115	3,104,000	
-50			758	110	3,761,000	
-51			724	105	4,080,000	
-52			827	120	2,980,000	Argon Atmosphere
-53			965	140	1,564,000	
-54			965	140	1,856,000	
-55			1,030	150	610,000	

Table 11-29. Axial Fatigue Data for $[0^\circ]_{12}$ B/Al, Unnotched, R = -1

Specimen Number	Test Temperature		Maximum Stress		Cycles	Comments
	K	(°F)	MN/m ²	(ksi)		
EU72-11	297	75	690	100	3,000	Did not fail
-12			655	95	229,000	
-13			638	92.5	<1,000	
-14			638	92.5	8,000	
-15			620	90	9,000	
-16			552	80	10,000,000	
-17			586	85	646,000	
-18			603	87.5	21,000	
-19			569	82.5	6,000	
-46			414	60	10,087,000	
EU72-38	505	450	425	61.7	12,000	Did not fail
-39			345	50	10,120,000	
-40			379	55	10,153,000	
-41			414	60	10,005,000	
-42			620	90	<1,000	
-43			483	70	1,332,000	
-44			552	80	51,000	
-45			586	85	5,000	

Table 11-30. Axial Fatigue Data for $[0^\circ]_6$ B/Al, Notched, $R = 0.1$

Specimen Number	Test Temperature		Maximum Stress		Cycles	Comments
	K	(°F)	MN/m ²	(ksi)		
EU71-10	297	75	1,000	145	76,000	
-11			896	130	4,634,000	
-12			827	120	4,546,000	
-13			758	110	10,002,000	Did not fail
-14			1,030	150	39,000	
-15			965	140	120,000	
-16			1,100	160	<1,000	
-17			931	135	1,469,000	
-18			793	115	1,761,000	
EU71-28	561	550	862	125	930,000	
-29	561	550	690	100	3,732,000	
-30	561	550	620	90	5,482,000	
-31	505	450	620	90	10,179,000	Did not fail
-32	505	450	862	125	996,000	
-33	561	550	827	120	1,057,000	
-34	561	550	965	140	60,000	
-35	561	550	896	130	330,000	
-36	561	550	758	110	2,974,000	

Table 11-31. Axial Fatigue Data for $[0^\circ]_{12}$ B/Al, Notched, $R = -1$

Specimen Number	Test Temperature		Maximum Stress		Cycles	Comments
	K	(°F)	MN/m ²	(ksi)		
EU71-1	297	75	586	85	310,000	Failed under doubler
-2			620	90	560,000	Failed under doubler
-3			655	95	887,000	Failed under doubler
-4			724	105	34,000	Failed under doubler
-5			758	110	9,000	
-6			793	115	3,000	Failed under doubler
-7			690	100	62,000	Failed under doubler
-8			552	80	12,486,000	Did not fail
-9			586	85	2,977,000	Failed under doubler
EU71-19A	505	450	552	80	6,000	
-20			483	70	18,000	
-21			414	60	4,253,000	
-22			448	65	3,931,000	
-23			566	82.1	4,000	
-24			379	55	10,829,000	
-25			517	75	9,000	
-26			465	67.5	2,398,000	
-27			431	62.5	554,000	

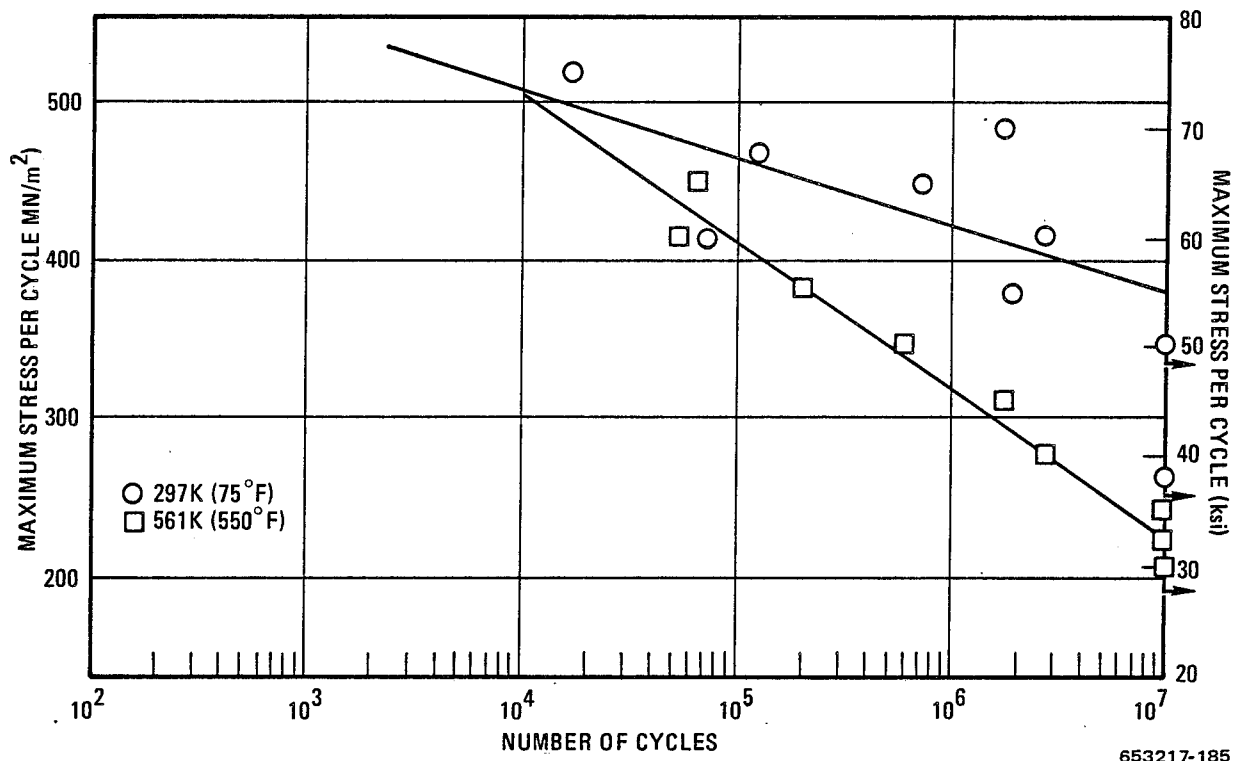


Figure 11-32 Axial Fatigue Properties of Unnotched $[0^\circ \pm 45^\circ]_s$ B/Al at a Stress Ratio, R , of 0.1

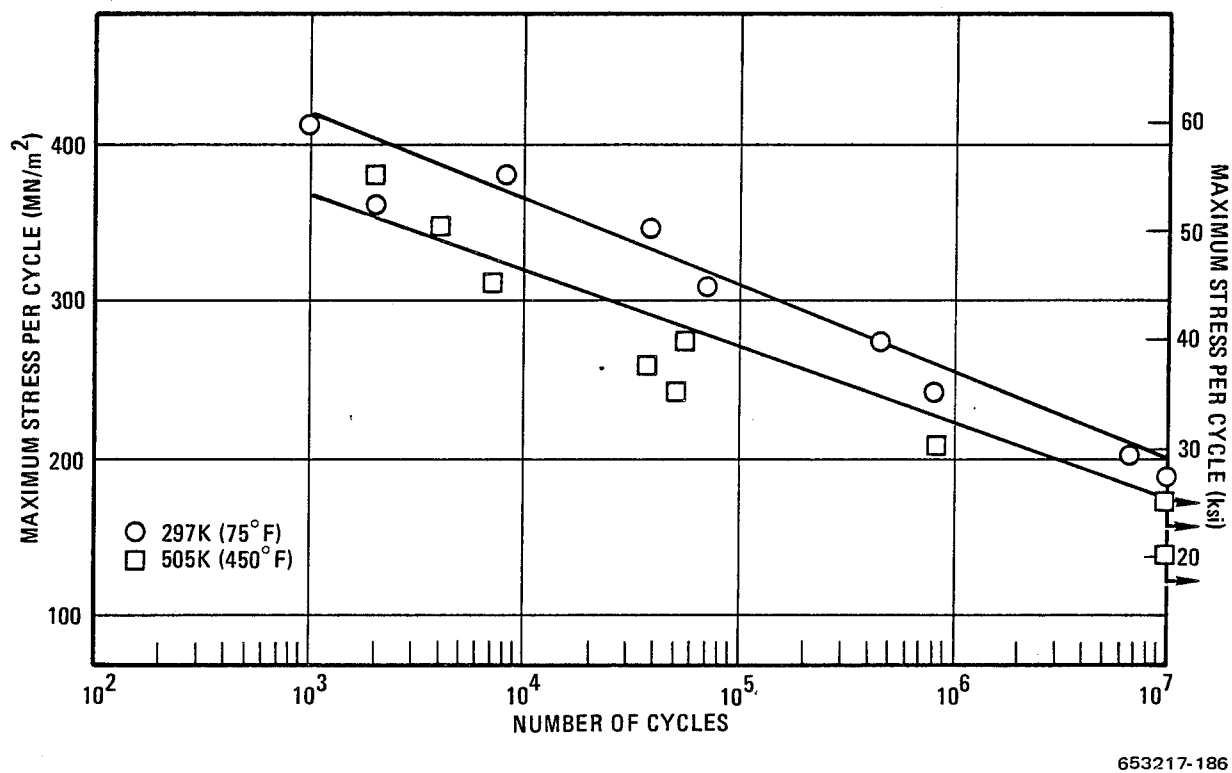


Figure 11-33 Axial Fatigue Properties of Unnotched $[0^\circ \pm 45^\circ]_{s2}$ B/Al at a Stress Ratio, R , of -1

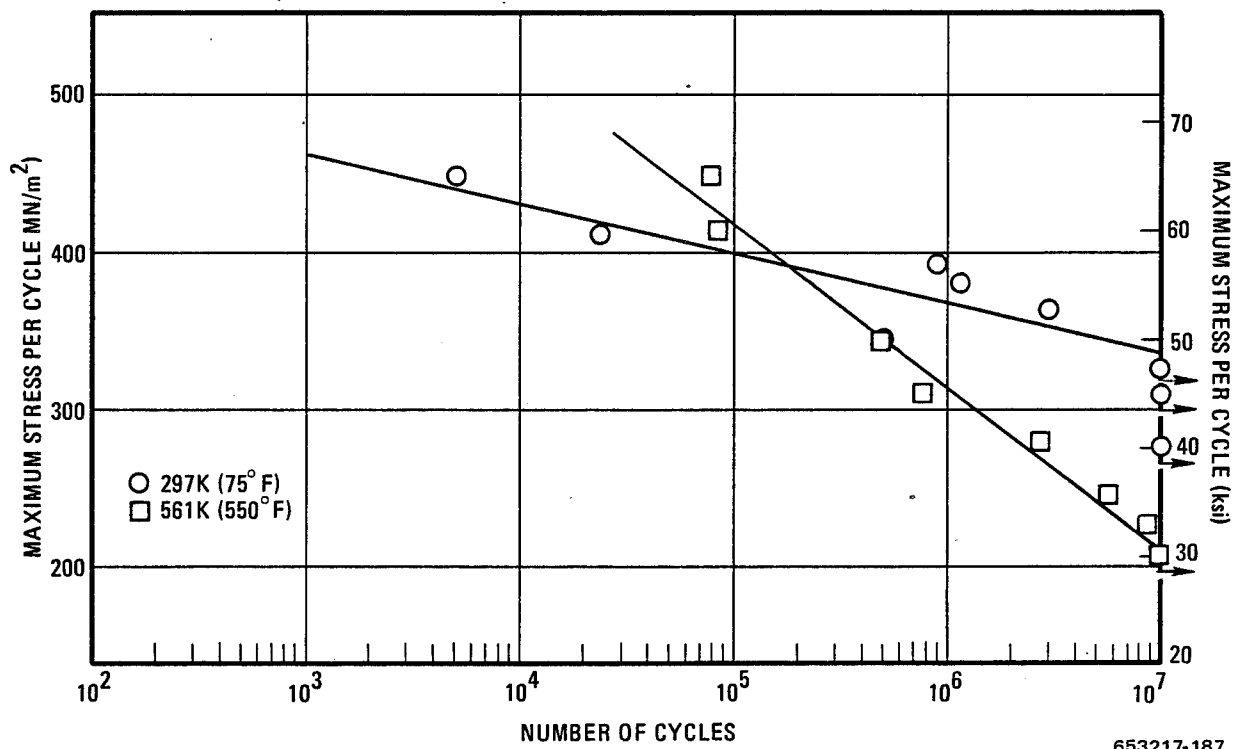


Figure 11-34 Axial Fatigue Properties of Notched $[0^\circ \pm 45^\circ]_s$ B/Al at a Stress Ratio, R , of 0.1

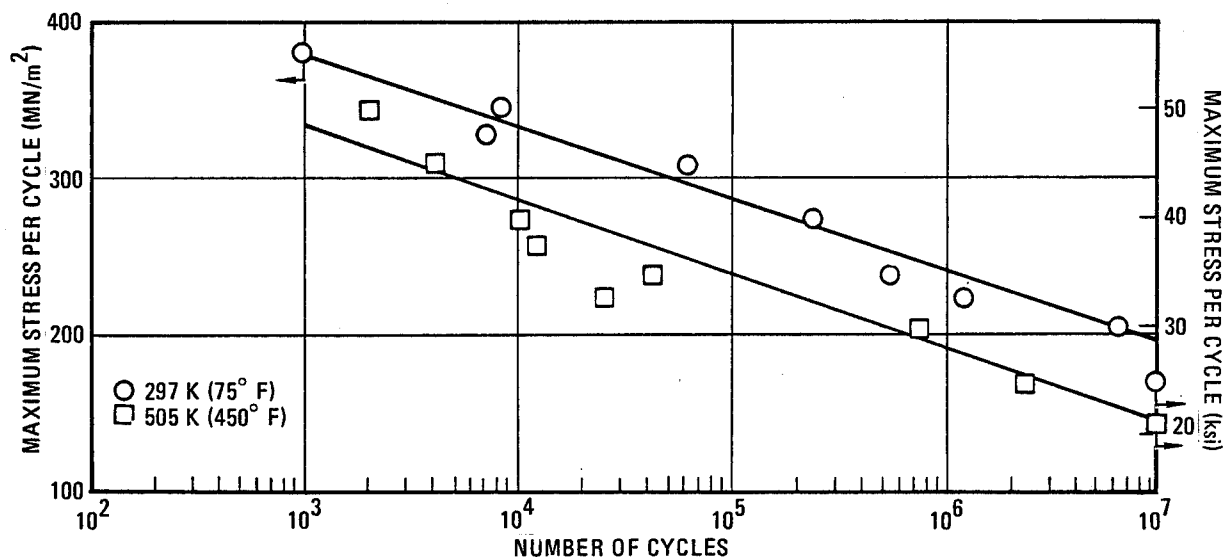


Figure 11-35 Axial Fatigue Properties of Notched $[0^\circ \pm 45^\circ]_{s2}$ B/Al at a Stress Ratio, R , of -1

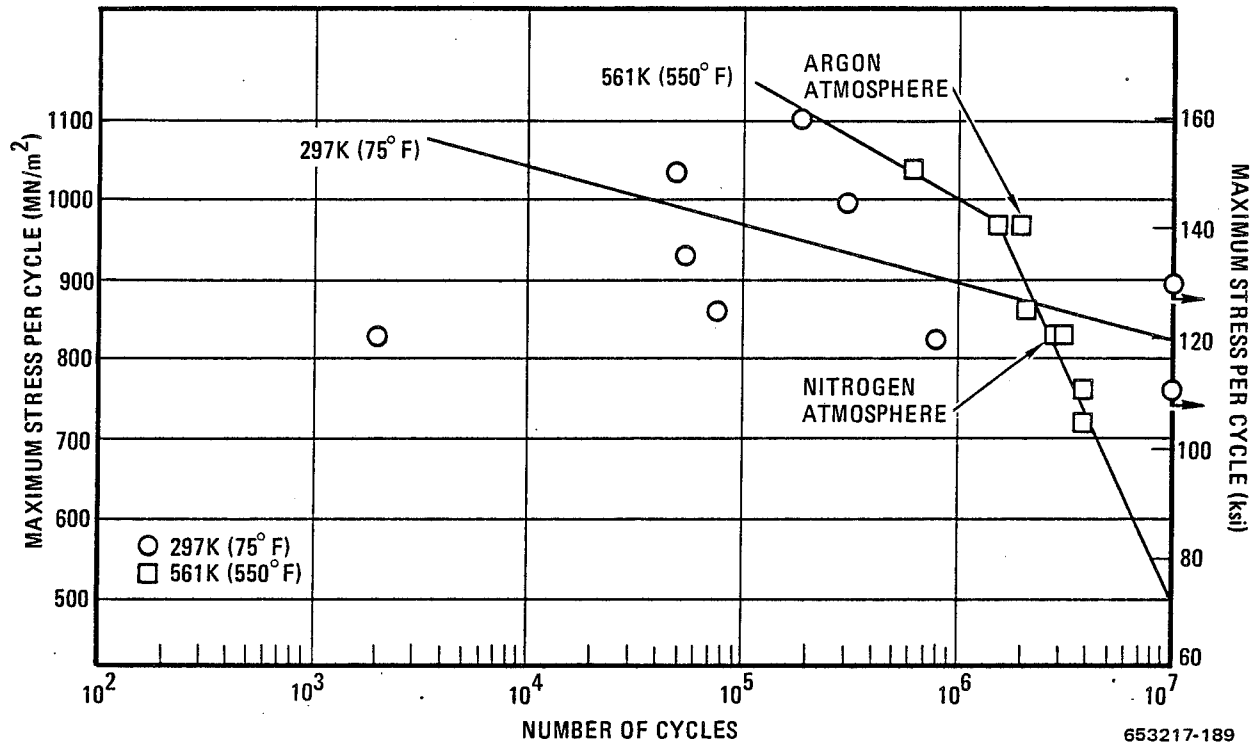


Figure 11-36 Axial Fatigue Properties of Unnotched $[0^\circ]_6$ B/Al at a Stress Ratio, R , of 0.1

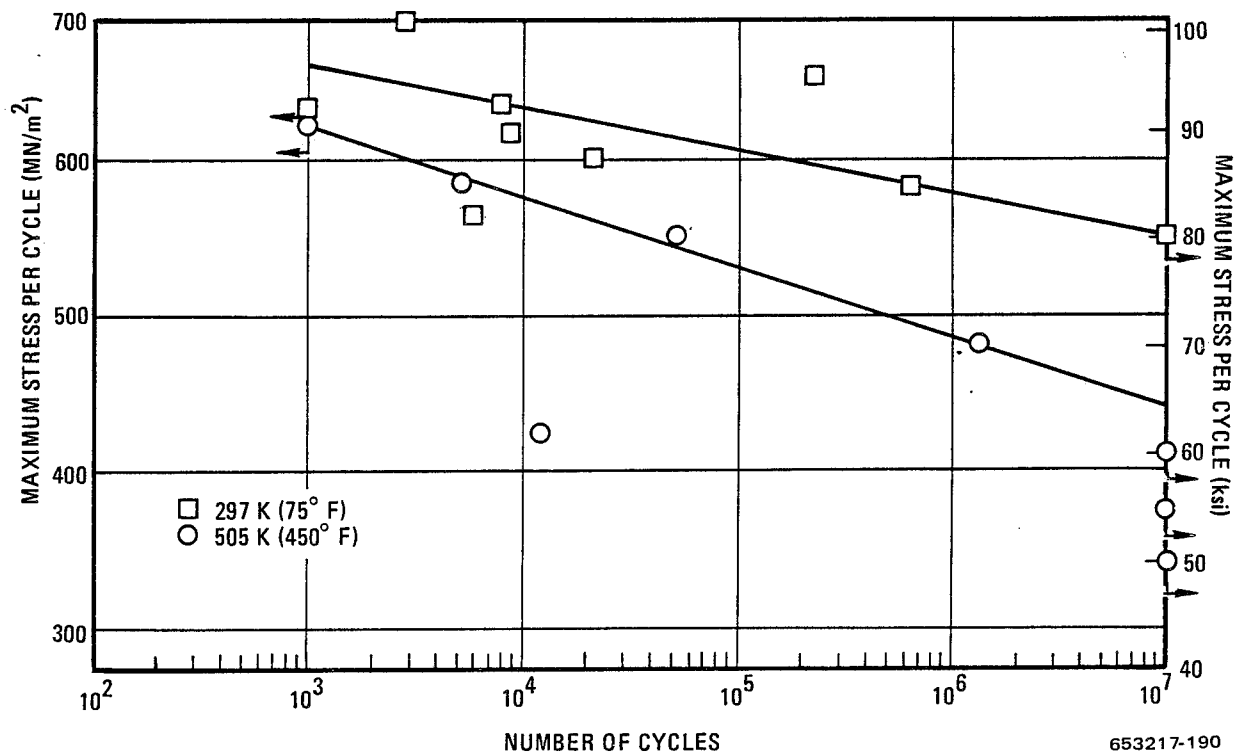
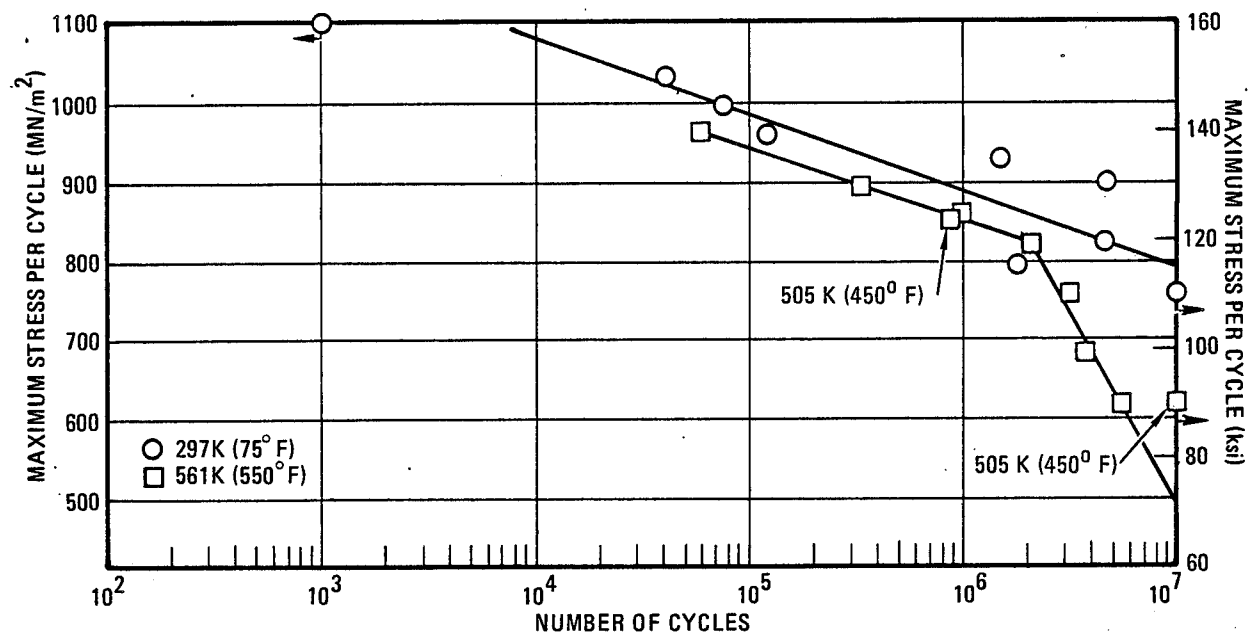
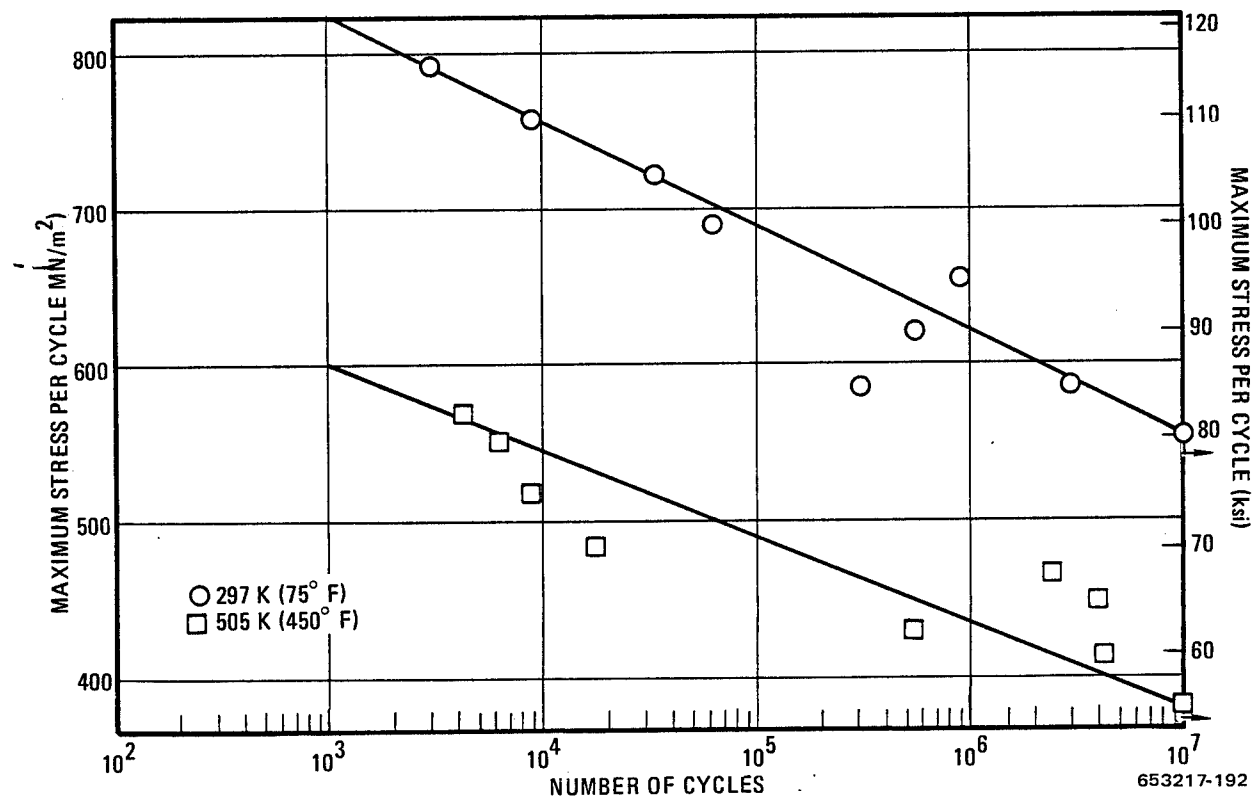


Figure 11-37 Axial Fatigue Properties of Unnotched $[0^\circ]_{12}$ B/Al at a Stress Ratio, R , of -1



653217-191

Figure 11-38 Axial Fatigue Properties of Notched $[0^\circ]_6$ at a Stress Ratio, R , of 0.1



653217-192

Figure 11-39 Axial Fatigue Properties of Notched $[0^\circ]_{12}$ B/Al at a Stress Ratio, R , of -1

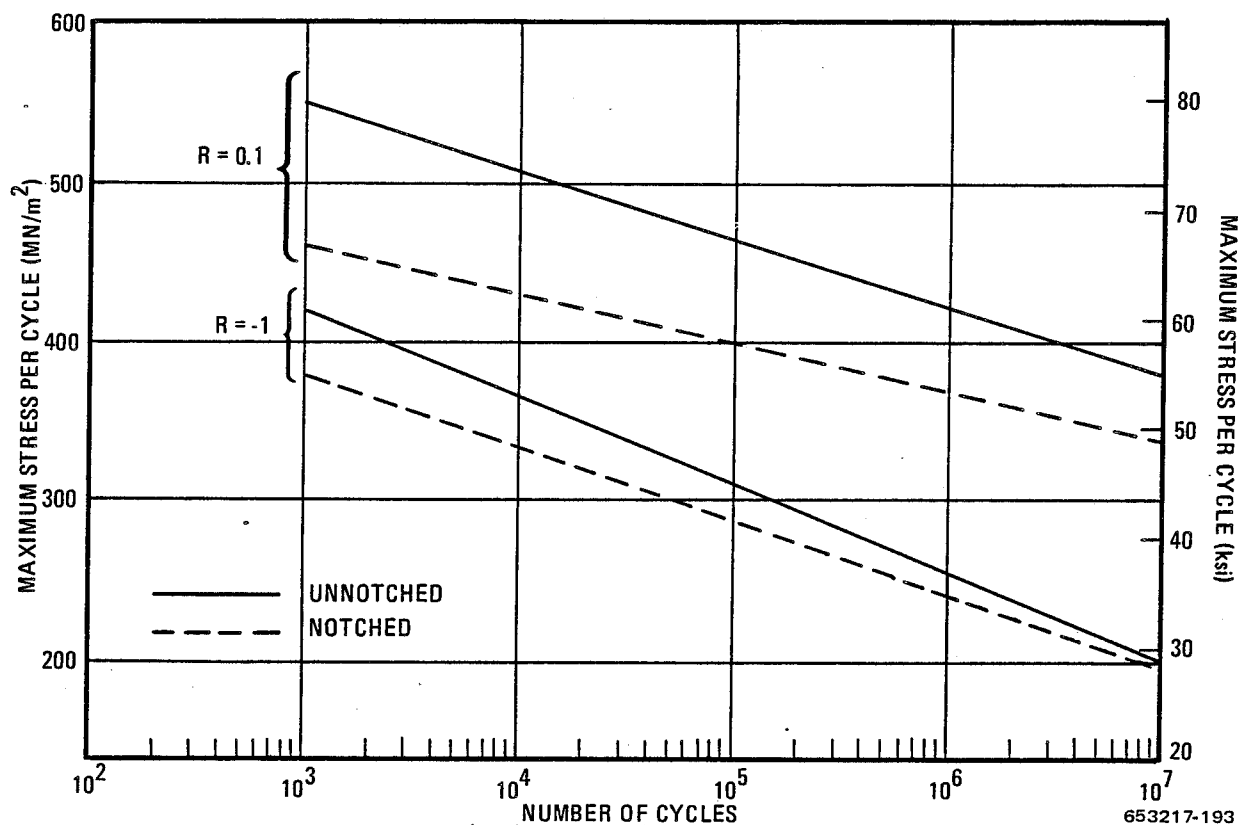


Figure 11-40 Axial Fatigue Properties of $[0^\circ \pm 45^\circ]$ B/Al at 297 K (75° F)

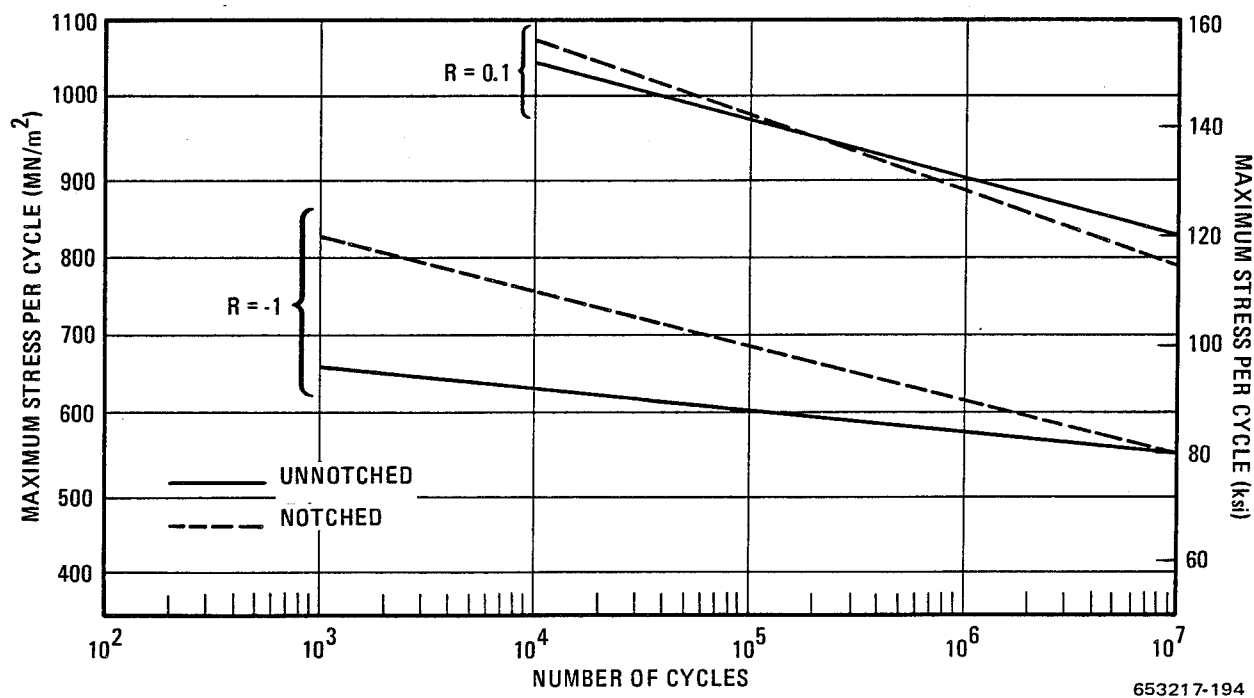


Figure 11-41 Axial Fatigue Properties of $[0^\circ]$ B/Al at 297 K (75° F)

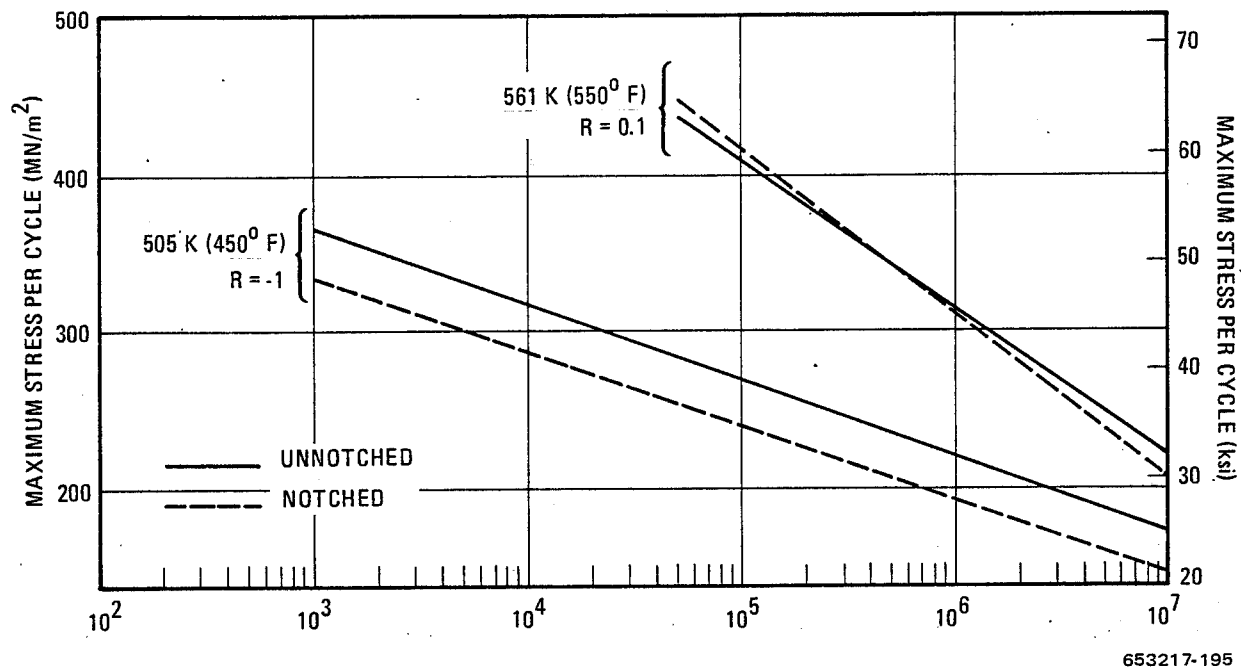


Figure 11-42 Axial Fatigue Properties of $[0^\circ \pm 45^\circ]$ B/Al at Elevated Temperatures

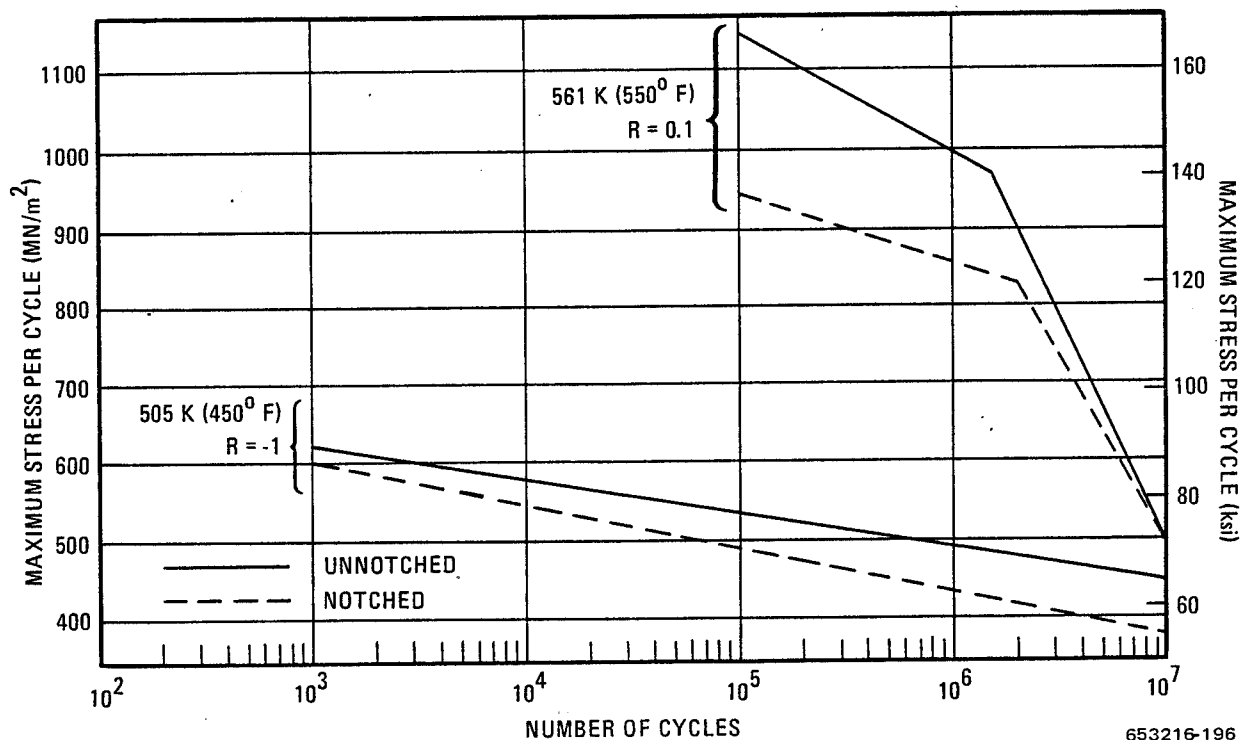


Figure 11-43 Axial Fatigue Properties of $[0^\circ]$ B/Al at Elevated Temperatures

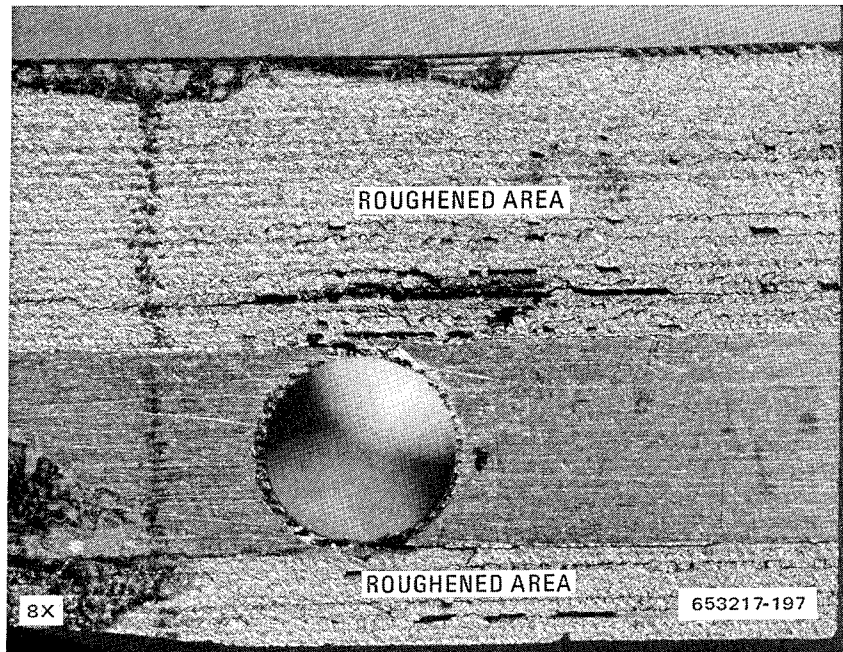


Figure 11-44 Surface Roughening of B/Al Specimen Fatigued at 561 K (550° F) in Air. (Roughening is confined to stressed areas on either side of the hole.)

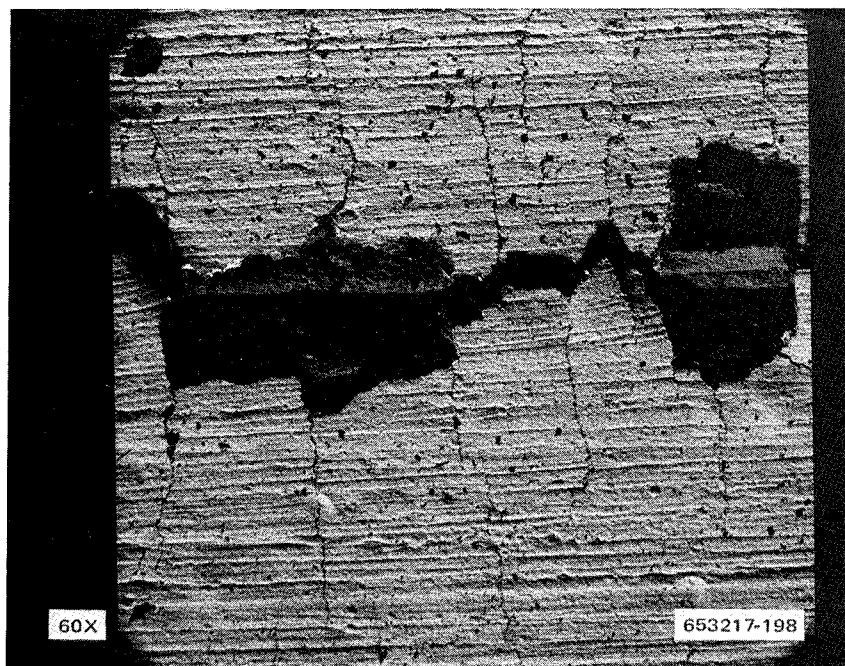


Figure 11-45 Area of Degraded B/Al Surface Showing Reticulation and Exposed (Aluminum-Covered) Boron Fiber

The surface appearance suggests that the degradation may have been caused by grain growth and embrittlement at the grain boundaries. A temperature gradient analysis of the hot zone of the furnace together with an examination of the degraded specimens indicated a minimum threshold temperature of 505 K (450° F) to 533 K (500° F) to cause matrix degradation. To better substantiate this, two of the specimens originally scheduled for 561 K (550° F) were fatigue tested at 505 K (450° F) under the same conditions (stress level and environment) as used on the 561 K (550° F) tests. Test data is reported in Table 11-29. Visual and metallographic examinations of the specimens revealed little or no matrix degradation at the lower temperature. The effect of environment was also briefly examined. Two fatigue tests were performed at 561 K (550° F) in an inert atmosphere (nitrogen gas for the first test and argon gas for the second one) to determine the effect, if any, on matrix degradation. The tests were run at the same temperature, stress levels, and for approximately the same number of cycles as previous tests performed in air (see Table 11-27). Visual and metallographic examinations indicated a significant decrease in matrix degradation. This implies that oxygen and/or moisture play an important role in the degradation process. One other test variable was stress level. For tests in air at 561 K (550° F) the effect was observed at all cyclic stress levels evaluated, although the number of cycles for degradation was substantially greater at the low stress levels than for the higher stress levels. A minimum threshold stress level was not determined. However, one is believed to be required since notched fatigue specimens (center hole notch) did not show matrix degradation in the unstressed areas (see Figure 11-44). Additional studies of the surface degradation problem, particularly effects of environment, should be conducted to identify the degradation mechanism and to develop solutions, e.g., protective coatings or change of matrix alloys.

A table similar to those presented earlier for both G/E and G/PI data has been prepared to show the percentage of the B/Al ultimate strengths at which the fatigue limit (or 10^7 cycles) occurred. The results for the eight B/Al fatigue curves are presented in Table 11-32. In comparing these data with those for the organic matrix materials, several differences are apparent. For tension-compression loading the B/Al system exhibits relatively higher fatigue limits than the organic matrix systems at both room and elevated temperatures. For tension-tension loading at room temperature the unidirectional B/Al data are comparable with those for G/E and G/PI while the crossply data are similar to the G/PI but lower than the G/E data. At 561 K (550° F) the B/Al was inferior to either the G/E at 450 K (350° F) or the G/PI at 505 K (450° F). In a comparison with similar data for the aluminum alloys listed in Table 11-13 the B/Al is superior. This is particularly apparent for the notched specimens. In like manner to the G/PI system, B/Al retains the excellent fatigue properties to 505 K (450° F), well above that for aluminum alloys. To show the same comparison with the Ti-6Al-4V alloy as was presented earlier for G/PI, Table 11-33 was prepared. The titanium alloy sheet data are the same as those listed in Table 11-23. With the exception of the unnotched, $R = 0.1$ results at 561 K (550° F) (surface degradation temperature) the B/Al is superior to the titanium alloy. This is particularly demonstrated by the notched fatigue data.

Table 11-32. Strength at Fatigue Limit or 10^7 Cycles Expressed as Percentage of Ultimate Tensile Strength for B/Al

Orientation	Specimen Configuration	Temperature K	Temperature (°F)	R Value	Fatigue Strength at 10^7 Cycles (%)
[0° ± 45°]	Unnotched	297	75	0.1	74
	Notched	297	75	.1	71
	Unnotched	561	550	.1	50
	Notched	561	550	.1	47
	Unnotched	297	75	-1.0	39
	Notched	297	75	-1.0	41
	Unnotched	505	450	-1.0	38
	Notched	505	450	-1.0	32
[0°]	Unnotched	297	75	.1	57
	Notched	297	75	.1	64
	Unnotched	561	550	.1	a38
	Notched	561	550	.1	a43
	Unnotched	297	75	-1.0	38
	Notched	297	75	-1.0	45
	Unnotched	505	450	-1.0	33
	Notched	505	450	-1.0	33

^aDetermined by extrapolation.

11.3.4 STACKING SEQUENCE EVALUATION. A limited program was conducted to investigate the effects of stacking sequence on the [0° ± 45°]_s family of laminates. Two systems, B/E and G/E, were evaluated. Room temperature tensile and fatigue tests (R = 0.1) were made on specimens of the following three laminate stacking sequences:

[0°, 45°, -45°, -45°, 45°, 0°]

[45°, 0°, -45°, -45°, 0°, 45°]

[45°, -45°, 0°, 0°, -45°, 45°]

Fabrication of the test panels and preparation of the tensile and fatigue specimens were accomplished using the same procedures described in Section 5. Tensile and fatigue tests were conducted using the techniques also described earlier.

Results of the tensile tests of the three stacking sequences for each material are given in Table 11-34. The data show that the position of the 0° layers in the layup appears to influence the

Table 11-33. Comparison of Strength at Fatigue Limit or 10^7 Cycles Expressed as Percentage of Ultimate Tensile Strength for B/Al and Ti-6Al-4V Titanium Alloy at Room and Elevated Temperatures

Specimen Configuration	R Value	Fatigue Strength at 10^7 Cycles (% of F_{tU})					
		Boron/Aluminum				Ti-6Al-4V Alloy	
		[0° ± 45°]		[0°]		Solution-treated and aged	
		297 K (75° F)	505 K (450° F)	297 K (75° F)	505 K (450° F)	297 K (75° F)	589 K (600° F)
Unnotched	0.1	74	b ₅₀	57	b ₃₈	50	52
^a Notched	0.1	71	b ₄₇	64	b ₄₃	23	29
Unnotched	-1.0	39	38	38	33	32	25
^a Notched	-1.0	41	32	45	33	16	19

^aB/Al, center notch, theoretical $K_t = 2.43$

Ti-6Al-4V Alloy, center notch, $K_t = 2.82$

^bTest Temperature was 561 K (550° F)

Table 11-34. Room Temperature Tensile Data for B/E and G/E Stacking Sequence Test Panels

Material System	Stacking Sequence	Tensile Strength MN/m ² (ksi)		Tensile Modulus GN/m ² (Msi)	
B/E	[0°, 45°, -45°] _s	525	76.2	66	9.6
		576	83.5	61	8.8
		550	79.8	63	9.2
	[45°, 0°, -45°] _s	556	80.6	63	9.2
		584	84.7	63	9.1
		570	82.6	63	9.2
	[45°, -45°, 0°] _s	576	83.5	61	8.9
		580	84.1	61	8.9
		578	83.8	61	8.9
	[0°, 45°, -45°] _s	506	73.4	48	6.9
		539	78.2	47	6.8
		523	75.8	47	6.8
G/E	[45°, 0°, -45°] _s	664	96.3	52	7.5
		652	94.5	52	7.5
		658	95.4	52	7.5
	[45°, -45°, 0°] _s	699	101.4	55	8.0
		675	97.9	56	8.1
		687	99.6	55	8.0

tensile strength of both systems. The strength is lowest with the 0° layers on the outside and increases as these layers move toward the center. The effect is small for B/E and may not be significant because of the very limited test data.

The fatigue tests were all carried out at room temperature at an R value of 0.1 using unnotched specimens. The test results are tabulated in Tables 11-35 and 11-36 and S-N curves are plotted in Figures 11-46 and 11-47. These limited data indicate that the position of the 0° layers in the composite has an effect on both tensile and fatigue strength. In like manner to the tensile results the fatigue properties are lowest with the 0° layers on the outside and highest with the 0° layers at the center. The S-N curves for the B/E system show the relationship between fatigue strength and stacking sequence quite clearly. The same effect, while apparent in the G/E curves, is not as distinct because of the increased scatter of the data.

Table 11-35. Room Temperature Axial Fatigue Data for B/E Stacking Sequence Test Panels, Unnotched, R = 0.1

Specimen Number	Stacking Sequence	Maximum Stress MN/m ² (ksi)		Cycles	Comments
A62-1	[0°, 45°, -45°] _s	448	65	<1,000	
-2		414	60	<1,000	
-3		379	55	3,000	
-4		345	50	294,000	
-5		379	55	178,000	
-6		345	50	132,000	
-7		310	45	3,015,000	
-8		310	45	10,145,000	Did not fail
-9		379	55	8,000	
A63-1	[45°, 0°, -45°] _s	448	65	2,000	
-2		414	60	81,000	
-3		379	55	2,372,000	Did not fail
-4		448	65	1,000	
-5		414	60	34,000	
-6		448	65	9,000	
-7		414	60	21,000	Failed under doubler
-8		379	55	5,733,000	
-9		396	57.5	111,000	
A61-1	[45°, -45°, 0°] _s	448	65	58,000	Failed under doubler
-2		414	60	407,000	
-3		431	62.5	16,000	
-4		448	65	4,000	Failed under doubler
-5		414	60	4,950,000	Did not fail
-6		483	70	<1,000	
-7		448	65	2,000	
-8		431	62.5	7,000	
-9		414	60	1,825,000	

Table 11-36. Room Temperature Axial Fatigue Data for G/E Stacking Sequence Test Panels, Unnotched, R = 0.1

Specimen Number	Stacking Sequence	Maximum Stress MN/m ² (ksi)		Cycles	Comments
B62-1	[0°, 45°, -45°] _s	379	55	13,000	
-2		414	60	39,000	
-3		448	65	36,000	
-4		483	70	<1,000	
-5		448	65	10,000	
-6		414	60	7,220,000	Did not fail
-7		431	62.5	<1,000	
-8		431	62.5	2,000	
-9		431	62.5	34,000	
B63-1	[45°, 0°, -45°] _s	483	70	2,000	
-2		448	65	34,000	
-3		483	70	1,000	
-4		517	75	<1,000	
-5		448	65	22,000	
-6		414	60	114,000	Failed under doubler
-7		414	60	2,306,000	Did not fail
-8		431	62.5	33,000	
-9		431	62.5	21,000	
B61-1	[45°, -45°, 0°] _s	379	55	2,001,000	Did not fail
-2		552	80	<1,000	
-3		517	75	<1,000	
-4		483	70	3,000	
-5		448	65	2,157,000	Did not fail
-6		483	70	1,000	
-7		465	67.5	3,000	
-8		465	67.5	3,000	
-9		448	65	2,295,000	Did not fail

The data presented in this section indicate that the [45°, -45°, 0°]_s sequence of the [0° ± 45°] family of laminates would have the best room temperature tensile and fatigue properties. For all testing of crossplied laminates on the balance of the test program, however, the stacking sequence that was selected was the [0°, 45°, -45°]_s sequence. The reason for this choice was that the joint strength to attachments, i.e., doublers, is much higher when made to an unidirectional ply than to an off-axis ply. Consequently, to minimize doubler bond failures in the various types of test specimens the [0°, 45°, -45°]_s layup was used for all crossplied panels.

11.3.5 POISSON'S RATIO EVALUATION. The final portion of the constant amplitude baseline fatigue study was a series of residual Poisson's ratio tests on specimens that survived 10 million fatigue cycles at room temperature at a stress ratio of -1. Determinations were made on unidirectional specimens of G/E, G/PI, and B/Al. Strain gage installation and test procedures were the same as those described in Section 7. The condition of the specimens (stress

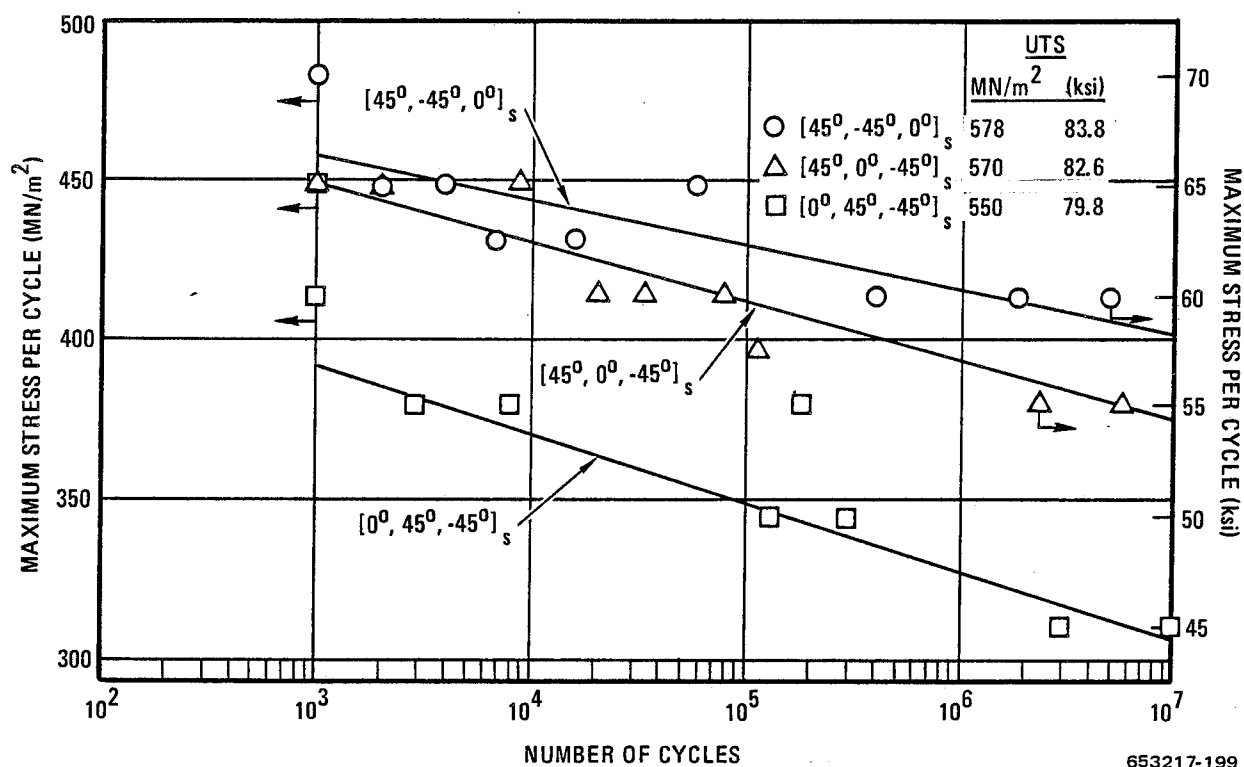


Figure 11-46 Axial Fatigue of B/E Laminates Showing Effect of Stacking Sequence, 297 K (75° F), R = 0.1

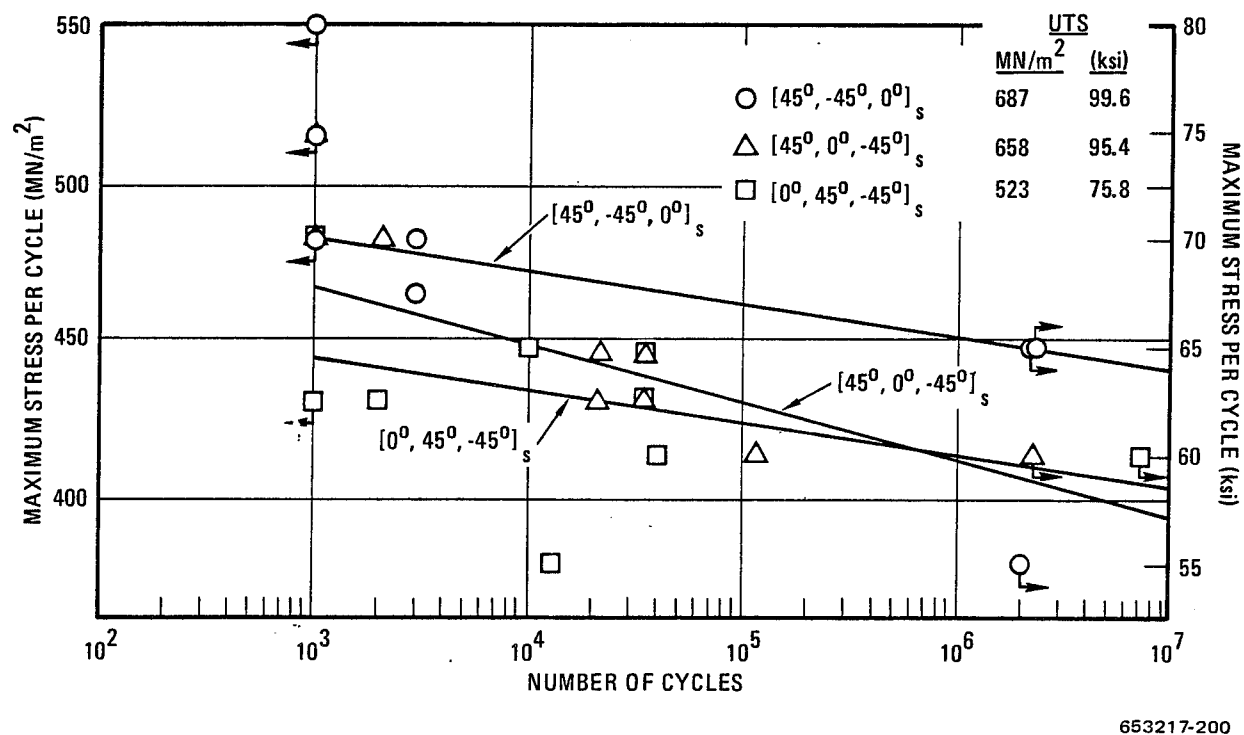


Figure 11-47 Axial Fatigue of G/E Laminates Showing Effect of Stacking Sequence, 297 K (75° F), R = 0.1

level and number of fatigue cycles) and the results of the Poisson's ratio tests are tabulated in Table 11-37. Also included are the tensile strength and modulus values obtained during the same tests. For the organic matrix materials, G/E and G/PI, the 10 million fatigue cycles appeared to have little effect on the value of Poisson's ratio. For the metal matrix system, B/Al, however, one specimen exhibited a drastic decrease in Poisson's ratio with the second showing a moderate loss. Modulus values were slightly lower after fatigue cycling for the G/E and G/PI systems. All of the specimens showed significant decreases in tensile strength. It should be pointed out, however, that the specimen configuration, 2.5 cm (1 in.) by 10.2 cm (4 in.) with a 1.3 cm (0.5 in.) gage section was not a good one for tensile testing and was not the one used for the baseline as received tests. Also, all but one of the specimens failed under the end doublers.

The purpose of these tests was to attempt to determine the amount of damage accumulated after 10 million stress cycles at different values of maximum stress. Based on the residual Poisson's ratio results alone, the resin matrix composite systems, G/E and G/PI, appear to have experienced only slight damage while the B/Al metal matrix system was significantly affected by the fatigue cycling. The more highly stressed B/Al specimen showed the greater decrease in Poisson's ratio. Additional testing would be required to verify these findings.

Table 11-37. Results of Residual Poisson's Ratio Testing of Run-Out Fatigue Specimens at Room Temperature

Material System	Specimen Number	Condition		Poisson's Ratio	Tensile Strength		Tensile Modulus	
		Number of Cycles	Fatigue Stress MN/m ²		(ksi)	MN/m ²	(ksi)	(GN/m ² (Msi))
G/E, [0°] ₁₂	—	Baseline		0.33	1540	224	141	20.4
	BU72-12	10.0 × 10 ⁶	483	70	.28	^a 1,100	^a 159	130
	BU72-15	12.6	414	60	.33	^a 1,000	^a 145	123
	BU72-16	10.2	448	65	.31	^a 1,280	^a 186	129
G/PI, [0°] ₁₂	—	Baseline		^b .39	1,190	172	126	18.3
	DU72-15	10.6	207	30	.41	^a 807	^a 117	118
	DU72-46	10.3	138	20	.33	^a 945	^a 137	117
B/Al, [0°] ₁₂	—	Baseline		.28	1,450	210	194	28.2
	EU72-16	10.0	552	80	.10	^a 470	^a 68	191
	EU72-46	10.1	414	60	.23	1,010	147	201

^aFailed under doubler

^b505 K (450° F) value

SECTION 12

FLIGHT SIMULATION TESTING

12.1 INTRODUCTION

The objective of this portion of the program was to subject in real time each of the four composite systems to the load-temperature history that would be experienced by a supersonic transport during its 50,000-hour life. To do this a flight simulation apparatus was constructed that was capable of loading a number of large specimens of each composite system using a random loading pattern while the specimens were heated to the temperatures corresponding to those expected to be encountered during flight. As the composites had different strengths and maximum use temperatures, it was necessary that the flight simulator be capable of providing the load and temperature suited to each composite. The apparatus had to be large enough to allow the testing of a number of replicates of each system to provide adequate statistical data for proper evaluation of the endurance of the material. In addition, the simulator had to be capable of automatically testing a large number of specimens reliably for an extended period of time.

A load spectrum was generated using the exceedance curves for a supersonic cruise aircraft, and this purely random spectrum was recorded on tape in a form suitable for load generation in real time so that 25,000 two-hour flights (50,000 hours) could be simulated. Each flight contained climb, cruise, descent, and landing loads with the temperatures corresponding to each portion of the flight. A typical load and temperature profile is shown in Figure 12-1.

The original intent of the program was to use the wearout model developed by Halpin (ref. 3) to predict the life and set the peak load levels for the flight simulation tests of all the composite systems. Once a random load spectrum had been generated, the test conditions for each composite system could be set by increasing or decreasing the magnitudes of the entire spectrum. This was done by setting the magnitude of the peak load in the spectrum. To set these peak loads, accelerated tests were run by increasing the frequency of the spectrum. A quarter of a lifetime and half a lifetime of loads were applied in 100 hours and 200 hours respectively. This was done with the specimens held at a constant temperature corresponding to what was considered to be the maximum use temperature for each individual composite system. These accelerated tests, referred to as short-term tests, were conducted so that the loads normally applied during a two-hour flight were applied in about one minute. Figure 12-2 shows a flight picked at random and plotted to show the nature of load variation as the specimen is held at its maximum use temperature. These data in conjunction with the baseline properties were to be used to calculate, by means of the wearout theory, the peak load to be applied during flight simulation testing of each composite. From the results of these short-term tests, however, it was determined that the wearout model could be used only on the B/E and G/E systems. The difficulty encountered for the G/PI and B/Al materials was that for the loads applied during accelerated testing the residual strength was observed to increase between one-quarter lifetime and one-half lifetime. This was contrary to the model, which is based on strength decreasing with time. The manner in which the flight simulation loads were determined for the G/PI and B/Al specimens as well as the details of the wearout analysis of the B/E and G/E specimens will be discussed later in the section.

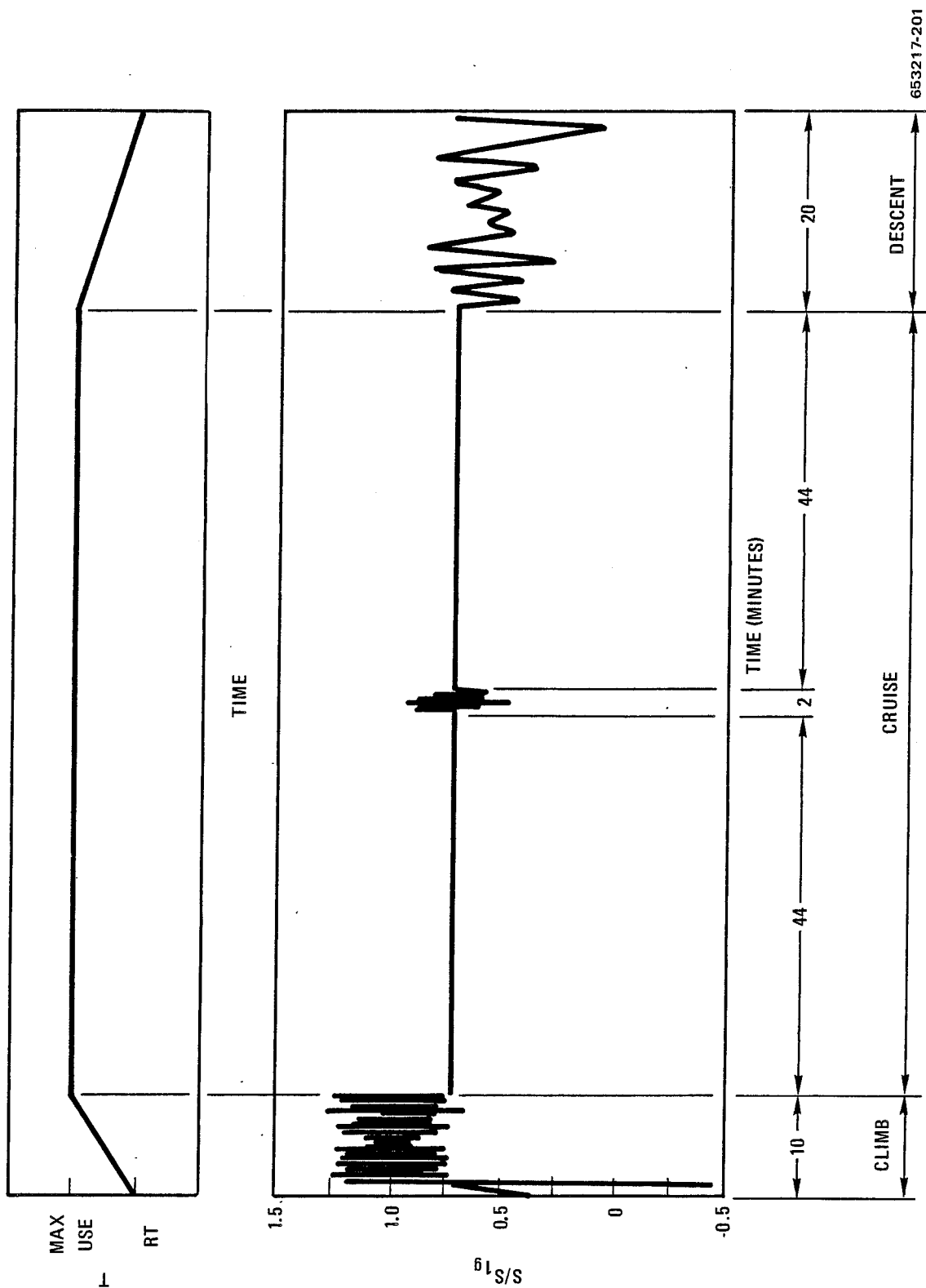


Figure 12-1 Typical Flight Simulation Cycle Showing Load and Temperature Profile

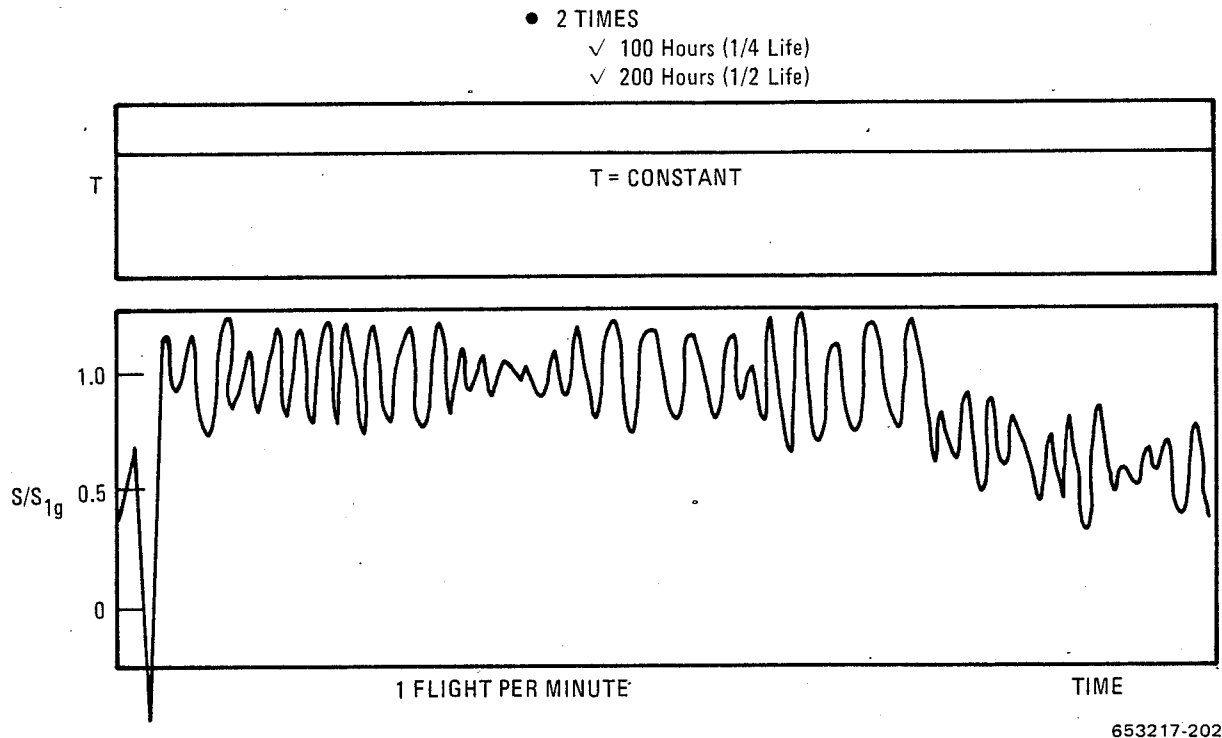


Figure 12-2 Typical Accelerated or Short-Term Flight Simulation Cycle Showing Loads and Temperature Profile

Following the short-term tests the four composite systems were subjected to the first 10,000 hours of flight simulation exposure, a number of specimens were removed from the apparatus, and residual property evaluations were conducted. The results of these tests have been analyzed and are presented in this section.

12.2 DESCRIPTION OF SIMULATOR

The flight simulation apparatus was built to test five composite materials and has the capability of cycling loads and temperatures on 100 test specimens simultaneously. The apparatus is divided into 10 independent test setups each of which contains 10 identical specimens. The flight simulation testing equipment is shown in Figure 12-3. There are 10 load frames, five of which are facing forward, and five more directly behind the front five. The small cabinet at the right of the simulator is the control console, which is shown in greater detail in Figure 12-4.

12.2.1 TEST FIXTURES. The test fixtures consist of 10 basic load frames, 10 whiffletree assemblies, attachment hardware for 100 specimens, 100 removable specimen stiffener assemblies, 20 heat lamp rack assemblies, and lateral support hardware.

The lateral support between a whiffletree assembly and its specimens is a beam containing five linear motion bearings. They allow motion in the load direction only. The travel of the clevis fitting, which passes through a bearing, is limited and adjustable in each direction. Specimen or

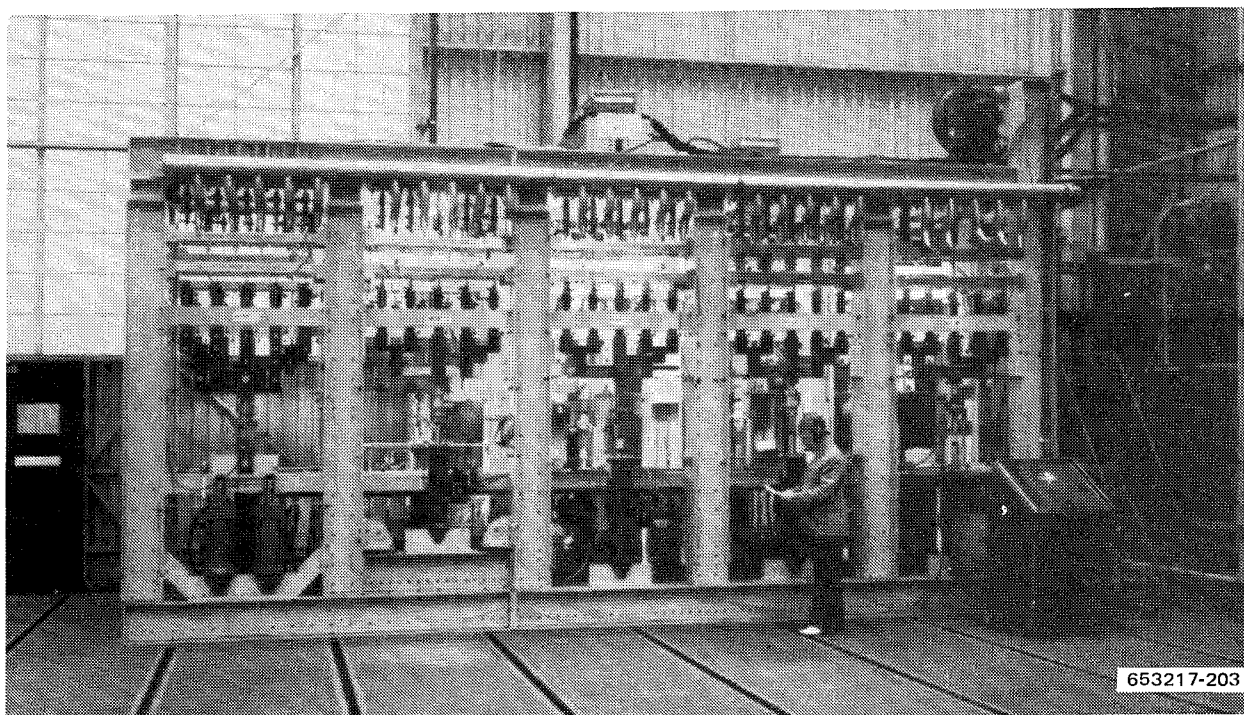


Figure 12-3 Flight Simulation Equipment

doubler failures are detected by means of microswitches activated when the clevis motion exceeds the preset values in either loading direction. Activation of a microswitch immediately dumps the hydraulic pressure and reduces the load to zero.

12.2.2 LOAD PROGRAMMER AND CONTROLLERS. The MTS digital load programmer and associated load controllers are shown in Figure 12-5. Ten of the 60 available controllers are used for the 10 basic load frames. The load programmer and controllers program and control the fatigue loading spectrum and synchronize the heating and cooling cycles.

12.2.3 PROGRAMMER SAFETY FEATURES. The load programmer provides the following self-checking features that automatically stop all test operations if activated.

- a. The load controller ERROR DETECTOR is activated if the error between the command and feedback system exceeds a preset value.
- b. Program HOLD is activated if a malfunction occurs in timing, parity, or the power supply.
- c. END OF PROGRAM code at the end of a punched tape places the program in "hold." If the test program is not manually restarted within a few minutes, all operations are deactivated.

12.2.4 HYDRAULIC SYSTEM. The hydraulic system consists of a hydraulic power source with oil reservoir level and oil temperature detectors, a manifold pressure dump valve, distribution manifolds and lines, and hydraulic actuating cylinders with pressure dump valves, filters, and servo valves.

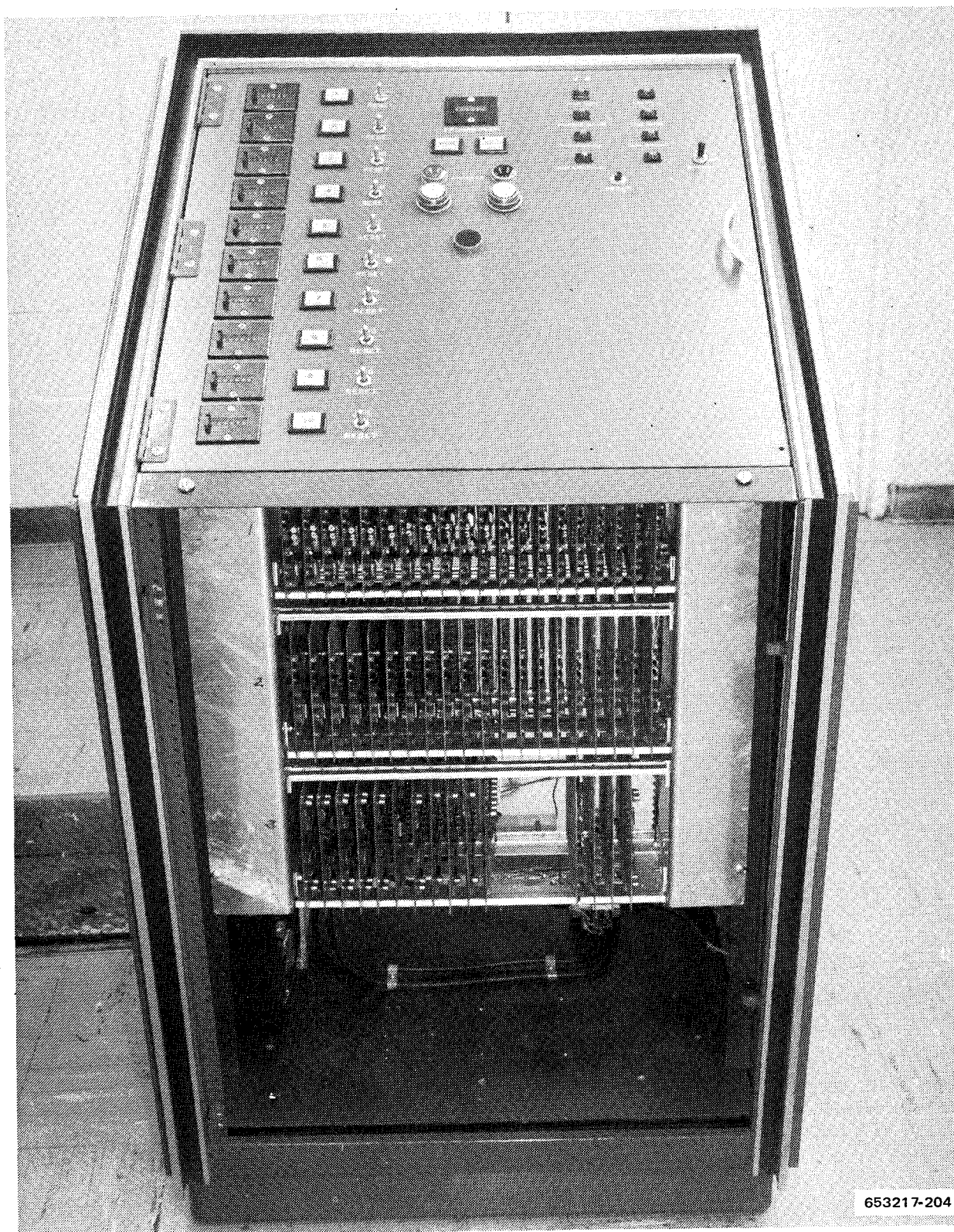


Figure 12-4 SCR Flight Simulation Apparatus — Control Console

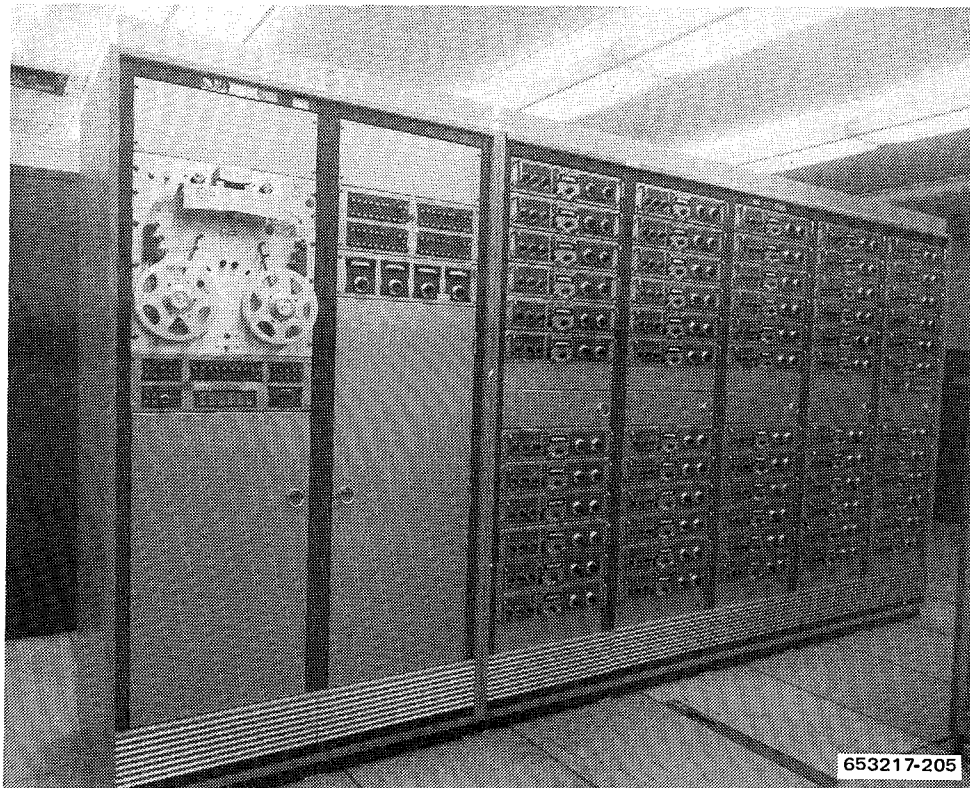
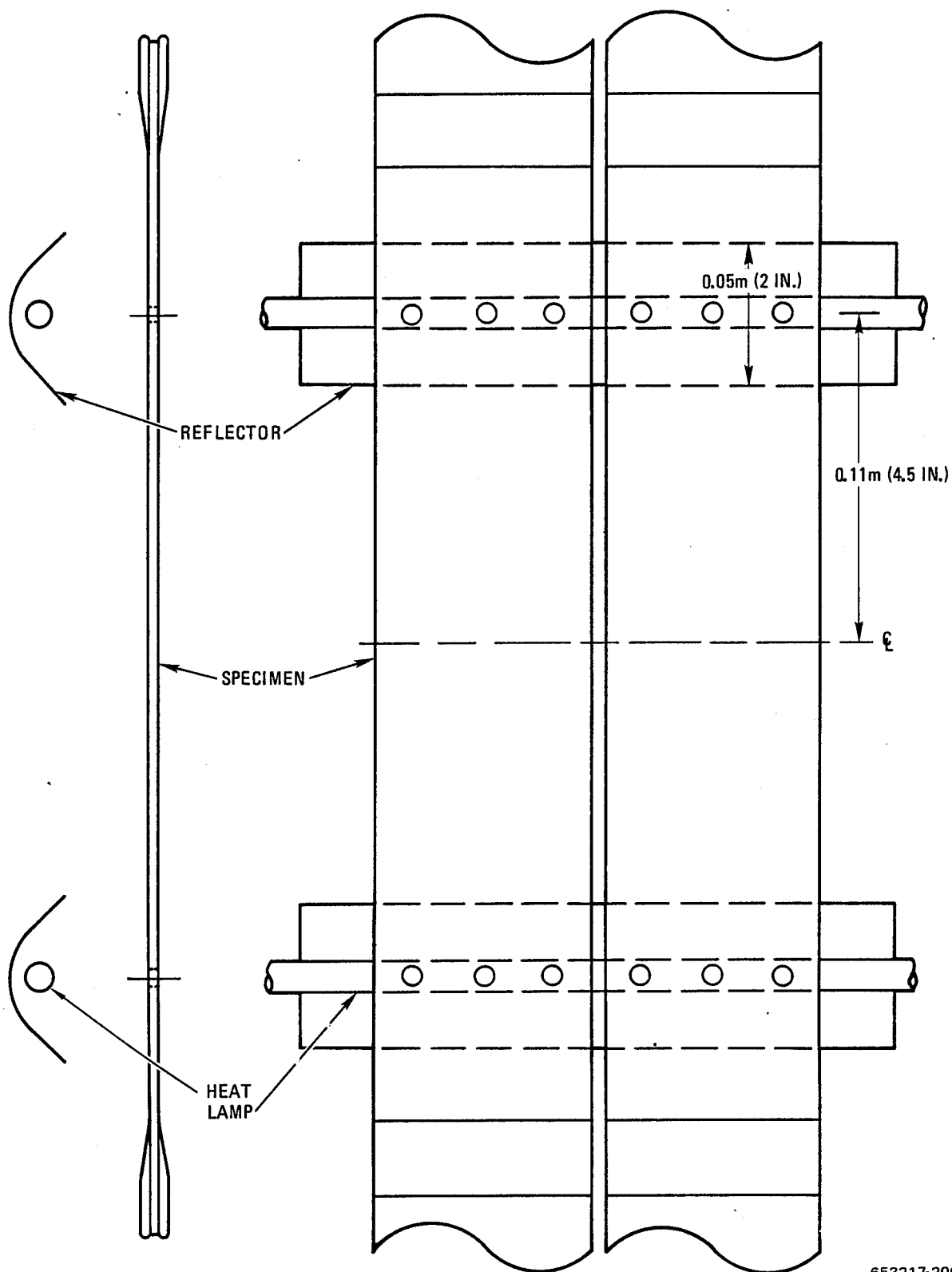


Figure 12-5 Programmer and Load Controllers

Two hydraulic power sources were used during the test program. One 50 gpm pump of the 200 gpm Pump Station was used for the short-term tests. A 7 gpm portable hydraulic pump was used for the long-term test.

12.2.5 HEATING SYSTEM. The test specimens are heated by 800-watt infrared quartz heat lamps. The heat is directed to the specimens by parabolic reflectors as shown in Figure 12-6. The lamps and reflectors are positioned so that they heat a 0.05 m (2 in.) strip on each half of the specimens. As discussed more fully in Section 12.3, this arrangement doubles the number of residual strength specimens that can be obtained from each long-term specimen. For each test setup, the five upper lamps and the five lower lamps are assembled in an upper rack and a lower rack. Each lamp rack is an independent heating system with its own temperature controller, control thermocouple, monitor thermocouple, and temperature error detection thermocouple.

The temperature cycling for the long-term test is synchronized with the loads by using the STEP code in the load programmer. STEP codes are programmed at the start and end of the heating period. The first STEP code activates the low temperature checking circuit for 10 milliseconds. If the specimen temperature is not less than 311 K (100° F), all test operations for that specific setup are deactivated. If the specimen temperature is less than 311 K (100° F), then power is applied to the heat lamps. The power is not controlled until the desired specimen



653217-206

Figure 12-6 Heating System Showing Arrangement of Specimens, Quartz Heatlamps, and Parabolic Reflectors

temperature is obtained. The temperature controller and its control thermocouple will maintain the desired temperature within ± 6 K (10° F). The temperature error detector thermocouple makes an independent and continuous check against over-temperature occurrences. (This thermocouple is also used by the low temperature checking circuit.) In case of an over-temperature occurrence, all test operations for that specific setup are deactivated. The second STEP code removes the power to the heat lamps, and the specimens are allowed to cool.

12.2.6 COOLING SYSTEM. A large centrifugal blower driven by a five horsepower motor provides the cooling air for the test specimens. The cooling air is distributed to 50 locations by a duct system. At each location a nozzle directs the cooling air to a pair of test specimens. Air flow at each location can be adjusted by physically changing the nozzle outlet area. These nozzles are shown near the top in Figure 12-3. Figure 12-7 is a closeup view of the nozzles in operation during the long-term tests.

12.2.7 CONTROL CONSOLE. The control console, shown in Figures 12-4 and 12-8, contains the temperature control and checking circuits, malfunction/shutdown logic circuits, and system control and indicator circuits.

The control console front panel contains the following controls and indicators.

- a. Ten setup counters to maintain the load programmer block count for each set up.
- b. Ten dump switches/indicators to manually dump or indicate an automatic dump or any setup.
- c. Ten JOG-RESET toggle switches to energize the hydraulics of each setup.
- d. PROGRAMMER counter to indicate load programmer block count.
- e. RUN and HOLD switches/indicators to provide remote control of load programmer.
- f. LOAD and UNLOAD switches and indicators to provide remote control of the hydraulic pump pressure to all setups.
- g. DUMP switch/indicator to completely shut down the hydraulic pump.
- h. OVER TEMPERATURE, LOW TEMPERATURE, SPECIMEN FAILURE, LOAD ERROR, RAM OVERTRAVEL, MANUAL LOCK indicators to indicate which malfunction caused a test to stop. The numbered setup indicator will also indicate which setup is related to the malfunction.

12.2.8 DATA RECORDING SYSTEM. All data are recorded on a high speed digital recorder. The 10 loads and 20 monitor thermocouples can be recorded on magnetic tape at a maximum sampling rate of six times per second. Data can then be printed out in engineering units.

Data are recorded periodically to confirm that loads appear to be reasonable and that the temperature cycle profile is correct. Loads cannot be confirmed exactly because the programmed loads are not known due to the random nature of the spectrum.

12.2.9 MONITOR/SAFETY SYSTEM. A Metrascope is used as a monitor and a limit detect safety system. Channels 1 through 10 display the tension loads up to 100% with the limits set to

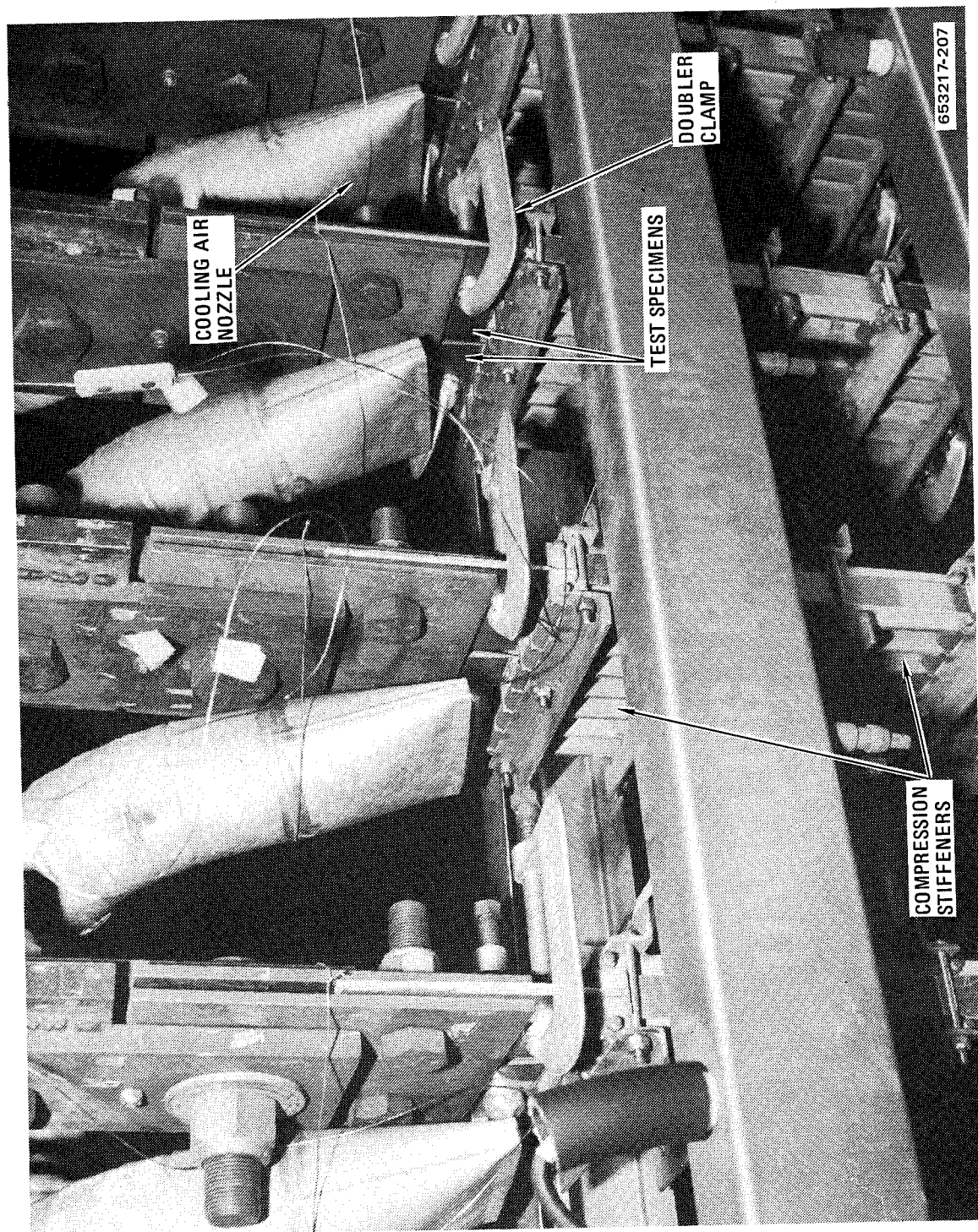


Figure 12-7 Closeup-View of Flight Simulation Apparatus Showing Cooling Air Nozzles, B/AI Doubler Clamps, and Compression Stiffeners

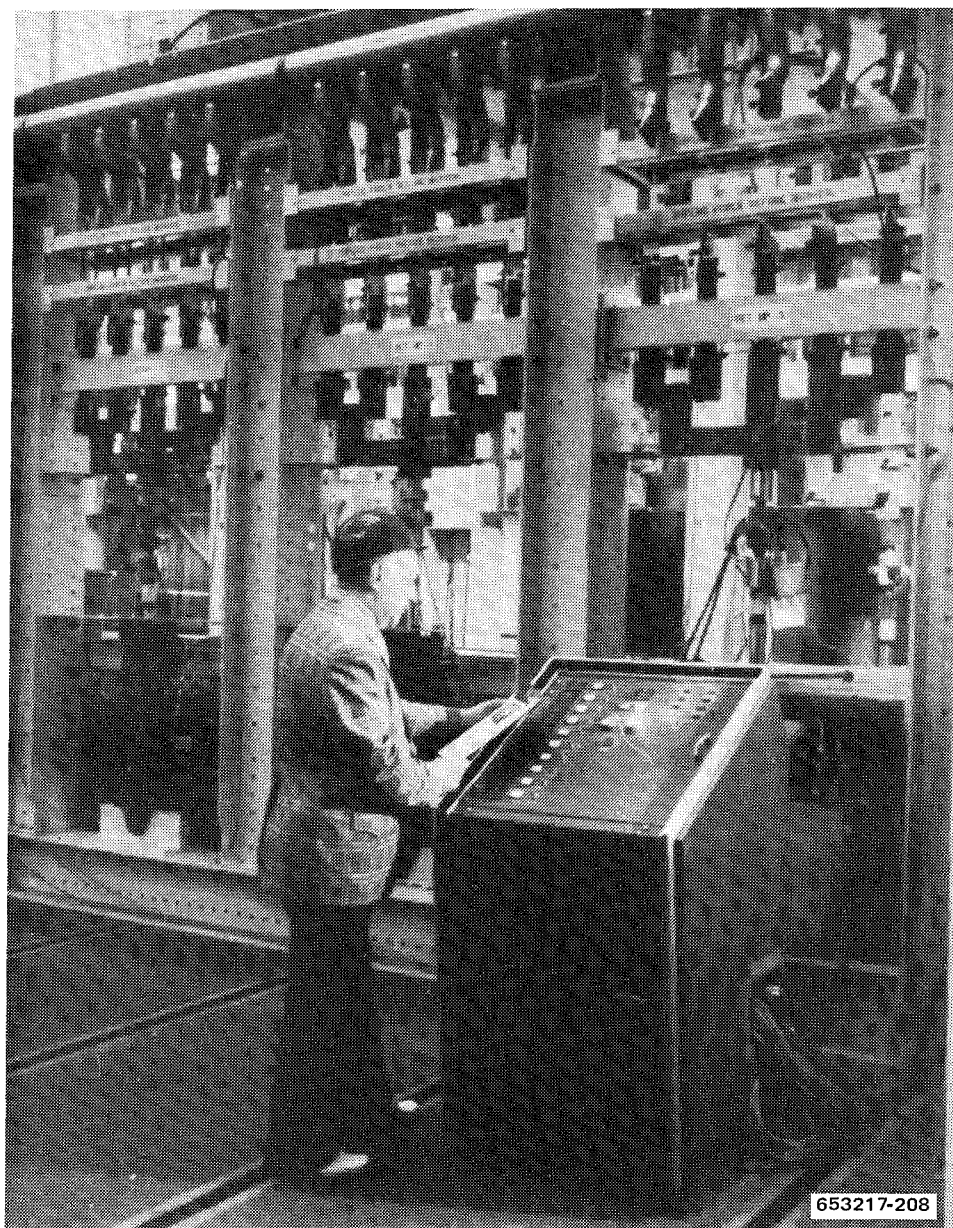


Figure 12-8 Control Console

105%. Channels 11 through 20 display the compression loads (1 through 10) up to 25% with the limits set at 30%. Channels 21 through 40 display the temperatures of each monitor thermocouple for each of the 20 lamp racks. The temperature limit is set 5% above the maximum temperature for a given setup.

If any limit is exceeded, the main electrical circuit breaker is thrown to its OFF position. All heat lamps go off, the hydraulic pressure at the manifold is dumped, the load programmer goes into HOLD, and all 10 setups are individually dumped. The channel that exceeded the limit is indicated by a flashing line on that channel.

12.2.10 CHECKOUT. Tests were performed to check out the loading mechanism and the distribution of loads by the whiffletree assemblies. A set of 10 strain gaged aluminum specimens was prepared and calibrated. The specimens were installed in the flight simulator and loaded to three load levels in the region of interest. Both the total applied load and the 10 individual loads were found to be within desired limits. The individual loads on each specimen were within $\pm 3\%$ of the desired load.

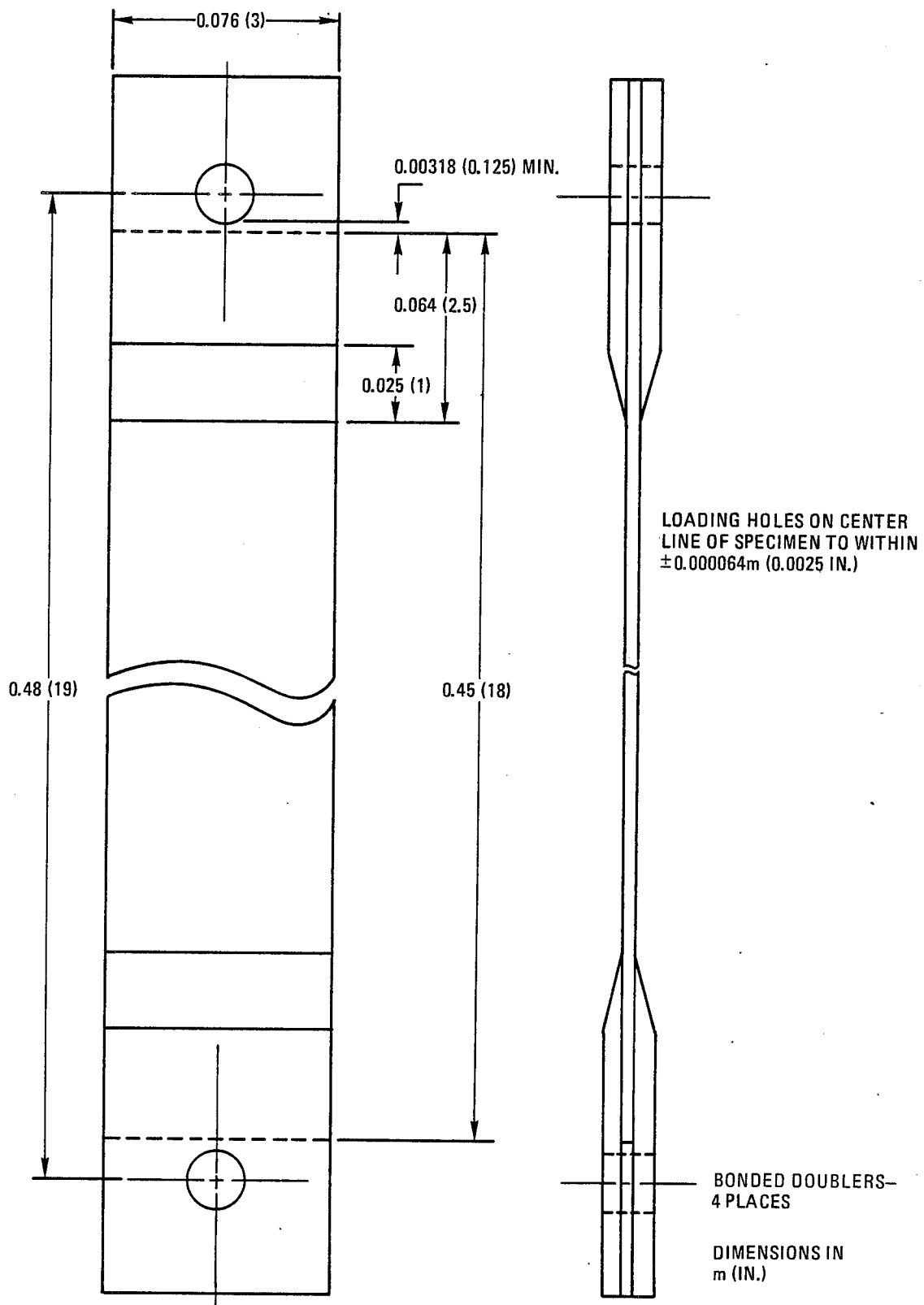
During checkout of the loading system, a dummy B/E short-term exposure specimen was intentionally loaded to failure in the simulator to determine the effects of individual specimen failures on the load levels of similar specimens within the same whiffletree arrangement. Each whiffletree contains five pairs of specimens. The specimens are loaded by a command from the programmer. This load program command signal is continuously compared to the signal from the load cell, and if the difference is more than a fixed amount, the loading mechanism shuts down. To check the response times of this arrangement in the event of specimen failure, the loads were monitored on two adjacent specimens, the specimen paired to the failed specimen, and one specimen in the adjacent pair. The strain gage and recorder arrangement used had a combined response time of well under 0.01 second. At failure, the load on the specimen paired to the failed specimen dropped to zero in 0.01 second. A compressive load of 10% of the tensile load was recorded for a duration of 0.01 second. The adjacent specimen lost about 20% of its tensile load for 0.02 second and recovered to 95% of the original load, which it maintained until the load was dumped at 0.18 second; the load then decayed linearly to zero in about 1 second.

12.2.11 AUTOMATIC OPERATION. To do long-term testing at the lowest cost and to be able to complete 50,000 hours testing in the shortest total time, the simulator must be automatic and be capable of operating unattended 75% of the time. Experience over the last several years shows that the simulator has operated on the average of 125 hours per week. This is about 75% of the time available. The monitoring and safety features are largely responsible for the off time. They are, however, very important in order to avoid destroying or damaging specimens during flight simulation testing. There are a number of other factors that have restricted the average run time to 125 hours per week. When equipment of this type is operated year after year, periodic maintenance must be performed. Recorders, heat lamps, hydraulic cylinders, bearings and electronic components must be serviced or replaced. The equipment must be shut down to remove broken specimens. When shutdown occurs in early evening or during the weekend, additional time is lost because the resin matrix specimens must be dried before operation is resumed.

Many weeks the simulator does run close to the 168 hours possible, but when we take a four-year period we find the long time average is close to 125 hours per week.

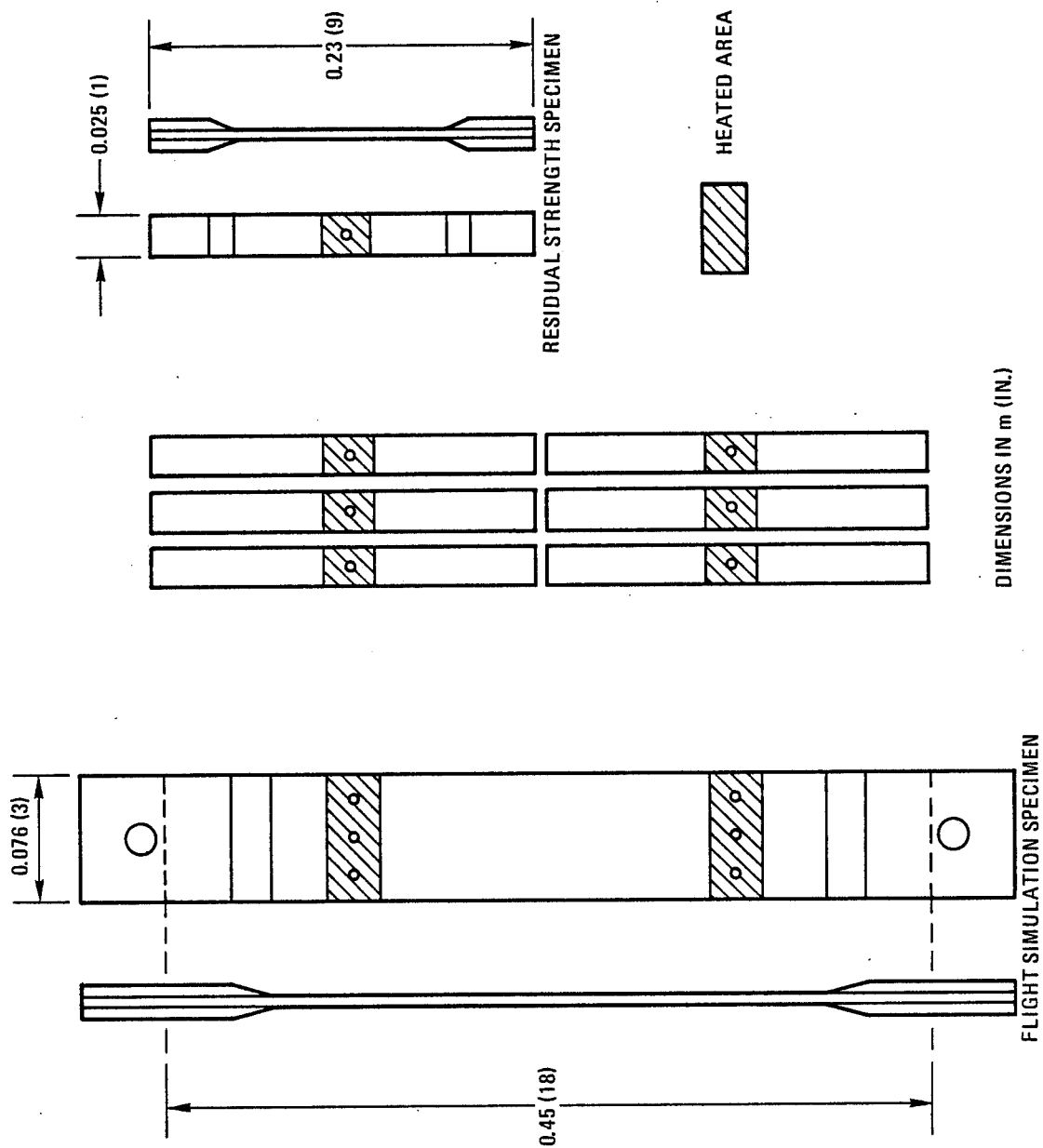
12.3 SPECIMEN CONFIGURATION

The unnotched specimen configuration for the long-term tests is shown in Figure 12-9. The composite portion of the specimen is 0.076 m (3 in.) by 0.46 m (18 in.). The tapered doublers bonded at each end of the specimen extend the overall length to 0.56 m (22 in.). Aluminum spacers of the same thickness as the composite are used to fill the gaps between the titanium doublers in the regions where the pin holes are located. The specimens are pin loaded to ensure uniform loading for the whiffletree arrangement used. Half of the resin matrix long-term specimens are prepared with notches consisting of 0.0064 m (0.25 in.) diameter holes. As shown in Figure 12-10, these holes are located so that they are centered in each of the six 0.025 m (1 in.) by 0.23 m (9 in.) post-test specimens to be cut from the notched long-term specimens after



653217-209

Figure 12-9 Long-Term Flight Simulation Specimen



653217-210

Figure 12-10 Cutting Plan for Post-Test of Notched Long-Term Specimens

flight simulation exposure. These specimens are used to determine the residual notched tensile or fatigue strength of the composite after flight simulation. The unnotched long-term specimens are also cut into smaller pieces for residual strength testing. The original plan was to cut each long-term specimen into twelve 0.013 m (0.5 in.) by 0.23 m (9 in.) post-test specimens. As discussed later, this plan was slightly modified as a result of the condition of the specimens at the completion of 10,000 hours of exposure. All of the post-test tensile and fatigue specimens will use bonded doublers as shown at the right in Figure 12-10. Two sets of quartz heat lamps 0.23 m (9 in.) apart are positioned so that they heat a 0.05 m (2 in.) strip on each half of the long-term specimen (see Figure 12-6). This arrangement places the 0.05 m (2 in.) heated zones at the centers of the post-test specimens. The edges of the heated zones are 0.025 m (1 in.) from the doublers so that the adhesive is not subjected to the operating temperature of the composite during simulation. Temperature measurements taken during testing showed the titanium end doublers to be approximately 69 K (125° F) cooler than the 408 K (275° F) heated zones of the epoxy specimens and approximately 117 K (210° F) cooler than the 505 K (450° F) heated zones of the G/PI and B/Al specimens. One modification was made to the B/Al specimens to increase the efficiency of heating during flight simulation exposure. The heated zones on the sides facing the quartz heat lamps were coated with flat black, heat resistant paint to reduce reflection from the aluminum surface.

The requirements for the short-term flight simulation specimens were less restrictive than for the long-term specimens because only residual tensile strength properties were to be obtained after the 100 and 200 hours of exposure. With this in mind a short-term specimen was designed that could be tensile tested after flight simulation with no further modifications, i.e., machining or doubler bonding. The specimen that was used is shown in Figure 12-11. A further advantage in using the 0.025 m (1 in.) wide specimen rather than the 0.076 m (3 in.) wide long-term configuration was a considerable savings in material. To satisfy the pin loading requirement of the flight simulation apparatus it was necessary to use the 0.05 m (2 in.) wide end doublers shown in Figure 12-11. The space between each set of doublers not occupied by the end of the composite material was filled with aluminum sheet of the same thickness as the composite. Also shown in Figure 12-11 is the notched specimen used for half of the resin matrix short-term tests. The 0.0064 m (0.25 in.) diameter holes, one in each half, are centered in the 0.05 m (2 in.) heated zones in like manner to the long-term specimens.

12.4 RANDOM LOAD SPECTRUM

The objective of the SCR spectrum generation task was to provide a load simulation that would be representative of flight conditions during the life of a supersonic cruise aircraft and would be acceptable and remain acceptable to all concerned parties during this long real-time flight simulation test program. Developments (ref. 38 and 39) in random flight-by-flight load simulation have produced a simple method for generating a random load sequence that matches the desired load-exceedance relationships on a mission segment basis. These studies have shown the importance of including the random character of the individual load, adhering to flight-by-flight profiles, and including the ground-air-ground load for each flight.

Several assumptions were made to define the loading spectrum. The mission profile and loads data were obtained from reference 1. These data were also used for the study described in reference 2. The life of a supersonic cruise aircraft was assumed to consist of 25,000 flights of two hours duration each. For this work, each flight was assumed to be an "operational flight" as defined by reference 1. Each flight consisted of a 10-minute climb, a 90-minute cruise, a 20-minute descent, and a single landing load. The number of loads per flight and the number of

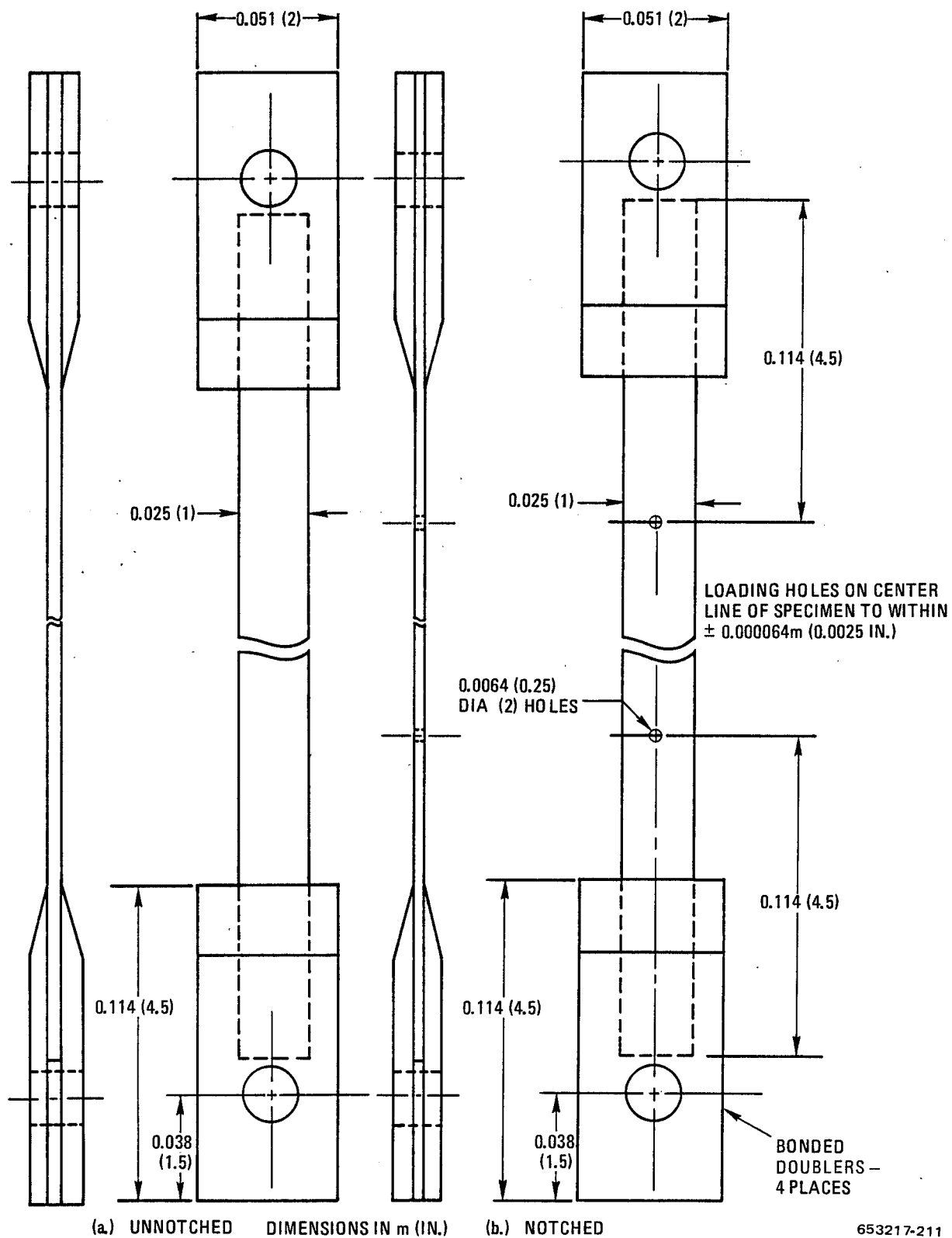


Figure 12-11 Short-Term Flight Simulation Specimens

loads in each of the segments were modeled after the reference 1 load sequence. However, the loads were randomized such that all the loads expected to occur in 10,000 flights were included. Since the 90-minute cruise was scheduled to include only about eight loads per flight, the mean load was held for 44 minutes before and after the imposition of a two-minute cruise loading period. The climb and descent loads were distributed over the entire climb and descent time.

To simulate the mission thermal profile for a Mach 3 cruise, an elevated temperature is applied to the specimens. From room temperature at the beginning of climb, the temperature is increased uniformly to the maximum use temperature for each material. Once the random load spectrum has been generated, the magnitude of the loads and the maximum use temperature or cruise temperature can be adjusted to suit each of the composite systems being studied. Both the load magnitudes and cruise temperatures were set using data from the baseline measurements and test data obtained by using the load spectrum at an accelerated rate. The loading rate was increased so that the loads normally occurring during a two-hour flight would occur in one minute. These accelerated tests are run at the cruise temperature and are referred to as short-term tests.

12.4.1 SPECTRUM GENERATION FOR THE LONG-TERM TESTS. The segment exceedance curves from reference 1 are shown in Figures 12-12, 12-13, and 12-14. The Gaussian process line needed for the random simulation is shown in each figure. The mapping function data are shown in Table 12-1.

The N_0 values for each segment were arrived at by the following argument. The long-term test simulation of reference 1 considered 10,000 flights. In this simulation it was desired to maintain the number of load values at 80 per flight. Since 20 dwell signals were required per flight to maintain the mean cruise load during heating and one landing load was included in each flight, there were 101 loads per flight for a total of 1.01 million loads for the 10,000 flights. For this work these 1.01 million loads are applied in 25,000 flights, thus requiring about 40 loads per flight. Since there are actually only 32 minutes of loading per two-hour flight, the overall cyclic frequency, N_p , of load values is calculated as:

$$\begin{aligned} N_p &= 40 \text{ cycles}/32 \text{ minutes} = 1.25 \text{ cpm} \\ &= 75,000 \text{ cycles}/1000 \text{ hours} \end{aligned}$$

The average number of mean crossings per unit time, N_0 , is defined as the product of the irregularity factor ($R = 0.9$) and N_p , giving:

$$N_0 = (0.9)N_p = 67,500 \text{ cycles}/1000 \text{ hours}$$

The 10-minute climb, 90-minute cruise, and 20-minute descent segments represent 31%, 6.25%, and 62.5% of the total loading time, respectively. For this program spectrum, the climb, cruise, and descent segments contain 70%, 12%, and 18% of the total number of loads. The N_0 values for each segment were calculated as:

$$\begin{aligned} N_0 (\text{Climb}) &= N_0 (0.7)/(0.31) = 152,000 \text{ cyc/kseg hr} \\ N_0 (\text{Cruise}) &= N_0 (0.12)/(0.0625) = 129,600 \text{ cyc/kseg hr} \\ N_0 (\text{Descent}) &= N_0 (0.18)/(0.625) = 19,440 \text{ cyc/kseg hr} \end{aligned}$$

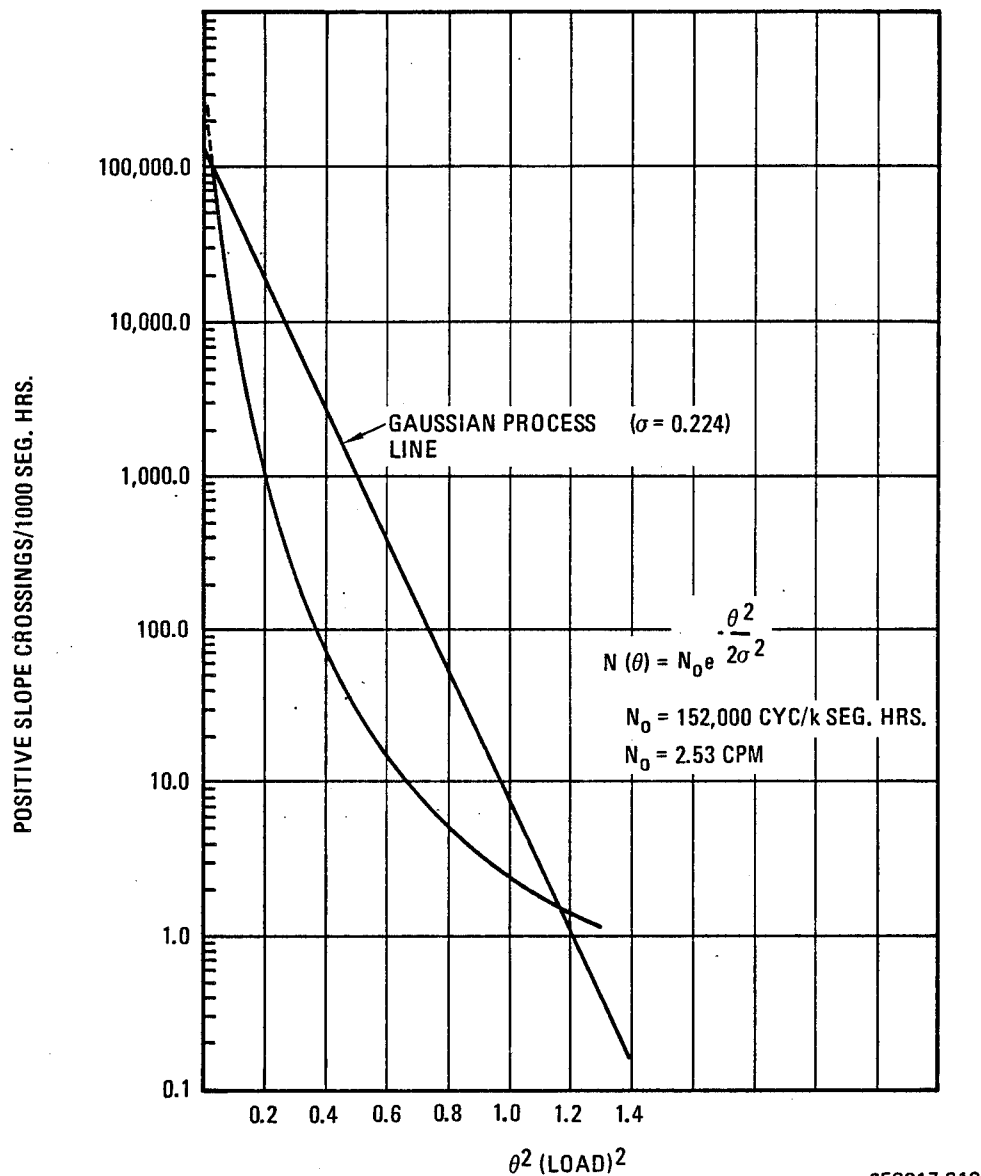


Figure 12-12 Climb Exceedance Curve

These values along with the other mission parameters were input to the General Dynamics Simulated History of Aircraft Missions (SHAM) computer procedure, which generated the load history (ref. 39). A typical mission is shown in Figure 12-15.

12.4.2 SPECTRUM FOR THE SHORT-TERM TESTS. To set the magnitudes of the long-term loads for each composite system some accelerated testing had to be done. This was done by increasing the frequency of loading to the point where a half of a lifetime of loads could be applied to specimens of each composite system in 200 hours. These groups of specimens were held at constant

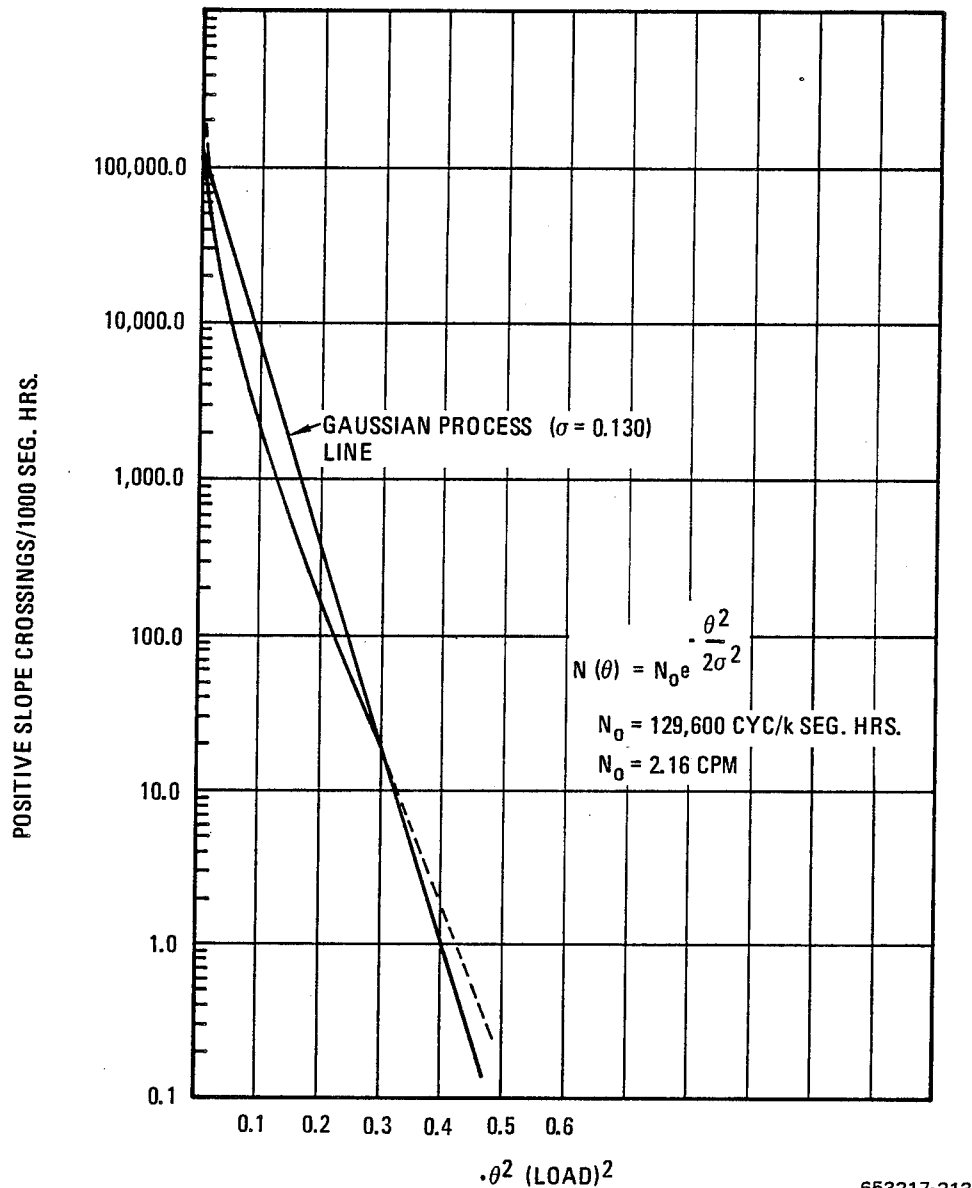


Figure 12-13 Cruise Exceedance Curve

temperatures. The temperatures chosen were their maximum use temperatures. These tests, which were run for 100 hours and 200 hours, are referred to as the short-term tests. The objective of the short-term tests was to apply as many mission loads as possible to the specimens in a short time. The random character of the loads, the flight-by-flight sequence, and the landing load were all maintained in the accelerated spectrum.

It can be shown that the minimum periods of the long-term test climb, cruise, and descent segments are 8.5, 10, and 66.25 sec/load, respectively. To obtain a maximum cyclic rate of 50 cpm,

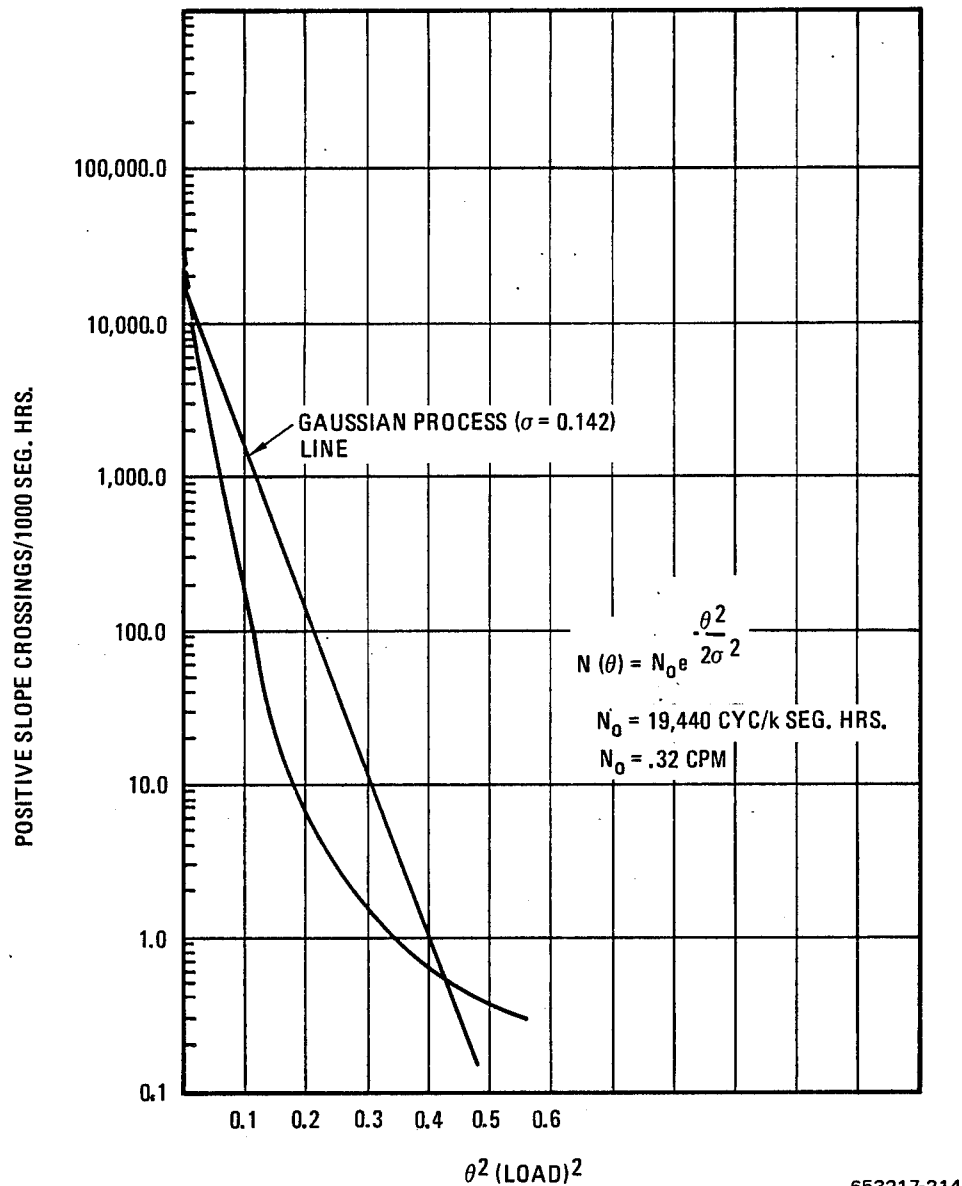


Figure 12-14 Descent Exceedance Curve

the minimum period for each segment should be 0.6 sec/load. The acceleration factors were thus calculated as:

$$(\text{AF}) \text{ climb} = 8.5/0.6 = 14.167$$

$$(\text{AF}) \text{ cruise} = 10/0.6 = 16.67$$

$$(\text{AF}) \text{ descent} = 66.25/0.6 = 110.417$$

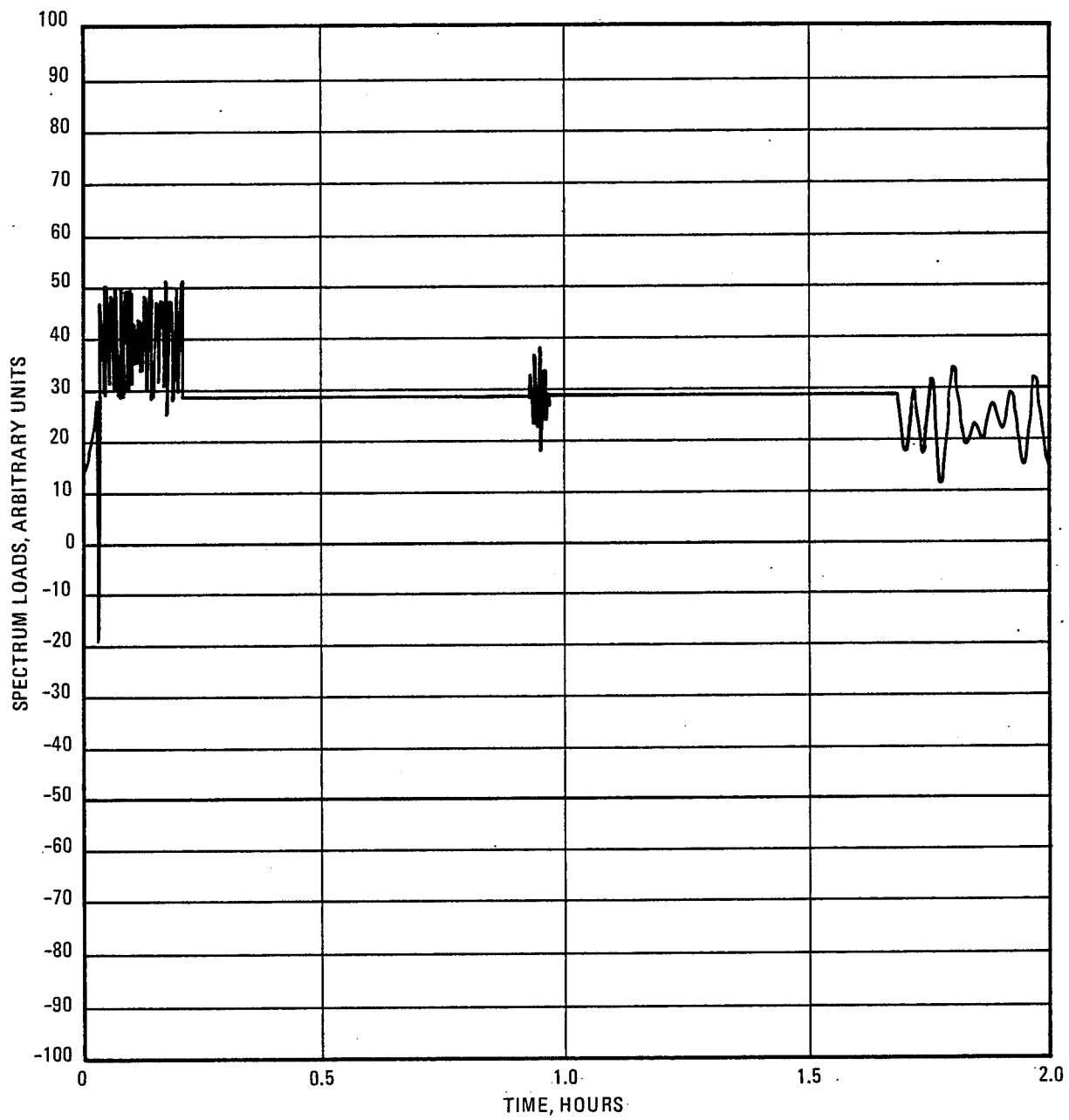
Table 12-1. Mapping Function Data

Crossing/ (k segment hr)	$\left(\begin{array}{c} \text{Gaussian} \\ \text{Load} \end{array} \right)^2$	$\left(\begin{array}{c} \text{Real} \\ \text{Load} \end{array} \right)^2$	Gaussian Load	Real Load	σ	N (cpm)
Climb Segment						
152,000	0	0	0	0	0.224	2.53
100,000	0.04	0.04	0.2	0.2		
10,000	.27	.095	.520	.308		
1,000	.50	.205	.707	.453		
100	.73	.375	.854	.612		
10	.96	.655	.980	.809		
5	1.03	.79	1.015	.889		
2	1.13	1.05	1.063	1.025		
1	1.2	1.43	1.095	1.196		
Cruise Segment						
130,000	0	0	0	0	.130	2.16
100,000	0.01	0.01	0.1	0.1		
10,000	.09	.045	.3	.212		
1,000	.165	.130	.406	.361		
100	.245	.225	.495	.474		
10	.32	.325	.576	.570		
1	.4	.425	.632	.652		
Descent Segment						
19,000	0	0	0	0	.142	0.324
8,500	.035	.035	.187	.187		
1,000	.12	.06	.346	.245		
100	.215	.12	.464	.346		
10	.305	.18	.552	.424		
3	.355	.24	.596	.490		
1	.4	.34	.632	.583		
0.5	.43	.44	.656	.663		

These acceleration factors and the long-term test mission data were input to the SHAM procedure to produce the short-term test history. A flight lasts about 60 seconds and is divided into approximately 25 climb loads in 42 seconds, six cruise loads in seven seconds, and seven descent loads and one landing load in 11 seconds. A typical load sequence is shown in Figure 12-16. The accelerated spectrum results in an overall rate of one minute per flight, so that in 100 hours of testing, about one fourth of a cruise aircraft lifetime (6000/25,000) can be imposed.

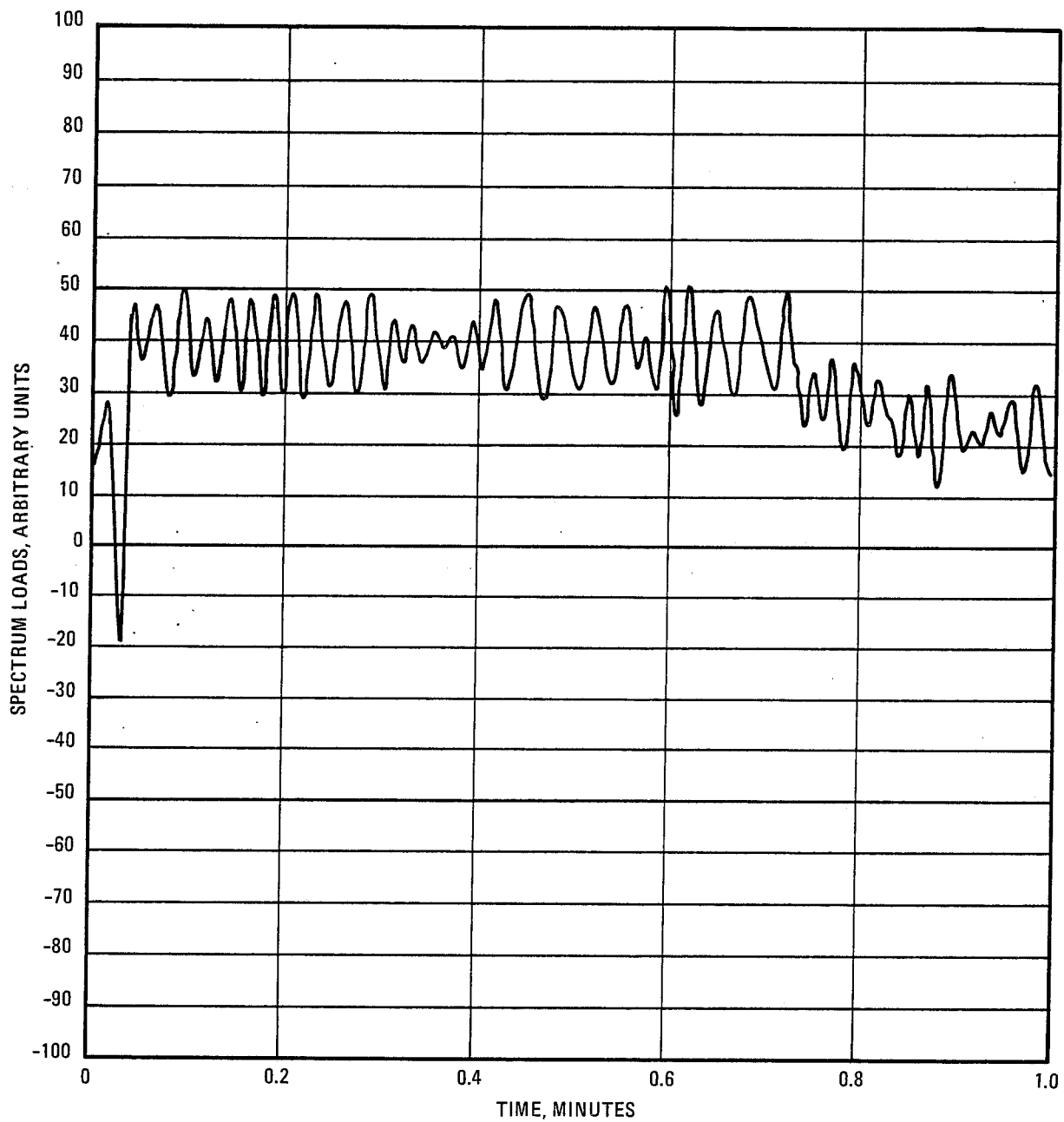
12.5 WEAROUT MODEL

At the time these tests were started a wearout model had been developed and used on epoxy matrix composite systems. The fatigue and residual strength data from the short-term service



653217-215

Figure 12-15 Typical Mission for Long-Term Testing



653217-216

Figure 12-16 Typical Mission for Short-Term Testing

history tests on two of the four composite systems, i.e., G/E and B/E specimens, were analyzed using the wearout model developed in references 3 and 40 and previously used in references 41 and 42.

The wearout or fatigue model is reviewed here and examples of its use will be given for the epoxy system in the section on short-term test results. This model is based on four assumptions (three physical and one mathematical form).

- a. Materials fail because of the presence of preexisting flaws.
- b. Flaws grow in a deterministic manner. The manner is determined by material properties, state, and magnitude of the stresses at the flaw perimeter; history of applied stress; and the thermal and mechanical history.
- c. The critical load for a structure is a function of instantaneous flaw state, and the distribution of residual strengths defines the flaw field statistics.
- d. Damage rate accumulation is of the functional form:

$$\frac{\partial C}{\partial t} = M \cdot C^r, \quad (1)$$

where C is the flaw length and r is the flaw growth rate exponent.

The residual strength function $F_R^{(t)}$ can be shown to have the form

$$F_R^{(t)} = \left[F_R^{(t_0)^{2(r-1)}} - A_4 (r-1) A_1^S (t-t_0) \right] \frac{1}{2(r-1)} \quad (2)$$

where:

$A_1 = F_{\max}/F_{\text{ref}}$, with F_{\max} being the truncation load a measure of rms stress and F_{ref} being a reference rms stress level.

The term A_4 is related to the history-dependent constant (M) in Equation (1).

The term r is the exponent of the flaw state (C) in Equation (1).

The term $-1/s$ is the slope of the $\ln F_{\max} - \ln t$ curve and is related to r .

The term t refers to time and t_0 is a reference time condition.

If the initial assumptions are correct, the results of varying stress history, environmental conditions, and geometry are contained in A_4 .

Note that Equation (2) is a strictly monotonic decreasing function of time. Therefore, time t must be measured after the initial stress relaxation occurs. If this point in time is considered to

be the time origin, $t = 0$, Equation (2) may be considered applicable for all positive values of t . $F(t = 0)$ is the initial static strength of the component possessing a Weibull (extreme value) distribution:

$$P(F(t_0) > F) = \exp \left\{ - \left(\frac{F}{\beta_0} \right)^{\alpha_0} \right\} \quad (3)$$

where α_0 and β_0 are the shape and scale parameters, respectively, for the Weibull distribution. Introducing the Weibull flaw distribution, Equation (3), into Equation (2) gives the time-varying residual strength distribution of the form:

$$P(F_R(t) > F_R) = \exp - \left[\frac{F_R^{2(r-1)} + (r-1) A_4 A_1^S t}{\beta_0^{2(r-1)}} \right]^{\frac{\alpha_0}{2(r-1)}} \quad (4)$$

for $F_R > F_{\max}$

$$P(0 < F_R(t) < F_{\max}) = 0$$

and

$$P(F_R(t) = 0) = 1 - P(F_R(t) > F_{\max})$$

The probabilistic Equation (4) does not involve the reference time t_0 , which appears in Equation (2), and agrees with Equation (3) when $t = 0$. For fixed time t , it follows from Equation (4) that the transformed variable $F_R(t)^{2(r-1)}$ has a truncated three-parameter Weibull distribution.

The distribution depicted in Equation (4) has a limiting form for $(F_{\max}/\beta_0)^{2(r-1)} \ll 1$, which gives the lifetime distribution as:

$$P(T > t) = P[F_R(t) > F_{\max}] = \exp - (t/\beta_f)^{\alpha_f} \quad (5)$$

where:

$$\alpha_f = \frac{\alpha_0}{2(r-1)} \quad (6)$$

$$\beta_f = \frac{\beta_0^{2(r-1)}}{(r-1) A_4 A_1^S} \quad (7)$$

If specimen behavior is found to be consistent with the model, the following responses would be expected.

- The lifetime shape parameter would be independent of rms stress, temperature, and humidity.
- Both the truncation load-endurance data and initial shape parameter to fatigue shape parameter relationship will yield consistent values of r .

c. Characteristic strengths and endurances will shift log-linearly.

The program used to fit the wearout model to the experimental data sample is based on minimizing the "error" between the prediction (model) and the data. The model parameters α_0 , β_0 , and t_0 and the experimental data are available as "known" values for input. The program uses an iteration procedure to minimize the error (variance). The iterative solution may be accomplished by determining either the value of "r" or of " A_4 " that gives a minimum error.

When the value of r is to be used in iteration, a value of A_4 must first be determined. The probabilistic model may be written in the form:

$$\frac{\left\{ \beta_0 \left[\ln \frac{1}{P} \right]^{\frac{1}{\alpha_0}} - F_R(t) \right\}^{2(r-1)}}{A_1^{2r(r-1)}} = A_4 (t-t_0)$$

where:

$$P = P(F_R(t) > F_R)$$

and

$$A_1^{2r} = 1$$

This equation is represented functionally as

$$f(P, F_R) = A_4 t$$

Therefore, the constant A_4 is the slope of the linear regression equation fitted to the empirical data. The iteration sequence is begun with an assumed value of "r" and repeated until the error term, i.e., the probabilistic squared difference between the model and the observed data, becomes a minimum.

The application of this model to the short-term test data will be shown in Section 12.6. At that time it will become clear how the parameters A_4 , s, and A_1 , are determined during the calculations.

α, β — Weibull shape and scale parameters for the distribution of the tensile data.

α_0, β_0 — Weibull parameters at time zero.

α_f, β_f — $\frac{\alpha_0}{2(r-1)}$, $\frac{\beta_0^{2(r-1)}}{(r-1)A_4A_1^S}$

α_T, β_T	— Weibull parameters at a temperature, T.
β_{RT}	— Room temperature value.
β_{MLE}	— Calculated using pooled α by formula $\beta = \left[\frac{\sum_{i=1}^n X_i^\alpha}{n} \right]^{\frac{1}{\alpha}}$ where n is number of specimens.
β_{LT}	— β for long term test.
σ	— Relates to slope of Gaussian process line. Slope = $-\frac{1}{2\sigma^2}$ See Figure 12-13.
Θ	— Load for exceedance curves expressed in number of g's.
a_T	— $\frac{\beta_T}{\beta_{RT}}$, ratio of β at temperature to β at room temperature.
A_1	— $\frac{F_{max}}{F_{ref}}$, where F_{max} is the truncation load, a measure of rms stress, and F_{ref} is a reference rms stress level.
A_4	— This term is related to the history dependent constant (M) in Equation (1).
C	— Flaw length.
f_c	— $(3)^{-\frac{1}{\alpha_0}}$ is the penalty for least of three as a function of the shape parameter, α_0 .
f_r	— $(100)^{-\frac{1}{\alpha}}$ is the risk factor obtained from failure statistics by assuming a 1% static failure rate is acceptable.
f_T	— Strength retention factor at elevated temperature obtained from the $\ln a_T$ versus T curve.
F	— Static strength.
$F_R(t)$	— Residual strength function.
g	— Acceleration due to gravity.
M	— Proportionality constant in Equation (1).
N_0	— $R N_p$ is the average number of mean crossings per unit time.
N_p	— Overall cyclic frequency of loads.

$P(F_R(t) > F_R)$	—	Probability function.
r	—	Flaw growth rate exponent.
R	—	Irregularity factor.
s	—	The term $-\frac{1}{s}$ is the slope of the $\ln F_{\max}$ versus $\ln t$ curve and is related to r .
t	—	Time. t_0 is a reference time condition.
T	—	Temperature.

12.6 SHORT-TERM FLIGHT SIMULATION

The short-term tests were intended to provide the data necessary to set reasonable load levels for the long-term tests. These load levels were extremely important to the success of the long-term tests. A selection that was too high could result in failure of all the specimens prior to completion of 50,000 hours of exposure. Conversely, a very low load level might result in neither specimen failures nor measureable changes in residual strength after 50,000 hours. The short-term tests were accomplished by accelerating the loading rate such that half a lifetime of loads was applied in 200 hours. During loading the specimens were exposed to the maximum use temperature for each composite material system. The loads for the short-term tests were set to induce some fatigue failures. Specimens that did not fail were tested for residual strength. These fatigue life and residual strength data were then used with the static baseline data to fit the wearout model and set the loads for the long-term tests.

The short-term tests were additionally intended to check out the flight simulation apparatus and to provide the modes and statistics of failure.

12.6.1 TEST PLAN AND PROCEDURES. For each material system a total of 40 specimens, in groups of 10, were subjected to the short-term flight simulation exposure tests. For B/Al, both unidirectional and $[0^\circ \pm 45^\circ]_s$ crossplied materials were tested while only $[0^\circ \pm 45^\circ]_s$ crossplied material was tested for the resin matrix systems. The unidirectional B/Al was included because its significantly higher transverse strength and transverse and shear moduli, than those of the resin systems, offer a much greater potential for structural applications. The originally scheduled unidirectional resin matrix specimens were changed to a notched $[0^\circ \pm 45^\circ]_s$ crossply configuration. Tests were conducted for time periods of 100 and 200 hours. At the accelerated rate of loading that was used, this represented one-fourth and one-half lifetimes respectively. All tests on any one system were conducted at the same temperature and load level.

Following the 100- and 200-hour exposures, all unfailed specimens were tested for residual tensile strength at the same temperature as used for the short-term tests.

12.6.1.1 Temperature Selection. Selection of the short-term test temperatures was to be based on the results of the baseline tensile tests. It was planned to select a temperature in the region just below that where a distinct change in the slope of the strength versus temperature curve

occurred. Generally, however, no distinct fall-off in strength was observed out to the maximum tensile test temperatures used for any of the materials. At the time that the short-term tests were ready to begin, the thermal aging exposures had not been running long enough to provide data for selection of the flight simulation temperatures. Data from the literature for use in selecting the maximum use temperatures for 50,000-hour service was also lacking. However, at the time that the long-term tests were expected to start it was thought that sufficient thermal aging data would then be available and that a rational selection of exposure temperatures could be made at that time. Therefore, the temperatures selected for the short-term tests were in the region covered by the thermal aging tests. For the epoxy systems 422 K (300° F) and for B/Al 505 K (450° F) were chosen. These temperatures were midway between those at which thermal aging exposures were currently in progress. To obtain a better comparison between the B/Al and the G/PI systems, 505 K (450° F) was also chosen for G/PI even though the mid-way temperature of the thermal aging tests was 533 K (500° F).

12.6.1.2 Selection of Short Term Loads. The loads for the short-term tests were set as high as possible to produce early fatigue failure and provide a basis for subsequent stress variations. The room temperature static ultimate strength is reduced by two independent factors to arrive at the desired load. One of these factors is strength retention at elevated temperature, f_T . It was obtained from a retention curve as described below. The other factor is a risk factor, f_r , and was obtained from failure statistics by assuming that a 1% static failure rate is acceptable.

Because no baseline tests were performed on B/E, its reduction factors were obtained from existing data. The procedure for the reduction of the G/E, G/PI, and B/Al data is described here.

The baseline data provides a starting point for setting the peak loads to be used during the short-term tests. The raw failure load data for a given material, notch condition, and temperature were fit with a Weibull distribution by linear regression to obtain the scale parameter, β , and the shape parameter, α . The temperature retention curve was plotted in the form of $\ln a_T$ versus temperature, where a_T is the ratio of β at a given temperature to β at room temperature. The portion of this curve that exhibits linearity permits statistical pooling of the data over that temperature range. The pooling was accomplished by scaling each data point (load value) to its raw β estimate and using this ratio as the random variable. The resulting α was the pooled α for that material and notch condition over the temperature range of interest. Using maximum likelihood estimation techniques, a better estimate of the β for each temperature was obtained from the original load data and the pooled α . These new β estimates were used to refine the $\ln a_T$ versus T curve so that the temperature factor, f_T , could be obtained directly from the plot. The risk factor, f_r , was calculated from the pooled α as the first failure of 100 samples, or

$$f_r = (100)^{-\frac{1}{\alpha}}$$

The permissible peak load was then the product:

$$\text{peak load} = f_r f_T \beta_{RT}$$

The procedure for load selection is demonstrated below using the baseline tensile data for unnotched $[0^\circ \pm 45^\circ]_s$ G/E in a typical calculation:

1. Fit a Weibull distribution to each set of raw load data (a distribution for each temperature, material, and notch condition).
2. Plot temperature retention in the form of a $\ln a_T$ versus T curve, where a_T is β_T/β_{RT} .
3. From Step 2, determine which sets of data may be pooled (based on linear part of $\ln a_T$ versus T curve).
4. Pool several temperatures by using X/β_T as the random variable. Obtain a pooled α for that material and notch condition.
5. Recompute β_T based on pooled α and original load data (use maximum likelihood estimator). Refine a_T versus T with β_{MLE} .
6. Compute risk factor based on 1% failure rate $f_r = (100)^{-\frac{1}{\alpha}}$
7. Find temperature retention factor (f_T) from refined a_T versus T .
8. Calculate peak load equal to $f_r f_T \beta_{RT}$.

Using the 35 tensile strength values in Table 12-2, the procedure is followed to calculate the peak short-term load for G/E.

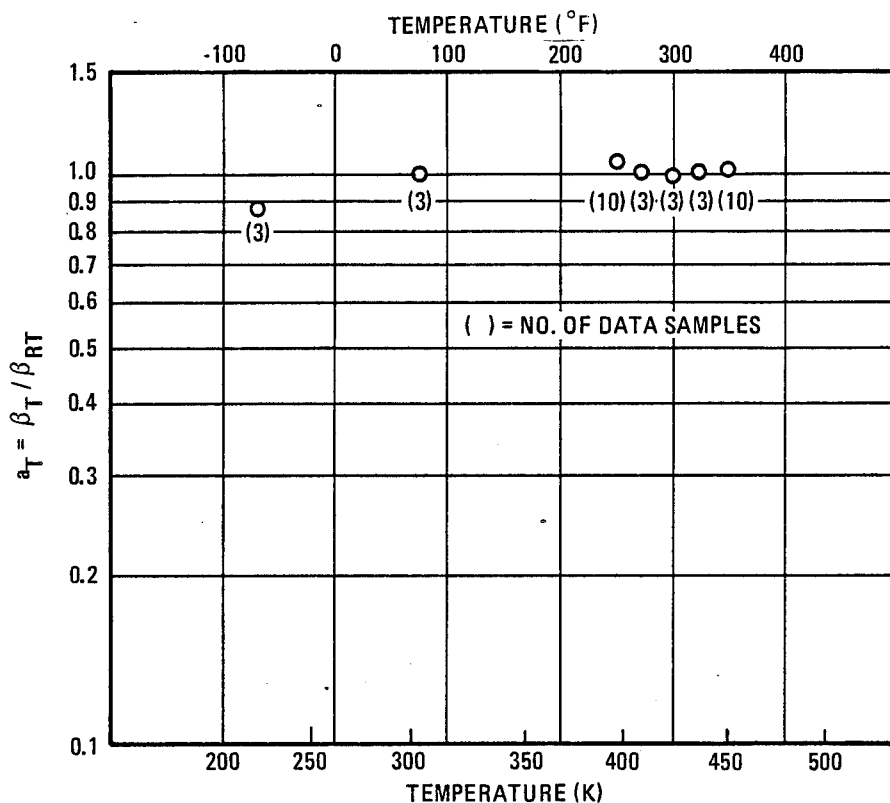
1. The β and α columns of the table list the value calculated from the data at each temperature.
2. Figure 12-17 shows a plot of $\ln a_T$ versus temperature using the values listed in the $a_T = \beta/\beta_{RT}$ column.
3. From Figure 12-17, it was determined to pool all the data.
4. All temperatures were used and the data shown in the Load/ β column was ordered and used to find a pooled α . The computer makes this calculation. However, for clarity the nature of this calculation is shown in Table 12-2 and the Weibull plot in Figure 12-18. The pooled α for this case is 12.71.
5. Recompute β_T based on $\alpha = 12.71$ and original load data for each temperature. The maximum likelihood estimator formula is

$$\beta = \left[\left(\sum_{i=1}^n X_i^\alpha \right) / N \right]^{1/\alpha}$$

Results of this calculation are shown in Table 12-2 in the β_{MLE} and β/β_{RT} columns. Now use this data to refine $\ln a_T$ versus T plot using β_{MLE} . These points leave Figure 12-17 essentially unchanged.

Table 12-2. Baseline Tensile Data — Unnotched $[0^\circ \pm 45^\circ]_s$ G/E

Specimen No.	Temperature		Load		μ		β		α	β/β_{RT}	Load/ β	β_{MLE}		β/β_{RT}
	K	(°F)	N	(lb)	N	(lb)	N	(lb)				N	(lb)	
BC01-1	218	-67	3870	870	4034	907	4190	942	11.79	0.89	0.96	4114	925	0.88
-2			3879	872							.93			
-3			4359	980							1.04			
BC01-6	297	75	5031	1131	4444	999	4702	1057	7.40	1.0	1.07	4684	1053	1.00
-7			3905	878							.83			
-8			4377	984							.93			
BC01-4	394	250	4257	957	4644	1044	4875	1096	9.61	1.04	.87	4991	1122	1.07
			4101	922							.84			
-16			3914	880							.80			
-22			4871	1095							1.00			
-23			4448	1000							.91			
-24			5782	1300							1.19			
-25			4804	1080							.99			
-26			4848	1090							.99			
-27			4670	1050							.96			
-28			4724	1062							.97			
BC01-9	408	275	4492	1010	4537	1020	4750	1068	9.34	1.01	.95	4710	1059	1.01
-10			4097	921							.86			
-17			5026	1130							1.06			
BC01-11	422	300	4919	1106	4635	1042	4790	1077	13.16	1.02	1.03	4715	1060	1.01
-18			4270	960							.89			
-19			4715	1060							.98			
BC01-12	436	325	4657	1047	4662	1048	4786	1076	17.09	1.02	.97	4715	1060	1.01
-13			5249	1180							1.03			
-20			4404	990							.92			
BC01-14	450	350	4008	901	4644	1044	4853	1091	10.49	1.03	.83	4862	1093	1.04
-15			4884	1098							1.01			
-21			4670	1050							.96			
-29			4715	1060							.97			
-30			4635	1042							.96			
-31			3941	886							.81			
-32			4270	960							.88			
-33			5293	1190							1.09			
-34			4670	1050							.96			
-35			5338	1200							1.10			



653217-217

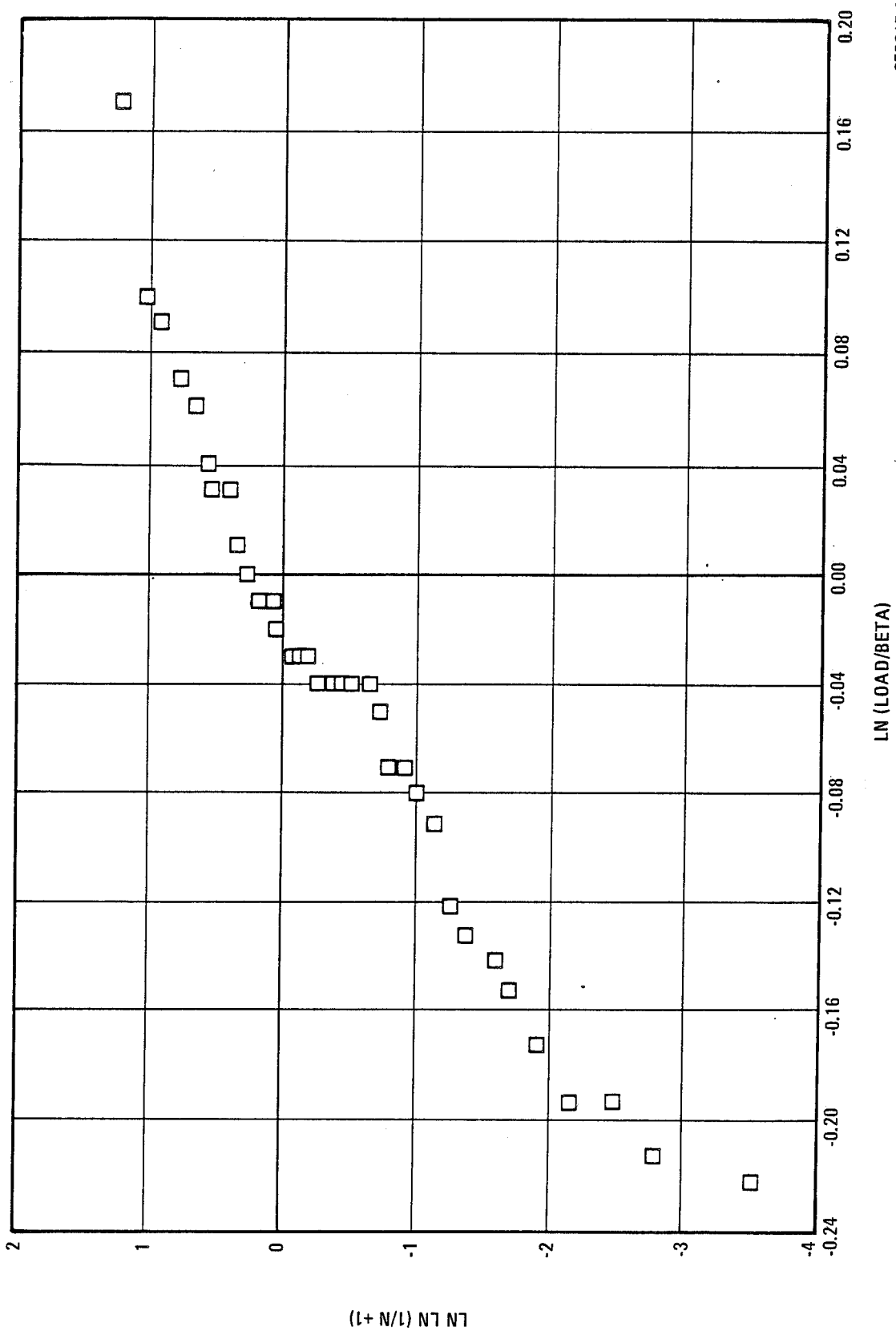
Figure 12-17 Strength Retention of Unnotched $[0^\circ \pm 45^\circ]_s$ G/E at Versus Temperatures

6. Risk factor based on 1% failure rate was then calculated as $f_r = (100)^{-\frac{1}{12.71}} = 0.70$.
7. The temperature retention factor was considered to be 1.0 for this case.
8. The peak load is equal to:

$$0.70 \times 1.0 \times [4684 \text{ N (1053 lb)}] = 3278 \text{ N (737 lb)}$$

Because the tensile specimens were 0.013 m (0.5 in.) wide, the peak load per inch is 6557 N (1474 lb).

In a similar manner the baseline test data for the other composite systems were analyzed for both the notched and unnotched cases. The B/AI data were calculated for unidirectional and crossplied materials. The reduction factors and calculated peak loads are given in Table 12-3.



653217-218

Figure 12-18 Plot of Pooled Data to Get α for G/E

Table 12-3. Summary of Reduction Factors, Loads, and Stresses for Short-Term Tests

Material	Condition			^a Peak Load		^b Landing Load		Peak Stress		Landing Stress		^c One g Stress	
		f_r	f_T	N	(lb)	N	(lb)	MN/m ²	(ksi)	MN/m ²	(ksi)	MN/m ²	(ksi)
B/E	Unnotched	0.79	0.80	6218	1398	-1557	-350	321	46.6	- 80	-11.7	161	23.3
	Notched	.79	.80	3483	783	- 872	-196	248	36.0	- 62	- 9.0	124	18.0
G/E	Unnotched	.70	1.0	6557	1474	-1637	-368	338	49.1	- 85	-12.3	169	24.6
	Notched	.68	1.0	3616	813	- 903	-203	249	36.1	- 62	- 9.0	125	18.1
B/Al	[0°] ₆	.77	.91	2531	5690	-6325	-1422	956	138.8	-239	-34.7	478	69.4
	[0° ± 45°] ₉	.71	.82	8451	1900	-2117	- 476	345	50.0	- 86	-12.5	173	25.0
G/PI	Unnotched	.68	1.0	4946	1112	-1237	- 278	207	30.1	- 52	- 7.5	104	15.1
	Notched	.68	1.0	2593	583	- 649	- 146	141	20.5	- 35	- 5.1	71	10.3

Note: Stresses based on the following thicknesses:

B/E, Unnotched:	0.00076 m (0.030 in.)
B/E, Notched:	.00074 m (.029 in.)
G/E, Unnotched:	.00076 m (.030 in.)
G/E, Notched:	.00076 m (.030 in.)
G/PI, Unnotched:	.00094 m (.036 in.)
G/PI, Notched:	.00089 m (.035 in.)
B/Al, [0°] ₆ :	.00104 m (.041 in.)
B/Al, [0° ± 45°] ₉ :	.00097 m (.038 in.)

^a Peak load = $f_r f_T \beta_{RT}$

^b Landing load is defined as negative 25% of peak load

^c One g stress is defined as 50% of peak stress

12.6.1.3 Test Procedure. Before installing the short-term specimens in the flight simulation apparatus, width and thickness measurements were determined, and the average cross-sectional areas were calculated for each set of 10. These areas were used to obtain the flight simulation stresses and, for specimens that did not fail, to calculate the residual tensile strengths after post-exposure testing. The specimens were then installed in the test machine, thermocouples were attached, the compression stiffening grids were bolted in place, and all resin-matrix specimens were heated to 422 K (300° F) for 24 hours to remove any absorbed moisture. Before starting the tests, each set of 10 specimens was proof loaded to the maximum load value that it would experience during the 100- or 200-hour, short-term exposure.

Once started, the short-term testing of any one set continued uninterrupted until completion unless specimen failure or equipment malfunction occurred. If the test was halted for 24 hours or more, an additional moisture bakeout of four hours was performed on all except the B/Al specimens.

At the completion of the 100- or 200-hour flight simulation exposures, the specimens were removed from the simulator and visually examined with a stereo microscope to check for changes in appearance or the presence of surface flaws such as cracks or delaminations. After the visual examination, the short-term specimens were tensile tested at the same temperatures

at which they had been exposed. Testing was performed in a Tinius-Olson Universal testing machine at a head rate of 0.0013 m (0.05 in.) per minute. Heating of the specimens was accomplished with two ring furnaces that encircled the specimen at the two areas that had been heated during the simulation exposures. This technique was used rather than an environmental chamber to prevent the possibility of premature failures in the doubler adhesive. The two ring furnaces were independently controlled by manually adjusting two power supplies. Temperature was monitored with thermocouples attached to the two test sections. The specimens were heated to the desired test temperature in approximately 10 minutes and then held at temperature for an additional 10 minutes before testing. Temperature was held to ± 3 K (5° F) during both the hold period and while testing. Figure 12-19 shows a specimen in the testing machine with the two ring furnaces in place. If the resin matrix specimens were not tensile tested within 48 hours of completion of the flight simulation exposure, they were given a bakeout treatment at 394 K (250° F) for at least 24 hours to remove any absorbed moisture.

12.6.1.4 Problem Areas. In addition to providing the data necessary to set the load levels for the long-term tests, the short-term test program was also intended to check out the loading facility and the suitability of specimen design and fabrication. Numerous deficiencies in the flight simulation apparatus were detected and corrective measures were taken. Some of the equipment problems included: malfunctioning of solid-state power control switches, voltage transients that interfered with the temperature control circuits, lack of proper safety valves in the hydraulic system, improperly positioned lamps and thermocouples, and intermittent shut-downs of the entire system caused by both electronic and mechanical difficulties with the programming systems. Because of the complexity of the flight simulation apparatus and the extremely long run times involved in the test program, it was not unexpected that equipment malfunctions and component wearouts would occur from time to time.

One problem involving support equipment rather than the simulator was caused by movement of the compression stiffeners (steel grids bolted to the specimens to prevent buckling), see Figure 12-7, during fatigue cycling. These fixtures tended to rotate slightly and/or ride too low on the specimens, leaving an unsupported column of composite approximately 0.0025 m (0.1 in.) long at the top. During the compressive loading portion of the cycle some buckling or bending could occur. It was most noticeable for the unidirectional B/Al where the compressive loads were considerably greater. Spacers were prepared that when inserted between the lower grips and the stiffeners, supported the stiffener, assured that they were centered about the specimen, and greatly reduced the unsupported column of composite material. The spacers also reduced rotation of the stiffeners during fatigue loading. One other problem caused by the compression fixtures was abrasion of the soft B/Al specimens during fatigue cycling (a form of fretting corrosion). The addition of the spacers reduced the relative movement between the stiffener and specimen and, thereby, eliminated much of the wearing. Further reduction in the abrasion of the aluminum surface of the B/Al specimens was accomplished by application of a stratified Teflon coating to the compression stiffeners. By the time these modifications were completed, however, considerable surface abrasion had occurred on the B/Al short-term specimens.

A problem encountered early in the testing of the B/Al short-term specimens was premature failure at the edge of the end doublers caused by undercutting of the B/Al during removal of excess adhesive when fitting the compression stiffeners. The problem was eliminated in the long-term tests by modifying the fabrication procedures. Another problem was a bond failure

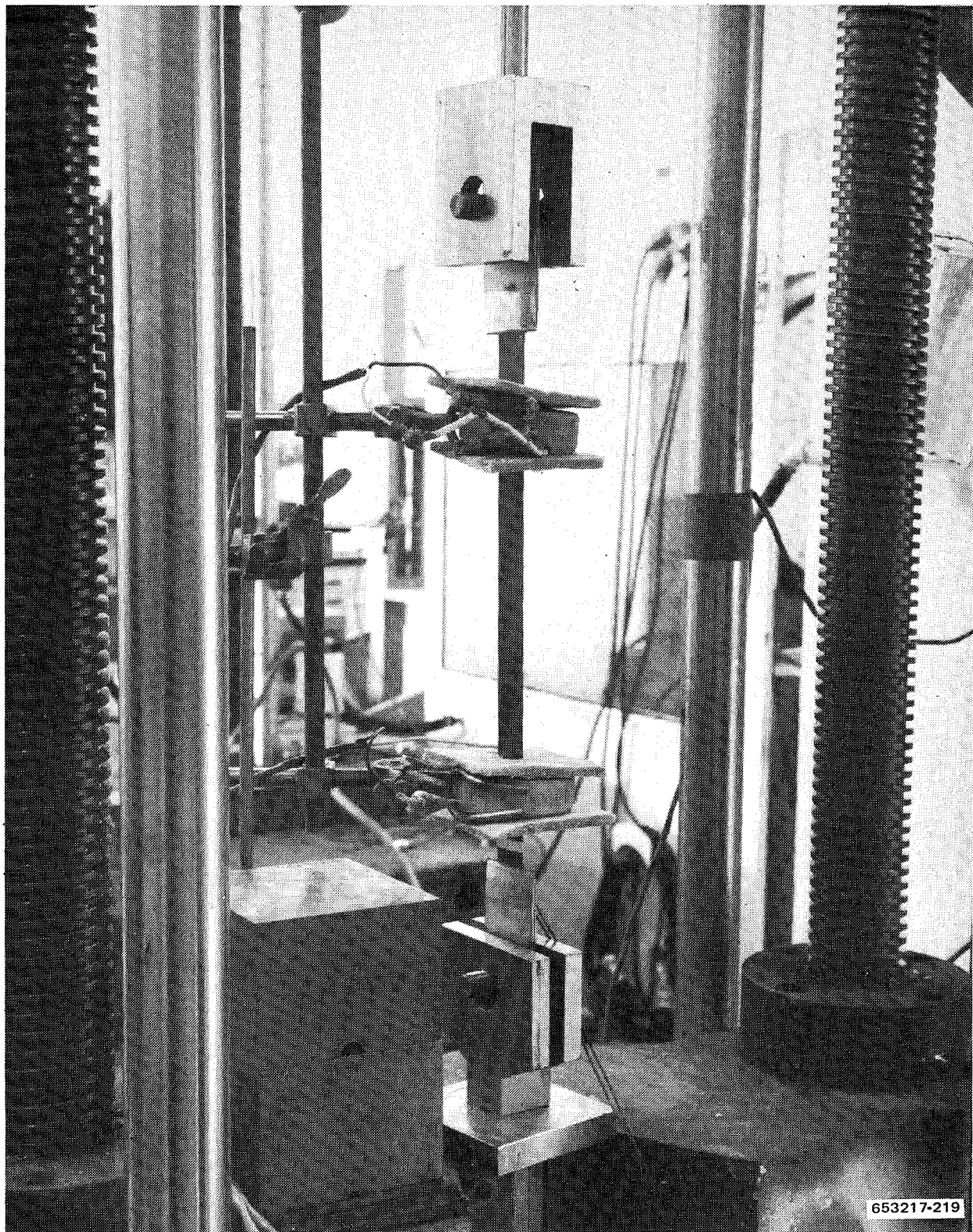


Figure 12-19 Test Setup for Residual Strength Determinations After 100-hr and 200-hr Short-Term Simulation Exposures

at the titanium doublers of the crossply specimens. A solution to this problem was found by installing a Ti-6Al-4V rivet on each end of the specimens through the titanium doublers and the B/Al material. A more difficult problem was the attachment of end doublers to the unidirectional specimens. For these specimens, the test loads were much higher than used for the crossply specimens with correspondingly higher shear stresses at the doublers. For unidirectional specimens, rivets did not solve the problem. Failures occurred in the doublers by shearout of the B/Al behind the rivets. Other techniques that were considered were brazing, diffusion bonding, diffusion braze bonding, spot welding, and mechanical clamping. The method selected was a clamping device on each end of the B/Al unidirectional short-term specimens. The clamp was placed near the tip of the doublers in the tapered portion. To assure uniform contact between the clamps and the doublers, flats were milled on each side at the contact areas. The purpose of the clamps was to increase the normal force reacting on the specimen and to decrease the tendency of the doublers to peel during flight cycle loading. An overall view of a B/Al specimen is shown in Figure 12-20 with a closeup view of the tapered section of the doubler shown in Figure 12-21. This technique proved to be successful for the short-term tests and was also used for the long-term testing of both the crossplied and unidirectional B/Al. Figure 12-7 shows the clamps in use during the long-term tests.

12.6.2 SHORT-TERM TEST RESULTS. Following the short-term flight simulation exposures, all specimens were removed from the test apparatus, examined visually, and then tensile tested for residual strength at the same temperature as was used for the flight simulation tests. The following sections describe the results of these examinations and tensile tests.

12.6.2.1 Post Simulation Examinations

B/E, $[0^\circ \pm 45^\circ]_s$, unnotched, 100 hours. After 100 hours the major change in the specimens was a distinct discoloring in the two heated zones of each specimen. These color changes were very

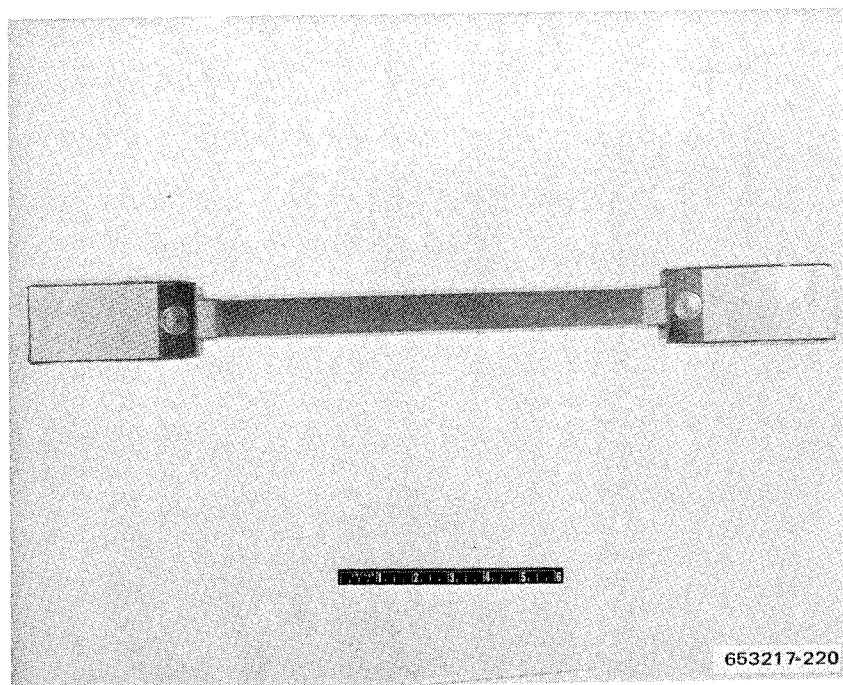


Figure 12-20 Overall View of B/Al Short-Term Specimen with Flats Milled in Titanium Doublers for Clamps

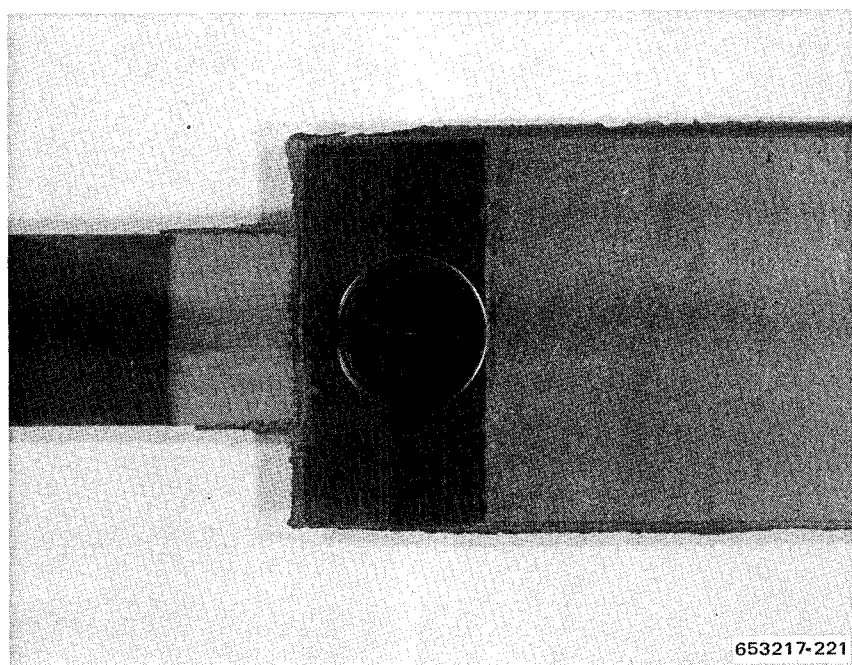


Figure 12-21 Closeup-View of Tapered Section of Titanium Doubler Showing Flat Area for Attaching Clamp

similar to those observed during the thermal aging tests at 450 K (350° F) and, hence, were considered normal for these exposure conditions. A slight amount of surface damage in the areas where the compression stiffeners supported the specimens was visible. No fibers were damaged, however, and the effect on the residual tensile properties was considered to be negligible.

B/E, $[0^\circ \pm 45^\circ]_s$, unnotched, 200 hours. The added 100 hours of flight simulation exposure did not change the appearance of these specimens from that described above.

B/E $[0^\circ \pm 45^\circ]_s$, notched 100 hours and 200 hours. The overall appearance of the notched specimens was identical to the unnotched samples previously discussed. In the vicinity of the notches, 0.0064 m (0.25 in.) diameter holes in the center of the heated areas, no apparent damage was visible. In machining these notches, by drilling with a diamond tool, a very small amount of chipping occurred on the back side of each hole. Small portions of some of the boron filaments were broken off, and several of the filaments were exposed where the epoxy matrix had been removed. No degradation of either the exposed filaments or the matrix was visible after the 100- or 200-hour exposures.

G/E, $[0^\circ \pm 45^\circ]_s$, unnotched, 100 hours. Seven of the 10 specimens in this group survived the 100 hours of exposure. Discoloration in the heated areas was not as noticeable as for the B/E specimens and, again, was quite similar to that found during thermal aging of G/E at 450 K (350° F). Only one of the seven specimens (BC84-7) experienced any visible damage. In this specimen, a small crack was found in the outer 0° ply in one of the heated areas. This crack and

delamination of the outer ply is shown in Figure 12-22, an edge view of the specimen. Also visible in the photo is a crack that passes through the second, third, and fourth plies and extends for several mm between the fourth and fifth plies. The effect of this flaw on the residual tensile strength, however, was minor (see Section 12.6.2.2, Table 12-6).

Three of the specimens in this set failed during the flight simulation exposure, one in 10.6 hours and the other two both at 54.2 hours. The first, BC84-6, is shown in Figure 12-23. While three breaks occurred along the length of the specimen, it is thought that the failure initiated in the heated zone. Multiple fractures of this type are common to these long specimens. This is especially true when failed in a "soft" test machine with the sudden release of a large amount of stored energy. The second specimen (BC84-2, 54.2 hours) also failed in one of the heated areas and was also a fatigue failure.

This specimen was of interest in that a crack had also formed at the other heated area but did not propagate sufficiently to fail the specimen at that location. An edge view of this crack is shown in Figure 12-24. The crack, while not deep, has extended through all six plies. Some delamination of the outer layers is also evident.

The third specimen (BC84-1, 54.2 hours), which was in the same set of two as BC84-2, failed in the doubler. Although it has been established that no transfer of load from a failed specimen to an adjacent one occurs, the failure of BC84-2 is thought to have been responsible in some unknown way for the apparently simultaneous failure of BC84-1. The time of failure and location of fracture make it improbable that this was a true random fatigue failure. Hence, this specimen was discounted in the data analysis.

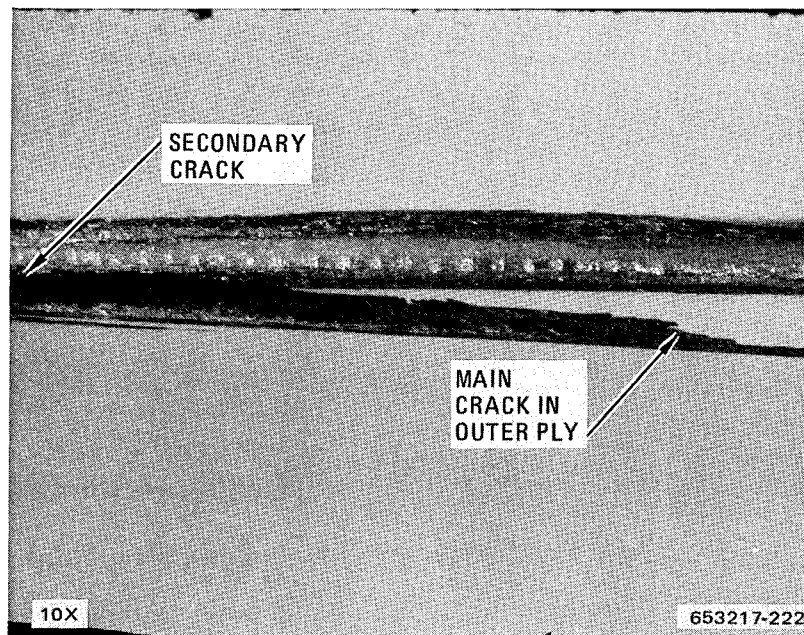


Figure 12-22 Edge Crack and Delamination in Specimen BC84-7, G/E, Unnotched, After 100-hr Simulation Exposure at 422 K (300° F)

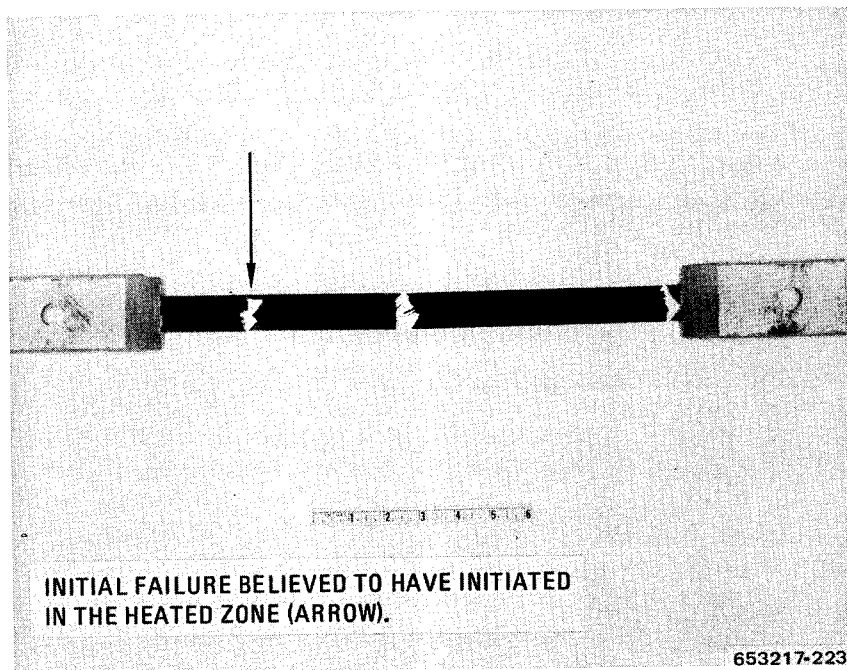


Figure 12-23 Specimen BC84-6, G/E, Unnotched

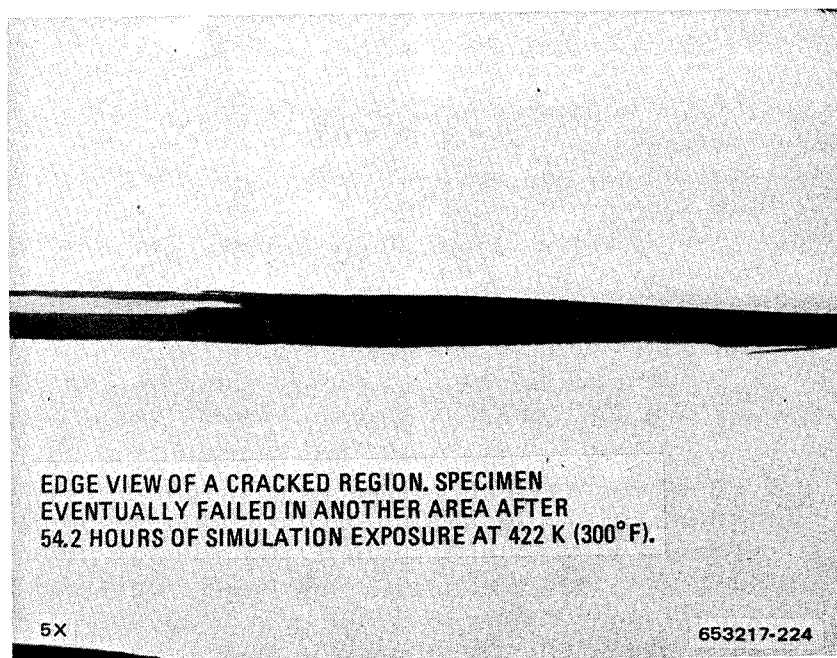


Figure 12-24 Specimen BC84-2, G/E, Unnotched

G/E $[0^\circ \pm 45^\circ]_s$, unnotched, 200 hours. These 10 specimens completed 200 hours with no failures. The specimens experienced color changes similar to the others of this system and minor abrasion from the compression stiffeners. No edge cracks were found except for some slight splintering of the outer plies in several of the specimens. These effects were small and were observed only at the edges.

G/E $[0^\circ \pm 45^\circ]_s$, notched, 100 hours. These 10 specimens completed 100 hours with no failures. The specimens experienced color changes similar to the unnotched specimens and minor abrasion from the compression stiffeners. Minor cracking of the inner surface of several of the holes was visible. With the exception of one specimen, these cracks were very shallow and did not appear to be very significant. The exception was specimen BF84-8, which contained a crack in the outer one or two plies extending from one of the holes for approximately 0.0025 m (0.1 in.). Figure 12-25 shows the location and extent of the crack on the surface of the specimen while Figure 12-26 shows the crack extending into the inner surface of the hole. Smaller branch cracks are also visible in the two middle plies. An overall view of this specimen is shown in Figure 12-27.

G/E, $[0^\circ \pm 45^\circ]_s$, notched, 200 hours. These specimens, all of which completed 200 hours, were very similar in appearance to the previous group. The only difference was at the inner surface of the holes. After 200 hours, the number of fine cracks was increased over that observed for the 100 hour specimens. These cracks were still small and quite shallow, however. These cracks, which were found in about half of the specimens, did not seem to influence the residual tensile properties.

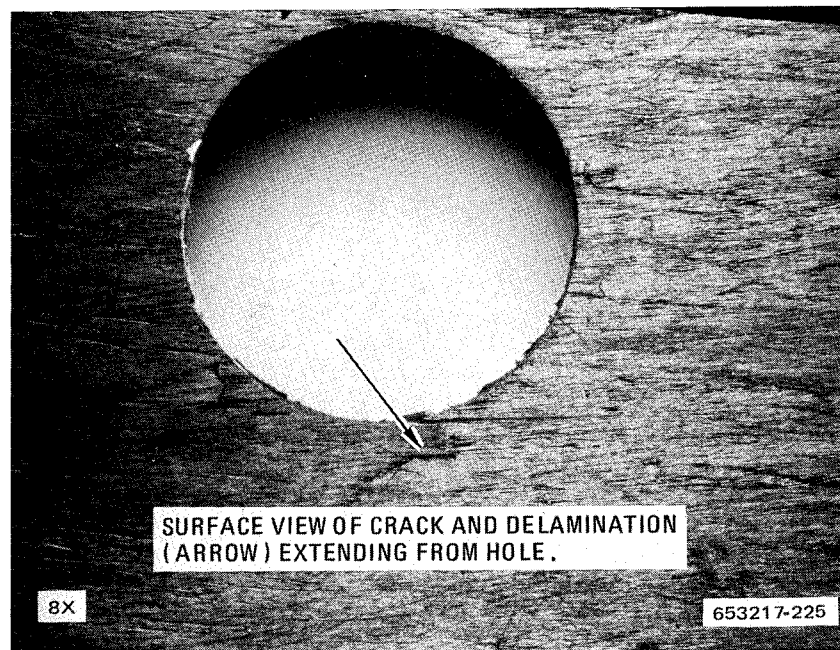


Figure 12-25 Specimen BF84-8, G/E, Notched, After 100-hr Simulation Exposure at 422 K (300° F)

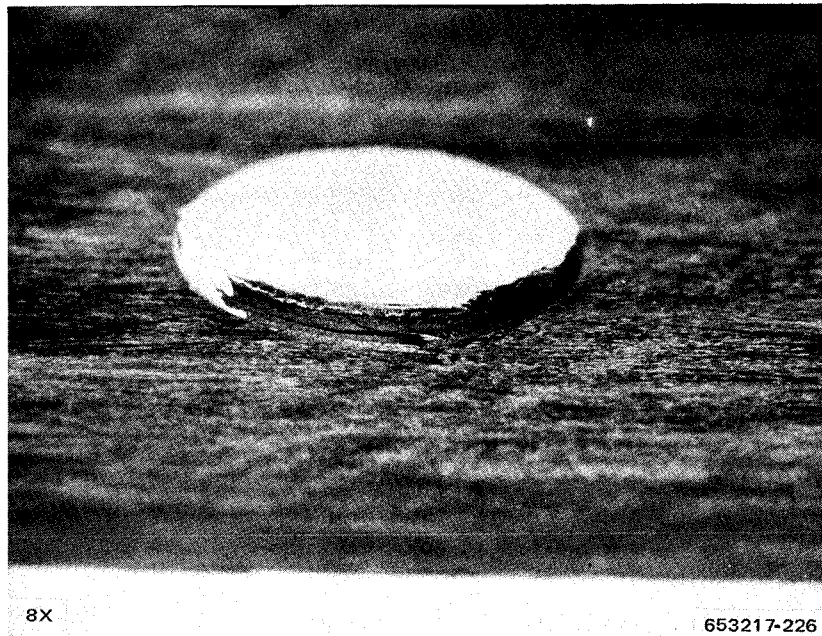


Figure 12-26 View of Main Crack and Several Branch Cracks at Edge of Hole in Specimen BF84-8, G/E, Notched, After 100-hr Simulation Exposure at 422 K (300° F)

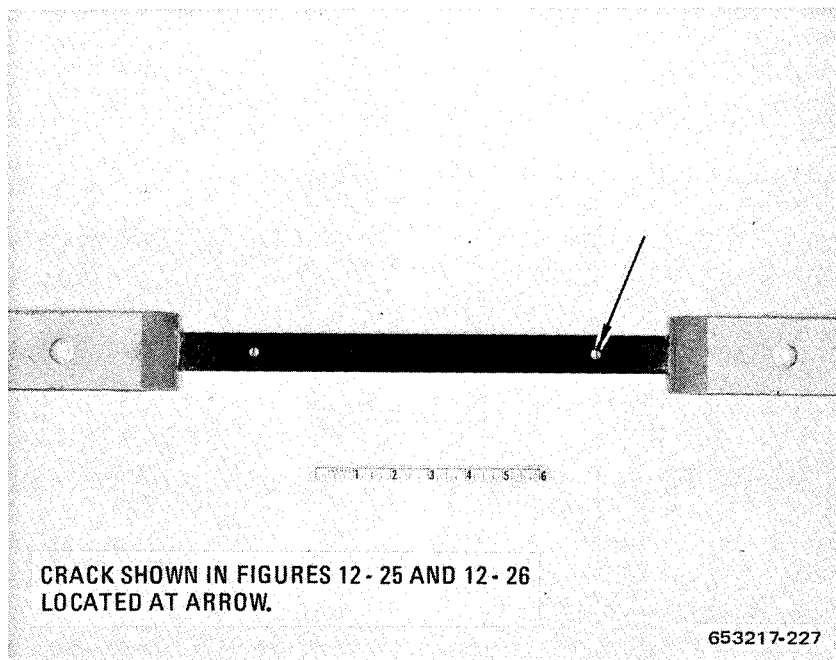


Figure 12-27 Overall View of Specimen BF84-8, G/E, Notched After 100-hr Simulation Exposure at 422 K (300° F)

B/Al, $[0^\circ \pm 45^\circ]_s$, unnotched, 100 hours. Examination of these specimens with a stereo microscope revealed the presence of numerous transverse cracks in the B/Al in the regions adjacent to the end doublers. These cracks were found in seven of the 10 specimens of this group. Figure 12-28 is an enlargement of the flawed area in one of these specimens. All of the transverse cracks were located in regions that had been undercut during the process of removing excess adhesive that had flowed from under the titanium end doublers during bonding. It was necessary to remove this adhesive so that the compression fixtures would fit securely to the test section between the doublers. The combination of a very hard adhesive and soft annealed aluminum led to the problem. Also, only about 0.00001 m (0.0004 in.) of aluminum covers the first layer of boron filaments, so that very little abrasion was required before exposing the boron filaments. The consequences of the undercutting of the specimens with the attendant transverse cracking were twofold. Examination of the specimen (EC84-9) that broke after 65.4 hours of exposure suggests that failure was premature and was caused by the growth of these transverse cracks in an abraded region. This is readily apparent from a comparison of the failed edge of specimen EC84-9 (Figure 12-29) with the transverse cracks shown in Figure 12-28. The second consequence of these transverse cracks was that residual strength testing of the exposed specimens in their present condition would probably be of little value because of the likelihood of premature failure of at least seven of the samples (those that were cracked). Therefore, rather than test the full size specimens, subsize coupons 0.013 m (0.5 in.) by 0.15 m (6 in.) were cut from an area adjacent to the end doublers, one from each short-term specimen. Figure 12-30 is a sketch showing the details of how the subsize specimens were prepared. Note that half of the heated test section is covered by one of the doublers on the subsize specimen. Cutting of the residual strength coupons in this manner had the advantage that they could be taken from undamaged areas of the short-term specimens. Several specimens showed surface damage where the compression stiffeners had been clamped. Again it was the low abrasion resistance of the soft aluminum that contributed to this surface damage.

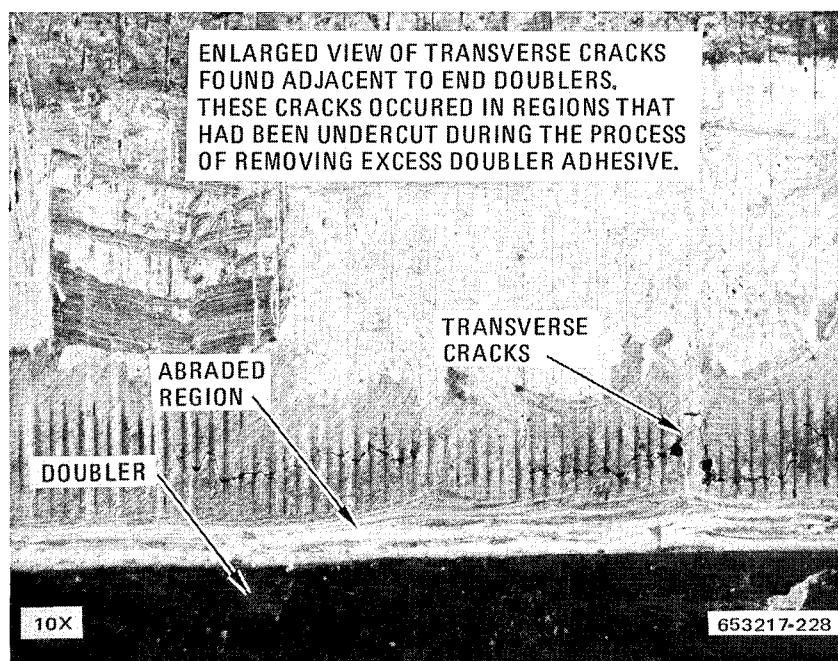


Figure 12-28 Specimen EC84-4, B/Al, Crossply, After 100-hr Simulation Exposure at 505 K (450° F)

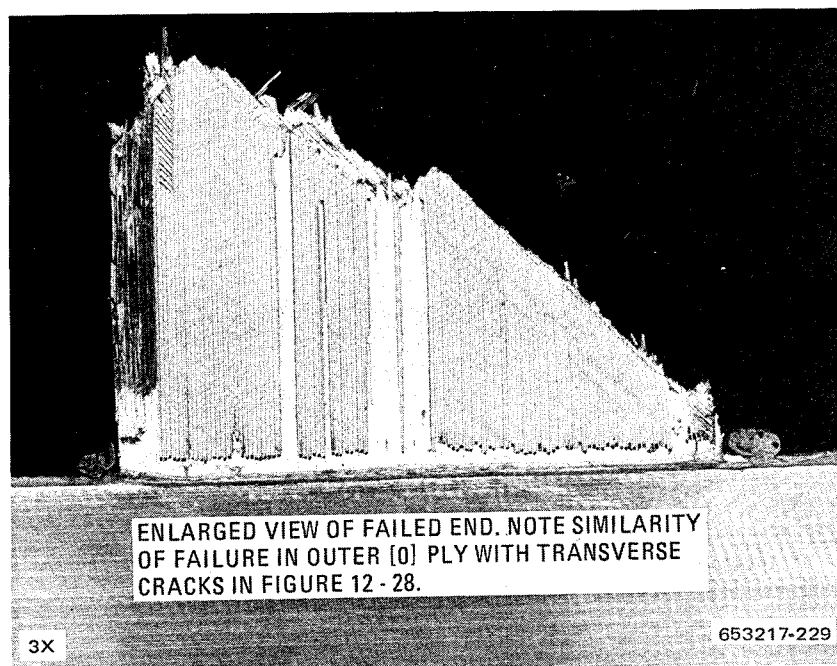
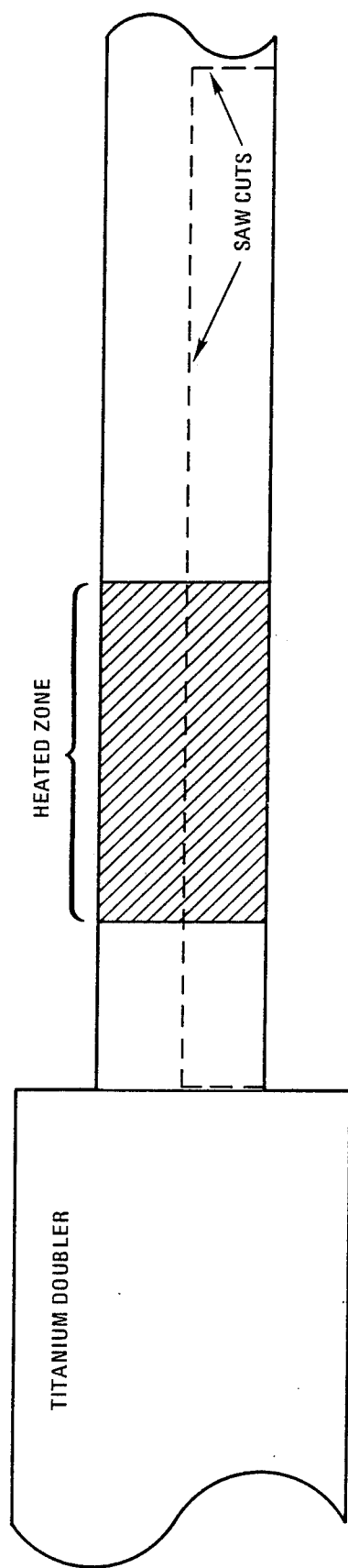


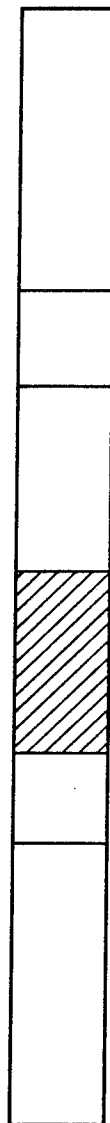
Figure 12-29 Specimen EC84-9, B/Al, Crossply, Which Failed After 65.4 hr of Simulation Exposure at 505 K (450° F)

B/Al, $[0^\circ \pm 45^\circ]$, unnotched, 200 hours. During the first 100 hours of exposure, doubler bond failures were experienced on five of the specimens. At the end of 100 hours, all specimens were removed from the apparatus, new doublers were attached where bond failures had occurred, and rivets were installed in the doublers of all 10 specimens. No more bond failures were observed during the remainder of the test. Four specimens did fail in the B/Al, however, before completing 200 hours of exposure. All four failed at the same time (one with 105 hours of test time and three with 136 hours). Three failed in the heated zones, and the fourth specimen failed about 0.008 m (0.3 in) from a doubler. Failure undoubtedly occurred during a very high load portion of the random load spectrum, but the probability of four true fatigue failures occurring simultaneously is quite small. All four specimens had abraded regions at the site of the fractures. Of these, three appeared to have been severe enough to possibly have initiated the fracture. Figure 12-31 shows one of these specimens. Fracture occurred 45° to the length of the specimen except in the region of the abrasion. Test coupons were cut from the heated areas of these specimens at the ends away from the fractures.

The remaining six specimens completed 200 hours without failures. Examination of these specimens with a stereo microscope revealed the wear marks caused by the relative motion of the specimens and compression stiffeners. This is a type of fretting corrosion that in aluminum is generally accompanied by a black powdery residue of aluminum oxide. The effect is clearly visible in Figure 12-31. Also noticeable on the specimens were numerous surface cracks located in the heated zones. An example of these cracks is shown in Figure 12-32. In all cases, these longitudinal cracks extend from regions where one or more of the outer layer boron fibers have fractured. Although not observed during the original examination, a recheck of the 100-hour,



(a) SHORT-TERM SPECIMEN



(b) SUBSIZE TENSILE SPECIMEN



653217-230

Figure 12-30 Cutting Plan for Obtaining Subsize Residual Strength Coupons from the B/Al Short-Term Specimens

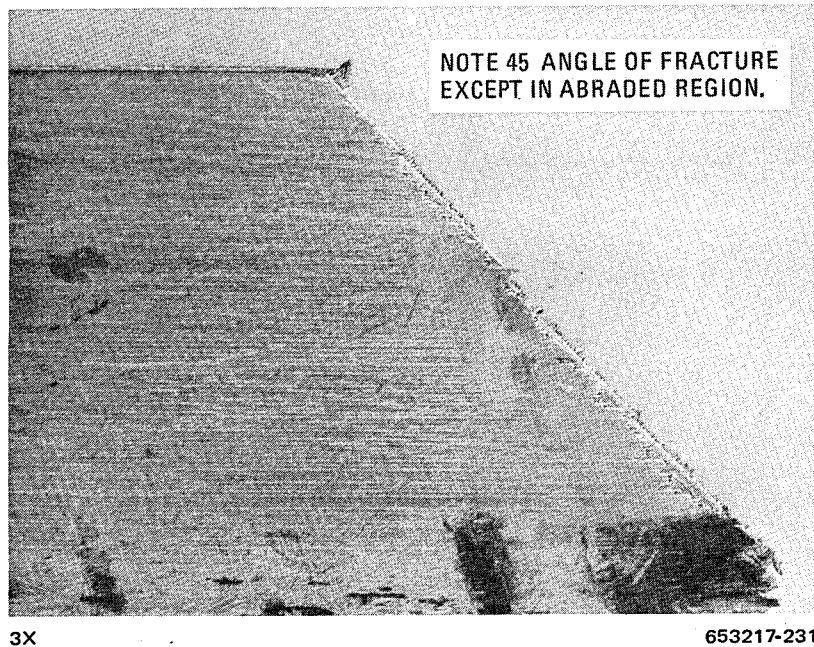


Figure 12-31 Enlarged View of Failed End of Specimen EC82-7, B/Al, Crossply, Which Failed After 135.8 hr of Simulation Exposure at 505 K (450° F)



Figure 12-32 Enlarged View of Surface Cracks Found in Heated Zones of B/Al Crossply Specimens After 200 hr of Simulation Exposure at 505 K (450° F), Specimen EC82-3

short-term specimens also revealed cracks of this type. For the 10 specimens, however, only two very small cracks were found. Apparently, the approximate time period required to form these cracks was between 100 and 200 hours. Similar surface cracking was observed during constant amplitude fatigue testing of B/Al at 561 K (550° F). The surface roughness seen on the fatigue specimens was not present on the short term specimens, however. For the few constant amplitude fatigue tests performed at 505 K (450° F) (same temperature as used for short-term tests), surface roughness was also not observed.

B/Al, [0°]₆, unnotched, 100 and 200 hours. Considerable difficulty was experienced during short-term testing of the unidirectional B/Al specimens. The major problem involved shear failures in the doubler bonds. These failures generally occurred at the upper bonds where test temperatures reached slightly higher values (406 K (270° F) maximum versus 372 K (210° F) maximum at the lower bond). The doubler bond failures were the result of the considerably higher loads required for the unidirectional material than were required for the crossplied B/Al specimens. These high loads, in combination with several other factors, also led to numerous failures in the B/Al. These included:

- a. Failures in the B/Al very close to the edge of the doublers. At the bottom end, these failures were initiated by the stiffening grids gouging into the soft aluminum during the compression load. Additional failures occurred at regions that had been undercut during the process of removing excess adhesive that had flowed from under the titanium end doublers during bonding. These failures occurred during the high tensile loads.
- b. The compression stiffening grids could ride too low on the specimens, leaving an unsupported column of B/Al approximately 0.0025 m (0.1 in.) long. During the compressive load, some buckling could occur. In severe cases, longitudinal splitting and/or failure occurred.
- c. Specimens that were riveted to increase doubler reliability all failed in the doublers by shearout of the B/Al behind the rivets.
- d. Abrasion of the soft aluminum surface of the specimens with eventual breakage of the underlying boron fibers was caused by movement of the stiffening grids during fatigue cycling. These damaged regions could ultimately initiate failure.

One of the objectives of the short-term tests was to uncover these testing problems and devise solutions prior to the start of the 50,000-hour, long-term test program. The mechanical clamping technique discussed earlier provided a very noticeable improvement in doubler bond reliability. Spacers inserted between the lower grips and compression stiffeners greatly decreased the unsupported column of B/Al and in turn reduced the incidence of compressive buckling failures. The combination of these spacers and the Teflon coating on the stiffeners significantly reduced the fretting fatigue abrasion of the soft aluminum surface of the B/Al specimens.

Because of these testing difficulties, the number of specimens that survived the 100- and 200-hour short-term exposures was less than originally planned. Nine specimens with 100 hours and six with 200 hours were available for residual strength testing. Several of the specimens were close to failure at one end as a result of small buckles. Many specimens also exhibited damage in the form of wear marks from stiffener abrasion and surface cracks and edge delaminations. It was possible, however, to cut subsize coupons, 0.013 m (0.5 in.) by 0.15

m (6 in.), from good areas of each of the short-term specimens as shown previously in Figure 12-30. The surface cracks were much less pronounced in the unidirectional specimens than observed in the 200-hour crossply specimens. Again no surface roughening similar to that found after fatigue testing at 516 K (550° F) was seen on the unidirectional short-term specimens.

G/PI, $[0^\circ \pm 45^\circ]_s$, unnotched, 100 hours. In like manner to the unidirectional B/Al, the number of unnotched G/PI short-term specimens was somewhat less than originally planned. The reasons for this were twofold:

- a. During proof loading of the G/PI system, nine of the unnotched specimens failed. These specimens, however, failed in a manner similar in appearance to the baseline tensile specimens. The reason for the premature failures was thought to be either: 1) an error in the applied load, or 2) lower than expected material strength. The first reason seemed unlikely as three independent strain measuring systems were used to monitor the loads. However, as a further check, 10 strain gaged dummy specimens of aluminum were installed in the flight simulation apparatus. Load checks in the region of interest indicated that the total applied load and the 10 individual loads were in agreement for all the measuring systems. To check the tensile properties of the panel (LRC-59) from which the short-term specimens were cut, two specimens were obtained from the small piece remaining from the panel. Several additional tensiles were also cut from the failed short-term specimens. These were then tensile tested at 505 K (450° F) using both a normal loading rate, 0.0013 m (0.05 in.) per minute, and a rate similar to that used during the proof test. The results, which were independent of load rate, showed the short-term panel to have an average tensile strength about 69 MN/m² (10 ksi) lower than the panel from which the baseline data were obtained. This same 69 MN/m² (10 ksi) lower value was found for the panel (LRC-60) that supplied the notched short-term specimens. Using the data from panels LRC-59 and 60 and that from additional specimens cut from the short-term specimens that had failed during the proof test, revised short-term loads were determined and testing was begun. However, because of the loss of the specimens during the first proof test, only seven specimens each were available for the 100-hour and 200-hour unnotched short-term exposures. No notched short-term specimens had failed so that full sets of 10 were available for the 100-hour and 200-hour time periods.
- b. During the short-term testing of the G/PI specimens, almost all the 200-hour unnotched specimens were failed during a compressive overload. The accident occurred as the result of an operator error when an incorrect hydraulic valve was opened. Testing was interrupted while seven additional specimens were fabricated from spare material. Again a full set of specimens could not be prepared because of a lack of extra material. Just before completing the short-term tests, another compressive overload occurred. This incident resulted in four additional specimen failures, three unnotched and one notched. The cause of the overload was traced to the load programmer. The malfunction, which could have occurred later during long-term testing, was corrected. Again, one objective of the short-term test program was to uncover the problems and equipment deficiencies that, if not found, could be very costly during the long-term test program.

The five unnotched specimens of this group completed the 100 hours of exposure with almost no change in color or surface texture. There was a slight amount of surface damage on four of

the specimens from the stiffening grids, but this was not believed to have had any effect on residual tensile properties. All of the specimens showed slight edge cracking, generally in the heated regions or near the doublers. A typical example can be seen in Figure 12-33. Again, these edge cracks probably did not affect the residual tensile strength, although in a compression or shear test they likely would have been important.

G/PI, $[0^\circ \pm 45^\circ]_s$, unnotched, 200 hours. The added 100 hours of flight simulation exposure did not change the appearance of these specimens from that described above.

G/PI, $[0^\circ \pm 45^\circ]_s$, notched, 100 hours and 200 hours. The overall appearance of the notched specimens was identical to the unnotched specimens previously discussed. Slight surface damage from the stiffening grids and shallow edge cracks were visible on most of the specimens. Figure 12-34 shows an edge view of one of the edge cracked specimens. During residual strength testing, failure occurred at the hole in this notched specimen approximately 0.004 m (1.6 in.) from the edge crack. Two of the 200-hour specimens also showed slight cracks at the holes. The cracks were small and were not thought to have been a factor during residual strength testing.

12.6.2.2 Residual Tensile Strength Data. Following the examination of the 100-hour and 200-hour short-term flight simulation specimens, residual tensile strength tests were conducted. These tensile tests were made at the same temperatures as the simulation exposures, 422 K (300° F) for the B/E and G/E systems and 505 K (450° F) for both the G/PI and B/Al materials. Full sets of residual strength data were obtained for the epoxies except for the

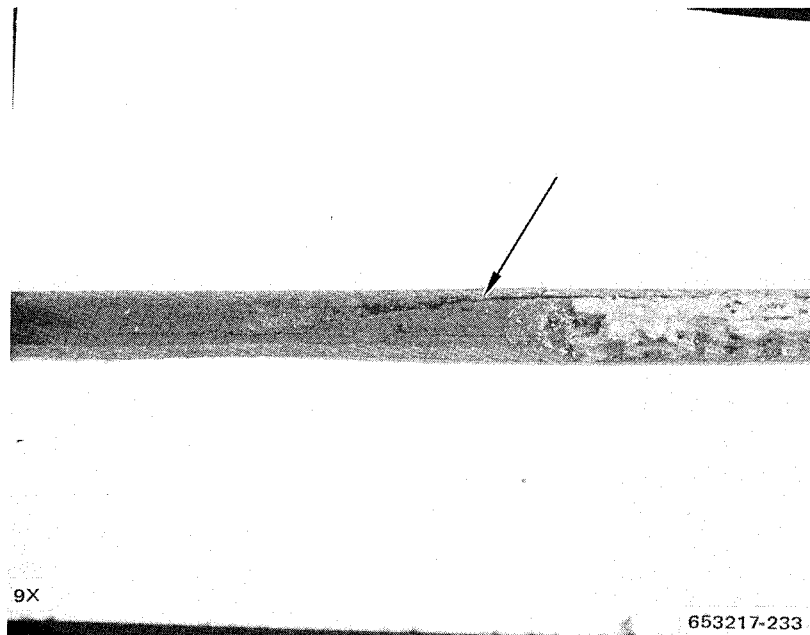


Figure 12-33 Edge Cracking (arrow) in Specimen DC82-5, G/PI, Unnotched, After 100-hr Simulation Exposure at 505 K (450° F)

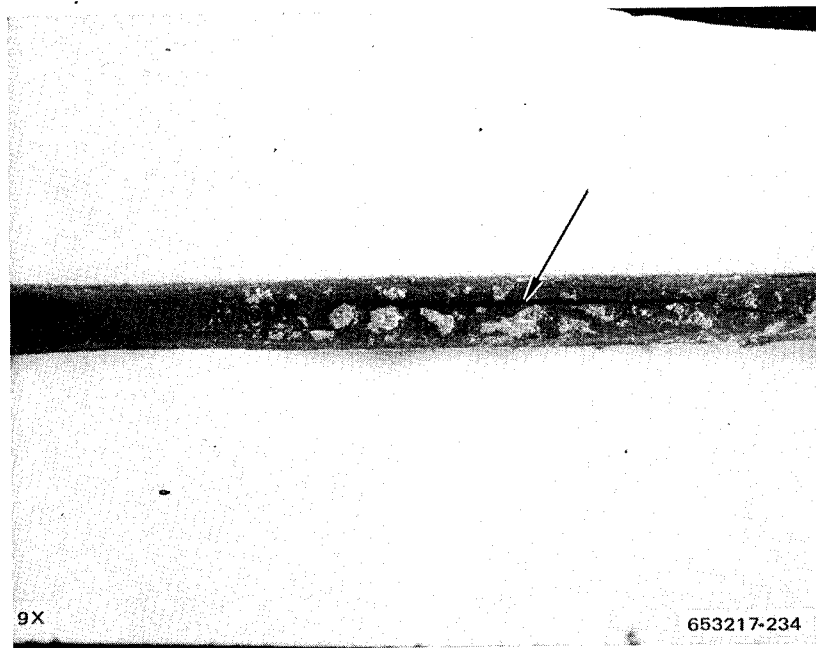


Figure 12-34 Edge Cracking (arrow) in Specimen DF81-5, G/PI, Notched, After 100-hr Simulation Exposure at 505 K (450° F)

100-hour unnotched G/E where three simulation failures occurred. Only partial sets of data were available from the G/PI and B/Al systems because of the numerous testing and material problems previously discussed in Section 12.6.2.1. The test results, both tensile strengths and failure loads, are given in Tables 12-4 and 12-5 for B/E, Tables 12-6 and 12-7 for G/E, Tables 12-8 and 12-9 for G/PI, and Tables 12-10 and 12-11 for B/Al. The widths of the unnotched resin matrix specimens were 0.025 m (1.0 in.). The notched specimens were also 0.025 m (1.0 in.) wide but with 0.0064 m (0.25 in.) diameter holes. All the B/Al residual strength specimens were 0.013 m (0.50 in.) in width.

Table 12-4. Short-Term Residual Strength Data, $[0^\circ \pm 45^\circ]_S$, B/E, Unnotched, Exposed at 422 K (300° F) and Tensile Tested at 422 K (300° F)

Specimen Number	Exposure Time (hr)	Load		Tensile Strength		
		kN	(kip)	MN/m ²	(ksi)	
AC82-1	100	10.7	2.415	541	78.4	
-2	100	10.7	2.405	553	80.2	
-3	100	10.7	2.410	552	80.1	
-4	100	8.94	2.010	474	68.8	
-5	100	9.83	2.210	523	75.9	
-6	100	9.65	2.170	502	72.8	
-7	100	10.2	2.300	539	78.2	
-8	100	9.92	2.230	516	74.8	
-9	100	9.90	2.225	518	75.2	
-10	100	10.0	2.250	533	77.3	
		ave	10.1	2.260	525	76.2
AC83-1	200	9.54	2.145	483	70.1	
-2	200	8.01	1.800	405	58.8	
-3	200	8.72	1.960	456	66.2	
-4	200	9.83	2.210	516	74.9	
-5	200	9.65	2.170	502	72.8	
-6	200	9.90	2.225	512	74.2	
-7	200	9.30	2.090	487	70.6	
-8	200	8.45	1.900	443	64.2	
-9	200	9.59	2.155	501	72.6	
-10	200	8.67	1.950	462	67.0	
		ave	9.17	2.060	477	69.1

Table 12-5. Short-Term Residual Strength Data, $[0^\circ \pm 45^\circ]_s$, B/E, Notched, Exposed at 422 K (300° F) and Tensile Tested at 422 K (300° F)

Specimen Number	Exposure Time (hr)	Load		Notched Tensile Strength		
		kN	(kip)	MN/m ²	(ksi)	
AF84-1	100	6.12	1.377	416	(a) 60.4	
-2	100	6.41	1.440	452	65.5	
-3	100	6.32	1.420	445	64.6	
-4	100	6.23	1.400	433	62.8	
-5	100	6.85	1.540	485	70.3	
-6	100	6.04	1.357	427	62.0	
-7	100	6.05	1.360	423	61.3	
-8	100	5.38	1.210	379	55.0	
-9	100	6.36	1.430	446	64.7	
-10	100	6.61	1.485	467	67.8	
		ave	6.24	1.400	437	63.4
AF82-1	200	5.96	1.340	420	60.9	
-2	200	6.49	1.458	451	65.4	
-3	200	5.98	1.345	430	62.3	
-4	200	4.98	1.120	354	51.4	
-5	200	6.32	1.420	471	68.3	
-6	200	6.41	1.440	475	68.9	
-7	200	5.78	1.300	419	60.7	
-8	200	5.78	1.300	419	60.7	
-9	200	5.69	1.280	403	58.4	
-10	200	5.56	1.250	412	59.8	
		ave	5.90	1.330	425	61.7

^a Net section strength, i.e., based on total width less hole diameter.

Table 12-6. Short-Term Residual Strength Data, $[0^\circ \pm 45^\circ]_s$, G/E, Unnotched, Exposed at 422 K (300° F) and Tensile Tested at 422 K (300° F)

Specimen Number	Exposure Time (hr)	Load		Tensile Strength		
		kN	(kip)	MN/m ²	(ksi)	
BC84-1	^a 54.2	—	—	—	—	
-2	^a 54.2	—	—	—	—	
-3	100	7.09	1.595	426	61.8	
-4	100	8.09	1.818	445	64.5	
-5	100	9.34	2.100	492	71.4	
-6	^a 10.6	—	—	—	—	
-7	100	8.94	2.010	^b 465	^b 67.4	
-8	100	11.1	2.499	565	81.9	
-9	100	8.45	1.900	460	66.7	
-10	100	9.96	2.240	501	72.7	
		ave	9.00	2.020	479	69.5
BC81-1	200	10.3	2.325	547	79.4	
-2	200	8.27	1.860	405	58.7	
BC82-3	200	10.0	2.250	552	80.1	
-4	200	9.74	2.190	523	75.8	
-5	200	7.34	1.650	381	55.2	
-6	200	6.56	1.475	365	52.9	
-7	200	9.67	2.175	484	70.2	
-8	200	8.10	1.820	420	60.9	
-9	200	10.1	2.260	516	74.8	
-10	200	9.56	2.150	501	72.6	
		ave	8.96	2.020	469	68.1

^a These specimens failed during flight simulation exposure testing.

^b This specimen had a small crack in the test section after the 100-hr simulation exposure. Failure during tensile testing occurred at this location.

Table 12-7. Short-Term Residual Strength Data, $[0^\circ \pm 45^\circ]_s$, G/E, Notched, Exposed at 422 K (300° F) and Tensile Tested at 422 K (300° F)

Specimen Number	Exposure Time (hr)	Load		Notched Tensile Strength		
		kN	(kip)	MN/m ²	(ksi)	
(a)						
BF84-1	100	5.69	1.280	403	58.4	
-2	100	5.36	1.205	405	58.8	
-3	100	6.05	1.360	439	63.6	
-4	100	5.60	1.260	412	59.7	
-5	100	6.29	1.415	434	62.9	
-6	100	6.05	1.360	424	61.5	
-7	100	6.29	1.415	436	63.2	
-9	100	5.78	1.300	425	61.6	
-10	100	6.00	1.350	450	65.2	
		ave	5.90	1.330	425	61.7
BF82-1	200	5.69	1.280	392	56.9	
-2	200	4.98	1.120	367	53.3	
-3	200	5.20	1.170	414	60.0	
-4	200	5.87	1.320	444	64.4	
-5	200	6.16	1.385	452	65.6	
-6	200	5.65	1.270	438	63.5	
-7	200	5.43	1.220	429	62.2	
-8	200	5.69	1.280	465	67.4	
-9	200	5.38	1.210	394	57.1	
-10	200	4.17	.937	343	49.8	
		ave	5.42	1.220	414	60.0

^a Net section strength, i.e., based on total width less hole diameter.

Table 12-8. Short-Term Residual Strength Data, $[0^\circ \pm 45^\circ]_s$, G/PI, Unnotched, Exposed at 505 K (450° F) and Tensile Tested at 505 K (450° F)

Specimen Number	Exposure Time (hr)	Load		Tensile Strength		
		kN	(kip)	MN/m ²	(ksi)	
DC81-12	100	8.12	1.825	402	58.3	
DC82-5	100	7.83	1.760	395	57.3	
-9	100	7.41	1.665	425	61.7	
-10	100	7.34	1.650	388	56.3	
-12	100	8.32	1.870	393	57.0	
		ave	7.80	1.750	401	58.1
DC85-2	200	7.03	1.580	316	45.9	
-4	200	7.34	1.650	339	49.1	
-5	200	7.58	1.705	384	55.7	
-7	200	7.03	1.580	348	50.5	
-9	200	7.90	1.775	426	61.8	
-10	200	7.72	1.735	368	53.4	
		ave	7.43	1.670	364	52.7

Table 12-9. Short-Term Residual Strength Data, $[0^\circ \pm 45^\circ]_s$, G/PI, Notched, Exposed at 505 K (450° F) and Tensile Tested at 505 K (450° F)

Specimen Number	Exposure Time (hr)	Load		Tensile Strength		
		kN	(kip)	MN/m ²	(ksi)	
(a)						
DF81-1	100	4.11	0.925	241	34.9	
-2	100	4.83	1.085	301	43.7	
-3	100	4.89	1.100	295	42.8	
-4	100	4.07	.915	240	34.8	
-5	100	5.38	1.210	325	47.1	
-6	100	4.71	1.060	294	42.6	
-7	100	4.29	.965	266	38.6	
-8	100	4.56	1.025	285	41.3	
-9	100	4.67	1.050	286	41.5	
-10	100	3.83	.860	234	34.0	
		ave	4.53	1.020	277	40.1
DF82-1	200	5.11	1.148	319	46.3	
-2	200	3.91	.880	236	34.2	
-3	200	5.60	1.260	328	47.6	
-4	200	4.20	.945	247	35.8	
-5	200	4.91	1.104	305	44.2	
-7	200	4.50	1.012	265	38.5	
-8	200	4.92	1.105	308	44.6	
-9	200	4.78	1.075	295	42.8	
-10	200	5.27	1.185	311	45.1	
		ave	4.80	1.080	290	42.1

^a Net section strength, i.e., based on total width less hole diameter.

Table 12-10. Short-Term Residual Strength Data, $[0^\circ \pm 45^\circ]_s$, B/Al, Unnotched, Exposed at 505 K (450° F) and Tensile Tested at 505 K (450° F)

Specimen Number	Exposure Time (hr)	Load		Tensile Strength	
		kN	(kip)	MN/m ²	(ksi)
EC84-1	100	7.56	1.700	604	87.6
-2	100	7.12	1.600	566	82.1
-3	100	7.34	1.650	574	83.3
-4	100	7.21	1.620	561	81.4
-5	100	5.78	1.300	457	66.3
-6	100	7.29	1.640	580	84.1
-7	100	6.56	1.475	519	75.3
-8	100	6.14	1.380	471	68.3
-9	^a 65.4	—	—	—	—
-10	100	7.07	1.590	556	80.7
		ave	6.90	543	78.8
EC82-1	^a 105	6.20	1.395	509	73.8
-2	^a 136	5.27	1.185	415	60.2
-3	200	5.12	1.150	401	58.1
-4	200	5.43	1.220	423	61.3
-5	200	5.72	1.285	434	63.0
-6	200	6.52	1.465	507	73.6
-7	^a 136	4.94	1.110	383	55.5
-8	200	4.25	.955	323	46.8
-9	200	4.49	1.010	348	50.5
-10	^a 136	6.83	1.535	521	75.6
		ave	5.48	426	61.8

^a These specimens failed during flight simulation exposure testing.

Table 12-11. Short-Term Residual Strength Data, $[0^\circ]_6$ B/Al, Unnotched, Exposed at 505 K (450° F) and Tensile Tested at 505 K (450° F)

Specimen Number	Exposure Time (hr)	Load		Tensile Strength	
		kN	(kip)	MN/m ²	(ksi)
EU85-1	100	17.6	3.950	1460	211
-3	100	19.0	4.280	1610	233
-6	100	17.8	4.010	1490	216
-9	100	17.3	3.900	1410	205
EU86-3	100	17.3	3.900	1390	201
-6	100	18.0	4.050	1550	225
EU87-11	100	21.8	4.910	1560	226
-12	100	21.7	4.880	1560	227
-14	100	12.5	2.820	882	128
	ave	18.1	4.080	1430	208
EU87-1	200	21.1	4.750	1460	211
-2	200	21.5	4.850	1520	221
-5	200	20.5	4.600	1450	210
-6	200	21.3	4.780	1520	221
-7	200	23.0	5.180	1630	236
-8	200	20.9	4.700	1480	214
	ave	21.4	4.810	1510	219

12.6.3 SHORT-TERM ANALYSIS. Using the residual strength measurements from Section 12.6.2 and the baseline data from Section 7.1.2, the peak loads for the long-term, real-time flight simulation tests were calculated. The wearout model equations discussed previously in Section 12.5 were programmed into a desk top computer (HP9830) to calculate the parameters r , A_4 , α_f , and β_f starting with α_0 , β_0 , and the short-term residual strength data. The results for G/E and B/E are listed in Table 12-12. For G/PI and B/Al the wearout model was not successful (to be discussed later). Since the long-term specimens were three times as wide as the short-term specimens they were expected to exhibit a reduced static strength. This expectation was based on the increase in complexity (least of three identical specimens). The strength reduction can also be thought of as a scaling effect since the long-term specimens have three times the stressed volume of the short-term specimens. The expected strength of the long-term specimen

is $\beta_{LT} = f_c \beta_{ST}$ where the scaling factor, $f_c = (3)^{\frac{-1}{\alpha_0}}$ is the penalty for least of three as a function of the shape parameter, α_0 . The values of f_c are listed in Table 12-12.

Table 12-12. Long-Term Model Parameters for B/E and G/E

Material	Condition	α_O	β_O		Short Term Peak Load		β_{LT}				Long Term Peak Load					
			kN/m	(kip/in)	kN/m	(kip/in)	r	A_4	α_f	β_f	f_c	kN/m	(kip/in)	A_1	kN/m	(kip/in)
B/E	Unnotched	19.5	403	2.300	245	1.398	5	131	2.44	1.50	0.95	383	2.185	0.94	230	1.314
	Notched	19.5	254	1.450	137	.783	5	2.77	2.44	1.76	.95	241	1.378	.96	132	.752
G/E	Unnotched	12.71	371	2.120	258	1.474	7	395	1.06	3.47	.92	341	1.950	.90	232	1.325
	Notched	12.03	226	1.288	142	.813	7	.564	1.00	6.16	.91	205	1.172	.93	132	.756

A few other assumptions are necessary to predict the loads applied in the long-term tests to achieve the desired results. The problem is to apply loads high enough to produce measureable effects without failing all specimens in fatigue. A reliability of 0.80 at one lifetime was the desired goal. In other words, one out of five specimens used for the long-term tests would be expected to fail in fatigue prior to the completion of the 50,000 hours of exposure.

One remaining parameter of the wearout model, s , must also be determined. The parameter, s , is the exponent on the stress or load ratio that defines the power law time response to changing loads. This parameter is obtained by subjecting specimens to various magnifications of the random spectrum to obtain a random S-N curve. The slope of the random S-N curve is $-\frac{1}{s}$.

Since no such tests were performed for the current program, s has been estimated from data in reference 41 and 42 to be 11.0. The assumption of s is not felt to be too serious in this case because the loads required for the desired long-term response are not very different from the loads applied in the short-term tests.

To calculate the appropriate A_1 for the desired results, Equations (5) and (7) (Section 12.5) are combined by eliminating β_f to arrive at:

$$A_1 = \left[\frac{\beta_o^{2(r-1)} (-\ln R)^{1/\alpha f}}{(r-1) A_4 t} \right] \frac{1}{s}$$

The results of this calculation are also listed in Table 12-12. Using the model parameters of Table 12-12 and the wearout model equations of Section 12.5 the peak long-term loads were obtained by an iteration process to give 80% survival at one lifetime (50,000 hours). These values are given in Table 12-12.

The computer was used to plot the wearout model curves shown in Figures 12-35 through 12-38 for the unnotched and notched G/E and B/E systems. The horizontal peak load lines have been set for 80% survival at one lifetime.

Wearout model curves could not be plotted for the G/PI and B/Al systems because the wearout model did not work for these materials. In some cases the short-term residual strength value, β , and the shape parameter, α , increased with time. The 200-hour or half lifetime residual strength values were actually higher than the 100-hour or quarter lifetime values, and the spread in the data was decreased. One method initially considered for determining the long-term peak loads for G/PI and B/Al was to take two-thirds of the "A" basis allowable tensile strength value for the particular composite considered. However, it was thought that this method did not place sufficient importance on the shape parameter, α , which for B/Al was higher than for G/PI. The method that was used was to essentially reapply the risk factor,

$f_r = (100)^{-\frac{1}{\alpha}}$, to the short-term peak load using the worst case α as determined from the baseline, 100-hour, or 200-hour strength data. This amounted to setting the long-term loads for these two systems by applying the square of the risk factor, f_r , times the complexity factor, f_c , to the baseline β for each system at the temperature at which the long-term simulation was to be performed. The results of these calculations for G/PI and B/Al are given in Table 12-13.

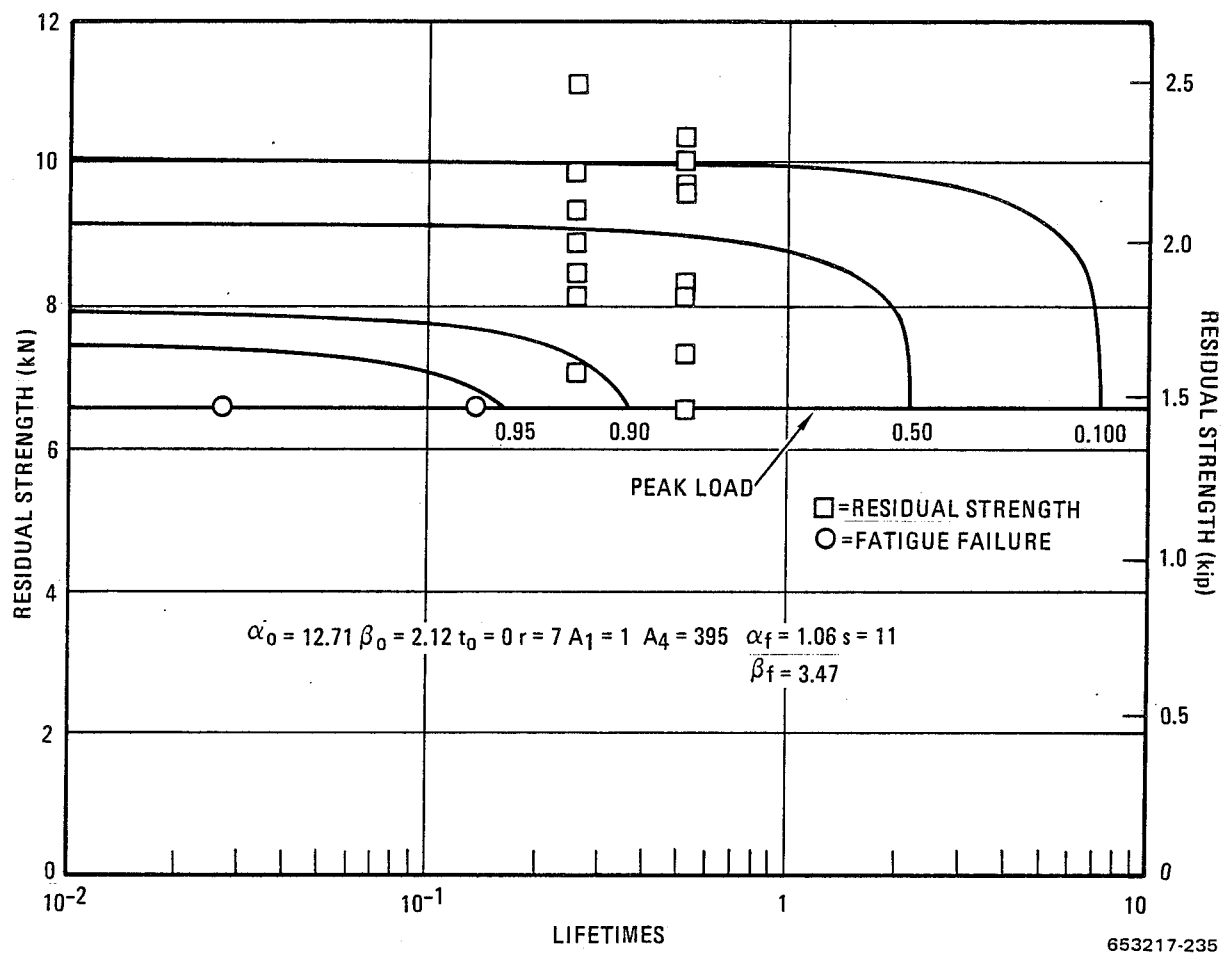


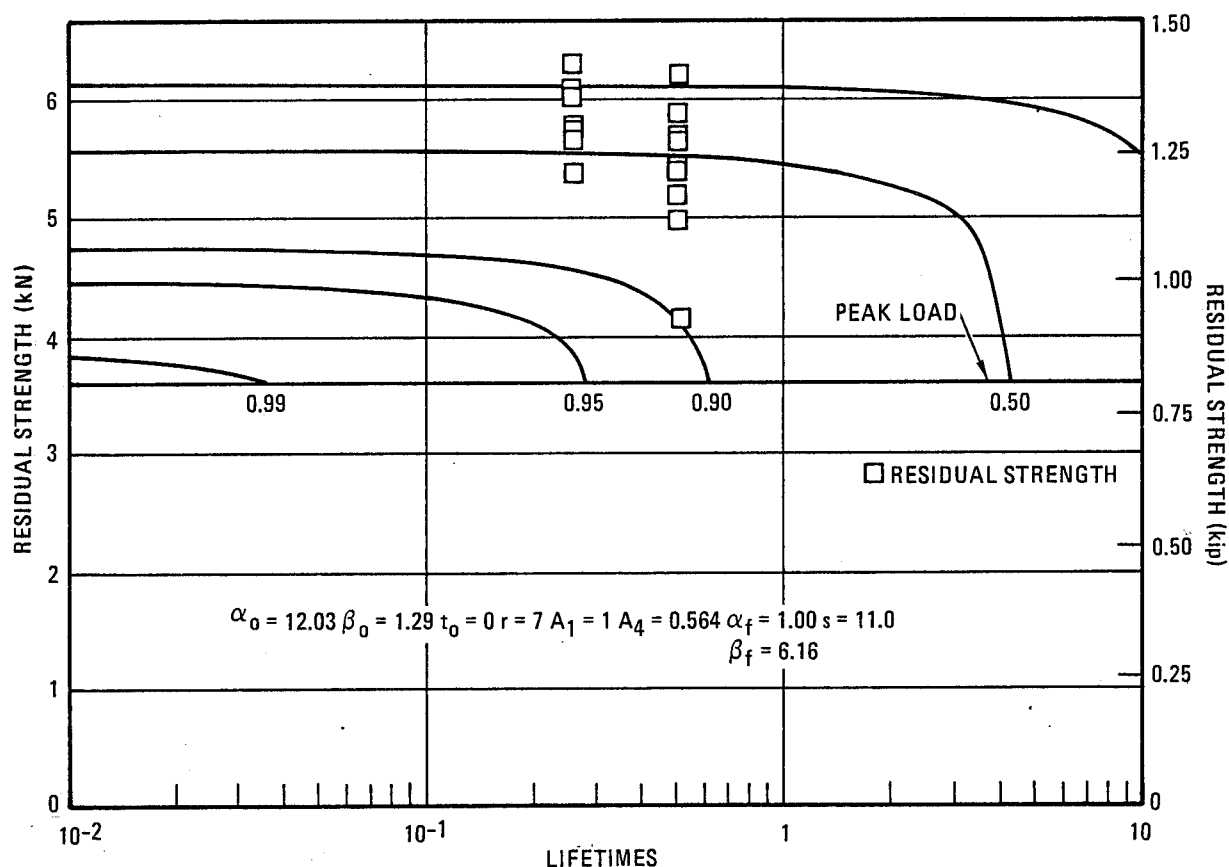
Figure 12-35 Wearout Model for Unnotched $[0^\circ \pm 45^\circ]_s$ G/E

Table 12-13. Long-Term Peak Loads for G/PI and B/Al

Material	Condition	^a β_T		α_T	f_r	f_r^2	f_c	^b Peak Load	
		kN/m	(kip/in)					kN/m	(kip/in)
G/PI	Unnotched	366	2.09	10.7	0.65	0.42	0.90	140	0.800
	Notched	233	1.33	10.0	.63	.40	.90	83.4	0.476
B/Al	$[0^\circ]_6$	1566	8.94	14.7	.73	.53	.93	778	4.44
	$[0^\circ \pm 45^\circ]_s$	427	2.44	13.6	.71	.51	.92	200	1.144

^a $\beta_T = f_T \beta_{RT}$ where $T = 505$ K (450° F)

^b Peak Load = $f_r^2 f_c \beta_T$



653217-236

Figure 12-36 Wearout Model for Notched $[0^\circ \pm 45^\circ]_s$ G/E

The peak long-term loads for the four materials, Tables 12-12 and 12-13, were used to calculate the peak, landing, and one g stresses presented in Table 12-14.

Table 12-14. Long-Term Peak Loads and Stresses

Material	Condition	Long-Term Peak Load		Total Peak Load for 0.076 m (3.0 in) Specimen		Peak Stress		Landing Stress		One g Stress	
		kN/m	(kip/in)	kN	(kip)	MN/m ²	(ksi)	MN/m ²	(ksi)	MN/m ²	(ksi)
B/E	Unnotched	230	1.314	17.5	3.94	302	43.8	-75.5	-10.9	151	21.9
	Notched	132	.752	10.1	2.26	239	34.6	-60.0	-8.7	120	17.3
G/E	Unnotched	232	1.325	17.7	3.98	305	44.2	-76.5	-11.1	153	22.1
	Notched	132	.756	10.1	2.27	232	33.6	-57.9	-8.4	116	16.8
G/PI	Unnotched	140	.800	10.7	2.40	153	22.2	-38.6	-5.6	76.5	11.1
	Notched	83.4	.476	6.36	1.43	125	18.2	-31.7	-4.6	63	9.1
B/Al	$[0^\circ]_6$	778	4.44	59.3	13.32	747	108.3	-187	-27.1	374	54.2
	$[0^\circ \pm 45^\circ]_s$	200	1.144	15.3	3.43	208	30.1	-51.7	-7.5	104	15.1

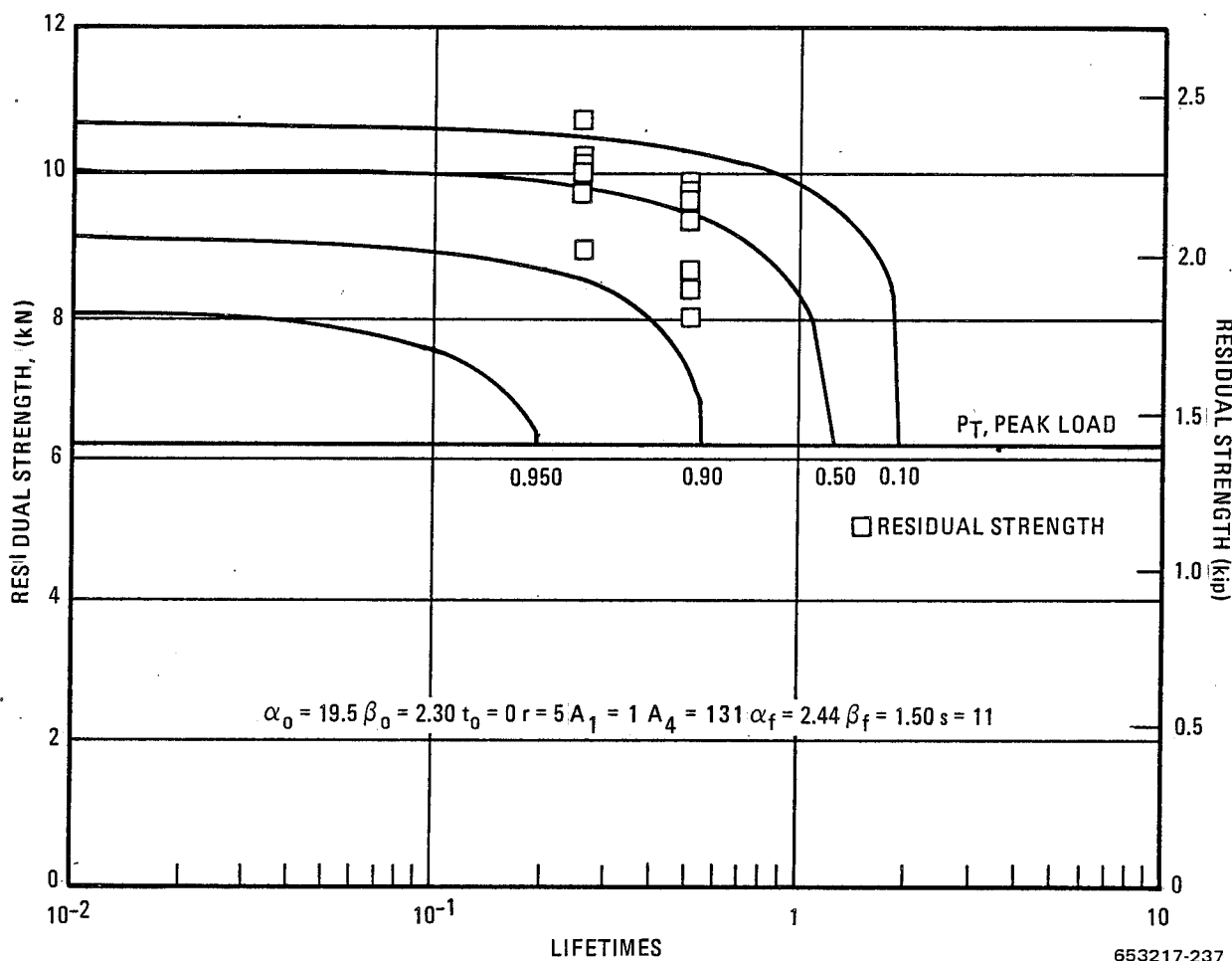
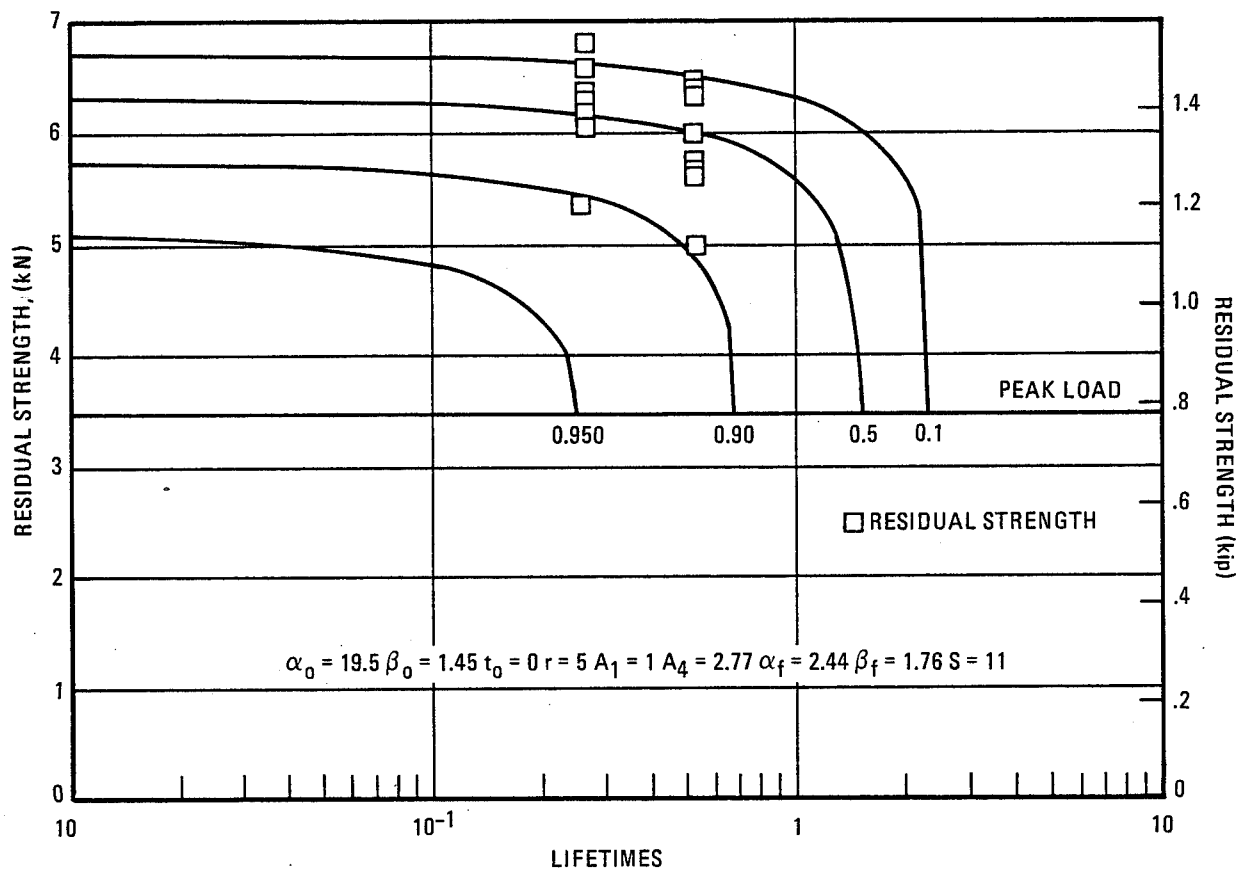


Figure 12-37 Wearout Model for Unnotched $[0^\circ \pm 45^\circ]_s$ B/E

12.7 LONG-TERM FLIGHT SIMULATION

The main emphasis of the entire program was on the long-term tests and that is why they were approached so carefully. The objective of the long-term test program was to determine the behavior of advanced composites in the operating environment of supersonic cruise aircraft. Specimens will be exposed for real-time periods of 10,000, 25,000, and 50,000 hours. The tests will be unsuccessful if the environmental conditions (loads or temperatures) are set either too high or too low. If the conditions can be set so that a given number fail by the end of the required 50,000 hours of exposure, not only will the behavior of the composites be determined but also a predictive capability will be demonstrated.

12.7.1 TEST PLAN AND PROCEDURES. For each material system, a total of 20 long-term specimens was installed in the flight simulation apparatus. The resin matrix specimens, B/E, G/E, and G/PI, were all fabricated from 6 ply panels having a $[0^\circ \pm 45^\circ]_s$ crossplied orientation. Ten were unnotched and 10 were notched (see Figures 12-9 and 12-10 for specimen configurations).



653217-238

Figure 12-38 Wearout Model for Notched $[0^\circ \pm 45^\circ]_s$ B/E

The B/A1 specimens, all of which were unnotched, were fabricated, half from 6 ply unidirectional and half from 6 ply $[0^\circ \pm 45^\circ]_s$ crossply panels. Five specimens from each material/orientation/configuration set were to be exposed for 10,000 hours (equivalent to 5000 of the two-hour flights) for the Phase I evaluation. The other five specimens of each set will remain in the simulation apparatus until 50,000 hours (25,000 flights) of exposure have been completed (Phase II). A modification to the Phase II test plan was the addition of three unnotched long-term specimens to each material/orientation set. These specimens were installed in the flight simulation apparatus after the 10,000-hour specimens were removed. The added specimens will be exposed for 25,000 hours to provide additional residual strength data between the originally scheduled 10,000- and 50,000-hour time periods.

The flight simulation cycle, shown earlier in Figure 12-1, is two hours in length and consists of three parts: climb, cruise, and descent. The time-temperature-load history of a typical flight is shown in Table 12-15. Each flight is concluded with one compressive load cycle. The load spectrum is applied in a random manner.

Table 12-15. Time-Temperature-Load History for Typical Long-Term Flight Simulation Cycle

Item	Climb (Heating)	Cruise (Held at Constant Temperature)			Descent (Cooling)
Time	10 minutes	44 minutes	2 minutes	44 minutes	20 minutes
^a Load	25 cycles	constant	6 cycles	constant	7 cycles

^aOne additional compressive load per two-hour flight.

The cruise portion of the simulation cycle was conducted at a constant temperature for each material system. The intent of the program was to select the temperature that was considered to be the maximum use temperature for each composite for long-time (50,000-hour) service. For the G/PI and B/Al materials, the short-term results and data from the thermal aging studies then in progress indicated that 505 K (450° F) was probably a good upper limit, and this temperature was selected. For the two epoxy systems, the short-term results obtained at 422 K (300° F) gave no reason to change the exposure temperature, and 1000-hour thermal aging data at 394 K (250° F) and 450 K (350° F), which was then available, also indicated no problem with the 422 K (300° F) temperature. Therefore, the long-term flight simulation exposures were begun using these temperatures for the cruise portions of the cycle. Shortly after starting the tests, the 5000-hour thermal aging results for the epoxy systems became available. The data indicated that severe degradation of the epoxy matrix with significant decreases in tensile strength had occurred at 450 K (350° F). No effects were observed at 394 K (250° F). Primarily because of the thermal aging data, but also as a result of discussions with various individuals who were well versed in composite usage and research and development, the maximum exposure temperature for the epoxy long-term tests was lowered to 408 K (275° F). At the time that the temperature was changed, the epoxy specimens had received only approximately 1000 hours of exposure.

Selection of the maximum load levels for the long-term flight simulation exposure tests has been discussed earlier in the short-term test results analysis section. A summary of the types and numbers of long-term specimens with the test conditions for each is given in Table 12-16.

Before installing the long-term specimens in the flight simulation apparatus, width and thickness measurements were made at several locations in the test sections of all specimens, and average cross-sectional areas were calculated for each set of specimens. These measurements were used to obtain the flight simulation stresses shown in Table 12-16 and could be used for the residual strength determinations for specimens that experienced surface degradation during the long-term exposure tests. The specimens were then installed in the test machine, thermocouples were attached, the compression stiffening grids were bolted in place, and all resin-matrix specimens were heated to their respective cruise temperatures and held for 24 hours to remove any absorbed moisture. Before starting the tests, each set of 10 specimens was proof loaded to the maximum value that would be experienced during the 50,000 hours of exposure to the random load spectrum.

Table 12-16. Summary of Long-Term Test Program

Material System	Orientation	Configuration	Number of Specimens			Cruise Temperature		Peak Stress	
			10,000 hr	25,000 hr	50,000 hr	K	(°F)	MN/m ²	(ksi)
B/E	[0° ± 45°] _s	Unnotched	5	3	5	408	275	302	43.8
		Notched	5	—	5	408	275	239	34.6
G/E	[0° ± 45°] _s	Unnotched	5	3	5	408	275	305	44.2
		Notched	5	—	5	408	275	232	33.6
G/PI	[0° ± 45°] _s	Unnotched	5	3	5	505	450	153	22.2
		Notched	5	—	5	505	450	125	18.2
B/Al	[0° ± 45°] _s	Unnotched	5	3	5	505	450	208	30.1
	[0°] ₆	Unnotched	5	3	5	505	450	747	108.3

At the completion of 10,000 hours of flight simulation testing, all unfailed Phase I specimens were removed from the simulator and visually examined with a stereo microscope to check for changes in appearance or the presence of surface flaws such as loose or bare fibers, cracks, or delaminations. Photographs were made of typical specimens and of those with significant changes in appearance as a result of the 10,000 hours of exposure. The large, 0.076 m (3 in.) by 0.46 m (18 in.), long-term specimens were then cut into smaller pieces, which were fabricated into various types of specimens and tested for determination of residual strength values.

12.7.2 LONG-TERM TESTING. Once started, the long-term tests were intended to continue uninterrupted 24 hours a day, seven days a week except for brief shutdowns to change the program tapes, retighten the B/Al doubler clamps, remove failed specimens, and provide equipment maintenance. Some unexpected problems did occur from time to time, however, and these often required extended amounts of downtime to correct. The monitoring and safety devices were also responsible for numerous shutdowns when test conditions tended to stray slightly from the allowable ranges. Any shutdown during nonworking hours could not be corrected until the next working day and could result in losses of one to sixteen hours of exposure (up to 62 hours on a weekend) depending on the time of shutdown. If the tests were halted for 24 hours or more an additional four hours were lost because of the moisture bakeout of the resin matrix specimens. At the completion of the short-term tests and at regular intervals during the long-term tests, the flight simulation apparatus was given an overhaul, which, as a minimum consisted of changing the piston rod seals in the hydraulic cylinders and replacing the quartz heat lamps. Any worn bearings or bushings in mechanical systems and any questionable electronic components were replaced as necessary.

The short-term test program was very successful in checking out the flight simulation apparatus, the suitability of the test specimen design, and the test procedures required to ensure long-time reliable operation during the long-term exposures. Many problems were uncovered and corrected. Some additional problems were encountered, however, after the long-term tests were begun. One problem that occurred with the compression stiffening grids affected only the long-term specimens. If the grids rotated slightly during testing, the attachment screws, see Figure 12-39, could bear against the specimen edges and in time could wear away a portion of

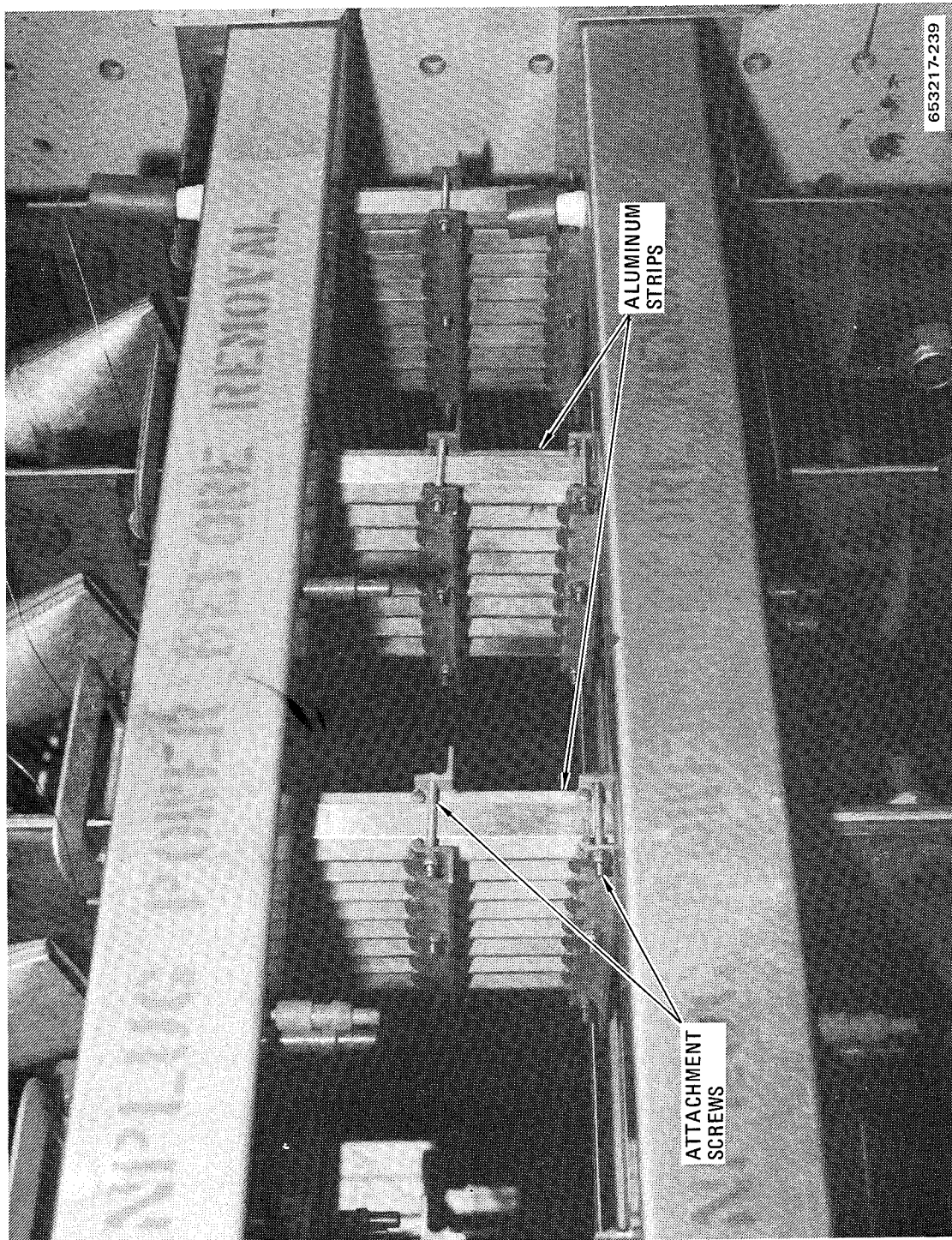


Figure 12-39 Closeup-View of Flight Simulation Apparatus Showing Attachment Screws for Compression Stiffeners and Aluminum Protection Strips

the material, forming an edge notch. This could not occur with the short-term specimens because of the much narrower widths involved. Several long-term specimens were found where the grid screws had begun to bear against the edges, but, with the exception of one G/E specimen, the effects were very slight. The G/E specimen failed prior to 10,000 hours with the failure location near one of the end doublers away from the heated zone. There was some edge damage in the vicinity of the fracture site, and this damage was believed to have been the cause of failure. The problem of the screws bearing against the specimen edges was eliminated by adding aluminum strips between the edges of the specimens and the attachment screws, Figure 12-39. During the short-term testing a problem of abrasion of the soft B/Al specimens during fatigue cycling was identified. This was caused by the relative motion of the specimens and compression stiffeners and led to a form of fretting corrosion. In an attempt to reduce this abrasion, the B/Al compression stiffeners were covered with a stratified Teflon coating. The technique helped to reduce the wearing of the surface, but at the completion of short-term testing the Teflon coating had worn away in several locations. It was also noted that the uncoated stiffener grids used on the short-term resin matrix specimens had also caused some abrasion of these specimens. Consequently, all of the grids were coated with new layers of Teflon for the long-term tests. However, because of the high cost of stratified Teflon coating an adhesive backed fiberglass/Teflon tape was used. This reduced, but did not eliminate, the surface wearing problem. One other problem has occurred with the unidirectional B/Al long-term specimens. From time to time specimens exhibit failures in the adhesive bonds between the B/Al and the titanium doublers. The adhesive, HT-424, which is quite porous, slowly oxidizes and eventually fails under the much larger loads used for the unidirectional B/Al. No damage is done to the specimens, but testing time is lost while the specimens are removed and new end doublers are attached. It is expected that this problem will continue throughout the test program. The remainder of the problems have been with the equipment and have involved periodic failure or erratic behavior of mechanical, electronic, or hydraulic components as a result of the rather severe service requirements of the flight simulation apparatus.

Periodically during the 10,000 hours of exposure in Phase I, the test specimens were examined in the test apparatus for changes in appearance or damage as a result of the simulation cycles. During two of these examinations all of the compression stiffening grids were removed so that the specimens could be studied more closely and, where desired, photographs could be made. It was during the first of these examinations that the problem of the grid screws bearing against the specimen edges was found. Figure 12-40 shows the most severe example of this edge damage. This specimen, BC92-4, later failed at 9669 hours but not at the edge notches. At the time of the first examination, the two epoxy systems had accumulated approximately 4500 hours of exposure and the G/PI and B/Al systems approximately 1700 hours. The results of the examination of the four composite systems were as follows:

- a. B/E—The two heated zones on each specimen were discolored and on several of the unnotched specimens exposed and broken boron fibers were visible. Several specimen also had shallow edge notches from the stiffener grid screws.
- b. G/E—Some slight discoloring of the heated zones was visible and several specimens were edge notched from the stiffener screws. At the time of this examination several of the unnotched specimens had already failed. The unfailed ones, however, appeared to be in good condition. None of the notched specimens had failed, but three of the 10 showed considerable damage in the form of cracks and delaminations at the edges and at the holes. Figure 12-41 shows the specimen with the most extensive damage (BF91-4). This specimen was removed because failure appeared imminent.

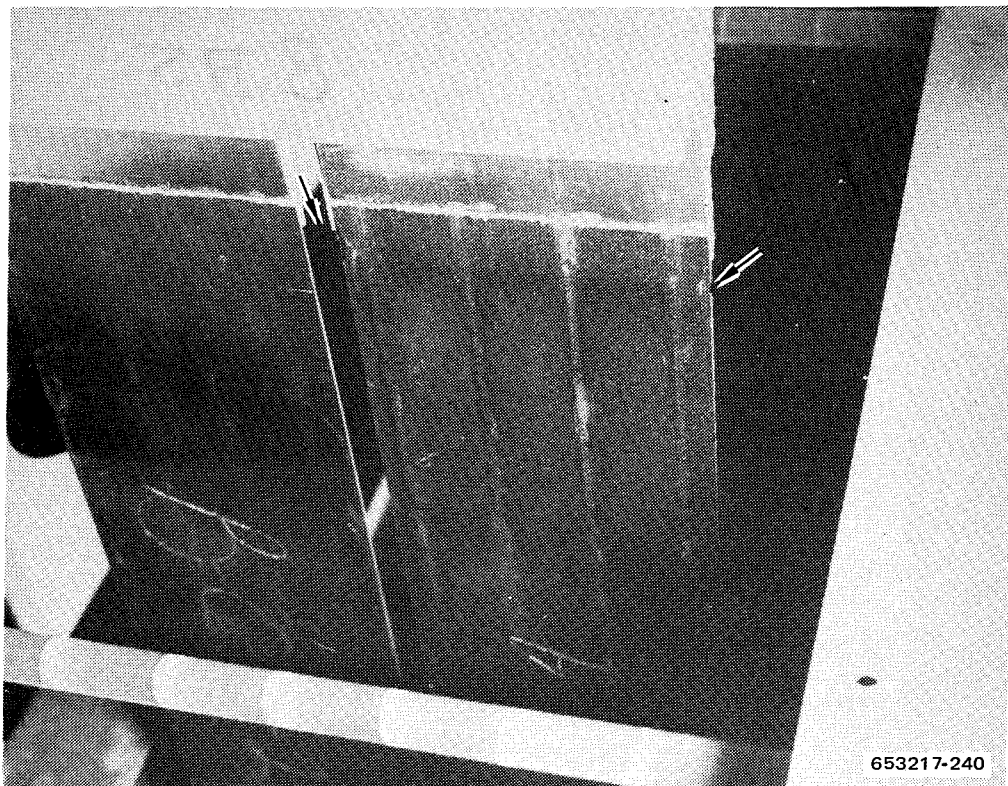


Figure 12-40 G/E Long-Term Specimen BC92-4 Showing Edge Damage (arrows) from Compression Stiffener Screws

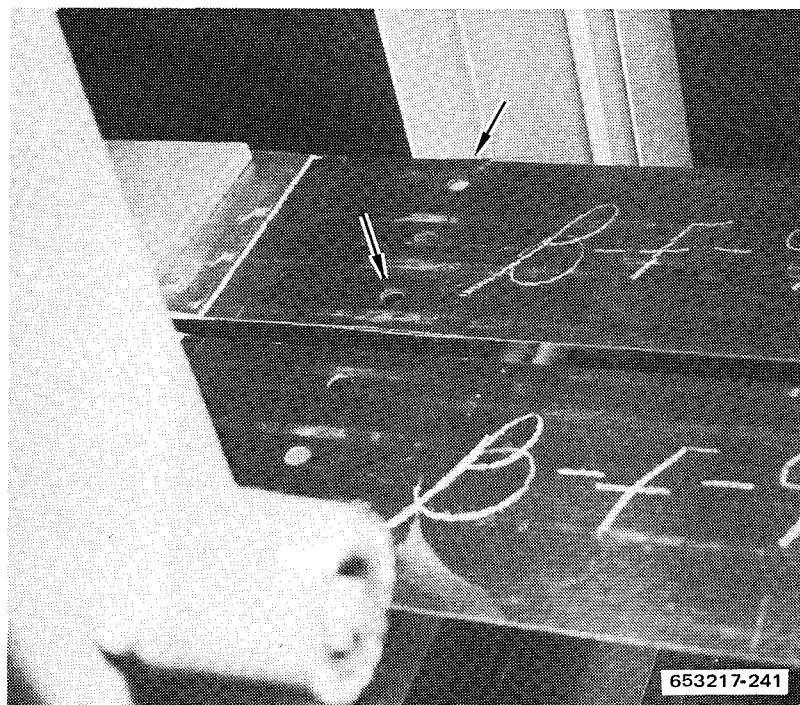


Figure 12-41 G/E Long-Term Specimen BF91-4 Showing Cracks and Delaminations (arrows) at Edges and Holes

- c. G/E—After 1700 hours of exposure the only visible changes were very slight wear marks on the edges of one of the unnotched specimens.
- d. B/Al—These specimen had also been exposed for only 1700 hours and were in good condition. Three specimens had slight edge notching from the stiffener screws and there was some surface abrasion from the stiffeners.

The next thorough examination was made just before the completion of 10,000 hours on the epoxy specimens (approximately 9000 hours for the epoxies and 6000 for the G/PI and B/Al specimens). The results of the examination of the four composite systems was as follows:

- a. B/E—These specimens showed the most damage as a result of the flight simulation exposures even though, in contrast to the G/E system, none had failed. The two heated zones on each specimen were discolored and in several instances showed exposed and broken fibers where portions of the epoxy resin had fallen away. In the notched B/E specimens some longitudinal surface cracks tangent to the holes were observed.
- b. G/E—At the time of this examination 11 of the 20 G/E specimens had failed or had been removed from the exposure apparatus because of showing significant damage. Of the remaining specimens the only visible effects were color changes in the heated zones at the top and bottom of each specimen and some small longitudinal cracks tangent to the holes in the notched specimens. These cracks were believed to extend only through the outer 0° ply in both the B/E and G/E specimens.
- c. G/PI—These specimens appeared to be in excellent condition with only slight color changes in the heated zones.
- d. B/Al—The only visible effects were longitudinal stripes on the surface where some of the Teflon tape from the stiffening grids had adhered.

Figures 12-42 through 12-45 are photographs of typical specimens of each composite material that were made during this examination with the specimens installed in the flight simulation apparatus. Only the B/E specimens, Figure 12-42, show any visible damage.

In setting the load levels for the long-term flight simulation tests, the expectation was for 80% of the specimens of each system to complete 50,000 hours of exposure. The 20% failure rate would amount to, on average, four specimens for each composite material system. In general, these failures would be expected to occur during Phase II of the test program. For the G/E system a much higher failure rate was observed. Twelve of the 20 G/E specimens either failed outright or were removed from test because of severe damage. Some of the badly damaged specimens were removed for further inspection and because of the likelihood of imminent failure were not returned. The others were in such poor condition that when a specimen in the same setup failed the damaged one was also removed to decrease the amount of equipment downtime. Table 12-17 lists the G/E specimens that did not survive the 10,000 hours of flight simulation and also shows the amount of exposure time logged when removed because of failure or significant degradation.

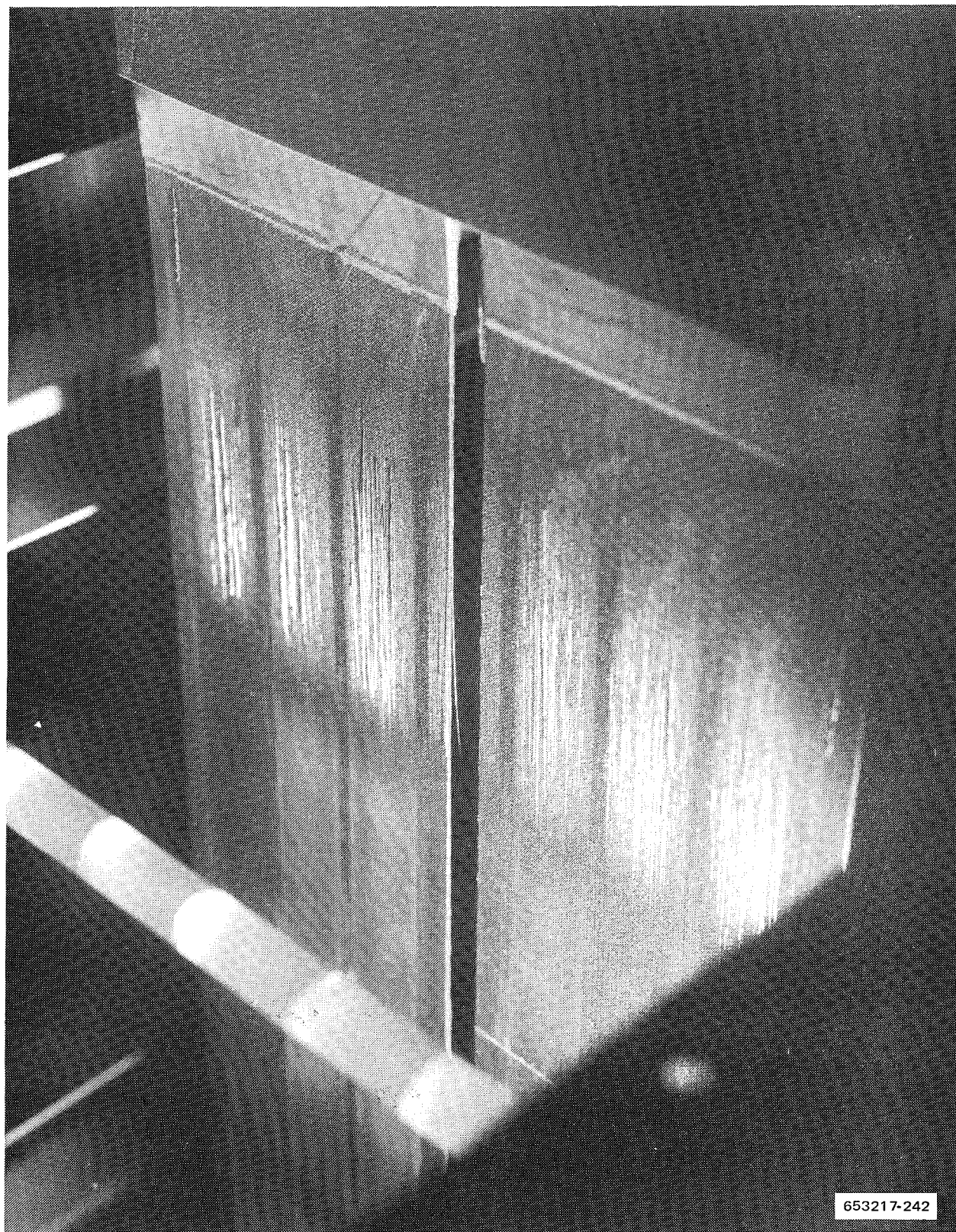


Figure 12-42 B/E Long-Term Specimens After Approximately 9000-hr of Exposure Showing Broken and Exposed Boron Fibers

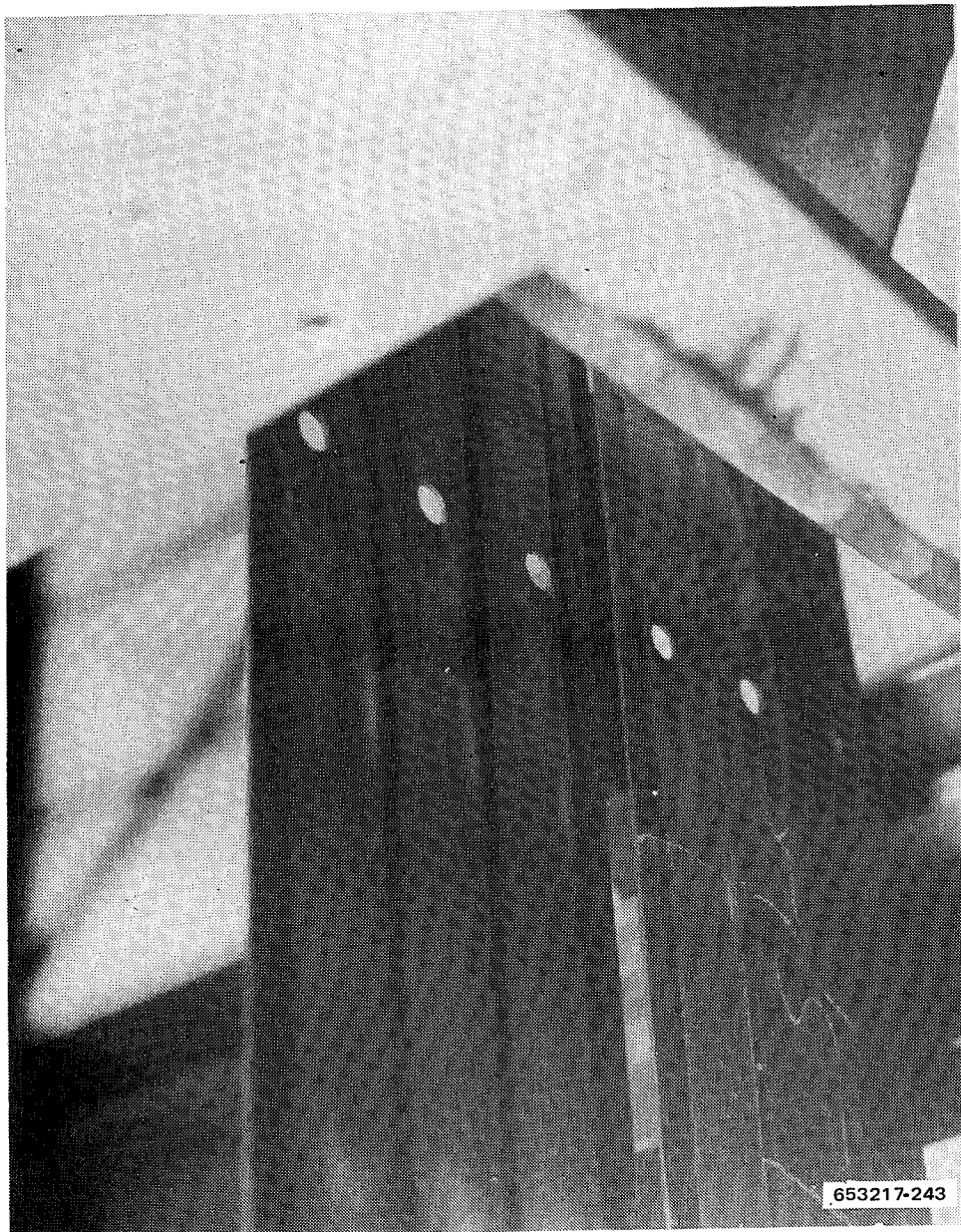


Figure 12-43 G/E Long-Term Specimens After Approximately 9000-hr of Exposure

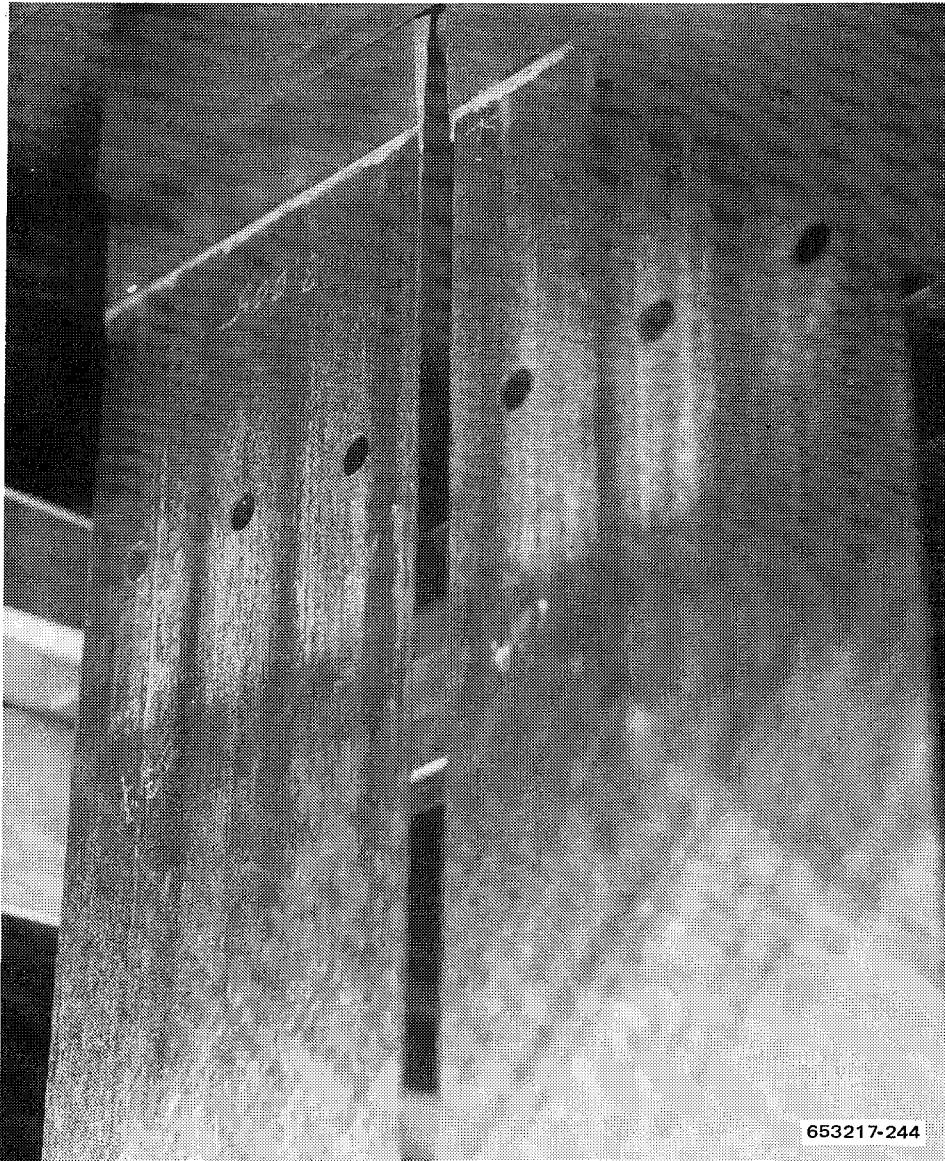


Figure 12-44 G/PI Long-Term Specimens After Approximately 6000-hr of Exposure

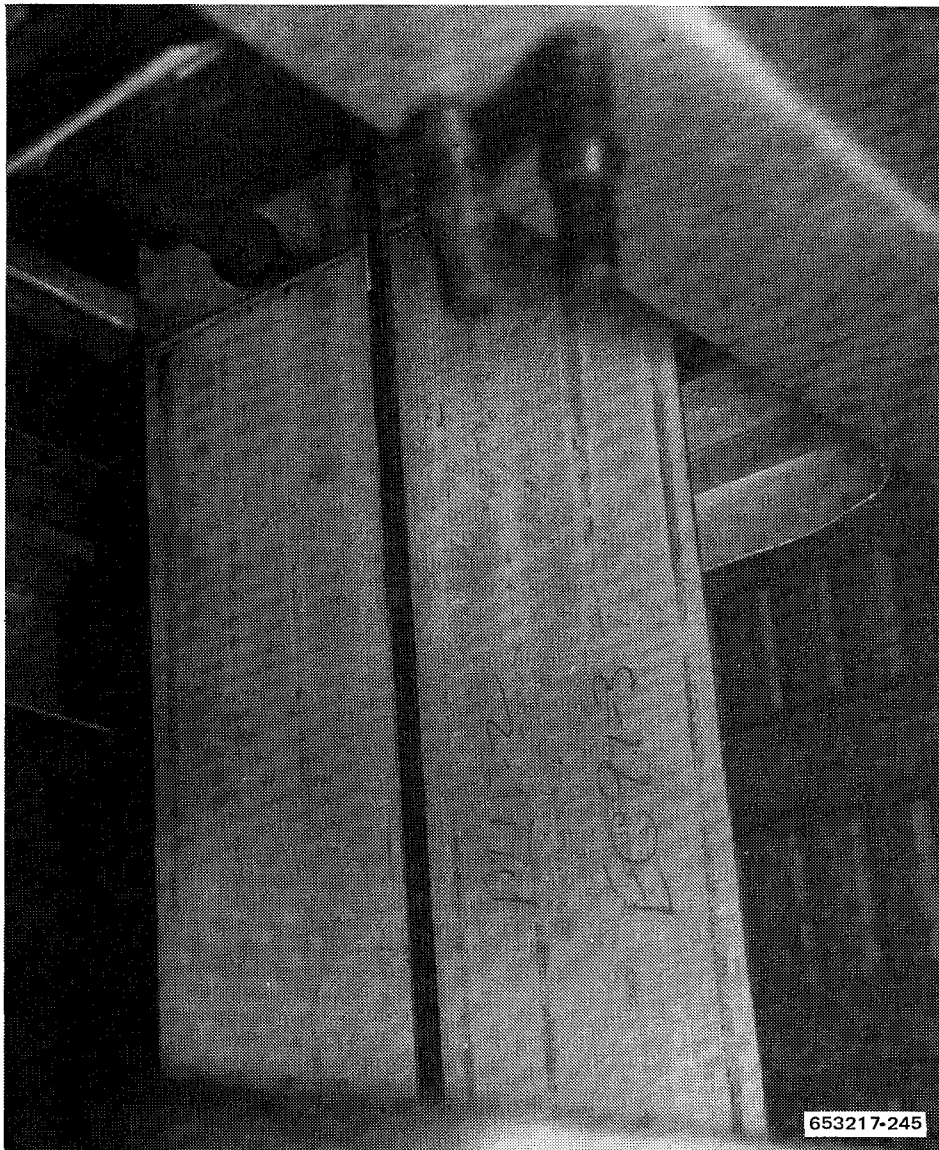


Figure 12-45 B/Al Long-Term Specimens After Approximately 6000-hr of Exposure

Table 12-17 G/E Long-Term Specimens Removed Because of Failure or Significant Degradation

Specimen No.	Type	Exposure (hr)	Failure or Damage Location
BC91-1	Unnotched	4515	Heated zone; failed
BC91-2	Unnotched	6683	Heated zone; not failed
BC91-3	Unnotched	6683	Heated zone; failed
BC91-4	Unnotched	4524	Heated zone; not failed
BC91-5	Unnotched	2696	Heated zone; failed
BC92-3	Unnotched	4053	Heated zone; failed
BC92-4	Unnotched	9669	Heated zone; failed
BC92-5	Unnotched	4524	Near doubler; failed
BF91-2	Notched	7520	Heated zone; failed
BF91-3	Notched	7520	Heated zone; not failed
BF91-4	Notched	4549	Heated zone; not failed
BF91-5	Notched	4549	Heated zone; not failed

All of the specimens except one failed in either the upper or lower heated zones. The specimens, which are 0.46 m (18 in.) long, are heated in two zones that are 0.11 m (4.5 in.) on either side of the centerline. Figure 12-46 shows three of the specimens, all of which failed in one of the heated sections. The two specimens with over 4000 hours of exposure also showed considerable damage in the heated zones opposite the failures in the form of edge delaminations. This can be seen in Figure 12-47. The 2669-hour specimen, BC91-5, did not show delamination in the unfailed heated zone. Another difference between the 2669-hour specimen and the two 4000-hour specimens of Figure 12-46 is the appearance of the fracture. The 2669-hour specimen has failed in a manner similar to the unexposed baseline specimens with little loss of the epoxy resin from around the graphite tows. After 4000 hours of exposure, however, the epoxy resin matrix has begun to crumble during failure leaving many bare graphite tows. Similar effects were observed during tensile testing of the 450 K (350° F) thermal age specimens after 5000 or more hours of exposure. Closeup views of the two different fracture appearances are shown in Figure 12-48 and Figure 12-49. The failure mechanism that was responsible for these early failures of the G/E specimens appeared to be a combination of several factors. Based on earlier thermal aging data the time at temperature, 4000 hours at 408 K (275° F), itself, is not sufficient to explain the brittle nature of the epoxy matrix. Added to this, however, are the effects of the thermal expansion stress during the 2000 thermal cycles and the tensile and compressive loads. As the matrix becomes embrittled as a result of oxidation the thermal and mechanical stresses act to produce microcracking and eventual loss of the outer epoxy layer. This can lead to accelerated oxidation as the filaments in the outer layers fail, thereby exposing the underlying resin to the oxidizing environment. The compressive load which occurs once per flight cycle is also important because of the lowered compressive resistance of the graphite

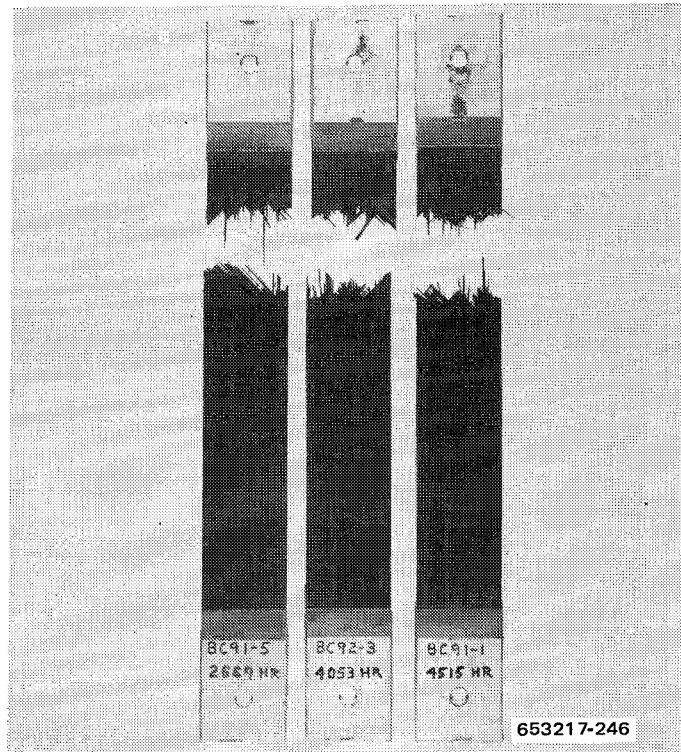


Figure 12-46 G/E Long-Term Specimens That Failed During Flight Simulation Testing Before Completion of 10,000-hr of Exposure

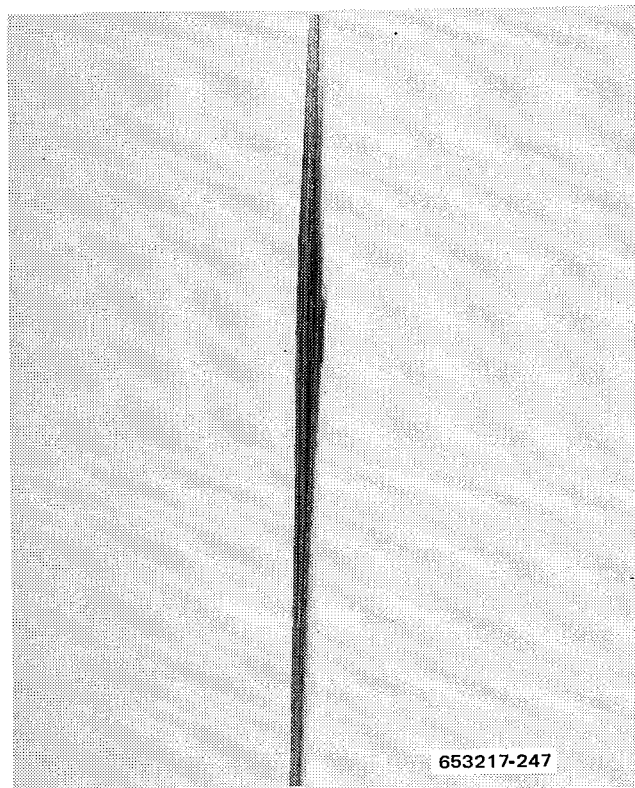


Figure 12-47 G/E Long-Term Specimen BC92-3 Showing Edge Delaminations in Heated Zone. (Specimen had failed at opposite heated zone after 4053-hr of exposure)

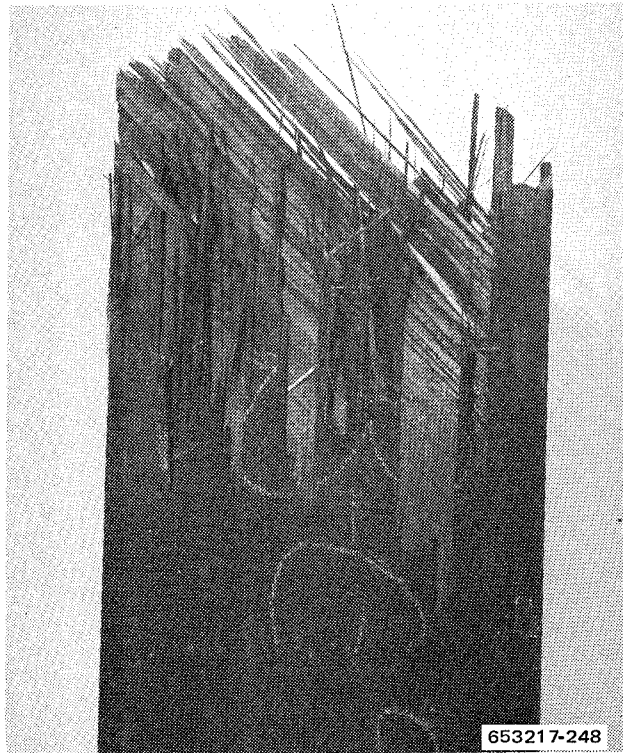


Figure 12-48 G/E Long-Term Specimen BC91-5 Showing Fracture Appearance After Failure in 2669-hr
(No significant loss of resin from around the graphite tows has occurred)

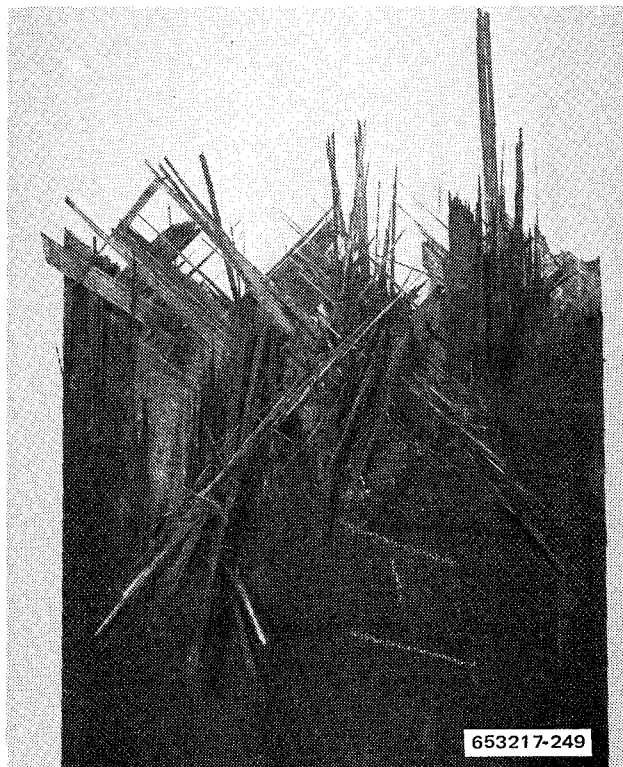


Figure 12-49 G/E Long-Term Specimen BC91-1 Showing Fracture Appearance After Failure in 4515-hr
(Loss of resin from around graphite tows is readily apparent)

tows as the matrix is degrading. It is these compressive loads that are responsible for the numerous delaminations observed in the heated zones of many of the specimens. A good example of a specimen that was about to fail by this mechanism is shown on the right in Figure 12-50. The edge view of the same specimen, Figure 12-51, shows clearly the loss of matrix on both surfaces with the exposed and broken graphite filaments and the extensive delamination caused by the compressive loading. This specimen would undoubtedly have failed very soon if it had not been removed from test.

The specimen on the left in Figure 12-50 was the only G/E specimen that did not fail in the heated zone. A closeup view of the fracture is shown in Figure 12-52. The arrows in the figure point to locations where stiffener grid screws could bear against the specimen edges if the grids rotated slightly. It appears likely that it was edge notches of this type that caused the early failure of specimen BC92-5. The fracture location and appearance were also quite different from the other failures.

One other specimen failure occurred during the long-term testing prior to completion of 10,000 hours. This was unidirectional B/Al specimen EU91-1 which failed out of the heated zone after 2454 hours. The specimen, shown in Figure 12-53, apparently failed because of a misaligned bearing in one branch of the whiffletree used to apply the fatigue loads. This caused the compressive loads to be misaligned with the axis of the specimen and resulted in the stiffening grid being pushed into the specimen at one end. Figure 12-54, a closeup of the fracture, shows where the four bearing surfaces of the stiffener were forced into the B/Al at the edge of the end doubler and initiated the failure.

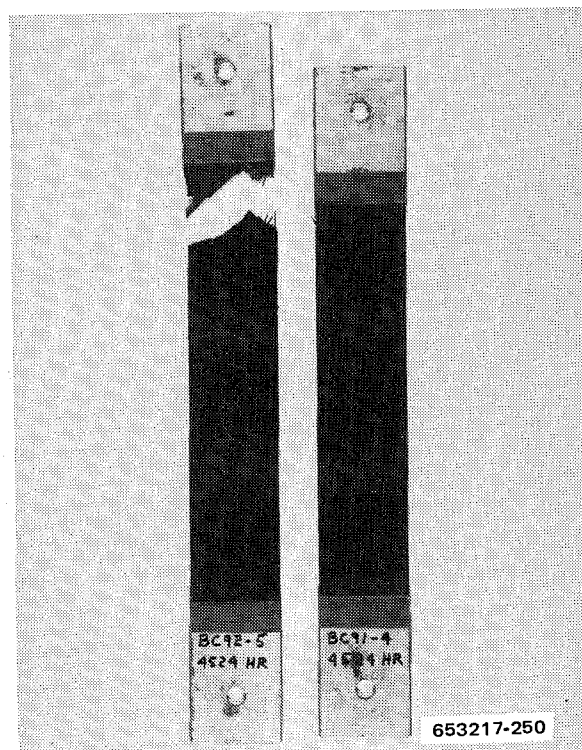


Figure 12-50 G/E Long-Term Specimens that were Removed from Test Before Completion of 10,000-hr of Exposure



Figure 12-51 Edge View of G/E Long-Term Specimen BC91-4 Showing Exposed and Broken Graphite Filaments and Extensive Delamination. (Specimen was removed from test after 4524-hr)

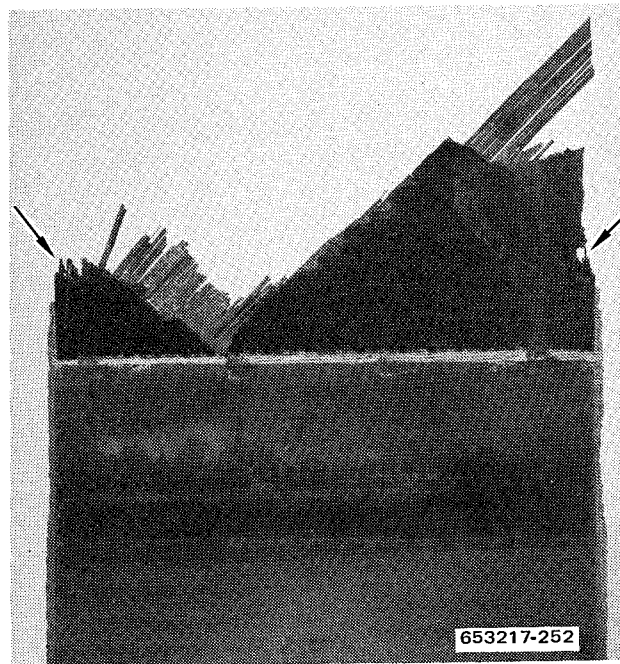


Figure 12-52 G/E Long-Term Specimen BC92-5 Showing Fracture Appearance After Failure in 4524-hr (Failure was probably the result of edge notches (at locations shown) caused by rotation of the compression stiffener grids)

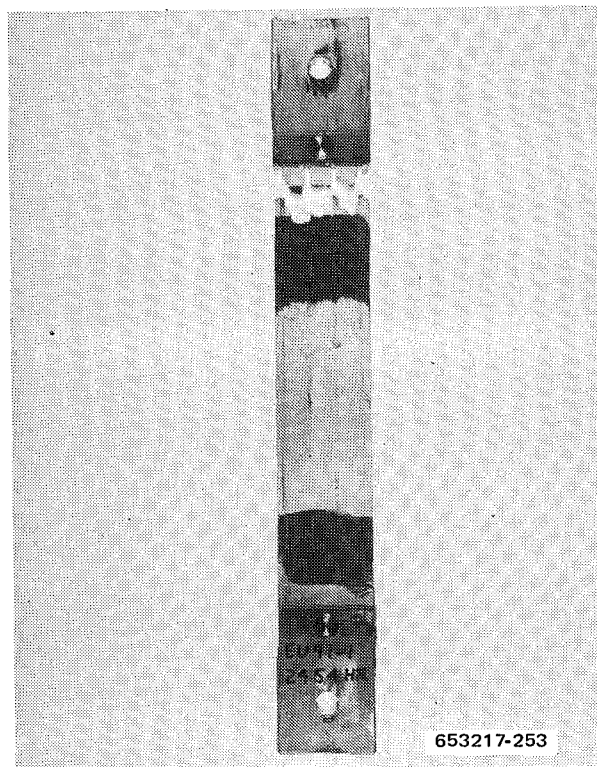


Figure 12-53 B/AI Long-Term Specimen that Failed During Flight Simulation Testing Before Completion of 10,000-hr of Exposure

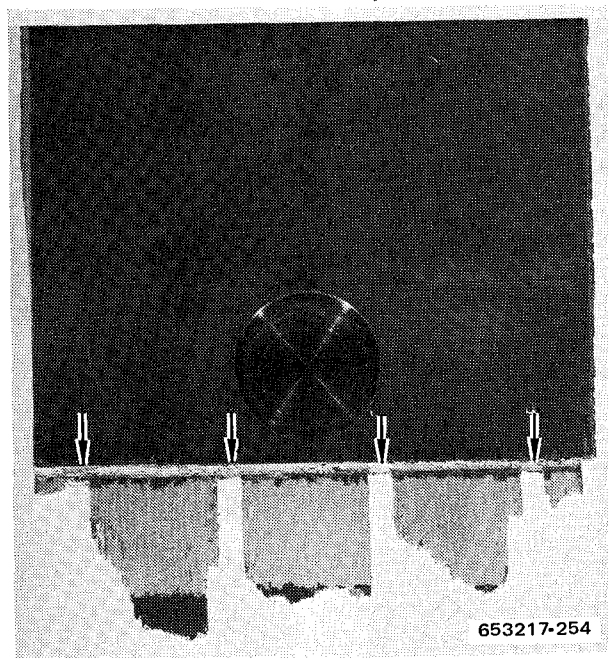


Figure 12-54 B/AI Long-Term Specimen EU91-1 Showing Fracture Appearance After Failure in 2454-hr (Failure was initiated at locations (arrows) where stiffener grid was forced into the B/AI)

None of the B/E or G/PI long-term specimens failed during the 10,000 hours of flight simulation exposure in Phase I.

12.7.3 LONG-TERM TEST RESULTS. At the completion of 10,000 hours of flight simulation exposure the Phase I long-term specimens were removed from the test apparatus. In addition, because of the high failure rate of the G/E and the extensive surface damage visible on the B/E, all remaining Phase II epoxy specimens were also removed. The revised flight simulation test plan for the B/E and G/E systems is described in Section 12.7.4. The specimens were examined visually with the aid of a stereo microscope and photographed. Based on the number and condition of the specimens and information gained during the overall test program, a residual strength testing plan was prepared. As will be discussed later, the test plan was somewhat different from the one originally scheduled. Cutting plans were prepared and the long-term specimens were machined into residual strength specimens, which were then tested. The results of the specimen examinations and residual strength tests are presented in the following sections.

12.7.3.1 Post Simulation Examinations

B/E, $[0^\circ \pm 45^\circ]_s$, unnotched and notched. All of the B/E specimens survived 10,000 hours of flight simulation exposure without fracture. The specimens did, however, experience considerable surface damage in the heated areas. The outer portions of the epoxy matrix had crumbled away in numerous places revealing the boron fibers, many of which had failed. In contrast to the G/E specimens no edge delaminations were observed at either the outside edges or at the holes in the notched specimens. Photographs showing both sides of three unnotched and three notched specimens are presented in Figures 12-55 to 12-58. The B/E laminates have a glass

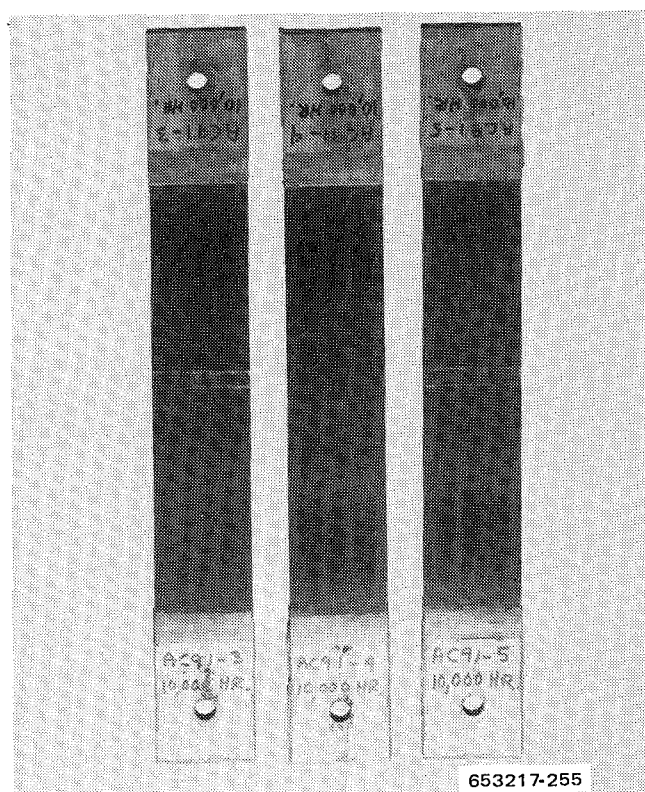


Figure 12-55 B/E Long-Term Specimens After 10,000-hr of Flight Simulation Exposure

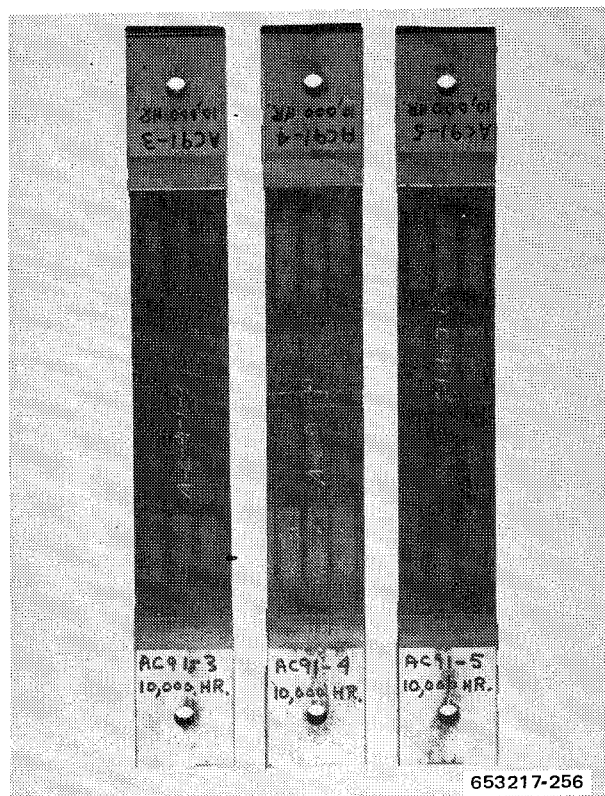


Figure 12-56 B/E Long-Term Specimens After 10,000-hr of Flight Simulation Exposure (Glass scrim cloth side)

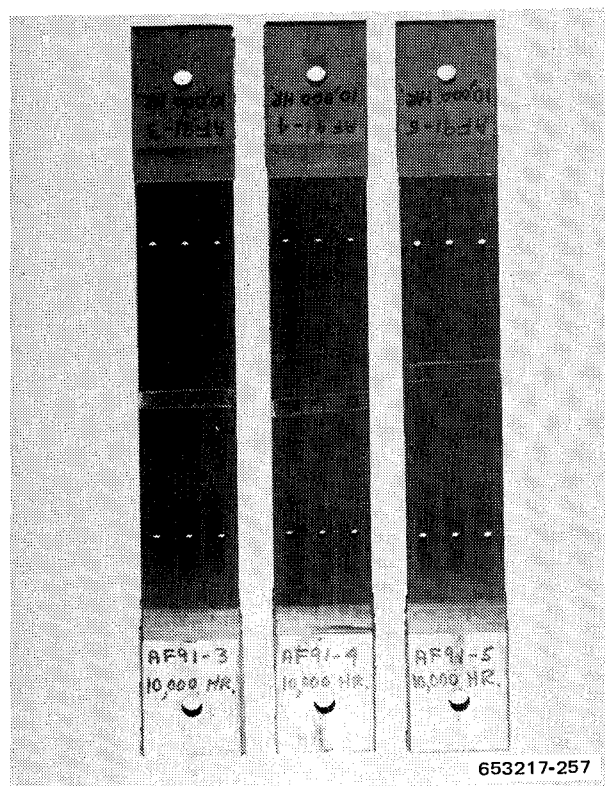


Figure 12-57 B/E Notched Long-Term Specimens After 10,000-hr of Flight Simulation Exposure

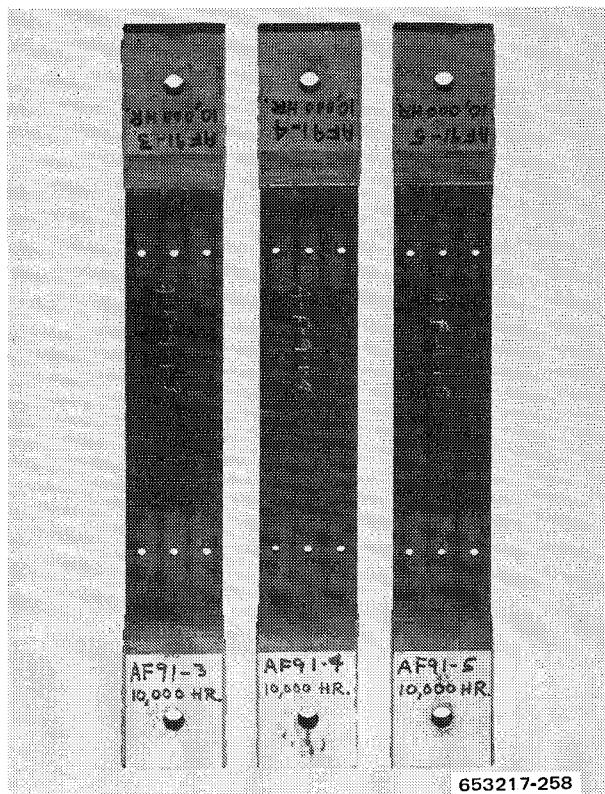


Figure 12-58 B/E Notched Long-Term Specimens After 10,000-hr of Flight Simulation Exposure (Glass scrim cloth side)

scrim cloth as the outer layer on one side. This side shows distinct color changes (to a light brown) in the heated zones. On the other side the epoxy resin has darkened somewhat, particularly in the heated zones. The effect of shielding of the surface by the compression stiffening grids is very evident. A few loosened and broken boron fibers are visible in Figure 12-55 and 12-57, the non scrim-cloth sides. A better view of these exposed boron fibers is shown in Figure 12-59 for an unnotched specimen and in Figure 12-60 for a notched specimen. These regions where the matrix has broken away at the surface and exposed the fibers were observed only in the heated zones in the areas not covered by the stiffening grids. Exposed fibers were also found in the heated areas on the scrim-cloth side of the B/E specimens, but these were generally hidden under the glass cloth. Figure 12-61 shows a closeup view of the heated zone on the scrim-cloth side. The disturbed areas of the glass cloth are caused by loosened and broken boron fibers beneath the cloth.

G/E, $[0^\circ \pm 45^\circ]_s$, unnotched and notched. Only two unnotched and six notched G/E specimens from the original 20 Phase I and Phase II specimens survived the 10,000 hours of exposure. The two unnotched specimens are shown in Figure 12-62 and 12-63. Unlike the failed specimens these appeared to be in reasonably good condition. No surface or edge cracks or delaminations were found. The heated zones had undergone some color changes particularly between the stiffening grids. These areas had a worn or eroded looking appearance and, in several places, the graphite tows were very close to being exposed as a result of the loss of the

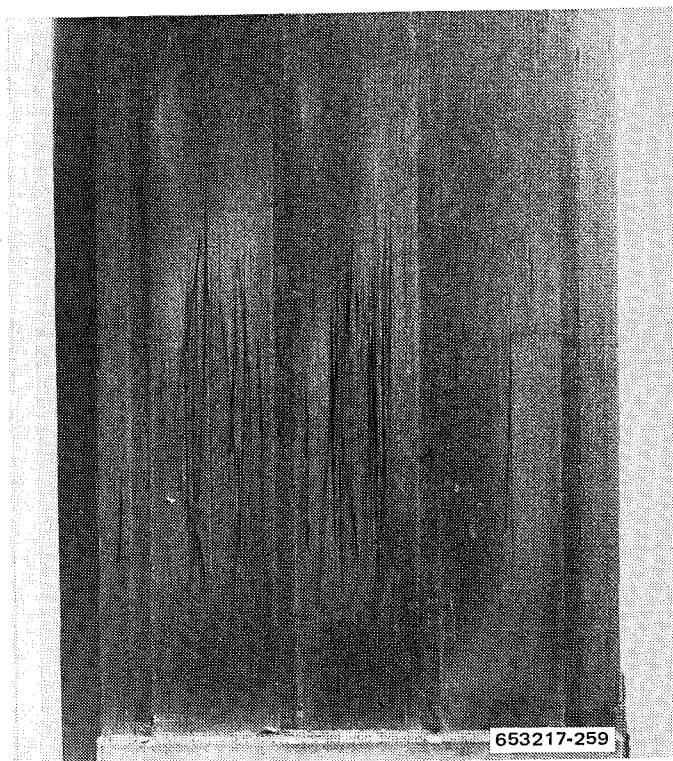


Figure 12-59 B/E Long-Term Specimen AC91-5 After 10,000-hr of Flight Simulation Exposure Showing Loosened and Broken Boron Fibers

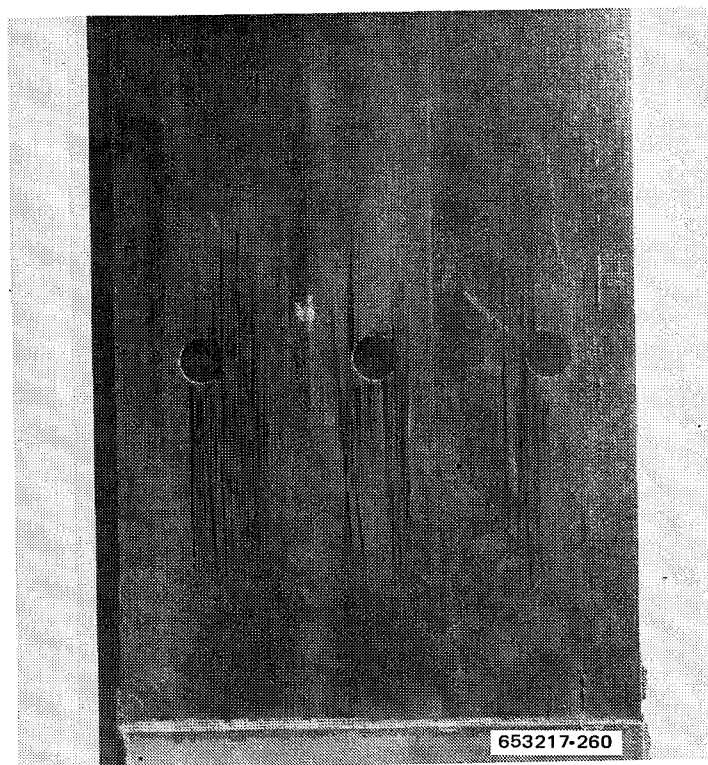


Figure 12-60 B/E Notched Long-Term Specimen AF91-5 After 10,000 hr of Flight Simulation Exposure Showing Loosened and Broken Boron Fibers

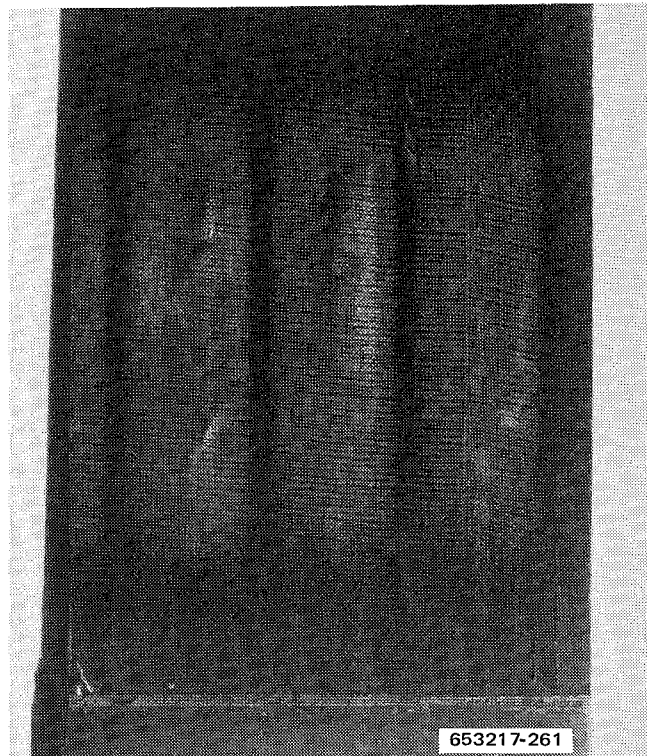


Figure 12-61 B/E Long-Term Specimen AC91-4 After 10,000 hr of Flight Simulation Exposure. (Glass scrim cloth side. The disturbed areas of the glass cloth are caused by loosened and broken boron fibers below the cloth)

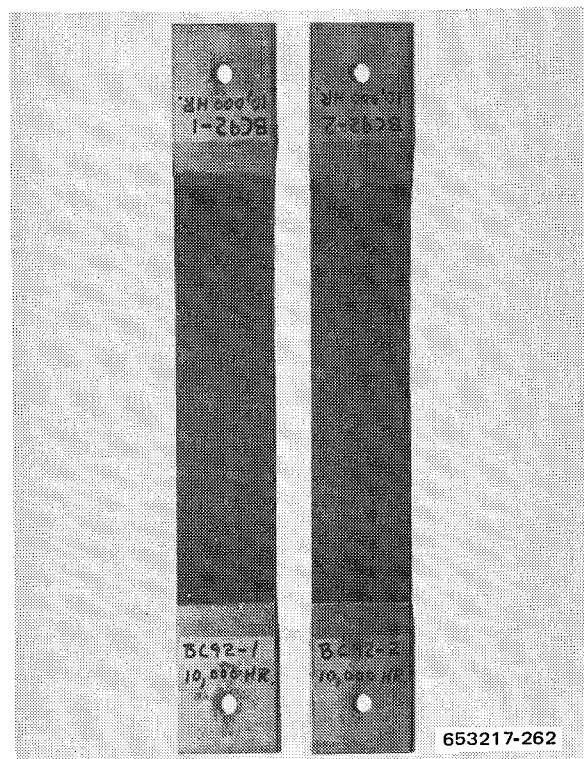


Figure 12-62 G/E Long-Term Specimens After 10,000 hr of Flight Simulation Exposure

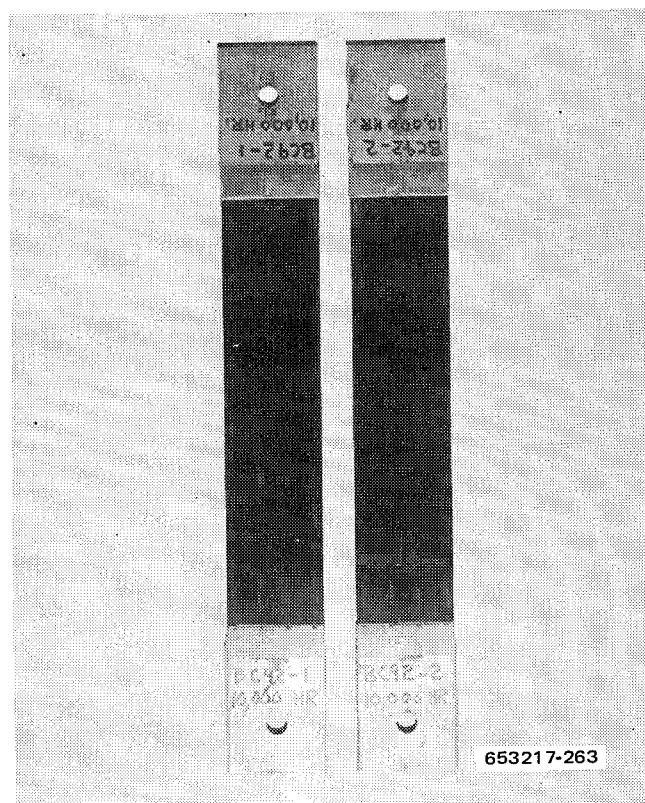


Figure 12-63 G/E Long-Term Specimens After 10,000 hr of Flight Simulation Exposure (Opposite sides of specimens in Figure 12-62)

epoxy matrix on the outer surface. The notched specimens that survived the 10,000 hours of flight simulation exposure were similar in appearance to the unnotched specimens except for some damage at the holes. Four of the specimens had longitudinal cracks near the holes and some delaminations at the edges of the holes. Two of the notched specimens that completed 10,000 hours are shown in Figure 12-64 and 12-65. Specimen BF92-3 is one with cracks at the holes but they are not readily visible in this photograph. The material on the surface of the specimens at one end is residue of the adhesive used to attach the thermocouples.

One of the specimens that appeared to be in good condition during the second inspection with the grids removed (9404 hours of exposure) is shown in Figure 12-66. Compressive failure in one of the heated zones occurred soon after the inspection, 9669 hours. No evidence of the impending failure was seen during the examination after 9404 hours. A higher magnification view of this specimen and two others that were removed from test prior to 10,000 hours because of severe damage is shown in Figure 12-67. The damage level in these specimens increases from left to right in the photograph. Inspection of the specimens suggests a failure mechanism slightly different from that proposed early in the test program and described in Section 12.7.2. In these specimens and also those in Figure 12-68, initial failure is thought to occur by delamination of the outer $[0^\circ]$ plies in the heated zones between the stiffening grids. The combination of thermal cycling stresses and the mechanical fatigue stresses acting at the ply interface overcomes the relatively low interlaminar strength, and delamination occurs. The

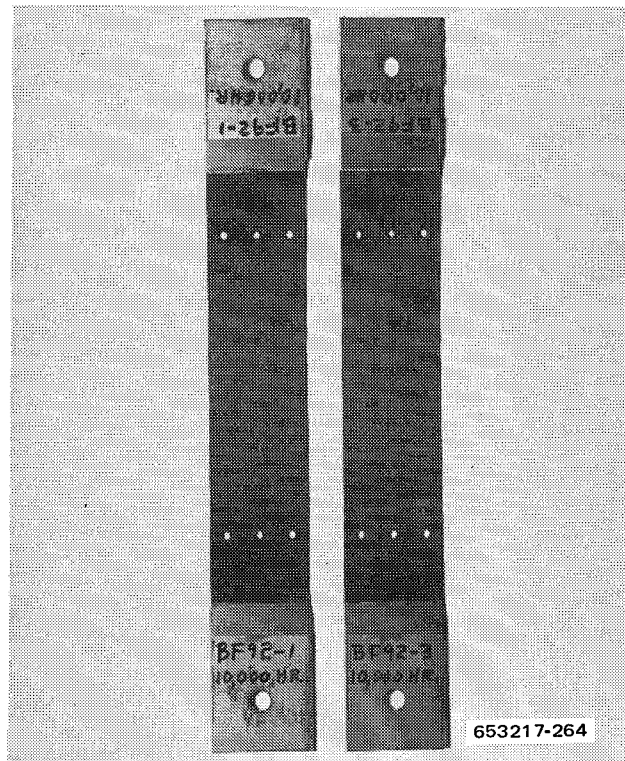


Figure 12-64 G/E Notched Long-Term Specimens After 10,000 hr of Flight Simulation Exposure

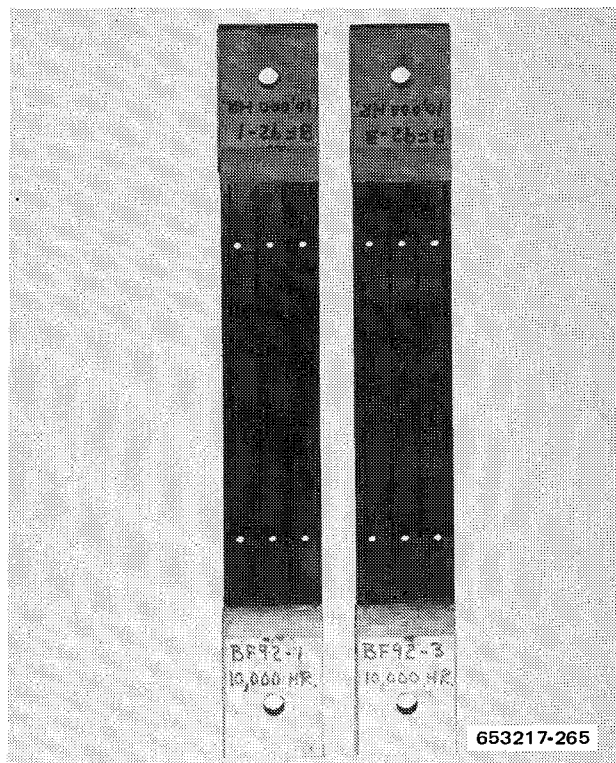


Figure 12-65 G/E Notched Long-Term Specimens After 10,000 hr of Flight Simulation Exposure (Opposite sides of specimens in Figure 12-64)

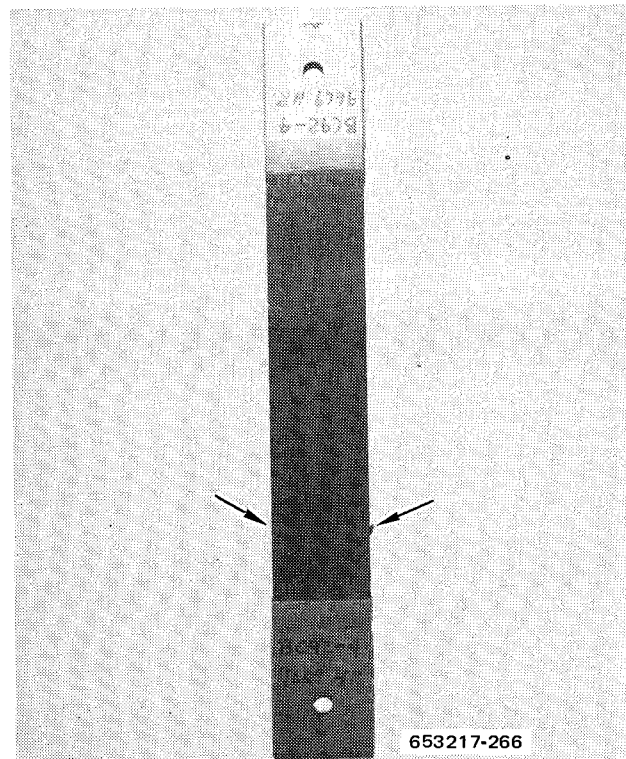


Figure 12-66 G/E Long-Term Specimen BC92-4 After 9669 hr of Flight Simulation Exposure. (Specimen failed (arrows) in compression at heated zone)

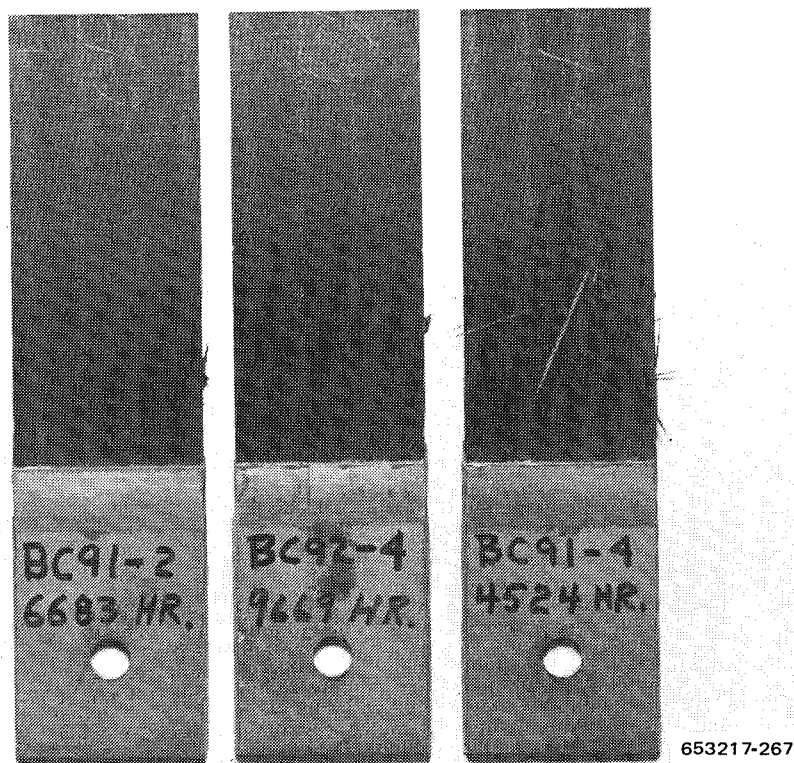


Figure 12-67 G/E Long-Term Specimens that were Removed from Test Before Completion of 10,000 hr of Exposure. (Increasing levels of damage in the specimens are visible in moving from left to right)

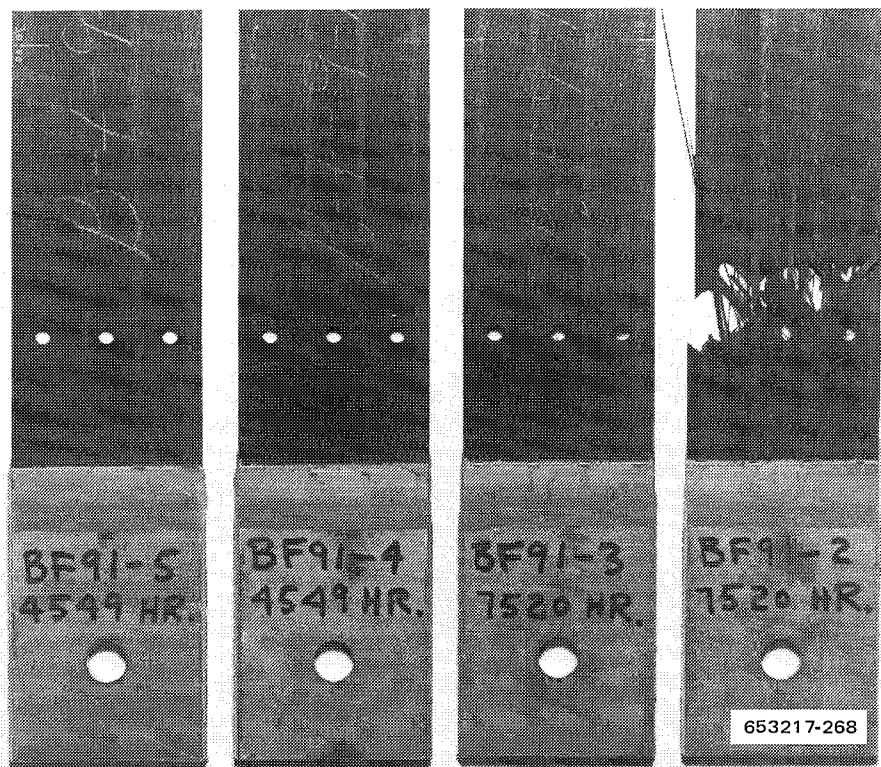


Figure 12-68 G/E Notched Long-Term Specimens that were Removed from Test Before Completion of 10,000 hr of Exposure. (Increasing levels of damage in the specimens are visible in moving from left to right)

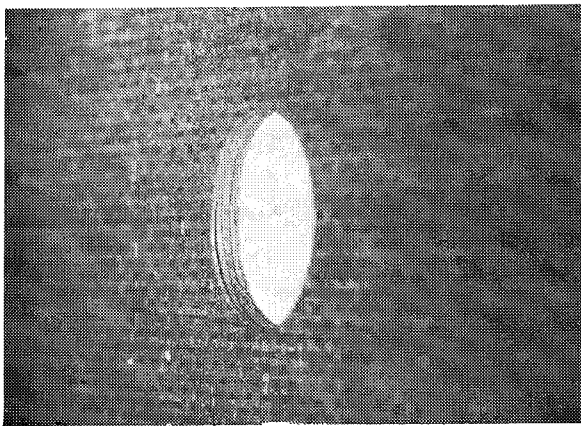
outer plies retain their strength during the tensile loads, but during the one compressive load per cycle all the load is carried by the low strength $\pm 45^\circ$ plies. At this point two effects occur. The $\pm 45^\circ$ plies begin to fail from the tensile and compressive fatigue loads, and oxidation with accompanying breaking up of the matrix of the outer plies is accelerated. The first specimen in Figure 12-63, BC91-2, was removed from test shortly after delamination of the outer plies occurred in the regions between the grids. Some damage to the inner $\pm 45^\circ$ plies was visible but the amount was small. The specimen still maintained its rigidity. In the regions that were beneath the .00318 m (0.125 in.) wide grids, transverse cracks can be seen. The second specimen, BC92-4, had sustained an increased amount of damage before being removed from test. Delamination and transverse cracking of the outer plies was much more extensive and the inner $\pm 45^\circ$ plies were badly broken. The specimen was no longer rigid and could easily be bent at the damaged heated zone. Some bare graphite fibers were also visible at the edges of the cracks and delaminations. These fibers were typical of those found in badly oxidized thermal aging test specimens, i.e., rather fuzzy appearing with no resin adhering to them. The final specimen in Figure 12-67, BC91-4, shows the greatest degree of degradation of the three. In addition to delamination of the outer plies and considerable inner ply damage, the surface has also experienced a great deal of tensile failure of the graphite fibers. Much of the epoxy resin matrix from the outer plies has oxidized and crumbled away, leaving bare graphite fibers exposed. This specimen had the least rigidity of the three. For these three specimens total time of flight simulation exposure was apparently not a factor in the onset of initial failure.

A similar set of the notched specimens showing varying degrees of damage is pictured in Figure 12-68. The first, BF91-5, shows the onset of delamination of the outer 0° plies, some longitudinal cracking near the holes, and some slight damage to the inner $[\pm 45^\circ]$ plies. The degree of delamination varies from one side of the specimen to the other. This can be seen from the closeup photographs of Figure 12-69. Severe delamination has occurred at one edge, a lesser amount in the center as shown at the three holes, and none at all at the opposite edge. The second specimen, BF91-4, had delaminated throughout the heated zone and shows increased longitudinal cracking and the onset of transverse cracking in the regions under the stiffening grids. The rigidity or resistance to bending at the heated zone has decreased somewhat. The third specimen, BF91-3, is very close to fracture with severe cracking of all the plies. The epoxy surface is heavily oxidized with many graphite fibers exposed. The specimen has almost no bending resistance across the notched region. The final specimen of the set, BF91-2, has fractured with considerable damage throughout the heated zone. In like manner to the 5000- and 10,000-hour 450 K (350° F) thermal aging specimens, many of the graphite fibers are visible as a result of the loss of the brittle oxidized epoxy resin.

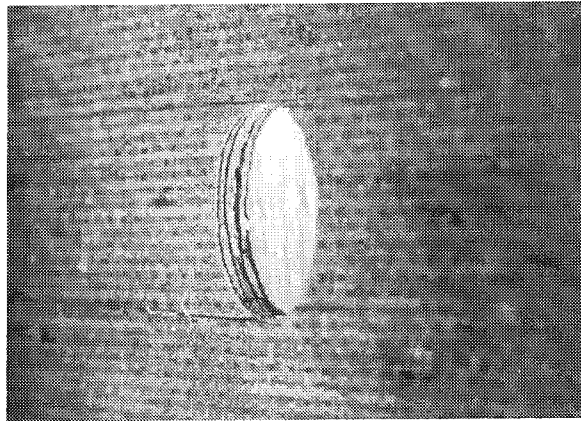
Figure 12-70 shows the effect of exposure time on the fracture appearance with respect to loss of resin from the graphite fibers. In 2669 hours, oxidation has not embrittled the matrix sufficiently to cause the resin to break away from the fibers during failure. The second specimen, BC91-1, after exposure of 4515 hours begins to show the bare graphite fibers caused by the crumbling away of the oxidized matrix. The effect increases with exposure time as can be seen in the other two specimens in Figure 12-70.

G/PI, $[0^\circ \pm 45^\circ]_s$, unnotched and notched. All of the Phase I G/PI long-term specimens completed 10,000 hours of flight simulation exposure. Photographs showing both sides of typical unnotched and notched specimens are presented in Figures 12-71 to 12-74. All of the specimens were discolored in the regions between the stiffening grids in the heated zones. All of the specimens also had exposed graphite fibers in these same areas. Generally the exposed fibers were found on the side of the specimen that faced the quartz heating lamps. However, for three specimens loose surface fibers were observed on both surfaces. Typically, these regions of exposed graphite fibers were approximately 0.025 m (1 in.) in length in the center of the heated zones. Figure 12-75 shows a closeup view of these damaged areas on an unnotched specimen and Figure 12-76 the same for a notched specimen. The amount of exposed fibers on the notched specimens was less than that found on the unnotched specimens. Some slight edge cracks were found in the heated zones of a few of the specimens. An example is shown in Figure 12-77. At 10,000 hours of exposure the edge cracks did not appear to be a serious problem. The appearance of the holes in the notched specimens was generally quite good. Slight horizontal cracks tangent to the holes were observed in three of the specimens. These were very short and appeared to extend only through the outer ply. Some slight delaminations or cracks were present in some of the holes, but, again, these also appeared to be very shallow and not a serious problem at this time.

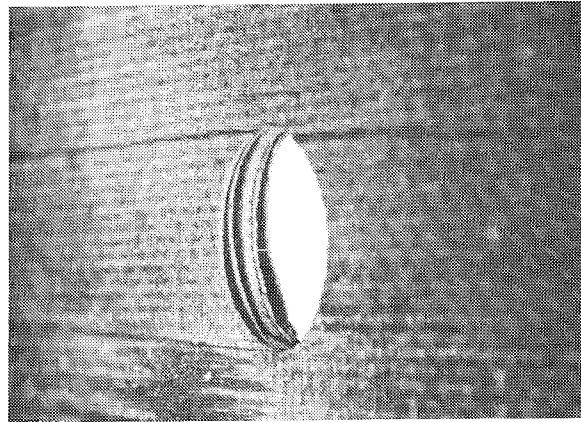
B/Al, $[0^\circ \pm 45^\circ]_s$ and $[0^\circ]_6$, unnotched. All of the $[0^\circ \pm 45^\circ]_s$ crossplied specimens and four of the five unidirectional B/Al long-term specimens completed 10,000 hours of exposure. Front and back views of typical specimens are shown in Figures 12-78 and 12-79 for crossply material and in Figures 12-80 and 12-81 for unidirectional material. The heated zones on the sides facing the quartz heat lamps have been coated with flat black, heat resistant paint to reduce reflection from the aluminum surface and thereby increase the efficiency of the heaters. The only



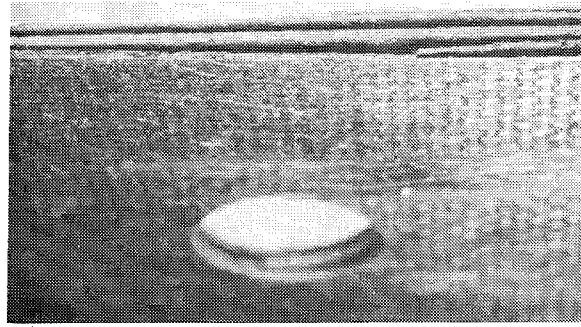
LEFT HOLE



CENTER HOLE



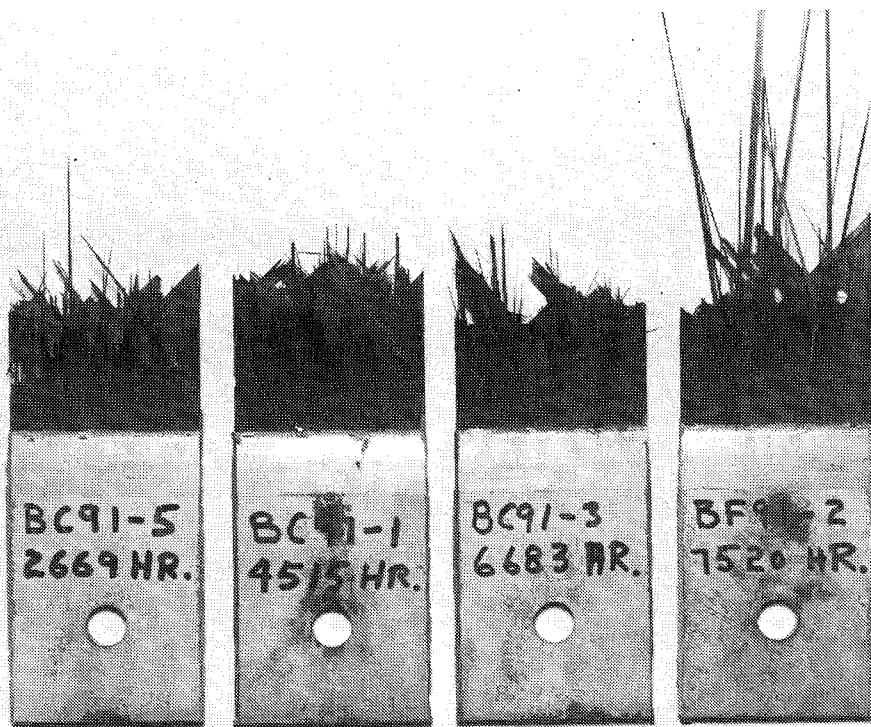
RIGHT HOLE



RIGHT EDGE

**Figure 12-69 G/E Notched Long-Term Specimen BF91-5 After 4549 hr of Flight Simulation Exposure
Showing Variation in Degree of Delamination Across Width of Specimen**

653217-269



653217-270

Figure 12-70 G/E Long-Term Specimens that Failed During Flight Simulation Testing Before Completion of 10,000 hr of Exposure. (Specimens show progressive loss of resin from the graphite fibers with exposure time)



653217-271

Figure 12-71 G/PI Long-Term Specimens After 10,000 hr of Flight Simulation Exposure



Figure 12-72 G/PI Long-Term Specimens After 10,000 hr of Flight Simulation Exposure (Opposite sides of specimens in Figure 12-71)

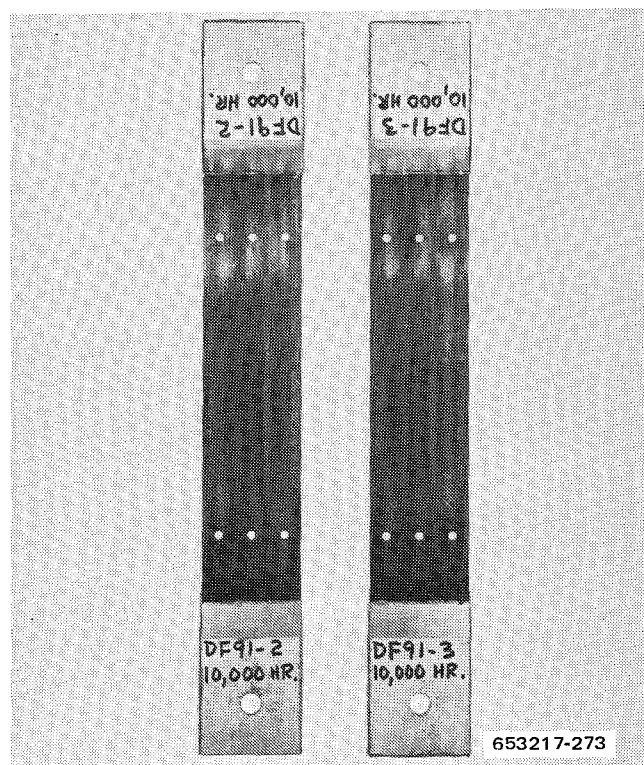


Figure 12-73 G/PI Notched Long-Term Specimens After 10,000 hr of Flight Simulation Exposure

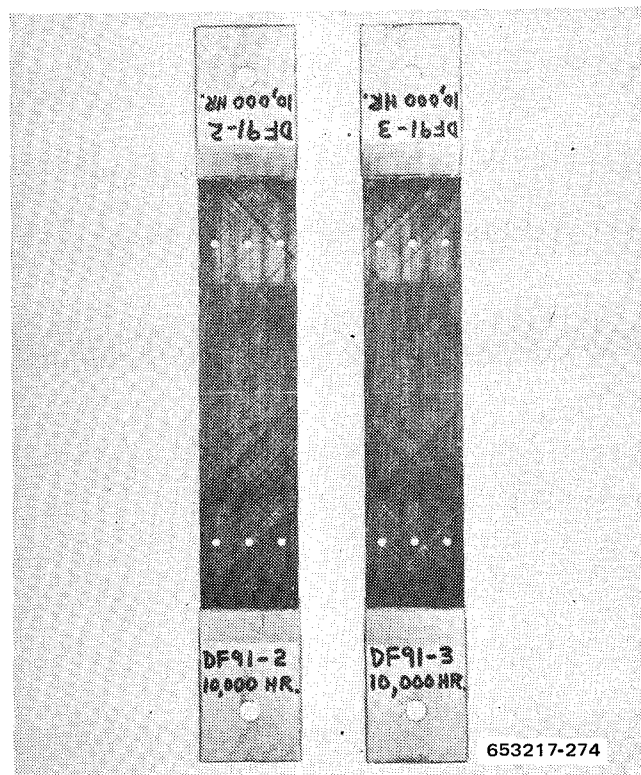


Figure 12-74 G/PI Notched Long-Term Specimens After 10,000 hr of Flight Simulation Exposure (Opposite sides of specimens in Figure 12-73)

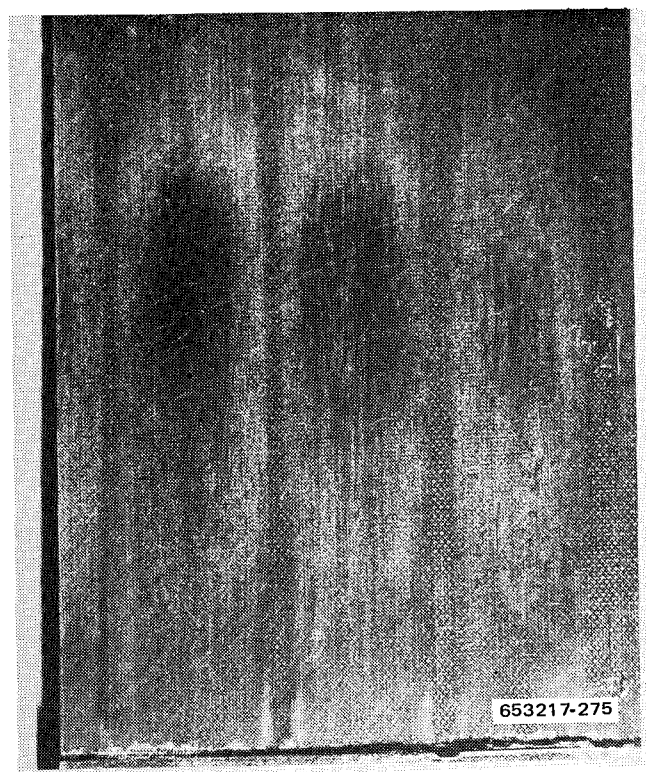


Figure 12-75 G/PI Long-Term Specimen DC91-3 After 10,000 hr of Flight Simulation Exposure Showing Exposed Graphite Fibers in Heated Zone

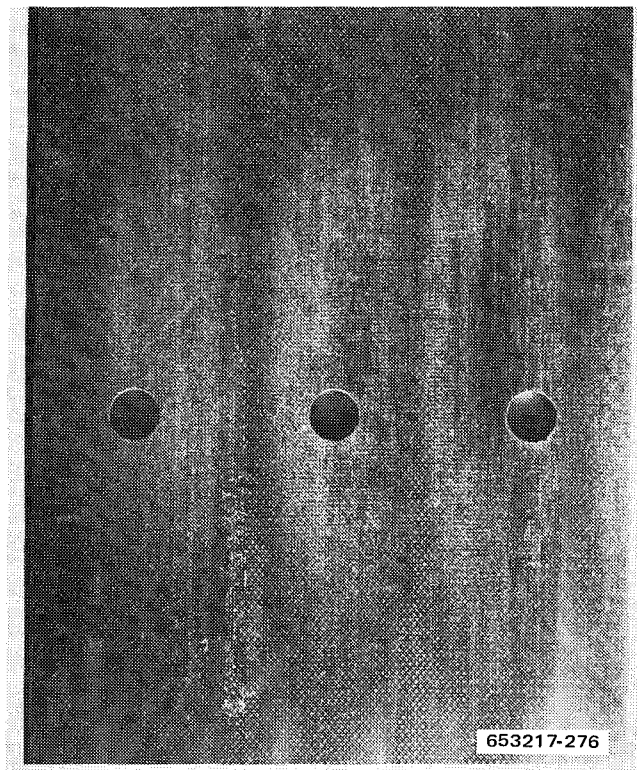


Figure 12-76 G/PI Notched Long-Term Specimen DF91-2 After 10,000 hr of Flight Simulation Exposure Showing Exposed Graphite Fibers in Heated Zone

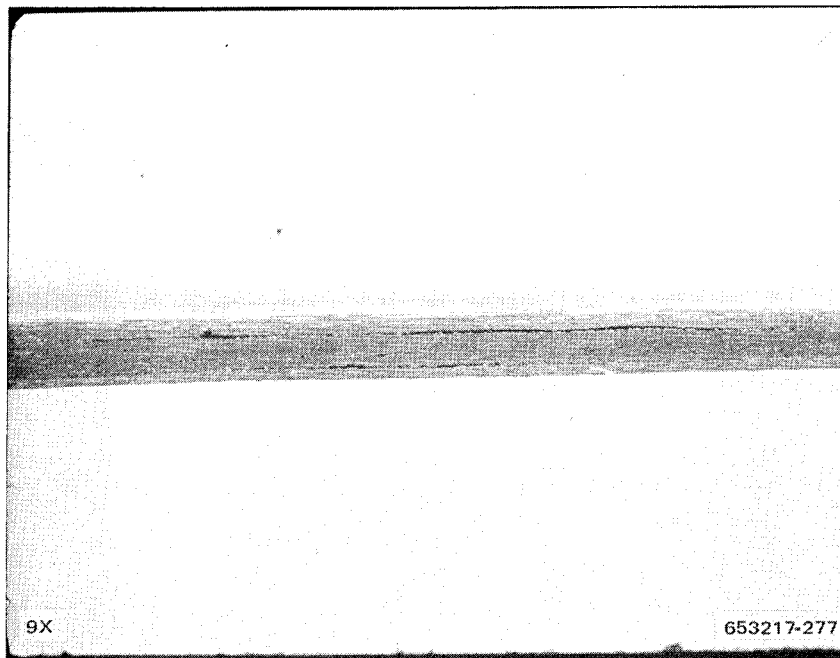


Figure 12-77 G/PI Long-Term Specimen DC91-1 Showing Slight Edge Cracks in Heated Zone After 10,000 hr of Flight Simulation Exposure

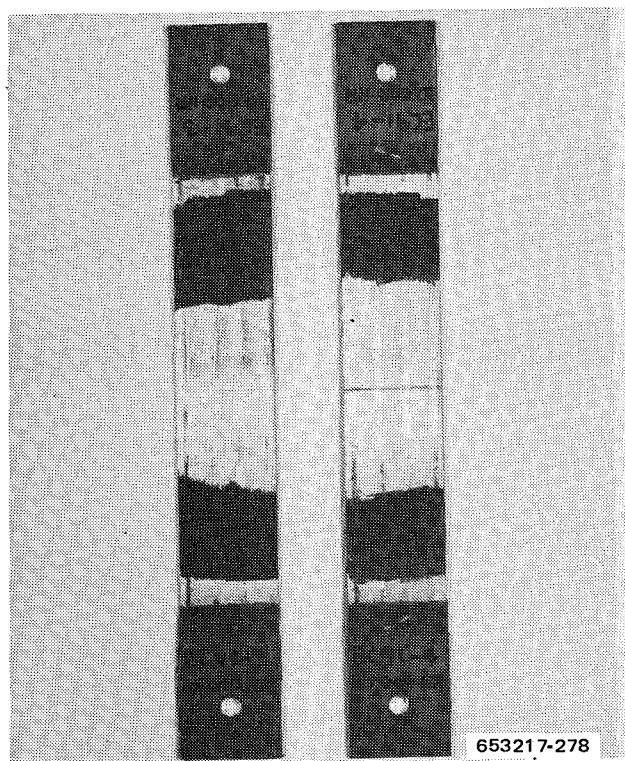


Figure 12-78 Crossply B/AI Long-Term Specimens After 10,000 hr of Flight Simulation Exposure

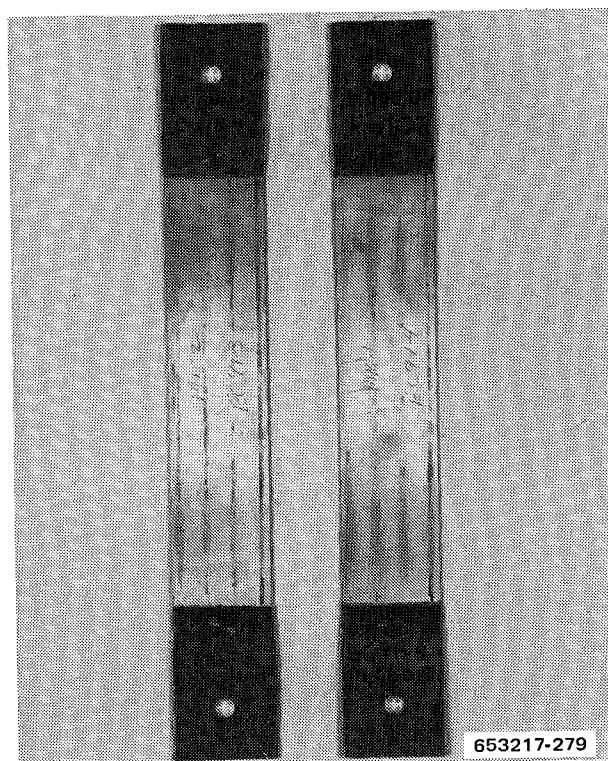


Figure 12-79 Crossply B/AI Long-Term Specimens After 10,000 hr of Flight Simulation Exposure (Opposite sides of specimens in Figure 12-78)

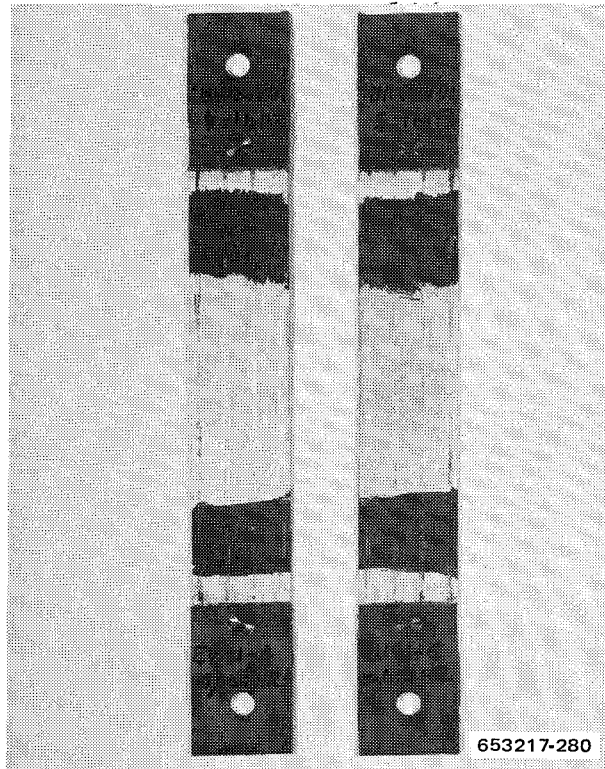


Figure 12-80 Unidirectional B/AI Long-Term Specimens After 10,000 hr of Flight Simulation Exposure

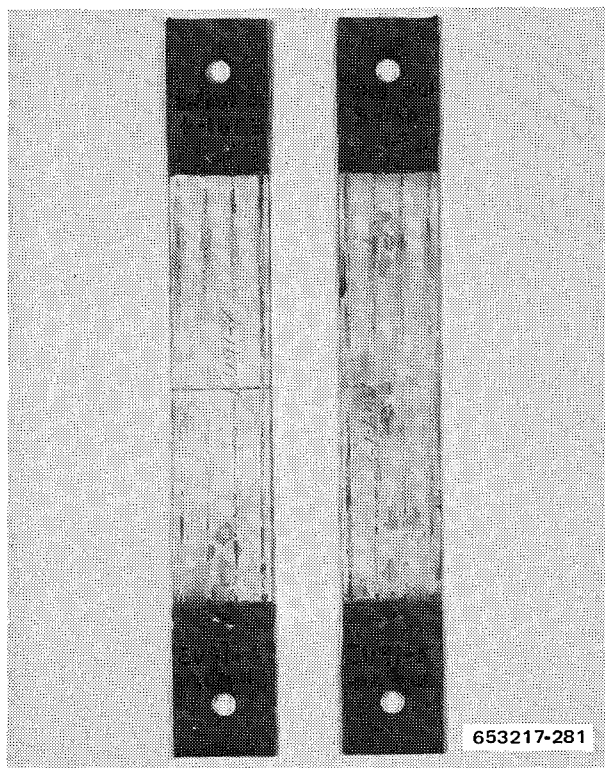
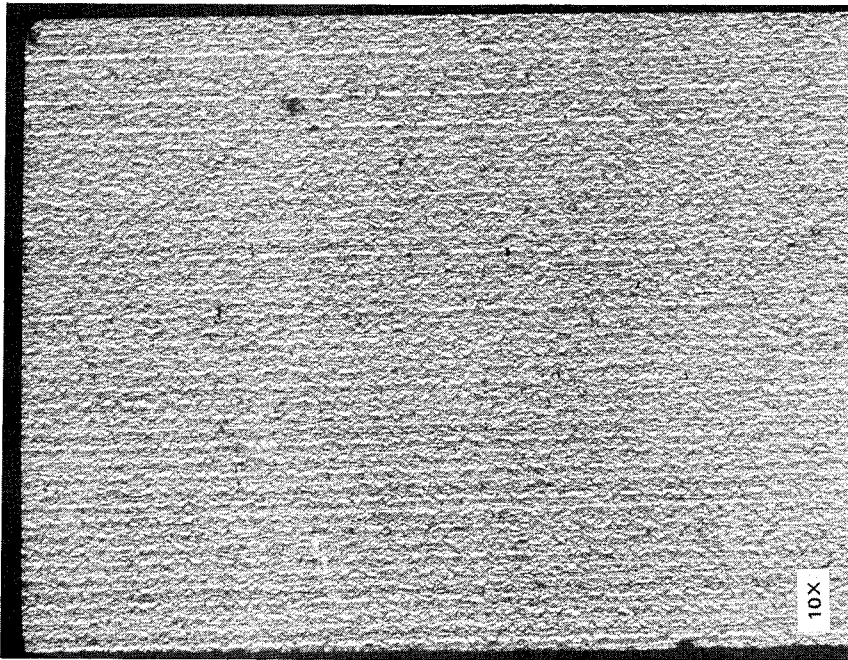


Figure 12-81 Unidirectional B/AI Long-Term Specimens After 10,000 hr of Flight Simulation Exposure (Opposite sides of specimens in Figure 12-80)

noticeable effects on these photographs are the vertical stripes where the stiffener grids were attached. These markings are residue from the Teflon coating on the grids, and in some areas, regions of wear where the soft aluminum surface has been eroded by the rubbing action of the stiffener during fatigue cycling. Careful examination of the surface in the heated zones reveals a roughened surface and some small shallow cracks. The effect is similar to, but not as extensive as, that observed in the specimens that were fatigue tested in air at 561 K (550° F). The surface roughening occurred on both sides but was more difficult to see on the painted side. A magnified view of the heated zone on the unpainted side of a crossplied specimen is shown in Figure 12-82. A photograph taken from the unheated center section of the same specimen is also shown in Figure 12-82 for comparison. The roughened surface was found on both the crossplied and the unidirectional specimens. One other observation was made on the unidirectional specimens. The specimens were flat except in the heated zones where the surface was very irregular (wavy) in the transverse direction. Edge cracks and delaminations were found in two of the crossplied specimens, generally in the heated zones. Figure 12-83 is an enlarged view of the worst area found on these two specimens. An ultrasonic C-scan of the same specimen is shown in Figure 12-84. The regions marked on the C-scan are the areas of the specimen where edge cracks were observed with a stereo microscope. The correlation was quite good. The C-scan indicates the cracks to extend approximately 0.006 m (0.25 in.) into the specimen.

12.7.3.2 Residual Strength Data. The original test plan for residual strength determinations assumed that all five specimens of each set would complete 10,000 hours of exposure and that all of the specimen width would be available for cutting into subsize specimens. For two of the materials, G/E and unidirectional B/Al, all of the Phase I specimens did not survive 10,000 hours. Also, earlier tests on material from the unfailed end of a G/E specimen, BC92-3, that had failed in 4053 hours showed considerable variation in tensile properties across the width of the specimen. Specimens that were shielded by the stiffening grids gave tensile values of 551 MN/m² (79.9 ksi) and 545 MN/m² (79.0 ksi) while a specimen that was cut from between the grids gave 163 MN/m² (23.5 ksi). Because of these results the decision was made to cut the specimens from the unnotched long-term specimens from the material between the grids. This reduced the number of 0.013 m (0.5 in.) wide residual strength specimens that could be obtained from one long-term specimen from 10 to six. For the notched long-term specimens the entire width was used (as was originally planned) so that the number of residual strength specimens remained the same (six per specimen). During the course of the test program, particularly for the thermal aging and the flight simulation tests, it became apparent that compressive and shear properties of the composites were of considerable importance in addition to the tensile characteristics toward which the study was primarily directed. The combination of these three factors 1) less than 100% survival, 2) loss of material from under grids, and 3) increased importance of residual compressive and shear properties resulted in a change in the residual strength test plan. Table 12-18 shows both the original and the revised plans for the G/E and B/E systems. Similar information for the G/PI and B/Al systems is listed in Table 12-19. The number of tests from the G/E unnotched long-term specimens was limited by the amount of material available (two and one-half specimens). Two specimens survived 10,000 hours and the unfailed end of BC92-4, which failed in 9669 hours, was undamaged and considered usable. The number of tests from the G/E notched, B/E unnotched, and B/E notched long-term specimens was intentionally kept small because the poor condition of the specimens



HEATED ZONE



CENTER SECTION

Figure 12-82 B/Al Long-Term Specimen EC91-1 After 10,000 hr of Flight Simulation Exposure Showing Roughened Surface Observed in Heated Zones (Photograph on right shows smooth surface of unheated center section for comparison)

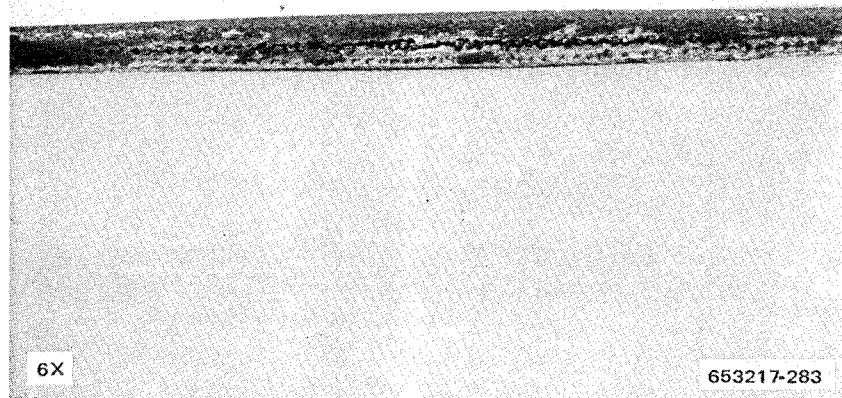
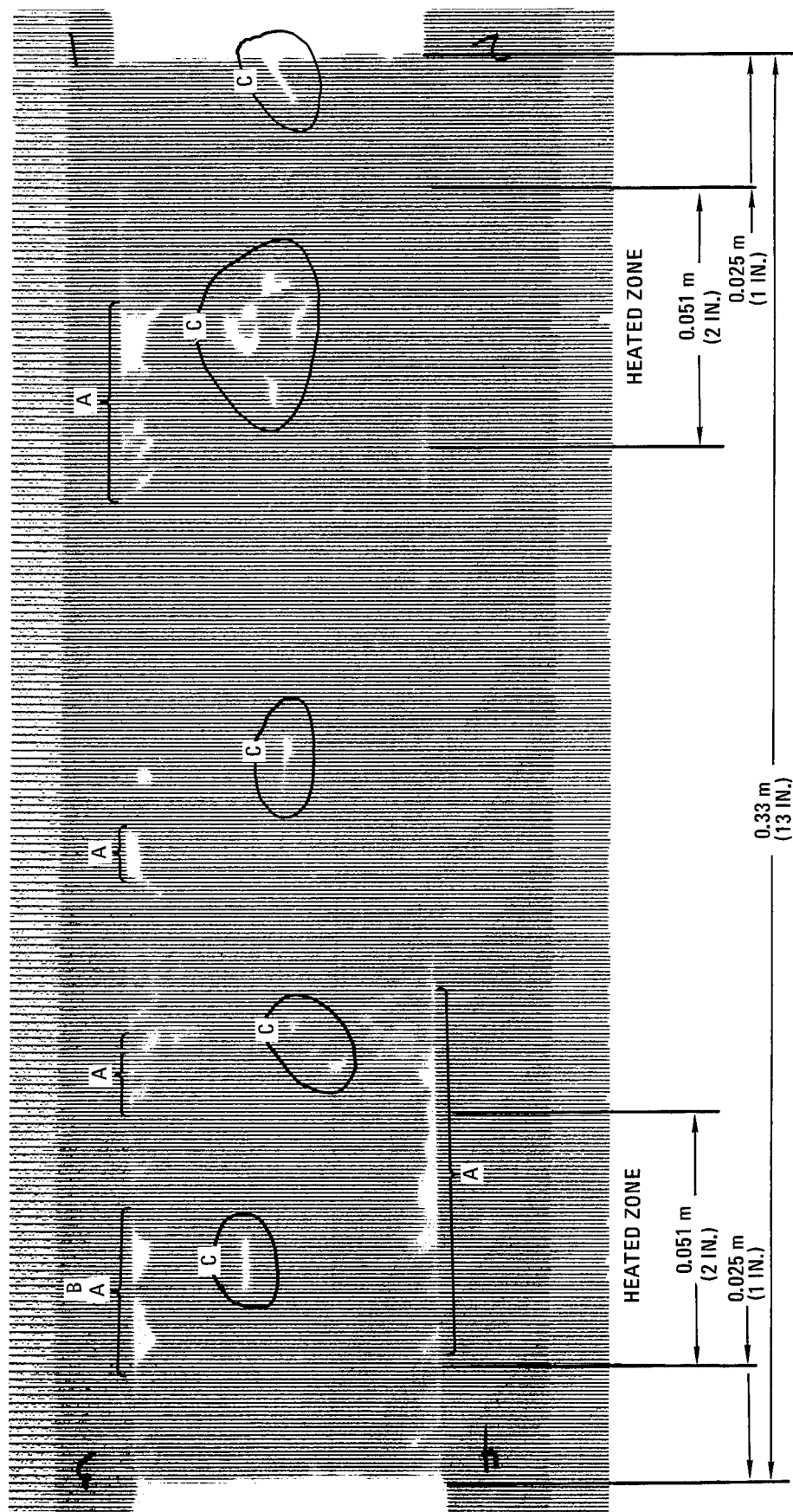


Figure 12-83 B/Al Long-Term Specimen EC91-1 After 10,000 hr of Flight Simulation Exposure Showing Edge Cracking in Heated Zone

did not appear to warrant a full scale residual strength test program. The 10,000 hour flight simulation exposure of the epoxy systems will be repeated using less severe test conditions as described in Section 12.7.4. The revised test plans for the G/PI and B/Al systems were developed to derive as much useful data as possible from a limited amount of test material, all of which was used.

All of the 0.013 m (0.5 in.) wide unnotched tensile and fatigue and B/Al notched tensile and shear specimens were cut from the 0.01 m (0.7 in.) wide portions of the flight simulation specimens between the stiffening grids. The approximate locations of these specimens (six per long-term specimen) can be seen in Figure 12-81 where the residue of the Teflon tape has outlined the location occupied by the grid during flight simulation testing. Bonding of doublers was required on only one end of each of the residual tensile and fatigue specimens as the titanium doubler from the flight simulation specimen was still attached to the other end.

The notched resin matrix flight simulation specimens were 0.073 m (3 in.) wide with three equally spaced 0.0064 m (0.25 in.) diameter holes across the width. Shearing of the specimens would produce three identical 0.025 m (1 in.) wide residual strength specimens with a centrally located hole. For composite material, however, the specimens must be cut with a saw having a finite blade width, approximately 0.0015 m (0.06 in.). Consequently, the notched tensile and fatigue specimens could be cut from the flight simulation specimen in at least three different ways: equal widths with offset holes; unequal widths with centered holes; and equal widths



A. EDGE CRACKS VISIBLE WITH STEREOGRAPHIC MICROSCOPE AT THESE LOCATIONS.

B. PHOTOGRAPH IN FIGURE 12-83 SHOWS THIS REGION.

C. THESE SPOTS CAUSED BY THERMOCOUPLE ADHESIVE THAT REMAINED ON SURFACE.

653217-284

Figure 12-84 Ultrasonic C-Scan of B/AI Long-Term Exposure Specimen EC91-1 After 10,000 hr of Flight Simulation Exposure (Size reduced by approximately 25%)

Table 12-18. Residual Strength Test Plan for Phase I B/E and G/E After 10,000 hr of Flight Simulation Testing

Material System	Flight Simulation Specimen Type	Test Type	Temperature		Number of Specimens	
			K	(°F)	Original Plan	Revised Plan
B/E	[0° ± 45°] _s Unnotched	Tensile	297	75	10	6
		Notched Tensile	297	75	10	0
		Fatigue	297	75	10	9
		Compressive	297	75	0	7
		Tensile	450	350	5	0
		Notched Tensile	450	350	5	0
	[0° ± 45°] _s Notched	Notched Tensile	297	75	10	6
		Notched Fatigue	297	75	10	9
		Notched Tensile	450	350	5	0
G/E	[0° ± 45°] _s Unnotched	Tensile	297	75	10	4
		Notched Tensile	297	75	10	0
		Fatigue	297	75	10	7
		Compressive	297	75	0	2
		Tensile	450	350	5	0
		Notched Tensile	450	350	5	0
	[0° ± 45°] _s Notched	Notched Tensile	297	75	10	6
		Notched Fatigue	297	75	10	9
		Notched Tensile	450	350	5	0

with centered holes. A check of reference 23 showed that the various configurations had very little difference in K_t factors. The one selected was specimens of equal widths with offset holes

in the two outer specimens. The difference in $\frac{\sigma_{\max}}{\sigma}$ values for the specimen with a centered hole and one with an offset hole was negligible (3.28 versus 3.30). Again, bonding of doublers was required on only one end.

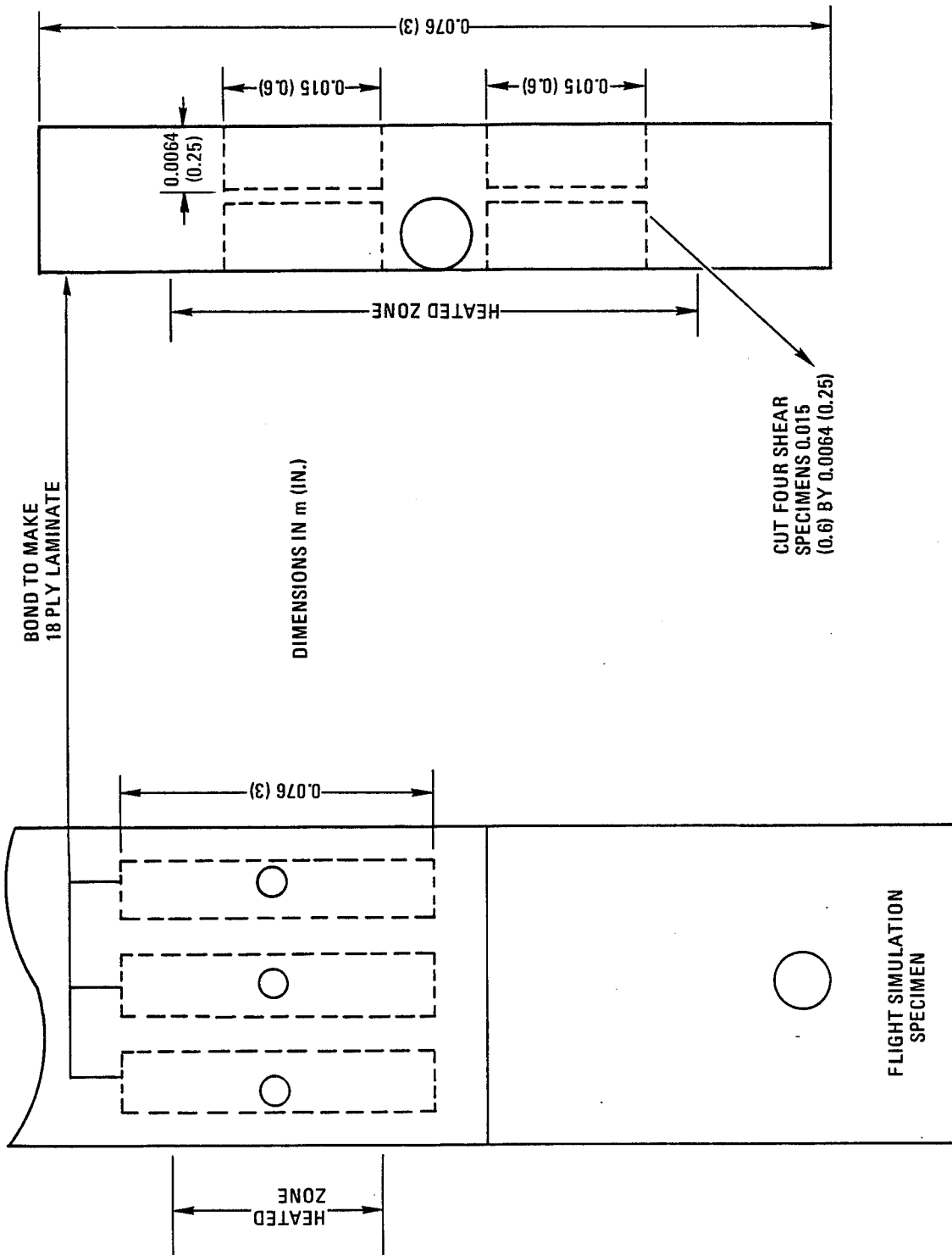
The residual compressive tests were performed using the specimen and test procedures described in Section 7. To get a sufficiently thick specimen for compressive testing from the 6 ply flight simulation specimens it was necessary to bond three or four layers together. From these 18 or 24 ply panels the 0.0064 m (0.25 in.) wide compressive specimens could be cut. Two specimens, made by laminating three or four 0.01 m (0.75 in.) wide pieces together, used the entire width of one end of a flight simulation specimen. Four compressive specimens, using one entire flight simulation specimen, were made for the crossplied B/E, G/PI, B/Al, and the unidirectional B/Al materials. The limited amount of G/E available allowed only two compressive specimens of this material. Since there were no failures of the B/E flight simulation specimens and the number of residual strength specimens was already reduced, sufficient material was

Table 12-19. Residual Strength Test Plan for Phase I G/PI and B/Al After 10,000 hr of Flight Simulation Testing

Material System	Flight Simulation Specimen Type	Test Type	Temperature		Number of Specimens	
			K	(°F)	Original Plan	Revised Plan
G/PI	[0° ± 45°] _s Unnotched	Tensile	297	75	10	5
		Notched Tensile	297	75	10	5
		Fatigue	297	75	10	9
		Compressive	297	75	0	4
		Tensile	505	450	5	5
		Notched Tensile	505	450	5	0
	[0° ± 45°] _s Notched	Notched Tensile	297	75	10	10
		Notched Fatigue	297	75	10	10
		Shear	297	75	0	4
		Notched Tensile	505	450	5	5
B/Al	[0° ± 45°] _s Unnotched	Tensile	297	75	10	4
		Notched Tensile	297	75	10	4
		Fatigue	297	75	10	8
		Compressive	297	75	0	4
		Tensile	505	450	5	4
		Notched Tensile	505	450	5	4
	[0°] ₆ Unnotched	Tensile	297	75	10	4
		Notched Tensile	297	75	10	4
		Fatigue	297	75	10	7
		Shear	297	75	5	3
		Compressive	297	75	0	4
		Tensile	505	450	5	0
		Notched Tensile	505	450	5	0
		Shear	505	450	5	0

available for another type of laminated compressive specimen. These were made by bonding four pieces together that were cut from the areas between the grids. Two flight simulation specimens provided enough material for three of the 0.0064 m (0.25 in.) wide compressive specimens. These two types of B/E compressive specimens were intended to show the effect of the stiffening grids on shielding the composite material during flight simulation exposure.

Residual interfiber shear strength tests were performed on the unidirectional B/Al material. No unidirectional resin matrix specimens were included in the flight simulation test program, however, and, therefore, no residual shear strength tests were originally scheduled. Examination of the failed G/E flight simulation specimens indicated that interlaminar shear strength played an important role in the premature failures and obtaining residual shear properties would be very useful. There was one half of a 10,000-hour notched G/PI simulation specimen that was not used for residual strength testing, and a method was devised to use this material to fabricate four short beam shear specimens. As shown in Figure 12-85 three strips were cut



653217-285

Figure 12-85 Plan for Cutting Short Beam Shear Specimen from G/PI Flight Simulation Specimen

from between the grid marks in the heated zone and bonded together to make an 18 ply laminate. The four short beam shear specimens, 0.015 m (0.60 in.) by 0.0064 m (0.25 in.), were cut from material just above and below the holes. As the heated zone in the simulation specimen was 0.05 m (2 in.) long and the holes 0.0064 m (0.25 in.) in diameter, there was sufficient room for cutting the specimens above and below the holes. The layout of the specimens was as shown in Figure 12-85.

B/E, $[0^\circ \pm 45^\circ]_s$, unnotched and notched. Residual tensile, notched tensile, and compressive data for B/E after 10,000 hours of flight simulation exposure are listed in Table 12-20. Elastic modulus values are included for all unnotched tensile and compressive tests. Compressive data are shown for the two methods of test specimen fabrication described earlier. Baseline tensile, notched tensile, and compressive values are also included in Table 12-20. Residual axial fatigue data at room temperature and a stress ratio, R , of 0.1 for unnotched and notched specimens are presented in Table 12-21, and S-N curves are plotted in Figures 12-86 and 12-87. Also included on the graphs are S-N curves (no data points) for unexposed material tested under the same conditions (presented earlier in Section 11, Baseline Fatigue Testing).

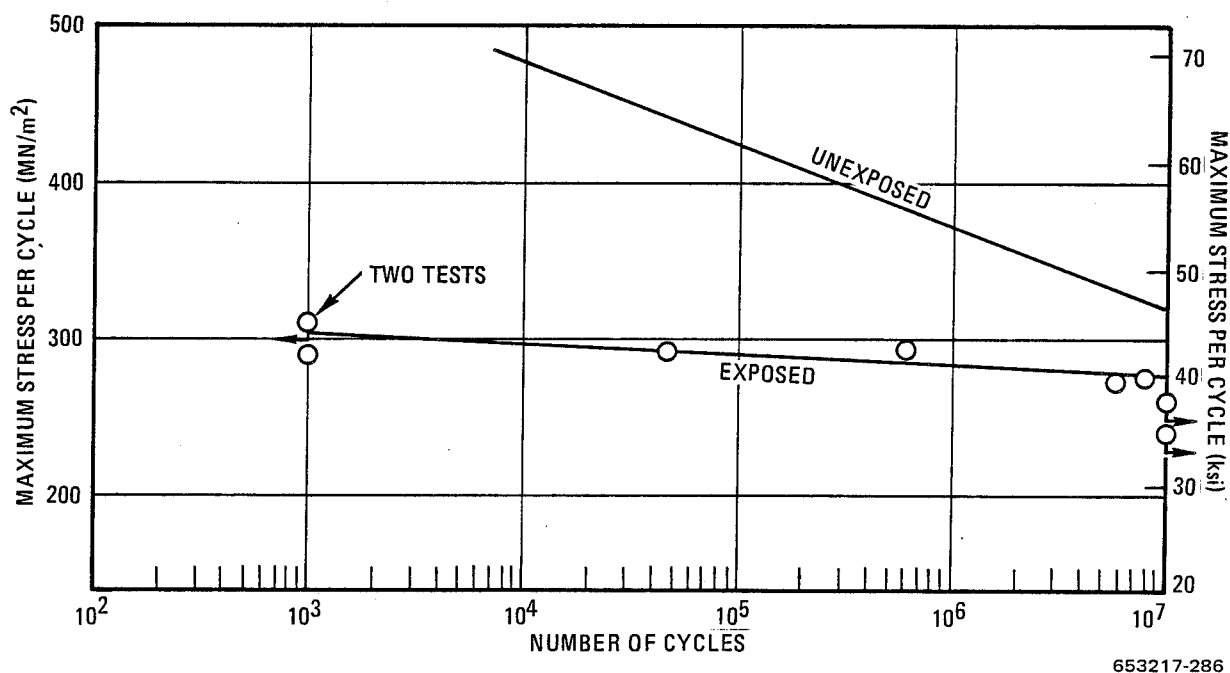


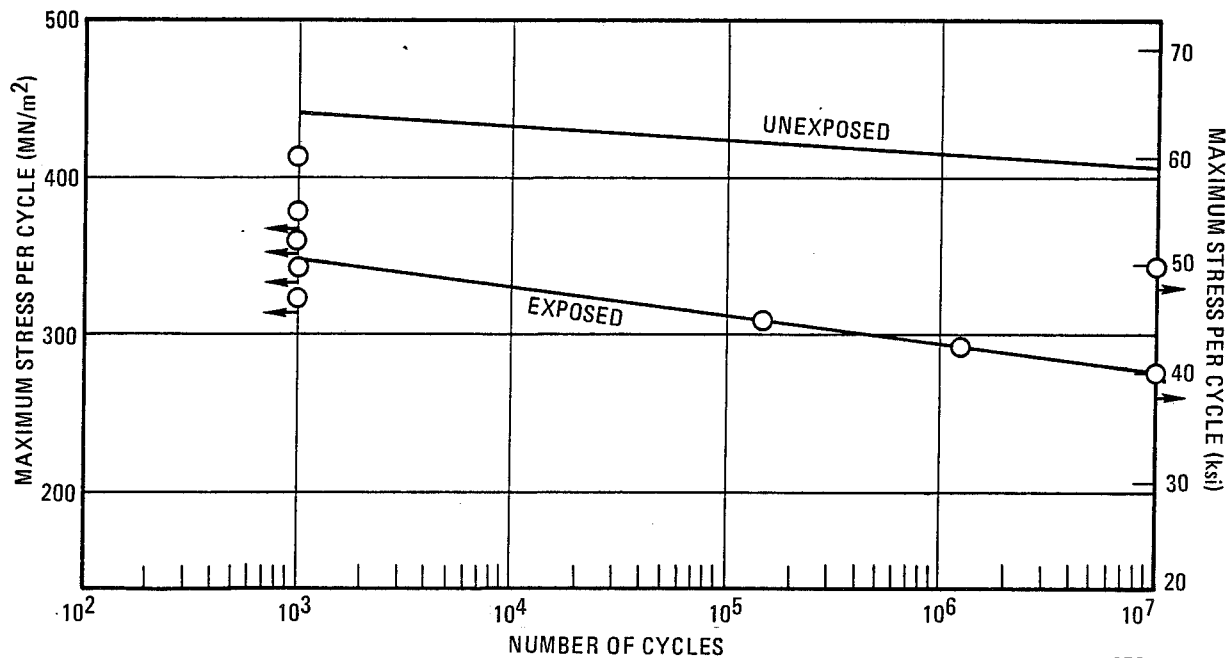
Figure 12-86 Axial Fatigue Properties of $[0^\circ \pm 45^\circ]_s$ B/E Before and After 10,000 hr Flight Simulation Exposure, 297 K (75° F), $R = 0.1$, Unnotched

Table 12-20. Strength and Modulus Properties of $[0^\circ \pm 45^\circ]_s$ B/E at 297 K (75° F) Before and After 10,000 hr of Flight Simulation Exposure

Specimen Number	Flight Simulation Specimen Number	Strength		Modulus	
		MN/m ²	(ksi)	GN/m ²	(Msi)
Unnotched Tensile: 10,000 hr					
A912-1	AC91-2	392	56.8	68.9	10.0
-2	-2	373	54.1	73.8	10.7
A913-1	-3	498	72.2	86.2	12.5
-2	-3	400	58.0	76.5	11.1
A914-1	-4	362	52.5	71.7	10.4
-2	-4	337	48.9	60.0	8.7
	av	394	57.1	72.8	10.6
Baseline	av	61.8	89.7	94.5	13.7
Notched Tensile: 10,000 hr					
AF913-1	AF91-3	452	65.6		
-2	-3	411	59.6		
-3	-3	412	59.7		
AF915-1	-5	315	45.7		
-2	-5	366	53.1		
-3	-5	424	61.5		
	av	397	57.5		
Baseline	av	461	64.2		
Compressive: 10,000 hr (entire specimen width used)					
A9C-1	AC91-1	834	120.9	84.1	12.2
-2	-1	934	135.4	82.0	11.9
-3	-1	834	120.9	86.2	12.5
-4	-1	1086	154.9	82.7	12.0
	av	918	133.0	83.8	12.2
Compressive: 10,000 hr (cut from between grids)					
A9C-5	AC91-5	741	107.5	79.3	11.5
-6	-5 & AC92-5	709	102.9	72.4	10.5
-7	AC92-5	754	109.3	82.0	11.9
	av	735	106.6	77.9	11.3
Baseline	av	1540	223.4	102	14.8

Table 12-21. Residual Axial Fatigue Data for $[0^\circ \pm 45^\circ]_s$ B/E at 297 K (75° F) After 10,000 hr of Flight Simulation Exposure, $R = 0.1$

Specimen Number	Flight Simulation Specimen Number	Specimen Type	Maximum Stress		Cycles	Comments
			MN/m ²	(ksi)		
A912-3	AC91-2	Unnotched	310	45	<1,000	
A913-3	-3		276	40	7,975,000	
-4	-3		293	42.5	47,000	
-5	-3		276	40	5,872,000	
-6	-3		310	45	<1,000	
A914-3	-4		293	42.5	600,000	
-4	-4		241	35	15,234,000	Did not fail
-5	-4		259	37.5	10,245,000	Did not fail
-6	-4		293	42.5	1,000	
AF913-4	AF91-3	Notched	345	50	10,000,000	Did not fail
-5	-3		414	60	1,000	
-6	-3		379	55	<1,000	
AF914-1	-4		362	52.5	<1,000	
-2	-4		345	50	<1,000	
-3	-4		328	47.5	<1,000	
AF915-4	-5		310	45	149,000	
-5	-5		293	42.5	1,213,000	
-6	-5		276	40	12,729,000	Did not fail



653217-287

Figure 12-87 Axial Fatigue Properties of $[0^\circ \pm 45^\circ]_s$ B/E Before and After 10,000 hr of Flight Simulation Exposure, 297 K (75° F), $R = 0.1$, Notched

The unnotched tensile strength was considerably lowered as a result of the 10,000 hours of flight simulation exposure while the notched strength was lowered only 10%. The notched properties of the resin matrix systems have generally shown smaller decreases than the unnotched after exposure. This may, in part, result from the method of specimen cutting where portions of the notched specimens had been shielded by the stiffening grids, whereas the unnotched specimens were cut from material between the grids. Compressive strength was degraded slightly more than the unnotched tensile strength. The residual compressive data also show the effect of the stiffening grid in protecting the underlying material. Specimens cut from the entire width had a compressive strength approximately one-third greater than specimens cut from between the grids. As shown in Figures 12-86 and 12-87, the fatigue properties were considerably lowered by the long-term exposure cycling.

G/E, $[0^\circ \pm 45^\circ]_s$, unnotched and notched. Residual tensile, notched tensile, compressive, and elastic modulus values for G/E after 10,000 hours of flight simulation exposure are listed in Table 12-22. Data for unexposed material are also included in the table. Residual axial fatigue

Table 12-22. Strength and Modulus Properties of $[0^\circ \pm 45^\circ]_s$ G/E at 297 K (75° F) Before and After 10,000 hr of Flight Simulation Exposure

Specimen Number	Flight Simulation Specimen Number	Strength		Modulus		
		MN/m ²	(ksi)	GN/m ²	(Msi)	
Unnotched Tensile: 10,000 hr						
B921-1	BC92-1	429	62.2	39	5.7	
-2	-1	427	62.0	46	6.7	
B922-1	-2	410	59.5	46	6.6	
-2	-2	411	59.6	50	7.2	
		av	419	60.8	45	6.6
Baseline		av	496	71.9	57	8.3
Notched Tensile: 10,000 hr						
BF911-1	BF91-1	413	59.9			
-2	-1	445	64.6			
-3	-1	377	54.7			
BF923-1	BF92-3	388	56.3			
-2	-3	470	68.2			
-3	-3	362	52.5			
		av	409	59.4		
Baseline		av	412	59.7		
Compressive: 10,000 hr (entire specimen width used)						
B9C-1	BC92-1	316	45.8	46	6.6	
-2	-1	293	42.5	47	6.8	
		av	304	44.2	46	6.7
Baseline		av	570	82.7	46	6.6

data at room temperature and a stress ratio, R , of 0.1 for unnotched and notched specimens are presented in Table 12-23, and S-N curves are plotted in Figures 12-88 and 12-89. S-N curves for unexposed material are shown on the fatigue plots for comparison.

Eight unnotched and four notched long-term specimens of G/E did not complete 10,000 hours of exposure, either because of complete failure or significant damage in the heated zones. In spite of this the residual tensile properties, particularly for the unnotched specimens, were not severely degraded. The compressive strength was, however, greatly affected. After 10,000 hours of flight simulation the compressive strength was reduced by approximately one-half. This decrease would be anticipated if the failure mechanism proposed for the specimens that did not survive the flight simulation exposures was correct. The residual fatigue properties were significantly lowered with the unnotched material again experiencing a greater decrease than the notched.

G/PI, $[0^\circ \pm 45^\circ]_s$, unnotched and notched. Results of the 297 K (75° F) and 505 K (450° F) tensile tests on unnotched and notched G/PI after 10,000 hours of flight simulation exposure are presented in Tables 12-24 and 12-25. Also included are the baseline data for comparison purposes. Two types of notched tensile specimens were tested. The first, Table 12-24, was cut from unnotched flight simulation specimens and was notched after exposure. The second, Table 12-25, was cut from the notched flight simulation specimens after being exposed in the notched condition. Table 12-26 gives the compressive and short beam shear data for G/PI before and after flight simulation exposure of 10,000 hours. Results of the residual fatigue tests on the unnotched and notched G/PI material at 297 K (75° F) and a stress ratio, R , of 0.1 are listed in Table 12-27 and plotted as S-N curves in Figures 12-90 and 12-91. Data for unexposed G/PI tested under the same conditions are shown on the fatigue plots for comparison.

Table 12-23. Residual Axial Fatigue Data for $[0^\circ \pm 45^\circ]_s$ G/E at 297 K (75° F) After 10,000 hr of Flight Simulation Exposure, $R = 0.1$

Specimen Number	Flight Simulation Specimen Number	Specimen Type	Maximum Stress		Cycles	Comments
			MN/m ²	(ksi)		
B922-3	BC92-2	Unnotched	379	55	<1,000	
-4	-2		345	50	6,968,000	
-5	-2		362	52.5	3,000	
-6	-2		328	47.5	1,000	
B924-1	BC92-4		310	45	4,000	
-2	-4	Notched	276	40	18,000	
-3	-4		224	32.5	10,466,000	Did not fail
BF925-1	BF92-5		276	40	1,829,000	
-2	-5		310	45	1,143,000	
-3	-5		345	50	2,000	
-4	-5		328	47.5	2,571,000	Bond failure
-5	-5		362	52.5	112,000	Bond failure
-6	-5		379	55	1,000	
BF923-4	-3		328	47.5	630,000	
-5	-3		362	52.5	1,662,000	
-6	-3		241	35	5,778,000	

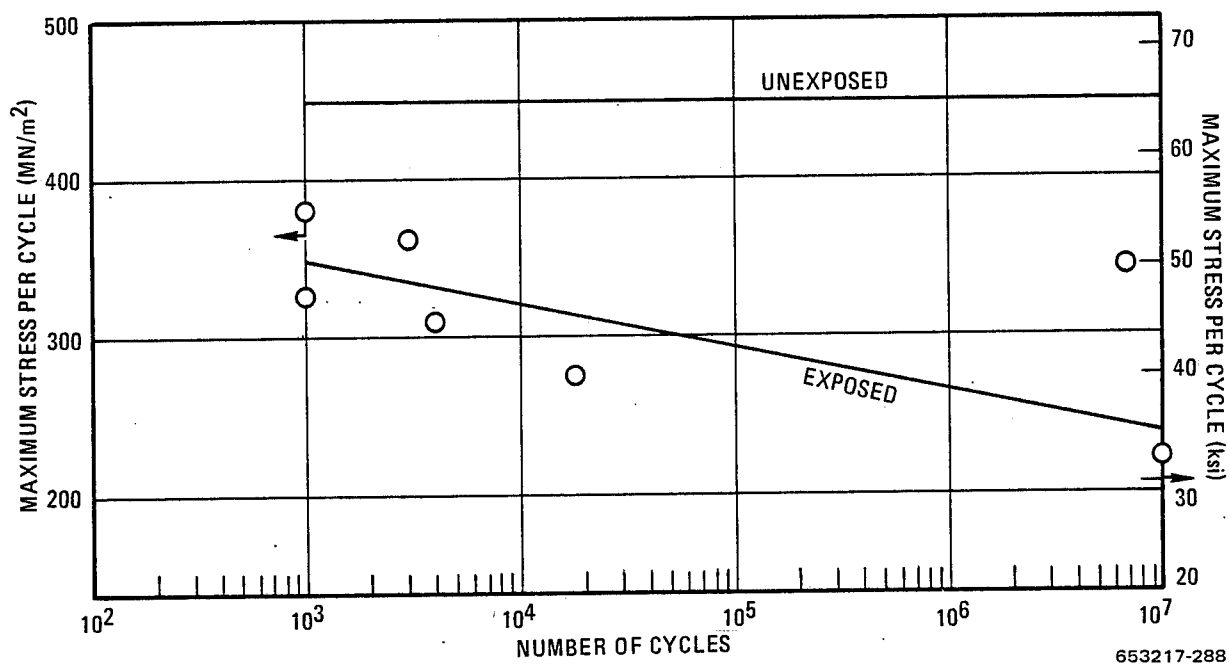


Figure 12-88 Axial Fatigue Properties of $[0^\circ \pm 45^\circ]_s$ G/E Before and After 10,000 hr of Flight Simulation Exposure, 297 K (75° F), $R = 0.1$, Unnotched

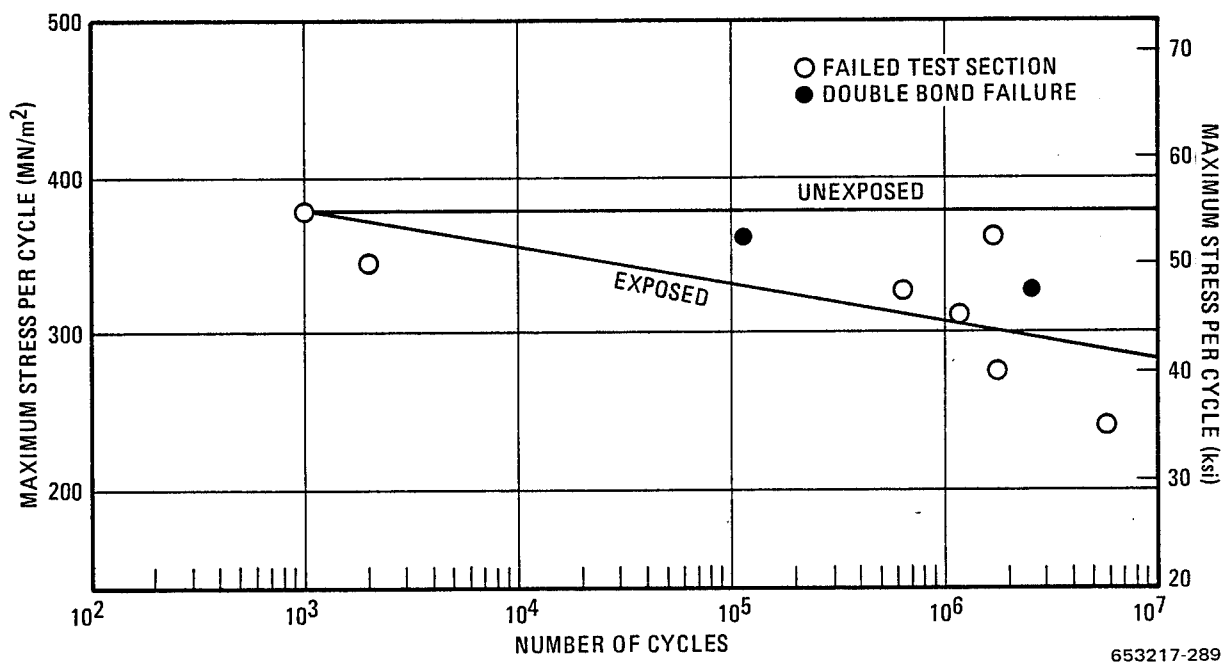


Figure 12-89 Axial Fatigue Properties of $[0^\circ \pm 45^\circ]_s$ G/E Before and After 10,000 hr of Flight Simulation Exposure, 297 K (75° F), $R = 0.1$, Notched

Table 12-24. Strength and Modulus Properties of $[0^\circ \pm 45^\circ]_s$ G/PI Before and After 10,000 hr of Flight Simulation Exposure. (Unnotched flight simulation specimen)

Specimen Number	Flight Simulation Specimen Number	Temperature		Strength		Modulus		
		K	(°F)	MN/m ²	(ksi)	GN/m ²	(Msi)	
Unnotched Tensile: 10,000 hr								
D912-1	DC91-2	297	75	405	58.8	47	6.8	
-2	-2			331	48.0	46	6.6	
-3	-2			225	32.7	41	5.9	
-4	-2			323	46.8	46	6.7	
-5	-2			510	74.0	—	—	
D914-6	-4			423	61.4	48	6.9	
D915-1	-5			372	54.0	46	6.7	
				av	370	53.7	46	6.6
Baseline				av	519	75.3	53	7.7
D912-6	DC91-2	505	450	334	48.5	36	5.2	
-1	-3			411	59.6	54	7.8	
-2	-3			303	43.9	42	6.1	
-3	-3			225	32.7	37	5.4	
-4	-3			296	43.0	41	6.0	
				av	314	45.5	42	6.1
Baseline				av	470	68.2	47	6.8
Notched Tensile: 10,000 hr								
D915-2	DC91-5	297	75	385	55.8			
-3	-5			198	28.7			
-4	-5			336	48.8			
-5	-5			346	50.2			
-6	-5			199	28.8			
				av	293	42.5		
Baseline				av	357	51.8		

Table 12-25. Notched Tensile Strength of $[0^\circ \pm 45^\circ]_s$ G/PI Before and After 10,000 hr of Flight Simulation Exposure. (Notched flight simulation specimen)

Specimen Number	Flight Simulation Specimen Number	Temperature		Strength		
		K	(°F)	MN/m ²	(ksi)	
Notched Tensile: 10,000 hr						
DF911-1	DF91-1	297	75	348	50.5	
-2	-1			427	61.9	
-3	-1			342	49.6	
-4	-1			315	45.7	
-5	-1			355	51.5	
-6	-1			247	35.8	
DF912-1	-2			261	37.8	
-2	-2			323	46.9	
-3	-2			376	54.5	
DF914-1	-4			271	39.3	
				av	326	47.4
Baseline				av	357	51.8
DF914-3	DF91-4	505	450	256	37.2	
-4	-4			294	42.7	
-5	-4			377	54.7	
-6	-4			397	57.6	
DF915-1	-5			336	48.7	
				av	332	48.2
Baseline				av	336	48.8

While no G/PI specimens failed during the 10,000 hours of flight simulation exposure, the unnotched tensile strength at both room and elevated temperatures decreased by about one-third. The residual notched tensile data appear to indicate a difference in the average amount of degradation depending on whether the notch was machined in the specimen before or after exposure. Those specimens that were notched after exposure showed a greater average decrease in strength. Further analysis of the data, however, indicates that the location from which the residual notched tensile specimen was cut from the flight simulation specimen may be more important. Six notched tensile specimens are cut from a flight simulation specimen, two from the center and four from the outer edges (see Figure 12-10 for cutting plan). The center specimens are shielded during exposure by two metal strips of the compressive stiffening grids while the outer specimens are each shielded by only one. The locations of these strips with respect to where the six residual strength specimens are cut can be seen in Figure 12-65. In addition to having two, presumably, higher strength portions, the center specimens are

Table 12-26. Compressive and Short Beam Shear Strength Properties of $[0^\circ \pm 45^\circ]_s$ G/PI at 297 K (75° F) Before and After 10,000 hr of Flight Simulation Exposure

Specimen Number	Flight Simulation Specimen Number	Strength		Modulus		
		MN/m ²	(ksi)	GN/m ²	(Msi)	
Compressive: 10,000 hr						
D9C-1	DC91-1	326	47.3	41	5.9	
-2	-1	299	43.3	41	6.0	
-3	-1	264	38.3	39	5.6	
-4	-1	274	39.7	41	5.9	
		av	291	42.2	40	5.8
Baseline		av	377	54.7	46	6.7
Short Beam Shear: 10,000 hr						
D9S-1	DF91-5	18	2.6			
-2	-5	18	2.6			
-3	-5	16	2.3			
-4	-5	17	2.4			
		av	17	2.5		
Baseline		av	37	5.4		

Table 12-27. Residual Axial Fatigue Data for $[0^\circ \pm 45^\circ]_s$ G/PI at 297 K (75° F) After 10,000 hr of Flight Simulation Exposure, R = 0.1

Specimen Number	Flight Simulation Specimen Number	Specimen Type	Maximum Stress		Cycles	Comments
			MN/m ²	(ksi)		
D913-5	DC91-3	Unnotched	293	42.5	<1,000	
-6	-3		241	35	<1,000	
D914-1	-4		207	30	<1,000	
-2	-4		172	25	12,262,000	Did not fail
-3	-4		190	27.5	10,256,000	Did not fail
-4	-4	Notched	198	28.75	<1,000	
-5	-4		190	27.5	10,269,000	Did not fail
DF912-4	DF91-2		276	40	1,099,000	
-5	-2		270	39.1	15,405,000	Did not fail
-6	-2		283	41.1	10,219,000	Did not fail
DF913-1	-3		345	50	<1,000	
-2	-3		310	45	4,000	
-3	-3		310	45	1,000	
-4	-3		293	42.5	53,000	
-5	-3		293	42.5	2,424,000	
-6	-3		293	42.5	<1,000	
DF914-2	-4		293	42.5	6,000	

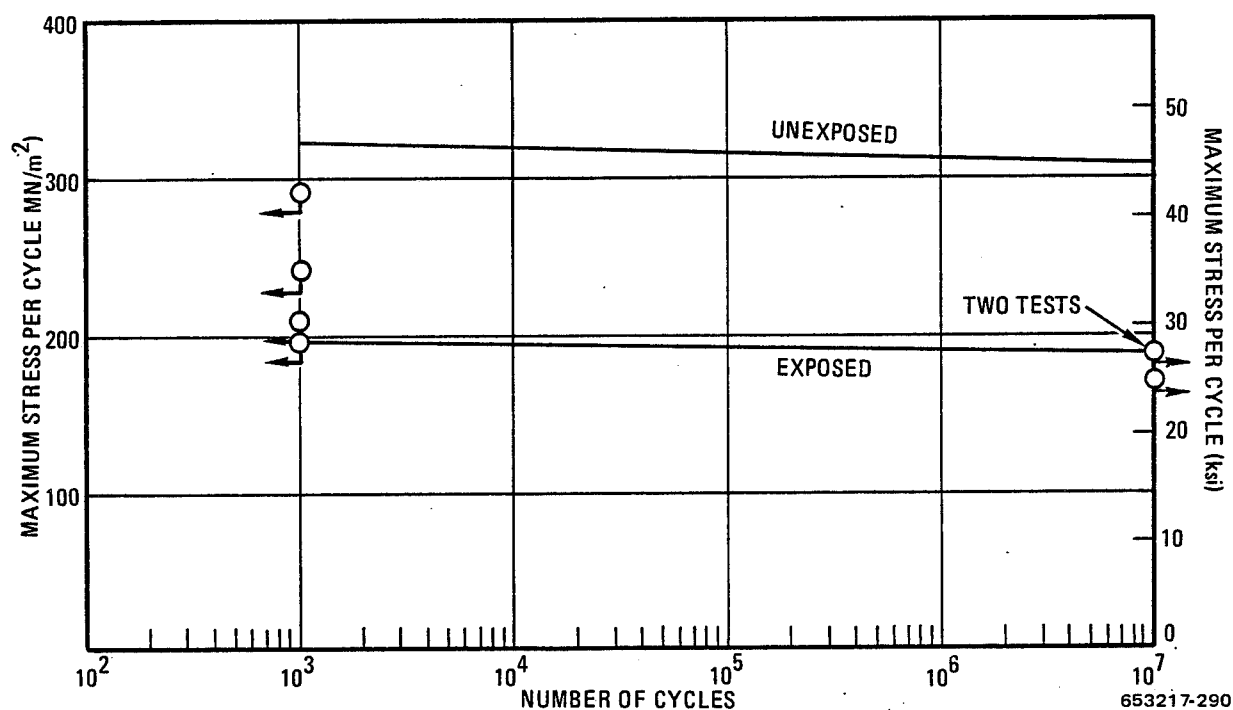


Figure 12-90 Axial Fatigue Properties of $[0^\circ \pm 45^\circ]_s$ G/PI Before and After 10,000 hr of Flight Simulation Exposure, 297 K (75° F), $R = 0.1$, Unnotched

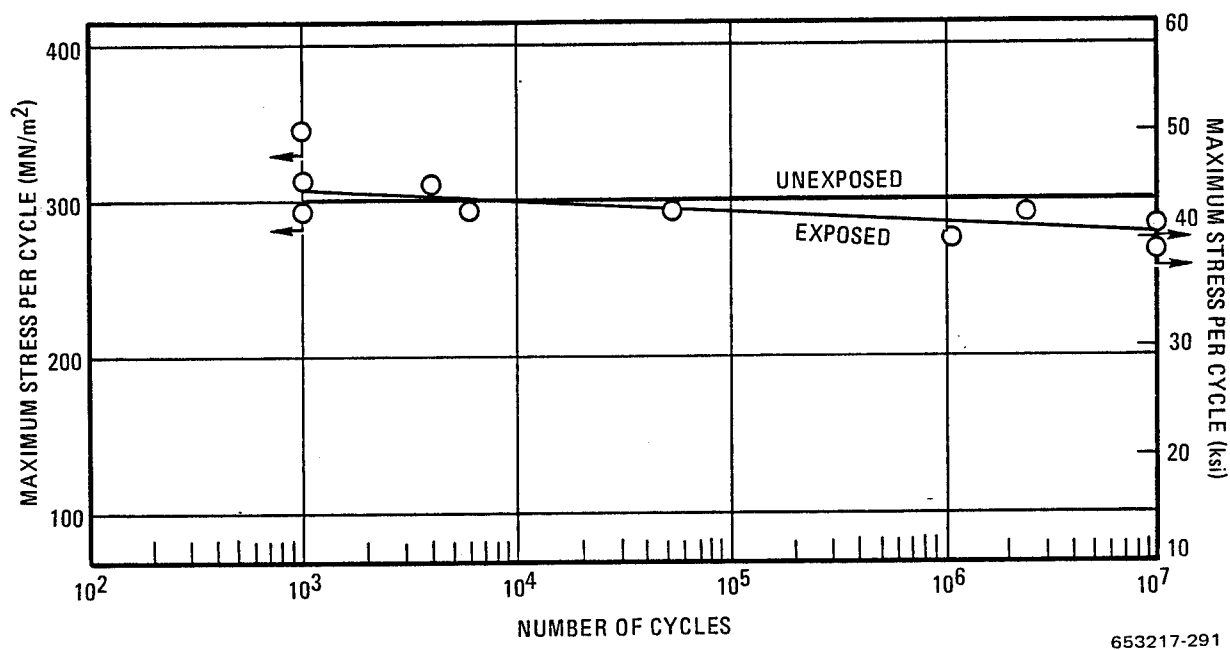


Figure 12-91 Axial Fatigue Properties of $[0^\circ \pm 45^\circ]_s$ G/PI Before and After 10,000 hr of Flight Simulation Exposure, 297 K (75° F), $R = 0.1$, Notched

symmetric with respect to these shielded portions. The outer specimens have a shielded portion on only one side of the center hole, and consequently, may experience uneven loading, which could initiate premature failure. To check out these effects the outer specimen (dash numbers 1, 3, 4, and 6) and center specimen (dash numbers 2 and 5) notched tensile strengths are compared in Table 12-28. The data are listed by temperature, without regard to whether the notches were introduced before or after flight simulation. For the room temperature tests, where sufficient data are available there is a distinct difference in the two types of specimens. The more heavily shielded center specimens were approximately 25% higher in notched tensile strength. In like manner to the G/E material, the G/PI experienced a significant reduction in compressive strength after 10,000 hours of exposure. The decrease was not as great as that for G/E, however, approximately 25% as compared to 50%. It is interesting to note that the loss in tensile strength was greater than that for compressive strength. Again, however, specimen location may be playing a role as the compressive specimens were prepared from the entire width of the specimens while the tensile specimens were cut from the unshielded areas. The residual short beam shear data indicate an apparent major reduction in interlaminar shear strength has occurred as a result of the 10,000 hours of flight simulation exposure. This degradation, if real, correlates well with the failure mechanism proposed earlier for the G/E specimens. The data, however, are limited, and the effect of bonding 6 ply laminates together to form 18 ply short beam shear specimens requires additional study to determine the usefulness of the results. The unnotched fatigue properties were greatly affected with a lowering of the S-N curve of approximately 40% over the entire range from 10^3 to 10^7 cycles. The notched fatigue strength, on the other hand, was just slightly lowered by the 10,000 hours of exposure.

Table 12-28. Effect of Specimen Location on Residual Notched Tensile Strength of $[0^\circ \pm 45^\circ]_s$ G/PI After 10,000 hr of Flight Simulation Exposure

Flight Simulation Specimen Number	Temperature		Outer Specimen Strength		Center Specimen Strength		
	K	(°F)	MN/m ²	(ksi)	MN/m ²	(ksi)	
DC91-5	297	75	198	28.7	385	55.8	
-5			336	48.8	346	50.2	
-5			199	28.8			
DF91-1	505	450	348	50.5	427	61.9	
-1			342	49.6	355	51.5	
-1			315	45.7			
-1			247	35.8			
-2			261	37.8	323	46.9	
-2			376	54.5			
-4			271	39.3			
			av	289	41.9	367	53.2
DF91-4			256	37.2	377	54.7	
-4			294	42.7			
-4			397	57.6			
-5			336	48.7			
			av	321	46.6	377	54.7

B/Al, $[0^\circ \pm 45^\circ]_s$ and $[0^\circ]_6$, unnotched. Results of the room and elevated temperature tensile tests on unnotched and notched B/Al before and after 10,000 hours of flight simulation exposure are presented in Tables 12-29 and 12-30. Residual compressive data for both crossply and unidirectional B/Al are presented in Table 12-31. No baseline compressive tests were conducted on either of the B/Al layups. Also included in Table 12-31 are interfiber shear strength data from unidirectional B/Al before and after flight simulation exposure. Results of the residual fatigue tests on the unnotched crossply and unidirectional B/Al material at 297 K (75° F) and a stress ratio, R, of 0.1 are listed in Table 12-32 and plotted as S-N curves in Figures 12-92 and 12-93. Fatigue curves for unexposed B/Al tested under the same conditions are also included in Figures 12-92 and 12-93 for comparison.

Table 12-29. Unnotched and Notched Tensile Properties of $[0^\circ \pm 45^\circ]_s$ B/Al Before and After 10,000 hr of Flight Simulation Exposure

Specimen Number	Flight Simulation Specimen Number	Temperature		Strength		Modulus		
		K	(°F)	MN/m ²	(ksi)	GN/m ²	(Msi)	
Unnotched Tensile: 10,000 hr								
EC911-1	EC91-1	297	75	409	59.3	103	15.0	
-2	-1			399	57.9	134	19.4	
-3	-1			406	58.9	160	23.2	
-4	-1			301	43.7	159	23.1	
				av	379	55.0	139	20.2
Baseline				av	516	74.8	154	22.4
EC911-5	EC91-1	505	450	264	38.3	—	—	
-6	-1			415	60.2	143	20.7	
EC912-1	-2			404	58.6	—	—	
-2	-2			359	52.1	—	—	
				av	360	52.3		
Baseline				av	452	65.6	121	17.6
Notched Tensile: 10,000 hr								
EC912-3	EC91-2	297	75	303	44.0			
-4	-2			478	69.4			
-5	-2			478	69.3			
-6	-2			364	52.8			
				av	406	58.9		
Baseline				av	479	69.5		
EC913-1	EC91-3	561	550	283	41.4			
-2	-3			303	44.0			
-3	-3			381	55.3			
-4	-3			354	51.3			
				av	330	47.9		
Baseline				av	443	64.3		

Table 12-30. Unnotched and Notched Tensile Properties of $[0^\circ]_6$ B/Al at 297 K (75° F) Before and After 10,000 hr of Flight Simulation Exposure

Specimen Number	Flight Simulation Specimen Number	Strength		Modulus	
		MN/m ²	(ksi)	GN/m ²	(Msi)
Unnotched Tensile: 10,000 hr					
EU913-1	EU91-3	1070	155	231	33.5
-2	-3	972	141	240	34.8
-3	-3	1000	145	170	24.6
-4	-3	1290	187	172	25.0
	av	1080	157	203	29.5
Baseline	av	1450	210	198	28.7
Notched Tensile: 10,000 hr					
EU913-5	EU91-3	869	126		
-6	-3	1080	157		
EU914-1	-4	896	130		
-2	-4	924	134		
	av	942	137		
^a Baseline	av	1220	177		

^aEstimated from notched tensile strength versus temperature curve for $[0^\circ]_6$ B/Al, Figure 7-20.

Table 12-31. Compressive and Interfiber Shear Strength Properties of B/Al at 297 K (75° F) Before and After 10,000 hr of Flight Simulation Exposure

Specimen Number	Flight Simulation Specimen Number	Orientation	Strength		Modulus		
			MN/m ²	(ksi)	GN/m ²	(Msi)	
Compressive: 10,000 hr							
EC9C-1	EC91-5	[0° ± 45°] _s	^a > 910	^a > 132	143	20.8	
-2	-5		^a > 1250	^a > 182	147	21.3	
-3	-5		^a > 1420	^a > 206	117	17.0	
-4	-5		^a > 1020	^a > 148	112	16.3	
			av			130	18.8
EU9C-1	EU92-4	[0°] ₆			212	30.7	
-2	-4		1550	225	197	28.5	
-3	-4		(a)	(a)	207	30.0	
-4	-4		1870	271	207	30.0	
			av	1570	227	206	29.8
Interfiber shear: 10,000 hr							
EU915-4	EU91-5	[0°] ₆	69.6	10.1			
-5	-5		72.4	10.5			
-6	-5		70.3	10.2			
			av	70.8	10.3		
Baseline			av	93.1	13.5		
^a Doubler bond shear failure.							

Table 12-32. Residual Unnotched Axial Fatigue Data for B/Al at 297 K (75° F) After 10,000 hr of Flight Simulation Exposure, R = 0.1

Specimen Number	Flight Simulation Specimen Number	Orientation	Maximum Stress		Cycles	Comments
			MN/m ²	(ksi)		
EC913-5	EC91-3	[0° ± 45°] _s	345	50	824,000	
-6	-3		379	55	130,000	
EC914-1	-4		310	45	1,789,000	
-2	-4		396	57.5	7,000	
-3	-4		276	40	13,704,000	Did not fail
-4	-4		362	52.5	190,000	
-5	-4		414	60	38,000	
-6	-4		293	42.5	2,986,000	
EU914-3	EU91-4	[0°] ₆	827	120	—	Equipment Malfunction
-4	-4		689	100	16,022,000	Did not fail
-5	-4		827	120	2,953,000	
-6	-4		862	125	2,377,000	
EU915-1	-5		965	140	27,000	
-2	-5		1000	145	133,000	
-3	-5		1070	155	28,000	

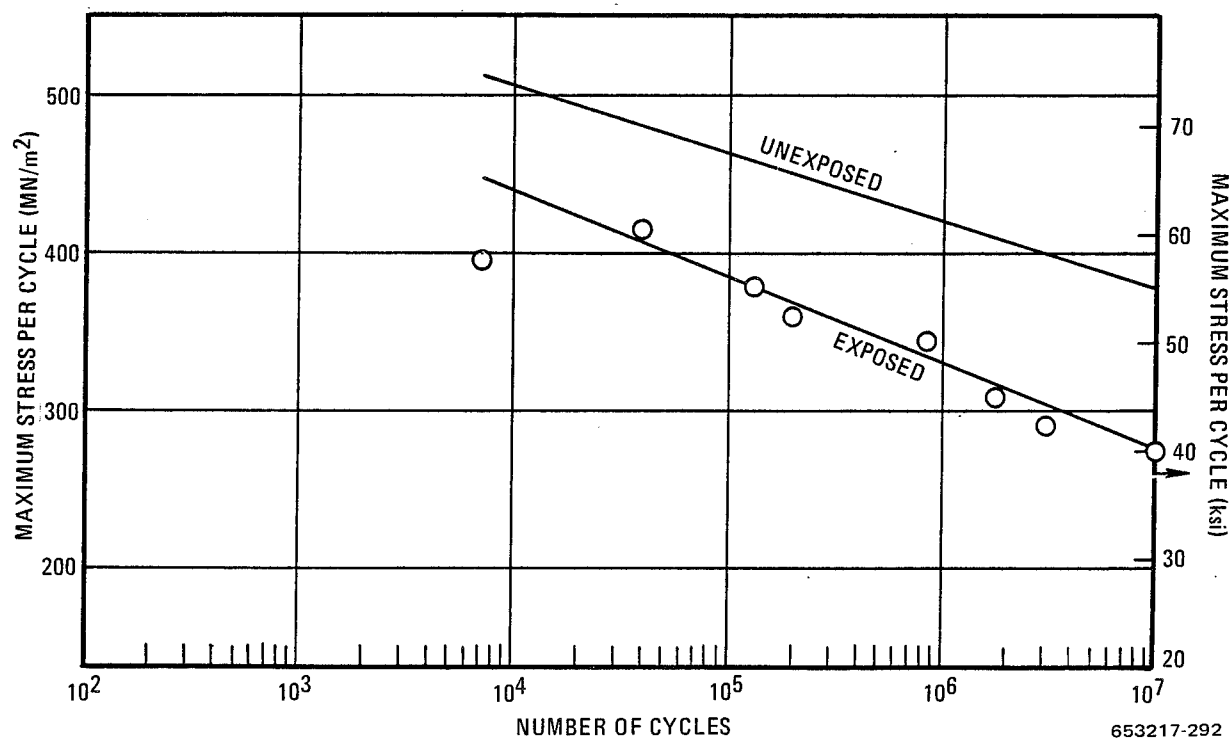


Figure 12-92 Axial Fatigue Properties of [0° ± 45°]_s B/Al Before and After 10,000 hr of Flight Simulation Exposure, 297 K (75° F), R = 0.1, Unnotched

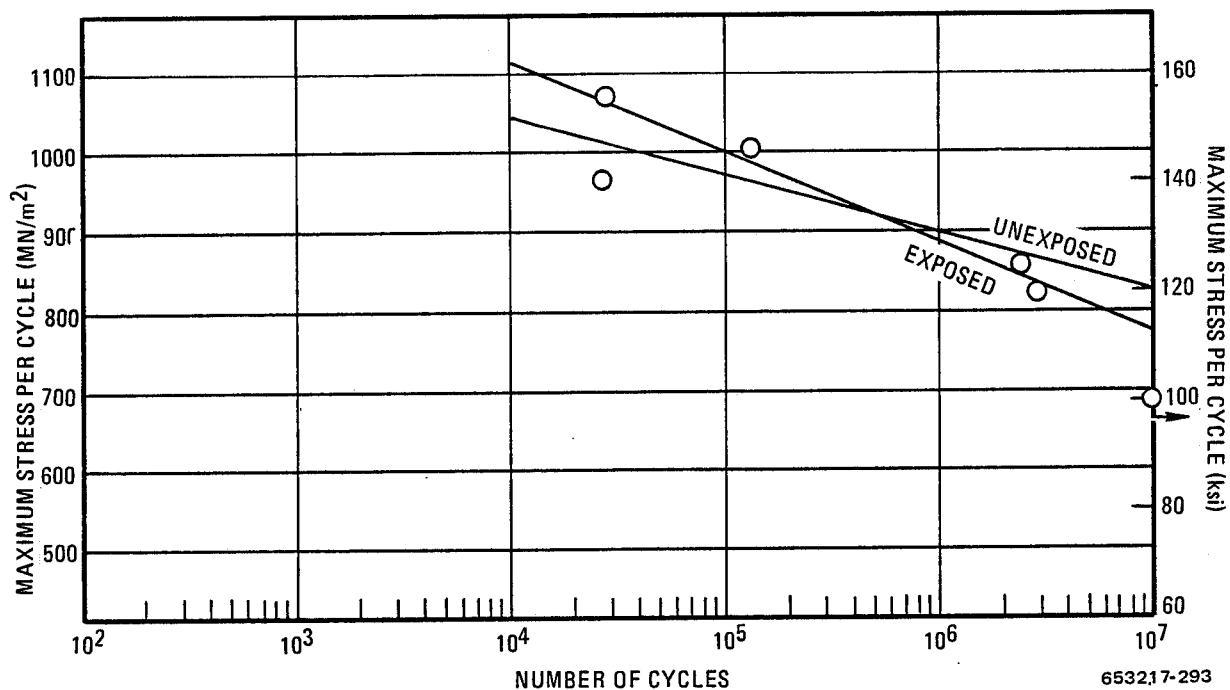


Figure 12-93 Axial Fatigue Properties of $[0^\circ]_6$ B/Al Before and After 10,000 hr of Flight Simulation Exposure, 297 K (75° F), $R = 0.1$, Unnotched

The B/Al system exhibited a loss in mechanical properties of approximately one-fourth after 10,000 hours of flight simulation exposure. This loss was generally observed for both unnotched and notched tensile strength of both crossplied and unidirectional layups and for interfiber shear strength of the unidirectional material. Tests conducted at both room and elevated temperatures gave similar results. Doubler bond shear failures were a problem with the B/Al compressive specimens. The crossply specimens were particularly bad with all failing prematurely in the doubler bonds. The failure loads were quite high, however, equal to a compressive stress in one of the crossply specimens of 1420 MN/m² (206 ksi). The residual fatigue results for the crossplied material showed a decrease of, again, approximately one-fourth in the runout stress (10⁷ cycles) after 10,000 hours of exposure. The unidirectional B/Al, on the other hand, showed very little change from the baseline fatigue data.

Table 12-33 summarizes the 10,000-hour, long-term flight simulation residual strength data obtained from the four composite systems. The percentage decrease in the various mechanical properties is listed for each material. The fatigue data are summarized in Table 12-34. In this table the fatigue strength at 10⁷ cycles, expressed as a percentage of the unexposed tensile strength, is compared for unexposed material and for that which has survived 10,000 hours of flight simulation exposure.

Table 12-33. Summary of 10,000-hr Flight Simulation Residual Strength Data

Material System	Property	Temperature		Property Loss (%)
		K	(°F)	
B/E [0° ± 45°] _s	F _{tu}	297	75	36
	E _t	297	75	23
	^a Notched F _{tu}	297	75	10
	F _{cu}	297	75	^b 40-52
	E _c	297	75	^b 18-24
G/E [0° ± 45°] _s	F _{tu}	297	75	15
	E _t	297	75	20
	^a Notched F _{tu}	297	75	1
	F _{cu}	297	75	47
	E _c	297	75	0
G/PI [0° ± 45°] _s	F _{tu}	297	75	29
	E _t	297	75	14
	F _{tu}	505	450	33
	E _t	505	450	10
	^c Notched F _{tu}	297	75	18
	^a Notched F _{tu}	297	75	8
	^a Notched F _{tu}	505	450	1
	F _{cu}	297	75	23
	E _c	297	75	13
	F _{su}	297	75	54
	F _{tu}	297	75	26
	E _t	297	75	10
	F _{tu}	505	450	20
B/Al [0° ± 45°] _s	^c Notched F _{tu}	297	75	15
	^c Notched F _{tu}	561	550	26
	F _{tu}	297	75	25
	E _t	297	75	0
B/Al [0°] ₆	F _{tu}	297	75	25
	E _t	297	75	0

Table 12-33. Summary of 10,000-hr Flight Simulation Residual Strength Data — Concluded

Material System	Property	Temperature K (°F)		Property Loss (%)
	^c Notched F_{tu}	297	75	23
	F_{su}	297	75	24

^aNotched flight simulation specimens

^bLoss greater for material cut from between grids

^cUnnotched flight simulation specimens

Table 12-34. Strength at Fatigue Limit or 10^7 Cycles Expressed as Percentage of Ultimate Tensile Strength Before and After 10,000 hr of Flight Simulation Exposure, $R = 0.1$, 297 K (75° F)

Material System	Specimen Configuration	Condition	Fatigue Strength at 10^7 Cycles (% of Unexposed F_{tu})
B/E [0° ± 45°] _s	Unnotched	Unexposed	52
		Exposed	45
	Notched	Unexposed	92
		Exposed	62
G/E [0° ± 45°] _s	Unnotched	Unexposed	90
		Exposed	49
	Notched	Unexposed	92
		Exposed	69
G/PI [0° ± 45°] _s	Unnotched	Unexposed	60
		Exposed	37
	Notched	Unexposed	84
		Exposed	78
B/Al [0° ± 45°] _s	Unnotched	Unexposed	74
		Exposed	54
B/Al [0°] ₆	Unnotched	Unexposed	57
		Exposed	53

12.7.4. PHASE II TEST PLAN. The test plan, as originally proposed, for the long-term flight simulation program was to expose 10 specimens of each material system for 10,000 hours in Phase I and 10 additional specimens for 50,000 hours in Phase II. The resin matrix specimens were all crossplied layups, half unnotched and half notched. The metal matrix specimens, B/Al, were equally divided between unidirectional and crossplied and were all unnotched. A modification was made to the test plan for Phase II by adding three more unnotched specimens of each material/orientation combination that would be exposed for 25,000 hours.

Because of the high failure rate of the G/E specimens and the extensive visual degradation of the B/E specimens, it became necessary to further modify the Phase II plan. All of the original B/E and G/E flight simulation specimens were removed, and new specimens were fabricated to replace them. These specimens, which were all unnotched, were installed in the simulator as follows:

Bay 5 5 B/E, 10,000-hr specimens
5 G/E, 10,000-hr specimens

Bay 6 3 B/E, 25,000-hr specimens
3 G/E, 25,000 hr specimens

Bay 7 5 B/E, 50,000-hr specimens
5 G/E, 50,000-hr specimens

The random load spectrum remained unchanged except that the load levels are now the average of those applied previously for the two epoxy materials. The change (shown below for the maximum tensile loads) is quite small, less than 1%.

Previous B/E load: 17.53 MN (3942 lb)

Previous G/E load: 17.68 MN (3975 lb)

Revised load: 17.60 MN (3958 lb)

An increase in testing efficiency will be possible by intermixing the two systems as the flight simulation exposures can be performed in three bays rather than the four required if the systems were run separately. This also frees a bay for possible new material additions in the future.

The maximum test temperature during flight simulation testing of B/E and G/E was reduced from 408 K (275° F) to 373 K (212° F). This temperature was determined from a log time versus 1/T plot of G/E thermal aging data obtained earlier in the program. The curve represents the time/temperature combinations at which significant degradation of the epoxy matrix begins. Extrapolation of the curve to 50,000 hours gave the new test temperature.

SECTION 13

THERMAL EXPOSURE TEST PROGRAM SUMMARY

This section presents an overview of the thermal exposure test programs with emphasis on trends observed for each of the materials. Specific tests included in the summary are the baseline tensile, compressive, and shear tests; the thermal aging tests; the short-term tests; the long-term test; and the baseline and post-flight simulation constant amplitude fatigue tests. The thermal aging tests are included in the summary even though they generally showed that significant aging effects occur at temperatures higher than the selected maximum use temperature. In the combined load/environment tests, some of the thermal aging effects were triggered at lower temperatures by the combination of load cycles, thermal cycles, and time at temperature.

Test data are presented in two ways. To aid the observation of trends, strength (stress) has been plotted as a function of the various tests performed, where the tests are ordered either in increasing test time or test sequence. Selected individual data have been plotted to observe data scatter. For the constant amplitude fatigue tests, the cyclic stress at 10^7 cycles (σ_{10^7}) has been plotted to indicate the relative severity of the effect of fatigue cycling. Ten million cycles were chosen in keeping with summary charts presented previously in both Sections 11 and 12. When fatigue effects are indicated by this simplified plotting method, the actual S-N curves should be referred to for more insight into the relative effects. In addition, to show the effects of the thermal exposures on specific properties, residual strengths have been compared to baseline strengths by means of bar charts. The bar charts have been prepared for crossply B/E, G/E, G/PI, and B/Al and unidirectional B/Al as these were the layups and materials for which flight simulation data were available. For the resin matrix composites, the residual notched tensile and notched fatigue values were obtained from notched flight simulation specimens. The residual notched tensile data for B/Al were obtained from material that was notched after flight simulation. The fatigue strengths shown on the bar charts were also for 10^7 cycles in keeping with summary charts presented previously in both Sections 11 and 12.

B/E, $[0^\circ \pm 45^\circ]$, unnotched. Figures 13-1 and 13-2 summarize the available tests for the unnotched B/E. As no baseline tensile testing was performed (except for three tests at room temperature), the mean strength at 422 K (300° F) was estimated to be 545 MN/m² (79 ksi) and the Weibull shape parameter, α , was obtained from reference 35 as 19.5. This value of α translates to a coefficient of variation of about 5%, and indicates that B/5505 B/E is a well-controlled repeatable composite system.

The short-term tests with a peak stress of 321 MN/m² (46.6 ksi), at a constant 422 K (300° F), showed the typical reduction in mean strength and increase in scatter with time. No fatigue failures occurred, and the residual strength failure mode was the same as that for the room temperature baseline tests.

Wearout analysis was performed to select the peak stress of 302 MN/m² (43.8 ksi) for the long-term tests.

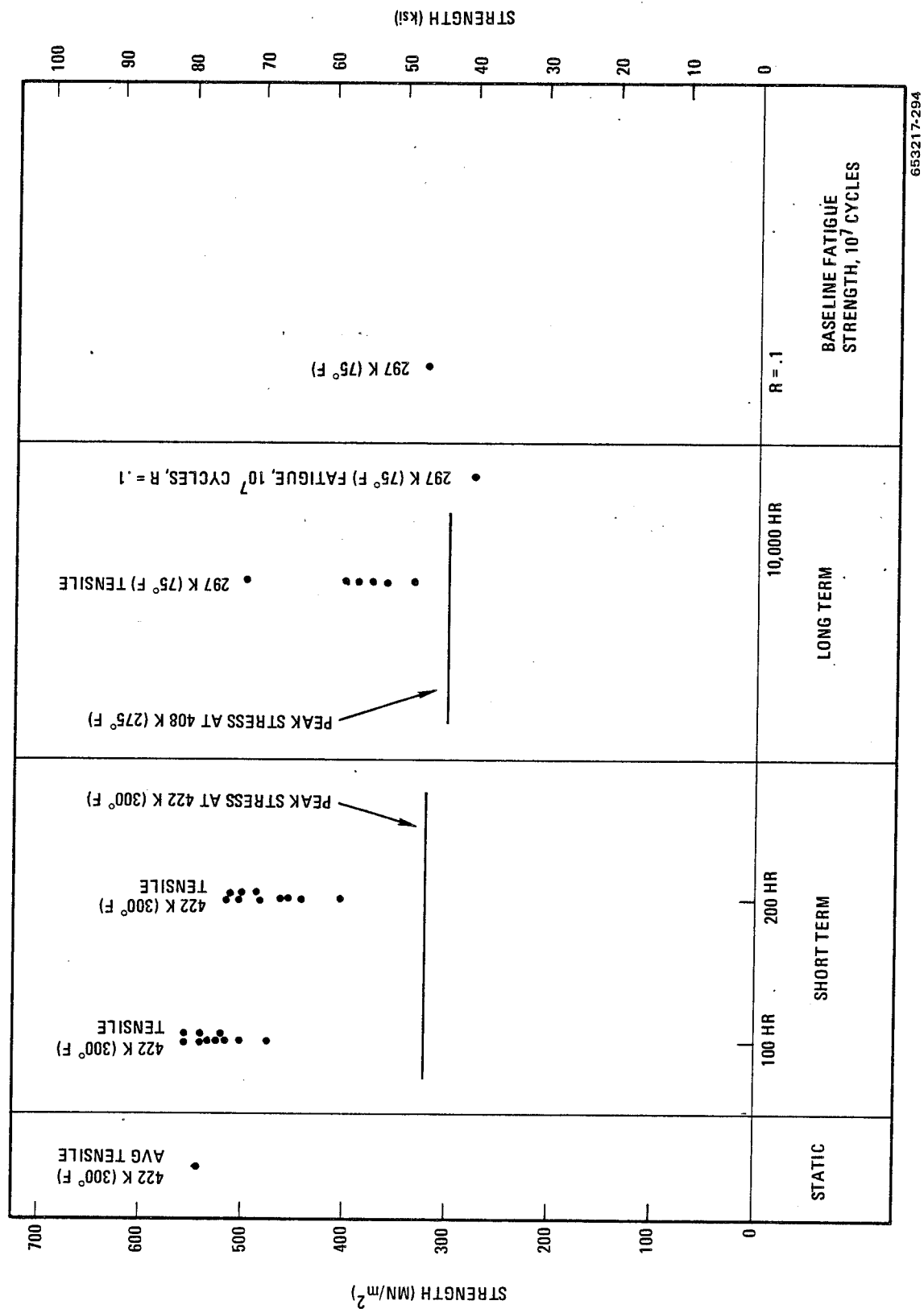


Figure 13-1 Unnotched [0° ± 45°] B/E

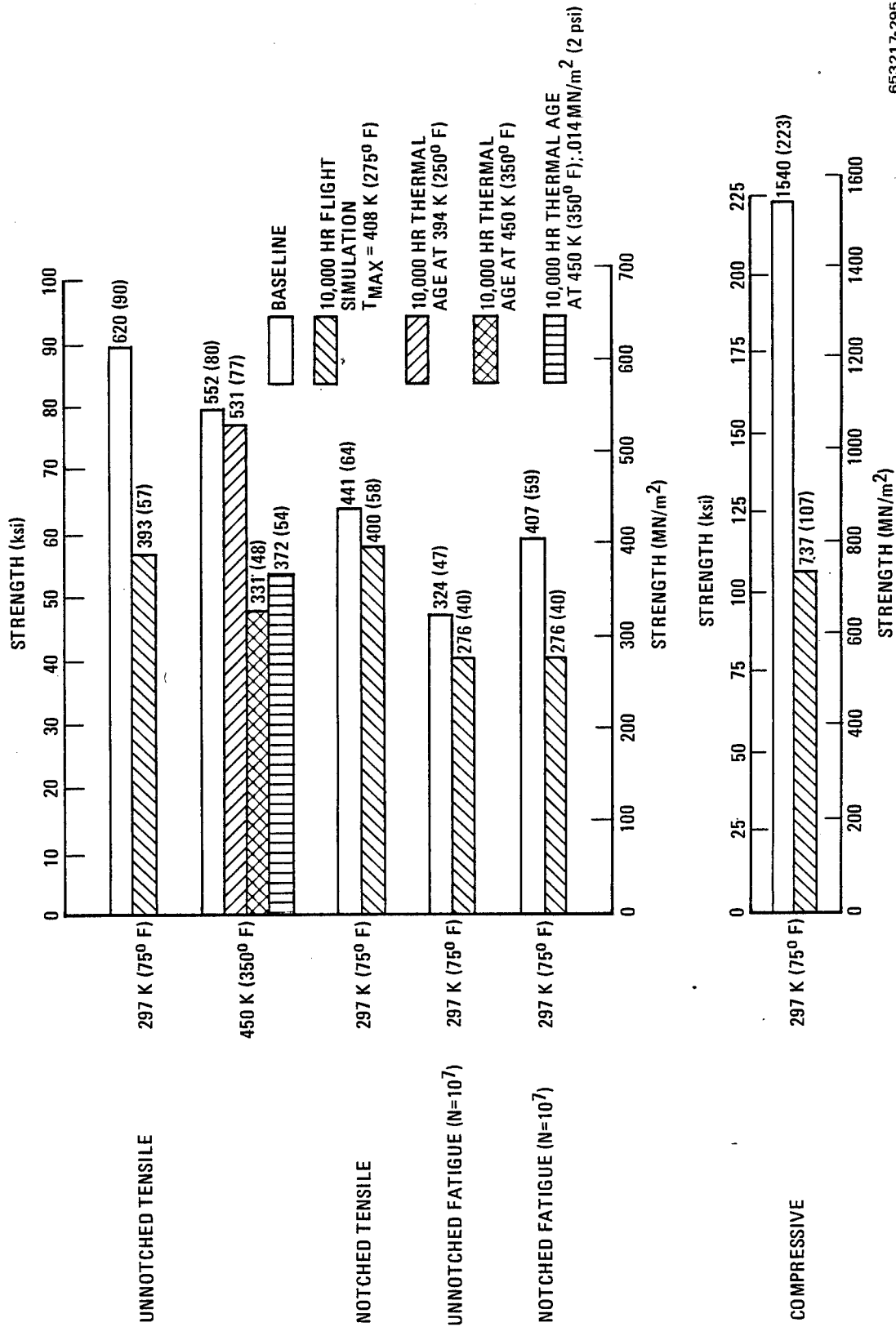


Figure 13-2 Summary of Residual Properties of [0° ± 45°] B/E After 10,000 hr of Exposure

After the first 1000 hours, the cruise temperature was lowered from 422 K (300° F) to 408 K (275° F). No fatigue failures occurred in the 10,000 hours of Phase I. Residual tensile strength tests showed more scatter than expected, with five specimens between 338 MN/m² (49 ksi) and 400 MN/m² (58 ksi) and one at 496 MN/m² (72 ksi). The average decrease at room temperature was approximately 35%. The residual compressive tests showed even greater reductions in properties with a decrease of slightly more than 50%. Although the residual strength failure mode was the same as the baseline, the specimens were severely oxidized in the heated zones. Recall that the wearout analysis had assumed that no thermal aging effects would be experienced below the apparent maximum use temperature. This assumption was violated by the long-term chemical and physical changes experienced by the epoxy resin. In the Phase II tests the cruise temperature has been changed to 373 K (212° F) for the epoxy systems. The thermal aging results (Figure 13-2) have shown that with no applied loads or temperature cycling no degradation of tensile properties, and probably none for compressive properties as well, occurs during 10,000 hours exposure at 394 K (250° F). However, at 450 K (350° F) significant tensile and severe compressive property degradation was observed. No thermal aging data were obtained at the flight simulation temperature of 422 K (300° F) or 408 K (275° F). The post long-term fatigue tests at $R = 0.1$ and 297 K (75° F) indicated a σ_{10^7} value of 276 MN/m² (40 ksi) compared to the baseline value of 324 MN/m² (47 ksi).

The combination of load, temperature, and thermal cycling has severely degraded the unnotched B/E specimens at a temperature at which thermal aging alone would probably not cause extensive damage.

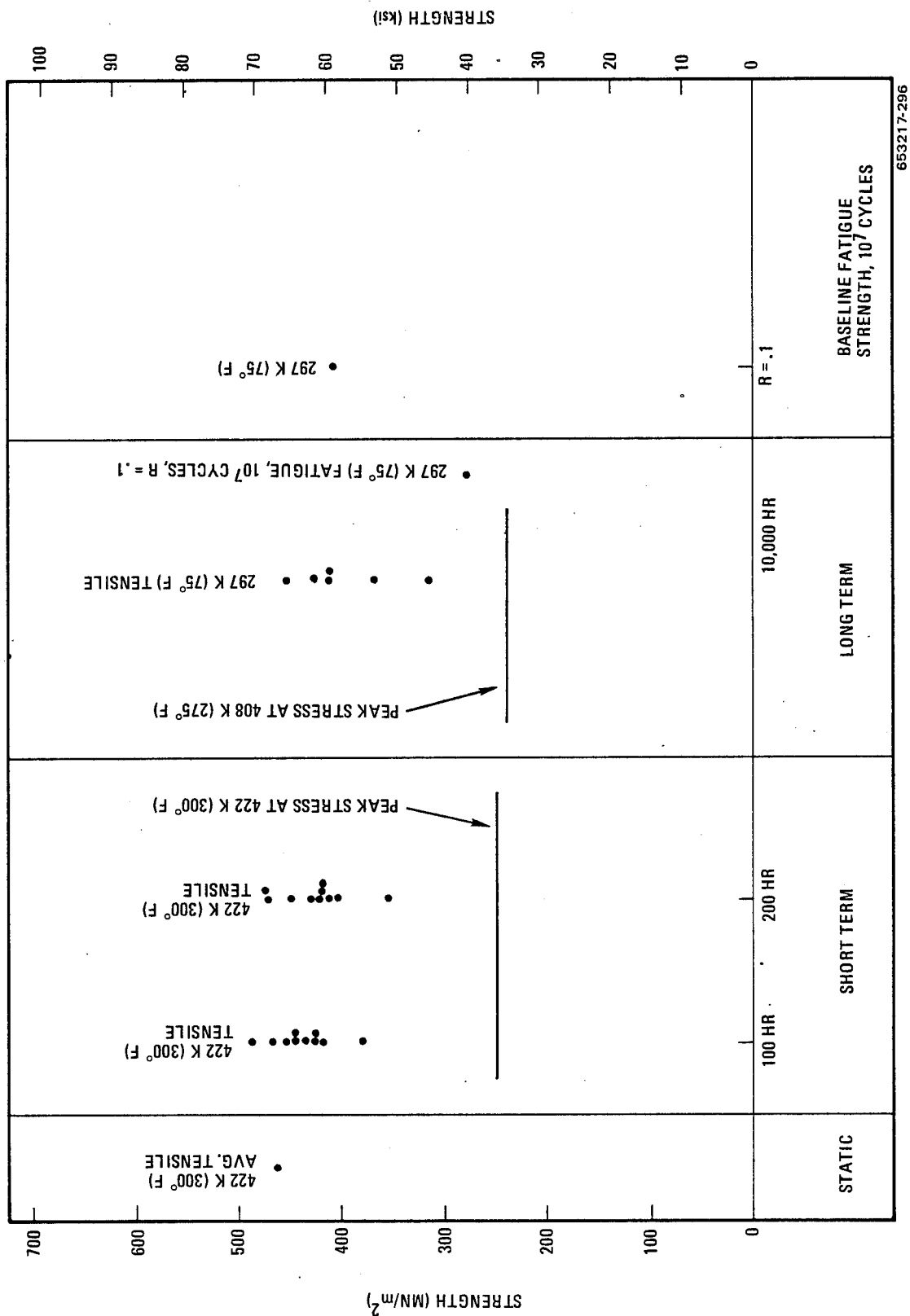
B/E, [0° ± 45°]_s, notched. Figure 13-3 summarizes the trend data for the notched B/E. The residual properties after flight simulation exposure are summarized in Figure 13-2.

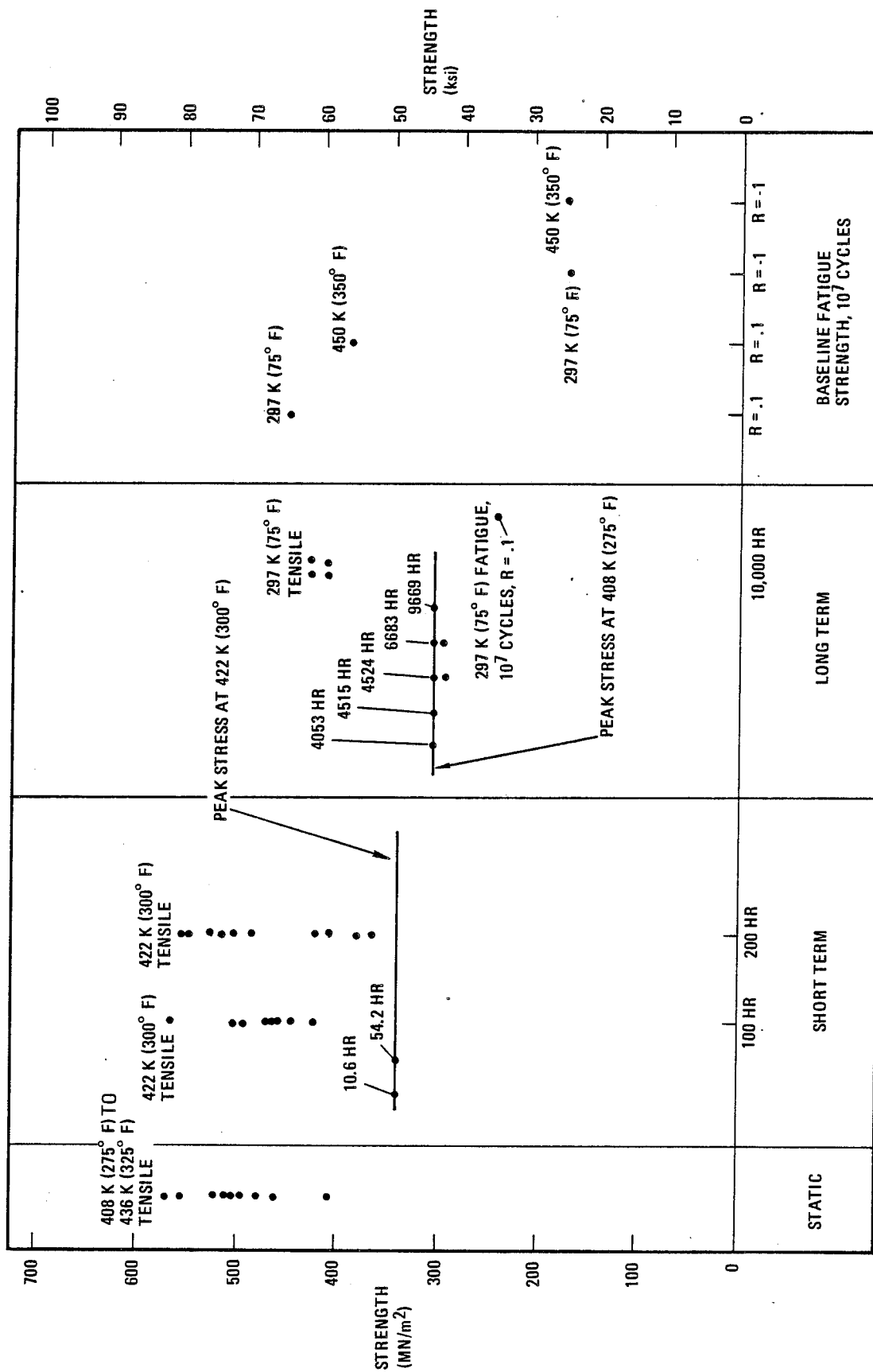
The 422 K (300° F) baseline mean strength was calculated to be about 462 MN/m² (67 ksi) net stress and the same α value of 19.5 was assumed. The short-term specimens were cycled to a peak stress of 248 MN/m² (36 ksi) at 422 K (300° F) and exhibited the typical wearout effects of reduced mean and increased scatter. Failure modes were net tension.

Wearout analysis was used to select the long-term peak stress of 239 MN/m² (34 ksi). The temperature of the cruise leg was reduced from 422 K (300° F) to 408 K (275° F) after about 1000 hours. No fatigue failures occurred in 10,000 hours. The residual strength specimens also failed in net tension with the values scattered between 317 MN/m² (46 ksi) and 455 MN/m² (66 ksi) and having an average value of 400 MN/m² (58 ksi). Again the epoxy resin sustained severe chemical and physical damage in the heated zones from the combination of load, temperature, and oxidation.

The $R = 0.1$ fatigue strengths for 10^7 cycles at 297 K (75° F) before and after the long-term tests were 407 MN/m² (59 ksi) and 276 MN/m² (40 ksi), substantiating the degrading effects of flight simulation exposure.

G/E, [0° ± 45°]_s, unnotched. The baseline mean strength of the G/E unnotched specimens at 408 K (275° F) to 436 K (325° F) (Figure 13-4) was about 496 MN/m² (72 ksi) with a calculated Weibull α of 12.7. This low value of shape parameter indicates poor reproducibility that impedes the clear interpretation of test trends.

Figure 13-3 Notched $[0^\circ \pm 45^\circ]_s$ B/E



653217-297

Figure 13-4 Unnotched [0° ± 45°], G/E

The short-term specimens were cycled to a peak stress of 338 MN/m² (49.1 ksi) at 422 K (300° F), and typical wearout was observed, including two early fatigue failures. Failure mode was net tension, the same as the baseline tests.

The wearout analysis was used to select the peak long-term stress of 305 MN/m² (44.2 ksi), and after 1000 hours, the cruise temperature was reduced to 408 K (275° F). Multiple fatigue failures occurred, principally by progressive delamination. The few residual strength results (Figures 13-4 and 13-5) showed only a slight reduction in the mean tensile strength but a drastic reduction in the mean compressive strength. The combination of severe oxidation and delamination growth during flight simulation exposure was a major impact to the program.

In like manner to the B/E system, thermal exposure without load at 450 K (350° F) produced severe degradation of the matrix and a very large decrease in tensile strength. No compressive tests were performed, but the appearance of the failed specimens indicated that compressive properties would also be poor. Thermal aging at 394 K (250° F) and at 450 K (350° F) at reduced pressure, however, gave no degradation in properties after at least 10,000 hours of exposure.

The post long-term test value of σ_{10^7} after $R = 0.1$ fatigue at room temperature was down to 241 MN/m² (35 ksi) from the 448 MN/m² (65 ksi) baseline. The low value of the baseline σ_{10^7} , 386 MN/m² (56 ksi), after $R = -1$ fatigue at 450 K (350° F) is probably attributable mostly to material variability. Constant amplitude fatigue at $R = 0.1$ during baseline testing was shown to produce severe reductions in strength. Compressive failure are suspected for these tests that produced σ_{10^7} values of 172 MN/m² (25 ksi) at 297 K (75° F) and 172 MN/m² (25 ksi) at 450 K (350° F). In hindsight, the test program, especially for the graphite systems, should have emphasized compressive effects.

G/E, [0° ± 45°]_s, notched. Broad scatter was again evident in the baseline notched G/E with an α value of 12.0 and a mean strength of about 414 MN/m² (60 ksi) (Figures 13-5 and 13-6).

The short-term tests, cycled to a peak stress of 249 MN/m² (36.1 ksi) at 422 K (300° F), produced no fatigue failures, but showed decreasing strength and increasing scatter. The residual strength failure mode was net tension.

After wearout analysis, the long-term specimens were cycled to a peak stress of 232 MN/m² (33.6 ksi). The temperature was again reduced from 422 K (300° F) to 408 K (275° F) after about 1000 hours. The badly oxidized residual tensile strength specimens retained a surprising amount of their original notched strength, exhibiting values from 358 MN/m² (52 ksi) to 469 MN/m² (68 ksi).

Again tensile fatigue testing did not discriminate the effects too well, with the post long-term test σ_{10^7} value ($R = 0.1$) at 297 K (75° F) being 283 MN/m² (41 ksi), compared to the baseline values of 379 MN/m² (55 ksi) and 345 MN/m² (50 ksi) at 297 K (75° F) and 450 K (350° F).

The stress ratio of $R = -1$ showed the much more severe effects of compression with σ_{10^7} values of 124 MN/m² (18 ksi) and 152 MN/m² (22 ksi) at 297 K (75° F) and 450 K (350° F) respectively, for the baseline tests.

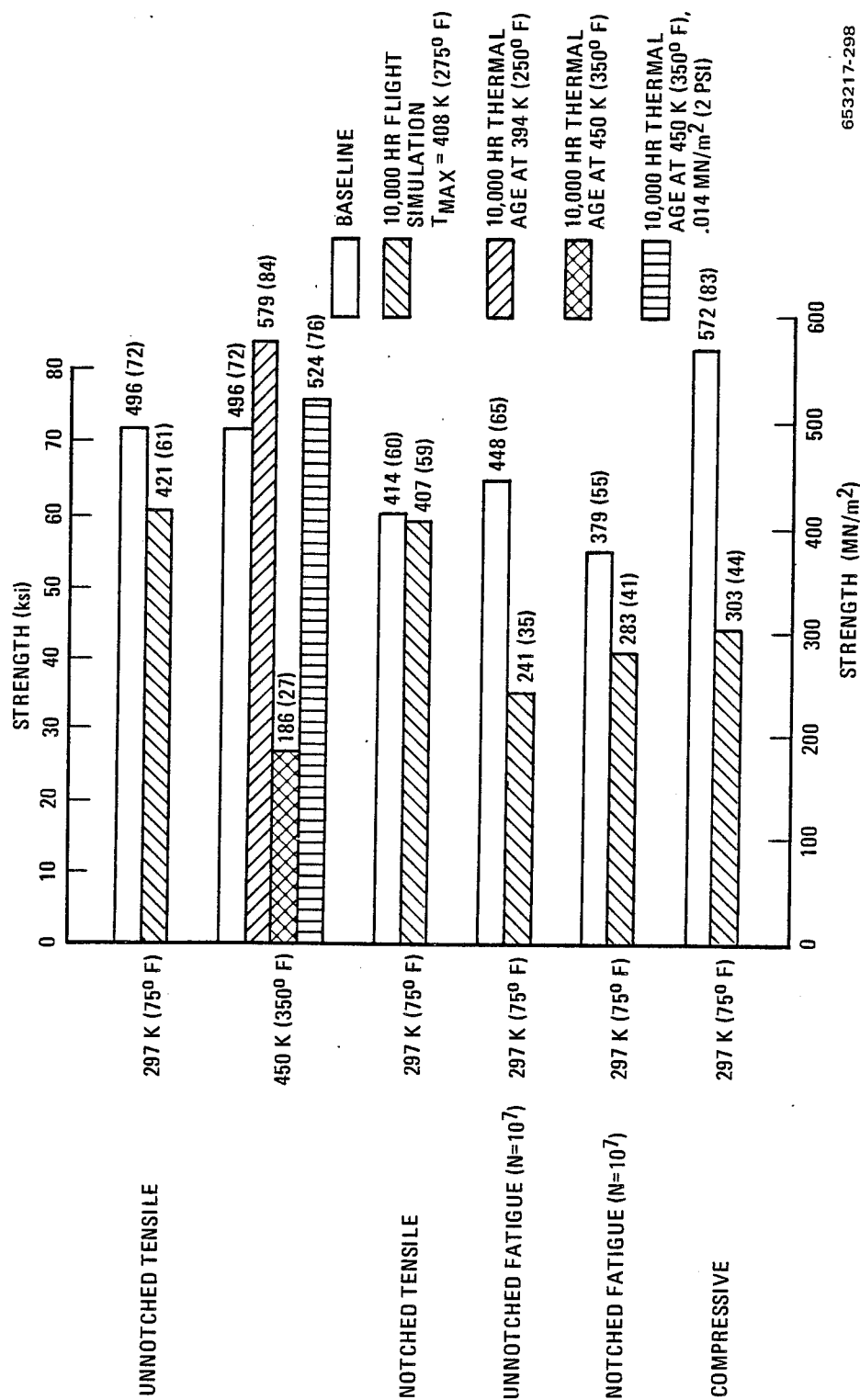
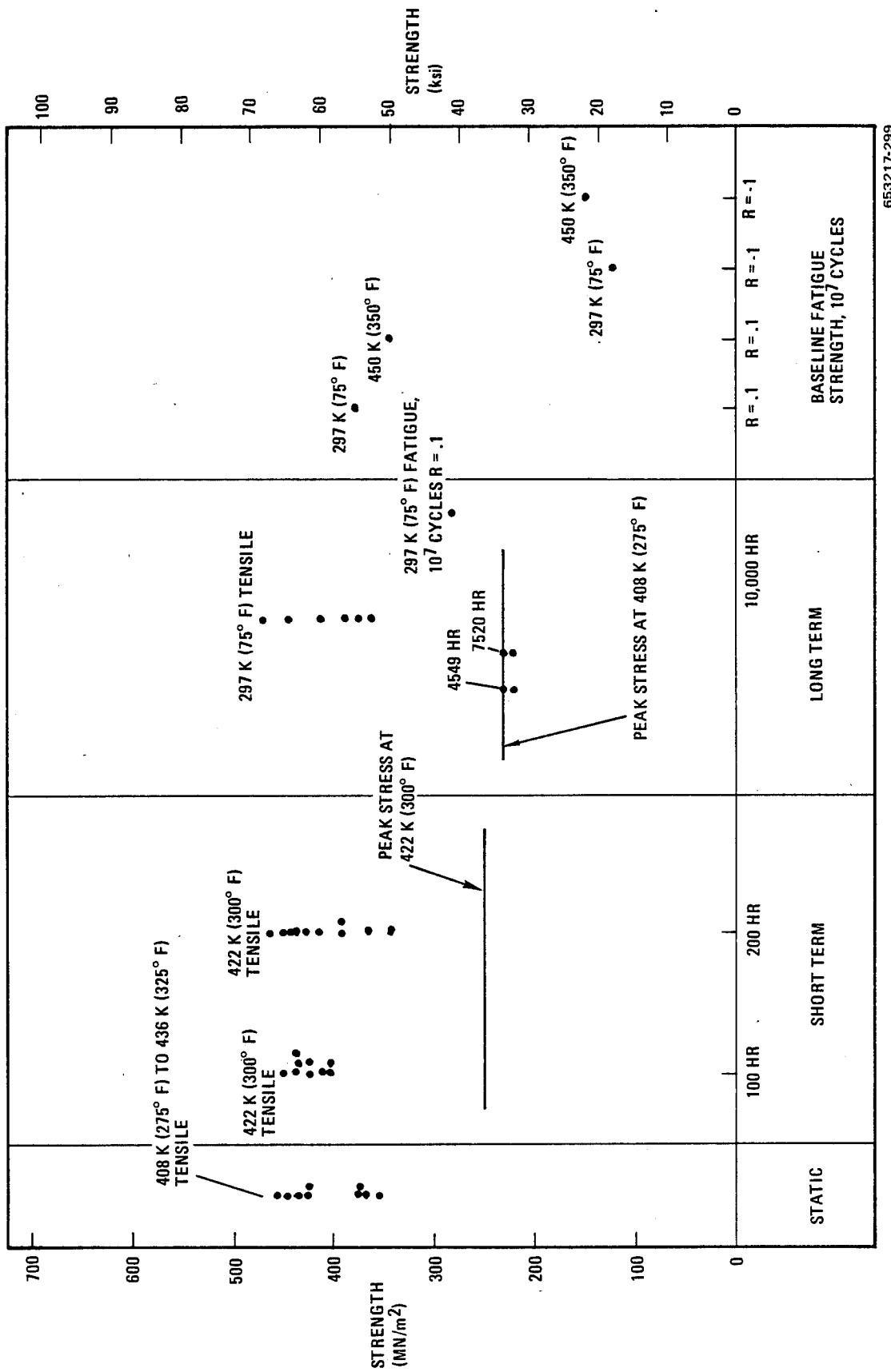


Figure 13-5 Summary of Residual Properties of $[0^\circ \pm 45^\circ]_s$ G/E After 10,000 hr of Exposure



653217-299

Figure 13-6 Notched [0° ± 45°], G/E

G/PI, $[0^\circ \pm 45^\circ]_s$, unnotched. The G/PI data is summarized in Figures 13-7 and 13-8. Baseline testing showed poor reproducibility, as exhibited by a mean strength at 505 K (450° F) of 469 MN/m² (68 ksi) and an α value of 12.15. Notice that one of the baseline specimens only reached 296 MN/m² (43 ksi). These panels had measured void contents up to 13%, so that defect sensitive failures modes could be greatly influenced by individual specimen quality.

The 505 K (450° F) short-term peak stress was originally selected to be 331 MN/m² (48 ksi), but nine out of 10 specimens failed the proof load at 283 MN/m² (41 ksi); consequently the stresses were reduced to a peak 207 MN/m² (30.1 ksi). Tests of the short-term panels showed that they were about 69 MN/m² (10 ksi) weaker than the baseline panel. Eventually, the short-term specimens exhibited typical wearout indications of decreasing strength and increasing scatter with test time.

The long-term test peak stress was reduced to 149 MN/m² (21.6 ksi), and at 505 K (450° F) maximum cruise temperature all specimens achieved 10,000 hours. Residual tensile strengths at 505 K (450° F) ranged from 228 MN/m² (33 ksi) to 414 MN/m² (60 ksi) and at 297 K (75° F) ranged from 228 MN/m² (33 ksi) to MN/m² (74 ksi). Reproducibility was quite poor, even though the failure mode remained tensile, and no aging or delamination affects were observed. Residual compressive strength was reduced by approximately the same degree as the tensile strength. This was in contrast to the epoxy systems where compressive strength was considerably more affected by flight simulation exposure than the tensile strength. The shear strength exhibited the greatest decrease with a loss of more than 50% after 10,000 hours of flight cycling. This may be an indication that G/PI flight simulation failures may occur early in the Phase II test program if the failure mechanism proposed for the epoxy systems is operative for the polyimide system as well.

The results of the 10,000-hour thermal aging exposures, Figure 13-8, clearly show the effect of aging temperature, with very little decrease in tensile strength when aged at 505 K (450° F) and almost a 50% reduction at 561 K (550° F).

The post long-term fatigue tests at $R = 0.1$ and 297 K (75° F) produced a σ_{10^7} value of only 193 MN/m² (28 ksi) as compared to the baseline values of 310 MN/m² (45 ksi) at 297 K (75° F) and 269 MN/m² (39 ksi) at 505 K (450° F). Panel-to-panel scatter may be influencing these results.

Again the effect of compressive stresses was demonstrated by the baseline fatigue tests at $R = -1$. Values of σ_{10^7} were 152 MN/m² (22 ksi) at 297 K (75° F) and 124 MN/m² (18 ksi) at 505 K (450° F).

G/PI, $[0^\circ \pm 45^\circ]_s$, notched. Even these notched specimens suffered from voids, porosity, and panel-to-panel variability. As shown in Figure 13-9, their mean strength at 505 K (450° F) was about 338 MN/m² (49 ksi). The Weibull α was 12.15.

The short-term peak stress was 141 MN/m² (20.5 ksi) at 505 K (450° F), and all specimens had about the same strength after 100 and 200 hours. Net tension failures were obtained from all specimens. The long-term peak stress was 125 MN/m² (18.1 ksi). All specimens survived this relatively low stress level. Residual notched tensile strengths at 505 K (450° F) ranged from 255 MN/m² (37 ksi) to 400 MN/m² (58 ksi), and at 297 K (75° F) they ranged from 248 MN/m²

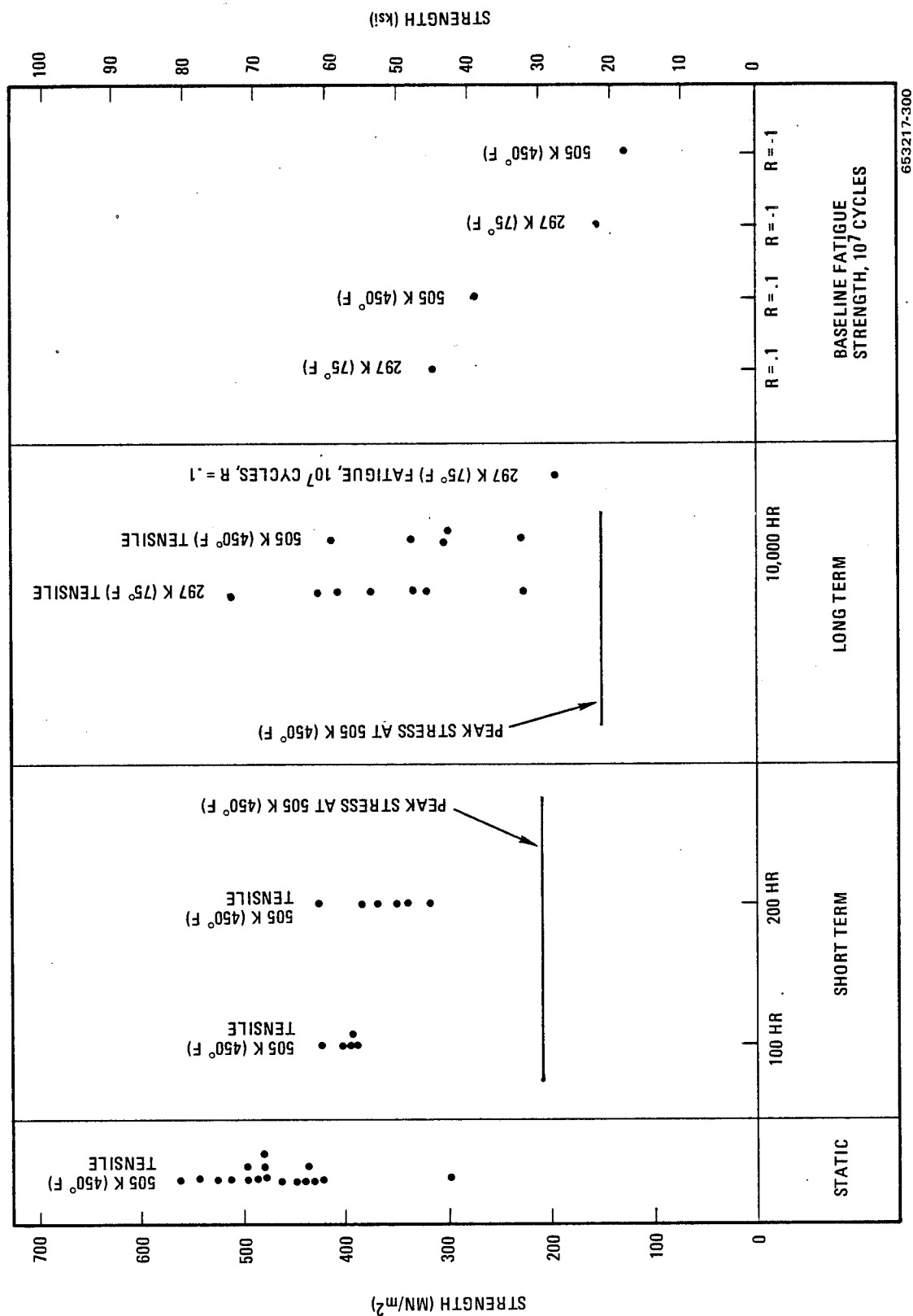


Figure 13-7 Unnotched $[0^\circ \pm 45^\circ]$, G/PI

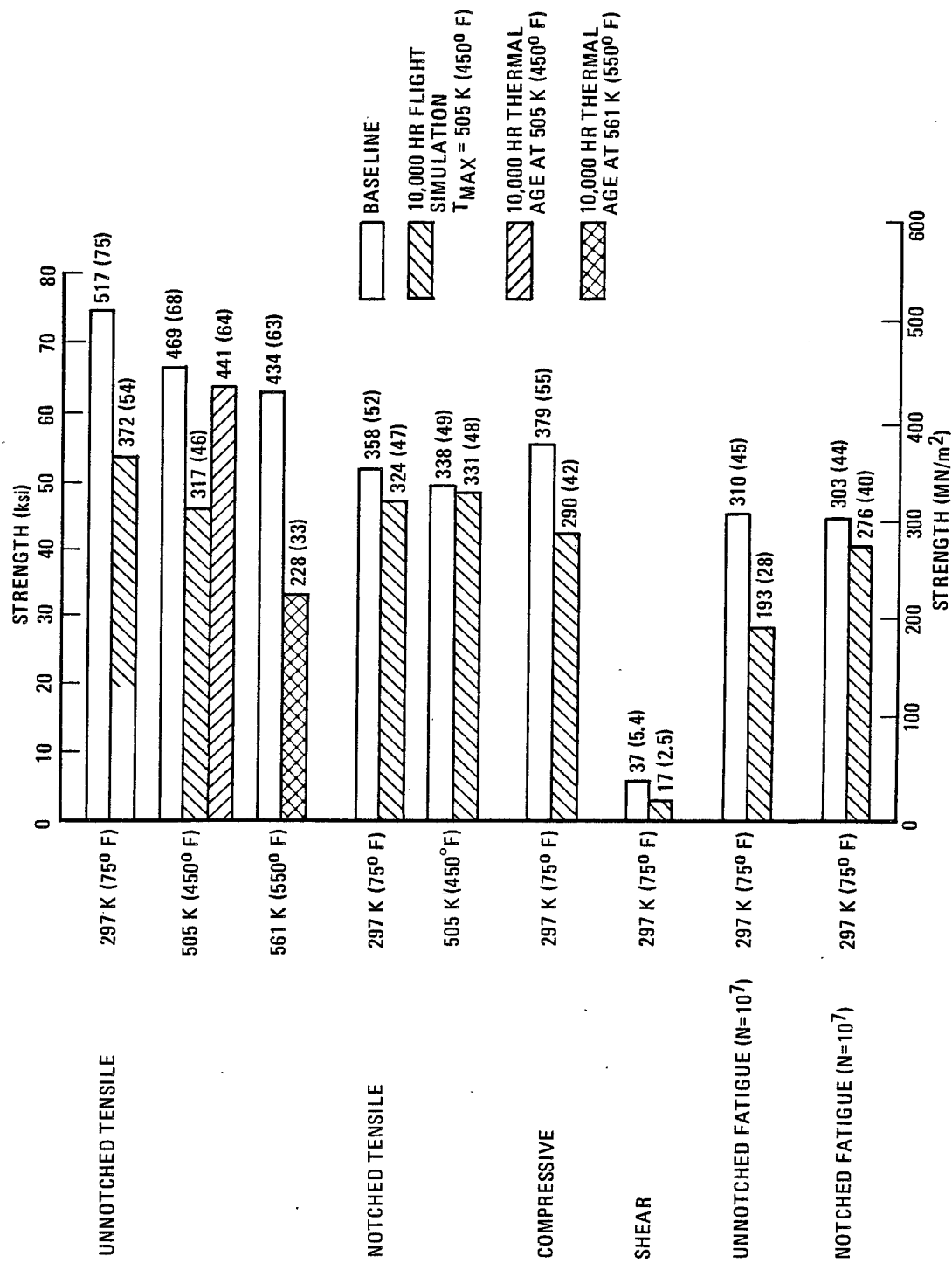


Figure 13-8 Summary of Residual Properties of $[0^{\circ} \pm 45^{\circ}]_s$ G/PI After 10,000 hr of Exposure

(36 ksi) to 428 MN/m² (62 ksi). No particular strength shift was seen, but the scatter was clearly increased. The decrease in the average notched tensile strength after 10,000 hours of flight simulation exposure was quite small compared with that observed for unnotched specimens (Figure 13-8). Similar differences in properties of notched and unnotched specimens of both B/E and G/E were also observed after 10,000 hours of flight simulation.

The post long-term notched fatigue test at $R = 0.1$ and 297 K (75° F) produced a σ_{10^7} of 276 MN/m² (40 ksi) as compared to a baseline value of 303 MN/m² (44 ksi) at 297 K (75° F) and 345 MN/m² (50 ksi) at 505 K (450° F). Panel variability is evidently operating here to confuse the trends.

The baseline reversed loading tests at $R = -1$ produced much lower σ_{10^7} values of 83 MN/m² (12 ksi) at 297 K (75° F) and 90 MN/m² (13 ksi) at 505 K (450° F), indicating the severe effect of compressive loading.

B/Al, [0° ± 45°]_s. Trend conclusions for B/Al were somewhat hampered by panel variability. Figures 13-10 and 13-11 summarize the data for the crossply layup. Static strength at 505 K (450° F) was about 455 MN/m² (66 ksi) with an α of 13.7.

The short-term specimens were cycled to a peak stress of 345 MN/m² (50 ksi) at 505 K (450° F). Fatigue failures occurred in both sets of specimens, and the two had quite different mean strengths. Note the one residual strength value of 323 MN/m² (46.8 ksi) which was below the peak cyclic stress.

The long-term specimens were cycled to only 208 MN/m² (30.1 ksi), and no fatigue failures were observed. The 505 K (450° F) residual tensile strengths were scattered from 262 MN/m² (38 ksi) to 414 MN/m² (60 ksi), and the 297 K (75° F) residuals scattered from 303 MN/m² (44 ksi) to 407 MN/m² (59 ksi). The aluminum surface appeared rough, and the fibers had been degraded by the 10,000 hours at 505 K (450° F). Residual compressive tests were not successful because of premature shear failures in the doubler bonds. However, the specimens did sustain quite high compressive stresses (well in excess of the tensile strength) before the doubler bond failure.

A significant portion of the degradation experienced by the B/Al during flight simulation exposure appears to be directly related to thermal aging effects and probably not a consequence of the fatigue loading and thermal cycling. While no 505 K (450° F) thermal aging data were available, interpolation of the 450 K (350° F) and 561 K (550° F) data, Figure 13-11, indicates that tensile strength losses equivalent to those determined after flight simulation could also have occurred during thermal aging at 505 K (450° F) for 10,000 hours. Similar effects were not observed for the resin matrix systems.

The post long-term fatigue at $R = 0.1$ and 297 K (75° F) produced a σ_{10^7} value of 276 MN/m² (40 ksi) as compared to the baseline values of 379 MN/m² (55 ksi) and 221 MN/m² (32 ksi) at 297 K (75° F) and 561 K (550° F) respectively. Again, the baseline reversed loading fatigue tests at $R = -1$ produced reductions in performance. The σ_{10^7} values were 200 MN/m² (29 ksi) and 173 MN/m² (25 ksi) at 297 K (75° F) and 505 K (450° F) respectively.

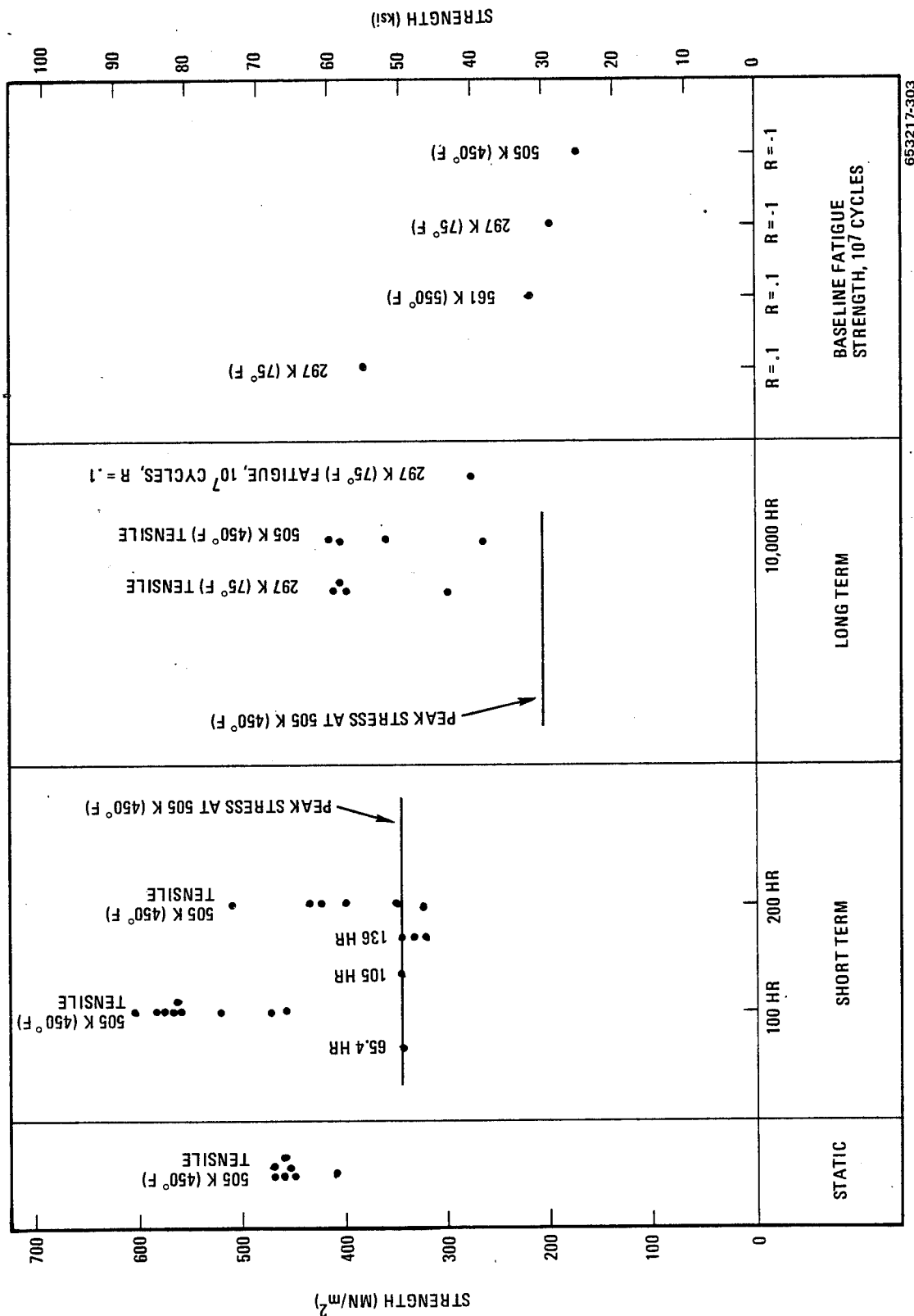


Figure 13-10 Unnotched [0° ± 45°], B/AI

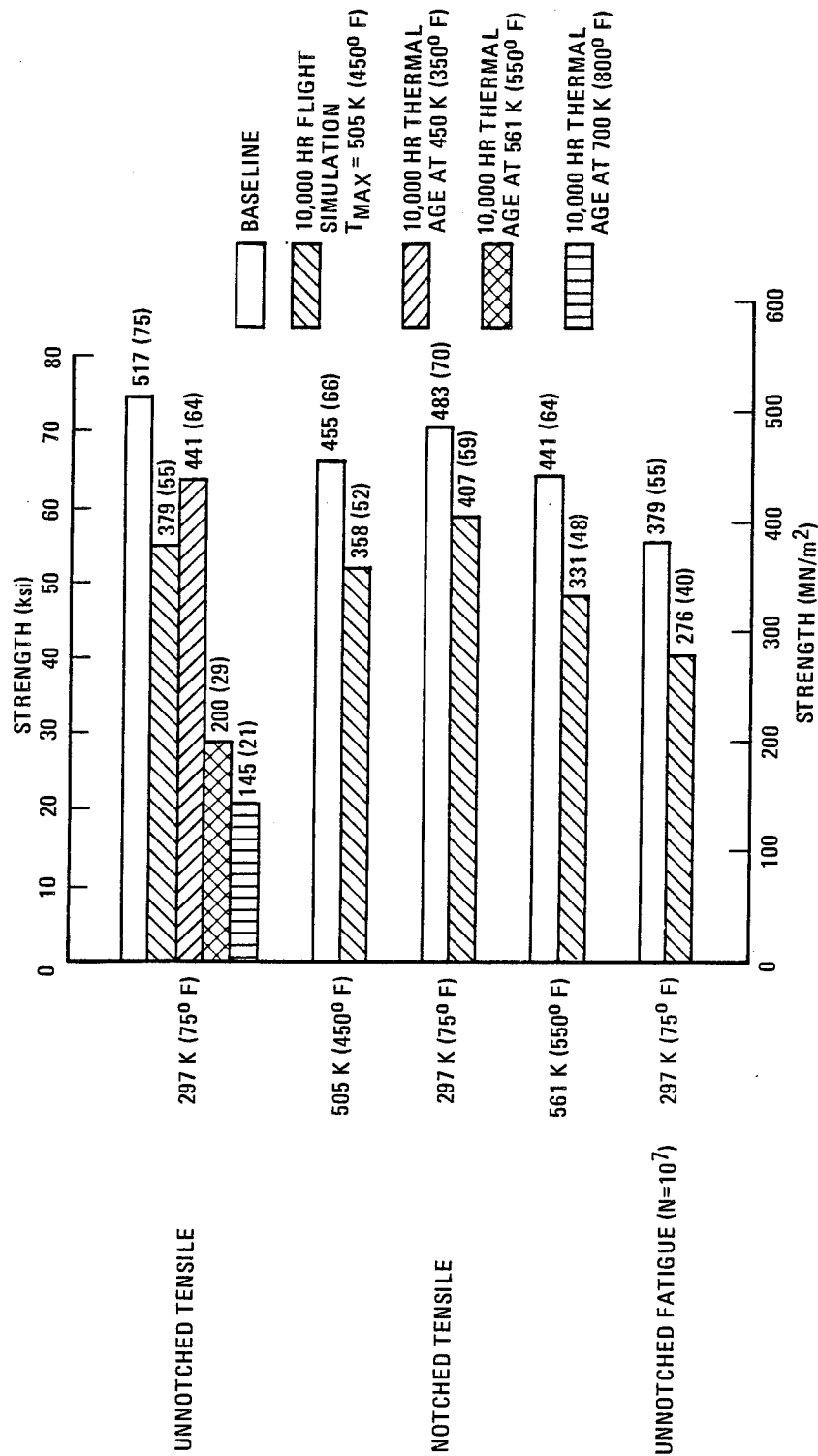


Figure 13-11 Summary of Residual Properties of $[0^\circ \pm 45^\circ]_s$ B/AI After 10,000 hr of Exposure

B/Al, [0°]₆. Figure 13-12 summarizes the trend data for the unidirectional B/Al. The residual properties after flight simulation and thermal aging exposures are summarized in Figure 13-13.

As no baseline tensile tests were conducted at 505 K (450° F), the 561 K (550° F) baseline data, shown in Figure 13-12, were used for selection of the short-term loads. A mean strength of 1300 MN/m² (188 ksi) was accompanied by a Weibull α of 17.55. Panel variability was again observed. The short-term specimens, cycled to a peak stress of 956 MN/m² (138.8 ksi) at 505 K (450° F), seemed to get stronger with time. One exception was an individual specimen reaching only 882 MN/m² (128 ksi) after 100 hours.

The long-term specimens were cycled to a peak stress of 747 MN/m² (108.3 ksi). The residual tensile, notched tensile, and shear strengths were degraded approximately 25% by the 10,000 hours at 505 K (450° F). Again surface roughness and fiber damage were apparent.

Again, as observed for the crossply B/Al, the decrease in unnotched tensile strength during 10,000 hours of flight simulation could be accounted for by thermal aging effects. In fact, this loss in strength was somewhat less than would be predicted for a 10,000 hour age at 505 K (450° F). The effect of thermal aging on matrix dominated properties, transverse tensile and interfiber shear, was nil except at 700 K (800° F) where oxidation of the boron fibers resulted in a 60% reduction of the interfiber shear strength.

Post long-term fatigue at $R = 0.1$ and 297 K (75° F) achieved a σ_{10^7} value of 772 MN/m² (112 ksi) compared with the 827 MN/m² (120 ksi) baseline value at 297 K (75° F) and the 455 MN/m² (66 ksi) baseline at 561 K (550° F). Scatter is again operating. The $R = -1$ baseline fatigue data again demonstrated compression degradation effects. The σ_{10^7} values were 552 MN/m² (80 ksi) at 297 K (75° F) and 441 MN/m² (64 ksi) at 505 K (450° F).

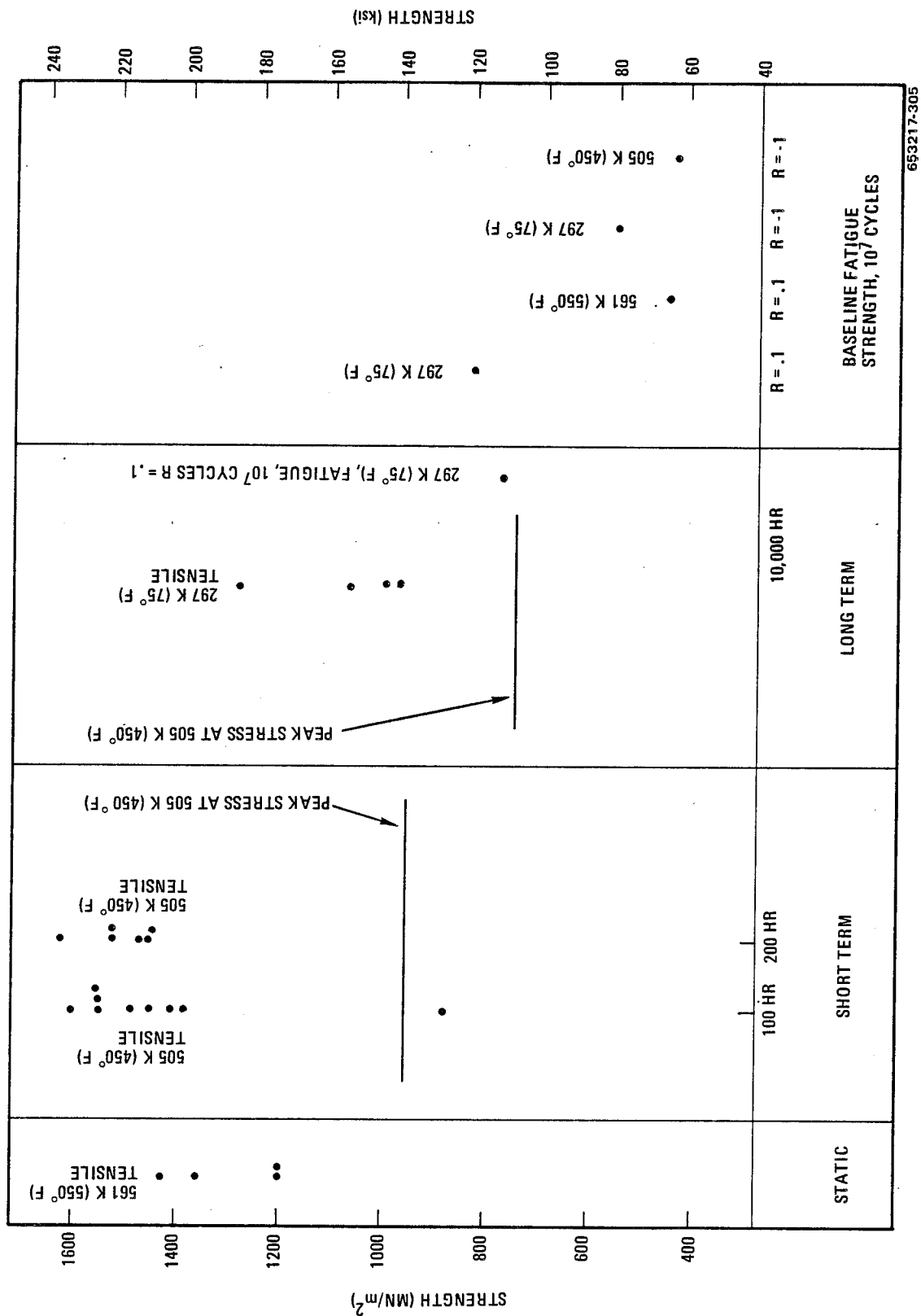
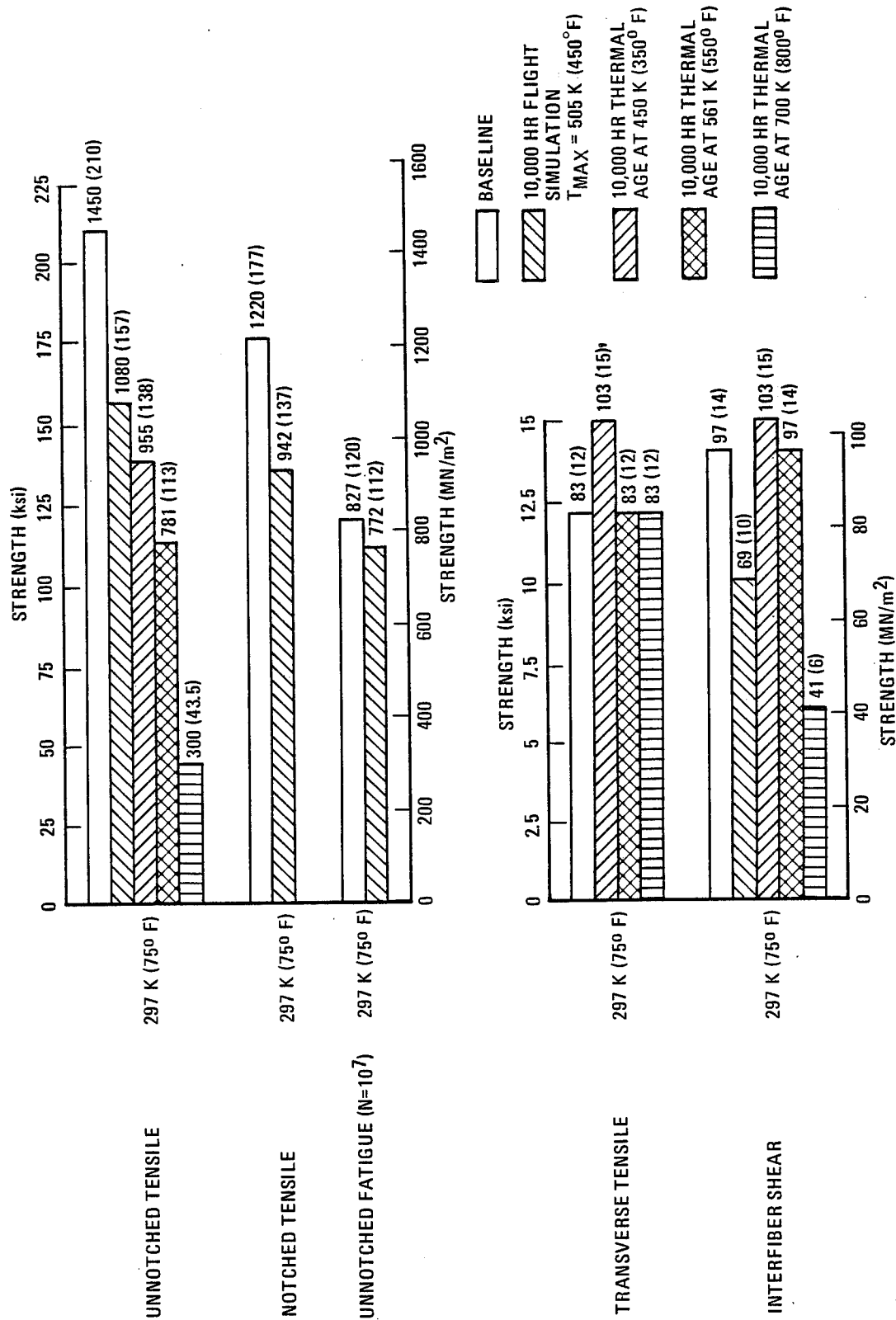


Figure 13-12 Unnotched [0°] B/AI



653217-306

Figure 13-13 Summary of Residual Properties of [0°]₆ B/AI After 10,000 hr of Exposure

SECTION 14

CONCLUSIONS

This report describes a program to characterize the properties of several types of advanced filamentary reinforced composite material systems before and after exposure to simulated supersonic cruise environments for real times of up to 50,000 hours. Because usage of the composites was intended for the lower wing surface of a supersonic aircraft, exposure loads and subsequent residual property measurements were largely tensile. Moisture effects were generally avoided by utilizing careful bakeout and storage procedures. Material behavior during these exposures and post exposure residual property tests provide exposure effects and reveal material failure modes and degradation mechanisms. In addition to the flight simulation exposures, the program provides extensive thermal and ambient aging data for times out to 50,000 hours. This Phase I report has presented considerable baseline fatigue, creep, fracture, and tensile data for all the systems and the flight simulation and thermal and ambient aging results for the first 10,000 hours of the 50,000-hour study. The observations and conclusions relating to these baseline measurements and the environmental exposure tests are summarized briefly below.

A-S/3501 G/E and B/5505 B/E should be limited to temperatures lower than 373 K (212° F) for cumulative exposures greater than 10,000 hours because of:

1. Early flight simulation test failures (due to compressive loading and thermal cycling combined with oxidation induced matrix degradation).
2. Loss of residual strength during flight simulation and thermal aging exposures (due to oxidation induced matrix degradation).
3. Moisture effects on elevated temperature strength (due to matrix degradation).

HT-S/710 G/PI should be limited to 505 K (450° F) for exposures greater than 10,000 hours because of:

1. Loss of residual tensile strength during thermal aging (due to oxidation induced matrix degradation).
2. Loss of residual strength, primarily matrix dominated, during flight simulation exposure (due to combined compressive and thermal stressing in conjunction with oxidation induced matrix degradation).

B/6061 B/Al should be limited to 505 K (450° F) for exposures greater than 10,000 hours because of:

1. Loss of residual tensile strength during thermal aging (due to interface diffusion induced fiber degradation). Some loss in strength can occur at temperatures as low as 450 K (350° F).

2. High temperature fatigue effects (matrix surface cracking and oxidation).
3. Loss of residual strength during flight simulation exposure (due to interface diffusion induced fiber degradation, matrix surface cracking, and oxidation).

B/P 105 AC B/PI is not suitable for this application because of severe matrix degradation during thermal aging and short-term flight simulation exposures at 505 K (450° F).

For the two epoxy systems the baseline and short-term flight simulation results were used in a wearout model to establish the long-term loading conditions. For the G/PI and B/Al materials, however, the wearout theory could not be applied because of inconsistent short-term data. The wearout model was based on a tensile failure mode and made no consideration for thermal effects. Phase I results for the epoxy systems indicated that a more comprehensive model was needed. This new model would be required to account for failure mechanism changes and thermal degradation during the course of the flight simulation exposures in order to more accurately predict complex real time exposure effects.

For the resin matrix systems, matrix degradation by oxidation was shown to be the primary cause of mechanical property losses during thermal aging. For G/E the extent of oxidation could readily be detected by metallographic techniques, especially with the SEM. Similar studies of G/PI revealed increased porosity and fiber-matrix separation accompanied by numerous fine cracks at the fiber-matrix interface. For the B/Al metal matrix system thermal aging strength decreases were primarily fiber related rather than caused by degradation of the aluminum matrix by oxidation.

Fatigue strength was found to be dependent on the stress ratio used in testing. Results for tension-compressive loading ($R = -1$) were considerably lower than those obtained for tension-tension loading ($R = 0.1$). The effect of a notch was generally to reduce the fatigue strength. However, some exceptions were observed at elevated temperature and additional studies are warranted. Severe degradation of the aluminum matrix was found after fatigue testing at 561 K (550° F). Testing in an argon or nitrogen atmosphere or lowering the temperature to 505 K (450° F) significantly decreases the matrix degradation.

Absorption of moisture by the epoxy systems caused a significant decrease in short time elevated temperature strength. Moisture effects were generally less damaging for the G/PI system, particularly for the ambient environment exposures.

Uncoated B/Al is subject to pitting and subsequent intergranular corrosion cracking when exposed for long periods in an industrial-seacoast environment. These corrosion cracks can seriously degrade the matrix controlled properties by acting as crack starters.

Boron or graphite reinforced composite materials with 0° plies aligned in the direction of loading undergo very little creep even at stress levels, which result in fracture in short exposure times. Because of the low creep strains observed in these materials it is suggested that stress rupture tests be substituted for creep measurements.

SECTION 15

REFERENCES

1. Imig, L. A.; and Illg, W.: Fatigue of Notched Ti-8Al-1Mo-1V Titanium Alloy at Room Temperature and 550°F (560°K) With Flight-by-Flight Loading Representative of a Supersonic Transport, NASA TND-5294, 1969.
2. Imig, L. A.; and Garrett, L. E.: Fatigue-Test Acceleration With Flight-by-Flight Loading and Heating to Simulate Supersonic-Transport Operation, NASA TND-7380, 1973.
3. Halpin, J. C.; Jerina, K. L.; and Johnson, T. A.: Analysis of the Test Methods for High Modulus Fibers and Composites, ASTM STP 521, American Society for Testing and Materials, 1973, pp. 5-64.
4. Structural Design Guide for Advanced Composite Applications, Second Edition, Advanced Composites Division, AFML, 1971.
5. Hertz, J.; Christian, J. L.; and Varlas, M.: Advanced Composite Applications for Spacecraft and Missiles, AFML-TR-71-186, 1972.
6. Christian, J. L.: Development and Evaluation of Advanced Metal-Matrix Composite Materials, Rep. GDC-ERR-1571, General Dynamics/Convair, 1970.
7. Forest, J. D.; and Christian, J. L.: Development and Application of Aluminum/Boron Composite Material, AIAA Paper No. 68-975, October 1968.
8. Christian, J. L.; and Jones, R. C.: Development and Evaluation of Improved Boron/Aluminum Composite Material, Rep. GDC-ERR-1450, General Dynamics/Convair, 1970.
9. Forest, J. D.; and Christian, J. L.: Development and Application of High Matrix Strength Aluminum/Boron, presented at ASM Metals Engineering Congress, October 1969.
10. Christian, J. L.: Material and Fabrication Development and Application Studies of Aluminum/Boron-Stainless Steel Composites, presented at ASME 15th Annual International Gas Turbine Conference, Brussels, Belgium, May 1970.
11. Miller, M. F.; Schaefer, W. H.; Weisinger, M. D.; et al: Development of Improved Metal-Matrix Fabrication Techniques for Aircraft Structures, AFML-TR-71-181, 1971.
12. Shockey, P. D.; Hofer, K. E.; Kaminski, B. E.; Lemon, G. H.; and McKague, E. L.: Development of Engineering Data for Advanced Composite Materials, Vol. I-Static and Thermophysical Properties, Vol. II-Fatigue and Load Rate Characteristics, AFML-TR-70-108, 1972.

13. Shockey, P. D.; Hofer, K. E.; and Wright, W. D.: Structural Airframe Application of Advanced Composite Materials, Vol. IV-Mechanical Properties-Static, AFML-TR-69-101, 1969.
14. Development of Engineering Data on the Mechanical and Physical Properties of Advanced Composites Materials, AMFL-TR-72-205 - Part I, 1972.
15. Advanced Composites Data for Aircraft Structural Design, Report No. NA-71-679-9, North American Rockwell, 1972.
16. Beeler, D. R.; and Chase, V. A.: Advanced Polyimide Composites, SAE Conference, Oct. 1968.
17. Vaughan, R. W.: Glass Reinforced P13N Polyimide Laminates Having Improved Processing Characteristics, 15th National SAMPE Conference, April 1969.
18. Vaughan, R. W.; Jones, R. J.; Sheppard, C. H.; and Burns, E. A.: Development of Low Void Polyimide Resin for Autoclave Processing of Glass and Graphite Reinforced Composites, National SAMPE Conference, Oct. 1971.
19. Petker, I.; et al: High-Strength, High-Modulus Filament-Reinforced Composites, AFML-TR-67-395, 1968.
20. Birchfield, E. B.; and Kollmansberger, R.: Develop Fabrication/Processing Techniques for High Temperature Advanced Composites for Use in Aircraft Structures, AFML-TR-72-91, 1972.
21. Scheck, W. G.: Development of Design Data for Graphite Reinforced Epoxy and Polyimide Composites, Rep. GDC-DBG70-005, General Dynamics/Convair, 1974.
22. Stuckey, J.; and Scheck, W. G.: Development and Evaluation of Graphite and Boron Polyimide Composites, National SAMPE Technical Conference, Oct. 1972, Palo Alto, California.
23. Peterson, R. E.: Stress Concentration Design Factors. John Wiley and Sons, Inc., 1953.
24. Waddoups, M. E.; Eisenmann, J. R.; and Kaminski, B. E.: Macroscopic Fracture Mechanics of Advanced Composite Materials. J. Composite Materials, 5, 1971, p. 446.
25. Konish, H. J., Jr.: A Study of Fracture Phenomena in Fiber Composite Laminates, AFML-TR-73-145, Vol. III, 1973.
26. Adsit, N. R.; and Waszczak, J. P.: Fracture Mechanics Correlation of Boron/Aluminum Coupons Containing Stress Risers, ASTM Symposium on Fracture Mechanics of Composites, 1974.
27. Paris, P. C.; and Sih, G. C.: Stress Analysis of Cracks. Fracture Toughness Testing and its Applications, ASTM STP 381, American Society for Testing and Materials, 1970, pp. 30-83.

28. Chase, V.; and Beeler, D.: Manufacturing Methods for Large High-Temperature Sandwich Structures, AFML-TR-70-211, 1970.
29. Jones, R. L.: Evaluation of Electron Scanning Microscopes, Rep. ERR-FW-1188, General Dynamics/Convair, 1972.
30. Metcalfe, A. G., ed.: Interfaces in Metal Matrix Composites, Academic Press, 1974.
31. Hertz, J.: Investigation Into the High Temperature Strength Degradation of Fiber-Reinforced Resin Composites During Ambient Aging, NASA CR-124290, 1973.
32. Shirrell, C. D.; Halpin, J. C.; and Browning, C. E.: Moisture — An Assessment of Its Impact on the Design of Resin Based Advanced Composites, Third Conf. on Fibrous Composites in Flight Vehicle Design, November 4-6, 1975, NASA TMX-3377, April 1976.
33. Schaefer, W. H.; and Christian, J. L.; et al.: Evaluation of the Structural Behavior of Filament Reinforced Metal Matrix Composites, AFML-TR-69-36, 1969.
34. Treadway, D. G.; Sutherland, W. M.; and Keller, E. E.: Aerospace Corrosion Prevention Studies, Rep. GDCA-ERR-1612, General Dynamics/Convair, 1971.
35. Shockey, P. D.; Anderson, J. D.; and Hofer, K. E.: Structural Airframe Application of Advanced Composite Materials - Vol. V, Mechanical Properties-Fatigue, AFML-TR-69-101, 1970.
36. Shockey, P. D.; and Hofer, K. E.: Development of Engineering Data for Advanced Composite Materials, Vol. II, Fatigue and Load Rate Characteristics, AFML-TR-70-108, 1972.
37. Military Standardization Handbook, Metallic Materials and Elements for Aerospace Vehicle Structures, MIL-HDBK-5B, Department of Defense, Washington, D. C., 1975.
38. Wolff, R. V.; and Lemon, G. H.: Reliability Prediction for Adhesive Bonds, AFML-TR-72-121, 1972.
39. Waddoups, M. E.; Wolff, R. V.; and Wilkins, D. J.: Reliability of Complex Large Scale Composite Structure-Proof of Concept, AFML-TR-73-160, 1973.
40. Halpin, J. C.; Johnson, T. A.; and Waddoups, M. E.: Kinetic Fracture Models and Structural Reliability, International Journal of Fracture Mechanics, Vol. 8, 1972.
41. Wolff, R. V.; and Lemon, G. H.: Reliability Prediction for Composite Joints-Bonded and Bolted, AFML-TR-74-197, 1974.
42. Wolff, R. V.; Wilkins, D. J.; Lemon, G. H.; Orringer, O. R.; and Shinozuka, M.: Life Assurance of Composite Structures, Vol. II - Technology, Vol. III -Element Characterization, AFFDL-TR-77-50, 1977.

APPENDIX A

AN ANALYSIS OF THE B/P105AC BORON POLYIMIDE SYSTEM

Approximately midway through Phase I of the program the decision was made to cancel all testing of the B/P105AC boron/polyimide system. The removal of the B/PI was based on very low tensile properties found for the majority of the panels and extensive thermal degradation observed during thermal aging and short-term flight simulation testing. The following is a brief description of the problems experienced with this material system, and what are believed to have been the reasons for the poor results.

In mid 1973, 28 kg (62 lb) of B/P105AC prepreg was ordered from AVCO Corporation with delivery expected in one to two months. Because of difficulties encountered by AVCO in obtaining the polyimide resin from the manufacturer, Ciba-Geigy, delivery was delayed until the end of 1973. Upon receipt of the prepreg, quality assurance testing was performed. The material was found to be acceptable. Two quality assurance panels were then fabricated. Before quality assurance testing could be completed, however, Ciba-Geigy informed us that they would no longer produce the P105AC resin (see letter on Page A-2), and as they were the only source of this material, testing was put on hold.

After a four-month delay, permission was received from NASA to resume fabrication and testing as it was thought that AVCO Corporation would obtain a license to produce the resin. The quality assurance panels were ultrasonically C-scanned, specific gravity and resin, fiber, and void contents were determined, and quality assurance mechanical property data were obtained. The results (see Tables 6-8 and 6-9) indicated the materials to be acceptable. Only the room temperature shear strength of the unidirectional material was on the low side, 55 MN/m² (8 ksi), compared to an expected value of about 69 to 83 MN/m² (10 to 12 ksi). Based on the quality assurance tests, the required number of full size panels were fabricated.

At about this time in the program, mid 1974, the start of short-term testing of B/PI had fallen well behind schedule. Since only crossplied specimens were to be used in the short-term tests, the main effort in baseline testing was, therefore, on the crossplied material. Baseline tensile and notched tensile tests were performed. Results are given in Tables A-1 and A-2. The data were typical of good material; consequently short-term specimens were prepared and installed in the flight simulation apparatus.

Baseline testing of the unidirectional material, which previously had been given low priority, was now started. Also during this time period, the end of 1974, results from the thermal aging tests were becoming available, and proof testing of the short-term specimens was begun. All three of these tests gave indications of a potential problem with the B/PI material system.

Unidirectional tensile strengths, Table A-3, were only half of what was considered normal. The notched unidirectional tensile strength, Table A-4, were somewhat higher but still unacceptable. The three notched specimens tested at room temperature gave particularly low values. These specimens and all of the unnotched specimens were cut from panel LRC-32. The remaining notched specimens were cut from panel LRC-34.

Plastics Operations

CIBA-GEIGY Corporation
Ardsley, New York 10502
914 478 3131

CIBA-GEIGY

November 15, 1973

Dear Customer,

It is necessary for us to discontinue one of our polyimide products, Pl05AC, when present stocks are exhausted. This is occasioned by the unanticipated withdrawal from commerce of one of the monomers required, thiodianiline. Pl05A, an earlier version, was replaced by Pl05AC early in 1973. The former product also was based on this monomer and cannot be re-introduced. Adhesive composition, LSU-1106, also containing thiodianiline is similarly affected.

Our Pl13N polyimide family contains no thiodianiline and is not affected. We encourage use of Pl13N in your applications. If changes in processing are required due to different flow characteristics, our Development & Applications Laboratory stands ready to render necessary assistance.

We are sorry for any inconvenience that this reluctant but unavoidable decision may have caused. CIBA-GEIGY appreciates your valued business and looks forward to providing continuing requirements for high quality engineering resins.

Very truly yours,



Stephen S. Hirsch
Manager, Business Development

SSH:jk

Table A-1. Baseline Tensile Properties [$0^\circ \pm 45^\circ$], B/PI

Specimen Number	Temperature		Tensile Strength		Tensile Modulus	
	K	(°F)	MN/m ²	(ksi)	GN/m ²	(Msi)
CC01-1	218	-67	450	65.3	88	12.7
-2			478	69.4	79	11.5
-3			513	74.4	84	12.2
			av 480	69.7	84	12.1
CC01-4	297	75	510	74.0	^a 105	^a 15.3
-5			505	73.2	^a 110	^a 16.0
-6			565	81.9	^a 91	^a 13.2
			av 527	76.4	102	14.8
CC01-7	505	450	490	71.1	^a 66	^a 9.5
-8			484	70.2	^a 66	^a 9.5
-9			547	79.4	^a 62	^a 9.0
-22			539	78.2	—	—
-23			518	75.2	—	—
-24			478	69.4	—	—
-25			538	78.1	—	—
-26			565	81.9	—	—
-27			549	79.6	—	—
-28			494	71.6	—	—
-29			443	64.2	—	—
-30			544	78.9	—	—
-31			525	76.2	—	—
-32			555	80.5	—	—
-33			562	81.5	—	—
-34			522	75.7	—	—
-35			494	71.7	—	—
			av 520	75.5	65	9.3
CC01-10	533	500	501	72.6	—	—
-11			465	67.5	—	—
-12			483	70.1	—	—
			av 483	70.1	—	—
CC01-13	561	550	446	64.7	^a 58	^a 8.4
-14			437	63.4	^a 55	^a 8.0
-15			447	64.8	^a 56	^a 8.1
			av 443	64.3	56	8.2
CC01-16	589	600	415	60.2	—	—
-17			452	65.6	—	—
-18			463	67.1	—	—
			av 443	64.3	—	—
CC01-19	616	650	444	64.4	—	—
-20			468	67.9	—	—
-21			482	69.9	—	—
			av 465	67.4	—	—

^a Strain gage measurement

Table A-2. Baseline Notched Tensile Properties of $[0^\circ \pm 45^\circ]_s$ B/PI

Specimen Number	Temperature		Notched Tensile Strength	
	K	(°F)	MN/m ²	(ksi)
CC02-1	218	-67	444 (a)	64.4
-2			432	62.7
-3			458	66.4
			av 445	64.5
CC02-4	297	75	503	73.0
-5			424	61.5
-6			404	58.6
			av 444	64.4
CC02-7	505	450	396	57.5
-8			379	54.9
-9			377	54.7
-22			383	55.5
-23			380	55.1
-24			342	49.6
-25			381	55.2
-26			379	54.9
-27			399	57.8
-28			372	54.0
-29			367	53.3
-30			372	54.0
-31			358	52.0
-32			369	53.5
-33			361	52.4
-34			356	51.6
-35			372	54.0
			av 373	54.1
CC02-10	533	500	416	60.4
-11			395	57.3
-12			423	61.3
			av 411	59.7
CC02-13	561	550	392	56.9
-14			398	57.7
-15			381	55.3
			av 390	56.6
CC02-16	589	600	396	57.5
-17			388	56.3
-18			388	56.3
			av 391	56.7
CC02-19	616	650	437	63.4
-20			425	61.7
-21			459	66.5
			av 440	63.9

^a Net section strength, i.e., based on total width less hole diameter.

Table A-3. Baseline Tensile Properties $[0^\circ]_6$ B/PI

Specimen Number	Temperature		Tensile Strength	
	K	(°F)	MN/m ²	(ksi)
CU01-22	505	450	848	123
-23			765	111
-24			717	104
-25			800	116
-26			772	112
-27			779	113
-28			945	137
-29			572	82.9
-30			657	95.3
			av	761
CU01-10	533	500	630	91.4
-11			627	91.0
-12			910	132
			av	722
CU01-16	561	550	510	74.0
-17			606	87.9
-18			331	48.0
			av	482
CU01-19	589	600	421	61.0
-20			690	100
-21			745	108
			av	619

Results of thermal aging exposures at 505 K (450° F) and 561 K (550° F) for times to 1000 hours were also very poor. Tensile testing of specimens aged for 500 hours gave low strength values with the specimens literally falling apart during the tests. Specimens aged 1000 hours failed by delamination during the doubler bonding operation and could not even be tested.

The third indication of unsatisfactory material came during the short-term tests. At 75% of the proof load used for the short-term exposures, four of the specimens failed. The stress levels were approximately 350 MN/m² (50 ksi), well below the average F_{tu} of 520 MN/m² (76 ksi) obtained from the baseline tests. The appearance of the failed specimens, which prior to proof loading had been baked out for 72 hours at 478 K (400° F) to remove any absorbed moisture, was similar to those from the thermal aging tests. The resin had crumbled away in the region of the failures leaving bare boron filaments.

At the beginning of the short-term testing of the G/PI system, a few of the B/PI specimens that had survived the proof test were included in with the G/PI specimens. One of these failed after only seven hours, while the remaining ones were badly damaged and about to fail. The appearance was similar to those described above with the resin breaking away from the boron filaments. Figure A-1 shows the heated area of one of the unfailed specimens. It is held together by the boron filaments with only a small amount of resin remaining.

Table A-4. Baseline Notched Tensile Properties of $[0^\circ]_6$ B/PI

Specimen Number	Temperature		Notched Tensile Strength	
	K	(°F)	MN/m ²	(ksi)
CU02-4	297	75	717 (a)	104
-5			557	80.8
-6			469	68.0
			av 581	84.3
CU02-7	505	450	669	97.1
-8			896	130
-9			862	125
-22			1250	181
-23			1320	191
-24			1190	173
-25			703	102
-26			1230	179
-27			1080	156
-28			1100	159
-29			1110	161
-30			1120	162
-31			903	131
-32			910	132
-33			882	128
-34			827	120
-35			862	125
			av 995	144
CU02-10	533	500	1240	180
-11			1200	174
-12			1070	155
			av 1170	170
CU02-13	561	550	1190	173
-14			1130	164
-15			952	138
			av 1090	158
CU02-16	589	600	979	142
-17			1110	161
-18			1040	151
			av 1040	151
CU02-19	616	650	910	132
-20			1010	146
-21			979	142
			av 966	140

^a Net section strength, i.e., based on total width less hole diameter.

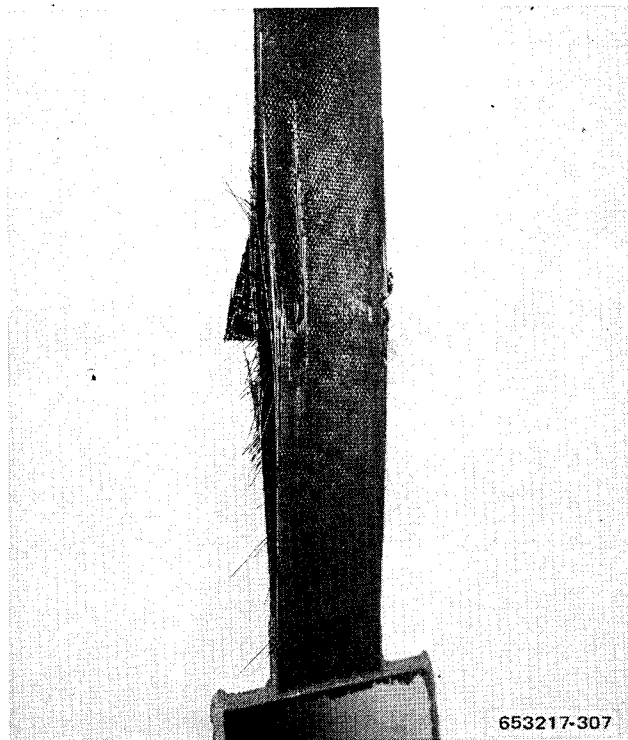


Figure A-1 Heated Area of B/PI Short-Term Specimen After Only 7 hr of Flight Simulation Exposure at 505 K (450° F)

To check the extent of the material problem and determine the cause, the following tasks were performed:

- a. Measured tensile properties of the remaining panels.
- b. Measured specific gravity, resin content, and fiber content of all tested panels.
- c. Conducted metallographic and SEM evaluations.

The results of the tensile tests are listed in Table A-5. Only two panels had acceptable tensile properties. LRC-33 and LRC-35. It was from LRC-33 that the crossplied baseline tensile specimens were cut.

Values of specific gravity, resin content, fiber content, and percent voids are listed in Table A-6. There appears to be no correlation between these values and the tensile data of Table A-6.

Two specimens were submitted for metallographic examination, one that had been thermal aged at 561 K (550° F) for 1000 hours, and a baseline tensile specimen. The aged specimen could not be sectioned or mounted as the resin matrix crumbled away during preparation. The tensile specimen, shown at 100X magnification in Figure A-2, revealed several points of interest and offered possible explanations for the poor behavior of the material. First, the spacing of the filaments within the plies was very nonuniform with many of the filaments touching each

Table A-5. Tensile Data for B/PI Panels Tested at 297 K (75° F)

Panel Number	Orientation	Tensile Strength		Intended Use (a)
		MN/m ²	(ksi)	
LRC-32	[0°] ₆	1100	159	0, 7
		965	140	
		896	130	
		av 987	143	
LRC-33	[0° ± 45°] _s	510	74.0	0
		505	73.2	
		565	81.9	
		av 527	76.4	
LRC-34	[0°] ₆	1360	198	0, 7
		1190	172	
		1160	169	
		av 1240	180	
LRC-35	[0° ± 45°] _s	530	76.8	0, 7
		512	74.2	
		512	74.2	
		av 518	75.1	
LRC-36	[0° ± 45°] _s	415	60.2	8
		410	59.4	
		av 412	59.8	
LRC-37	[0° ± 45°] _s	461	66.8	8
		486	70.5	
		av 474	68.6	
LRC-38	[0° ± 45°] _s	387	56.2	8
		389	56.4	
		av 388	56.3	
LRC-39	[0°] ₆	917	133	1, 5
		917	133	
		876	127	
		av 906	131	
LRC-40	[0° ± 45°] _s	412	59.7	0, 5
		415	60.2	
		432	62.6	
		av 420	60.8	
LRC-41	[0° ± 45°] _s	360	52.2	1
		395	57.3	
		av 378	54.7	

Table A-5. Tensile Data for B/PI Panels Tested at 297 K (75° F) — Concluded

Panel Number	Orientation	Tensile Strength		Intended Use (a)
		MN/m ²	(ksi)	
LRC-42	[0° ± 45°] _s	436	63.2	9
		437	63.4	
		av 436	63.3	
LRC-43	[0° ± 45°] _s	398	57.7	9
		412	59.7	
		av 405	58.7	

^a 0 Baseline

1 Thermal Aging

2 Ambient Aging

5 Creep

7 Fatigue

8 Short-term Exposure

9 Long-term Exposure

Table A-6. Specific Gravities and Resin, Fiber, and Void Contents of B/PI Panels

Panel Number	Orientation	Specific Gravity	Resin Content (wt %)	Fiber Content	Void Content (vol. %)
				(wt %) (a)	
LRC-32	[0°] ₆	1.98	28.4	71.6	3.6
LRC-33	[0° ± 45°] _s	1.97	32.5	67.5	0.8
LRC-34	[0°] ₆	1.93	26.9	73.1	7.0
LRC-35	[0° ± 45°] _s	1.94	30.6	69.4	3.8
LRC-37	[0° ± 45°] _s	1.91	33.5	66.5	3.4
LRC-38	[0° ± 45°] _s	1.98	26.3	73.7	4.7
LRC-39	[0°] ₆	1.98	27.0	73.0	4.2
LRC-40	[0° ± 45°] _s	1.90	37.2	62.8	1.0
LRC-41	[0° ± 45°] _s	1.91	31.0	69.0	4.9

^a Includes approximately 9% glass fiber from scrim cloth.

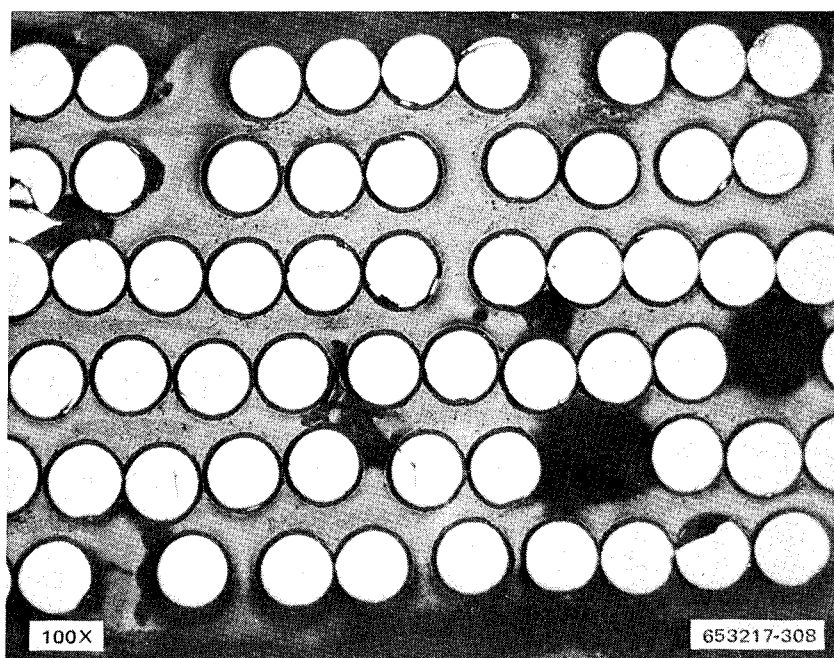


Figure A-2 Photomicrograph of a Transverse Section of $[0^\circ]_6$ B/PI Showing Nonuniform Filament Spacing and an Indication of Poor Bonding of the Resin to the Boron Filaments

other. For example, in this photomicrograph, as many as six touching filaments in a row can be seen. Efficient distribution of stresses within a composite and, hence, high strength, particularly in the transverse directions, requires good bonding of the matrix to the filaments with a minimum of filament-to-filament contact. The second, and more important feature of the photomicrograph, was the apparent lack of contact or bonding between the fibers and the resin matrix. This is difficult to show conclusively with a light microscope with its poor depth of field. Because of the significance of this apparent lack of bonding, additional examinations were made using a scanning electron microscope (SEM), an instrument with excellent depth of field.

The photomicrographs in Figures A-3 and A-4 clearly show examples of the separation between filaments and the matrix in both unidirectional and crossplied specimens. Further evidence of poor bonding of the resin to the boron is shown in Figures A-5 and A-6 by the pullout of the filaments from the matrix and the fact that the filaments are smooth with almost no resin adhering to the surface.

It is this lack of bonding of the resin to the filaments that is believed to have been responsible for the poor tensile behavior of the B/P105AC system. Whether the problem was caused by the filaments (dirty or contaminated surface, for example) or by the resin is not known. There had been reported during this time period, however, instances of the P105AC resin going bad in storage, and this may well have been the case for the batch of material evaluated on this program.

The reason for the unsatisfactory performance of the specimens during thermal aging and short-term flight simulation was apparently a combination of two effects. These were the poor bonding of the matrix to the filaments discussed above combined with a resin matrix material that was not capable of extended service at 505 K (450° F).

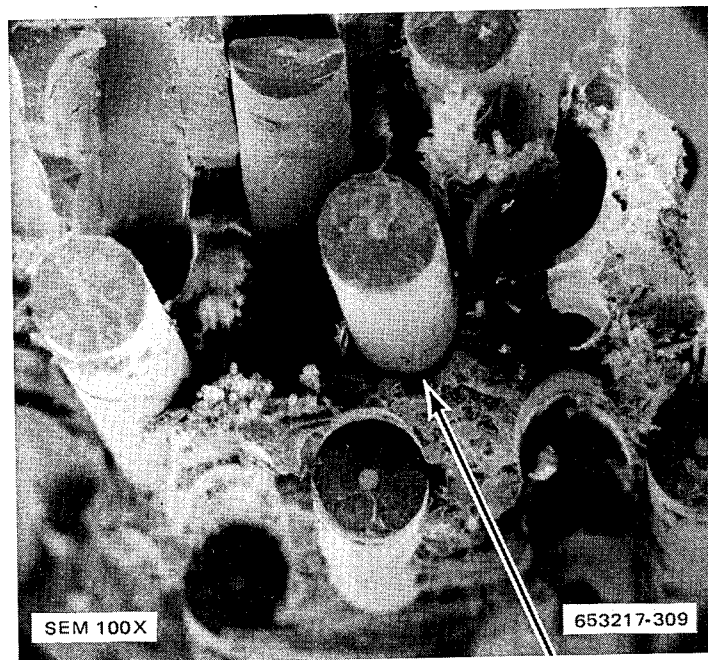


Figure A-3 Fracture Surface of $[0^\circ]_6$ B/PI Tensile Specimen Showing (arrow) Poor Bonding Between Boron Filament and Resin Matrix

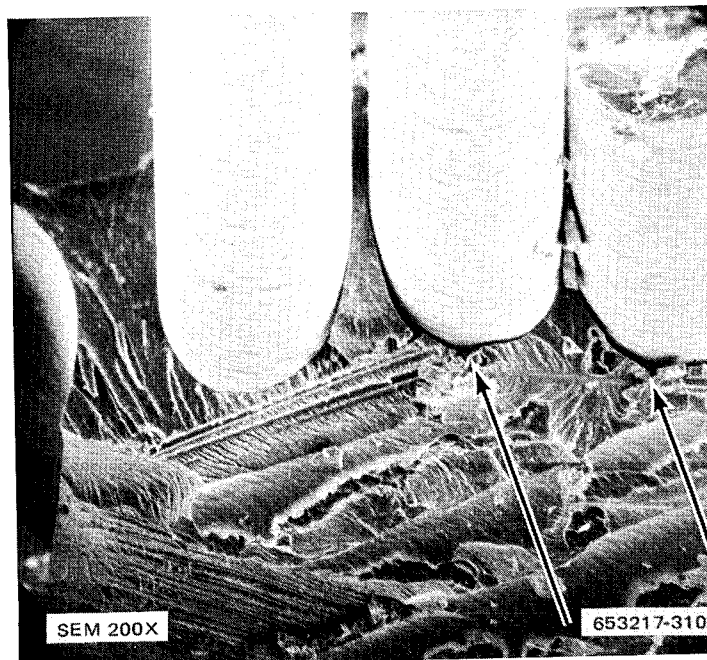


Figure A-4 Fracture Surface of $[0^\circ \pm 45^\circ]_6$ B/PI Tensile Specimen Showing (arrows) Poor Bonding Between Filaments and Resin Matrix

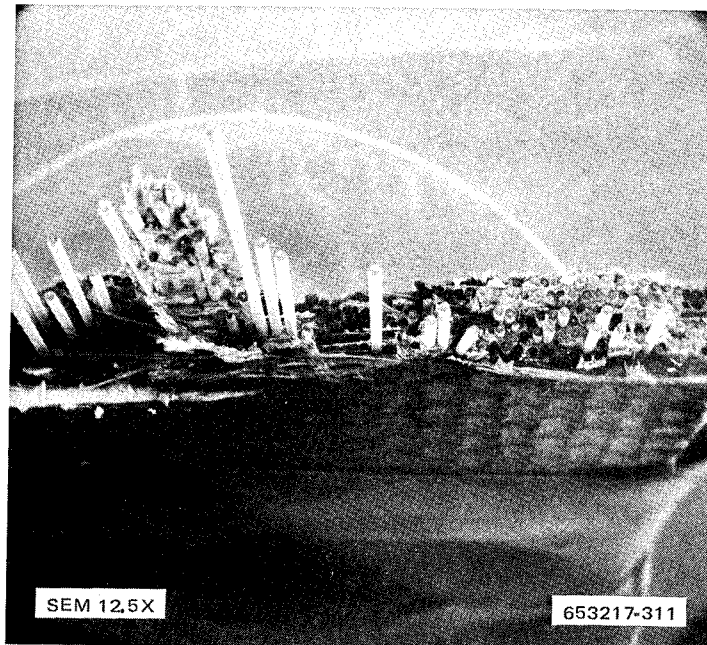


Figure A-5 Fracture Surface of $[0^\circ]_6$ B/PI Tensile Specimen Showing Pullout of the Boron Filaments from the Matrix (an indication of poor matrix-to-filament bond)



Figure A-6 B/PI $[0^\circ]_6$ Specimen Tensile Tested at 505 K (450° F) After a 500-hr Thermal Age at 505 K (450° F). (Most of the resin has broken away, leaving bare boron filaments and scrim cloth)

APPENDIX B

QUALITY ASSURANCE TEST PROCEDURES

B.1 PREPREG VOLATILE CONTENT

Cut three specimens of the material, each approximately 0.051 by 0.051 m (2.0 by 2.0 in.), from an area of the sample away from the edges. The specimen may be any shape that will fit into a preweighed and fired crucible or disposable aluminum dish but may not be rolled up or more than one ply. Weigh each crucible on an analytical balance to the nearest 0.1 mg (W_2). Place the test specimen in the crucible and record the total weight to the nearest 0.1 mg (W_1). Place the crucible containing the specimen in a preheated air circulating oven (for epoxy resin use 436 K (325° F) for 15 ± 1 minutes and for polyimide resin use 450 K (350° F) for 20 ± 1 minutes), cool to room temperature, and weigh to the nearest 0.1 mg (W_3). The mean value of the three volatile determinations calculated as follows was reported:

$$\text{Volatile Content, weight percent} = \frac{W_1 - W_3}{W_1 - W_2} \times 100$$

where:

W_1 = Weight of crucible plus specimen before volatile removal

W_2 = Weight of crucible

W_3 = Weight of crucible plus specimen after volatile removal

B.2 PREPREG RESIN SOLIDS AND FIBER CONTENT

Cut three specimens of the material, each approximately 0.051 by 0.051 m (2.0 by 2.0 in.), from an area of the sample away from the edges. Weigh a specimen to the nearest 0.1 mg (W_1), place in a 300 ml tall-form beaker, and add 25 ml of dimethyl formamide (DMF) technical grade. Place the beaker on a hot plate and heat to boiling for 10 to 15 minutes. Remove the beaker from the hot plate and allow to cool to room temperature. Pour off the DMF, being careful not to lose any fibers. Rinse the fiber residue two or three times in acetone. After removing most of the acetone, place the fibers in a tared aluminum cup (throwaway type) and dry for 30 minutes minimum in an oven at 436 K (325° F). Determine the weight of fibers (W_2) to the nearest 0.1 mg and record. The mean value of three fiber and resin solids content determinations calculated as follows was reported:

$$\text{Fiber Content, weight percent} = \frac{W_2}{W_1} \times 100$$

$$\text{Resin plus volatiles, weight percent} = 100 - \frac{W_2}{W_1} \times 100$$

$$\text{Resin Solids Content, weight percent} = 100 - \frac{W_2}{W_1} \times 100 - \text{Volatile Content}$$

where:

W_1 = weight of specimen

W_2 = weight of fibers

Volatile Content = See Section B.1

B.3 PREPREG RESIN FLOW

Cut six pieces of style 181 glass fabric, 0.10 by 0.10 m (4.0 by 4.0 in.) square, for bleeder and two squares of Teflon coated glass fabric of the same size, for separator. Weigh to the nearest 0.1 mg (W_1) on an analytical balance. Cut two pieces of the material to be tested 0.051 by 0.051 m (2.0 by 2.0 in.) and weigh with the separator and bleeder to the nearest 0.1 mg (W_2). Cross ply the two specimens and sandwich them between the separator and the bleeder with the bleeder on the outside. Place in a preheated press and cure for $15 \pm 1_0$ minutes under 0.69 MN/m^2 (100 psig) at 436 K (325° F) for the epoxy system and at 450 K (350° F) for the polyimide system. Remove the crossply test specimen from the separator and bleeder. Weigh the separator plus bleeder to the nearest 0.1 mg (W_3). The mean value of three flow determinations calculated as follows was reported:

$$\text{Percent Flow} = \frac{W_3 - W_1}{W_2 - W_1} \times 100$$

where:

W_1 = Weight of glass fabric plus Teflon coated glass fabric

W_2 = Weight of glass fabric, Teflon coated glass fabric, and specimens

W_3 = Weight of glass fabric plus Teflon coated glass fabric after cure

B.4 LAMINATE SPECIFIC GRAVITY

The method used for determining the specific gravity of the laminates was by displacement of water. The test procedure was in accordance with Federal Test Method Standard No. 406, Method 5011. Cut three pieces of the laminate to be tested 0.013 by 0.013 m (0.5 by 0.5 in.). Using an analytical balance and a specific gravity bridge, weigh the specimen in air (W_1) and in distilled water (W_2) at $296 \pm 1.1 \text{ K}$ ($73.5 \pm 2^\circ \text{ F}$). The mean value of three specific gravity determinations calculated as follows was reported:

$$\text{Specific Gravity} = \frac{W_1}{W_1 - W_2}$$

where:

W_1 = weight of specimen in air

W_2 = weight of specimen in water

B.5 LAMINATE RESIN AND FIBER CONTENT

The test specimen was approximately 0.013 by 0.013 m (0.5 by 0.5 in.) by laminate thickness. The cured resin and fiber content was determined by acid/peroxide digestion as follows:

1. Weigh the test specimen to the nearest 0.1 mg (W_1), place in a 300 ml tall-form beaker, and add 20 ml of concentrated sulfuric acid. Place the beaker on a hot plate and heat the acid until vigorous fuming occurs.
2. When the composite is visibly disintegrated and resin particles and fibers are dispersed throughout the sulfuric solution, carefully add the hydrogen peroxide (50% strength) dropwise down the side of the beaker. Rubber gloves and a fume hood with appropriate safety glass shield shall be used throughout the addition, and precautions shall be taken as recommended by the applicable safety regulations and procedures for handling hydrogen peroxide.
3. The reaction is considered complete when the hot sulfuric acid solution below the fibers becomes clear and colorless. At this point add two more ml of hydrogen peroxide to the solution, and heat the solution to fumes for another 10 minutes to ensure complete decomposition of the polymer. Remove the beaker from the hot plate, and allow to cool to 294 to 300 K (70° to 80° F) and then place in an ice bath.
4. Collect fibers by vacuum filtration through a medium-porosity, sintered-glass crucible that has been weighed to nearest 0.1 mg (W_2). After the sulfuric acid has been filtered off, wash the fibers in the crucible thoroughly with 600 ml of distilled water, adding a few milliliters at a time. Verify removal of sulfuric acid traces by checking pH of the filtrate drops.
5. Remove the crucible from the filtering system and place in an open beaker in an oven at 422 K (300° F) for 45 minutes. After drying, cool the crucible in a desiccator and weigh to the nearest 0.1 mg (W_3).

The resin and fiber content were calculated according to the following equations:

$$\text{Resin Content, weight percent} = \frac{W_1 - (W_3 - W_2)}{W_1} \times 100$$

$$\text{Fiber Content, weight percent} = \frac{W_3 - W_2}{W_1} \times 100$$

where:

W_1 = Weight of test specimen

W_2 = Weight of crucible

W_3 = Weight of crucible plus fibers after acid/peroxide digestion

B.6 B/Al LAMINATE FIBER VOLUME

The test specimen was approximately 0.013 m (0.5 by 0.5 in.) by laminate thickness. The fiber volume was determined as follows:

1. Wash, dry, and weigh the test specimen to the nearest 0.1 mg (W_1).
2. Leach the fibers from the samples in a 50% solution of sodium hydroxide at approximately 339 K (150° F).
3. Wash, dry, and weigh the collected fibers to the nearest 0.1 mg (W_2).

Assuming a density of 2700 kg/m³ for the aluminum and a density of 2510 kg/m³ for the 5.6 mil boron, the volume percentages of fibers were calculated according to the following equation:

$$\text{Fiber Volume, volume percent} = \frac{\frac{W_2}{\rho_F}}{\frac{W_1 - W_2}{\rho_A} + \frac{W_2}{\rho_F}} \times 100$$

where:

W_1 = Weight of test specimen

W_2 = Weight of fibers

ρ_F = Density of fibers

ρ_A = Density of aluminum

B.7 LONGITUDINAL FLEXURAL STRENGTH

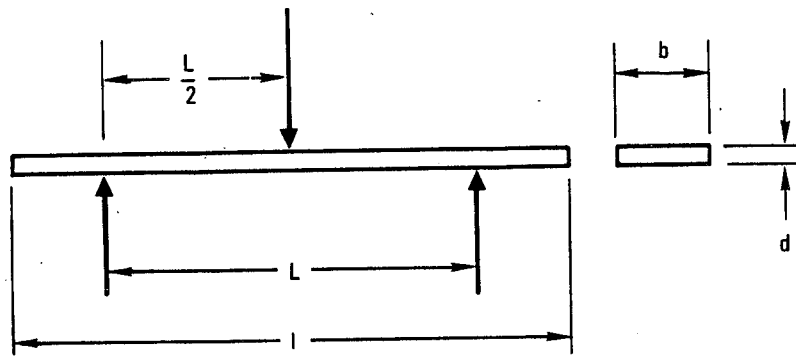
The test method used for determining longitudinal flexural strength was generally in accordance with ANSI/ASTM D 790-71 and Federal Test Method Standard No. 406, Method 1031. Specimens were cut with the fibers aligned parallel to the longitudinal axis. The specimen configuration with the loading geometry is shown in Figure B-1. Testing was done with three point loading using a span to thickness ratio of 32 to 1. The specimens, with the smooth side up, were loaded to failure at 0.0025 m (0.10 in.) per minute crosshead speed in standard test machines (Instron, Tinius-Olsen, or Baldwin). The longitudinal flexural strengths were calculated according to the following formula:

$$F_L = \frac{3PL}{2bd^2}$$

where:

F_L = Ultimate longitudinal flexural strength

P = Maximum load carried by the specimen



Specimen Dimensions

Length (l) = 0.076 m (3.0 in.)

Width (b) = 0.01270 m (0.500 in.)

Thickness (d) = Approximately 0.0015 m (0.060 in.)

Span/Thickness Ratio ($\frac{L}{d}$) = 32 to 1

Loading head and reaction supports are 0.00635 m (0.250 in.) diameter steel rod

Overhang must be the same over each end

653217-313

Figure B-1. Longitudinal Flexural Specimen

L = Support span

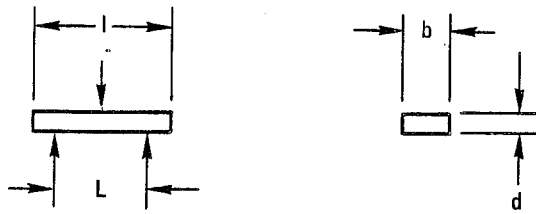
b = Specimen width

d = Specimen thickness

B.8 SHORT BEAM SHEAR STRENGTH

The test method used for determining short beam shear strength was generally in accordance with ANSI/ASTM D2344-76. Specimens were cut with the fibers aligned parallel to the longitudinal axis. The specimen configuration with the loading geometry is shown in Figure B-2. Testing was done with three point loading using a span to thickness ratio of 4 to 1. The specimens, with the smooth side up, were loaded to failure at 0.0025 m (0.10 in.) per minute crosshead speed in standard test machines (Instron, Tinius-Olsen, or Baldwin). The short beam shear strengths were calculated according to the following formula:

$$\tau = \frac{3P}{4bd}$$



Specimen Dimensions

Length (l) = 0.0152 m (0.60 in.)

Width (b) = 0.00635 m (0.250 in.)

Thickness (d) = Approximately 0.0015 m (0.060 in.)

Span/Thickness Ratio ($\frac{L}{d}$) = 4 to 1

Loading head and reaction supports are 0.00318 m (0.125 in.) diameter steel rod

Overhang must be the same over each end

653217-314

Figure B-2. Short Beam Shear Specimen

where:

τ = Ultimate short beam shear strength

P = Maximum load carried by the specimen

b = Specimen width

d = Specimen thickness